

Nonlinear Structural Analysis

©Filip C. Filippou
University of California, Berkeley

Department of Civil and Environmental Engineering

Contents

1	Event to Event Linear Elastic, Perfectly Plastic Analysis	1
1.1	Introduction	1
1.1.1	Analysis Methods	2
1.1.2	Incremental Loading and Analysis	2
1.1.3	Event-to-Event Incremental Analysis	2
1.1.4	Limitations of Event-to-Event Analysis	2
1.1.5	Linear Response Increment with Force Method of Analysis	3
1.1.6	Event-to-Event Analysis with Displacement Method	3
1.1.7	Linear Response Increment with Displacement Method of Analysis	3
1.1.8	Proportionality of Linear Response	4
1.1.9	Principle of Linear Superposition	4
1.2	Linear Elastic Response Limit	5
1.2.1	Range of Linear, Elastic Structural Response	5
1.2.2	Limit Load Factor for Linear, Elastic Response	5
1.3	Event-to-Event Analysis	6
1.3.1	Notation	6
1.3.2	Summary of Key Relations for Linear Response Increment	6
1.3.3	Initialization of Incremental Analysis	7
1.3.4	Linear Response Increment to First Event	7
1.3.5	Linear Response Increment from Event k to the Next	8
1.3.6	Linear Response Increment from First to Second Event	8
1.3.7	Comments on Incremental Relations	9
1.3.8	Linear Step from Event k to Event $k + 1$	9
1.4	Examples	9
	Example 1.1 Simple Truss	9
	Example 1.2 Column-Girder Assembly	13
1.5	Unloading Response	16
1.5.1	Inelastic material behavior	16
1.5.2	Inelastic element behavior	17
1.5.3	Inelastic structural behavior	17
1.5.4	Plastic Deformations at Second Event of 2-dof Truss	18
1.6	Unloading from Plastic Deformation State	18

1.6.1	Basic Forces of 2-dof Truss upon Complete Load Removal	20
1.7	Computer Implementation of Event-To-Event Analysis	21
1.7.1	Typical linear response increment from event k to next event	21
	Example 1.3 Event-to-Event Analysis of Portal Frame	23
2	Introduction to Nonlinear Geometry	27
2.1	Overview	27
2.2	Nonlinear Kinematics of Truss Element	31
2.2.1	Definition of Deformation	31
2.2.2	Green-Lagrange Deformation for Truss	32
2.2.3	Relative Importance of Terms in Green-Lagrange Deformation	34
2.2.4	Comparison of Deformation Measures	34
2.3	Single Degree-of-Freedom Truss Example	35
2.3.1	Kinematic Relations	36
2.3.2	Equilibrium Equations	38
2.3.3	Element Force-Deformation Relation	39
2.3.4	Truss Resisting Force \mathbf{P}_r	40
2.3.5	Static and Kinematic Summary	41
2.4	Structure Stiffness Matrix	42
2.4.1	Material Stiffness of Single Dof Truss	43
2.4.2	Geometric Stiffness Of Single Dof Truss	43
2.4.3	Summary and Observations about Tangent Stiffness	44
	Example 2.1 Instability of Shallow Truss	44
	Example 2.2 Prestressed Horizontal Cable	46
	Example 2.3 Linear Buckling Load of Truss/Beam	51
2.5	Conclusions from Single Dof Examples	52
3	Nonlinear Solution Methods I	53
3.1	Introduction	53
3.2	Solution of One Nonlinear Equation	53
3.2.1	Newton-Raphson Algorithm for One Nonlinear Equation	54
3.2.2	Newton-Raphson Solution for Structural Problem	54
	Example 3.1 Nonlinear Solution for Single dof Truss under Given Load	55
3.3	Mathematical Preliminaries	56
3.4	Solution of a System of Nonlinear Equations	57
3.4.1	Newton-Raphson Algorithm for System of Nonlinear Equations	58
3.4.2	Newton-Raphson Solution for Structural Problem	58
	Example 3.2 Nonlinear Solution of Two dof Truss under Given Load	60
3.5	Multi-Step Incremental Analysis	71
3.5.1	Introduction	71
3.5.2	Single Load Step	72

3.5.3	Multi-Step Load Application	74
3.6	Modified Newton and Quasi-Newton Methods	77
3.7	Load Factor Control	77
3.7.1	Load Factor Control for Predictor Phase	78
3.7.2	Load Factor Control during Equilibrium Corrections	80
3.8	Convergence Criterion	82
3.9	Implementation of Nonlinear Solution Strategy in FEDEASLab	83
3.9.1	Loading	83
3.9.2	State of the Structure	84
3.9.3	Control of Iterative Solution	84
3.9.4	Functions and Scripts for Iterative Solution	85
4	Nonlinear Geometry of Plane Frames	89
4.1	Introduction	89
4.2	Basic Force-Deformation Relations for Linear Element Geometry	91
4.2.1	Deformation-Force Relation for Linear Elastic Material	91
4.2.2	Force-Deformation Relation for Linear Elastic Material	93
4.2.3	Conclusion	94
4.3	Force-Deformation Relation for Nonlinear Element Geometry	94
4.3.1	Tensile Axial Basic Force q_1	97
4.3.2	Compressive Axial Basic Force q_1	97
4.3.3	Basic Stiffness Matrix Coefficients	100
4.3.4	Summary	102
4.4	Corotational Formulation of Plane Frame Element	104
4.4.1	Nonlinear Kinematics	104
4.4.2	Variation of Deformations	106
4.4.3	Incremental Kinematic Matrix	108
4.4.4	Nonlinear Statics	110
4.4.5	Tangent stiffness matrix	111
4.5	Truss Effect Approximation of Nonlinear Chord Geometry	113
4.5.1	Introduction	113
4.5.2	Derivation	114
4.5.3	Summary	115
4.6	Linear Stability Analysis	116
4.6.1	Introduction	116
4.6.2	Assumptions	117
4.6.3	Structure Stiffness Contributions	117
4.6.4	Linear Eigenvalue Problem	118
4.6.5	Examples	119
Example 4.1	Cantilever Column	119
Example 4.2	Partially Restrained Cantilever Column	126

Example 4.3 Simply Supported Column	129
4.6.6 Effective Length Factor K	133
4.6.7 Conclusions about Linear Buckling Analysis	134
4.7 Second Order Elastic Analysis	135
Example 4.4 Cantilever Column under Vertical and Lateral Force	135
Example 4.5 Restrained Cantilever Column under Vertical and Lateral Force	139
4.7.1 Magnification Factor	145
4.7.2 Summary for Second Order Elastic Analysis	146
Example 4.6 Three Story-One Bay Steel Frame under Gravity and Lateral Loads	147
4.8 Second Order Linear Elastic, Perfectly Plastic Analysis	151
Example 4.7 Cantilever Column	151
Example 4.8 Column-Girder Assembly with Gravity Column	154
5 Path-Independent Nonlinear Material and Section Response	157
5.1 Introduction	157
5.2 Material State Determination	157
5.3 Simple Nonlinear Material Models	158
5.3.1 Bilinear Model	158
5.3.2 Giuffré, Menegotto, Pinto (GMP) Model (1970-1973)	158
5.3.3 Concrete Model by Mander, Priestley, Park (1992)	160
5.4 Section Response	161
5.4.1 Section Kinematics	161
5.4.2 Section Equilibrium	162
5.4.3 Section Tangent Stiffness	163
5.4.4 Section Stiffness under Linear Elastic Response	164
5.4.5 Section Stiffness under Nonlinear Material Response	165
5.5 Numerical Integration	165
5.5.1 Simpson and Trapezoidal Integration Rules	166
5.5.2 Midpoint integration rule	168
5.5.3 Gaussian Quadrature	168
Example 5.1 Numerical Evaluation of Integral	169
5.6 Section State Determination	169
Example 5.2 Section Forces s for Given Deformations e	172
5.7 Section Analysis	174
5.7.1 Formulation	174
5.7.2 Section Analysis Problems	175
5.7.3 First Section Analysis Problem	176
5.7.4 Second Section Analysis Problem	176
Example 5.3 Section Deformations e for Given Section Forces s	177
Example 5.4 Incremental Response of Rectangular Section	181
5.7.5 Third Section Analysis Problem: Moment-Curvature Analysis	182

5.7.6	Moment-Curvature Analysis	183
Example 5.5	Section Moment For Given Curvature κ and Normal Force N	184
Example 5.6	Moment-Curvature Relation of Rectangular Section	186
5.8	Moment-Curvature Relation	186
5.8.1	Elastic-Perfectly Plastic Material Response	187
5.8.2	Bilinear Elastic Material Response	189
5.8.3	Numerical Evaluation of Moment-Curvature Response	192
5.8.4	Moment-Curvature Relation of RC Section	196
5.9	Limit N - M Surface for Perfect Plasticity	197
5.9.1	Exact Solution for Rectangular Section	197
5.9.2	Numerical Solution for Rectangular Section	199
5.9.3	Plastic Limit Surface for Wide Flange Section	199
5.9.4	Ultimate Strength Surface for RC Rectangular Section	203
	Example 5.7 Collapse Load Factor of Column under Eccentric Axial Force	206
6	Path-Independent Nonlinear Frame Elements	211
6.1	Introduction	211
6.2	Plane and Space Truss Element	211
6.2.1	Displacement Formulation of Nonlinear Basic Truss Element	211
Example 6.1	Simple Truss	214
6.2.2	Force Formulation of Nonlinear Basic Truss Element	219
6.2.3	Parallel Spring Model	223
6.2.4	Series Spring Model	225
Example 6.2	Nonlinear Truss with Series Material	229
6.2.5	Applications	233
6.2.6	Conclusions	235
6.3	Beam Elements	236
6.3.1	Introduction	236
6.3.2	Force-Displacement Response of Cantilever Beam	236
6.3.3	Approximation of Load-Displacement Response of Cantilever Beam	243
6.3.4	Some Simple Nonlinear Beam Models	244
6.3.5	Linear Elastic, Perfectly Plastic Beam Element	244
Example 6.3	State Determination for LEPP Beam	247
6.3.6	Two (Parallel) Component Beam Model	253
6.3.7	One-Component (Series) Beam Model	258
Example 6.4	State Determination of One Component Model	262
6.3.8	Series Beam Model with Offset Nonlinear Springs	266
6.3.9	Conclusions about Beam Models	269
6.3.10	Evaluation of Beam Models under General Moment Distributions	270

Chapter 1

Event to Event Linear Elastic, Perfectly Plastic Analysis

1.1 Introduction

The objective of this chapter is to extend the linear analysis methods to the multi-linear step response determination process of a structural model under increasing loads up to incipient collapse. Each linear step is of finite size under linear equilibrium, linear kinematics, and under certain conditions of nonlinear material response.

The chapter, therefore, serves as a brief introduction of key concepts of nonlinear structural analysis within the simple framework of a sequence of finite step size linear analyses. It also helps to introduce the concept of residual deformations and displacements upon complete removal of applied loads. *The stress state of the structure after complete removal of applied loads corresponds to the superposition of homogeneous static solutions satisfying the compatibility conditions. Note that the residual plastic deformations need to be included for a non-trivial homogeneous solution to result.*

A linear elastic, perfectly-plastic basic force-deformation relation under linear equilibrium and linear kinematics leads to a piecewise linear structural response characterized by a sudden stiffness change when a plastic hinge forms and linear response segments from one plastic hinge appearance to the next.

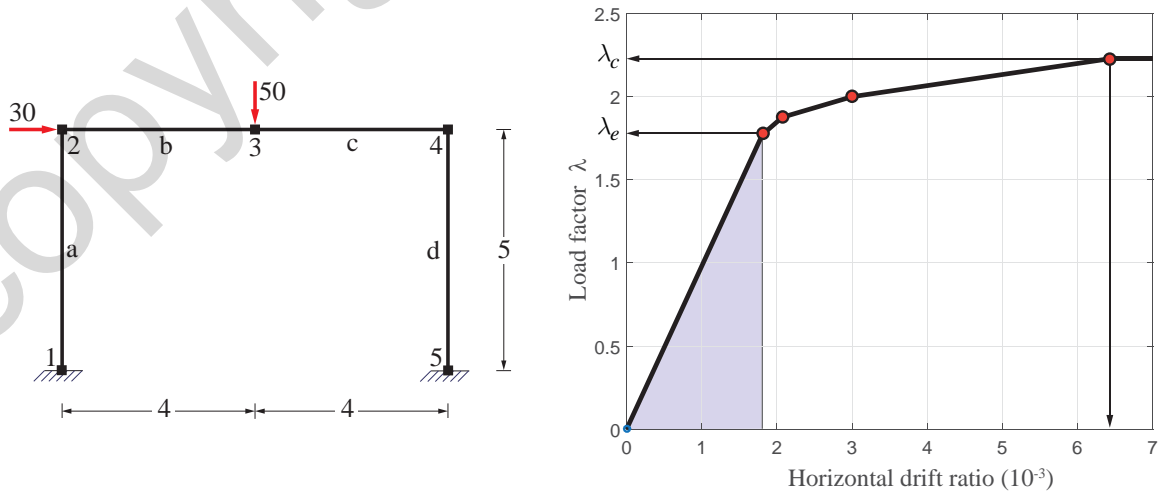


Fig. 1.1: Piecewise linear response of portal frame under incremental loading

Fig. 1.1 shows the relation between load factor λ and the horizontal story drift for the one-story portal frame of Example 5.3 of from the CE220 Reader.

1.1.1 Analysis Methods

We can use the force or the displacement method of analysis for the linear structural response determination from one event to the next but need to consider the following aspects of the problem:

- 1) Incremental load application.
- 2) Update of structure properties after each event.
- 3) Storage of information at each event to allow moving forward to the next.
- 4) Accumulation of displacement increments of each linear segment.

1.1.2 Incremental Loading and Analysis

To describe the incremental load application we recall the definition of the applied nodal force vector \mathbf{P}_f

$$\mathbf{P}_f = \lambda \mathbf{P}_{ref} \quad (1.1)$$

with \mathbf{P}_{ref} representing the spatial nodal force distribution or load pattern and λ the load factor. In linear structural analysis we assumed that the load factor λ is equal to 1, so that we did not distinguish \mathbf{P}_f from \mathbf{P}_{ref} . We will now *increment* the load factor λ until the collapse load factor λ_c while keeping the nodal force distribution \mathbf{P}_{ref} constant, and determine the response of the structure under incremental loading up to incipient collapse.

The response determination of the structural model under incremental loading is known as incremental analysis.

1.1.3 Event-to-Event Incremental Analysis

For the *event-to-event incremental analysis* the incremental solution process proceeds from one event to the next with a linear step of finite size in between.

Whereas this method has been proposed as general solution strategy for the response of structures with piecewise linear behavior, it is used here only for introducing the concept of incremental analysis and for extending linear response calculations to the simple case of *structures with linear elastic, perfectly-plastic basic force-deformation relations*. This text uses general nonlinear solution strategy methods and makes reference to the event-to-event solution strategy only in the context of the state determination of certain beam elements with nonlinear material response.

1.1.4 Limitations of Event-to-Event Analysis

The piecewise linear event-to-event analysis is based on several assumptions that limit its range of application for general problems of nonlinear analysis. These assumptions ensure that the response from one event to the next is linear:

- 1) Linear kinematics.

- 2) Linear statics; \mathbf{P} - Δ equilibrium can be accounted for with some effort, as will be discussed later in this text.
- 3) The nonlinearity of material response is represented by *discrete events*. In particular, the nonlinear basic element response is limited to the formation of perfectly-plastic hinges. Under the assumption that the flexural basic forces represent the maximum internal forces of an element, the flexural plastic hinges form only at the element ends.

In reality, the nonlinear basic element response is a continuous process that is affected by the interaction of the internal forces or stress resultants, like the interaction of the axial and shear force with the bending moment in plane frame elements. Moreover, global dof displacements and structural deformations may become large enough to require use of nonlinear geometry. In this case, the load-displacement response of the structure is *continuously nonlinear*, even for piecewise linear material response.

1.1.5 Linear Response Increment with Force Method of Analysis

For a typical linear response increment from one hinge formation to the next we set up the governing relation between the basic forces of the structural model \mathbf{Q} and the applied nodal forces \mathbf{P}_f with the help of the force influence matrix $\bar{\mathbf{B}}$.

This relation can be set up either through the force method or the displacement method of analysis.

The use of the force method of analysis may be advantageous if the location of the plastic hinges is known from the plastic analysis with the upper or lower bound theorem. Selecting the redundant basic forces to coincide with the plastic hinge locations leads to the reduction of the degree of static indeterminacy of the structure every time a plastic hinge forms. More importantly, the linear solution after each event simply involves the removal of the homogeneous solution for the redundant force at the new plastic hinge location, without affecting the particular and the other homogeneous solutions. Thus, not only is the size of the compatibility conditions reduced by one at each event, but the particular and homogeneous solutions only need to be set up once at the beginning of the entire analysis.

1.1.6 Event-to-Event Analysis with Displacement Method

We present here the details of the event-to-event analysis with the displacement method, since this is the method of choice in the few commercial software packages that use the method for push-over analysis. The presentation is limited to a monotonically increasing load factor under the assumption that once a plastic hinge forms it cannot close during the subsequent increment of the load factor.

1.1.7 Linear Response Increment with Displacement Method of Analysis

Without initial forces \mathbf{P}_0 the equations of equilibrium at the free dofs are

$$\mathbf{P}_f = \mathbf{K} \mathbf{U}_f \quad (1.2)$$

and the basic forces can be determined with

$$\mathbf{Q} = \mathbf{K}_s (\mathbf{A}_f \mathbf{U}_f) \quad (1.3)$$

Substituting the solution for the free dof displacements from (1.2) into (1.3) gives

$$\mathbf{Q} = (\mathbf{K}_s \mathbf{A}_f \mathbf{K}^{-1}) \mathbf{P}_f$$

which can be written in compact form as

$$\mathbf{Q} = \bar{\mathbf{B}} \mathbf{P}_f \quad (1.4)$$

where $\bar{\mathbf{B}}$ is the $nq \times nf$ basic force influence matrix of the structural model that relates the basic element forces \mathbf{Q} with the applied nodal forces \mathbf{P}_f .

1.1.8 Proportionality of Linear Response

Under linear kinematics and linear statics the kinematic matrix \mathbf{A}_f is constant. Under linear elastic material response the collection of element stiffness matrices \mathbf{K}_s is also constant. The basic force influence matrix $\bar{\mathbf{B}}$ is, therefore, constant.

This means that the basic forces \mathbf{Q} are proportional to the applied forces \mathbf{P}_f . Expressing \mathbf{P}_f in terms of the reference force distribution \mathbf{P}_{ref} gives

$$\begin{aligned} \mathbf{Q} &= \bar{\mathbf{B}}(\lambda \mathbf{P}_{ref}) \\ \mathbf{Q} &= \lambda(\bar{\mathbf{B}} \mathbf{P}_{ref}) \\ \mathbf{Q} &= \lambda \mathbf{Q}' \end{aligned} \quad (1.5)$$

where \mathbf{Q}' are the basic forces under the reference force distribution \mathbf{P}_{ref}

$$\mathbf{Q}' = \bar{\mathbf{B}} \mathbf{P}_{ref} \quad (1.6)$$

This means that the basic forces \mathbf{Q} can be determined by scaling the reference forces \mathbf{Q}' under the reference load distribution \mathbf{P}_{ref} with load factor λ as long as the plastic capacity of the basic forces is not exceeded.

1.1.9 Principle of Linear Superposition

(1.5) implies that the basic forces under two reference force distributions with different load factors can be expressed as

$$\mathbf{Q} = \lambda_a \mathbf{Q}'_a + \lambda_b \mathbf{Q}'_b \quad (1.7)$$

where \mathbf{Q}'_a are the basic forces under the reference force distribution $\mathbf{P}_{ref}^{(a)}$, and \mathbf{Q}'_b the basic forces under the reference force distribution $\mathbf{P}_{ref}^{(b)}$.

(1.7) is known as *principle of linear superposition*.

The principle of linear superposition holds as long as the basic forces \mathbf{Q} to not exceed the corresponding plastic capacity.

1.2 Linear Elastic Response Limit

1.2.1 Range of Linear, Elastic Structural Response

Elastic material response is characterized by the ability of the material to return to its initial deformation state upon complete removal of stress.

By extension, an elastic structure is able to return to its initial deformation state after complete removal of the applied loads.

Linear structural response arises when the global dof displacements \mathbf{U}_f and the associated element deformations \mathbf{V} are small so that linear kinematics and linear equilibrium is an accurate approximation, and as long as the basic element forces \mathbf{Q} remain within the linear, elastic range of material behavior. Under these conditions we speak of *linear elastic analysis*.

Under the assumption of a linear elastic, perfectly-plastic material resulting in a linear elastic, perfectly-plastic basic force-deformation relation $\mathbf{q}\text{-}\mathbf{v}$ we establish the load factor λ_e that represents the upper limit of linear, elastic response of a structural model under the reference load distribution \mathbf{P}_{ref} .

1.2.2 Limit Load Factor for Linear, Elastic Response

We recall first the definition of the plastic capacities \mathbf{Q}_{pl} for basic forces \mathbf{Q} with \mathbf{Q}_{pl}^+ and \mathbf{Q}_{pl}^- denoting the absolute value of the plastic capacity under positive and negative \mathbf{Q} , respectively.

For the comparison of the basic forces \mathbf{Q} with the corresponding plastic capacities \mathbf{Q}_{pl} we introduce an integer index m ranging from 1 to nq , where nq is the total number of basic forces in the structural model, thus corresponding to the length of vectors \mathbf{Q} and \mathbf{Q}_{pl} .

Linear elastic element response requires that each basic force \mathbf{Q}_m does not exceed the corresponding plastic capacity $\mathbf{Q}_{pl,m}$

$$|\mathbf{Q}_m| \leq \mathbf{Q}_{pl,m} \quad (1.8)$$

without explicit distinction of the positive and negative plastic capacity at this point. With the basic forces \mathbf{Q}' under the reference load distribution \mathbf{P}_{ref} according to (1.6), (1.8) gives

$$\lambda |\mathbf{Q}'_m| \leq \mathbf{Q}_{pl,m}^{\text{sgn}} \quad (1.9)$$

where the superscript sgn is shorthand for denoting the plastic capacity matching the sign of \mathbf{Q}'_m , i.e. \mathbf{Q}_{pl}^+ for positive \mathbf{Q}'_m and \mathbf{Q}_{pl}^- for negative \mathbf{Q}'_m . For the following derivations we, therefore, introduce the following shorthand

$$\text{sgn} = \text{sgn}(\mathbf{Q}'_m)$$

To find the largest load factor λ_m satisfying (1.9) we turn it into an equality. Substituting the relation

$$|\mathbf{Q}'_m| = \text{sgn } \mathbf{Q}'_m$$

in (1.9) gives

$$\lambda_m \operatorname{sgn} \mathbf{Q}'_m = \mathbf{Q}_{pl,m}^{\operatorname{sgn}}$$

Multiplying both sides with sgn and noting that $\operatorname{sgn}^2 = 1$ gives

$$\lambda_m \mathbf{Q}'_m = \operatorname{sgn} \mathbf{Q}_{pl,m}^{\operatorname{sgn}} \quad (1.10)$$

From (1.10) we conclude that the basic force component m remains within the linear elastic range as long as $\lambda \leq \lambda_m$.

For *all basic force components* to remain within the linear elastic range so that the structure remains linear elastic under the reference load distribution \mathbf{P}_{ref} the load factor λ in (1.9) *cannot exceed the smallest λ_m value*. The limit load factor λ_e for linear elastic response, therefore, is

$$\lambda_e = \lambda_{p_1} = \min(\lambda_m) = \min\left(\frac{\operatorname{sgn} \mathbf{Q}_{pl,m}^{\operatorname{sgn}}}{\mathbf{Q}'_m}\right) \quad (1.11)$$

where λ_{p_1} is the value of load factor λ when the first plastic hinge forms at p_1 .

For numerical calculations of large structures we note the danger of dividing by zero in the denominator of (1.11). We, therefore, make use of an alternative form of writing (1.11)

$$\lambda_e = \lambda_{p_1} = \frac{1}{\max\left(\frac{\mathbf{Q}'_m}{\operatorname{sgn} \mathbf{Q}_{pl,m}^{\operatorname{sgn}}}\right)} = \frac{1}{\max(\mathbf{DC}'_m)} \quad (1.12)$$

The ratio of the basic force \mathbf{Q}_m at m under the applied loads to the corresponding plastic capacity value $\mathbf{Q}_{pl,m}$ is known as *demand-capacity* or *DC* ratio at m . \mathbf{DC}' is the demand-capacity ratio under the reference load distribution \mathbf{P}_{ref} .

The limit load factor λ_e for linear, elastic response is the inverse of the largest DC ratio of all basic forces under the reference load distribution \mathbf{P}_{ref} .

1.3 Event-to-Event Analysis

1.3.1 Notation

Incremental analysis requires special notation for the increments of force and displacement variables and for identifying these variables at each event. We adopt the following notation:

- 1) We denote the increment or change of a variable with prefix Δ .
- 2) We identify variables at specific events by the event counter in parentheses as a superscript. Thus, $\mathbf{U}_f^{(1)}$ denotes the free dof displacements at the first event, and $\lambda^{(2)}$ the load factor at the second event.

1.3.2 Summary of Key Relations for Linear Response Increment

The relations for a linear response increment with the displacement method are:

- 1) Current stiffness determination of small structural models with

$$\mathbf{K} = \mathbf{A}_f^T \mathbf{K}_s \mathbf{A}_f \quad (1.13)$$

or by direct assembly of element contributions.

- 2) Displacement determination under reference load distribution \mathbf{P}_{ref}

$$\mathbf{P}_{ref} = \mathbf{K} \mathbf{U}'_f \quad (1.14)$$

- 3) Basic force determination under reference load distribution \mathbf{P}_{ref}

$$\mathbf{Q}' = \mathbf{K}_s (\mathbf{A}_f \mathbf{U}'_f) \quad (1.15)$$

Under the applied forces $\mathbf{P}_f = \lambda \mathbf{P}_{ref}$ the free dof displacements are $\mathbf{U}_f = \lambda \mathbf{U}'_f$ and the basic forces are $\mathbf{Q} = \lambda \mathbf{Q}'$.

1.3.3 Initialization of Incremental Analysis

Under the assumption that only the reference load distribution \mathbf{P}_{ref} acts on the structure we set

$$\lambda^{(0)} = 0$$

and assume that the initial state corresponds to the unstressed structure so that

$$\begin{aligned} \mathbf{U}'_f &= \mathbf{0} \\ \mathbf{Q}^{(0)} &= \mathbf{0} \end{aligned}$$

1.3.4 Linear Response Increment to First Event

- 1) Set up initial stiffness and solve for \mathbf{U}'_f and \mathbf{Q}' under \mathbf{P}_{ref}

$$\begin{aligned} \mathbf{K}^{(0)} &= \mathbf{A}_f^T \mathbf{K}_s^{(0)} \mathbf{A}_f \\ \mathbf{P}_{ref} &= \mathbf{K}^{(0)} \mathbf{U}'_f^{(0)} \\ \mathbf{Q}'^{(0)} &= \mathbf{K}_s^{(0)} [\mathbf{A}_f \mathbf{U}'_f^{(0)}] \end{aligned}$$

- 2) Determine load factor $\lambda^{(1)} = \lambda_{p_1}$ for first plastic hinge to form (first event)

$$\lambda^{(1)} = \lambda_{p_1} = \frac{1}{\max(\mathbf{D}\mathbf{C}'_m)}$$

- 3) Determine the free dof displacements \mathbf{U}_f and the basic forces \mathbf{Q} at first event

$$\begin{aligned}\mathbf{U}_f^{(1)} &= \lambda^{(1)} \mathbf{U}_f'^{(0)} \\ \mathbf{Q}^{(1)} &= \lambda^{(1)} \mathbf{Q}'^{(0)}\end{aligned}\quad (1.16)$$

1.3.5 Linear Response Increment from Event k to the Next

Once a hinge forms at a particular location p_k at event k the stiffness matrix of the corresponding element changes. *For subsequent load factor increments* the element behaves as if it had a basic force release at that location.

The structure stiffness matrix needs to be reformed to account for the change. It represents the *incremental linear stiffness matrix* from the current to the next event. For large structures it is easier to subtract the change of the element stiffness matrix contribution to the structure stiffness matrix for the element with the new plastic hinge.

To determine the *load factor increment* $\Delta\lambda$ to the next event we modify (1.10) with the basic force increments from the current to the next event, namely

$$\mathbf{Q}_m^{(k)} + \Delta\lambda_m \mathbf{Q}_m'^{(k)} = \text{sgn } \mathbf{Q}_{pl,m}^{\text{sgn}} \quad (1.17)$$

where \mathbf{Q}' are the basic forces *for the structure with modified stiffness after event k* under the reference load distribution \mathbf{P}_{ref} .

1.3.6 Linear Response Increment from First to Second Event

- 1) Insert a hinge at location p_1 and update the corresponding basic element stiffness. Set up current stiffness and solve for \mathbf{U}_f' and \mathbf{Q}' under \mathbf{P}_{ref}

$$\begin{aligned}\mathbf{K}^{(1)} &= \mathbf{A}_f^T \mathbf{K}_s^{(1)} \mathbf{A}_f \\ \mathbf{P}_{ref} &= \mathbf{K}^{(1)} \mathbf{U}_f'^{(1)} \\ \mathbf{Q}'^{(1)} &= \mathbf{K}_s^{(1)} \left[\mathbf{A}_f \mathbf{U}_f'^{(1)} \right]\end{aligned}$$

- 2) Determine the *load factor increment* $\Delta\lambda$ to the second event with (1.17)

$$\Delta\lambda^{(1)} = \min \left[\Delta\lambda_m^{(1)} \right] = \min \left[\frac{\text{sgn } \mathbf{Q}_{pl,m}^{\text{sgn}} - \mathbf{Q}_m^{(1)}}{\mathbf{Q}_m'^{(1)}} \right] \quad (1.18)$$

- 3) Determine load factor λ , \mathbf{U}_f and basic forces \mathbf{Q} at second event

$$\begin{aligned}\lambda^{(2)} &= \lambda^{(1)} + \Delta\lambda^{(1)} \\ \mathbf{U}_f^{(2)} &= \mathbf{U}_f^{(1)} + \Delta\lambda^{(1)} \mathbf{U}_f'^{(1)} \\ \mathbf{Q}^{(2)} &= \mathbf{Q}^{(1)} + \Delta\lambda^{(1)} \mathbf{Q}'^{(1)}\end{aligned}\quad (1.19)$$

1.3.7 Comments on Incremental Relations

(1.18) and (1.19) can be interpreted as resetting the origin of the load-displacement response of the structure to the first event. Under this viewpoint the basic element forces $\mathbf{Q}^{(1)}$ at the first event are *initial forces* for the subsequent response that *reduce* the available basic force plastic capacity to $[\operatorname{sgn} \mathbf{Q}_{pl,m}^{\text{sgn}} - \mathbf{Q}_m^{(1)}]$. We call this the *residual plastic capacity*. Note that *sgn is the sign of \mathbf{Q}'_m* .

$\Delta\lambda$ is the *load factor increment* to the second event, and the same is true for the corresponding free dof displacements and basic forces. These increments need to be added to the values at the first event to get the *total values* at the second event according to equation (1.19).

It is worth noting that the minimum in equation (1.20) extends over all m basic forces *except* p_1 , otherwise the algorithm will keep selecting p_1 as the "next event", since $\Delta\lambda$ is zero at that location, and thus smallest.

1.3.8 Linear Step from Event k to Event $k + 1$

After inserting hinges at locations p_1 through p_k and updating the basic stiffness of all elements we set up current stiffness and solve for \mathbf{U}'_f and \mathbf{Q}' under \mathbf{P}_{ref}

$$\begin{aligned}\mathbf{K}^{(k)} &= \mathbf{A}_f^T \mathbf{K}_s^{(k)} \mathbf{A}_f \\ \mathbf{P}_{ref} &= \mathbf{K}^{(k)} \mathbf{U}'_f^{(k)} \\ \mathbf{Q}'^{(k)} &= \mathbf{K}_s^{(k)} [\mathbf{A}_f \mathbf{U}'_f^{(k)}]\end{aligned}$$

We determine the *load factor increment* $\Delta\lambda$ to the next event

$$\Delta\lambda^{(k)} = \min \left[\Delta\lambda_m^{(k)} \right] = \min \left[\frac{\operatorname{sgn} \mathbf{Q}_{pl,m}^{\text{sgn}} - \mathbf{Q}_m^{(k)}}{\mathbf{Q}'_m^{(k)}} \right] \quad (1.20)$$

We determine load factor, free dof displacements and basic forces at next event

$$\begin{aligned}\lambda^{(k+1)} &= \lambda^{(k)} + \Delta\lambda^{(k)} \\ \mathbf{U}'_f^{(k+1)} &= \mathbf{U}'_f^{(k)} + \Delta\lambda^{(k)} \mathbf{U}'_f^{(k)} \\ \mathbf{Q}^{(k+1)} &= \mathbf{Q}^{(k)} + \Delta\lambda^{(k)} \mathbf{Q}'^{(k)}\end{aligned} \quad (1.21)$$

1.4 Examples

Example 1.1 Simple Truss

The simple truss in Fig. 1.2 consists of four elements with axial stiffness $EA = 10,000$, so that

$$\mathbf{k}^{(a)} = \frac{EA}{L_a} = 1666.7 \quad \mathbf{k}^{(b)} = \frac{EA}{L_b} = 1000 \quad \mathbf{k}^{(c)} = \frac{EA}{L_c} = 1250 \quad \mathbf{k}^{(d)} = \frac{EA}{L_d} = 1000$$

The truss elements have the same plastic capacity in tension and compression, $Q_{pl}^+ = 15$, $Q_{pl}^- = 15$.

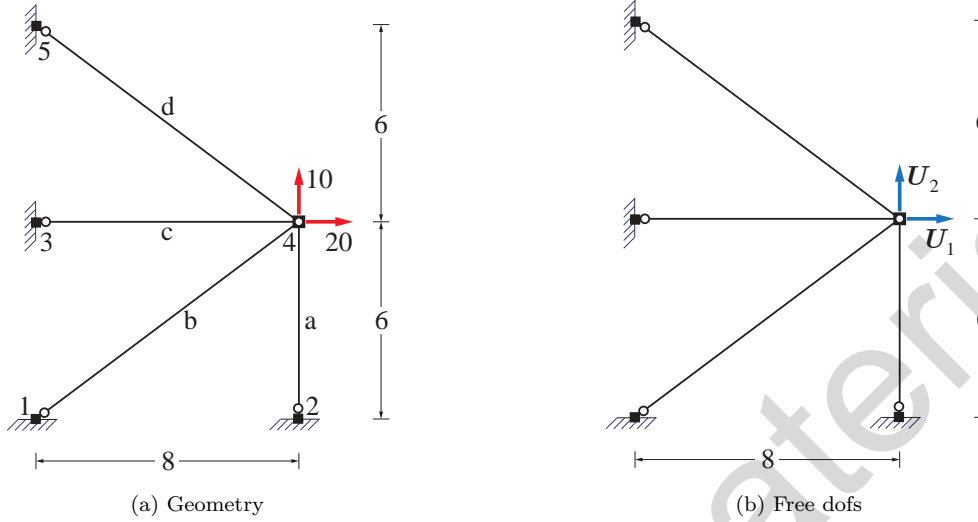


Fig. 1.2: Four element plane truss

The truss has two free dofs. It is subjected to a load pattern represented by the following reference vector

$$\mathbf{P}_{ref} = \begin{pmatrix} 20 \\ 10 \end{pmatrix}$$

(a) Initial Stiffness Matrix

With all elements in the linear elastic range the free dof stiffness matrix \mathbf{K} of the truss is made up of four element contributions

$$\mathbf{K} = \mathbf{K}^{(a)} + \mathbf{K}^{(b)} + \mathbf{K}^{(c)} + \mathbf{K}^{(d)}$$

with

$$\begin{aligned} \mathbf{K}^{(a)} &= \frac{EA}{L_a} \begin{bmatrix} 0 & 0 \\ 0 & 1 \end{bmatrix} & \mathbf{K}^{(b)} &= \frac{EA}{L_b} \begin{bmatrix} (0.8)^2 & 0.8 \cdot 0.6 \\ 0.6 \cdot 0.8 & (0.6)^2 \end{bmatrix} \\ \mathbf{K}^{(c)} &= \frac{EA}{L_c} \begin{bmatrix} 1 & 0 \\ 0 & 0 \end{bmatrix} & \mathbf{K}^{(d)} &= \frac{EA}{L_d} \begin{bmatrix} (-0.8)^2 & (-0.8) \cdot (0.6) \\ 0.6 \cdot (-0.8) & (0.6)^2 \end{bmatrix} \end{aligned}$$

(b) Linear Response Increment to First Event

With all truss elements in the linear elastic range the initial stiffness matrix of the simple truss is

$$\mathbf{K}^{(0)} = \mathbf{K}^{(a)} + \mathbf{K}^{(b)} + \mathbf{K}^{(c)} + \mathbf{K}^{(d)} = \begin{bmatrix} 2530 & 0 \\ 0 & 2387 \end{bmatrix}$$

Solving for the free dof displacements \mathbf{U}'_f and the basic forces \mathbf{Q}' under \mathbf{P}_{ref} gives

$$\begin{aligned} \mathbf{U}'^{(0)} &= [7.905 \quad 4.19]^T \cdot 10^{-3} \\ \mathbf{Q}'^{(0)} &= [6.98 \quad 8.84 \quad 9.88 \quad 3.81]^T \end{aligned}$$

The load factor to the first event is determined from the demand-capacity ratios DC' under \mathbf{P}_{ref} according to (1.12)

$$\lambda^{(1)} = \min(2.15, 1.70, 1.52, 3.94) = 1.52$$

We conclude that the first plastic hinge forms in element c and scale the free dof displacements \mathbf{U}'_f and the basic forces \mathbf{Q}' with the load factor $\lambda^{(1)}$ to establish the free dof displacements \mathbf{U}_f and the basic forces \mathbf{Q} at the first event according to (1.16)

$$\begin{aligned}\mathbf{U}'^{(1)}_f &= \lambda^{(1)} \mathbf{U}'^{(0)}_f = [12 \quad 6.36]^T \cdot 10^{-3} \\ \mathbf{Q}'^{(1)} &= \lambda^{(1)} \mathbf{Q}'^{(0)} = [10.60 \quad 13.42 \quad 15 \quad 5.78]^T\end{aligned}$$

(c) Linear Response Increment from First to Second Event

For the load factor increment past $\lambda^{(1)}$ we set up the stiffness matrix of the simple truss without the contribution of element c

$$\mathbf{K}^{(1)} = \mathbf{K}^{(a)} + \mathbf{K}^{(b)} + \mathbf{0} + \mathbf{K}^{(d)} = \begin{bmatrix} 1280 & 0 \\ 0 & 2387 \end{bmatrix}$$

Solving for the free dof displacements \mathbf{U}'_f and the basic forces \mathbf{Q}' under \mathbf{P}_{ref} gives

$$\begin{aligned}\mathbf{U}'^{(1)}_f &= [15.625 \quad 4.19]^T \cdot 10^{-3} \\ \mathbf{Q}'^{(1)} &= [6.98 \quad 15.01 \quad 0 \quad 9.99]^T\end{aligned}$$

The load factor increment to the second event is determined from the demand-capacity ratios DC' under \mathbf{P}_{ref} according to (1.18) after accounting for the residual plastic capacity of elements a, b, and d at the first event

$$\Delta\lambda^{(1)} = \min(0.63, 0.105, -0.92) = 0.105$$

We conclude that the second plastic hinge forms in element b and scale the free dof displacements \mathbf{U}'_f and the basic forces \mathbf{Q}' with the load factor increment $\Delta\lambda^{(1)}$ and add them to those at the first event to establish the free dof displacements \mathbf{U}_f and the basic forces \mathbf{Q} at the second event according to (1.19)

$$\begin{aligned}\lambda^{(2)} &= \lambda^{(1)} + \Delta\lambda^{(1)} = 1.52 + 0.105 = 1.62 \\ \mathbf{U}'^{(2)}_f &= \mathbf{U}'^{(1)}_f + \Delta\lambda^{(1)} \mathbf{U}'^{(1)}_f = [13.648 \quad 6.802]^T \cdot 10^{-3} \\ \mathbf{Q}^{(2)} &= \mathbf{Q}^{(1)} + \Delta\lambda^{(1)} \mathbf{Q}'^{(1)} = [11.34 \quad 15 \quad 15 \quad 6.84]^T\end{aligned}$$

(d) Linear Response Increment from Second to Third Event

For the load factor increment past $\lambda^{(2)}$ we set up the stiffness matrix of the simple truss without the contribution of elements b and c

$$\mathbf{K}^{(2)} = \mathbf{K}^{(a)} + \mathbf{0} + \mathbf{0} + \mathbf{K}^{(d)} = \begin{bmatrix} 640 & -480 \\ -480 & 2027 \end{bmatrix}$$

Solving for the free dof displacements \mathbf{U}'_f and the basic forces \mathbf{Q}' under \mathbf{P}_{ref} gives

$$\mathbf{U}'^{(2)}_f = \begin{bmatrix} 42.5 & 15 \end{bmatrix}^T \cdot 10^{-3}$$

$$\mathbf{Q}'^{(2)} = \begin{bmatrix} 25 & 0 & 0 & 25 \end{bmatrix}^T$$

The load factor increment to the third event is determined from the demand-capacity ratios DC' under \mathbf{P}_{ref} according to (1.20) after accounting for the residual plastic capacity of elements a and d at the second event

$$\Delta\lambda^{(2)} = \min(0.147, -0.327) = 0.147$$

We conclude that the third plastic hinge forms in element a and scale the free dof displacements \mathbf{U}'_f and the basic forces \mathbf{Q}' with the load factor increment $\Delta\lambda^{(2)}$ and add them to those at the second event to establish the free dof displacements \mathbf{U}_f and the basic forces \mathbf{Q} at the third event according to (1.21)

$$\lambda^{(3)} = \lambda^{(2)} + \Delta\lambda^{(2)} = 1.62 + 0.147 = 1.77$$

$$\mathbf{U}_f^{(3)} = \mathbf{U}_f^{(2)} + \Delta\lambda^{(2)} \mathbf{U}'^{(2)}_f = \begin{bmatrix} 19.875 & 9 \end{bmatrix}^T \cdot 10^{-3}$$

$$\mathbf{Q}^{(3)} = \mathbf{Q}^{(2)} + \Delta\lambda^{(2)} \mathbf{Q}'^{(2)} = \begin{bmatrix} 15 & 15 & 15 & 10.5 \end{bmatrix}^T$$

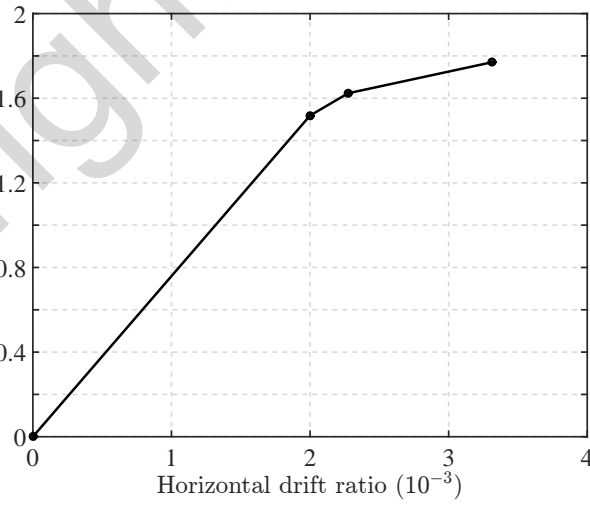


Fig. 1.3: Relation between load factor λ and lateral drift for simple truss

(e) Incipient collapse

After the third event the stiffness matrix of the simple truss without the contribution of elements a, b and c

$$\mathbf{K}^{(3)} = \mathbf{0} + \mathbf{0} + \mathbf{0} + \mathbf{K}^{(d)} = \begin{bmatrix} 640 & -480 \\ -480 & 360 \end{bmatrix}$$

is singular. We conclude that the structure has reached the state of incipient collapse under the load factor $\lambda^{(3)}$ and it forms a mechanism under any subsequent free dof displacement increment without a further increase of the basic forces $\mathbf{Q}^{(3)}$.

Fig. 1.3 shows the relation between the load factor λ and the lateral drift of the truss that is determined with $\mathbf{U}_1/6$.

Example 1.2 Column-Girder Assembly

The column-girder assembly in Fig. 1.4 consists of three elements with flexural stiffness stiffness $EI = 50,000$ so that

$$\frac{EI}{L_a} = 10,000 \quad \frac{EI}{L_b} = \frac{EI}{L_c} = 12,500$$

The column element has plastic capacity $Q_{pc} = 180$ under positive or negative flexural basic force, while the girder elements have plastic capacity $Q_{pg} = 120$ under positive or negative flexural basic force. The elements are assumed to be inextensible with very large axial capacity. Moreover, it is assumed that the presence of an axial force in the column does not affect the plastic flexural capacity.

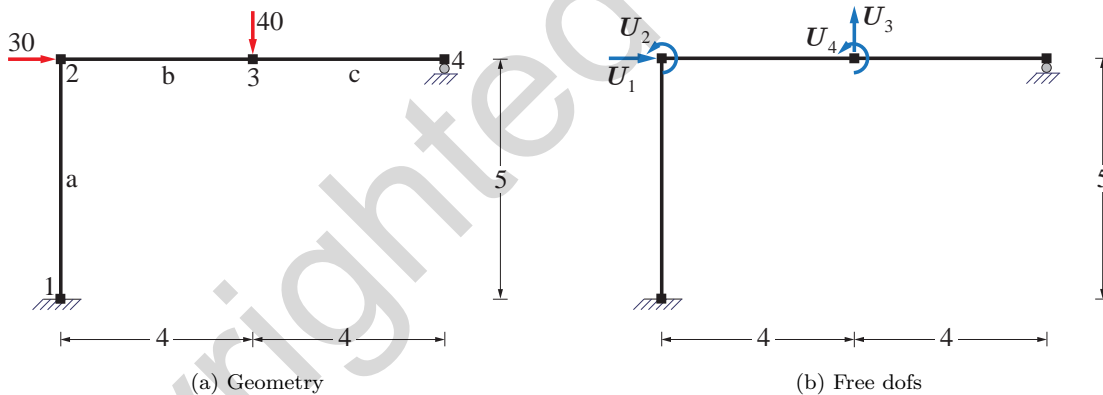


Fig. 1.4: Girder-column assembly

The column-girder assembly has 4 independent free dofs. It is subjected to a load pattern represented by the following reference vector

$$\mathbf{P}_{ref} = \begin{pmatrix} 30 \\ 0 \\ -40 \\ 0 \end{pmatrix}$$

(a) Initial Stiffness Matrix

With all elements in the linear elastic range the free dof stiffness matrix \mathbf{K} of the column-girder assembly is made up of three element contributions

$$\mathbf{K} = \mathbf{K}^{(a)} + \mathbf{K}^{(b)} + \mathbf{K}^{(c)}$$

with

$$\mathbf{K}^{(a)} = \frac{EI}{L_a} \begin{bmatrix} \frac{12}{L_a^2} & \frac{6}{L_a} & 0 & 0 \\ \frac{6}{L_a} & 4 & 0 & 0 \\ 0 & 0 & 0 & 0 \\ 0 & 0 & 0 & 0 \end{bmatrix} \quad \mathbf{K}^{(b)} = \frac{EI}{L_b} \begin{bmatrix} 0 & 0 & 0 & 0 \\ 0 & 4 & -\frac{6}{L_b} & 2 \\ 0 & -\frac{6}{L_b} & \frac{12}{L_b^2} & -\frac{6}{L_b} \\ 0 & 2 & -\frac{6}{L_b} & 4 \end{bmatrix} \quad \mathbf{K}^{(c)} = \frac{EI}{L_c} \begin{bmatrix} 0 & 0 & 0 & 0 \\ 0 & 0 & 0 & 0 \\ 0 & 0 & \frac{3}{L_c^2} & \frac{3}{L_c} \\ 0 & 0 & \frac{3}{L_c} & 3 \end{bmatrix}$$

(b) *Linear Response Increment to First Event*

With all frame elements in the linear elastic range the initial stiffness matrix of the column-girder assembly is

$$\mathbf{K}^{(0)} = \mathbf{K}^{(a)} + \mathbf{K}^{(b)} + \mathbf{K}^{(c)} = \begin{bmatrix} 4.8 & 12 & 0 & 0 \\ 12 & 90 & -18.75 & 25 \\ 0 & -18.75 & 11.72 & -9.38 \\ 0 & 25 & -9.38 & 87.5 \end{bmatrix} \cdot 10^3$$

Solving for the free dof displacements \mathbf{U}'_f and the basic forces \mathbf{Q}' under \mathbf{P}_{ref} gives

$$\mathbf{U}'^{(0)}_f = \begin{bmatrix} 17.99 & -4.7 & -10.78 & 0.19 \end{bmatrix}^T \cdot 10^{-3}$$

$$\mathbf{Q}'^{(0)} = \begin{bmatrix} 121.96 & 28.04 & -28.04 & 94.02 & -94.02 \end{bmatrix}^T$$

The load factor to the first event is determined from the demand-capacity ratios DC' under \mathbf{P}_{ref} according to (1.12)

$$\lambda^{(1)} = \min(1.48, 6.42, 4.28, 1.28, 1.28) = 1.28$$

We conclude that the first plastic hinge forms at girder midspan and scale the free dof displacements \mathbf{U}'_f and the basic forces \mathbf{Q}' with the load factor $\lambda^{(1)}$ to establish the free dof displacements \mathbf{U}_f and the basic forces \mathbf{Q} at the first event according to (1.16)

$$\mathbf{U}_f^{(1)} = \lambda^{(1)} \mathbf{U}'^{(0)}_f = \begin{bmatrix} 22.96 & -5.99 & -13.75 & 0.24 \end{bmatrix}^T \cdot 10^{-3}$$

$$\mathbf{Q}^{(1)} = \lambda^{(1)} \mathbf{Q}'^{(0)} = \begin{bmatrix} 155.6 & 35.99 & -35.79 & 120 & -120 \end{bmatrix}^T$$

(c) *Linear response increment from first to second event*

With a hinge at girder midspan there is no stiffness contribution of element c for the load increment from the first to the second event. Moreover, the stiffness contribution of element b changes to

$$\mathbf{K}'^{(b)} = \frac{EI}{L_b} \begin{bmatrix} 0 & 0 & 0 & 0 \\ 0 & 3 & -\frac{3}{L_b} & 0 \\ 0 & -\frac{3}{L_b} & \frac{3}{L_b^2} & 0 \\ 0 & 0 & 0 & 0 \end{bmatrix}$$

to account for the presence of a plastic hinge at end j of the element. Consequently, the incremental linear stiffness of the column-girder assembly is

$$\mathbf{K}^{(1)} = \mathbf{K}^{(a)} + \mathbf{K}'^{(b)} + \mathbf{0} = \begin{bmatrix} 4.8 & 12 & 0 & 0 \\ 12 & 77.5 & -9.38 & 0 \\ 0 & -9.38 & 2.34 & 0 \\ 0 & 0 & 0 & 0 \end{bmatrix} \cdot 10^3$$

Solving for the free dof displacements \mathbf{U}'_f and the basic forces \mathbf{Q}' under \mathbf{P}_{ref} gives

$$\mathbf{U}'^{(1)} = \begin{bmatrix} 65 & -23.5 & -111.07 & 27.77 \end{bmatrix}^T \cdot 10^{-3}$$

$$\mathbf{Q}'^{(1)} = \begin{bmatrix} 310 & -160 & 160 & 0 & 0 \end{bmatrix}^T$$

The load factor increment to the second event is determined from the demand-capacity ratios DC' under \mathbf{P}_{ref} according to (1.18) after accounting for the residual plastic capacity at ends i and j of element a and the residual plastic capacity at end i of element b at the first event

$$\Delta\lambda^{(1)} = \min(0.08, 0.90, 0.97, -, -) = 0.08$$

We conclude that the second plastic hinge forms at the column base and scale the free dof displacements \mathbf{U}'_f and the basic forces \mathbf{Q}' with the load factor increment $\Delta\lambda^{(1)}$ and add them to those at the first event to establish the free dof displacements \mathbf{U}_f and the basic forces \mathbf{Q} at the second event according to (1.19)

$$\lambda^{(2)} = \lambda^{(1)} + \Delta\lambda^{(1)} = 1.28 + 0.08 = 1.36$$

$$\mathbf{U}_f^{(2)} = \mathbf{U}_f^{(1)} + \Delta\lambda^{(1)} \mathbf{U}'^{(1)} = \begin{bmatrix} 28.07 & -7.83 & -22.47 & 2.42 \end{bmatrix}^T \cdot 10^{-3}$$

$$\mathbf{Q}^{(2)} = \mathbf{Q}^{(1)} + \Delta\lambda^{(1)} \mathbf{Q}'^{(1)} = \begin{bmatrix} 180 & 23.23 & -23.23 & 120 & -120 \end{bmatrix}^T$$

(d) Incipient Collapse

With the formation of a plastic hinge at the base of the column element its incremental stiffness contribution to the column-girder assembly becomes

$$\mathbf{K}'^{(a)} = \frac{EI}{L_a} \begin{bmatrix} \frac{3}{L_a^2} & \frac{3}{L_a} & 0 & 0 \\ \frac{3}{L_a} & 3 & 0 & 0 \\ 0 & 0 & 0 & 0 \\ 0 & 0 & 0 & 0 \end{bmatrix}$$

The incremental linear stiffness of the column-girder assembly after the second event is

$$\mathbf{K}^{(2)} = \mathbf{K}'^{(a)} + \mathbf{K}'^{(b)}$$

We conclude that the structure has reached the state of incipient collapse under the load factor $\lambda^{(2)}$ and it forms a mechanism under any subsequent free dof displacement increment without a further increase of the basic forces $\mathbf{Q}^{(2)}$.

Fig. 1.5 shows the relation between the load factor λ and the lateral drift ratio of the column-girder assembly, which is the ratio of the horizontal translation \mathbf{U}_1 to the column height of 5 units.

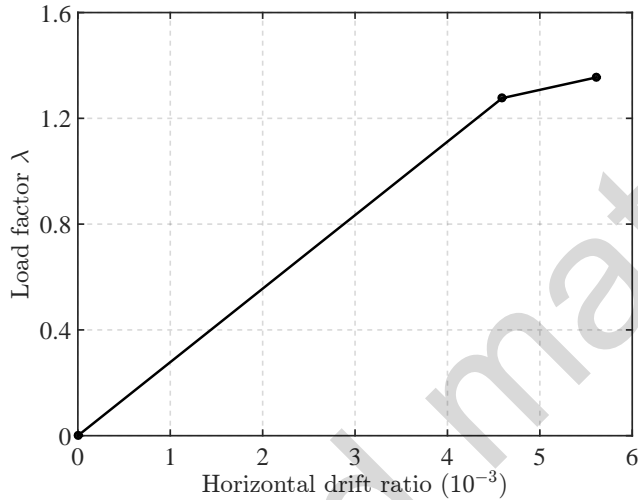


Fig. 1.5: Relation between load factor λ and lateral drift ratio for column-girder assembly

1.5 Unloading Response

In this section we address the following aspects of the event-to-event linear elastic, perfectly plastic analysis of structures:

- 1) Material response upon unloading.
- 2) Determination of plastic hinge deformations at each event.
- 3) Stress and deformation state of the structure upon complete removal of applied forces after the formation of one or more plastic hinges.

1.5.1 Inelastic material behavior

Fig. 1.6(a) shows the stress-strain relation for *linear inelastic, perfectly-plastic response*. Such stress-strain relation is a good approximation of the behavior of metallic materials. The arrow in the branches of the relation indicates the direction of deformation for a typical loading-unloading cycle involving plastic deformation. Upon stress removal the material *unloads linearly with slope equal to the initial slope E*. This is called *elastic unloading*. The permanent strain offset at zero stress is the plastic strain ε_p .

Fig. 1.6(b) shows that the total strain ε is the sum of an elastic and a plastic strain contribution

$$\varepsilon = \varepsilon_e + \varepsilon_p = \frac{1}{E}\sigma + \varepsilon_p \quad (1.22)$$

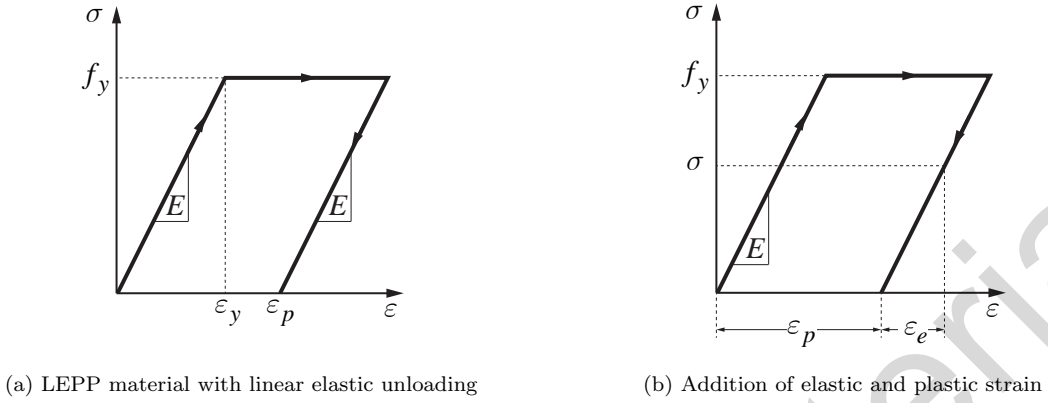


Fig. 1.6: Linear elastic, perfectly plastic (LEPP) material response with linear elastic unloading

where ε_e is the elastic strain and ε_p is the plastic strain. The latter is the difference between total strain ε and elastic strain ε_e

$$\varepsilon_p = \varepsilon - \frac{1}{E}\sigma \quad (1.23)$$

1.5.2 Inelastic element behavior

We recall that the total element deformations \mathbf{v} are the sum of deformations \mathbf{v}_ε of continuous nature and deformations \mathbf{v}_h at releases. With the symbol \mathbf{v}_{hp} for the deformations at plastic hinges we get

$$\mathbf{v} = \mathbf{v}_\varepsilon + \mathbf{v}_{hp} = \mathbf{f} \mathbf{q} + \mathbf{v}_{hp} \quad (1.24)$$

under the assumption of linear behavior for \mathbf{v}_ε with \mathbf{f} the initial element flexibility matrix. Regular release deformations \mathbf{v}_h are a special case of plastic hinge deformations which are always present, because the release cannot transfer any force.

The plastic element deformations can be expressed as

$$\mathbf{v}_{hp} = \mathbf{v} - \mathbf{f} \mathbf{q} \quad (1.25)$$

and we note the similarity of this relation with (1.23).

1.5.3 Inelastic structural behavior

For the collection of element deformations \mathbf{V} for the entire structural model we get the relation

$$\mathbf{V} = \mathbf{V}_\varepsilon + \mathbf{V}_{hp} = \mathbf{F}_s \mathbf{Q} + \mathbf{V}_{hp} \quad (1.26)$$

with \mathbf{F}_s the collection of initial element flexibility matrices. The collection of plastic deformations for the entire structural model then is

$$\mathbf{V}_{hp} = \mathbf{V} - \mathbf{F}_s \mathbf{Q} \quad (1.27)$$

and we note the similarity of this relation with (1.23) and (1.25).

Noting that the element deformations \mathbf{V} satisfy the kinematic relations with the global dof displacements we get

$$\mathbf{V}_{hp} = \mathbf{A}_f \mathbf{U}_f - \mathbf{F}_s \mathbf{Q} \quad (1.28)$$

in the absence of restrained dof displacements.

We can now return to the examples of the event-to-event analysis and determine the plastic deformations at each event either with (1.28) for the entire structure or with (1.25) element-by-element.

1.5.4 Plastic Deformations at Second Event of 2-dof Truss

From Example 1.1(c) we have the following response variables at the occurrence of the second event

$$\begin{aligned}\mathbf{U}_f^{(2)} &= \begin{bmatrix} 13.648 & 6.802 \end{bmatrix}^T \cdot 10^{-3} \\ \mathbf{Q}^{(2)} &= \begin{bmatrix} 11.34 & 15 & 15 & 6.84 \end{bmatrix}^T\end{aligned}$$

with

$$\mathbf{A}_f = \begin{bmatrix} 0 & 1 \\ 0.8 & 0.6 \\ 1 & 0 \\ 0.8 & -0.6 \end{bmatrix}$$

we get

$$\mathbf{V}^{(2)} = \mathbf{A}_f \mathbf{U}_f^{(2)} = \begin{bmatrix} 6.802 & 15.000 & 13.648 & 6.837 \end{bmatrix}^T \cdot 10^{-3}$$

and the plastic deformations \mathbf{V}_{hp} are with (1.28) or, better, with (1.25)

$$\mathbf{V}_{hp}^{(2)} = \begin{bmatrix} 0 & 0 & 1.648 & 0 \end{bmatrix}^T \cdot 10^{-3} \quad (1.29)$$

noting that the hinge in element b is about to form, while the hinge in element c has formed in the preceding event and has undergone some plastic deformation.

1.6 Unloading from Plastic Deformation State

We are interested in establishing the state of the structure after first increasing the load factor λ past λ_e , so that at least one plastic hinge forms, and then removing completely the applied loads by setting the load factor λ equal to zero. *During unloading the elements behave linearly with stiffness equal to the initial stiffness.* Fig. 1.7 shows the linear elastic unloading of the simple truss of Example 1.1 from a state between the formation of the second and the third plastic hinge. \mathbf{U}_1 denotes the horizontal translation in the figure and $\mathbf{U}_1^{(u)}$ is the horizontal translation value upon complete load removal.

As Fig. 1.6 shows, *the plastic deformations do not change during the unloading process.* Denoting the stress and deformation state of the structure with superscript u and assuming that unloading initiates at event k gives

$$\begin{aligned}\mathbf{U}_f^{(u)} &= \mathbf{U}_f^{(k)} - \lambda^{(k)} \mathbf{U}_f'^{(0)} \\ \mathbf{Q}^{(u)} &= \mathbf{Q}^{(k)} - \lambda^{(k)} \mathbf{Q}'^{(0)}\end{aligned} \quad (1.30)$$

where

$$\begin{aligned}\mathbf{U}'^{(0)}_f &= \mathbf{K}^{(0)} \setminus \mathbf{P}_{ref} \\ \mathbf{Q}'^{(0)} &= \mathbf{K}_s^{(0)} [\mathbf{A}_f \mathbf{U}'^{(0)}_f]\end{aligned}\quad (1.31)$$

using the Matlab® \ operator to denote the solution of the equilibrium equations.

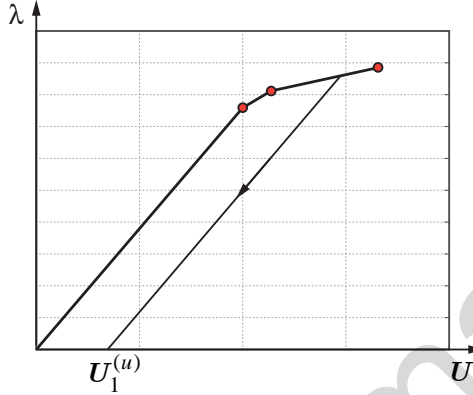


Fig. 1.7: Linear elastic unloading of simple truss after second hinge forms

We get the plastic element deformations on complete load removal with (1.28)

$$\mathbf{V}_{hp}^{(u)} = \mathbf{A}_f \mathbf{U}_f^{(u)} - \mathbf{F}_s^{(0)} \mathbf{Q}^{(u)}$$

Substituting the expressions for \mathbf{U}_f and \mathbf{Q} from (1.30) gives

$$\begin{aligned}\mathbf{V}_{hp}^{(u)} &= \mathbf{A}_f [\mathbf{U}_f^{(k)} - \lambda^{(k)} \mathbf{U}'^{(0)}_f] - \mathbf{F}_s^{(0)} [\mathbf{Q}^{(k)} - \lambda^{(k)} \mathbf{Q}'^{(0)}] \\ &= \mathbf{A}_f \mathbf{U}_f^{(k)} - \mathbf{F}_s^{(0)} \mathbf{Q}^{(k)} - \lambda^{(k)} [\mathbf{A}_f \mathbf{U}'^{(0)}_f - \mathbf{F}_s^{(0)} \mathbf{Q}'^{(0)}]\end{aligned}$$

On account of the second equation of (1.31) the expression in square brackets on the right hand side of the last equation is zero so that

$$\boxed{\mathbf{V}_{hp}^{(u)} = \mathbf{A}_f \mathbf{U}_f^{(k)} - \mathbf{F}_s^{(0)} \mathbf{Q}^{(k)} = \mathbf{V}_{hp}^{(k)}}$$

confirming that the plastic element deformations on complete load removal do not change from the values at event k at which unloading initiated.

Because the applied loads are removed upon complete unloading, there are no applied forces at the free dofs of the structure for this state. *Consequently, the basic forces $\mathbf{Q}^{(u)}$ constitute a homogeneous equilibrium state or self-stress state.*

With knowledge of the plastic element deformations $\mathbf{V}_{hp}^{(u)}$ this stress state can be established from the satisfaction of the compatibility conditions

$$\mathbf{0} = \bar{\mathbf{B}}_x^T \mathbf{V} = \bar{\mathbf{B}}_x^T [\mathbf{V}_\varepsilon + \mathbf{V}_{hp}^{(u)}] = \bar{\mathbf{B}}_x^T [\mathbf{F}_s \mathbf{Q}^{(u)} + \mathbf{V}_{hp}^{(u)}]$$

Substituting $\bar{\mathbf{B}}_x \mathbf{Q}_x$ for $\mathbf{Q}^{(u)}$ in the last equation gives

$$\mathbf{0} = \bar{\mathbf{B}}_x^T [\mathbf{F}_s \bar{\mathbf{B}}_x \mathbf{Q}_x + \mathbf{V}_{hp}^{(u)}] \rightarrow \mathbf{Q}_x = -\mathbf{F}_{xx}^{-1} [\bar{\mathbf{B}}_x^T \mathbf{V}_{hp}^{(u)}] \quad (1.32)$$

furnishing the equation for determining the redundant basic forces and with them $\mathbf{Q}^{(u)} = \bar{\mathbf{B}}_x \mathbf{Q}_x$. The basic forces $\mathbf{Q}^{(u)}$ are known as *residual forces* and are present in most structures as the result of construction loads. They appear as residual stresses in steel beam profiles as the result of plastic deformations during manufacturing.

1.6.1 Basic Forces of 2-dof Truss upon Complete Load Removal

We determine now the basic forces of the 2-dof truss under the assumption that the load is completely removed following the second event. With the plastic deformations from (1.29) we get

$$\mathbf{V}_{hp}^{(u)} = \mathbf{V}_{hp}^{(2)} = [0 \quad 0 \quad 1.648 \quad 0]^T \cdot 10^{-3}$$

The selection of the basic forces \mathbf{Q}_3 and \mathbf{Q}_4 as redundant basic forces gives the following homogeneous static solutions

$$\bar{\mathbf{B}}_x = \begin{bmatrix} 0.75 & 1.20 \\ -1.25 & -1.00 \\ 1.00 & 0 \\ 0 & 1.00 \end{bmatrix}$$

(1.32) gives

$$\mathbf{F}_{xx} = \begin{bmatrix} 2.700 & 1.790 \\ 1.790 & 2.864 \end{bmatrix} 10^{-3} \quad \bar{\mathbf{B}}_x^T \mathbf{V}_{hp}^{(u)} = \begin{pmatrix} 1.648 \\ 0 \end{pmatrix} 10^{-3} \rightarrow \mathbf{Q}_x = \begin{pmatrix} -1.042 \\ 0.652 \end{pmatrix}$$

With the redundant basic forces \mathbf{Q}_x the residual basic forces $\mathbf{Q}^{(u)}$ are

$$\mathbf{Q}^{(u)} = \bar{\mathbf{B}}_x \mathbf{Q}_x = \begin{pmatrix} 0 \\ 0.652 \\ -1.042 \\ 0.652 \end{pmatrix}$$

These basic forces agree with the result of (1.30) for $k = 2$

$$\mathbf{Q}^{(u)} = \mathbf{Q}^{(2)} - \lambda^{(2)} \mathbf{Q}'^{(0)} = \begin{pmatrix} 11.34 \\ 15 \\ 15 \\ 6.84 \end{pmatrix} - 1.62 \begin{pmatrix} 6.98 \\ 8.84 \\ 9.88 \\ 3.81 \end{pmatrix} = \begin{pmatrix} 0 \\ 0.652 \\ -1.042 \\ 0.652 \end{pmatrix}$$

with the values for $\mathbf{Q}^{(2)}$ and $\lambda^{(2)}$ from Section(c) and the values for $\mathbf{Q}'^{(0)}$ from Section (b) of Example 1.1. It is worth recalling that at the second event, the element c has undergone plastic deformation, whereas element b has just reached its axial plastic capacity without any plastic deformation.

1.7 Computer Implementation of Event-To-Event Analysis

The preceding discussion reveals a characteristic of nonlinear structural analysis: *a typical linear step needs to be repeated several times until the target load or displacement of the structure is reached.* The target load may be the collapse load, while the target displacement may be past incipient collapse with the kinematics of the collapse mechanism superimposed on the deformation state of the structure at incipient collapse.

While calculations for a typical linear step may be carried out by hand for a small structural model, insight into the behavior of the structure under incremental analysis can only be gained from the completion of all steps up to the target load or displacement. Consequently, the ability to program a typical linear step becomes indispensable for nonlinear analysis.

At this point the instructor of a course on nonlinear structural analysis has two options: (a) use commercial software and try to match his understanding of what its elements and procedures do with the theoretical tidbits of a typical manual for commercial software, or, (b) program a flexible tool for *education and research*. The author followed the second path by creating the Matlab® toolbox [FEDEASLab](#) for education and research in the nonlinear analysis of structures. The graduate students who contributed to particular functions will be given the appropriate credit when these are discussed.

1.7.1 Typical linear response increment from event k to next event

Here is the summary of a linear step in the event-to-event analysis process for linear elastic, perfectly-plastic element basic force-deformation response:

- 1) Set up the current stiffness of the structural model with basic force releases at all p_k locations where plastic hinges appeared in the events through k

$$\mathbf{K}^{(k)} = \mathbf{A}_f^T \mathbf{K}_s^{(k)} \mathbf{A}_f$$

- 2) Solve for the free dof displacements \mathbf{U}'_f and the basic forces \mathbf{Q}' under reference load

$$\begin{aligned}\mathbf{U}'_f^{(k)} &= \mathbf{K}^{(k)} \backslash \mathbf{P}_{ref} \\ \mathbf{Q}'^{(k)} &= \mathbf{K}_s^{(k)} \left[\mathbf{A}_f \mathbf{U}'_f^{(k)} \right]\end{aligned}$$

- 3) Determine the DC ratio under the reference load at locations m without plastic hinge

$$DC'_m = \frac{\mathbf{Q}'_m^{(k)}}{\operatorname{sgn} \mathbf{Q}_{pl,m}^{\operatorname{sgn}} - \mathbf{Q}_m^{(k)}}$$

- 4) Determine the *load factor increment* $\Delta\lambda^{(k)}$ to next event

$$\Delta\lambda^{(k)} = \frac{1}{\max(DC'_m)}$$

- 5) Update the load factor, the free dof displacements and the basic forces to next event

$$\begin{aligned}\lambda^{(k+1)} &= \lambda^{(k)} + \Delta\lambda^{(k)} \\ \mathbf{U}_f^{(k+1)} &= \mathbf{U}_f^{(k)} + \Delta\lambda^{(k)} \mathbf{U}_f'^{(k)} \\ \mathbf{Q}^{(k+1)} &= \mathbf{Q}^{(k)} + \Delta\lambda^{(k)} \mathbf{Q}'^{(k)}\end{aligned}$$

- 6) Determine the plastic deformations at next event

$$\mathbf{V}_{hp}^{(k+1)} = \mathbf{A}_f \mathbf{U}_f^{(k+1)} - \mathbf{F}_s^{(0)} \mathbf{Q}^{(k+1)}$$

where $\mathbf{F}_s^{(0)}$ is the collection of *initial element flexibility matrices*.

Box 1.1 shows the Matlab® implementation of the above process from the unstressed state until complete or partial collapse of the structural model.

```
% step by step analysis until full or partial collapse
while (rank(Af(ind_e,ind_n))==length(ind_n))
    KsAf = Fs(ind_e,ind_e)\Af(ind_e,ind_n);
    Kf = Af(ind_e,ind_n)*KsAf;
    Ufe = zeros(nf,1);
    Ufe(ind_n) = Kf\Pref(ind_n);
    Qe = zeros(nq,1);
    Qe(ind_e,:) = KsAf*Ufe(ind_n);
    Qplres = sign(Qe(ind_e)+eps).*Qpl(ind_e)-Qh(ind_e,k);
    DC = zeros(nq,1);
    DC(ind_e) = Qe(ind_e)./Qplres;
    new_hinge = find(max(DC)-DC < eps*max(DC));
    Dlamda = 1/DC(new_hinge(1));
    lamdah(k+1) = lamdah(k) + Dlamda;
    Ufh(:,k+1) = Ufh(:,k) + Dlamda.*Ufe;
    Qh(:,k+1) = Qh(:,k) + Dlamda.*Qe;
    Iph = [Iph new_hinge'];
    ind_t = setdiff(1:nf,ind_n);
    Ufh(ind_t,k+1) = Ufh(ind_t,k);
    Vph(:,k+1) = Af*Ufh(:,k+1) - Fs*Qh(:,k+1);
    ind_e = setdiff(ind_e,new_hinge');
    [i,j] = find([Pref Af(ind_e,:)'']);
    ind_n = unique(i);
    % increment step counter
    k = k+1;
end
```

Box 1.1: Event-to-event analysis implementation from unstressed state to complete or partial collapse

A more involved implementation was accomplished with the help of former graduate student Dr. Chin-Long Lee¹ in the function `Event2Event_NLAnalysis` with the following syntax:

```
[lamdah,Qh,Ufh,Vph,Iph] = Event2Event_NLAnalysis ('lg',Model,ElemData,Loading)
```

The function accommodates P - Δ geometry by specifying 'ng' in lieu of 'lg' in the first input argument of the function. The next two input arguments are familiar from the course on linear analysis: `Model` is a data structure with model geometry and element type information, and `ELEMData` is a data structure with the element properties. The data structure `Loading` contains information about the

¹ Lecturer at the University of Canterbury, New Zealand

applied loading. The event-to-event analysis looks for the reference load vector P_{ref} for the applied loads to be factored, and for the load vector P_i for applied nodal forces that remain constant during the load application process. The default value of the latter is zero.

The function returns the load factor values for the events in row vector λ_{mdah} and the index of plastic hinge locations in the array I_{ph} . The second row of this array, if present, contains the index of the second hinge in a double hinge configuration. Q_h , U_{fh} , and V_{ph} are arrays with the history of the basic forces, the free dof displacements and the plastic element deformations at the events, with the first column corresponding to the initial, unstressed and undeformed state. Consequently, $Q_h(:, 3)$ corresponds to the basic forces when the second plastic hinge forms, and $U_{fh}(3, 5)$ gives the free dof displacement at dof #3 when the fourth plastic hinge forms. For generality it is better to use the dof numbering in $Model.DOF$ to access the displacement value at a particular dof, e.g. $Model.DOF(3, 2)$ refers to the dof number for the vertical translation at node 3.

The arrays Q_h , U_{fh} , and V_{ph} can be used with the **FEDEASLab** plotting functions to create plot sequences and animations. An interesting application is the function **Animate_EventSequence** which creates a plot series of the deformed shape of the structure with animation of the plastic hinge formation sequence. The function syntax is

```
Animate_EventSequence (Model, ElemdData, Ufh, Qh)
```

Example 1.3 Event-to-Event Analysis of Portal Frame

The following figures show the results of the linear elastic, perfectly-plastic event-to-event analysis of the portal frame from Example 5.3 of the course on linear structural analysis. Fig. 1.8(a) shows the geometry of the portal frame and the reference values of the applied nodal forces. The following analysis assumes that the vertical and the horizontal force are incremented simultaneously until the complete collapse mechanism with the plastic hinges in Fig. 1.8(b) forms. Fig. 1.8(b) shows the free dof numbering and the numbering of plastic hinge deformations. The sequence of plastic hinges given by I_{ph} is: at 6, at 4, at 8 and finally at 1.

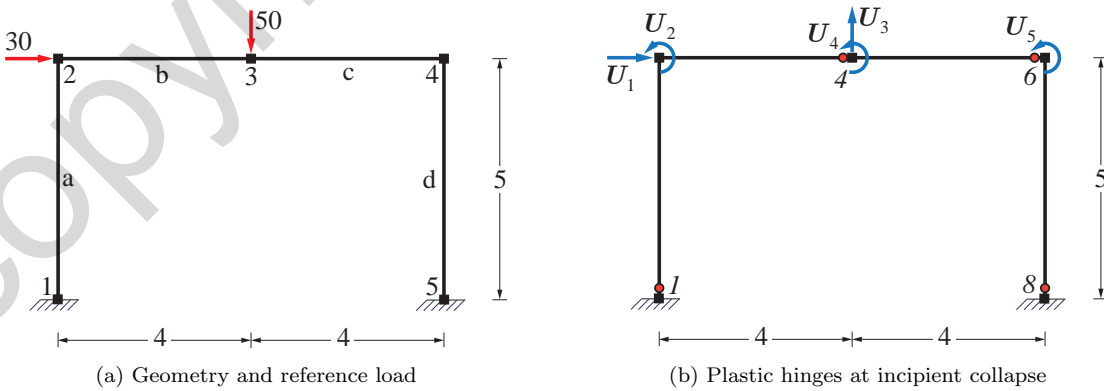


Fig. 1.8: Portal frame

Fig. 1.9 shows the relation between the load factor λ of the reference nodal force vector P_{ref} and the horizontal drift ratio, i.e. the ratio of the horizontal translation to the story height. The analysis

assumes that the frame elements are inextensible with very large plastic axial capacity. The analysis also assumes that the axial force in the frame elements does not affect the plastic flexural capacity. The interaction between axial force and bending moment will be studied in a later chapter. The event of a new plastic hinge forming is marked in the load-displacement relation of Fig. 1.9 with a marker. The load is removed following the formation of the last hinge and before the onset of the collapse mechanism. A marker denotes the point of complete unloading with a residual horizontal drift ratio slightly larger than 0.004 in Fig. 1.9.

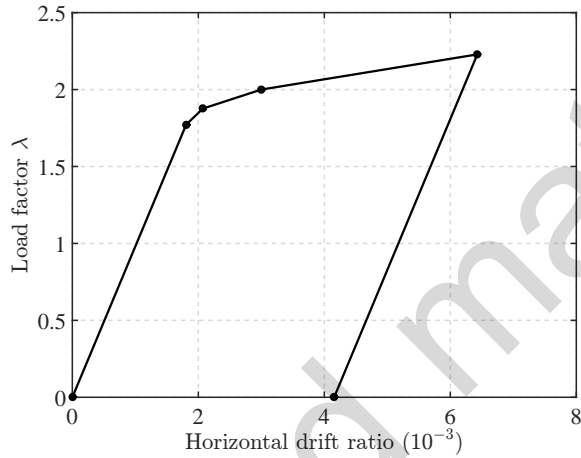


Fig. 1.9: Relation between load factor λ and horizontal drift ratio for portal frame

Fig. 1.10 shows the deformed shape and the corresponding bending moment distribution at each event. The magnification factor for the deformed shapes in Fig. 1.10(a) is 30. The plot of each bending moment distribution is scaled to the same value so that the moment value remains constant at a plastic hinge location during subsequent load incrementation to provide insight to the process of *moment redistribution* under increasing load. This process is most evident for girder element b and column element d in Fig. 1.10(b).

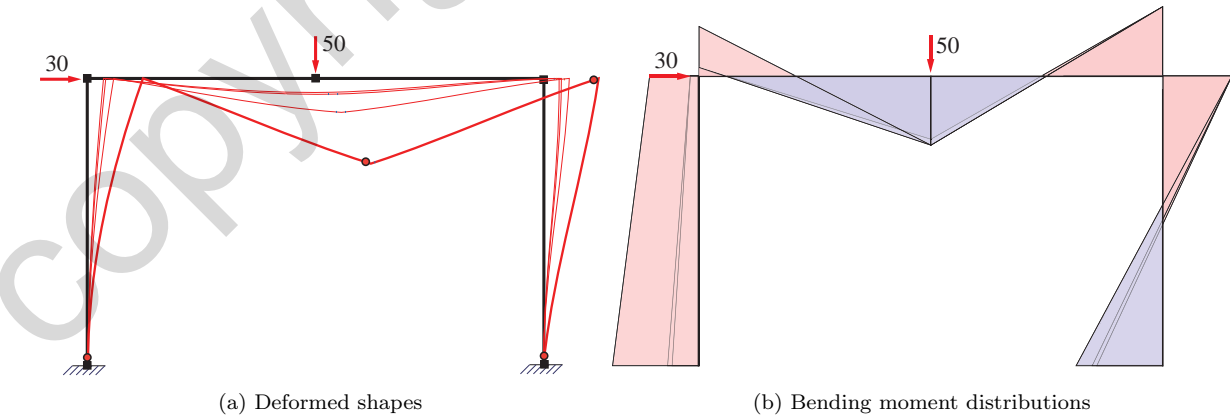


Fig. 1.10: Deformed shape and bending moment distribution at each event

Fig. 1.11 shows the deformed shape of the portal frame under complete removal of the applied nodal forces following the formation of the last hinge, as Fig. 1.9 shows. The tangent continuity at 1 is evident in the deformed shape, since the last hinge did not open. In contrast, there are residual plastic deformations at the other three plastic hinges, as is clearly evident in Fig. 1.11(a) by the discontinuous tangent of the deformed shape at these locations. The corresponding bending moment distribution in Fig. 1.11(b) corresponds to the *homogeneous basic force state* given by the redundant basic force values in (1.32). Because the degree of static indeterminacy of the portal frame is 3, the homogeneous basic force state at complete unloading results from the linear combination of 3 homogeneous solutions for the static relations of the portal frame.

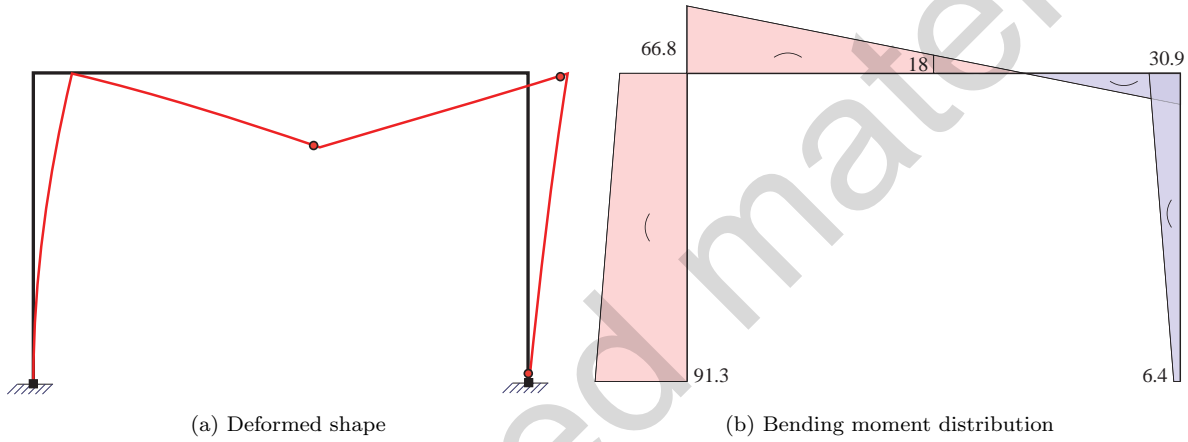


Fig. 1.11: State of portal frame upon complete unloading at formation of last hinge

Fig. 1.12(a) shows the plastic hinge deformation history with the hinges numbered in the order of their appearance. Fig. 1.12(b) shows the relation between basic force and corresponding *total element deformation* for the four plastic hinges. Both figures show that the last hinge does not undergo any plastic deformation without collapse mechanism displacement.

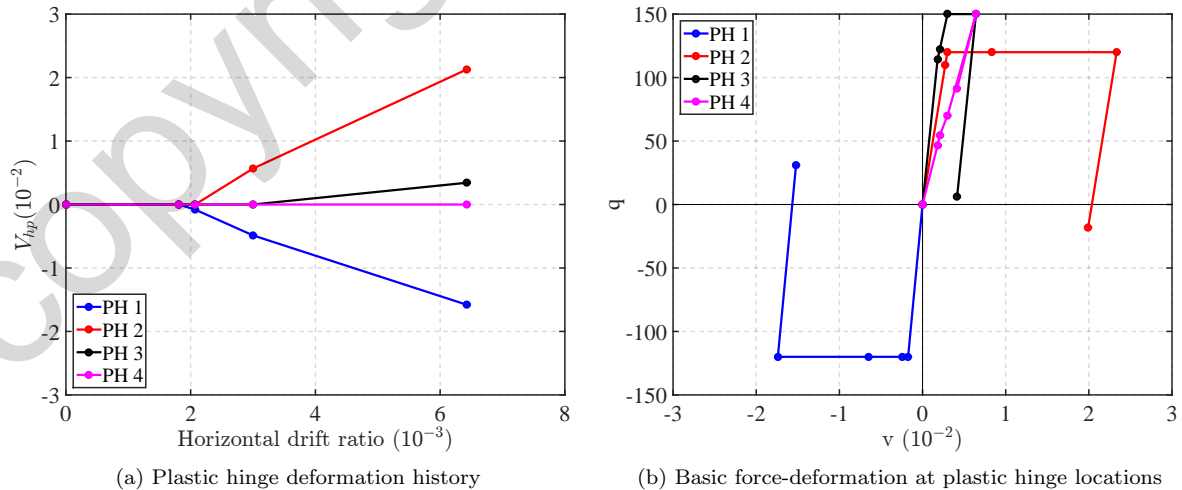


Fig. 1.12: Plastic hinge deformation history and basic force-deformation relation

It is worth noting that the basic force-deformation relation for the third hinge exhibits a bilinear branch before reaching the plastic capacity of the hinge. The reason is left as a challenge for the reader.

Fig. 1.13 shows the relation between lateral force load factor and average roof drift ratio for an 8-story steel frame designed according to the EC4 recommendations for a student project. The designers did an excellent job to distribute the plastic hinges at the girder ends over the entire height of the building before the onset of the collapse mechanism. The lateral force distribution follows an inverted triangle over the height of the building.

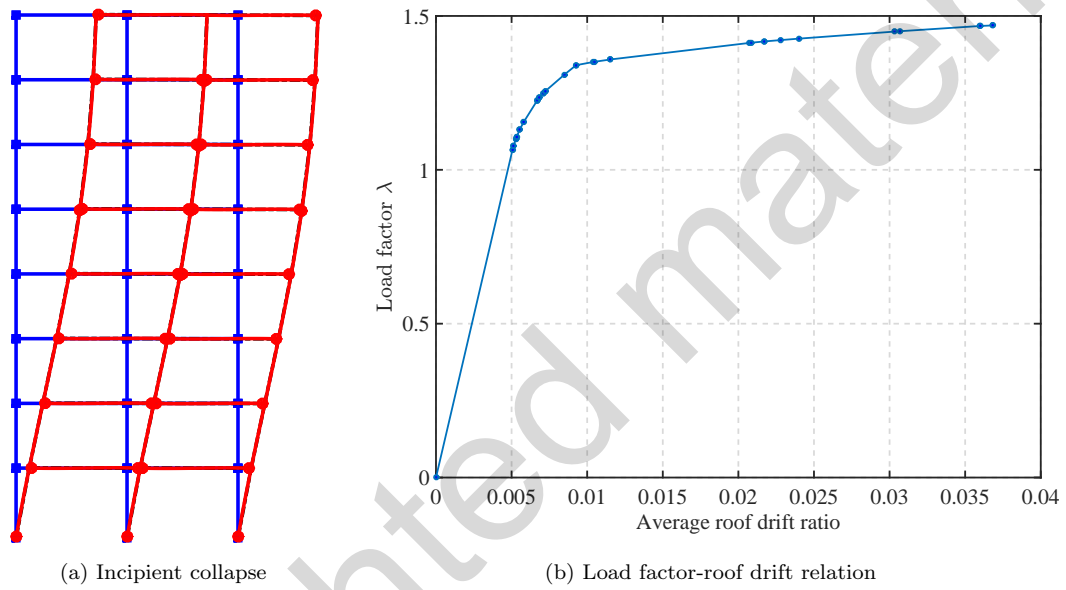


Fig. 1.13: Event-to-event pushover of 8-story steel frame under inverted triangular lateral force distribution

Chapter 2

Introduction to Nonlinear Geometry

2.1 Overview

Structural analysis is based on three pillars: (a) kinematics, (b) statics, and (c) the constitutive force-deformation relations for the material. Depending on whether a pillar of structural analysis is linear (L) or nonlinear (NL) we distinguish the following categories of nonlinear structural analysis.

Case	Kinematics	Statics	Material
Linear analysis	L	L	L
NL material	L	L	NL
NL geometry	NL	NL	L
2nd order with LM	L	NL	L
2nd order with NLM	L	NL	NL
NL geometry+material	NL	NL	NL

Table 2.1: Summary of nonlinear analysis options

The case of approximate nonlinear statics for frame elements while kinematics remains linear is known as *2nd order analysis* or *P-Δ analysis*. The case that kinematics is nonlinear while statics is linear does not make sense.

In a discrete structural model we distinguish the structural kinematics from the element kinematics:

- Structural kinematics refers to the relation between the global dof displacements and the intra-node deformations. The latter are the *deformations of the discrete structural model*.
- Element kinematics refers to the relations between the element deformations \mathbf{v} and the strain tensor $\boldsymbol{\epsilon}(x, y, z)$ at a material point (x, y, z) of the element. In the following we limit ourselves to the uniaxial normal strain ε_x and drop the subscript x for brevity of notation.

Similarly, we distinguish the structural statics from the element statics:

- Structural statics refers to the relation between the element end forces \mathbf{p} in the global coordinate system that directly contribute to the node equilibrium equations and the basic element forces \mathbf{q} . The element end forces \mathbf{p} and the basic element forces \mathbf{q} satisfy the equilibrium relations for *the element free body*.

- Element statics refers to the relations between the basic element forces \mathbf{q} and the stress $\sigma(x, y, z)$ at a material point (x, y, z) of the element. In the following we limit ourselves to the uniaxial normal stress σ_x and drop the subscript x for brevity of notation.

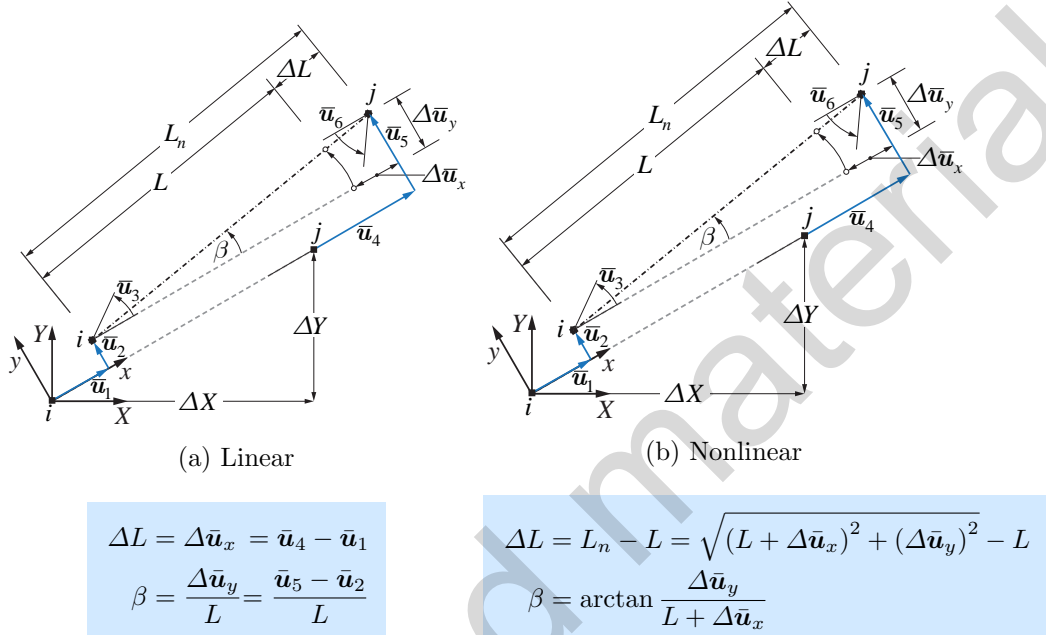


Fig. 2.1: Linear vs. nonlinear structural kinematics

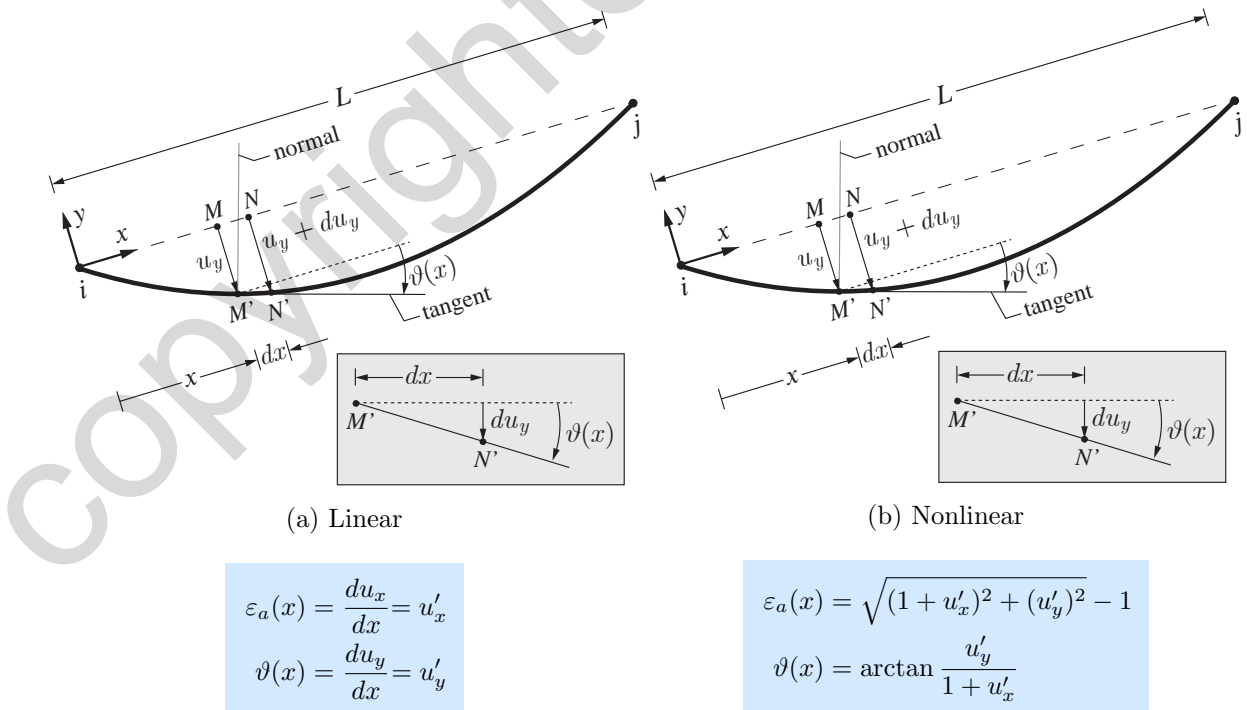


Fig. 2.2: Linear vs. nonlinear frame element kinematics

Fig. 2.1 shows the distinction between linear and nonlinear structural kinematics for a line element. Because of the compatibility of the element end displacements with the corresponding node displacements, the intra-node deformations for a plane frame element are the change of distance ΔL and the chord rotation angle β . Fig. 2.1(b) shows the general definition for ΔL and β under large *relative translations* Δu_x and Δu_y , while Fig. 2.1(a) shows the linear approximation for ΔL and β under the assumption of small relative translations Δu_x and Δu_y *relative to the original distance* L .

Fig. 2.2 shows the distinction between linear and nonlinear kinematics for a frame element. In the figure $u_x(x)$ denotes the translation in x of a point of the reference axis for the straight frame element and $u_y(x)$ denotes the translation in y . If the *derivative of the translation* $u_x(x)$ with respect to x is large relative to 1 and the derivative of the translation $u_y(x)$ with respect to x is larger than 10^{-2} , Fig. 2.2(b) shows the general definition for the normal strain $\varepsilon_a(x)$ of the reference axis and the angle $\vartheta(x)$ of the tangent to the deformed shape relative to the element chord. Fig. 2.2(a) shows the linear approximation for $\varepsilon_a(x)$ and $\vartheta(x)$ under the assumption that u'_x is small relative to 1 and u'_y is smaller than 10^{-2} . Note the similarity of the nonlinear kinematic relations in Fig. 2.2(b) with the kinematic relations for the intra-node deformations in Fig. 2.1(b).

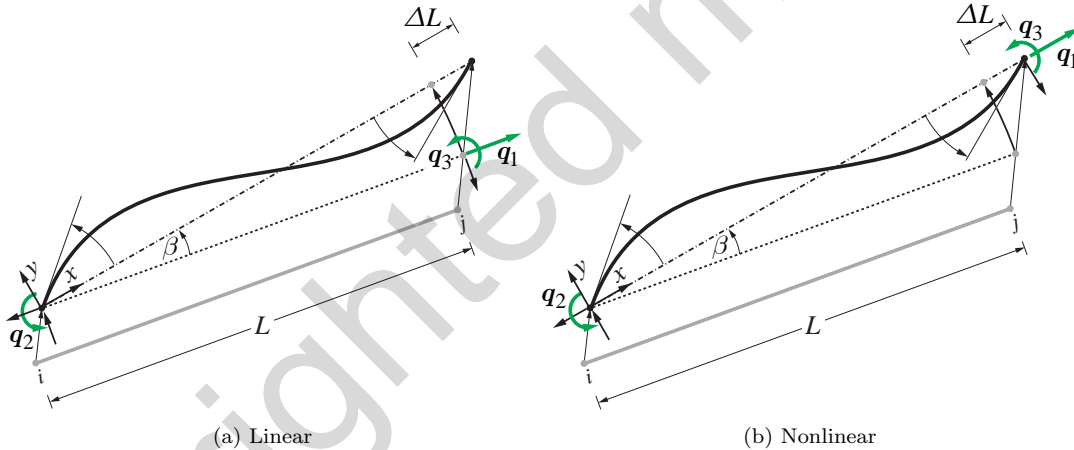


Fig. 2.3: Linear vs. nonlinear structural statics

Fig. 2.3 shows the distinction between linear and nonlinear structural statics for a frame element. Under linear statics in Fig. 2.3(a) the equilibrium of the element free body is satisfied in the *original, undeformed configuration* so that the transformation to the element end forces in the global coordinate system involves the direction cosines of the original element chord orientation. Under nonlinear statics in Fig. 2.3(b) the equilibrium of the element free body is satisfied in the *deformed configuration by defining the basic element forces relative to the chord in its position under large displacements*. This approach to nonlinear structural statics is known as *corotational formulation*. With this definition of basic element forces to the element end forces in the global coordinate system involves the direction cosines of the element chord orientation in the deformed configuration. The latter include the relative end translations of the element, so that the direction cosines change continuously during the incremental deformation of the structure under incremental loading.

Fig. 2.4 shows the distinction between linear and nonlinear frame element statics. Under linear statics in Fig. 2.4(a) the equilibrium of the internal element forces $N(x)$, $V(x)$ and $M(x)$ is satisfied

for a segment of length dx of the *undeformed element reference axis*. The internal axial force $N(x)$ and the bending moment $M(x)$ are the integrals of the normal stress distribution over the element section normal to the element axis at x . The shear force V results from equilibrium considerations under the assumptions of the Euler-Bernoulli beam theory that plane sections remain plane after deformation. Under nonlinear statics in Fig. 2.4(b) the equilibrium of the internal element forces $N(s)$, $V(s)$ and $M(s)$ is now satisfied for a segment of length ds of the *deformed element axis* where s is the independent variable that measures the arc distance from the origin of the element coordinate system $x-y$.

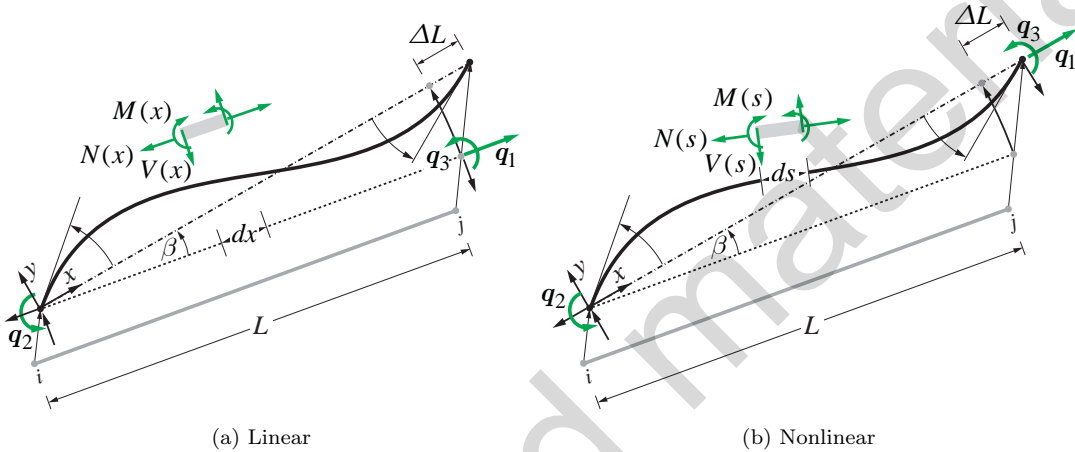


Fig. 2.4: Linear vs. nonlinear element statics

From the preceding discussion we conclude that *nonlinear kinematics* theoretically involves both, nonlinear structural and element kinematics, and the same is true for *nonlinear statics*. Noting the similarity of the nonlinear kinematic relations in Fig. 2.2(b) with the kinematic relations for the intra-node deformations in Fig. 2.1(b) it becomes clear that the former relations can be approximated by discrete relations after the subdivision of a single element into several subelements and the same is true for the static relations. Intuitively we conclude that we may be able to dispense with nonlinear kinematics and statics for the element and limit ourselves to the nonlinear structural kinematics for the intra-node deformations and the nonlinear structural statics for the entire element free body.

We plan to use this approach to nonlinear kinematics and statics throughout this text, but defer to a later chapter the confirmation of the accuracy of this assumption. For now we introduce a few phenomena of the nonlinear geometric response of structures with the help of the plane truss element. We note that *nonlinear geometry* implies that both structural kinematics and statics are nonlinear.

After introducing two deformation measures and deriving the nonlinear kinematic relations of the general plane and space truss element we use a single degree-of-freedom (dof) truss to illustrate the consistent derivation of the equilibrium equations in the deformed configuration with the principle of virtual work. From the equilibrium equations we derive the stiffness matrix of the structure by differentiating the vector of resisting forces \mathbf{P}_r .

The derivation of the truss element stiffness matrix shows that under nonlinear geometry considerations it consists of two contributions: (a) the material stiffness, and (b) the geometric stiffness. The

geometric stiffness is proportional to the axial basic force of the element and alters the behavior of the structure significantly:

- 1) under a tensile axial force the geometric stiffness stiffens the structure under nonlinear geometry considerations, as demonstrated by prestressed cables and membranes, and may render an initially unstable structure stable in the original configuration.
- 2) By contrast, a compressive element force softens the structure under nonlinear geometry considerations and can lead to several interesting instability phenomena. In particular, a compressive force of a certain magnitude may render an initially stable structure unstable in the original configuration.

2.2 Nonlinear Kinematics of Truss Element

Before the following derivations we recall that the element deformations \mathbf{v} are always equal to the intra-node deformations because of the compatibility the element end displacements with the corresponding node displacements. The truss element has a single deformation, its change of length v_1 . Correspondingly, the only intra-node deformation of interest is the change of distance ΔL of the two nodes to which the truss element connects. For brevity of notation we drop the subscript 1 from the element deformation vector \mathbf{v} and denote it as the scalar v .

Because rotations are of no relevance for structural models with truss elements, we do not include them in the following introduction and number the four independent end translations for the plane truss element $\mathbf{u}_1 \dots \mathbf{u}_4$, or, the six independent end translations for the space truss element $\mathbf{u}_1 \dots \mathbf{u}_6$.

2.2.1 Definition of Deformation

Fig. 2.5 shows two nodes i and j undergoing large displacements \mathbf{u} . The plane truss element chord is shown with a dashed line to illustrate that the element is not yet inserted between the nodes. Because of the one-to-one equality between element end translations and node translations we denote the node translations in Fig. 2.5 with lower case letters. For the numbering we note that node i corresponds to truss element end i and node j to truss element j , respectively.

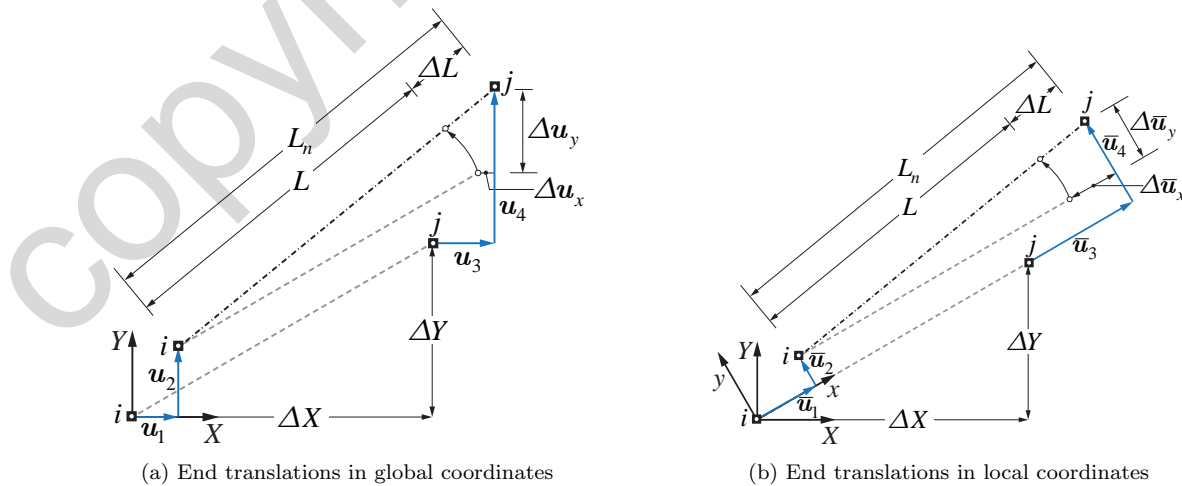


Fig. 2.5: Intra-node deformations under large translations

We are interested in expressing the change of distance ΔL between nodes i and j in terms of the node translations \mathbf{u} . To this end we can either express the relative end translations in global coordinates, as Fig. 2.5(a) shows, or, express first the end translations in local coordinates, as Fig. 2.5(b) shows, and then use the rotation transformation between local and global vector components to transform the translations to the global coordinate system.

Before embarking on the task we define the change of distance ΔL in two ways. The first definition is rather intuitive, namely

$$\Delta L_{RE} = L_n - L \quad (2.1)$$

and we give it the name *rotated engineering deformation* and use the subscript RE to identify it whenever necessary.

The second definition for the change of distance ΔL has its origin in continuum mechanics and is known by the name of *Green-Lagrange*. It is

$$\Delta L_{GL} = \frac{1}{2L} (L_n^2 - L^2) \quad (2.2)$$

We use the subscript GL to identify it whenever necessary. We will demonstrate shortly that there is little difference in the two definitions for the change of distance in practical structural engineering applications.

From end translation compatibility considerations the axial element deformation v is equal to the change of length ΔL and we use $v = \Delta L$ in the following:

- 1) For the Green-Lagrange deformation

$$v_{GL} = \frac{1}{2L} (L_n^2 - L^2) \quad (2.3)$$

- 2) For the rotated engineering definition

$$v_{RE} = L_n - L \quad (2.4)$$

For both deformation definitions we need to establish the new distance L_n between nodes i and j . Before doing so we state the assumption that normal strain of the truss element is small so that $\varepsilon_a = \frac{du_x}{dx}$ leading to

$$v = \Delta \bar{\mathbf{u}}_x = \int_0^L \varepsilon_a dx \quad (2.5)$$

This means that the *truss element kinematics are assumed linear while the structural kinematics are nonlinear*.

2.2.2 Green-Lagrange Deformation for Truss

According to (2.3) the Green-Lagrange deformation requires the square of the distance L_n between nodes i and j after deformation and it equal to the deformed length of the truss element. With the translation components $\bar{\mathbf{u}}$ in the local reference system in Fig. 2.5(b) we use the Pythagorean theorem to express the square of the deformed element length L_n

$$L_n^2 = (L + \Delta\bar{\mathbf{u}}_x)^2 + (\Delta\bar{\mathbf{u}}_y)^2 = L^2 \left[\left(1 + \frac{\Delta\bar{\mathbf{u}}_x}{L}\right)^2 + \left(\frac{\Delta\bar{\mathbf{u}}_y}{L}\right)^2 \right] \quad (2.6)$$

where $\Delta\bar{\mathbf{u}}_x = \bar{\mathbf{u}}_3 - \bar{\mathbf{u}}_1$ and $\Delta\bar{\mathbf{u}}_y = \bar{\mathbf{u}}_4 - \bar{\mathbf{u}}_2$. With (2.6) the Green-Lagrange deformation in (2.3) becomes

$$v_{GL} = \frac{1}{2L} (L_n^2 - L^2) = \frac{L}{2} \left[\left(1 + \frac{\Delta\bar{\mathbf{u}}_x}{L}\right)^2 + \left(\frac{\Delta\bar{\mathbf{u}}_y}{L}\right)^2 - 1 \right]$$

After expanding the square of the first term in the square brackets we get

$$v_{GL} = \Delta\bar{\mathbf{u}}_x + \frac{(\Delta\bar{\mathbf{u}}_x)^2}{2L} + \frac{(\Delta\bar{\mathbf{u}}_y)^2}{2L} \quad (2.7)$$

The expression for the Green-Lagrange deformation in (2.7) consists of the linear kinematic term $\Delta\bar{\mathbf{u}}_x$ and two quadratic terms of the relative translations. Expressing the translation vector components in the local coordinate system in terms of the vector components in the global coordinate system gives

$$\begin{aligned} \Delta\bar{\mathbf{u}}_x &= \frac{\Delta X}{L} \Delta\mathbf{u}_x + \frac{\Delta Y}{L} \Delta\mathbf{u}_y \\ \Delta\bar{\mathbf{u}}_y &= -\frac{\Delta Y}{L} \Delta\mathbf{u}_x + \frac{\Delta X}{L} \Delta\mathbf{u}_y \end{aligned} \quad (2.8)$$

where $\Delta\mathbf{u}_x = \mathbf{u}_3 - \mathbf{u}_1$ and $\Delta\mathbf{u}_y = \mathbf{u}_4 - \mathbf{u}_2$. Adding up the square of the two equations in (2.8) and noting that the sum of the square of the direction cosines $\frac{\Delta X}{L}$ and $\frac{\Delta Y}{L}$ is equal to 1 leads to the conclusion that

$$(\Delta\bar{\mathbf{u}}_x)^2 + (\Delta\bar{\mathbf{u}}_y)^2 = (\Delta\mathbf{u}_x)^2 + (\Delta\mathbf{u}_y)^2$$

Consequently, the truss element deformation v_{GL} can be expressed in terms of the end translation components in the global reference system

$$v_{GL} = \frac{\Delta X}{L} \Delta\mathbf{u}_x + \frac{\Delta Y}{L} \Delta\mathbf{u}_y + \frac{(\Delta\mathbf{u}_x)^2}{2L} + \frac{(\Delta\mathbf{u}_y)^2}{2L} \quad (2.9)$$

The same result can be arrived at by expressing the deformed element length L_n directly in terms of the relative end translation components in the global coordinate system. We note that the linear term in (2.9) leads to the kinematic relation $v = \mathbf{a}_g \cdot \mathbf{u}$ with

$$\mathbf{a}_g = \begin{bmatrix} -\frac{\Delta X}{L} & -\frac{\Delta Y}{L} & \frac{\Delta X}{L} & \frac{\Delta Y}{L} \end{bmatrix}$$

The extension of the preceding relations to the space truss element is straightforward. The Green-Lagrange deformation becomes with (2.7)

$$v_{GL} = \Delta\bar{\mathbf{u}}_x + \frac{(\Delta\bar{\mathbf{u}}_x)^2}{2L} + \frac{(\Delta\bar{\mathbf{u}}_y)^2}{2L} + \frac{(\Delta\bar{\mathbf{u}}_z)^2}{2L} \quad (2.10)$$

and noting that

$$(\Delta\bar{\mathbf{u}}_x)^2 + (\Delta\bar{\mathbf{u}}_y)^2 + (\Delta\bar{\mathbf{u}}_z)^2 = (\Delta\mathbf{u}_x)^2 + (\Delta\mathbf{u}_y)^2 + (\Delta\mathbf{u}_z)^2$$

the kinematic relation between truss element deformation and element end translations in the global reference system becomes

$$v_{GL} = \frac{\Delta X}{L} \Delta \mathbf{u}_x + \frac{\Delta Y}{L} \Delta \mathbf{u}_y + \frac{\Delta Z}{L} \Delta \mathbf{u}_z + \frac{(\Delta \mathbf{u}_x)^2}{2L} + \frac{(\Delta \mathbf{u}_y)^2}{2L} + \frac{(\Delta \mathbf{u}_z)^2}{2L}$$

The linear contribution v_L of the truss element deformation is the inner product of the direction cosines of the undeformed element configuration with the vector of relative end translation components in the global reference system

$$v_L = \frac{\Delta X}{L} \Delta \mathbf{u}_x + \frac{\Delta Y}{L} \Delta \mathbf{u}_y + \frac{\Delta Z}{L} \Delta \mathbf{u}_z = \begin{bmatrix} \frac{\Delta X}{L} & \frac{\Delta Y}{L} & \frac{\Delta Z}{L} \end{bmatrix} \begin{pmatrix} \Delta \mathbf{u}_x \\ \Delta \mathbf{u}_y \\ \Delta \mathbf{u}_z \end{pmatrix}$$

Thus, the linear contribution v_L of the truss element deformation v is the projection of the relative end translation components in the global reference system *onto the element axis in the undeformed configuration*.

2.2.3 Relative Importance of Terms in Green-Lagrange Deformation

To study the relative contribution of the terms of the Green-Lagrange deformation we convert it to dimensionless form by dividing it with the original element length L . This gives an axial strain ε that is equivalent to the Green-Lagrange strain definition of continuum mechanics. We limit the assessment of the relative importance of the terms to the plane truss element, but the discussion for the space truss element is analogous.

$$\varepsilon_{GL} = \frac{v_{GL}}{L} = \frac{\Delta \bar{\mathbf{u}}_x}{L} + \frac{1}{2} \left(\frac{\Delta \bar{\mathbf{u}}_x}{L} \right)^2 + \frac{1}{2} \left(\frac{\Delta \bar{\mathbf{u}}_y}{L} \right)^2 \quad (2.11)$$

In structural applications the linear term $\Delta \bar{\mathbf{u}}_x/L$ is of the order of 10^{-3} to 10^{-2} . Consequently, the first quadratic term is of the order 10^{-6} to 10^{-4} and may be safely neglected. The second quadratic term is approximately equal to the *chord rotation* of the truss element and can assume values up to 10^{-1} in flexible structures like cable roofs and membranes. *It may, therefore, be of the same order of magnitude as the linear term and should not be neglected.*

We conclude that the second quadratic term in (2.11) becomes significant for $\Delta \bar{\mathbf{u}}_y/L$ values greater than 10^{-2} . The second quadratic term is the only term present in horizontal cables and membranes under transverse loads.

We will discuss the effect of this term with an example later in this chapter.

2.2.4 Comparison of Deformation Measures

For the comparison of the Green-Lagrange deformation in (2.3) with the rotated engineering deformation in (2.4) we approximate the deformed element length L_n by power series expansion of the square root arising from (2.6). We have

$$L_n = L \sqrt{\left(1 + \frac{\Delta \bar{u}_x}{L}\right)^2 + \left(\frac{\Delta \bar{u}_y}{L}\right)^2} = L \left[1 + \frac{\Delta \bar{u}_x}{L} + \frac{1}{2} \left(\frac{\Delta \bar{u}_y}{L}\right)^2 + \text{h.o.t}\right] \quad (2.12)$$

with $\sqrt{1+x} \approx 1 + \frac{1}{2}x - \frac{1}{8}x^2$ for small x relative to 1. The rotated engineering deformation, therefore, becomes

$$v_{RE} = L_n - L \approx \Delta \bar{u}_x + \frac{(\Delta \bar{u}_y)^2}{2L} \quad (2.13)$$

The engineering strain is obtained from the engineering deformation v_{RE} by dividing the latter with the original element length L . It gives

$$\varepsilon_{RE} = \frac{L_n - L}{L} \approx \frac{\Delta \bar{u}_x}{L} + \frac{1}{2} \left(\frac{\Delta \bar{u}_y}{L}\right)^2 \quad (2.14)$$

Because of the relative insignificance of the first quadratic term in (2.11) in structural applications we conclude that the two strain/deformation measures are practically the same. We will confirm this conclusion with a subsequent example.

We plan to use the Green-Lagrange deformation in this introductory discussion of nonlinear geometry phenomena, because of the simplicity of the resulting terms for a truss element, but we switch to the rotated engineering deformation for the nonlinear geometry description of the frame element in a later chapter.

2.3 Single Degree-of-Freedom Truss Example

Instead of proceeding with the general derivation of the static relations between the end forces \mathbf{p} and the basic force q of the truss element in the deformed configuration and the subsequent derivation of the truss element stiffness matrix in global coordinates, we present this process first in the simpler setting of a single dof truss and address the derivation of the response of the general truss element in the next chapter. The one dof truss example also offers the opportunity to discuss several nonlinear geometry phenomena in a simple context.

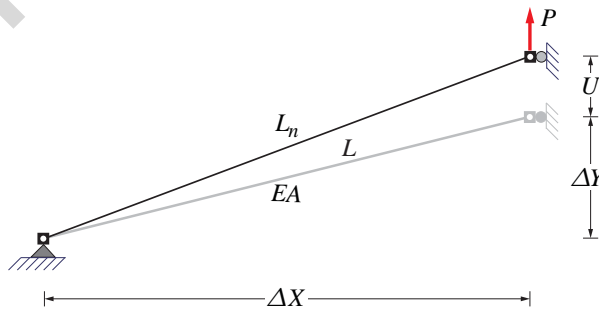


Fig. 2.6: Geometry of single dof truss

We consider the single dof truss in Fig. 2.6¹. For brevity of notation we drop the subscript from the applied force P and the corresponding displacement U , since we are dealing with a single dof and the

¹ The truss and the following derivations follow the discussion in the book by M.A. Crisfield, pp. 57–65, where a rotated log strain that is suitable for large strains is also discussed.

force and displacement variables of the problem are scalars. The geometric variables of the problem are the direction cosines of the undeformed structural configuration $\Delta X/L$ and $\Delta Y/L$.

Keeping $\Delta X = 8$ constant we study the effect of two values of ΔY on the truss force-displacement response under an upward and a downward force P :

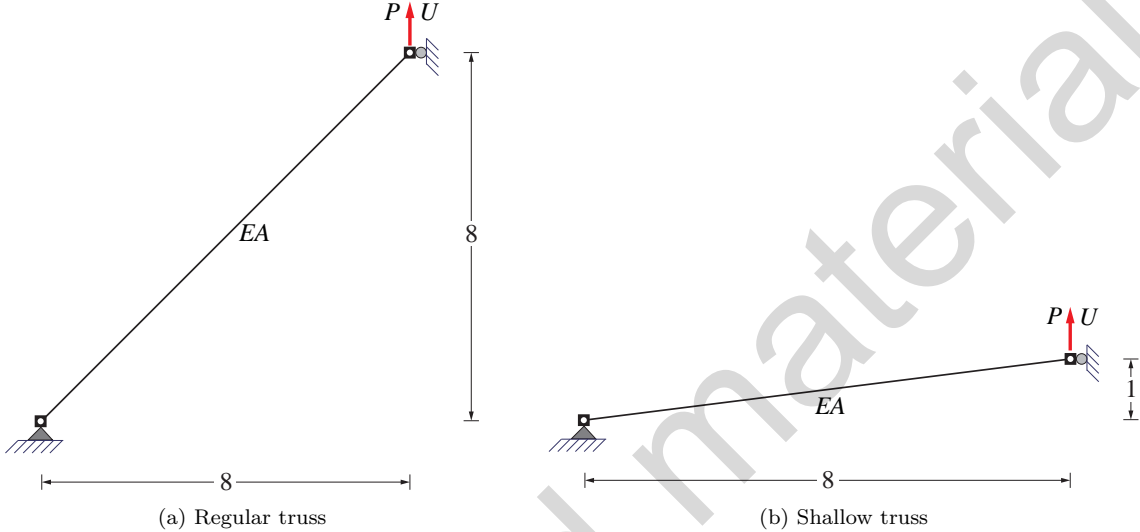


Fig. 2.7: Regular and shallow truss geometry

- 1) A value of $\Delta Y = 8$ represents a single dof truss with an inclination of 45 deg in the undeformed configuration. We call the truss in Fig. 2.7(a) *regular*.
- 2) A value of $\Delta Y = 1$ represents the *shallow* single dof truss in Fig. 2.7(b).

2.3.1 Kinematic Relations

The square of the deformed element length L_n in (2.6) becomes for the single dof truss in Fig. 2.6

$$L_n^2 = \Delta X^2 + (\Delta Y + U)^2 = L^2 + 2\Delta YU + U^2$$

using the fact that $\Delta X^2 + \Delta Y^2 = L^2$. The Green-Lagrange deformation of the truss element is

$$v_{GL} = \frac{1}{2L} (L_n^2 - L^2) = \frac{\Delta Y}{L}U + \frac{U^2}{2L} \quad (2.15)$$

and the rotated engineering deformation is

$$v_{RE} = L_n - L = \sqrt{L^2 + 2\Delta YU + U^2} - L \quad (2.16)$$

The linear deformation is

$$v_L = \frac{\Delta Y}{L}U \quad (2.17)$$

For the regular truss in Fig. 2.7(a) with $\Delta X = 8$ and $\Delta Y = 8$ we compare the Green-Lagrange, rotated engineering, and linear deformation measures from (2.15), (2.16) and (2.17), respectively, in

Fig. 2.8 for a range of values U such that v/L does not exceed 10%. The comparison in Fig. 2.8 leads to the conclusion that there is little difference between linear and nonlinear deformations.

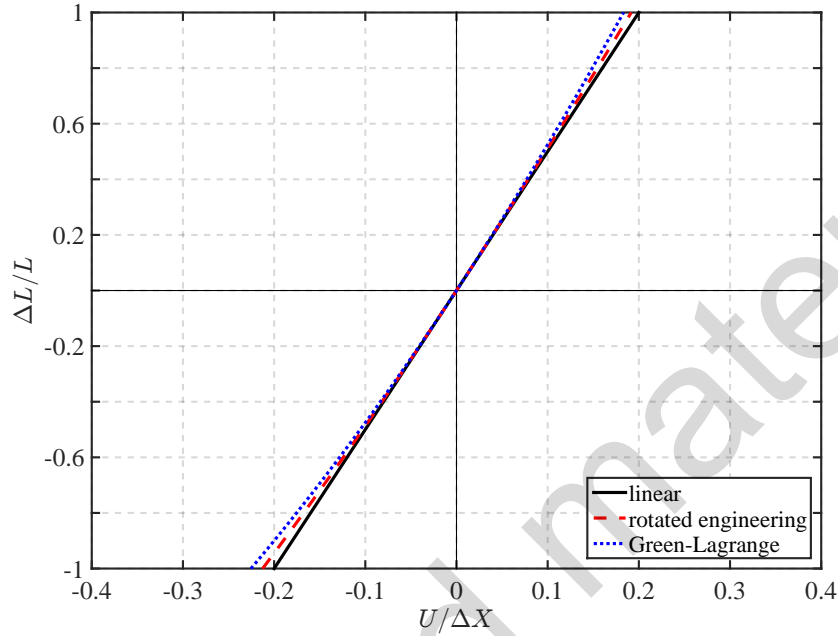


Fig. 2.8: Comparison of deformation measures for regular truss

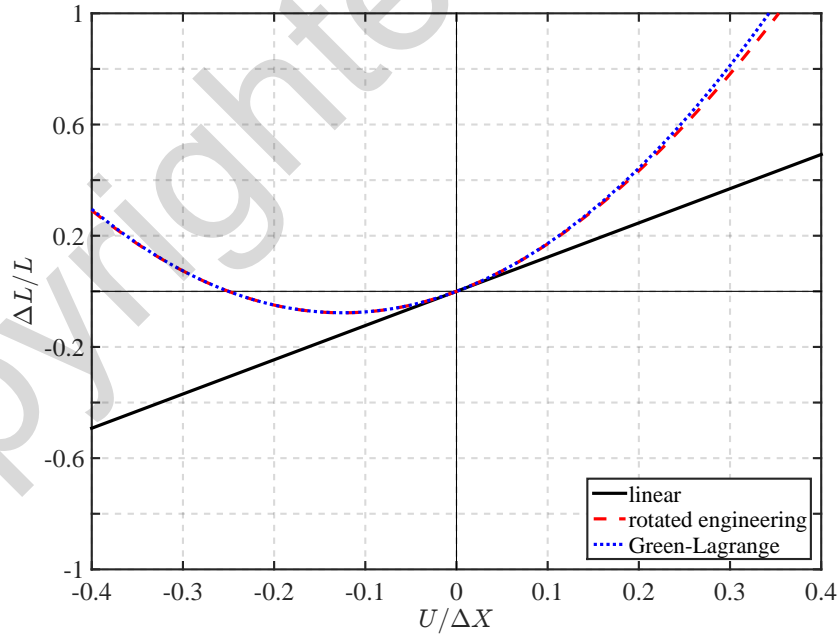


Fig. 2.9: Comparison of deformation measures for shallow truss

For the shallow truss in Fig. 2.7(b) with $\Delta X = 8$ and $\Delta Y = 1$ we compare the Green-Lagrange, rotated engineering, and linear deformation measures from (2.15), (2.16) and (2.17), respectively, in

Fig. 2.9 for a range of values U such that v/L does not exceed 10%. The comparison in Fig. 2.9 leads to the conclusion that there is significant difference between the linear deformation on the one hand and the nonlinear deformations on the other. The nonlinear deformations show very little difference among each other.

2.3.2 Equilibrium Equations

We set up the equilibrium equations of the single dof truss with the principle of virtual work (virtual displacements). *For satisfying the equilibrium equations in the deformed configuration we select a suitable compatible virtual displacement field with a unit value at the dof of interest by taking the variation of the kinematic relation of the problem for the single independent free dof.*

We define first the variation δ of a function $g(x)$ of a scalar variable x with

$$\delta g = \frac{dg}{dx} \delta x \quad (2.18)$$

The Green-Lagrange and rotated engineering deformation of the truss element is a function of the deformed element length, which in turn is a function of the single global dof displacement U for the example at hand. We invoke the chain rule of differentiation and establish first the deformation variation with respect to the deformed element length. We have for the Green-Lagrange deformation

$$\delta v_{GL} = \delta \left(\frac{L_n^2 - L^2}{2L} \right) = \frac{L_n}{L} \delta L_n$$

For the variation of the rotated engineering deformation we have

$$\delta v_{RE} = \delta (L_n - L) = \delta L_n$$

With $L_n = \sqrt{\Delta X^2 + (\Delta Y + U)^2}$ we obtain

$$\delta L_n = \frac{1}{2\sqrt{\dots}} 2(\Delta Y + U) \delta U = \frac{\Delta Y + U}{L_n} \delta U$$

and the variations of Green-Lagrange and rotated engineering deformation become

$$\delta v_{GL} = \frac{L_n}{L} \frac{\Delta Y + U}{L_n} \delta U = \frac{\Delta Y + U}{L} \delta U \quad (2.19)$$

$$\delta v_{RE} = \frac{\Delta Y + U}{L_n} \delta U \quad (2.20)$$

For the single dof truss we write the equilibrium equation at the global dof with the principle of virtual displacements. The external work is

$$\delta \mathcal{W}_e = (\delta U) P$$

The internal work is

$$\delta \mathcal{W}_i = -(\delta v) q$$

Upon substitution of (2.19) and (2.20) into $\delta\mathcal{W} = \delta\mathcal{W}_e + \delta\mathcal{W}_i = 0$ we obtain the equilibrium equation for the two kinematic assumptions. For the Green-Lagrange kinematics we get

$$P - P_r = 0 \rightarrow P - \frac{\Delta Y + U}{L}q = 0 \quad (2.21)$$

and for the rotated engineering kinematics we get

$$P - P_r = 0 \rightarrow P - \frac{\Delta Y + U}{L_n}q = 0 \quad (2.22)$$

Setting $U = 0$ in either one of (2.21) or (2.22) gives the equilibrium equation for the single dof truss under linear statics

$$P - P_r = 0 \rightarrow P - \frac{\Delta Y}{L}q = 0 \quad (2.23)$$

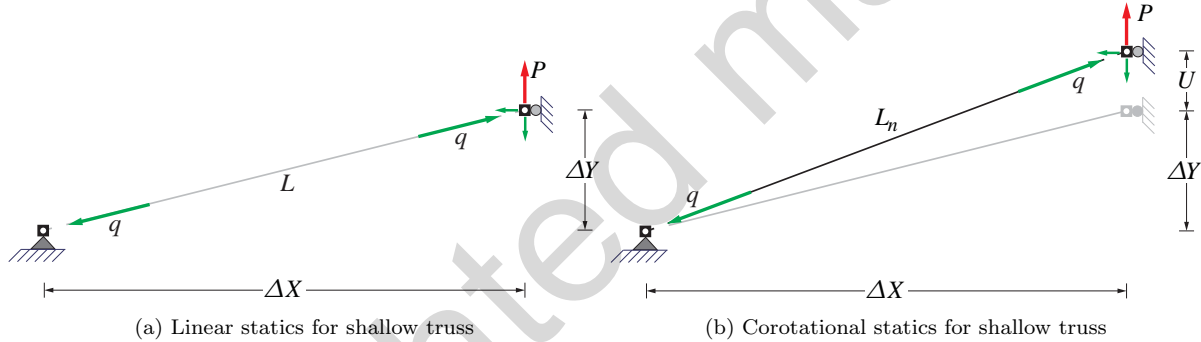


Fig. 2.10: Regular and shallow truss geometry

Fig. 2.10(a) gives the interpretation of the single dof equilibrium equation for the shallow truss under linear statics: the basic force q acts along the undeformed element axis, so that the corresponding end force component in Y involves the direction cosine $\frac{\Delta Y}{L}$ of the undeformed element axis orientation. Fig. 2.10(b) gives the interpretation of the single dof equilibrium equation for the shallow truss under corotational statics, i.e. nonlinear statics that are work consistent with the rotated engineering deformation: the basic force q acts along the deformed element axis, so that the corresponding end force component in Y involves the direction cosine $\frac{\Delta Y+U}{L}$ of the deformed element axis orientation under the free dof displacement U .

2.3.3 Element Force-Deformation Relation

After kinematics and statics we introduce the third pillar of structural analysis, material response, so that we can proceed with the response determination of a structure under nonlinear geometry conditions.

We assume that the material is linear elastic and that the stress is proportional to strain. Since two different strain measures were introduced, two stress measures result: *the engineering stress proportional to the engineering strain*, and the *2nd Piola-Kirchhoff (PK) stress proportional to the Green-Lagrange strain*. For clarity we use the same subscripts, RE and GL, as for the deformations. The basic force of

the truss element for the two cases is

$$q = q_{GL} = (EA)\varepsilon_{GL} = \left(\frac{EA}{L}\right) v_{GL} \quad (2.24)$$

$$q = q_{RE} = (EA)\varepsilon_{RE} = \left(\frac{EA}{L}\right) v_{RE} \quad (2.25)$$

where A is the element area in the undeformed configuration.

2.3.4 Truss Resisting Force P_r

The combination of kinematics, statics, and material response results in the relation between the resisting force P_r and the single dof displacement U .

For Green-Lagrange kinematics we get

$$P_r = \frac{\Delta Y + U}{L} q_{GL} = \frac{\Delta Y + U}{L} \left(\frac{EA}{L}\right) \left(\frac{\Delta Y}{L} U + \frac{U^2}{2L}\right) \quad (2.26)$$

for rotated engineering kinematics we get

$$P_r = \frac{\Delta Y + U}{L_n} q_{RE} = \frac{\Delta Y + U}{L_n} \left(\frac{EA}{L}\right) (L_n - L) \quad (2.27)$$

with $L_n = \sqrt{\Delta X^2 + (\Delta Y + U)^2}$. For linear kinematics, statics, and material response we get

$$P_r = \frac{\Delta Y}{L} q_L = \frac{\Delta Y}{L} \left(\frac{EA}{L}\right) \left(\frac{\Delta Y}{L} U\right) \quad (2.28)$$

We investigate the relation between force and single dof displacement first for the regular truss in Fig. 2.7(a). Noting that $P = P_r$ we depict the relation between the applied force P and the resulting global dof translation U in Fig. 2.11 where the curves for Green-Lagrange, rotated engineering, and linear kinematics correspond to (2.26), (2.27) and (2.28), respectively. We note that appreciable differences arise only for $U/\Delta X$ values greater than 0.1 for which the relative deformations exceed the linear elastic limit of typical structural materials.

Next we investigate the relation between force and single dof displacement for the shallow truss in Fig. 2.7(b). The relation is depicted in Fig. 2.12 for Green-Lagrange, rotated engineering, and linear kinematics according to (2.26), (2.27) and (2.28), respectively. We note that appreciable differences between linear and nonlinear geometry arise very early in the response, both, under positive U and under negative U . We also note the significant difference of the response for an upward translation (positive value) from the response under a downward translation (negative value). In the former case the resisting force is monotonically increasing, whereas in the latter case the force at first increases in absolute value, but then reaches a limit value and starts decreasing. In order to be able to study in more detail this interesting phenomenon we derive the tangent stiffness matrix of the single dof truss in the following section.

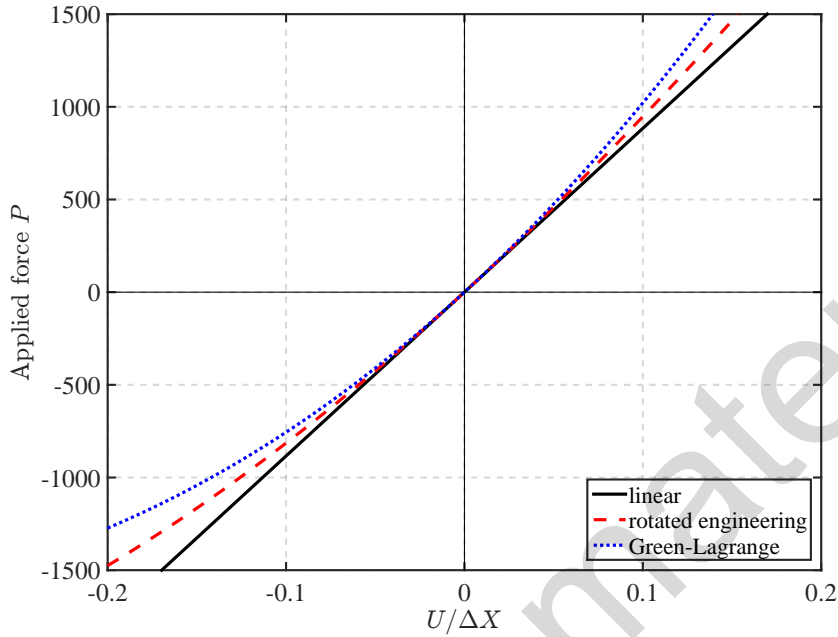


Fig. 2.11: Applied force-vertical translation relation of regular truss for different deformation measures

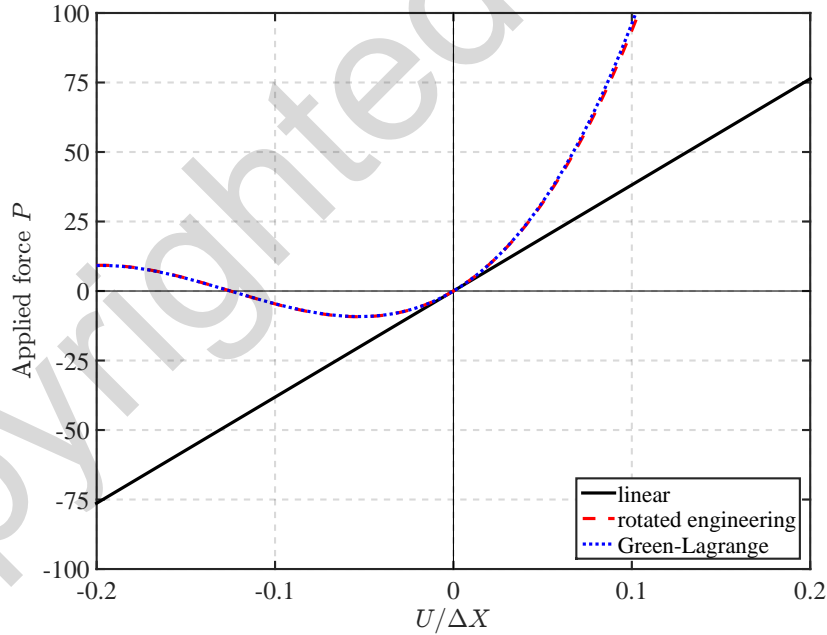


Fig. 2.12: Applied force-vertical translation relation of shallow truss for different deformation measures

2.3.5 Static and Kinematic Summary

The different deformation measures with the corresponding static relations according to the principle of virtual work are summarized in Table 2.2. The basic force-deformation relation includes the effect of an initial prestressing force q_0 .

Kinematics	Variation	Statics	Basic force q
$v_L = \frac{\Delta Y}{L} U$	$\delta v_L = \frac{\Delta Y}{L} \delta U$	$P_r = \frac{\Delta Y}{L} q_L$	$q_L = \frac{EA}{L} \left(\frac{\Delta Y}{L} U \right) + q_0$
$v_{GL} = \frac{\Delta Y}{L} U + \frac{U^2}{2L}$	$\delta v_{GL} = \frac{\Delta Y + U}{L} \delta U$	$P_r = \frac{\Delta Y + U}{L} q_{GL}$	$q_{GL} = \frac{EA}{L} \left(\frac{\Delta Y}{L} U + \frac{U^2}{2L} \right) + q_0$
$v_{RE} = L_n - L$	$\delta v_{RE} = \frac{\Delta Y + U}{L_n} \delta U$	$P_r = \frac{\Delta Y + U}{L_n} q_{RE}$	$q_{RE} = \frac{EA}{L} (L_n - L) + q_0$

Table 2.2: Kinematic and static relations for single dof truss

- 1) In structural mechanics different strain measures can be defined depending on strain magnitude and other considerations. In this course we restrict ourselves to small strains under *moderate and large displacements*. For this kind of problem the Green-Lagrange deformation (strain) and (rotated) engineering deformation (strain) are most commonly used.
- 2) The consistent derivation of work-equivalent stress measures and basic forces is based on the principle of virtual displacements. *Nonlinear equilibrium equations should be set up accordingly*.
- 3) Nonlinear kinematics and statics, that is nonlinear geometry, are very important for the study of shallow structures (reticulated roofs, shells and domes and prestressed cables and membranes).

2.4 Structure Stiffness Matrix

For the detailed study of the structural response of the single dof truss we derive the tangent stiffness K_t at the single independent free dof.

The typical coefficient \mathbf{K}_{ij} of the structural stiffness matrix in linear structural analysis represents the resisting force at global dof i due to a unit displacement at dof j . Such interpretation is possible because the stiffness matrix is constant and, thus, independent of the global dof displacements.

In the general case that the stiffness matrix \mathbf{K} depends on the global dof displacements \mathbf{U} a typical stiffness coefficient \mathbf{K}_{ij} represents *the change of the resisting force* at global dof i due to *a change in the displacement* at dof j . If the displacement change is finite, the resulting stiffness coefficient belongs to the *secant stiffness matrix* of the structural model. If it is possible to take the displacement change to the limit of a differential change, the resulting stiffness coefficient belongs to the *tangent stiffness matrix* of the structural model. The tangent stiffness matrix \mathbf{K}_t , therefore, is

$$\mathbf{K}_t = \frac{\partial \mathbf{P}_r}{\partial \mathbf{U}} \quad (2.29)$$

We define the partial derivative of the resisting force vector \mathbf{P}_r in terms of the displacement vector \mathbf{U} in the following chapter and plan to use it subsequently. For now we limit ourselves to the derivative of the scalar resisting force P_r with respect to the single displacement U to get the scalar stiffness K_t as

$$K_t = \frac{dP_r}{dU}$$

In the derivation of the tangent stiffness for the single dof truss we limit ourselves to Green-Lagrange nonlinear kinematics because of the simpler form of the resulting expressions. The rotated engineering deformation gives similar results, as will be discussed in the chapter on nonlinear geometry of frames.

The derivative of the resisting force P_r in (2.26) with respect to U after accounting for the fact that q is a function of U gives

$$K_t = \frac{dP_r}{dU} = \frac{\Delta Y + U}{L} \frac{dq}{dU} + \frac{1}{L} q = K_m + K_g \quad (2.30)$$

The first term on the right hand side of (2.30) represents the material stiffness K_m which arises from the differentiation of the basic force q with respect to U , while the truss element orientation is kept constant at the current position. The second term represents the geometric stiffness K_g , which arises from the differentiation of the orientation of the basic force q , while the value of it is kept constant. The geometric stiffness, therefore, arises from *the change in the direction of the line of application of the basic force q* .

2.4.1 Material Stiffness of Single Dof Truss

The basic force q depends on the deformation v through the material constitutive relation. v , in turn, depends on the displacement U by kinematics. With the chain rule of differentiation we get

$$K_m = \frac{\Delta Y + U}{L} \left(\frac{dq}{dv} \right) \left(\frac{dv}{dU} \right)$$

and with the relation between deformation v and global dof displacement U for the Green-Lagrange deformation we get

$$K_m = \left(\frac{\Delta Y + U}{L} \right) \left(\frac{dq}{dv} \right) \left(\frac{\Delta Y + U}{L} \right)$$

For linear elastic material response we have that $\frac{dq}{dv} = \frac{EA}{L}$ so that the material stiffness finally becomes

$$K_m = \left(\frac{\Delta Y + U}{L} \right) \left(\frac{EA}{L} \right) \left(\frac{\Delta Y + U}{L} \right) \quad (2.31)$$

It is worth noting that the tangent stiffness of the single dof truss under linear kinematics results from (2.31) by setting $U = 0$.

2.4.2 Geometric Stiffness Of Single Dof Truss

The geometric stiffness contribution to the tangent stiffness of the single dof truss in (2.30) is directly proportional to the value of the axial basic force q . We generalize the relation between the axial basic

force q and the corresponding axial deformation v with the inclusion of an initial prestressing force q_0 . Upon substitution of the relation between the deformation v and the single dof displacement U of the truss model from (2.15) we have

$$q = \frac{EA}{L}v_{GL} + q_0 = \frac{EA}{L} \left(\frac{\Delta Y}{L}U + \frac{U^2}{2L} \right) + q_0$$

The geometric stiffness of the single dof truss in (2.30) thus becomes

$$K_g = \frac{1}{L}q = \frac{1}{L} \left[\frac{EA}{L} \left(\frac{\Delta Y}{L}U + \frac{U^2}{2L} \right) + q_0 \right] \quad (2.32)$$

2.4.3 Summary and Observations about Tangent Stiffness

The tangent stiffness K_t of the single dof truss is made up of two contributions, the material stiffness K_m from (2.31) and the geometric stiffness K_g from (2.32)

$$K_t = K_m + K_g = \left(\frac{\Delta Y + U}{L} \right) \left(\frac{EA}{L} \right) \left(\frac{\Delta Y + U}{L} \right) + \frac{1}{L} \left[\frac{EA}{L} \left(\frac{\Delta Y}{L}U + \frac{U^2}{2L} \right) \right] \quad (2.33)$$

The study of the expressions for K_m in (2.31) and K_g in (2.32) leads to the following conclusions:

- 1) The material stiffness is *non-negative*.
- 2) The geometric stiffness is *positive* for a tensile force q , and *negative* for a compressive force q .
- 3) A geometric stiffness is present even under zero displacement, as long as the truss element is prestressed with an initial force q_0 .
- 4) The material stiffness is equal to the stiffness of the simple truss under linear kinematics and statics for $U = 0$.
- 5) The geometric and the material stiffness have a "symmetric" form, a fact to be confirmed with a multi-dof example in a subsequent chapter.

In the following we specialize the results of this example to three special cases: first, we study in more detail the response of the shallow truss under a *downward force*. Then, we study the response of a horizontal truss under a tensile prestressing force (prestressed cable). Finally, we study the response of a horizontal truss with an additional spring in the middle under a compressive force (linear buckling).

Example 2.1 Instability of Shallow Truss

We study the shallow truss in Fig. 2.13(a) under a *downward force* and focus on the relation between the single dof displacement U and the resisting force P_r (or the applied force P) as well as the relation between U and the tangent stiffness K_t with its contributions K_m and K_g . Because of the symmetric characteristics of the structural model in Fig. 2.13(a), we use only half the model for the study under a downward force P , as shown in Fig. 2.13(b). For the following discussion and results we consider the downward force P and the corresponding down translation U as *positive*.

Fig. 2.14 shows the relation between the relative downward translation U/L and the relative change of length or distance $\Delta L/L = v$ for the Green-Lagrange, rotated engineering, and linear deformation

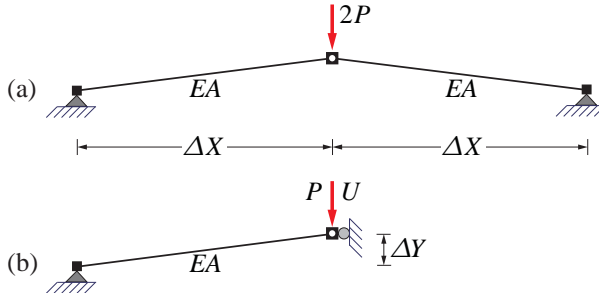
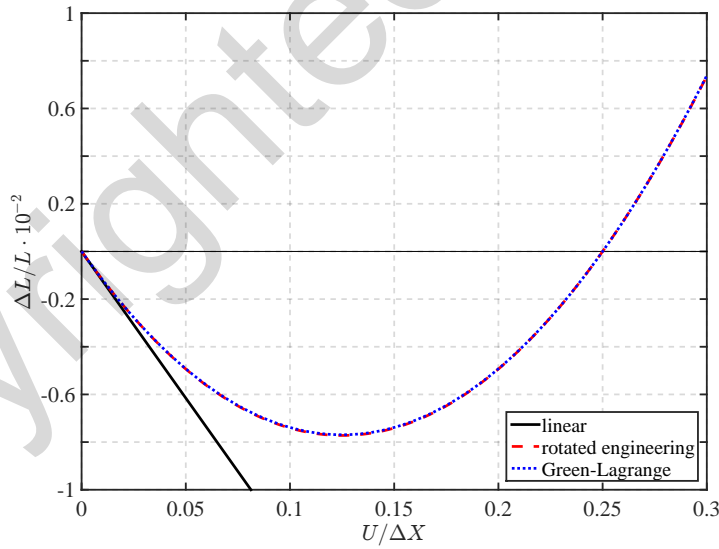


Fig. 2.13: Shallow truss under nodal force at midspan

v from (2.15), (2.16) and (2.17), respectively. L is the undeformed length of the truss element. The following figures assume $\Delta X = 8$ and $\Delta Y = 1$ in agreement with the geometry of the shallow truss in Fig. 2.7. It is clear from Fig. 2.14 that nonlinear kinematics plays a very important role for a downward midspan translation of the shallow truss in Fig. 2.13(a). The same is true for other shallow structures like arches and domes. As the point of load application translates downward the truss shortens up to a maximum value, which is attained when the truss element becomes horizontal. As the apex of the shallow truss translates further downward the truss shortening reduces and recovers its original length when the downward translation becomes equal to $U = 0.25L = 2$, which corresponds to the symmetric position of the apex relative to the horizontal. For a downward translation beyond this point the truss elongates.

Fig. 2.14: Relation between relative deformation and relative displacement $U/\Delta X$ for shallow truss

The governing equations for the resisting force P_r and the tangent stiffness K_t from (2.26) and (2.33), respectively, are

$$\begin{aligned} P_r &= \frac{\Delta Y + U}{L} q = \frac{\Delta Y + U}{L} \left[\frac{EA}{L} \left(\frac{\Delta Y}{L} U + \frac{U^2}{2L} \right) \right] \\ K_t &= K_m + K_g = \left(\frac{\Delta Y + U}{L} \right) \left(\frac{EA}{L} \right) \left(\frac{\Delta Y + U}{L} \right) + \frac{1}{L} \left[\frac{EA}{L} \left(\frac{\Delta Y}{L} U + \frac{U^2}{2L} \right) \right] \end{aligned} \quad (2.34)$$

under the assumption that the initial prestressing force q_0 is zero. For the shallow truss we have that $\Delta X = 8$ and $\Delta Y = 1$. These relations were already studied for an upward and a downward force. Here we limit ourselves to the latter case.

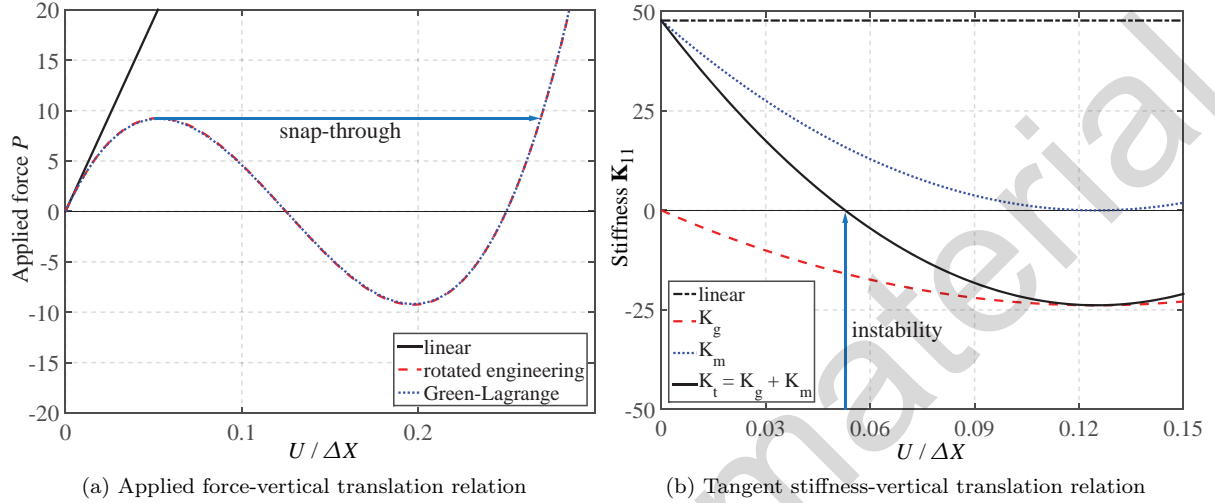


Fig. 2.15: Applied force and tangent stiffness dependence of shallow truss on downward translation

Fig. 2.15(a) shows the relation between the downward applied force P and the corresponding single dof translation U for Green-Lagrange, rotated engineering, and linear kinematics according to (2.26), (2.27) and (2.28), respectively, noting that $P = P_r$. The applied force reaches a maximum value (limit value) at a specific downward translation U , at which point the force-displacement relation has a horizontal tangent reflecting the fact that the tangent stiffness is zero at this point and the structure becomes unstable. This applied force value is known as nonlinear stability limit and the instability phenomenon experienced by the shallow truss is known as *snap-through*. This name derives from the fact that the truss snaps-through the horizontal position to a new equilibrium position under constant force, as shown by the arrow in the figure. Clearly, this process is dynamic in nature, because snap-through occurs very quickly. Moreover, it is unlikely that an actual structure can survive this process intact, so that the response past the snap-through instability limit is of only theoretical interest. What is important from a practical standpoint is the determination of the nonlinear stability limit or snap-through force value.

Fig. 2.15(b) shows the dependence of the material and geometric stiffness of the shallow truss on the vertical translation U according to (2.34). The linear stiffness is constant. The material stiffness is equal to the linear stiffness at $U = 0$ and then decreases quadratically to zero for $U = -\Delta Y$ (horizontal position). Beyond this point it increases again quadratically. The geometric stiffness is equal to zero at $U = 0$ because $q = 0$. With increasing downward translation q is increasing in compression and the geometric stiffness is negative, until its minimum value at $U = -\Delta Y$ (horizontal position). Snap-through instability sets in when the total stiffness $K_m + K_g$ becomes zero at $U = 0.05\Delta X$ approximately.

Example 2.2 Prestressed Horizontal Cable

This example concerns the response of a prestressed horizontal cable with a span of $2L = 400$ units in Fig. 2.16(a). The truss is prestressed with an initial tensile force $q_0 = \sigma_0 A$, which is kept constant,

while the cable is subjected to an increasing transverse nodal force of $2P$ at midspan. σ_0 is the initial prestress and A is the cable area.

The model has a single independent vertical translation dof at midspan on account of symmetry. While it may appear that the cable is unstable in the horizontal translation when resting on a roller at both ends, the symmetric horizontal deformation mode ensures a zero translation at midspan, so that the model of half the cable in Fig. 2.16(b) is clearly stable.

We focus again on the relation between the single dof of translation U and the resisting force P_r (or applied force P) as well as the relation between U and the tangent stiffness K_t and its contributions K_m and K_g . Because of symmetry, we analyze again only half of the structure, as shown in Fig. 2.16(b). Consequently, the resulting values for the applied force P and the tangent stiffness K_t should be doubled to $2P$ and $2K_t$ for the structure in Fig. 2.16(a). The downward applied force and the downward midspan translation *are assumed positive* for the following results and figures.

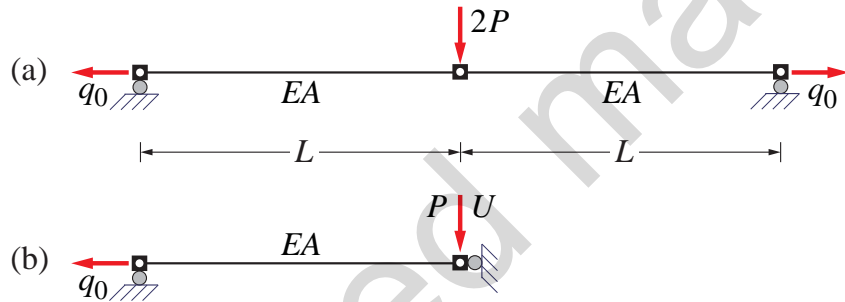


Fig. 2.16: Prestressed horizontal cable under transverse load

With $\Delta Y = 0$ in (2.15) we have that the Green-Lagrange deformation is

$$v_{GL} = \frac{U^2}{2L}$$

The governing equations from Table 2.2 and (2.33) simplify to

$$P_r = \frac{U}{L}q = \frac{U}{L} \left[\frac{EA}{L} \left(\frac{U^2}{2L} \right) + q_0 \right] \quad (2.35)$$

and

$$K_t = K_m + K_g = \left(\frac{U}{L} \right) \left(\frac{EA}{L} \right) \left(\frac{U}{L} \right) + \frac{1}{L} \left[\frac{EA}{L} \left(\frac{U^2}{2L} \right) + q_0 \right] \quad (2.36)$$

We observe first that the Green-Lagrange deformation v_{GL} of the cable contains only a quadratic term. This means that the linear deformation is zero and that the structure is *unstable* in the horizontal, undeformed position under the assumption of linear geometry. Under the assumption of nonlinear geometry the stiffness matrix of the structure is zero at the undeformed position, *unless the geometric stiffness effect of an initial prestressing force is accounted for*. In such case, the structure is *stable* in the undeformed position. We conclude that the rank of the kinematic matrix \mathbf{A}_f does not suffice to judge the stability of a structure, as was assumed in linear structural analysis. Instead, the smallest eigenvalue of

the stiffness matrix needs to be greater than zero, a fact that will be used in later chapters to establish the stability limit of structures.

(a) Effect of Initial Prestressing Force

We rewrite the resisting force and the tangent stiffness of the prestressed horizontal cable by separating the effect of the cable stiffness EA from that of the initial prestressing force q_0 . We obtain from (2.35)

$$P_r = EA \frac{1}{2} \left(\frac{U}{L} \right)^3 + q_0 \frac{U}{L}$$

We factor out the influence of the cable area A by replacing q_0 with $\sigma_0 A$ to get

$$P_r = A \left[E \frac{1}{2} \left(\frac{U}{L} \right)^3 + \sigma_0 \frac{U}{L} \right] \quad (2.37)$$

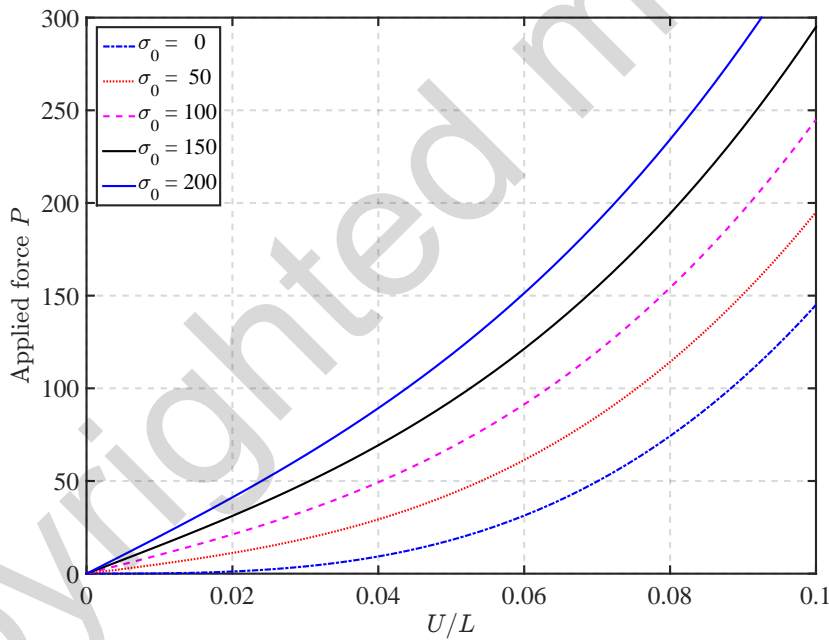


Fig. 2.17: Effect of initial prestress on force-translation relation of prestressed horizontal cable

Fig. 2.17 plots the relation between the applied force $P = P_r$ and the midspan translation U according to (2.37) for different initial prestress values. The cable has an elastic modulus E of 29,000 units, and an area A of 10 units. We conclude that for typical structural deflections in service (U/L around 1/400) the linear term due to prestressing provides the dominant contribution to the resisting force for typical metallic materials, e.g. steel with $E = 29,000$ ksi and initial prestress σ_0 of about 145 ksi for 250K strands, i.e. 60% of the ultimate strength. For higher prestress values the resisting force is practically linear even up to rather large deflections of $U/L = 0.04$.

Separating the effect of the cable stiffness EA from that of the initial prestressing force q_0 in the tangent stiffness expression in (2.36) or, alternatively, taking the derivative of the resisting force in (2.37)

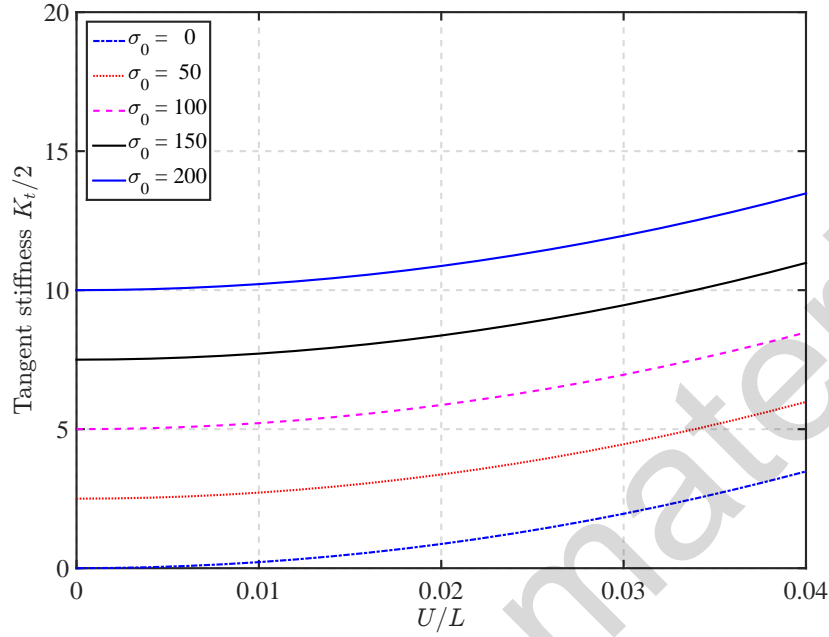


Fig. 2.18: Effect of initial prestress on transverse stiffness of prestressed horizontal cable

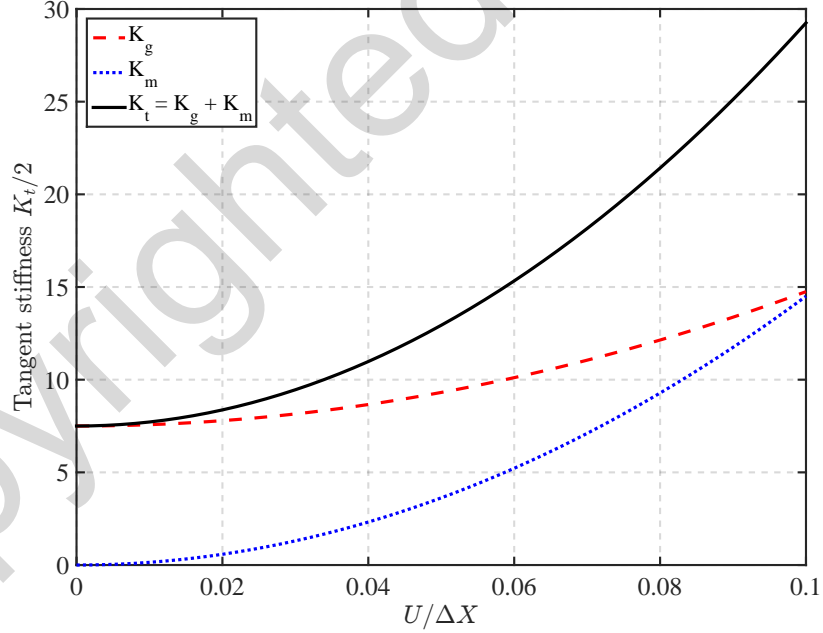


Fig. 2.19: Material and geometric stiffness contributions for prestressed horizontal cable

with respect to U gives

$$K_t = \frac{A}{L} \left[E \frac{3}{2} \left(\frac{U}{L} \right)^2 + \sigma_0 \right] \quad (2.38)$$

which confirms the earlier conclusion about the effect of the prestressing force: for small to moderate deflections the tangent stiffness is dominated by the presence of the prestress σ_0 . We confirm this fact with a plot of the transverse tangent stiffness value at cable midspan for the range of U/L from 0 to 0.04 in Fig. 2.18.

Fig. 2.19 plots the stiffness contributions K_m and K_g of the prestressed horizontal cable according to (2.36) for $E = 29,000$, $A = 10$, and $\sigma_0 = 150$ units.

(b) Effect of Cable Area A

Without initial prestress the cable force-displacement response is highly nonlinear, as shown in Fig. 2.20. Significant resistance can be developed by cables of large diameter, as long as large displacements can be tolerated. Note the zero tangent stiffness of the horizontal cable with $U = 0$.

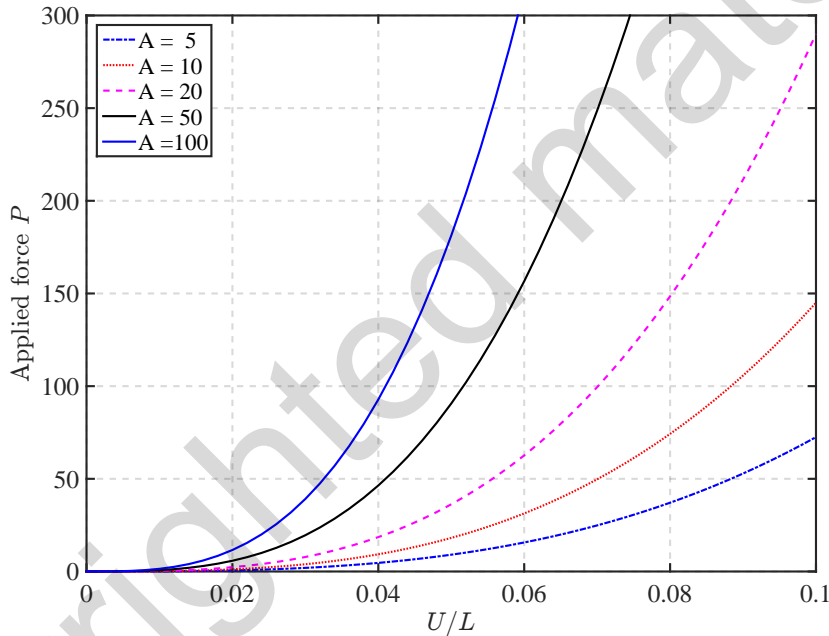


Fig. 2.20: Effect of cable area A on vertical force-translation relation of prestressed horizontal cable

(c) A Note on Prestressing - Pretensioning vs. Post-Tensioning

Fig. 2.21 illustrates the structural models corresponding to the pretensioning of a high-strength cable to clarify the prestressed cable model of Fig. 2.16.

The model in Fig. 2.21(b) represents the cable during the stressing operation. The cable is supported on a roller at one end to allow its free elongation during stressing to an initial force q_0 . For retaining the symmetry of the model we assume the configuration in Fig. 2.21 with the zero horizontal translation at midspan instead of one support. In Fig. 2.21(c) the cable is *released* from the stressing jacks after inserting a spring k_s that represents the elastic stiffness of the medium surrounding the cable. This medium is typically a concrete member and the force transfer between cable and concrete is provided either by an anchorage device or by the bond of the grout in the cable duct. Because of the horizontal force equilibrium at the free dof with the spring, the cable force drops to the value q_r , the prestressing force *after release* which is equal to

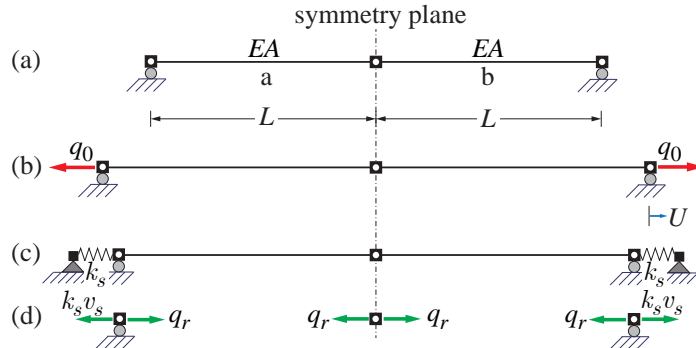


Fig. 2.21: Pre-tensioning of high strength cable

$$q_r = q_0 \left(\frac{k_s}{k_s + \frac{EA}{L}} \right)$$

The preceding sequence of events describes the process of cable pretensioning, which takes place in precast plants. In this case the prestressing jack applying the initial force q_0 in Fig. 2.21(b) holds the cable against a fixed support until the concrete cast around the stressed cable hardens for the cable to be released. In post-tensioning the cable is prestressing jack acts against the member to be prestressed, so that the cable force is gradually increased to the value q_r in the model of Fig. 2.21(c). In this case the cable never experiences the force q_0 . Nonetheless, the separate models for stressing and release in Fig. 2.21 help clarify even the post-tensioning operation. The initial prestressing force q_0 is used for all subsequent loading, if the displacements are measured relative to the state in Fig. 2.21(b). The slight discrepancy in the cable length in Fig. 2.21(b) relative to the undeformed length L in Fig. 2.21(a) is neglected in the calculations.

Example 2.3 Linear Buckling Load of Truss/Beam

The final example of this introduction into phenomena caused by the nonlinear geometry of structures involves the horizontal truss of the preceding example with the addition of a spring with axial stiffness k_s at midspan in Fig. 2.22(a). We use the same considerations as for the preceding example regarding the horizontal stability of the structural model in the horizontal direction, which is ensured in the model of half the structure in Fig. 2.22(b).

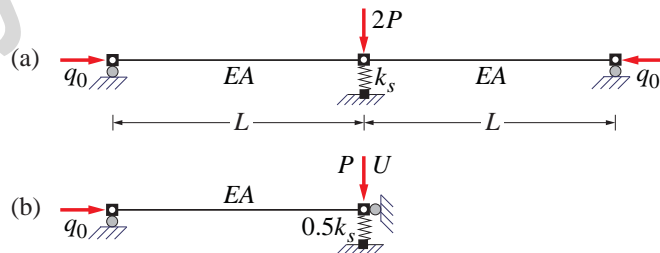


Fig. 2.22: Horizontal truss with transverse spring under compression force

In contrast to the preceding example, the structural model of the truss element under initial compression q_0 in Fig. 2.22(b) is stable on account of the lateral spring with stiffness $0.5k_s$. Interestingly, it turns out that under consideration of the geometric stiffness of the truss element we can show that it becomes unstable in the undeformed configuration, i.e. at $U = 0$ under a certain value of the initial compressive force q_0 .

To study this problem we set up first the tangent stiffness K_t at the independent translation dof U in Fig. 2.22(b). To this end we combine the terms involving the axial stiffness EA in the tangent stiffness expression of the horizontal truss element in (2.34) and add the axial stiffness of the transverse spring in Fig. 2.22(b) to get

$$K_t = \frac{1}{L} \left[EA \frac{3}{2} \left(\frac{U}{L} \right)^2 + q_0 + \frac{k_s L}{2} \right] \quad (2.39)$$

For the stability *in the undeformed configuration* of the truss model with the transverse axial spring in (2.34) we set $U = 0$ in (2.39) to get for the tangent stiffness K_t at the independent translation dof

$$K_t = \frac{1}{L} \left[q_0 + \frac{k_s L}{2} \right]$$

It is immediately clear that K_t is zero for $q_0 = -0.5k_s L$. This value represents the *linear buckling load* of the simple truss with the transverse axial spring in (2.34). The buckling load is called linear because it renders the structure unstable in the undeformed configuration. Nonetheless, it should be clear that the buckling study requires the *inclusion of the geometric stiffness of the elements of the structural model*.

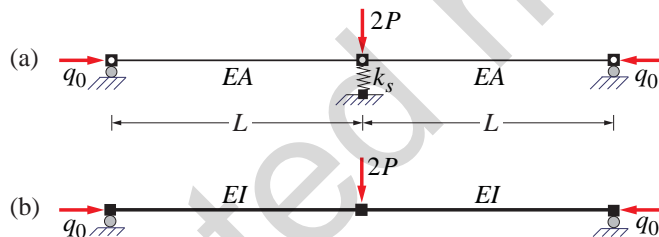


Fig. 2.23: Equivalence of spring with transverse stiffness of beam at midspan

The axial spring at midspan can be thought of as representing the transverse flexural stiffness of a pinned-pinned beam or column, as shown in Fig. 2.23. The linear buckling load we determined is then an approximation of the buckling load of a pinned-pinned column, because the flexural stiffness of the member is "lumped" at the transverse axial spring. We return to this problem when discussing the linear buckling load of structural models in the chapter on nonlinear geometry of frames.

2.5 Conclusions from Single Dof Examples

We encountered three phenomena from the study of structures with nonlinear geometry:

- 1) Shallow trusses, frames and domes are susceptible to a phenomenon of *nonlinear instability* called snap-through instability. *To arrive at the critical load we trace the load-displacement response until the stiffness matrix becomes singular.* We will encounter other types of nonlinear instability later, but the method of determining the critical load remains the same. This family of phenomena is known as *nonlinear buckling* problems.
- 2) Prestressed cables possess positive geometric stiffness under a tensile force that renders *apparently unstable structures* under linear geometry *stable* under inclusion of the geometric stiffness.
- 3) *Apparently stable structures* under linear geometry become unstable under inclusion of the geometric stiffness, if the elements are under compression. Because this phenomenon arises in the undeformed, original configuration of the structure, this instability problem is known as *linear buckling analysis*.

Chapter 3

Nonlinear Solution Methods I

3.1 Introduction

The equilibrium equation for the single dof truss in Section 2.3.2 has the form

$$P - P_r(U) = 0 \quad (3.1)$$

where P denotes the applied force and P_r the resisting force at the single dof. The latter is a component of the basic element force q , which depends on the element deformation v , which, in turn, depends on the free dof displacement U . Under nonlinear kinematics and statics the resisting force P_r is a nonlinear function of the free dof displacement U even for linear elastic material response.

We were able to study the response of the single dof truss for introducing a few nonlinear geometry phenomena in Chapter 2 by supplying a range of displacement values U and determining the corresponding resisting force P_r and tangent stiffness K_t of the single dof truss. For multi-dof structural models this is clearly not possible, because the applied forces are specified and the free dof displacements need to be determined. We are, therefore, faced with solving a system of nonlinear equations for the unknown free dof displacements \mathbf{U}_f . Before studying solution methods for this problem we discuss the simpler version of it with one unknown displacement U in (3.1).

3.2 Solution of One Nonlinear Equation

Because nonlinear equations appear in different contexts in structural analysis and not only for the solution of equilibrium equations we write (3.1) in a general form as

$$g(x) = 0 \quad (3.2)$$

where x is the independent variable and $g(x)$ the nonlinear function of it.

While closed form solutions exist for a few simple nonlinear functions $g(x)$, only numerical solutions are possible for the general case. In seeking such a solution we use a Taylor series expansion of the function $g(x)$ about an arbitrary point x_0 . x_0 is assumed to be sufficiently close to the solution of $g(x) = 0$ so that it can be thought of as an initial estimate for it. The Taylor series expansion about x_0 gives

$$g(x) = g(x_0) + g'(x_0)(x - x_0) + \frac{1}{2!}g''(x_0)(x - x_0)^2 + \text{h.o.t.} \quad (3.3)$$

where g' denotes the function derivative $\frac{dg}{dx}$. Truncating the expansion after the linear term gives a *linear approximation* for it in the form

$$g(x) \approx g(x_0) + g'(x_0)(x - x_0) \quad (3.4)$$

Following Newton/Raphson (NR)(1690) we propose to use the linear approximation of the function $g(x)$ to determine a *better estimate* for the solution of the nonlinear equation $g(x) = 0$, i.e. we use

$$g(x_0) + g'(x_0)(x - x_0) = 0 \quad (3.5)$$

with the result x_1

$$x_1 = x_0 - \frac{g(x_0)}{g'(x_0)} \quad (3.6)$$

to get an improved estimate for the solution of $g(x) = 0$.

With the new solution estimate x_1 we check the error of the nonlinear equation $g(x_1)$. If the error is larger than desired, we repeat the following process

$$x_{i+1} = x_i - \frac{g(x_i)}{g'(x_i)} \quad (3.7)$$

for $i = 1 \dots n$ until the error is smaller than a specified tolerance. This iterative process converges to the solution with any desired level of accuracy, *as long as the function $g(x)$ is smooth in the vicinity of the solution and the initial estimate x_0 is not too far from the final answer.*

3.2.1 Newton-Raphson Algorithm for One Nonlinear Equation

The algorithmic form of the iterative process for the solution of the nonlinear equation $g(x) = 0$ is

- 1) Given the nonlinear equation $g(x) = 0$ with an initial guess x_0 for the solution.
- 2) For $i = 0 \dots n$ determine the function value $g(x_i)$ and the derivative $g'(x_i)$ at x_i
- 3) Determine a correction to the previous solution estimate $\Delta x_i = -\frac{g(x_i)}{g'(x_i)}$
- 4) Update the solution estimate $x_{i+1} = x_i + \Delta x_i$
- 5) Return to step 2 until the error is smaller than a specified tolerance $|g(x_{i+1})| \leq \text{tol}$.

The NR algorithm converges to the solution *quadratically* if the function $g(x) = 0$ is smooth near the solution and the initial estimate x_0 is not too far from it. Quadratic convergence means that $|g(x_{i+1})| \leq \mu |g(x_i)|^2$, or, alternatively, $|x^* - x_{i+1}| \leq \mu^* |x^* - x_i|^2$ where x^* denotes the solution. μ and μ^* are constants whose value need not concern us.

3.2.2 Newton-Raphson Solution for Structural Problem

We apply the NR algorithm to the equilibrium equation of the single dof truss in (3.1). Calling the difference between the applied force P and the resisting force P_r the force unbalance P_u at the free dof we write the nonlinear equilibrium equation for the single dof truss in the form

$$P_u(U) = \lambda P_{ref} - P_r(U) = 0 \quad (3.8)$$

after replacing the applied force P by the product of the load factor λ with the reference force value P_{ref} .

Before stating the algorithm for the solution of (3.8) we set up the derivative for the function $P_u(U)$. It is

$$\frac{dP_u}{dU} = -\frac{dP_r}{dU} = -K_t$$

under the assumption that the reference load does not depend on the displacement U . This is true for *conservative loading* that maintains its direction while the structure deforms, with an additional term arising for the derivative for *non-conservative loading*.

The NR solution algorithm for the solution of (3.8) takes the following form:

- 1) Given the nonlinear equation $P_u(U) = 0$ with an initial guess for the solution U_0 .
- 2) For $i = 0 \dots m$ determine the function value $P_u(U_i)$ and its derivative $-K_t(U_i)$.
- 3) Determine the correction to the previous solution estimate $\Delta U_i = K_t(U_i) \setminus P_u(U_i)$.
- 4) Update the solution estimate $U_{i+1} = U_i + \Delta U_i$.
- 5) Return to step 2 until the equilibrium error (force unbalance at free dof) is smaller than a specified tolerance, i.e. $|P_u(U_{i+1})| \leq \text{tol}$.

In the determination of the correction in step (3) of the algorithm we made use of Matlab's \ operator to express the solution of a system of linear equations by Gauss elimination. This is, however, not necessary here, because we are dealing with a scalar equation.

For the structural problem a suitable initial guess for the solution is $U_0 = 0$, the unstressed state of the structure, as long as the load factor λ is not too large. We plan to address this issue in more detail later in the chapter.

Example 3.1 Nonlinear Solution for Single dof Truss under Given Load

We demonstrate the nonlinear solution algorithm for the single dof shallow truss of Fig. 2.13 under a downward vertical force $P_f = \lambda P_{ref}$ of 8 units, as shown in Fig. 3.1. The axial stiffness EA of the truss element is 25,000. The equation to be solved is

$$P_u(U) = (-8) - P_r(U) = 0 \quad (3.9)$$

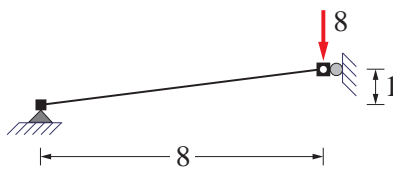


Fig. 3.1: Shallow single dof truss under given vertical force $P_f = \lambda P_{ref}$

with the following expressions for the resisting force P_r from (2.26) and for the tangent stiffness K_t from (2.33)

$$P_r = \frac{\Delta Y + U}{L} \left(\frac{EA}{L} \right) \left(\frac{\Delta Y}{L} U + \frac{U^2}{2L} \right)$$

$$K_t = \left(\frac{\Delta Y + U}{L} \right) \left(\frac{EA}{L} \right) \left(\frac{\Delta Y + U}{L} \right) + \frac{1}{L} \left[\frac{EA}{L} \left(\frac{\Delta Y}{L} U + \frac{U^2}{2L} \right) \right]$$

With the initial guess $U_0 = 0$ and the relations

$$\begin{aligned} P_u(U_i) &= (-8) - P_r(U_i) \\ \Delta U_i &= \frac{P_u(U_i)}{K_t(U_i)} \\ U_{i+1} &= U_i + \Delta U_i \end{aligned}$$

the results of the NR iteration algorithm are summarized in Table 3.1.

Iteration i	U_i	$P_u(U_i)$	$K_t(U_i)$	ΔU_i	U_{i+1}
0	0	-8	47.706	-0.168	-0.168
1	-0.168	-1.9	25.718	-0.074	-0.242
2	-0.242	-0.315	17.309	-0.018	-0.260

Table 3.1: Iteration results for equilibrium solution of single dof truss

The final solution estimate after 3 iteration steps is $U_3 = -0.260$ and the corresponding error of the equilibrium equation is $P_u(U_3) = -0.018$. The process is depicted in Fig. 3.2 with the downward applied force and vertical translation plotted shown positive.

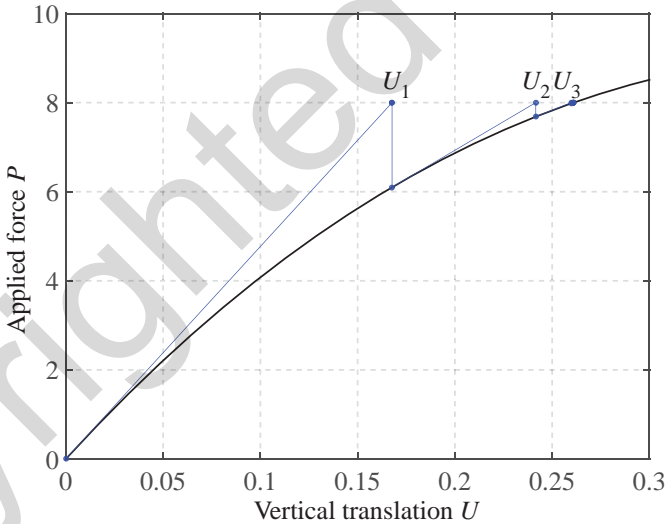


Fig. 3.2: Steps of Newton-Raphson iteration algorithm for single dof truss

3.3 Mathematical Preliminaries

We define the *gradient* ∇g of a scalar function $g(\mathbf{x})$ of n variables $\mathbf{x}_1, \mathbf{x}_2, \dots, \mathbf{x}_n$

$$\nabla g = \begin{pmatrix} \frac{\partial g}{\partial \mathbf{x}_1} \\ \frac{\partial g}{\partial \mathbf{x}_2} \\ \vdots \\ \frac{\partial g}{\partial \mathbf{x}_n} \end{pmatrix} \quad \text{or} \quad \nabla g_i = \frac{\partial g}{\partial \mathbf{x}_i} \quad (3.10)$$

We define the *Jacobian* \mathbf{J} of a vector-valued function $\mathbf{g}(\mathbf{x})$ with components $\mathbf{g}_1, \mathbf{g}_2, \dots, \mathbf{g}_m$ of n variables $\mathbf{x}_1, \mathbf{x}_2, \dots, \mathbf{x}_n$

$$\mathbf{J} = \begin{bmatrix} \frac{\partial \mathbf{g}_1}{\partial \mathbf{x}_1} & \frac{\partial \mathbf{g}_1}{\partial \mathbf{x}_2} & \cdots & \frac{\partial \mathbf{g}_1}{\partial \mathbf{x}_n} \\ \frac{\partial \mathbf{g}_2}{\partial \mathbf{x}_1} & \frac{\partial \mathbf{g}_2}{\partial \mathbf{x}_2} & \cdots & \frac{\partial \mathbf{g}_2}{\partial \mathbf{x}_n} \\ \vdots & \vdots & \ddots & \vdots \\ \frac{\partial \mathbf{g}_m}{\partial \mathbf{x}_1} & \frac{\partial \mathbf{g}_m}{\partial \mathbf{x}_2} & \cdots & \frac{\partial \mathbf{g}_m}{\partial \mathbf{x}_n} \end{bmatrix} \quad \text{or} \quad \mathbf{J}_{ij} = \frac{\partial \mathbf{g}_i}{\partial \mathbf{x}_j} \quad (3.11)$$

The gradient is a vector of n components and the Jacobian is an $m \times n$ matrix.

Note that to be consistent with the definition of the gradient of a scalar function as a vector, the Jacobian consists of the stacking of the transpose of the gradient of each function component, i.e.

$$\mathbf{J} = \begin{bmatrix} (\nabla \mathbf{g}_1)^T \\ \vdots \\ (\nabla \mathbf{g}_m)^T \end{bmatrix} \quad (3.12)$$

The variation of a vector-valued function $\mathbf{g}(\mathbf{x})$ with components $\mathbf{g}_1, \dots, \mathbf{g}_m$ of n variables $\mathbf{x}_1, \dots, \mathbf{x}_n$ is

$$\delta \mathbf{g} = \frac{\partial \mathbf{g}_i}{\partial \mathbf{x}_j} \delta \mathbf{x} = \mathbf{J} \delta \mathbf{x} \quad (3.13)$$

where \mathbf{J} is the Jacobian of the function.

3.4 Solution of a System of Nonlinear Equations

For the solution of equilibrium equations of multi-degree-of-freedom (mdof) structural models we consider the extension of the NR iterative solution strategy to a system of n nonlinear equations in n unknowns. Mathematically, we express the system of nonlinear equations as a vector \mathbf{g} of nonlinear functions $\mathbf{g}_1, \mathbf{g}_2 \dots \mathbf{g}_n$ of the vector \mathbf{x} with unknown components $x_1, x_2, \dots x_n$. With this notation we seek the solution of the system of nonlinear equations

$$\mathbf{g}(\mathbf{x}) = \mathbf{0}$$

We use the Taylor series expansion of the vector valued function \mathbf{g} about an arbitrary point x_0 . x_0 is assumed to be sufficiently close to the solution of $\mathbf{g}(\mathbf{x}) = \mathbf{0}$ so that it can be thought of as an initial estimate for it. The Taylor series expansion about x_0 gives

$$\mathbf{g}(\mathbf{x}) = \mathbf{g}(x_0) + \mathbf{g}'(x_0)(\mathbf{x} - \mathbf{x}_0) + \frac{1}{2!}\mathbf{g}''(x_0)(\mathbf{x} - \mathbf{x}_0)^2 + \text{h.o.t.} \quad (3.14)$$

where $\mathbf{g}' = \frac{\partial \mathbf{g}}{\partial \mathbf{x}}$ is the Jacobian of the vector valued function $\mathbf{g}(\mathbf{x})$. Truncating the Taylor series expansion of the function after the linear term gives a *linear approximation* for the function value $\mathbf{g}(\mathbf{x})$ at \mathbf{x} in the form

$$\mathbf{g}(\mathbf{x}) \approx \mathbf{g}(x_0) + \mathbf{J}_0(\mathbf{x} - \mathbf{x}_0) \quad (3.15)$$

where \mathbf{J}_0 is shorthand for $\mathbf{J}(x_0)$, the value of the Jacobian at x_0 .

Following Newton/Raphson (NR)(1690) we propose to use the linear approximation of the function $\mathbf{g}(\mathbf{x})$ to determine *a better estimate* for the solution of the nonlinear equation $\mathbf{g}(\mathbf{x}) = 0$, i.e. we use

$$\mathbf{g}(\mathbf{x}_0) + \mathbf{g}'(\mathbf{x}_0) (\mathbf{x} - \mathbf{x}_0) = 0 \quad (3.16)$$

Note the notation distinction between x_1 as the first component of vector \mathbf{x} and \mathbf{x}_1 as *the first linear correction* of the initial solution estimate \mathbf{x}_0 .

The solution of the linear system of equations in (3.16) gives for the linear correction \mathbf{x}_1 .

$$\mathbf{x}_1 = \mathbf{x}_0 - \mathbf{J}_0 \backslash \mathbf{g}(\mathbf{x}_0) \quad (3.17)$$

making use of the Matlab solve operator \backslash to express the solution of the system of linear equations by Gauss elimination. With the new solution estimate \mathbf{x}_1 we check the error of the system of nonlinear equations $\mathbf{g}(\mathbf{x}_1)$. If the error is larger than desired, we repeat the following process

$$\mathbf{x}_{i+1} = \mathbf{x}_i - \mathbf{J}_i \backslash \mathbf{g}(\mathbf{x}_i) \quad (3.18)$$

for $i = 1 \dots n$ until the error is smaller than a specified tolerance. \mathbf{J}_i is shorthand for $\mathbf{J}(\mathbf{x}_i)$.

3.4.1 Newton-Raphson Algorithm for System of Nonlinear Equations

The algorithmic form of the iterative process for the solution of the system of n nonlinear equations $\mathbf{g}(\mathbf{x}) = 0$ in n unknowns x_1, x_2, \dots, x_n is

- 1) Given the system of nonlinear equations $\mathbf{g}(\mathbf{x}) = 0$ with an initial guess for the solution \mathbf{x}_0 .
 - 2) For $i = 0 \dots m$ determine the function value $\mathbf{g}(\mathbf{x}_i) = 0$ and the Jacobian $\mathbf{J}(\mathbf{x}_i)$ at \mathbf{x}_i .
 - 3) Determine a correction to the previous solution estimate $\Delta \mathbf{x}_i = -\mathbf{J}(\mathbf{x}_i) \backslash \mathbf{g}(\mathbf{x}_i)$.
 - 4) Update the solution estimate $\mathbf{x}_{i+1} = \mathbf{x}_i + \Delta \mathbf{x}_i$.
 - 5) Return to step 2 until the error is smaller than a specified tolerance $\|\mathbf{g}(\mathbf{x}_{i+1})\| \leq \text{tol}$.
- where $\|\cdot\|$ denotes a suitable vector norm such as the Euclidean norm

$$\|\mathbf{g}\|_2 = \sqrt{\mathbf{g}^T \mathbf{g}} \quad (3.19)$$

The NR algorithm converges to the solution *quadratically* if the function $\mathbf{g}(\mathbf{x}) = 0$ is smooth near the solution and the initial estimate \mathbf{x}_0 is not too far from it. Quadratic convergence means that

$$\|\mathbf{g}(\mathbf{x}_{i+1})\| \leq \mu \|\mathbf{g}(\mathbf{x}_i)\|^2 \quad \text{or} \quad \|\mathbf{x}^* - \mathbf{x}_{i+1}\| \leq \mu^* \|\mathbf{x}^* - \mathbf{x}_i\|^2$$

where \mathbf{x}^* denotes the solution of the nonlinear system of equations $\mathbf{g}(\mathbf{x}) = 0$, while μ and μ^* are constant scalars whose value need not concern us.

3.4.2 Newton-Raphson Solution for Structural Problem

In structural analysis the system of nonlinear equations to be solved are the equilibrium equations at the free dofs of the structural model. In this case the function \mathbf{g} is the force unbalance between the applied forces \mathbf{P}_f and the resisting forces \mathbf{P}_r with the free dof displacements as the unknowns. Limiting ourselves to a single load pattern for the moment we express the applied forces \mathbf{P}_f as the product of the

load distribution vector \mathbf{P}_{ref} with the load factor λ and write

$$\mathbf{P}_u(\mathbf{U}) = \lambda \mathbf{P}_{ref} - \mathbf{P}_r(\mathbf{U}) = \mathbf{0} \quad (3.20)$$

noting explicitly the dependence of \mathbf{P}_r on the displacement \mathbf{U} . In the following we assume that the displacements \mathbf{U}_d at the restrained dofs of the model are equal to zero, so that the dependence of the resisting forces \mathbf{P}_r on \mathbf{U} reduces to a dependence on \mathbf{U}_f . With the assumption that the applied forces are *conservative* and do not depend on the displacements \mathbf{U} the equilibrium equations at the free dofs become

$$\mathbf{P}_u(\mathbf{U}_f) = \lambda \mathbf{P}_{ref} - \mathbf{P}_r(\mathbf{U}_f) = \mathbf{0} \quad (3.21)$$

For the NR algorithm we need the Jacobian of the force unbalance vector \mathbf{P}_u . It is

$$\mathbf{J} = \frac{\partial \mathbf{P}_u}{\partial \mathbf{U}} = -\frac{\partial \mathbf{P}_r}{\partial \mathbf{U}_f} = -\mathbf{K}_{tf}$$

where \mathbf{K}_{tf} is the tangent stiffness at the free dofs of the structural model. We drop the second subscript whenever the relevant dofs for the stiffness matrix are clear from the context and write explicitly

$$\mathbf{K}_t = \begin{bmatrix} \frac{\partial P_{r_1}}{\partial U_1} & \frac{\partial P_{r_1}}{\partial U_2} & \cdots & \frac{\partial P_{r_1}}{\partial U_n} \\ \frac{\partial P_{r_2}}{\partial U_1} & \frac{\partial P_{r_2}}{\partial U_2} & \cdots & \frac{\partial P_{r_2}}{\partial U_n} \\ \vdots & \vdots & \ddots & \vdots \\ \frac{\partial P_{r_n}}{\partial U_1} & \frac{\partial P_{r_n}}{\partial U_2} & \cdots & \frac{\partial P_{r_n}}{\partial U_n} \end{bmatrix} \quad (3.22)$$

The tangent stiffness coefficient \mathbf{K}_{ij} is, therefore, the *partial derivative* of the resisting force at dof i of the structural model with respect to the free dof displacement at dof j , or,

$$\mathbf{K}_{ij} = \frac{\partial P_{r_i}}{\partial U_j}$$

where we dropped the subscript t from the stiffness for brevity of notation.

The NR algorithm for the solution of the system of nonlinear equilibrium equations is

- 1) Given the nonlinear equation $\mathbf{P}_u(\mathbf{U}_f) = \mathbf{0}$ with an initial guess for the solution \mathbf{U}_0 .
- 2) For $i = 0 \dots m$ determine the value of $\mathbf{P}_u(\mathbf{U}_i)$ and the Jacobian of the resisting forces $\mathbf{K}_t(\mathbf{U}_i)$.
- 3) Determine a correction to the previous solution estimate $\Delta \mathbf{U}_i = \mathbf{K}_t(\mathbf{U}_i) \setminus \mathbf{P}_u(\mathbf{U}_i)$.
- 4) Update the solution estimate $\mathbf{U}_{i+1} = \mathbf{U}_i + \Delta \mathbf{U}_i$.
- 5) Return to step 2 until the error norm is smaller than a specified tolerance $\|\mathbf{P}_u(\mathbf{U}_{i+1})\| \leq \text{tol}$.

In the algorithm summary we used $\mathbf{U} = \mathbf{U}_f$ for simplicity of notation. We point out the notation distinction between U_1 which denotes the first component of the displacement vector \mathbf{U} , i.e. the displacement at dof 1, and \mathbf{U}_1 which denotes the first linear correction for the displacement vector \mathbf{U} during the NR solution algorithm.

We stress that the force unbalance vector \mathbf{P}_u and the tangent stiffness \mathbf{K}_t depend on the current free dof displacements \mathbf{U}_i , as explicitly indicated with parentheses.

The following aspects of the NR algorithm require further elaboration:

- 1) *The initial guess for the solution:* unless the estimate is close to the solution the algorithm may not reach a solution and diverge away from it. For a structural model a good initial guess is the undeformed configuration with $\mathbf{U}_f = \mathbf{0}$ as long as the load factor λ is not too large.
- 2) Every iteration requires the determination of the resisting force vector of the structural model and its Jacobian. This process is known as *structure state determination*.
- 3) Because the tangent stiffness matrix \mathbf{K}_t changes at every iteration, the system of linear equations need to be solved anew every time.
- 4) A suitable convergence criterion is very important; in the algorithm summary we used the norm of the unbalanced force vector, but this may not be the most suitable measure when the components of the unbalanced force vector have very different magnitude, as is the case in structural models with force and moment dofs.

Example 3.2 Nonlinear Solution of Two dof Truss under Given Load

To demonstrate the application of the NR solution algorithm we modify the single dof shallow truss of Example 3.1 by converting the simple support to a roller with a horizontal spring of axial stiffness k_s in Fig. 3.3. With this modification the structural model has two independent free dofs, U_1 and U_2 and consists of a truss element with nonlinear Green-Lagrange kinematics, and an axial spring with stiffness $k_s = 50,000$. Because the only displacement affecting the spring is oriented along the spring axis, we assume that the spring follows linear kinematics and statics in the following.

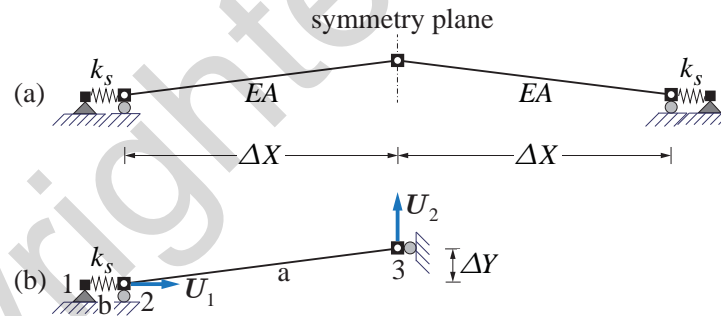


Fig. 3.3: Two free dof shallow truss

(a) Kinematics

For the truss element a we note that $\Delta u_x = -U_1$ and $\Delta u_y = U_2$. Substituting into (2.9) gives the Green-Lagrange deformation v_a

$$v_a = (-U_1) \frac{\Delta X}{L} + U_2 \frac{\Delta Y}{L} + \frac{1}{2L} [(-U_1)^2 + U_2^2] \quad (3.23)$$

The linear deformation of the spring b in terms of the free global dof displacements U_1 and U_2 is

$$v_b = U_1 \quad (3.24)$$

(b) Free dof Equilibrium Equations

We set up the equilibrium equations first by the principle of virtual displacements. To this end we set up the variation of the element deformations v_a and v_b in terms of the free dof displacements U_1 and U_2 . With the expression for the variation of \mathbf{g} in (3.13) we get for the variation of v_a

$$\begin{aligned}\delta v_a &= \frac{\partial v_a}{\partial U_1} \delta U_1 + \frac{\partial v_a}{\partial U_2} \delta U_2 \\ \delta v_a &= \left(-\frac{\Delta X}{L} + \frac{U_1}{L} \right) \delta U_1 + \left(\frac{\Delta Y}{L} + \frac{U_2}{L} \right) \delta U_2\end{aligned}\quad (3.25)$$

The variation of the spring deformation v_b is simply

$$\delta v_b = \delta U_1$$

The external virtual work $\delta \mathcal{W}_e$ is

$$\delta \mathcal{W}_e = \delta U_1 P_1 + \delta U_2 P_2$$

The internal virtual work $\delta \mathcal{W}_i$ is

$$\delta \mathcal{W}_i = -(\delta v_a q_a + \delta v_b q_b)$$

From $\delta \mathcal{W} = \delta \mathcal{W}_e + \delta \mathcal{W}_i = 0$ we obtain

$$\delta U_1 P_1 + \delta U_2 P_2 - (\delta v_a q_a + \delta v_b q_b) = 0$$

Substituting the deformation variation for elements a and b we get

$$\delta U_1 \left[P_1 - \left(-\frac{\Delta X}{L} + \frac{U_1}{L} \right) q_a - q_b \right] + \delta U_2 \left[P_2 - \left(\frac{\Delta Y}{L} + \frac{U_2}{L} \right) q_a \right] = 0 \quad (3.26)$$

Because the principle of virtual work states that equilibrium is satisfied if (3.26) holds for *arbitrary virtual displacements* $\delta \mathbf{U}$ it results that the expression in each bracket needs to be equal to zero. This furnishes the equilibrium equations at the free dofs of the 2-dof shallow truss. They are

$$\begin{aligned}P_1 - \left(-\frac{\Delta X}{L} + \frac{U_1}{L} \right) q_a - q_b &= 0 \\ P_2 - \left(\frac{\Delta Y}{L} + \frac{U_2}{L} \right) q_a &= 0\end{aligned}\quad (3.27)$$

The resisting forces \mathbf{P}_r at the free dofs, therefore, are

$$\begin{aligned}P_{r1} &= \left(-\frac{\Delta X}{L} + \frac{U_1}{L} \right) q_a + q_b \\ P_{r2} &= \left(\frac{\Delta Y}{L} + \frac{U_2}{L} \right) q_a\end{aligned}\quad (3.28)$$

These can be written in compact form as

$$\mathbf{P}_r = \begin{pmatrix} P_{r1} \\ P_{r2} \end{pmatrix} = \begin{bmatrix} -\frac{\Delta X + U_1}{L} & 1 \\ \frac{\Delta Y + U_2}{L} & 0 \end{bmatrix} \begin{pmatrix} q_a \\ q_b \end{pmatrix} = \mathbf{A}_f^T(\mathbf{U}_f) \mathbf{Q} \quad (3.29)$$

noting the explicit dependence of the transpose of the kinematic matrix \mathbf{A}_f on the free dof displacements \mathbf{U}_f . The basic forces q_a and q_b result from the basic force-deformation relations

$$\begin{aligned} q_a &= \frac{EA}{L} v_a = \frac{EA}{L} \left[-U_1 \frac{\Delta X}{L} + U_2 \frac{\Delta Y}{L} + \frac{1}{2L} (U_1^2 + U_2^2) \right] \\ q_b &= k_s v_b = k_s U_1 \end{aligned} \quad (3.30)$$

after substituting v_a and v_b from the kinematic relations (3.23) and (3.24).

(c) Tangent Stiffness Matrix

For the NR solution strategy we set up the tangent stiffness matrix \mathbf{K}_t with

$$\mathbf{K}_t = \begin{bmatrix} \frac{\partial P_{r1}}{\partial U_1} & \frac{\partial P_{r1}}{\partial U_2} \\ \frac{\partial P_{r2}}{\partial U_1} & \frac{\partial P_{r2}}{\partial U_2} \end{bmatrix}$$

We proceed to differentiate each resisting force in (3.28) with respect to each independent free dof displacement. We have

$$\begin{aligned} \mathbf{K}_{11} &= \frac{\partial P_{r1}}{\partial U_1} = \left(-\frac{\Delta X}{L} + \frac{U_1}{L} \right) \frac{\partial q_a}{\partial U_1} + \frac{1}{L} q_a + \frac{\partial q_b}{\partial U_1} \\ \mathbf{K}_{12} &= \frac{\partial P_{r1}}{\partial U_2} = \left(-\frac{\Delta X}{L} + \frac{U_1}{L} \right) \frac{\partial q_a}{\partial U_2} + \frac{\partial q_b}{\partial U_2} \\ \mathbf{K}_{21} &= \frac{\partial P_{r2}}{\partial U_1} = \left(\frac{\Delta Y}{L} + \frac{U_2}{L} \right) \frac{\partial q_a}{\partial U_1} \\ \mathbf{K}_{22} &= \frac{\partial P_{r2}}{\partial U_2} = \left(\frac{\Delta Y}{L} + \frac{U_2}{L} \right) \frac{\partial q_a}{\partial U_2} + \frac{1}{L} q_a + \frac{\partial q_b}{\partial U_2} \end{aligned} \quad (3.31)$$

From the basic force-deformation relation in (3.30) we get

$$\begin{aligned} \frac{\partial q_a}{\partial U_1} &= \frac{EA}{L} \left(-\frac{\Delta X}{L} + \frac{U_1}{L} \right) \\ \frac{\partial q_a}{\partial U_2} &= \frac{EA}{L} \left(\frac{\Delta Y}{L} + \frac{U_2}{L} \right) \\ \frac{\partial q_b}{\partial U_1} &= k_s \\ \frac{\partial q_b}{\partial U_2} &= 0 \end{aligned} \quad (3.32)$$

These relations can also be written in compact form

$$\frac{\partial \mathbf{Q}}{\partial \mathbf{U}_f} = \begin{bmatrix} \frac{\partial q_a}{\partial U_1} & \frac{\partial q_a}{\partial U_2} \\ \frac{\partial q_b}{\partial U_1} & \frac{\partial q_b}{\partial U_2} \end{bmatrix} = \begin{bmatrix} EA & 0 \\ 0 & k_s \end{bmatrix} \begin{bmatrix} -\frac{\Delta X + U_1}{L} & \frac{\Delta Y + U_2}{L} \\ 1 & 0 \end{bmatrix} = \mathbf{K}_s \mathbf{A}_f(\mathbf{U}_f)$$

Substituting (3.32) into (3.31) gives the tangent stiffness coefficients

$$\begin{aligned}\mathbf{K}_{11} &= \left(-\frac{\Delta X}{L} + \frac{U_1}{L}\right) \frac{EA}{L} \left(-\frac{\Delta X}{L} + \frac{U_1}{L}\right) + k_s + \frac{1}{L} q_a \\ \mathbf{K}_{21} &= \left(-\frac{\Delta X}{L} + \frac{U_1}{L}\right) \frac{EA}{L} \left(\frac{\Delta Y}{L} + \frac{U_2}{L}\right) \\ \mathbf{K}_{12} &= \left(\frac{\Delta Y}{L} + \frac{U_2}{L}\right) \frac{EA}{L} \left(-\frac{\Delta X}{L} + \frac{U_1}{L}\right) \\ \mathbf{K}_{22} &= \left(\frac{\Delta Y}{L} + \frac{U_2}{L}\right) \frac{EA}{L} \left(\frac{\Delta Y}{L} + \frac{U_2}{L}\right) + \frac{1}{L} q_a\end{aligned}$$

The tangent stiffness matrix \mathbf{K}_t thus is

$$\mathbf{K}_t = \frac{EA}{L} \begin{bmatrix} \left(\frac{-\Delta X + U_1}{L}\right)^2 & \left(\frac{-\Delta X + U_1}{L}\right) \left(\frac{\Delta Y + U_2}{L}\right) \\ \left(\frac{-\Delta X + U_1}{L}\right) \left(\frac{\Delta Y + U_2}{L}\right) & \left(\frac{\Delta Y + U_2}{L}\right)^2 \end{bmatrix} + \begin{bmatrix} k_s & 0 \\ 0 & 0 \end{bmatrix} + \begin{bmatrix} \frac{1}{L} & 0 \\ 0 & \frac{1}{L} \end{bmatrix} q_a \quad (3.33)$$

The tangent stiffness matrix is made up of two contributions: the material stiffness \mathbf{K}_m which depends on the material properties of the truss element and the spring

$$\mathbf{K}_m = \frac{EA}{L} \begin{bmatrix} \left(\frac{-\Delta X + U_1}{L}\right)^2 & \left(\frac{-\Delta X + U_1}{L}\right) \left(\frac{\Delta Y + U_2}{L}\right) \\ \left(\frac{-\Delta X + U_1}{L}\right) \left(\frac{\Delta Y + U_2}{L}\right) & \left(\frac{\Delta Y + U_2}{L}\right)^2 \end{bmatrix} + \begin{bmatrix} k_s & 0 \\ 0 & 0 \end{bmatrix} \quad (3.34)$$

with the element a and b contributions listed separately, and the geometric stiffness \mathbf{K}_g

$$\mathbf{K}_g = \begin{bmatrix} \frac{1}{L} & 0 \\ 0 & \frac{1}{L} \end{bmatrix} q_a \quad (3.35)$$

We note that the spring does not contribute to the geometric stiffness because of the assumption of linear statics for it.

(d) Compact General Formulation

The resisting force vector \mathbf{P}_r and the tangent stiffness \mathbf{K}_t for the two-dof truss can be derived more concisely with the use of vector differentiation. We demonstrate the process by first defining the derivative of the element deformations \mathbf{V} with respect to the free dof displacements \mathbf{U}_f . We have

$$\frac{\partial \mathbf{V}}{\partial \mathbf{U}_f} = \begin{bmatrix} \frac{\partial v_a}{\partial U_1} & \frac{\partial v_a}{\partial U_2} \\ \frac{\partial v_b}{\partial U_1} & \frac{\partial v_b}{\partial U_2} \end{bmatrix}$$

With the kinematic relations (3.23) and (3.24) it results

$$\frac{\partial \mathbf{V}}{\partial \mathbf{U}_f} = \begin{bmatrix} -\frac{\Delta X + U_1}{L} & \frac{\Delta Y + U_2}{L} \\ 1 & 0 \end{bmatrix} = \mathbf{A}_f(\mathbf{U}_f) \quad (3.36)$$

with the definition

$$\mathbf{A}_f(\mathbf{U}_f) = \frac{\partial \mathbf{V}}{\partial \mathbf{U}_f} \quad (3.37)$$

Following (3.13) the variation of the element deformations $\delta \mathbf{V}$ is

$$\delta \mathbf{V} = \frac{\partial \mathbf{V}}{\partial \mathbf{U}_f} \delta \mathbf{U}_f = \mathbf{A}_f(\mathbf{U}_f) \delta \mathbf{U}_f$$

The principle of virtual displacements gives with $\mathcal{W}_e = \delta \mathbf{U}_f \mathbf{P}_f$ and $\mathcal{W}_i = -\delta \mathbf{V}^T \mathbf{Q}$

$$\delta \mathbf{U}_f \mathbf{P}_f - \delta \mathbf{V}^T \mathbf{Q} = 0 \quad \rightarrow \quad \delta \mathbf{U}_f (\mathbf{P}_f - \mathbf{A}_f^T(\mathbf{U}_f) \mathbf{Q}) = 0$$

Because this relation must hold for arbitrary virtual displacements $\delta \mathbf{U}_f$ for the structural system to be in equilibrium we conclude that

$$\mathbf{P}_f - \mathbf{A}_f^T(\mathbf{U}_f) \mathbf{Q} = \mathbf{0}$$

obtaining thus the equilibrium equations at the free dofs of the structure $\mathbf{P}_f - \mathbf{P}_r(\mathbf{U}_f) = \mathbf{0}$ with

$$\mathbf{P}_r = \mathbf{A}_f^T(\mathbf{U}_f) \mathbf{Q}$$

in agreement with the conclusion for (3.29).

The tangent stiffness matrix \mathbf{K}_t is given by

$$\mathbf{K}_t = \frac{\partial \mathbf{P}_r}{\partial \mathbf{U}_f} = \mathbf{A}_f^T(\mathbf{U}_f) \frac{\partial \mathbf{Q}}{\partial \mathbf{U}_f} + \frac{\partial \mathbf{A}_f^T(\mathbf{U}_f)}{\partial \mathbf{U}_f} \mathbf{Q} \quad (3.38)$$

The first contribution is the material stiffness \mathbf{K}_m noting that

$$\frac{\partial \mathbf{Q}}{\partial \mathbf{U}_f} = \frac{\partial \mathbf{Q}}{\partial \mathbf{V}} \frac{\partial \mathbf{V}}{\partial \mathbf{U}_f} = \mathbf{K}_s \mathbf{A}_f(\mathbf{U}_f)$$

where we made use of (3.37) and defined

$$\frac{\partial \mathbf{Q}}{\partial \mathbf{V}} = \begin{bmatrix} \frac{\partial q_a}{\partial v_a} & \frac{\partial q_a}{\partial v_b} \\ \frac{\partial q_b}{\partial v_a} & \frac{\partial q_b}{\partial v_b} \end{bmatrix} = \begin{bmatrix} \frac{\partial q_a}{\partial v_a} & 0 \\ 0 & \frac{\partial q_b}{\partial v_b} \end{bmatrix} = \begin{bmatrix} EA & 0 \\ 0 & k_s \end{bmatrix} = \mathbf{K}_s$$

after noting that the basic force of each element depends only on its deformation. The material stiffness \mathbf{K}_m thus becomes

$$\mathbf{K}_m = \mathbf{A}_f^T(\mathbf{U}_f) \mathbf{K}_s \mathbf{A}_f(\mathbf{U}_f) \quad (3.39)$$

The substitution of $\mathbf{A}_f(\mathbf{U}_f)$ for the two-dof truss from (3.36) gives the material stiffness in (3.34).

The second contribution to the tangent stiffness \mathbf{K}_t in (3.38) is the geometric stiffness \mathbf{K}_g of the two-dof truss. It is

$$\mathbf{K}_g = \frac{\partial \mathbf{A}_f^T(\mathbf{U}_f)}{\partial \mathbf{U}_f} \mathbf{Q}$$

For the partial derivative of the matrix \mathbf{A}_f^T we note that it consists of two columns with the first column multiplying the basic force q_a of element a and the second column the basic force q_b of element b. We,

therefore, have

$$\frac{\partial \mathbf{A}_f^T(\mathbf{U}_f)}{\partial \mathbf{U}_f} \mathbf{Q} = \frac{\partial}{\partial \mathbf{U}_f} \begin{bmatrix} \frac{-\Delta X + U_1}{L} \\ \frac{\Delta Y + U_2}{L} \end{bmatrix} q_a + \frac{\partial}{\partial \mathbf{U}_f} \begin{bmatrix} 1 \\ 0 \end{bmatrix} q_b$$

For the derivative of the columns of the \mathbf{A}_f matrix we note that these are vectors and we follow the definition for the Jacobian of the vector function \mathbf{g} in (3.11) to get

$$\mathbf{K}_g = \begin{bmatrix} \frac{1}{L} & 0 \\ 0 & \frac{1}{L} \end{bmatrix} q_a$$

in agreement with the result in (3.34).

(e) Direct Assembly Formulation

The preceding derivations of the resisting force \mathbf{P}_r and the stiffness matrix \mathbf{K}_t for the two-dof truss are insightful and suitable for this small structural model with only two free dofs. This process is, however, tedious for a large structural model because it cannot be as easily automated. For this case the direct stiffness implementation furnishes the necessary modularity and automation. We derive the method for the case in hand.

In the direct assembly formulation the kinematic relations are set up in two steps: (a) first the element deformation v is related to the element end displacements \mathbf{u} ; (b) then, the element end displacements \mathbf{u} are set equal to the displacements \mathbf{U}_f of the global free dofs corresponding to the particular element. The latter relation can be conveniently expressed with the help of the Boolean matrix \mathbf{A}_b (see CE220 course reader).

$$\mathbf{u}^{(el)} = \mathbf{A}_b^{(el)} \mathbf{U}_f$$

where we limit the displacement vector \mathbf{U} to the free dofs only. We note that (2.9) gives the relation between the element deformation v and the end displacements \mathbf{u} for the plane truss under Green-Lagrange kinematics:

$$v_{GL} = \frac{\Delta X}{L} \Delta u_x + \frac{\Delta Y}{L} \Delta u_y + \frac{(\Delta u_x)^2}{2L} + \frac{(\Delta u_y)^2}{2L}$$

The principle of virtual work furnishes the equilibrium equations at the free dofs of the structural model:

$$\delta \mathbf{U}_f^T \mathbf{P}_f = \sum_{el} \delta \mathbf{u}^{(el)T} \mathbf{p}^{(el)} \rightarrow \delta \mathbf{U}_f^T \left(\mathbf{P}_f - \sum_{el} \mathbf{A}_b^{(el)T} \mathbf{p}^{(el)} \right) = 0$$

with the summation of the internal work extending over the number el of elements for the structural model. Because the virtual work equation holds for arbitrary virtual displacements $\delta \mathbf{U}_f$ the free dof equilibrium equations are

$$\mathbf{P}_f - \sum_{el} \mathbf{A}_b^{(el)T} \mathbf{p}^{(el)} = \mathbf{0}$$

and we recognize the resisting forces \mathbf{P}_r as the sum of the element resisting force contributions

$$\mathbf{P}_r = \sum_{el} \mathbf{P}_r^{(el)} = \sum_{el} \mathbf{A}_b^{(el)T} \mathbf{p}^{(el)} \quad (3.40)$$

The tangent stiffness matrix of the structure is the Jacobian of the resisting force vector \mathbf{P}_r

$$\mathbf{K}_t = \frac{\partial \mathbf{P}_r}{\partial \mathbf{U}_f} = \sum_{el} \mathbf{A}_b^{(el)T} \frac{\partial \mathbf{p}^{(el)}}{\partial \mathbf{u}^{(el)}} \frac{\partial \mathbf{u}^{(el)}}{\partial \mathbf{U}_f} = \sum_{el} \mathbf{A}_b^{(el)T} \mathbf{k}_e^{(el)} \mathbf{A}_b^{(el)}$$

where \mathbf{k}_e is the tangent element stiffness matrix in global reference with the definition

$$\mathbf{k}_e = \frac{\partial \mathbf{p}}{\partial \mathbf{u}} \quad (3.41)$$

The tangent stiffness matrix of the structure \mathbf{K}_t can thus be formed by direct assembly and summation of the element stiffness matrix contributions according to

$$\mathbf{K}_t = \sum_{el} \mathbf{A}_b^{(el)T} \mathbf{k}_e^{(el)} \mathbf{A}_b^{(el)} \quad (3.42)$$

All that remains to be done now is to establish the end forces \mathbf{p} and the tangent element stiffness \mathbf{k}_e of the plane truss element for Green-Lagrange nonlinear geometry.

(f) Green-Lagrange Plane Truss Element

We use the principle of virtual work to set up the static relations of the Green-Lagrange plane truss element

$$\delta \mathbf{u}^T \mathbf{p} = \delta v^T q$$

To this end we need the variation of the element deformation v . Following (3.13) the variation of the element deformation v with respect to the element end displacements \mathbf{u} is

$$\delta v = \frac{\partial v}{\partial \mathbf{u}} \delta \mathbf{u} = \mathbf{a}_g(\mathbf{u}) \delta \mathbf{u}$$

where we defined the derivative of the deformation v with respect to the element end displacements \mathbf{u} as the *kinematic matrix* $\mathbf{a}_g(\mathbf{u})$ of the truss. For the kinematic matrix we have in detail

$$\frac{\partial v}{\partial \mathbf{u}} = \begin{bmatrix} \frac{\partial v}{\partial u_1} & \frac{\partial v}{\partial u_2} & \frac{\partial v}{\partial u_3} & \frac{\partial v}{\partial u_4} \end{bmatrix}$$

Proceeding with the derivatives of v in (2.9) for each end displacement component $u_1 \dots u_4$ we get

$$\begin{aligned} \frac{\partial v}{\partial u_1} &= \frac{\partial v}{\partial (\Delta u_x)} \frac{\partial (\Delta u_x)}{\partial u_1} = \frac{\Delta X + \Delta u_x}{L} (-1) = -\frac{\Delta X + \Delta u_x}{L} \\ \frac{\partial v}{\partial u_2} &= \frac{\partial v}{\partial (\Delta u_y)} \frac{\partial (\Delta u_y)}{\partial u_2} = \frac{\Delta Y + \Delta u_y}{L} (-1) = -\frac{\Delta Y + \Delta u_y}{L} \\ \frac{\partial v}{\partial u_3} &= \frac{\partial v}{\partial (\Delta u_x)} \frac{\partial (\Delta u_x)}{\partial u_3} = \frac{\Delta X + \Delta u_x}{L} (-1) = -\frac{\Delta X + \Delta u_x}{L} \\ \frac{\partial v}{\partial u_4} &= \frac{\partial v}{\partial (\Delta u_y)} \frac{\partial (\Delta u_y)}{\partial u_4} = \frac{\Delta Y + \Delta u_y}{L} (-1) = -\frac{\Delta Y + \Delta u_y}{L} \end{aligned}$$

The Green-Lagrange kinematic matrix $\mathbf{a}_g(\mathbf{u})$ for the plane truss is

$$\mathbf{a}_g(\mathbf{u}) = \frac{\partial v}{\partial \mathbf{u}} = \begin{bmatrix} -\frac{\Delta X + \Delta u_x}{L} & -\frac{\Delta Y + \Delta u_y}{L} & \frac{\Delta X + \Delta u_x}{L} & \frac{\Delta Y + \Delta u_y}{L} \end{bmatrix} \quad (3.43)$$

Under linear kinematics the kinematic matrix $\mathbf{a}_g(\mathbf{u})$ simplifies to

$$\mathbf{a}_g = \begin{bmatrix} -\frac{\Delta X}{L} & -\frac{\Delta Y}{L} & \frac{\Delta X}{L} & \frac{\Delta Y}{L} \end{bmatrix}$$

and *does not depend on the element end displacements \mathbf{u}* . Because the kinematic matrix \mathbf{a}_g is constant under linear kinematics it follows that

$$\frac{\partial v}{\partial \mathbf{u}} = \mathbf{a}_g = \text{const} \rightarrow \mathbf{v} = \mathbf{a}_g \mathbf{u}$$

Substituting into the virtual work equation for the element gives

$$\delta \mathbf{u}^T \mathbf{p} = \delta v^T q = \delta \mathbf{u}^T \mathbf{a}_g^T(\mathbf{u}) q$$

For arbitrary virtual displacements $\delta \mathbf{u}$ we conclude that

$$\mathbf{p} = \mathbf{a}_g^T(\mathbf{u}) q \quad \text{or} \quad \mathbf{p} = \begin{bmatrix} -\frac{\Delta X + \Delta u_x}{L} \\ -\frac{\Delta Y + \Delta u_y}{L} \\ \frac{\Delta X + \Delta u_x}{L} \\ \frac{\Delta Y + \Delta u_y}{L} \end{bmatrix} q \quad (3.44)$$

We note that the static relation between the basic force q and the element end forces \mathbf{p} in the undeformed, original configuration of the element is

$$\mathbf{p} = \begin{bmatrix} -\frac{\Delta X}{L} \\ -\frac{\Delta Y}{L} \\ \frac{\Delta X}{L} \\ \frac{\Delta Y}{L} \end{bmatrix} q$$

The tangent stiffness matrix \mathbf{k}_e of the plane truss element in global coordinates is

$$\begin{aligned} \mathbf{k}_e = \frac{\partial \mathbf{p}}{\partial \mathbf{u}} &= \frac{\partial [\mathbf{a}_g^T(\mathbf{u}) q]}{\partial \mathbf{u}} = \mathbf{a}_g^T(\mathbf{u}) \frac{\partial q}{\partial \mathbf{u}} + \frac{\partial [\mathbf{a}_g^T(\mathbf{u})]}{\partial \mathbf{u}} q \\ &= \mathbf{a}_g^T(\mathbf{u}) \frac{\partial q}{\partial v} \frac{\partial v}{\partial \mathbf{u}} + \frac{\partial [\mathbf{a}_g^T(\mathbf{u})]}{\partial \mathbf{u}} q \\ &= \mathbf{a}_g^T(\mathbf{u}) \frac{\partial q}{\partial v} \mathbf{a}_g(\mathbf{u}) + \frac{\partial [\mathbf{a}_g^T(\mathbf{u})]}{\partial \mathbf{u}} q \\ &= \mathbf{k}_m + \mathbf{k}_g \end{aligned}$$

where \mathbf{k}_m is the material stiffness and \mathbf{k}_g the geometric stiffness of the element in the global reference system. Subscript t is dropped from the element stiffness matrix for brevity of notation.

The material stiffness of the truss element is

$$\mathbf{k}_m = \mathbf{a}_g^T(\mathbf{u}) \frac{\partial q}{\partial v} \mathbf{a}_g(\mathbf{u}) = \frac{EA}{L} \begin{bmatrix} \mathbf{N} & -\mathbf{N} \\ -\mathbf{N} & \mathbf{N} \end{bmatrix} \quad (3.45)$$

with

$$\mathbf{N} = \begin{bmatrix} \left(\frac{\Delta X + (\Delta u_x)}{L} \right)^2 & \left(\frac{\Delta X + (\Delta u_x)}{L} \right) \left(\frac{\Delta Y + \Delta u_y}{L} \right) \\ \left(\frac{\Delta Y + \Delta u_y}{L} \right) \left(\frac{\Delta X + (\Delta u_x)}{L} \right) & \left(\frac{\Delta Y + \Delta u_y}{L} \right)^2 \end{bmatrix} \quad (3.46)$$

The geometric stiffness matrix of the Green-Lagrange element is

$$\mathbf{k}_g = \frac{\partial [\mathbf{a}_g^T(\mathbf{u})]}{\partial \mathbf{u}} q = \frac{\partial}{\partial \mathbf{u}} \begin{bmatrix} -\frac{\Delta X + \Delta u_x}{L} \\ -\frac{\Delta Y + \Delta u_y}{L} \\ \frac{\Delta X + \Delta u_x}{L} \\ \frac{\Delta Y + \Delta u_y}{L} \end{bmatrix} q$$

The most convenient way of performing the differentiation of $\mathbf{a}_g(\mathbf{u})$ is

$$\mathbf{k}_g = \left\{ \frac{\partial}{\partial (\Delta u_x)} \begin{bmatrix} -\frac{\Delta X + \Delta u_x}{L} \\ -\frac{\Delta Y + \Delta u_y}{L} \\ \frac{\Delta X + \Delta u_x}{L} \\ \frac{\Delta Y + \Delta u_y}{L} \end{bmatrix} \frac{\partial \Delta u_x}{\partial \mathbf{u}} + \frac{\partial}{\partial \Delta u_y} \begin{bmatrix} -\frac{\Delta X + \Delta u_x}{L} \\ -\frac{\Delta Y + \Delta u_y}{L} \\ \frac{\Delta X + \Delta u_x}{L} \\ \frac{\Delta Y + \Delta u_y}{L} \end{bmatrix} \frac{\partial \Delta u_y}{\partial \mathbf{u}} \right\} q$$

Noting that

$$\begin{aligned} \frac{\partial \Delta u_x}{\partial \mathbf{u}} &= \frac{\partial (\mathbf{u}_3 - \mathbf{u}_1)}{\partial \mathbf{u}} = \begin{bmatrix} -1 & 0 & 1 & 0 \end{bmatrix} \\ \frac{\partial \Delta u_y}{\partial \mathbf{u}} &= \frac{\partial (\mathbf{u}_4 - \mathbf{u}_2)}{\partial \mathbf{u}} = \begin{bmatrix} 0 & -1 & 0 & 1 \end{bmatrix} \end{aligned}$$

With the above expressions the geometric stiffness matrix becomes

$$\mathbf{k}_g = \frac{q}{L} \begin{bmatrix} 1 & 0 & -1 & 0 \\ 0 & 1 & 0 & -1 \\ -1 & 0 & 1 & 0 \\ 0 & -1 & 0 & 1 \end{bmatrix} = \frac{q}{L} \begin{bmatrix} \mathbf{I} & -\mathbf{I} \\ -\mathbf{I} & \mathbf{I} \end{bmatrix} \quad (3.47)$$

where \mathbf{I} is the 2×2 identity matrix.

For a tensile force in the truss element the diagonal terms of the geometric stiffness are positive (stiffening effect), while for a compression force they are negative (softening or destabilizing effect).

A negative geometric stiffness may render the structure unstable at a specific applied force value.

Under linear geometry the tangent stiffness matrix of the plane truss is constant with $\mathbf{k}_g = \mathbf{0}$ and \mathbf{k}_m given by (3.45) with \mathbf{N} given by

$$\mathbf{N} = \begin{bmatrix} \left(\frac{\Delta X}{L}\right)^2 & \left(\frac{\Delta X}{L}\right)\left(\frac{\Delta Y}{L}\right) \\ \left(\frac{\Delta Y}{L}\right)\left(\frac{\Delta X}{L}\right) & \left(\frac{\Delta Y}{L}\right)^2 \end{bmatrix} \quad (3.48)$$

(g) Application of Direct Assembly to Two Dof Truss

The resisting forces \mathbf{P}_r are

$$\mathbf{P}_r = \begin{pmatrix} p_1^{(a)} + p_3^{(b)} \\ p_4^{(a)} \end{pmatrix} = \begin{pmatrix} -\frac{\Delta X + \Delta u_x}{L} \\ \frac{\Delta Y + \Delta u_y}{L} \end{pmatrix} q_a + \begin{pmatrix} 1 \\ 0 \end{pmatrix} q_b$$

Substituting $\Delta u_x = -U_1$ and $\Delta u_y = U_2$ gives

$$\mathbf{P}_r = \begin{pmatrix} -\frac{\Delta X - U_1}{L} \\ \frac{\Delta Y + U_2}{L} \end{pmatrix} q_a + \begin{pmatrix} 1 \\ 0 \end{pmatrix} q_b$$

in agreement with (3.28).

The tangent stiffness \mathbf{K}_t is

$$\begin{aligned} \mathbf{K}_t &= \begin{bmatrix} \mathbf{k}_{11} & \mathbf{k}_{14} \\ \mathbf{k}_{41} & \mathbf{k}_{44} \end{bmatrix}^{(a)} + \begin{bmatrix} \mathbf{k}_{33} & 0 \\ 0 & 0 \end{bmatrix}^{(b)} \\ &= \frac{EA}{L} \begin{bmatrix} \left(\frac{\Delta X + \Delta u_x}{L}\right)^2 & -\left(\frac{\Delta X + \Delta u_x}{L}\right)\left(\frac{\Delta Y + \Delta u_y}{L}\right) \\ -\left(\frac{\Delta X + \Delta u_x}{L}\right)\left(\frac{\Delta Y + \Delta u_y}{L}\right) & \left(\frac{\Delta Y + \Delta u_y}{L}\right)^2 \end{bmatrix} + \begin{bmatrix} \frac{1}{L} & 0 \\ 0 & \frac{1}{L} \end{bmatrix} q_a + \begin{bmatrix} k_s & 0 \\ 0 & 0 \end{bmatrix} \\ &= \frac{EA}{L} \begin{bmatrix} \left(\frac{\Delta X - U_1}{L}\right)^2 & -\left(\frac{\Delta X - U_1}{L}\right)\left(\frac{\Delta Y + U_2}{L}\right) \\ -\left(\frac{\Delta X - U_1}{L}\right)\left(\frac{\Delta Y + U_2}{L}\right) & \left(\frac{\Delta Y + U_2}{L}\right)^2 \end{bmatrix} + \begin{bmatrix} \frac{1}{L} & 0 \\ 0 & \frac{1}{L} \end{bmatrix} q_a + \begin{bmatrix} k_s & 0 \\ 0 & 0 \end{bmatrix} \end{aligned}$$

in agreement with (3.33).

(h) Summary of Governing Relations

Before embarking on the response determination of the two dof truss with the NR algorithm we summarize the governing relations:

1) Kinematics

$$\begin{aligned} v_a &= (-U_1) \frac{\Delta X}{L} + U_2 \frac{\Delta Y}{L} + \frac{1}{2L} [(-U_1)^2 + U_2^2] \\ v_b &= U_1 \end{aligned}$$

2) Basic force-deformation relations

$$\begin{aligned} q_a &= \frac{EA}{L} v_a \\ q_b &= k_s v_b \end{aligned}$$

3) Equilibrium at free dofs

$$\mathbf{P}_f - \begin{pmatrix} -\frac{\Delta X - U_1}{L} \\ \frac{\Delta Y + U_2}{L} \end{pmatrix} q_a + \begin{pmatrix} 1 \\ 0 \end{pmatrix} q_b = \mathbf{0}$$

4) Tangent stiffness matrix at free dofs

$$\mathbf{K}_t = \frac{EA}{L} \begin{bmatrix} \left(\frac{\Delta X - U_1}{L}\right)^2 & -\left(\frac{\Delta X - U_1}{L}\right)\left(\frac{\Delta Y + U_2}{L}\right) \\ -\left(\frac{\Delta X - U_1}{L}\right)\left(\frac{\Delta Y + U_2}{L}\right) & \left(\frac{\Delta Y + U_2}{L}\right)^2 \end{bmatrix} + \begin{bmatrix} \frac{1}{L} & 0 \\ 0 & \frac{1}{L} \end{bmatrix} q_a + \begin{bmatrix} k_s & 0 \\ 0 & 0 \end{bmatrix}$$

(i) Response to Given Load

We present now the determination of the free dof displacements \mathbf{U}_f for the two dof truss under the given downward force of 8 units in Fig. 3.4. Assuming that the loading in Fig. 3.4 constitutes the reference force vector the applied forces \mathbf{P}_f at the free dofs are

$$\mathbf{P}_f = \lambda \mathbf{P}_{ref} = (1) \begin{pmatrix} 0 \\ -8 \end{pmatrix} = \begin{pmatrix} 0 \\ -8 \end{pmatrix}$$

for a load factor $\lambda = 1$.

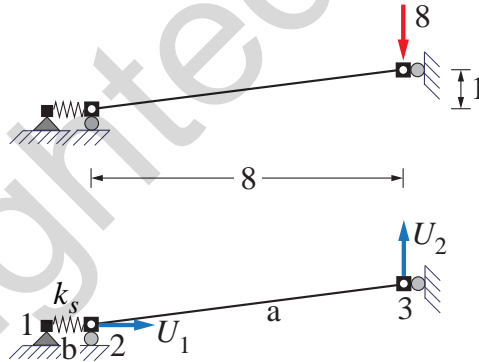


Fig. 3.4: Two free dof shallow truss

We use the unstressed structure as the initial guess $\mathbf{U}_0 = \mathbf{0}$ for the solution. With the following notation for the key relations of the NR solution algorithm

$$\mathbf{P}_u(\mathbf{U}_i) = \begin{pmatrix} 0 \\ -8 \end{pmatrix} - \mathbf{P}_r(\mathbf{U}_i)$$

$$\Delta \mathbf{U}_i = \mathbf{K}_t(\mathbf{U}_i) \backslash \mathbf{P}_u(\mathbf{U}_i)$$

$$\mathbf{U}_{i+1} = \mathbf{U}_i + \Delta \mathbf{U}_i$$

Table 3.2 presents the results of the calculations with the use of the Matlab® \ operator to denote the solution of the linear system of two equilibrium equations in two unknowns by Gauss elimination.

The iterative NR solution process converges to the solution

Iteration i	\mathbf{U}_i	$\mathbf{P}_u(\mathbf{U}_i)$	$\mathbf{K}_t(\mathbf{U}_i)$	$\Delta\mathbf{U}_i$	\mathbf{U}_{i+1}
0	$\begin{pmatrix} 0 \\ 0 \end{pmatrix}$	$\begin{pmatrix} 0 \\ -8 \end{pmatrix}$	$\begin{bmatrix} 53053 & -382 \\ -382 & 47.7 \end{bmatrix}$	$\begin{pmatrix} -0.0013 \\ -0.1779 \end{pmatrix}$	$\begin{pmatrix} -0.0013 \\ -0.1779 \end{pmatrix}$
1	$\begin{pmatrix} -0.0013 \\ -0.1779 \end{pmatrix}$	$\begin{pmatrix} 6.033 \\ -2.044 \end{pmatrix}$	$\begin{bmatrix} 53047 & -314 \\ -314 & 25 \end{bmatrix}$	$\begin{pmatrix} -0.0004 \\ -0.0868 \end{pmatrix}$	$\begin{pmatrix} -0.0017 \\ -0.2647 \end{pmatrix}$
2	$\begin{pmatrix} -0.0017 \\ -0.2647 \end{pmatrix}$	$\begin{pmatrix} 1.437 \\ -0.414 \end{pmatrix}$	$\begin{bmatrix} 53044 & -281 \\ -281 & 15.5 \end{bmatrix}$	$\begin{pmatrix} -0.0001 \\ -0.0291 \end{pmatrix}$	$\begin{pmatrix} -0.0018 \\ -0.2938 \end{pmatrix}$
3	$\begin{pmatrix} -0.0018 \\ -0.2938 \end{pmatrix}$	$\begin{pmatrix} 0.161 \\ -0.043 \end{pmatrix}$	$\begin{bmatrix} 53043 & -270 \\ -270 & 12.5 \end{bmatrix}$	$\begin{pmatrix} -0.0000 \\ -0.0037 \end{pmatrix}$	$\begin{pmatrix} -0.0018 \\ -0.2976 \end{pmatrix}$
4	$\begin{pmatrix} -0.0018 \\ -0.2976 \end{pmatrix}$	$\begin{pmatrix} 0.003 \\ -0.001 \end{pmatrix}$	$\begin{bmatrix} 53043 & -268 \\ -268 & 12.15 \end{bmatrix}$	$\begin{pmatrix} -0.00000 \\ -0.00006 \end{pmatrix}$	$\begin{pmatrix} -0.0018 \\ -0.2976 \end{pmatrix}$

Table 3.2: Results for iterative solution of equilibrium equations for two dof truss

$$\mathbf{U}_f = \begin{pmatrix} -0.0018 \\ -0.2976 \end{pmatrix}$$

to within 4 significant digits. The force unbalance vector \mathbf{P}_u is also very small. With the given free dof displacement values we can determine the element deformations v_a and v_b , proceed to determine the corresponding basic forces q_a and q_b and use the equilibrium equations at the restrained dofs to determine the support reactions:

$$\begin{aligned} \mathbf{R}_1 - \mathbf{p}_1^{(b)} &= 0 & \mathbf{R}_1 &= -q_b \\ \mathbf{R}_2 - \mathbf{p}_2^{(b)} &= 0 & \mathbf{R}_2 &= 0 \\ \mathbf{R}_3 - \mathbf{p}_2^{(a)} &= 0 & \rightarrow \quad \mathbf{R}_3 &= -\frac{\Delta Y + U_2}{L} q_a \\ \mathbf{R}_4 - \mathbf{p}_3^{(a)} &= 0 & \mathbf{R}_4 &= \frac{\Delta X - U_1}{L} q_a \end{aligned}$$

Finally, we check the global equilibrium of the structure *in the deformed configuration*.

3.5 Multi-Step Incremental Analysis

3.5.1 Introduction

In the preceding discussion of the NR solution algorithm for the system of nonlinear equilibrium equations we assumed that the nodal forces are applied in a single load increment or step by specifying the reference load vector \mathbf{P}_{ref} and a load factor λ . Consequently, we used the unstressed state of the structure as the initial guess for the iterative solution. With this approach we cannot be sure that the initial guess is close to the solution of the equilibrium equations under the given nodal forces, and thus cannot guarantee that the algorithm will converge. Moreover, there may be more than one displacement solution for given applied forces, as is the case for the snap-through problem of the shallow truss who

load-displacement response is shown in Fig. 2.15(a). To address the risk that the initial guess may not be close to the solution of the equilibrium equations we apply the given nodal forces *in several increments and use the solution for each increment as the initial guess for the next.*

3.5.2 Single Load Step

Before discussing the *multi-step incremental analysis* we revisit the calculation steps for a *single load step* of the NR solution algorithm from Section 3.4.2.

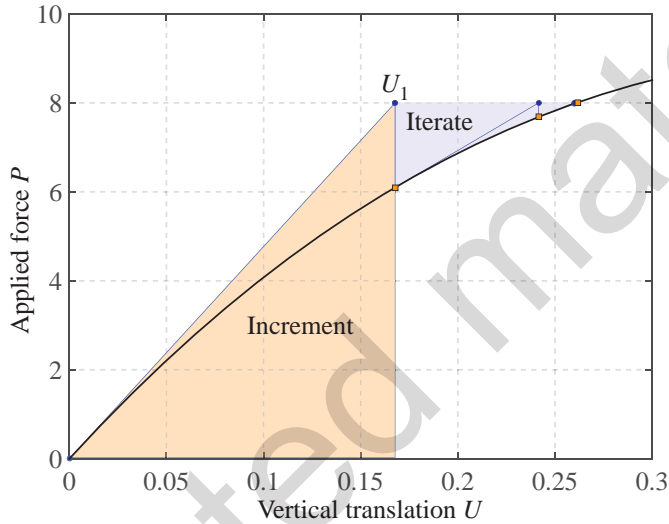


Fig. 3.5: Iterative solution algorithm for single dof truss under a single load step

Given the reference load vector \mathbf{P}_{ref} and the load factor λ the calculation steps of the NR solution algorithm are:

- 1) Set up the applied nodal force vector $\mathbf{P}_f = \lambda \mathbf{P}_{ref}$.
- 2) Make an initial guess for the solution \mathbf{U}_0 ; for a single load step $\mathbf{U}_0 = 0$ is a logical choice.
- 3) For $i = 0 \dots n$
 - a. *Structure State Determination:* determine the resisting forces $\mathbf{P}_r(\mathbf{U}_i)$ and the tangent stiffness matrix $\mathbf{K}_t(\mathbf{U}_i)$.
 - b. Determine the *nodal force unbalance or equilibrium error* $\mathbf{P}_u(\mathbf{U}_i) = \mathbf{P}_f - \mathbf{P}_r(\mathbf{U}_i)$.
 - c. Determine the correction to the previous solution estimate $\Delta\mathbf{U}_i = \mathbf{K}_t(\mathbf{U}_i) \backslash \mathbf{P}_u(\mathbf{U}_i)$.
 - d. Update the solution estimate $\mathbf{U}_{i+1} = \mathbf{U}_i + \Delta\mathbf{U}_i$.

Repeat steps (a)-(d) until the error norm is smaller than a specified tolerance.
- 4) On convergence determine the resisting forces for the final displacements.

We group the steps for the first solution correction separately from the subsequent corrections and restate the process as follows:

- 1) Set up the applied nodal force vector $\mathbf{P}_f = \lambda \mathbf{P}_{ref}$.
- 2) Make an initial guess for the solution \mathbf{U}_0 ; for a single load step $\mathbf{U}_0 = 0$ is a logical choice.
- 3) *Structure State Determination*: determine the resisting forces $\mathbf{P}_r(\mathbf{U}_0)$ and the tangent stiffness matrix $\mathbf{K}_t(\mathbf{U}_0)$.
- 4) Determine the *nodal force unbalance or equilibrium error* $\mathbf{P}_u(\mathbf{U}_0) = \mathbf{P}_f - \mathbf{P}_r(\mathbf{U}_0)$.
- 5) Determine the first correction to the initial solution estimate $\Delta\mathbf{U}_1 = \mathbf{K}_t(\mathbf{U}_0) \setminus \mathbf{P}_u(\mathbf{U}_0)$.
- 6) Update the solution estimate $\mathbf{U}_1 = \mathbf{U}_0 + \Delta\mathbf{U}_0$.
- 7) For $i = 1 \dots n$
 - a. *Structure State Determination*: determine the resisting forces $\mathbf{P}_r(\mathbf{U}_i)$ and the tangent stiffness matrix $\mathbf{K}_t(\mathbf{U}_i)$.
 - b. Determine the *nodal force unbalance or equilibrium error* $\mathbf{P}_u(\mathbf{U}_i) = \mathbf{P}_f - \mathbf{P}_r(\mathbf{U}_i)$.
 - c. Determine the correction to the previous solution estimate $\Delta\mathbf{U}_i = \mathbf{K}_t(\mathbf{U}_i) \setminus \mathbf{P}_u(\mathbf{U}_i)$.
 - d. Update the solution estimate $\mathbf{U}_{i+1} = \mathbf{U}_i + \Delta\mathbf{U}_i$.

Repeat steps (a)-(d) until the error norm is smaller than a specified tolerance.
- 8) On convergence determine the resisting forces for the final displacements.

Fig. 3.5 depicts the steps of the solution algorithm for a single load step of the shallow truss from Example 2.1. Steps (2)-(6) represent the *incrementation phase* of the algorithm that imposes the applied nodal forces \mathbf{P}_f and determines a linear correction $\Delta\mathbf{U}_1$ of the initial solution estimate \mathbf{U}_0 . If the structural response were linear, the force unbalance $\mathbf{P}_u(\mathbf{U}_1)$ between the applied forces \mathbf{P}_f and the resisting forces $\mathbf{P}_r(\mathbf{U}_1)$ would be numerically equal to zero and the subsequent iterations would not be required. In fact, we note that the force unbalance $\mathbf{P}_u(\mathbf{U}_0) = \mathbf{P}_f - \mathbf{P}_0$, where \mathbf{P}_0 are the initial forces that include the effect of element loading and support displacements.

For nonlinear structural response, as depicted in Fig. 3.5, the force unbalance $\mathbf{P}_u(\mathbf{U}_1)$ most probably exceeds the tolerance of the convergence criterion, so that *further corrections of the solution estimate* are required. This is the *iteration phase* of the nonlinear solution algorithm consisting of as many repetitions of steps 7(a)-(d) as required to satisfy the convergence criterion.

Finally, step (8) of the algorithm is conditional on the convergence of the iterations. In such case the final displacement values resulting from the iterative algorithm are *committed* to memory. These values are used for the determination of the basic element forces and the corresponding resisting forces \mathbf{P}_r are used for the determination of the support reactions and the check of global equilibrium, if necessary. This phase of the algorithm is known as *final state updating*.

The incrementation phase of the solution algorithm is also known as the *predictor phase*, while the iteration phase is also known as the *corrector phase* of the iterative solution process.

The intermediate solution estimates of the iterative algorithm are represented by square markers Fig. 3.5. The force unbalance between the applied nodal force of 8 units and the resisting force \mathbf{P}_r of each solution estimate is represented by the vertical distance between the round marker and the square marker for a particular displacement value. These markers move closer together during the iterative phase of the algorithm, until they numerically coincide. Note that the basic element forces and with them the internal element forces and support reactions correspond to the state of the structure at the

square marker. This is of considerable importance for subsequent discussions of alternative strategies for the solution of the nonlinear equilibrium equations.

3.5.3 Multi-Step Load Application

The NR algorithm of the last section has the limitation that the external forces are applied in a single load step, requiring that we have an approximate idea for the magnitude of the load factor λ that can be resisted by the structure under investigation. With this approach we obtain only a single load factor-displacement response pair, so that establishing the response under different load factors would involve repeating the process by with the same initial guess \mathbf{U}_0 each time. Because the NR iteration process is only guaranteed to converge in the "vicinity" of the solution, the distance between the initial guess \mathbf{U}_0 and the final displacement vector should not be too large. This is, however, very hard to ensure with this process. To overcome this limitation we introduce an *multi-step incremental solution strategy*.

In a multi-step incremental load analysis we apply the external forces gradually by increasing the load factor from one load step to the next. We use the solution of the preceding load step as the initial "guess" for the iterative solution algorithm of the next load step. By keeping the load factor increment small we ensure that the initial "guess" is not too distant from the solution, thus improving the chances for success of the NR algorithm significantly. In fact, if the algorithm does not converge to the solution within a specified number of iterations, we can reduce the load factor increment and try again. Even so, there is no guarantee of success, so the deployment of a variety of strategies becomes necessary for the most challenging nonlinear response problems, as will be discussed later in this chapter.

For describing the multi-step incremental load analysis we introduce the load step counter k with values $1 \dots n_{step}$ and write for the applied forces $\mathbf{P}_f^{(k)}$ at load step k

$$\mathbf{P}_f^{(k)} = \mathbf{P}_f^{(k-1)} + \Delta\lambda \mathbf{P}_{ref} \quad (3.49)$$

where $\Delta\lambda$ is the load factor increment and $\mathbf{P}_f^{(0)} = \mathbf{0}$. To identify the load and response variables at a given load step k in the following discussion we use the load step counter k in parentheses as a superscript of the corresponding variable whenever necessary.

At first we assume that the load factor increment $\Delta\lambda$ is constant so that $\Delta\lambda = \Delta\lambda_0$, with the load factor increment $\Delta\lambda_0$ specified at the beginning of the multi-step incremental analysis.

Taking advantage of the separation of the NR algorithm into a *load incrementation phase*, *an equilibrium iteration phase*, and a *final updating phase* we summarize in the following the calculation steps of the multi-step incremental analysis under the assumption that the structural model geometry and element properties as well as the reference load vector \mathbf{P}_{ref} are given at the start of the analysis. The initial load factor increment $\Delta\lambda = \Delta\lambda_0$ must also be specified.

The calculation steps are:

Start with $\mathbf{P}_f^{(0)} = \mathbf{0}$ and initial guess $\mathbf{U}^{(0)} = \mathbf{0}$.

For $k = 1 \dots n_{step}$ with given load factor $\Delta\lambda = \Delta\lambda_0$ and applied force distribution \mathbf{P}_{ref} .

- 1) **Load Incrementation:** update the applied forces $\mathbf{P}_f^{(k)} = \mathbf{P}_f^{(k-1)} + \Delta\lambda \mathbf{P}_{ref}$.
- 2) Use the solution at $k - 1$ as initial guess $\mathbf{U}_0^{(k)} = \mathbf{U}^{(k-1)}$.
- 3) *Structure State Determination:* determine $\mathbf{P}_r^{(k)} = \mathbf{P}_r(\mathbf{U}_0^{(k)})$ and $\mathbf{K}_t^{(k)} = \mathbf{K}_t(\mathbf{U}_0^{(k)})$.
- 4) Determine the nodal force unbalance $\mathbf{P}_u^{(k)} = \mathbf{P}_f^{(k)} - \mathbf{P}_r^{(k)}$.
- 5) Determine the first correction to the initial solution estimate $\Delta\mathbf{U}_0^{(k)} = \mathbf{K}_t^{(k)} \setminus \mathbf{P}_u^{(k)}$.
- 6) Update the solution estimate $\mathbf{U}_1^{(k)} = \mathbf{U}_0^{(k)} + \Delta\mathbf{U}_0^{(k)}$.
- 7) **Equilibrium Iterations**
For $i = 1 \dots n$ and constant k without superscript (k) except for \mathbf{P}_f .
 - a. *Structure State Determination:* determine $\mathbf{P}_r(\mathbf{U}_i)$ and $\mathbf{K}_t(\mathbf{U}_i)$.
 - b. Determine the nodal force unbalance $\mathbf{P}_u(\mathbf{U}_i) = \mathbf{P}_f^{(k)} - \mathbf{P}_r(\mathbf{U}_i)$.
 - c. Determine the solution correction $\Delta\mathbf{U}_i = \mathbf{K}_t(\mathbf{U}_i) \setminus \mathbf{P}_u(\mathbf{U}_i)$.
 - d. Update the solution estimate $\mathbf{U}_{i+1} = \mathbf{U}_i + \Delta\mathbf{U}_i$.
 Repeat steps (a)-(d) until the error norm satisfies the specified tolerance.
- 8) On convergence of the equilibrium iterations determine the resisting forces for the final $\mathbf{U}^{(k)}$.

The following figures show the response of the single dof shallow truss from Example 2.1. For this case the exact solution for the resisting force P_r is available in (2.26) and can be plotted in each figure. The multi-step incremental analysis terminates for all cases at $\lambda = 1$, so that the constant load factor increment $\Delta\lambda$ is equal to the inverse of the number of load steps $nstep$.

Fig. 3.6 shows two cases of incremental analysis with equilibrium iterations using a stringent check for the equilibrium error with a tolerance value of 10^{-16} . Fig. 3.6(a) results from 2 load steps with load factor increment $\Delta\lambda_0$ of 0.5 and Fig. 3.6(b) results from 4 load steps with load factor increment $\Delta\lambda_0$ of 0.25. The intermediate steps of the algorithm are depicted with round markers while a square marker is used for the solution of each load step.

It is worth noting that a large tolerance value `tol` skips iteration and moves to the application of the next load increment. *This represents a linear estimate for each load increment without iterative correction of the error of the nonlinear equilibrium equations. It is equivalent to a step of linear analysis.*

From the comparison of Fig. 3.6(b) with Fig. 3.6(a) we conclude that more iterations are required for the larger load factor increment. Moreover, larger load factor increment results in fewer load-displacement pairs and, thus, less information about the structural response evolution.

Fig. 3.7 shows two cases of incremental analysis *without equilibrium iterations*. This can be achieved with the specification of a very large tolerance value of 10^{12} for the check of the equilibrium error during iterations. Fig. 3.7(a) results from 4 load steps with load factor increment $\Delta\lambda_0$ of 0.25 and Fig. 3.7(b) results from 10 load steps with load factor increment $\Delta\lambda_0$ of 0.10. The round markers in the figure correspond to the external force-vertical translation pair of the linear solution for each load step, and the square markers to the resisting force-vertical translation pair. The basic element forces, the

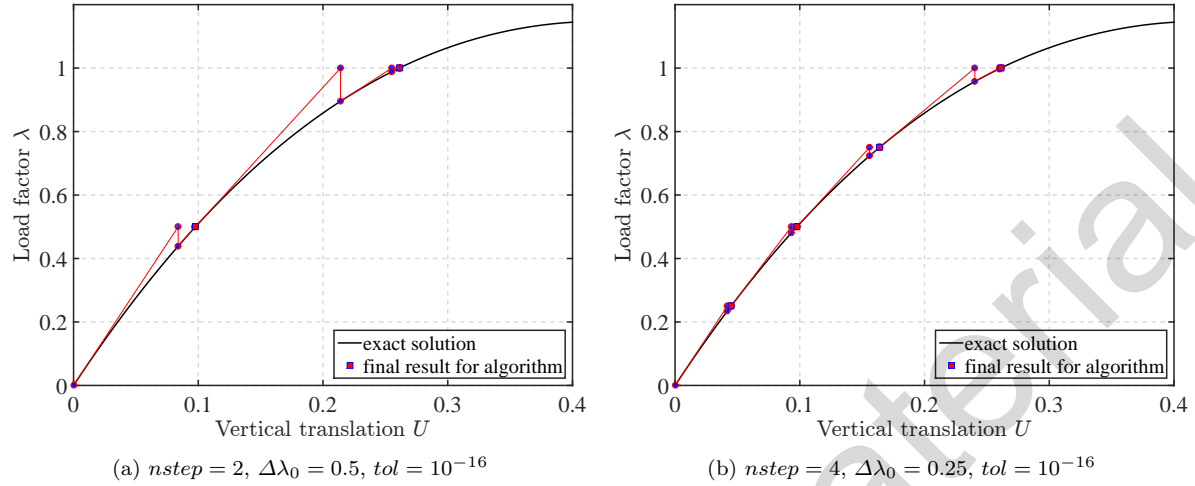
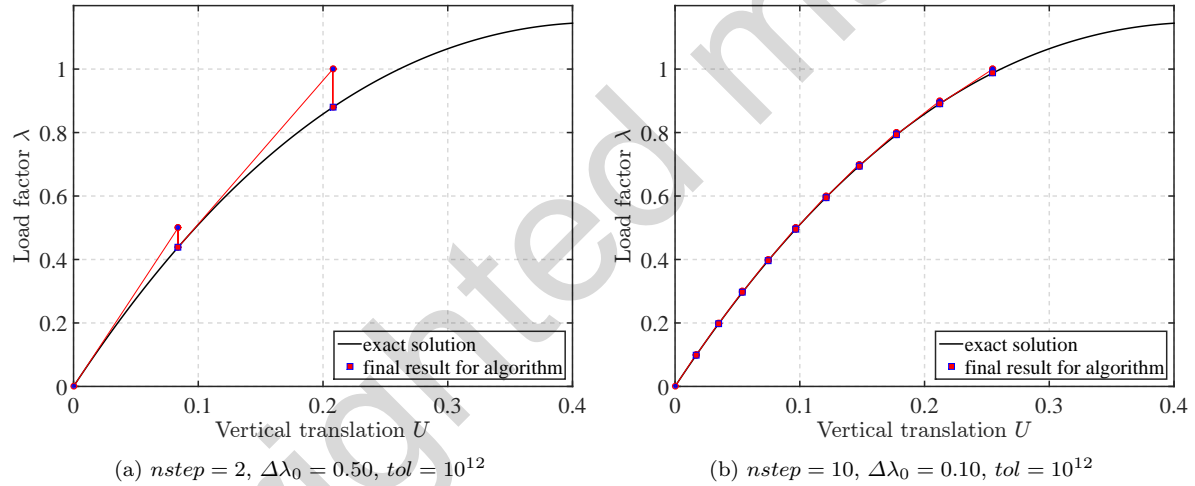


Fig. 3.6: Multi-step incremental analysis of single dof truss from Example 2.1 with equilibrium iterations

Fig. 3.7: Multi-step incremental analysis of single dof truss from Example 2.1 *without equilibrium iterations*

internal forces and the support reactions correspond to the square marker, so that the global equilibrium error from the discrepancy between the applied nodal forces and the support reactions increases with each load step, as is clear in Fig. 3.7(a). We speak of the *drift* between the applied nodal forces and the resisting forces or, in other words, of the increase of the equilibrium error during the incremental analysis. Fig. 3.7(b) shows that it is possible to minimize the drift between the applied nodal forces and the resisting forces by reducing the load factor increment. The multi-step incremental analysis without equilibrium correction is of interest in nonlinear dynamic analysis under earthquake excitation for which the step size is very small in order to capture the acceleration changes in the ground motion record. Moreover, the structural response is cyclic so that the drift between the applied and the resisting forces does not increase with the number of load steps.

3.6 Modified Newton and Quasi-Newton Methods

The Newton-Raphson algorithm requires that the current tangent stiffness matrix be used at every iteration of each load step. This ensures the *quadratic convergence* of the numerical solution estimates to the solution of each load step. Depending on the size of the problem and the available computer architecture this may be a very expensive proposition.

Consequently, the following variants to the NR algorithm have been proposed:

- 1) **Modified Newton method.** In this case the tangent stiffness matrix is not updated at every iteration but only every so often based on a criterion. Specific cases of the modified Newton algorithm involve updating the stiffness matrix only at the beginning of each load step or not updating the stiffness matrix at all. The latter case is known as initial stiffness method. If the stiffness matrix is not updated, the last triangular decomposition of the stiffness matrix is used for the solution of the equilibrium equations with significant savings in the number of operations.
- 2) **Accelerated Modified Newton method.** The convergence of the modified Newton method can be significantly improved with various acceleration schemes. A class of acceleration schemes uses Krylov subspaces to improve the solution estimate during equilibrium iterations while keeping the stiffness matrix constant during the load step. A proposal by M. Scott and G.L. Fenves in the May 2010 issue of the ASCE Journal of Structural Engineering on pp. 473-480 is implemented in OpenSees. The authors claim that it is particularly suitable for dynamic progressive collapse simulations.
- 3) **Quasi-Newton method.** Instead of using the tangent stiffness matrix secant stiffness approximations of the inverse of the stiffness matrix from the displacement vectors of previous iterations are used. Among the best known quasi-Newton methods is the BFGS method, which was originally developed for nonlinear optimization problems. For a brief description of the method consult pp. 759-761 in the book by K.J. Bathe "Nonlinear Finite Element Procedures", which has references to the original papers.

3.7 Load Factor Control

So far we have assumed that the load factor increment $\Delta\lambda$ remains constant and equal to the specified value $\Delta\lambda_0$ during the incrementation of the applied load. This has the disadvantage that the resulting displacement increments change with the state of the structure: for stiffness softening response the displacement increments get larger under increasing load with the risk that the equilibrium iterations may fail to converge as the response gets closer to the limit load of the structure. For the stiffness hardening response of cable and membrane structures the displacement increments get smaller under increasing load, thus increasing the cost of the analysis. A procedure for automatically adjusting the load factor during incremental analysis is, therefore, important for numerical stability and computational efficiency.

Furthermore, we have assumed that the applied force vector *remains constant* during the iterative phase of the algorithm. This assumption makes it impossible to determine the limit load and capture the post-peak response of the structure, as it arises for strength softening materials and nonlinear geometry effects.

In the following we turn our attention to the solution of these two problems of load factor control which are independent. Consequently, we deal first with the load factor control during incrementation and subsequently with the load factor control during equilibrium iterations. We call the former the *predictor phase*, and the latter the *corrector phase* of the nonlinear solution algorithm.

3.7.1 Load Factor Control for Predictor Phase

The key idea for adjusting the load factor during load incrementation is to relate it to the stiffness of the structure at the beginning of each load step so as to reduce the factor when the stiffness "decreases" and increase it when the stiffness "increases". Because the stiffness of a multi-dof structural model is a matrix, it is not clear how to measure the change of stiffness. One approach is to use the smallest eigenvalue, but an eigenvalue analysis is computationally expensive. A rather efficient way of judging the stiffness characteristics of a large structure is to determine the work in the direction of the reference load vector \mathbf{P}_{ref} . A measure of this work is the *stiffness parameter* S_p proposed by P. Bergan and his collaborators in a paper published in 1973¹. They define the stiffness parameter by

$$S_p = \mathbf{P}_{ref}^T \mathbf{U}_t = \mathbf{P}_{ref}^T (\mathbf{K}_t \backslash \mathbf{P}_{ref}) \quad (3.50)$$

where \mathbf{U}_t is the resulting free dof displacement vector under the reference load vector \mathbf{P}_{ref} . \mathbf{U}_t is, therefore, called the *tangential displacement vector*.

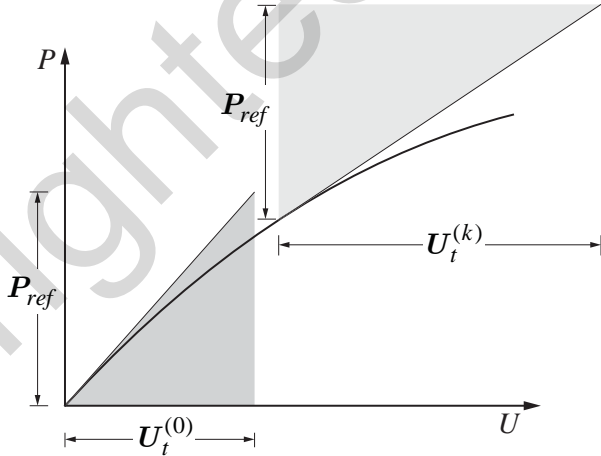


Fig. 3.8: Definition of current stiffness parameter S_p

Fig. 3.8 shows the representation of the current stiffness parameter for the nonlinear response of a one dof model. In this case the triangle area in the figure corresponds to $\frac{1}{2}S_p^{(0)}$ for the initial state, and to $\frac{1}{2}S_p^{(k)}$ for load step k . For the response of a multi-dof model a graphical representation is not possible.

For a constant reference load vector \mathbf{P}_{ref} during the incremental analysis, (3.50) shows that the value of the stiffness parameter depends *the inverse of the tangent stiffness matrix* \mathbf{K}_t . In fact, the softer

¹ P. G. Bergan, et al. (1978). "Solution techniques for nonlinear finite element problems." International Journal for Numerical Methods in Engineering 12(11), pp. 1677–1696

the response the larger the value of the tangential displacement vector, and thus the higher the stiffness parameter, as shown schematically in Fig. 3.8.

Bergan et al. (1978) proposed the following relation for adjusting the load factor increment in load step k

$$\Delta\lambda^{(k)} = \Delta\lambda^{(0)} \left[\frac{S_p^{(0)}}{S_p^{(k)}} \right]^\gamma \quad (3.51)$$

where $S_p^{(0)}$ is the stiffness parameter at the *start of the incremental analysis*, and $S_p^{(k)}$ the stiffness parameter at the *beginning of load step k*. In (3.51) we used $\Delta\lambda^{(0)}$ to refer to the initial load factor increment $\Delta\lambda_0$ for consistency with the notation that a superscript in parentheses denotes the load step.

A reasonable range for the value for exponent γ in (3.51) is from 0.8 to 1.5, with a value of 1 suitable for most cases. A higher exponent value results in a more rapid change of the load factor increment.

For any exponent value other than 1, it is necessary to use the absolute value of the stiffness parameter ratio in (3.51). Because the sign of the stiffness parameter plays an important role in reversing the load factor increment for strength softening problems like the snap-through instability problem, we introduce the sign of the stiffness parameter in equation (3.51) and obtain

$$\Delta\lambda^{(k)} = \Delta\lambda^{(0)} \text{sign} \left[S_p^{(k)} \right] \left| \frac{S_p^{(0)}}{S_p^{(k)}} \right|^\gamma$$

For the case that $\gamma = 1$ (3.51) simplifies to

$$\Delta\lambda^{(k)} = \Delta\lambda^{(0)} \left[\frac{S_p^{(0)}}{S_p^{(k)}} \right] \quad (3.52)$$

For accommodating the change of the load factor increment during the predictor phase of the multi-step incremental analysis algorithm we need to modify the order of steps (1)-(6) in the algorithm on pp. 75 and insert the determination of the load factor increment $\Delta\lambda^{(k)}$. To explain the required changes we modify first the load increment in (3.49) to

$$\mathbf{P}_f^{(k)} = \mathbf{P}_f^{(k-1)} + \Delta\lambda^{(k)} \mathbf{P}_{ref} \quad (3.53)$$

The displacement correction of the linear predictor phase of the algorithm can then be written as

$$\begin{aligned} \Delta\mathbf{U}_0^{(k)} &= \mathbf{K}_t^{(k)} \backslash \mathbf{P}_u^{(k)} = \mathbf{K}_t^{(k)} \backslash \left[\mathbf{P}_f^{(k)} - \mathbf{P}_r^{(k)} \right] \\ &= \mathbf{K}_t^{(k)} \backslash \left[\mathbf{P}_f^{(k-1)} + \Delta\lambda^{(k)} \mathbf{P}_{ref} - \mathbf{P}_r^{(k)} \right] \\ &= \mathbf{K}_t^{(k)} \backslash \left[\mathbf{P}_f^{(k-1)} - \mathbf{P}_r^{(k)} \right] + \Delta\lambda^{(k)} \left[\mathbf{K}_t^{(k)} \backslash \mathbf{P}_{ref} \right] \\ &= \Delta\mathbf{U}_r + \Delta\lambda^{(k)} \mathbf{U}_t^{(k)} \end{aligned} \quad (3.54)$$

$\Delta\mathbf{U}_r$ is the displacement correction for the equilibrium error under the forces at the end of the last load step, which is tolerance related, and $\mathbf{U}_t^{(k)}$ are the tangential displacements for the current load step.

The incrementation phase of the algorithm on pp. 75 is then modified to the following steps:

Start with $\mathbf{P}_f^{(0)} = \mathbf{0}$ and initial guess $\mathbf{U}^{(0)} = \mathbf{0}$.

For $k = 1 \dots nstep$ with given load factor $\Delta\lambda = \Delta\lambda_0$ and applied force distribution \mathbf{P}_{ref} .

- 1) **Load Incrementation.** Use the solution at $k - 1$ as initial guess $\mathbf{U}_0^{(k)} = \mathbf{U}^{(k-1)}$.
- 2) Determine $\mathbf{P}_r^{(k)} = \mathbf{P}_r(\mathbf{U}_0^{(k)})$ and $\mathbf{K}_t^{(k)} = \mathbf{K}_t(\mathbf{U}_0^{(k)})$.
- 3) Determine $\mathbf{U}_t^{(k)} = \mathbf{K}_t^{(k)} \setminus \mathbf{P}_{ref}$ and $\Delta\mathbf{U}_r = \mathbf{K}_t^{(k)} \setminus (\mathbf{P}_f^{(k-1)} - \mathbf{P}_r^{(k)})$.
- 4) Use the current stiffness parameter $S_p^{(k)} = \mathbf{P}_{ref}^T \mathbf{U}_t^{(k)}$ to determine $\Delta\lambda^{(k)}$ with (3.52) and update the applied force vector $\mathbf{P}_f^{(k)} = \mathbf{P}_f^{(k-1)} + \Delta\lambda^{(k)} \mathbf{P}_{ref}$.
- 5) Determine $\Delta\mathbf{U}_0^{(k)} = \Delta\mathbf{U}_r + \Delta\lambda^{(k)} \mathbf{U}_t^{(k)}$.
- 6) Update the solution $\mathbf{U}_1^{(k)} = \mathbf{U}_0^{(k)} + \Delta\mathbf{U}_0^{(k)}$.

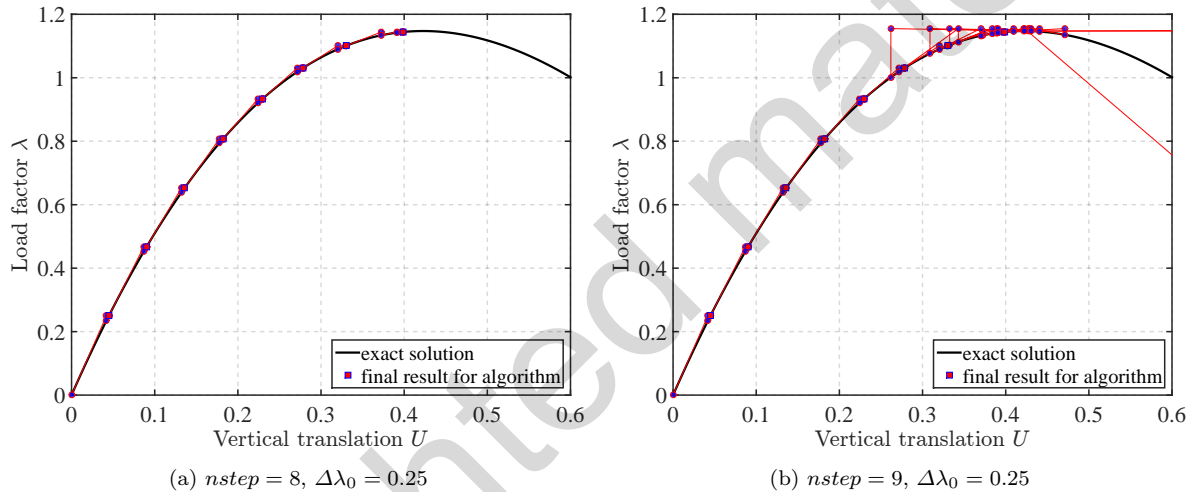


Fig. 3.9: Incremental analysis of single dof truss from Example 2.1 with load factor control during incrementation

With load factor control during incrementation and an appropriately small initial load factor increment $\Delta\lambda_0$ the multi-step incremental analysis of the shallow, single dof truss from Example 2.1 approaches the snap-through limit load in Fig. 3.9(a). Another increment, however, results in the failure of the iterative algorithm with iterations "flip-flopping" about the vertical translation corresponding to the snap-through limit load factor in Fig. 3.9(b). This happens because the load factor increment remains unchanged during iterations, so that the iterative algorithm is unable to advance past the point of maximum load.

3.7.2 Load Factor Control during Equilibrium Corrections

The multi-step incremental analysis of the single dof shallow truss in Fig. 3.9 makes it clear that it is not possible to establish the exact snap-through limit load of the shallow truss let alone get past it by controlling the load factor only during the predictor phase of the algorithm. For determining the limit load and for tracing the post-peak response of structures with strength loss caused by instability or material failure *load factor control during iterations is required*.

To accommodate load factor control during iterations we relax the constraint that the applied force vector $\mathbf{P}_f^{(k)}$ remain constant during the equilibrium iterations of the nonlinear solution algorithm on

pp. 80. We express the variation of the applied nodal forces \mathbf{P}_f during the equilibrium iterations with

$$\mathbf{P}_{f,i}^{(k)} = \mathbf{P}_{f,i-1}^{(k)} + \Delta\lambda_i^{(k)} \mathbf{P}_{ref} \quad (3.55)$$

with subscript i denoting the equilibrium iteration counter consistent with the notation of the algorithm on pp. 75. After noting that all nodal forces in (3.55) refer to load step k with $\mathbf{P}_{f,0}^{(k)} = \mathbf{P}_f^{(k)}$ in (3.53) we write

$$\mathbf{P}_{f,i} = \mathbf{P}_{f,i-1} + \Delta\lambda_i \mathbf{P}_{ref} \quad (3.56)$$

The displacement correction $\Delta\mathbf{U}_i$ of the equilibrium correction phase of the algorithm on pp. 80 can then be written as

$$\begin{aligned} \Delta\mathbf{U}_i &= \mathbf{K}_t(\mathbf{U}_i) \setminus \mathbf{P}_u(\mathbf{U}_i) = \mathbf{K}_{t,i} \setminus (\mathbf{P}_{f,i} - \mathbf{P}_{r,i}) \\ &= \mathbf{K}_{t,i} \setminus (\mathbf{P}_{f,i-1} + \Delta\lambda_i \mathbf{P}_{ref} - \mathbf{P}_{r,i}) \\ &= \mathbf{K}_{t,i} \setminus (\mathbf{P}_{f,i-1} - \mathbf{P}_{r,i}) + \Delta\lambda_i (\mathbf{K}_{t,i} \setminus \mathbf{P}_{ref}) \\ &= \Delta\mathbf{U}_{r,i} + \Delta\lambda_i \mathbf{U}_{t,i} \end{aligned} \quad (3.57)$$

where $\Delta\mathbf{U}_{r,i}$ is the displacement correction for the equilibrium error under the forces at the end of the last iteration, and $\mathbf{U}_{t,i}$ is the tangential displacement vector for the current iteration.

Several proposals are available in the literature for controlling the load factor increment $\Delta\lambda_i$ according to (3.57). We present only a few with the comment that differences between these arise only in special cases.

- 1) Displacement control of particular dof m (m component in parentheses)

$$\text{from } \Delta\mathbf{U}_{i(m)} = 0 = \Delta\mathbf{U}_{r,i(m)} + \Delta\lambda_i \mathbf{U}_{t,i(m)} \rightarrow \Delta\lambda_i = -\frac{\Delta\mathbf{U}_{r,i(m)}}{\mathbf{U}_{t,i(m)}}$$

- 2) Minimum of the displacement increment norm².

$$\text{from } \frac{\partial}{\partial \Delta\lambda_i} (\Delta\mathbf{U}_i^T \Delta\mathbf{U}_i) = 0 \rightarrow \Delta\lambda_i = -\frac{\mathbf{U}_{t,i}^T \Delta\mathbf{U}_{r,i}}{\mathbf{U}_{t,i}^T \mathbf{U}_{t,i}}$$

This method is used in the solution script `S_One_Iteration`.

- 3) Constant external work³.

$$\text{from } \mathbf{P}_{ref}^T \Delta\mathbf{U}_i = 0 \rightarrow \Delta\lambda_i = -\frac{\mathbf{P}_{ref}^T \Delta\mathbf{U}_{r,i}}{\mathbf{P}_{ref}^T \mathbf{U}_{t,i}}$$

- 4) Arc-length control⁴. A quadratic equation results for $\Delta\lambda_i$.

² Chan, S. L. (1988). "Geometric and material non-linear analysis of beam-columns and frames using the minimum residual displacement method." International Journal for Numerical Methods in Engineering 26, pp. 2657-2669

³ Powell, G. and J. Simons (1981). "Improved iteration strategy for nonlinear structures." International Journal for Numerical Methods in Engineering 17, pp. 1455-1467

⁴ Crisfield, M. A. (1981). "A Fast Incremental/Iterative Solution Procedure that Handles 'Snap Through'." Computers and Structures 13, pp. 55-62

Further details on load factor control strategies can be found in a summary paper⁵. Methods 1 and 4 are the best known leading to the somewhat misleading name "displacement control method" or "arc-length control method" for all load factor control methods. This text uses the name *load factor control method*, which also encompasses methods 2 and 3 as well as other proposals.

With the modification of (3.57) for the load factor increment during the equilibrium iteration phase of the nonlinear solution algorithm in 80 the post-peak response of the shallow truss can be traced, as Fig. 3.10(a) shows. The load factor control during iterations is based on the minimum of the displacement increment norm. In the figure the response is limited to 15 load steps which suffice to demonstrate the ability of the algorithm to trace the post-peak response of the shallow truss.

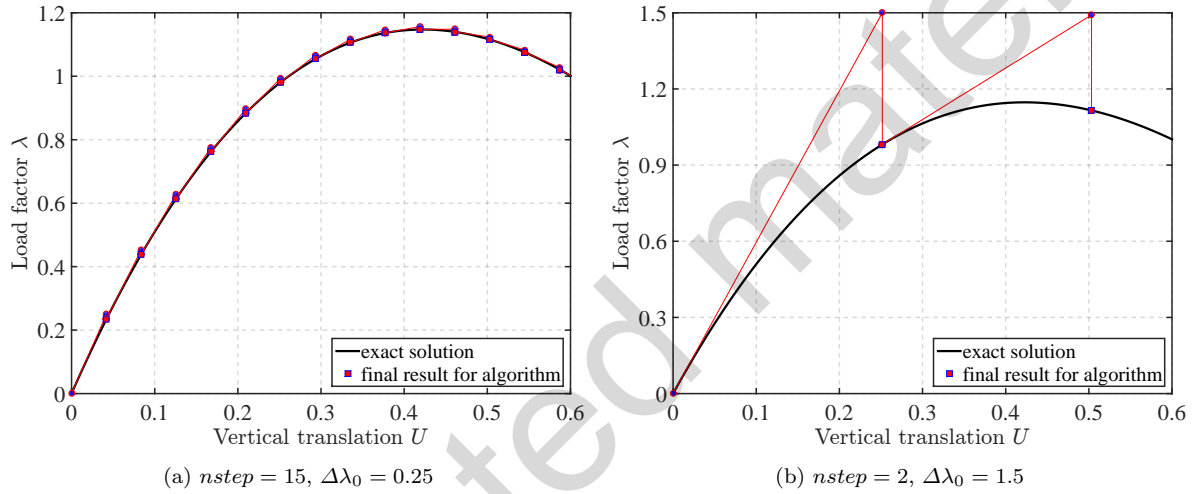


Fig. 3.10: Incremental analysis of single dof truss from Example 2.1 with load factor control

Fig. 3.10(b) shows that for the single dof problem the load factor control criterion of minimizing the displacement increment norm amounts to maintaining the displacement of the free dof constant during iterations. The figure also illustrates that the choice of the initial load factor $\Delta\lambda_0$ is no longer critical for convergence for this problem.

3.8 Convergence Criterion

It is possible to check the convergence of the equilibrium iterations either with the Euclidean norm of the force unbalance vector at iteration i $\|\mathbf{P}_u(\mathbf{U}_i)\| \leq \text{tol}$, or with the Euclidean norm of the displacement correction $\|\Delta\mathbf{U}_i\| \leq \text{tol}$. In such case it is better to use relative force or displacement measures by dividing with a reference value such as the reference force vector or the total displacement

$$\frac{\|\mathbf{P}_u\|}{\|\mathbf{P}_{ref}\|} \leq \text{tol} \quad \text{or} \quad \frac{\|\Delta\mathbf{U}_i\|}{\|\mathbf{U}_i\|} \leq \text{tol}$$

For frames the force vector contains forces and moments and the displacement vector contains translations and rotations whose magnitude may be significantly different depending on the units used. To

⁵ Clarke, M. J. and G. J. Hancock (1990). "A study of incremental-iterative strategies for non-linear analyses." Int. Journ. Num. Meth. Engrg. 29, pp. 1365-1391

overcome this problem it is strongly recommended to use the work increment to check convergence. The convergence criterion for iteration i then is

$$\frac{\Delta \mathbf{U}_i^T \mathbf{P}_{u,i}}{\Delta \mathbf{U}_0^T \mathbf{P}_{u,0}} \leq \text{tol} \quad (3.58)$$

where subscript 0 refers to the variable value after the linear predictor step. **FEDEASLab** uses the work increment criterion to check convergence. An appropriate tolerance value for this criterion is $\text{tol} = 10^{-16}$ in (3.58).

3.9 Implementation of Nonlinear Solution Strategy in **FEDEASLab**

The discussion in this chapter makes clear that the efficient, modular and user friendly implementation of solution methods for determining the nonlinear response of structural models is based on the following considerations:

- 1) The principle of linear superposition for load combination does not hold under nonlinear response. Consequently, the spatial distribution of each load type needs to be stored. Similarly, the history of load application needs to be stored for each load pattern.
- 2) The incremental nonlinear response requires that the state of the structure be saved from one step to the next including element history variables for path dependent nonlinear material response.
- 3) The iterative solution algorithm needs to keep track of displacement increments, load factor variations. It also needs to allow for the flexibility of modifying the solution strategy by updating the current stiffness matrix or not as well as updating the load factor increment or not depending on user instructions.

To address these needs three new data structures join the data structure **Model** with model geometry information and the data structure **ElementData** with element property information in **FEDEASLab**:

- 1) **Loading**: the fields of this data structure hold load and displacement patterns and load and acceleration time histories.
- 2) **State**: the fields of this data structure hold information about the current state of the structure, such as current stiffness, global dof displacements and their increments, as well as information about the element history variables for tracing path dependent response.
- 3) **SolStrat**: the fields of this data structure hold variables for controlling the iterative solution strategy for the nonlinear equilibrium equations of the structural model.

Finally, a sixth data structure **Post** contains information about the structure and the element response to be used for *post-processing*: free dof displacements, basic element forces and deformations, plastic deformations, etc.

3.9.1 Loading

In linear elastic analysis the principle of linear superposition holds, so that a single applied nodal force vector suffices.

In nonlinear analysis the principle does not hold, so that the spatial distribution of each load type needs to be stored separately in a **Loading** data structure. The latter also includes load time histories for

the application of multiple loads during the incremental analysis. The data structure loading is created by the function `Create>Loading` with the syntax is: `Loading = Create>Loading (Model, Pe, Ue)`. `Pe` is an array of the form `nnum,dir,patnum` for the specification of the applied nodal forces with `nnum` the node number, `dir` the direction of the applied load in the order, force in X , Y and Z (if present), followed by moment about X , Y and Z (if present), and `patnum` the applied load pattern id. `Ue` is an array of similar form with the array `Pe` for the imposed displacements at the restrained dofs.

3.9.2 State of the Structure

In linear elastic analysis by the displacement method of analysis the response of the structural model is described by the independent dof displacements \mathbf{U} .

In nonlinear analysis displacement increments from the solution of the last load step as well as displacement increments from the last iteration need to be stored. In transient analysis free dof velocities and accelerations also need to be stored. Finally, other nodal response variables may be useful in applications, e.g. temperature for thermal analysis.

To store all these response variables **FEDEASLab** uses the data structure `State`. `State` also holds the stiffness matrix `K` in fields `Kf` and `Kfd`, its LU decomposition in fields, `KL`, `KU`, `KP`, and element history variables in fields `Past` and `Pres`.

Finally, `State` also holds the real or pseudo-response time in field `Time`, the current load factor(s) λ in field `lambda`, the resisting forces `Pr` in field `Pr` and the element response in field `Elem`. The latter is a cell array with information about the current state of element `el` in the field `Elem{el}`.

3.9.3 Control of Iterative Solution

In linear elastic analysis by the displacement method of analysis the applied nodal forces and support displacements can be applied in a single load step. Because the governing equilibrium equations are *linear* in the independent dof displacements \mathbf{U} , a direct solution is possible *without iteration*.

In nonlinear analysis by the displacement method of analysis a *multi-step incremental analysis* for the applied nodal forces and support displacements is required. Because the governing equilibrium equations are *nonlinear* in the independent dof displacements \mathbf{U} , *an iterative solution algorithm is required*.

The preceding figures demonstrate that the iterative solution algorithm can take many forms. The particular selection depends on the fields of data structure `SolStrat`.

The information in `SolStrat` is organized in five fields:

- 1) `ConvFlag`: true (1) or false (0) if the convergence criterion is met.
- 2) `IncrStrat`: contains subfields for the incrementation phase of the solution algorithm. Those relevant for the basic case of incremental static analysis are:
 - a. `Dlam0`: initial load factor increment(s).
 - b. `StifUpdt`: 'yes' or 'no'.
 - c. `LFCtrl`: 'yes' or 'no'.
- 3) `IterStrat`: contains subfields for the iteration phase of the solution algorithm. Those relevant for this text are:
 - a. `tol`: convergence tolerance.
 - b. `maxiter`: maximum number of iterations before giving up

- c. **StifUpdt**: 'yes' or 'no'.
 - d. **LFCtrl**: 'yes' or 'no'.
- 4) **Hist**: not relevant for this course.

3.9.4 Functions and Scripts for Iterative Solution

The different stages of the iterative solution algorithm for the nonlinear equilibrium equations of the structural model are implemented in 6 separate **FEDEASLab** functions: **Initialize_State**, **Initialize_SolStrat**, **Initialize**, **Increment**, **Iterate**, **Update_State**.

These take one or more arguments consisting of **Model**, **ElemData**, **Loading**, **State**, **SolStrat** and return either **State** or **SolStrat** or both.

For ease of use in this course these functions are "wrapped" in 4 scripts. The scripts check for the existence of one or more of the following variables in the Matlab® workspace and set the value of the corresponding variables of the data structure **SolStrat**: **Dlam0**, **maxiter**, **tol**, **StifUpdt**, **LFCtrl**.

Specifically:

- 1) **S_Initialize**: the script checks for the existence of **Dlam0**, **maxiter**, **tol**, and **LFCtrl** and calls the function **Initialize_SolStrat** to initialize the solution strategy data structure with default values and overwrite these with values specified by the user; then it calls the function **Initialize_State** to initialize the state of the structural model with zero displacements and finally calls the function **Initialize** for determining the initial stiffness and setting up load factor control parameters, if **LFCtrl** = 'yes'. The script also calls the function **Structure** for determining and storing the initial response values of the elements in **Post** for later post-processing.
- 2) **S_Increment**: the script checks for the existence of **Dlam0**, **StifUpdt** and **LFCtrl**, overwrites the corresponding variables in the field **IncrStrat** of the data structure **SolStrat** and calls the function **Increment**.
- 3) **S_Iterate**: the script checks for the existence of **maxiter**, **tol**, **StifUpdt** and **LFCtrl**, overwrites the corresponding variables in the field **IterStrat** of the data structure **SolStrat** and calls the function **Iterate**.
- 4) **S_Update_State**: the script calls the function **Update_State**, saves output information in the data structure **Post**, and updates the plot counter.

Fig. 3.11-Fig. 3.19 show the scripts corresponding to the multi-step incremental analysis cases that were discussed in Section 3.5 and Section 3.7. To facilitate the understanding of the scripts the resulting intermediate steps and the final result of the corresponding iterative solution strategy are shown in the figure on the right. For brevity of notation the variable name **ConvFlag** is used in lieu of the actual variable name **SolStrat.ConvFlag**.

It is worth noting that to bypass the phase of iterative equilibrium corrections one can either specify a very large tolerance for the convergence criterion in Fig. 3.13, or do not invoke the script **S_Iterate** in Fig. 3.14 and Fig. 3.15.

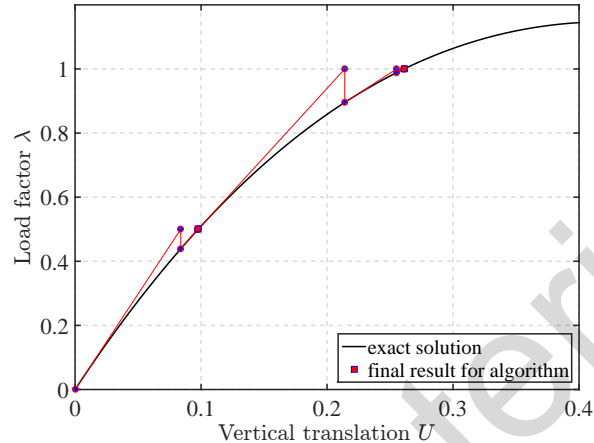
```

nstep    = 2;
Dlam0   = 1/nstep;
tol     = 1e-16;
maxiter = 10;

S_Initialize

for k = 1:nstep
  S_Increment;
  S_Iterate;
  if (ConvFlag)
    S_Update_State;
end
end

```



(a) Except from script file

(b) Intermediate steps and result of solution strategy

Fig. 3.11: Response of single dof shallow truss of Fig. 2.13 with classical NR strategy

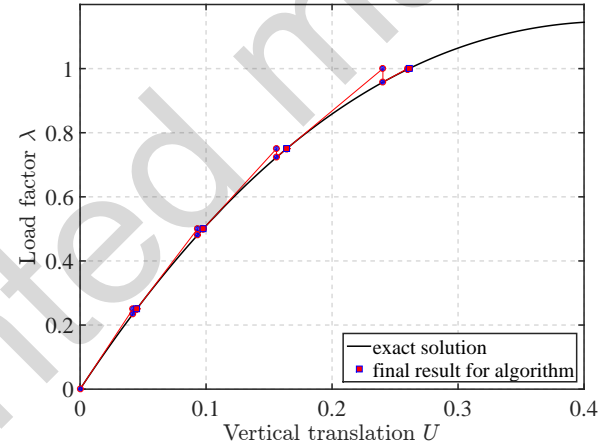
```

nstep    = 4;
Dlam0   = 1/nstep;
tol     = 1e-16;
maxiter = 10;

S_Initialize

for k = 1:nstep
  S_Increment;
  S_Iterate;
  if (ConvFlag)
    S_Update_State;
end
end

```



(a) Except from script file

(b) Intermediate steps and result of solution strategy

Fig. 3.12: Response of single dof shallow truss of Fig. 2.13 with classical NR strategy

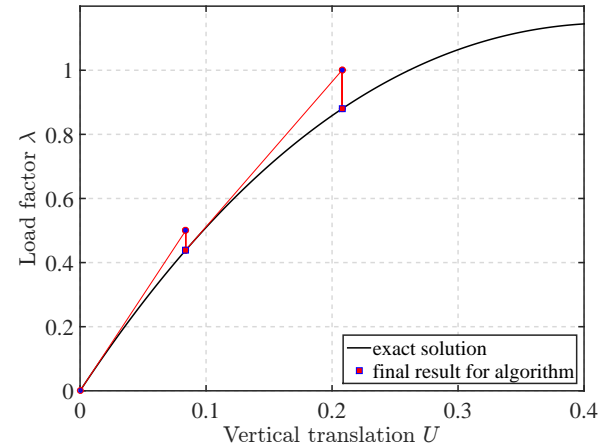
```

nstep    = 2;
Dlam0   = 1/nstep;
tol     = 1e+16;
maxiter = 10;

S_Initialize

for k = 1:nstep
  S_Increment;
  S_Iterate;
  if (ConvFlag)
    S_Update_State;
end
end

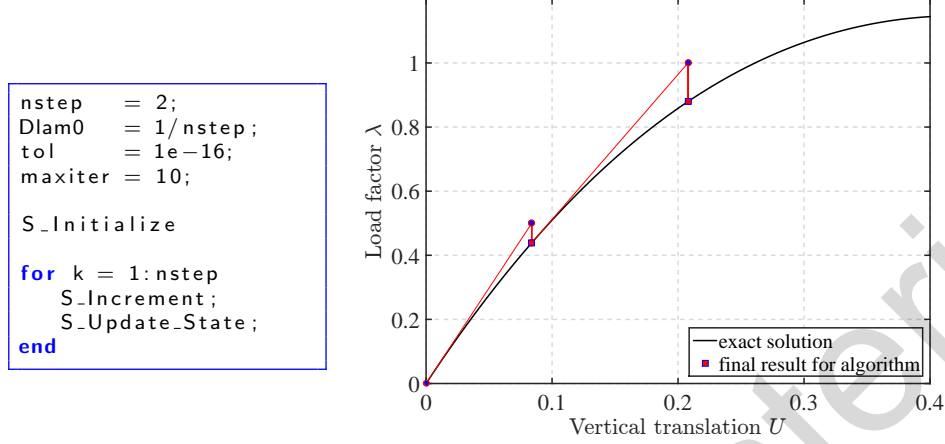
```



(a) Except from script file

(b) Intermediate steps and result of solution strategy

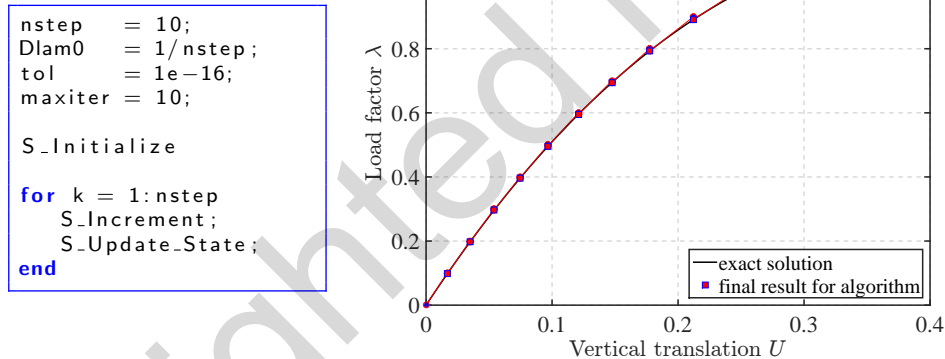
Fig. 3.13: Response of single dof shallow truss of Fig. 2.13 without equilibrium iterations



(a) Except from script file

(b) Intermediate steps and result of solution strategy

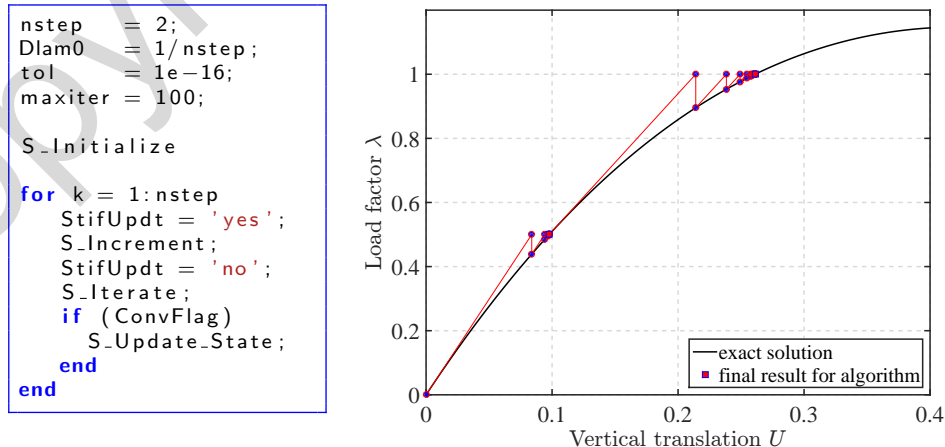
Fig. 3.14: Response of single dof shallow truss of Fig. 2.13 without equilibrium iterations



(a) Except from script file

(b) Intermediate steps and result of solution strategy

Fig. 3.15: Response of single dof shallow truss of Fig. 2.13 without equilibrium iterations



(a) Except from script file

(b) Intermediate steps and result of solution strategy

Fig. 3.16: Response of single dof shallow truss of Fig. 2.13 with constant stiffness during iterations

```

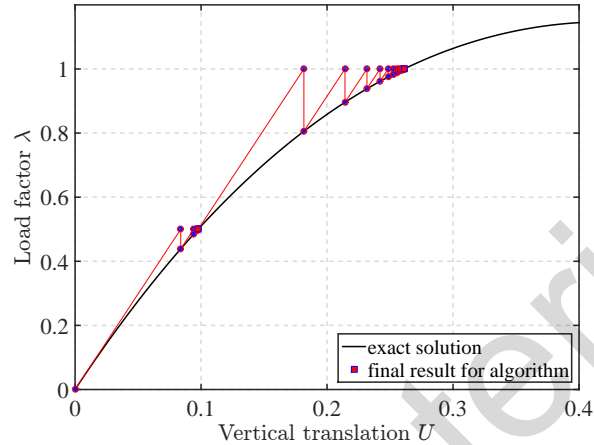
nstep    = 2;
Dlam0   = 1/nstep;
tol     = 1e-16;
maxiter = 100;

S_Initialize

for k = 1:nstep
    StifUpdt = 'no';
    S_Increment;
    StifUpdt = 'no';
    S_Iterate;
    if (ConvFlag)
        S_Update_State;
    end
end

```

(a) Except from script file



(b) Intermediate steps and result of solution strategy

Fig. 3.17: Response of single dof shallow truss of Fig. 2.13

```

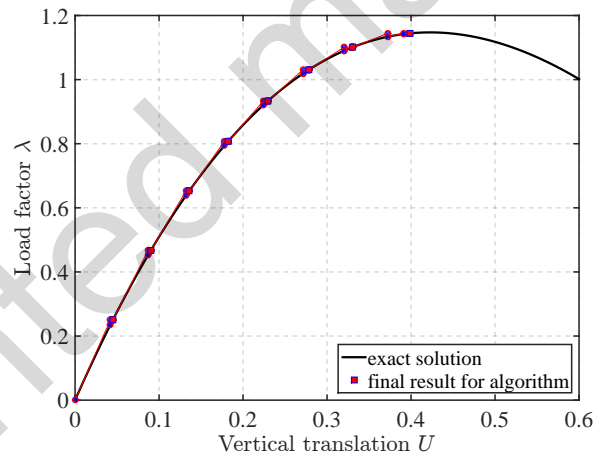
nstep    = 8;
Dlam0   = 0.25;
tol     = 1e-16;
maxiter = 10;

LFCtrl = 'yes';
S_Initialize

for k = 1:nstep
    LFCtrl = 'yes';
    S_Increment;
    LFCtrl = 'no';
    S_Iterate;
    if (ConvFlag)
        S_Update_State;
    end
end

```

(a) Except from script file



(b) Intermediate steps and result of solution strategy

Fig. 3.18: Response of single dof shallow truss of Fig. 2.13

```

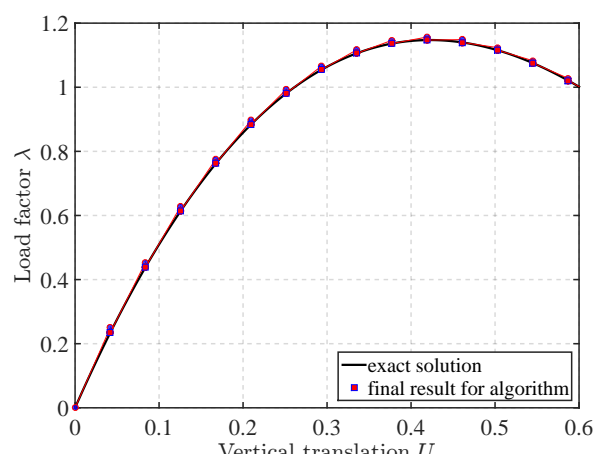
nstep    = 14;
Dlam0   = 0.25;
tol     = 1e-16;
maxiter = 10;

LFCtrl = 'yes';
S_Initialize

for k = 1:nstep
    LFCtrl = 'yes';
    S_Increment;
    LFCtrl = 'yes';
    S_Iterate;
    if (ConvFlag)
        S_Update_State;
    end
end

```

(a) Except from script file



(b) Intermediate steps and result of solution strategy

Fig. 3.19: Response of single dof shallow truss of Fig. 2.13

Chapter 4

Nonlinear Geometry of Plane Frames

4.1 Introduction

In Chapter 2 we introduced key concepts of structural response under nonlinear geometry with the help of the Green-Lagrange truss element. We discussed the effect of tensile prestressing in stiffening the structural response, and the phenomenon of structural instability under a compressive axial force. In this chapter we investigate the nonlinear geometry effects of two-dimensional frame elements with emphasis on instability phenomena under compressive axial forces.

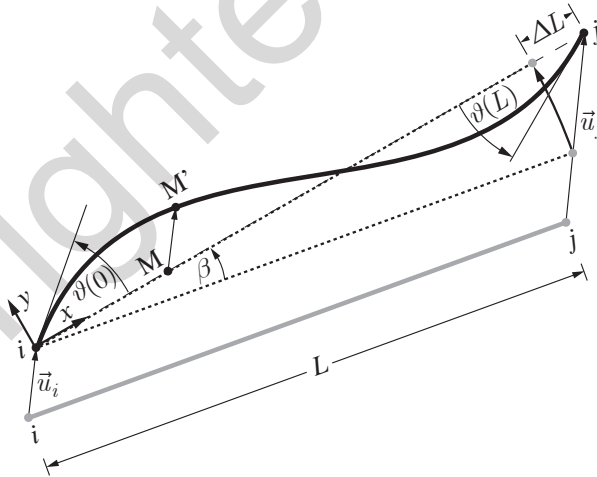


Fig. 4.1: Corotational basic system for element kinematics

We base the derivation for the nonlinear geometry of plane frame elements on the *corotational formulation*. This approach postulates that the large displacement kinematics of the element can be decomposed into the kinematics relative to a reference frame x - y that follows the element as it deforms, and the rigid body motion of this frame. Fig. 4.1 shows the x -axis of the corotational reference frame lining up with the element chord following its translation and rotation. The y -axis of the reference frame is normal to the x -axis so as to form a right handed Cartesian coordinate system with the z -axis pointing towards the viewer. The reference frame is called the *basic system*.

With reference to Fig. 4.1 we recall the discussion in Section 2.1 about element kinematics vs. structural kinematics: the former addresses the relation between the axial strain and curvature of the element axis relative to the corotational reference frame, while the latter address the relation between the element deformations \mathbf{v} and the end displacements \mathbf{u} in the global reference system.

It is convenient to assume that the strain and curvature are small relative to the reference frame, so as to keep the element kinematics linear, but this is not necessary, as will be discussed subsequently. With linear element kinematics the effect of large displacements is accounted for only in the relation between the element deformations \mathbf{v} and the end displacements \mathbf{u} in the global reference system. This is very convenient from the implementation standpoint because different plane frame element types can use the same transformation of the end variables for the inclusion of nonlinear geometry effects under large displacements.

There is a large body of work on the nonlinear kinematics of the plane frame element in the basic system and we pursue this briefly in this chapter not only for reference to alternative approaches, but also for deriving the discretization requirements for neglecting the nonlinear kinematics of the plane frame element in the basic system.

The corollary to the assumption of nonlinear deformations in the basic element system is that the equilibrium needs to be satisfied in the deformed element configuration. In this case Fig. 4.2 shows that the axial basic element force \mathbf{q}_1 affects the bending moment $M(x)$ and, consequently, the flexural stiffness coefficients of the basic stiffness matrix \mathbf{k} . This is a case of *nonlinear element statics*.

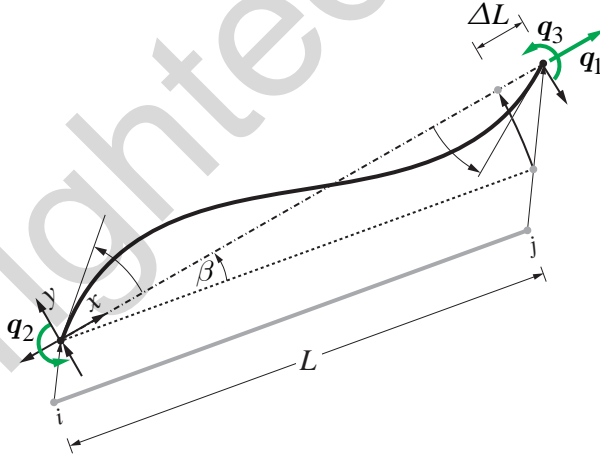


Fig. 4.2: Nonlinear statics for basic element system

Fig. 4.2 also shows the equilibrium of the basic system and the transformation of the element end forces from the basic to the global reference system requires that the change of element length ΔL and the rotation of the element chord through angle β be accounted for. This is a case of *nonlinear structural statics*.

In summary we distinguish two nonlinear geometry effects for the plane frame element:

- 1) The effect of the axial basic force \mathbf{q}_1 on the flexural response of the basic system relative to the corotational frame. This effect derives from the kinematic and static relations of the element being nonlinear.

- 2) The effect of the nonlinear geometric transformation for the rigid body translation and rotation of the basic system involving a nonlinear kinematic relation between the element deformations \mathbf{v} and end displacements \mathbf{u} (nonlinear structural kinematics) while also accounting for the change of length ΔL and the chord rotation β in the equilibrium relations between the basic element forces \mathbf{q} and the element end forces \mathbf{p} in the global reference system.

The first effect is related to the relative distance of the deformed element shape from the *element chord* and is called the *element geometry effect* in the following. *If this distance is significant relative to the element length L , the nonlinear kinematic and static relations should be included in the derivation of the element force-deformation relation. If this distance is small relative to the element length L , then it suffices to consider linear kinematic and static relations; these result in the force-deformation relations of linear analysis for the plane frame element.*

The second effect is related to the relative translations of the element ends and is called the *chord geometry effect*. If the relative translations of the element ends are significant relative to the element length, the relation between the element deformations \mathbf{v} and the element end displacements \mathbf{u} is nonlinear, as is the relation between the basic element forces \mathbf{q} and the end forces \mathbf{p} . We have already encountered this effect in the study of the nonlinear geometry of the Green-Lagrange truss element in Chapter 2. If the relative translations of the element ends are small relative to the element length, the structural kinematic and static relations are linear.

In classical structural analysis, which treats structural models without subdivision of structural members into elements, the first effect is known as *P- δ* or *little P-delta effect*, while a simple approximation of the second effect is known as *P- Δ* or *big P-Delta effect*.

This terminology is confusing for *discrete structural models with structural members subdivided into multiple elements*. To avoid ambiguity this text makes use of the following terminology with reference to an element of the discrete structural model and not a structural member of the structure:

- The term *P- δ* geometry refers to the nonlinear element geometry effect.
- The term *P- Δ* refers to the approximate method for the nonlinear chord geometry effect.
- The accurate treatment of nonlinear structural kinematics and statics is called nonlinear chord geometry effect.

In the next section we review the linear kinematics and statics of a plane frame element and summarize the resulting deformation force-relations for linear elastic material response. Subsequently, we extend this study to plane frame element with *moderate deformations* relative to the reference frame.

4.2 Basic Force-Deformation Relations for Linear Element Geometry

4.2.1 Deformation-Force Relation for Linear Elastic Material

We summarize briefly the relations from Linear Structural Analysis. From

$$\begin{aligned}\varepsilon_a(x) &= \frac{du_x}{dx} = u'_x \\ \vartheta(x) &= \frac{du_y}{dx} = u'_y\end{aligned}\tag{4.1}$$

it follows

$$\begin{aligned}\mathbf{v}_1 &= \int_0^L \varepsilon_a(x) dx \\ \mathbf{v}_2 &= - \int_0^L \left(1 - \frac{x}{L}\right) \kappa(x) dx \quad \rightarrow \quad \mathbf{v} = \int_0^L \mathbf{b}^T(x) \mathbf{e}(x) dx \\ \mathbf{v}_3 &= \int_0^L \left(\frac{x}{L}\right) \kappa(x) dx\end{aligned}\tag{4.2}$$

where the section deformation vector $\mathbf{e}(x)$ for the Euler-Bernoulli plane frame element theory consists of the axial strain at the reference axis $\varepsilon_a(x)$ and the curvature $\kappa(x)$, because shear deformations are neglected. Details of the derivation are available in Chapter 3 of the text on Linear Structural Analysis.

The static relations between the internal forces at a section x and the basic element forces \mathbf{q} can be set up either from the equilibrium of the left free body of the plane frame element in Fig. 4.3

$$N(x) = \mathbf{q}_1 = \text{const} \tag{4.3a}$$

$$M(x) = -\mathbf{q}_2 \left(1 - \frac{x}{L}\right) + \mathbf{q}_3 \frac{x}{L} \tag{4.3b}$$

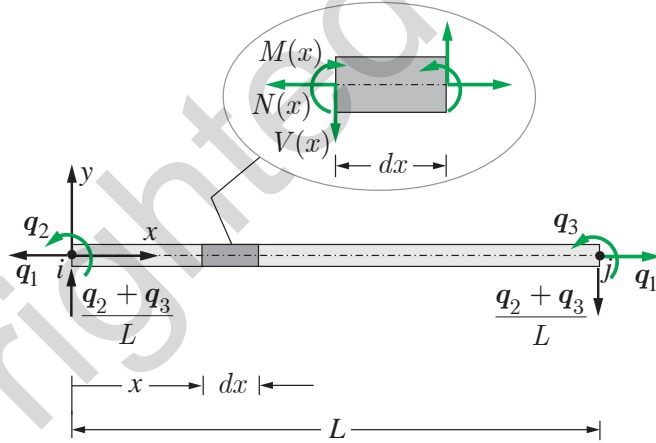


Fig. 4.3: Element free body equilibrium - Relation between internal and basic element forces

or, from equilibrium equations of the differential element with length dx

$$\begin{aligned}\frac{dN(x)}{dx} &= 0 \\ \frac{d^2M(x)}{dx^2} &= 0\end{aligned}\tag{4.4}$$

with the solution

$$N(x) = C_1$$

$$M(x) = C_2 + C_3 x$$

(4.3) results after determining the integration constants C_1 , C_2 and C_3 with the force boundary conditions.

Finally, the relation between basic element forces \mathbf{q} and element deformations \mathbf{v} requires postulating a material relation. For linear elastic material response the following linear relation between section deformations \mathbf{e} and section forces \mathbf{s} results for the Euler-Bernoulli beam

$$N(x) = EA(x) \varepsilon_a(x) \quad (4.5a)$$

$$M(x) = EI(x) \kappa(x) \quad (4.5b)$$

where we neglected initial section deformations for the sake of simplicity.

We can also write these relations in inverse form

$$\varepsilon_a(x) = \frac{N(x)}{EA(x)} \quad (4.6a)$$

$$\kappa(x) = \frac{M(x)}{EI(x)} \quad (4.6b)$$

After substituting (4.3) into (4.6) and the result into (4.2) we obtain the following deformation-force relations for the plane frame element with linear elastic material response without initial deformations

$$\mathbf{v}_1 = \mathbf{q}_1 \int_0^L \frac{1}{EA(x)} dx \quad (4.7a)$$

$$\mathbf{v}_2 = \mathbf{q}_2 \int_0^L \frac{(1 - \frac{x}{L})^2}{EI(x)} dx - \mathbf{q}_3 \int_0^L \frac{(1 - \frac{x}{L})(\frac{x}{L})}{EI(x)} dx \quad (4.7b)$$

$$\mathbf{v}_3 = -\mathbf{q}_2 \int_0^L \frac{(\frac{x}{L})(1 - \frac{x}{L})}{EI(x)} dx + \mathbf{q}_3 \int_0^L \frac{(\frac{x}{L})^2}{EI(x)} dx \quad (4.7c)$$

which can be written in compact form as

$$\mathbf{v} = \mathbf{f}\mathbf{q} \quad (4.8)$$

with the following coefficients for the element flexibility matrix \mathbf{f}

$$\begin{aligned} \mathbf{f}_{11} &= \int_0^L \frac{1}{EA(x)} dx \\ \mathbf{f}_{22} &= \int_0^L \frac{(1 - \frac{x}{L})^2}{EI(x)} dx & \mathbf{f}_{23} &= \int_0^L \frac{(\frac{x}{L} - 1)(\frac{x}{L})}{EI(x)} dx \\ \mathbf{f}_{32} &= \int_0^L \frac{(\frac{x}{L})(\frac{x}{L} - 1)}{EI(x)} dx & \mathbf{f}_{33} &= \int_0^L \frac{(\frac{x}{L})^2}{EI(x)} dx \end{aligned} \quad (4.9)$$

For a homogeneous, prismatic plane frame element the equations (4.9) give the exact element flexibility matrix \mathbf{f} . Its inverse is the stiffness matrix \mathbf{k} of the basic plane frame element for linear elastic material response under linear geometry.

4.2.2 Force-Deformation Relation for Linear Elastic Material

It is alternatively possible to derive the *force-deformation* relation of a *a homogeneous, prismatic plane frame element* by substituting the linear kinematic relations from (4.1) into the section force-deformation relations in (4.5) and then into the differential equilibrium equations in (4.4) to get

$$\begin{aligned}\frac{d}{dx} \left[EA(x) \frac{du_x(x)}{dx} \right] &= 0 \\ \frac{d^2}{dx^2} \left[EI(x) \frac{d^2 u_y(x)}{dx^2} \right] &= 0\end{aligned}\tag{4.10}$$

The solution of these differential equations with appropriate displacement and force boundary conditions gives the force-deformation relations of the plane frame element. For the general case of a tapered plane frame element there is no closed form solution, but approximate solutions can be derived with the assumption of suitable displacement interpolation functions following the concepts of finite element theory.

For a homogeneous, prismatic plane frame element with $EA = \text{const}$ and $EI = \text{const}$ the differential equations (4.10) simplify to

$$EA \frac{d^2 u_x(x)}{dx^2} = 0\tag{4.11a}$$

$$EI \frac{d^4 u_y(x)}{dx^4} = 0\tag{4.11b}$$

The homogeneous solution of (4.11a) for $u_x(x)$ is a linear polynomial

$$u_x(x) = C_{11}x + C_{12}$$

and the homogeneous solution of (4.11b) for $u_y(x)$ is a cubic polynomial

$$u_y(x) = C_{21}x^3 + C_{22}x^2 + C_{23}x + C_{24}\tag{4.12}$$

C_{11} , C_{12} , and $C_{21} \dots C_{24}$ are constants to be determined from displacement and force boundary conditions. This approach gives the basic force-deformation relation and the stiffness matrix of the plane frame element.

4.2.3 Conclusion

The integral relations between the element deformations \boldsymbol{v} and the basic element forces \boldsymbol{q} in (4.7) are accurate to within the numerical accuracy of the integration scheme for a tapered element with variable EA and EI and should be the method of choice for the case of linear geometry.

The differential equations in (4.11) can be more extended to the case of nonlinear element geometry for a homogeneous, prismatic plane frame element under moderate deformations, as will be discussed next.

4.3 Force-Deformation Relation for Nonlinear Element Geometry

Fig. 4.4 shows the deformed shape of a plane element with the translations $u_x(x)$ and $u_y(x)$ measured relative to the corotational reference frame that moves with the element chord as it translates and rotates. Considering the axial deformation ε_a as the change of length of an infinitesimal segment $M-N$ of length dx we can write

$$\varepsilon_a(x) = \frac{ds - dx}{dx}$$

where ds is the length of the infinitesimal segment $M'-N'$ after deformation. Using the Pythagorean theorem for expressing the deformed length ds gives

$$\varepsilon_a(x) = \sqrt{(1 + u'_x)^2 + (u'_y)^2} - 1$$

After expanding the square root into a power series about 1 and truncating higher order terms than quadratic gives

$$\varepsilon_a(x) \approx u'_x + \frac{1}{2}(u'_y)^2$$

The approximation is quite accurate for $u'_x \leq 5 \cdot 10^{-3}$ and $u'_y \leq 5 \cdot 10^{-2}$.

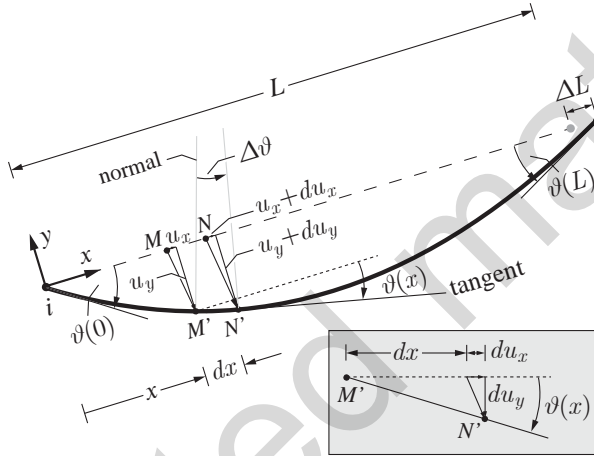


Fig. 4.4: Element deformations in the corotational reference frame

For the angle $\theta(x)$ of the tangent to the deformed shape relative to the chord we get

$$\vartheta(x) = \arctan \frac{u'_y}{1 + u'_x} \approx u'_y$$

The approximation is again quite accurate for $u'_x \leq 5 \cdot 10^{-3}$ and $u'_y \leq 5 \cdot 10^{-2}$. The curvature $\kappa(x)$ of the deformed element shape then is

$$\kappa(x) \approx \frac{d\vartheta(x)}{dx} = u''_y \quad (4.13)$$

For deriving the equilibrium equations of the differential segment of length dx in the deformed configuration (nonlinear element statics) there are two approaches: (a) use the principle of virtual work with a variation of the axial strain and curvature, and (b) set up the equilibrium of the differential segment in the deformed configuration. We pursue the second approach in the following which is less mathematical.

Fig. 4.5 shows a differential segment of the plane frame element in the deformed configuration. The axial force N is the normal stress resultant and the shear force V is the shear stress resultant. In the deformed configuration segment of length ds these are, therefore, oriented parallel and normal to the tangent at the deformed element shape, respectively, as the figure insert shows. For setting up the equilibrium equations in the deformed configuration the forces H and T parallel and normal to the

element chord in the deformed configuration, respectively, are a more suitable choice than the stress resultants N and V .

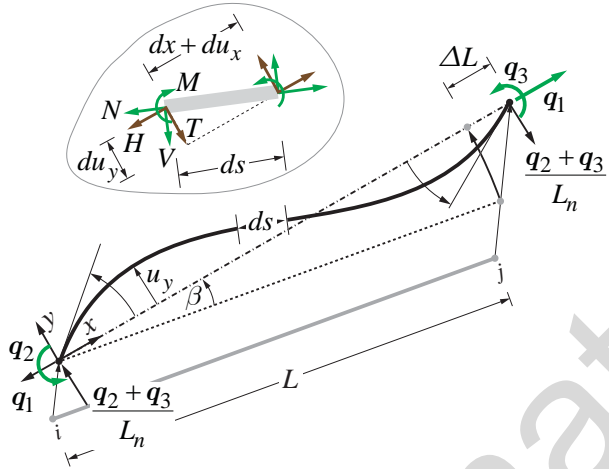


Fig. 4.5: Equilibrium of differential segment in deformed configuration

The infinitesimal segment equilibrium in the insert of Fig. 4.5 gives

$$\begin{aligned} H(x + dx) - H(x) &= 0 \\ T(x + dx) - T(x) &= 0 \\ M(x + dx) - M(x) + T(x)(dx + du_x) - H du_y &= 0 \end{aligned} \quad (4.14)$$

Dividing the equilibrium equations by dx and taking $dx \rightarrow 0$ gives the following differential equations

$$\frac{dH}{dx} = 0 \quad (4.15a)$$

$$\frac{dT}{dx} = 0 \quad (4.15b)$$

$$\frac{dM}{dx} + T(x) \left(1 + \frac{du_x}{dx} \right) - H \frac{du_y}{dx} = 0 \quad (4.15c)$$

Substituting (4.15b) into (4.15c) and neglecting $\frac{du_x}{dx}$ as small relative to 1 gives

$$\frac{d^2M}{dx^2} - H \frac{d^2u_y}{dx^2} = 0 \quad (4.16)$$

Because the horizontal force $H(x)$ is constant on account of (4.15a) and equal to q_1 at the boundary, we can rewrite the last equation as follows

$$\frac{d^2}{dx^2} \left[M(x) - q_1 u_y(x) \right] = 0 \quad (4.17)$$

Substituting the kinematic relation (4.13) between curvature and transverse displacement $u_y(x)$ into the moment-curvature relation (4.5b) for linear elastic material behavior, and the latter into (4.17) gives

$$\frac{d^2}{dx^2} \left[EI(x) \frac{d^2u_y}{dx^2} - q_1 u_y(x) \right] = 0 \quad (4.18)$$

For a homogeneous, prismatic plane frame element with $EI=\text{const}$ we get

$$\frac{d^2}{dx^2} \left[\frac{d^2 u_y}{dx^2} - \frac{q_1}{EI} u_y(x) \right] = 0$$

which upon introduction of the parameter $\bar{\psi}^2 = \frac{q_1}{EI}$ becomes

$$\frac{d^2}{dx^2} \left[\frac{d^2 u_y}{dx^2} - \bar{\psi}^2 u_y(x) \right] = 0 \quad (4.19)$$

4.3.1 Tensile Axial Basic Force q_1

For a tensile basic force $q_1 > 0$ we have

$$\frac{d^2}{dx^2} \left(\frac{d^2 u_y}{dx^2} - \bar{\psi}^2 u_y \right) = 0 \quad (4.20)$$

We assume an exponential function $u_y(x) = C e^{\xi x}$ for the solution and substitute it into the differential equation (4.20) to get

$$(\xi^4 - \bar{\psi}^2 \xi^2) C e^{\xi x} = 0 \quad (4.21)$$

We conclude that the solution of the differential equation needs to satisfy

$$\xi^4 - \bar{\psi}^2 \xi^2 = 0$$

The last equation has a double root $\xi = 0$, and two distinct roots $\xi = \pm \bar{\psi}$. With these roots the solution of the differential equation becomes

$$u_y(x) = C_1 e^{\bar{\psi}x} + C_2 e^{-\bar{\psi}x} + C_3 x + C_4 \quad (4.22)$$

or, better with hyperbolic trigonometric functions

$$u_y(x) = C_1 \sinh(\bar{\psi}x) + C_2 \cosh(\bar{\psi}x) + C_3 x + C_4 \quad (4.23)$$

4.3.2 Compressive Axial Basic Force q_1

For a compressive basic force $q_1 < 0$ we have

$$\frac{d^2}{dx^2} \left(\frac{d^2 u_y}{dx^2} + \bar{\psi}^2 u_y \right) = 0 \quad \text{with} \quad \bar{\psi} = \sqrt{\frac{|q_1|}{EI}} \quad (4.24)$$

The assumption of an exponential function $u_y(x) = C e^{\xi x}$ for the solution gives

$$(\xi^4 + \bar{\psi}^2 \xi^2) EI C e^{\xi x} = 0 \quad (4.25)$$

We conclude that the solution of the differential equation needs to satisfy

$$\xi^4 + \bar{\psi}^2 \xi^2 = 0$$

The last equation has a double root $\xi = 0$, and two distinct roots $\xi = \pm i\bar{\psi}$ where i is the imaginary unit defined by $i = \sqrt{-1}$. With these roots the solution of the differential equation becomes

$$u_y(x) = C_1 e^{i\bar{\psi}x} + C_2 e^{-i\bar{\psi}x} + C_3 x + C_4 \quad (4.26)$$

or, better with trigonometric functions

$$u_y(x) = C_1 \sin(\bar{\psi}x) + C_2 \cos(\bar{\psi}x) + C_3 x + C_4 \quad (4.27)$$

With the dimensionless parameter $\psi = \bar{\psi}L$ we get the final form for $u_y(x)$

$$u_y(x) = C_1 \sin\left(\frac{\psi x}{L}\right) + C_2 \cos\left(\frac{\psi x}{L}\right) + C_3 \frac{x}{L} + C_4 \quad (4.28)$$

The boundary conditions for the basic element express the fact that the transverse translation of the basic element relative to the chord is zero at the element ends, and the slope of the tangent to the deformed shape relative to the chord is equal to the element deformations v_2 and v_3 , as Fig. 4.6 shows.

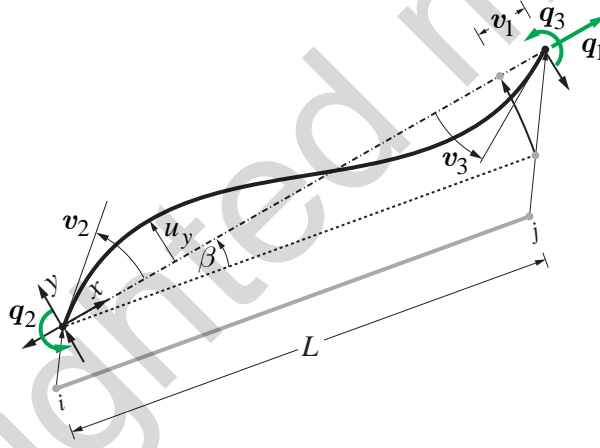


Fig. 4.6: Element deformations and basic forces in the corotational frame of the plane frame element

$$\begin{aligned} u_y(x = 0) &= 0 \\ u_y(x = L) &= 0 \\ \frac{du_y}{dx}(x = 0) &= v_2 \\ \frac{du_y}{dx}(x = L) &= v_3 \end{aligned} \quad (4.29)$$

We limit ourselves to the case with compressive basic force q_1 and substitute the general homogeneous solution from (4.28) and its derivative

$$\frac{du_y(x)}{dx} = \frac{\psi}{L} C_1 \cos\left(\frac{\psi x}{L}\right) - \frac{\psi}{L} C_2 \sin\left(\frac{\psi x}{L}\right) + C_3 \frac{1}{L}$$

into the boundary conditions in (4.29) to get

$$\begin{aligned}
 C_1(0) + C_2(1) &+ C_3(0) + C_4 = 0 \\
 C_1 \sin \psi + C_2 \cos \psi &+ C_3(1) + C_4 = 0 \\
 \frac{\psi}{L} C_1(1) - \frac{\psi}{L} C_2(0) &+ \frac{1}{L} C_3 = \mathbf{v}_2 \\
 \frac{\psi}{L} C_1 \cos \psi - \frac{\psi}{L} C_2 \sin \psi + \frac{1}{L} C_3 &= \mathbf{v}_3
 \end{aligned}
 \rightarrow
 \begin{bmatrix}
 0 & 1 & 0 & 1 \\
 \sin \psi & \cos \psi & 1 & 1 \\
 \frac{\psi}{L} & -\frac{\psi}{L} & \frac{1}{L} & 0 \\
 \frac{\psi}{L} \cos \psi & -\frac{\psi}{L} \sin \psi & \frac{1}{L} & 0
 \end{bmatrix}
 \begin{pmatrix}
 C_1 \\
 C_2 \\
 C_3 \\
 C_4
 \end{pmatrix}
 = \begin{pmatrix}
 0 \\
 0 \\
 \mathbf{v}_2 \\
 \mathbf{v}_3
 \end{pmatrix}$$

We solve for the four constants $C_1 \dots C_4$ and obtain

$$\begin{aligned}
 C_1 &= \frac{1 - \psi \sin \psi - \cos \psi}{\psi (2 - 2 \cos \psi - \psi \sin \psi)} \mathbf{v}_2 L + \frac{\cos \psi - 1}{\psi (2 - 2 \cos \psi - \psi \sin \psi)} \mathbf{v}_3 L \\
 C_2 &= \frac{\sin \psi - \psi \cos \psi}{\psi (2 - 2 \cos \psi - \psi \sin \psi)} \mathbf{v}_2 L + \frac{\psi - \sin \psi}{\psi (2 - 2 \cos \psi - \psi \sin \psi)} \mathbf{v}_3 L \\
 C_3 &= \frac{\psi (1 - \cos \psi)}{\psi (2 - 2 \cos \psi - \psi \sin \psi)} \mathbf{v}_2 L + \frac{\psi (1 - \cos \psi)}{\psi (2 - 2 \cos \psi - \psi \sin \psi)} \mathbf{v}_3 L \\
 C_4 &= \frac{\psi \cos \psi - \sin \psi}{\psi (2 - 2 \cos \psi - \psi \sin \psi)} \mathbf{v}_2 L + \frac{\sin \psi - \psi}{\psi (2 - 2 \cos \psi - \psi \sin \psi)} \mathbf{v}_3 L
 \end{aligned} \tag{4.30}$$

Substituting the kinematic relation (4.13) between curvature and transverse displacement $u_y(x)$ into the moment-curvature relation (4.5b) for linear elastic material behavior we get

$$M(x) = EI \frac{d^2 u_y}{dx^2}$$

which with the second derivative of the solution $u_y(x)$ from (4.28) becomes

$$M(x) = -EI \left(\frac{\psi}{L}\right)^2 \left[C_1 \sin\left(\frac{\psi x}{L}\right) + C_2 \cos\left(\frac{\psi x}{L}\right) \right]$$

Substituting the above expression into the boundary conditions

$$\begin{aligned}
 \mathbf{q}_2 &= -M(x=0) \\
 \mathbf{q}_3 &= M(x=L)
 \end{aligned}$$

gives

$$\begin{aligned}
 \mathbf{q}_2 &= EI \left(\frac{\psi}{L}\right)^2 C_2 \\
 \mathbf{q}_3 &= -EI \left(\frac{\psi}{L}\right)^2 (C_1 \sin \psi + C_2 \cos \psi)
 \end{aligned}$$

Substituting C_1 and C_2 from (4.30) in (4.31) and collecting terms gives

$$\begin{aligned}
 \mathbf{q}_2 &= \frac{EI}{L} \frac{\psi (\sin \psi - \psi \cos \psi)}{2 - 2 \cos \psi - \psi \sin \psi} \mathbf{v}_2 + \frac{EI}{L} \frac{\psi (\psi - \sin \psi)}{2 - 2 \cos \psi - \psi \sin \psi} \mathbf{v}_3 \\
 \mathbf{q}_3 &= \frac{EI}{L} \frac{\psi (\psi - \sin \psi)}{2 - 2 \cos \psi - \psi \sin \psi} \mathbf{v}_2 + \frac{EI}{L} \frac{\psi (\sin \psi - \psi \cos \psi)}{2 - 2 \cos \psi - \psi \sin \psi} \mathbf{v}_3
 \end{aligned} \tag{4.31}$$

which can be written in compact form

$$\begin{pmatrix} \mathbf{q}_2 \\ \mathbf{q}_3 \end{pmatrix} = \frac{EI}{L} \begin{bmatrix} A & B \\ B & A \end{bmatrix} \begin{pmatrix} \mathbf{v}_2 \\ \mathbf{v}_3 \end{pmatrix} \quad (4.32)$$

with the flexural stiffness coefficients A and B given by

$$A = \frac{\psi(\sin \psi - \psi \cos \psi)}{2 - 2 \cos \psi - \psi \sin \psi} \quad B = \frac{\psi(\psi - \sin \psi)}{2 - 2 \cos \psi - \psi \sin \psi} \quad (4.33)$$

For a plane frame element with a moment release at end j we substitute the fourth boundary condition in (4.29) by the condition $M(x = L) = 0$. After determining the constants $C_1 \dots C_4$, substituting into the expression for $M(x)$ and setting $\mathbf{q}_2 = -M(x = 0)$ we get

$$\mathbf{q}_2 = \frac{EI}{L} C \mathbf{v}_2 \quad \text{with} \quad C = \frac{\psi^2 \sin \psi}{\sin \psi - \psi \cos \psi} \quad (4.34)$$

The flexural stiffness coefficients A , B and C of the plane basic frame element under nonlinear element geometry are functions of ψ where

$$\psi = \bar{\psi}L = \sqrt{\frac{|\mathbf{q}_1|}{EI}}L = \sqrt{\frac{|\mathbf{q}_1|L^2}{EI}} \quad (4.35)$$

We conclude that the flexural stiffness coefficients of the plane basic frame element are *nonlinear functions* of the axial basic force \mathbf{q}_1 , the element length L , and the flexural stiffness EI .

4.3.3 Basic Stiffness Matrix Coefficients

Expanding the flexural stiffness coefficients A , B , and C into power series about $\psi = 0$ gives the following approximations in terms of powers of ψ :

$$\begin{aligned} A &= 4 - \frac{2}{15}\psi^2 + O(\psi^4) \\ B &= 2 + \frac{1}{30}\psi^2 + O(\psi^4) \\ C &= 3 - \frac{1}{5}\psi^2 + O(\psi^3) \end{aligned}$$

We note that

$$\begin{aligned} A &\rightarrow 4 \quad \text{as} \quad \psi \rightarrow 0 \\ B &\rightarrow 2 \quad \text{as} \quad \psi \rightarrow 0 \\ C &\rightarrow 3 \quad \text{as} \quad \psi \rightarrow 0 \end{aligned}$$

This can also be confirmed with L'Hospital's rule on the exact expressions for A , B , and C in (4.33) and (4.34). The values for A , B , and C for $\psi = 0$ correspond to the flexural stiffness coefficients of the basic

homogeneous, prismatic plane frame element with linear geometry (consult equations 8.14 and 8.18 in CE220 reader).

Truncating the flexural stiffness coefficients after the quadratic term gives

$$\begin{aligned} A &\approx 4 - \frac{2}{15}\psi^2 \\ B &\approx 2 + \frac{1}{30}\psi^2 \\ C &\approx 3 - \frac{1}{5}\psi^2 \end{aligned} \quad (4.36)$$

This approximation of the flexural stiffness coefficients is known as *second order* with first order representing the constant stiffness coefficients of the linear theory.

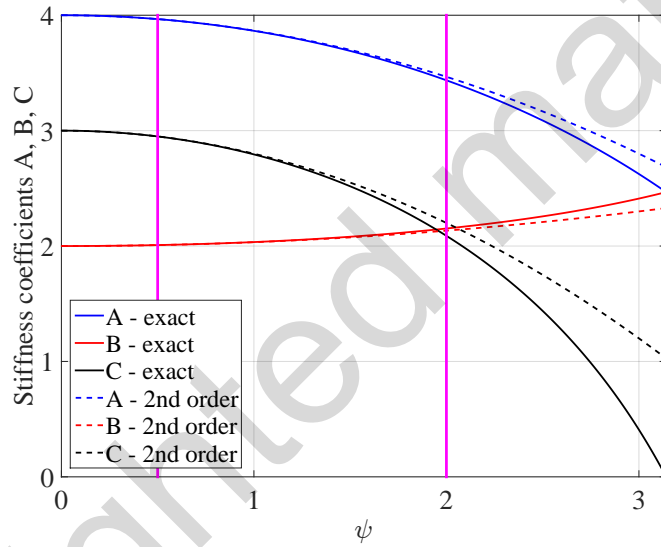


Fig. 4.7: Dependence of stiffness coefficients A , B , and C on ψ according to (4.33), (4.34) and (4.36)

Substituting $\psi^2 = \frac{|q_1|L^2}{EI}$ from (4.35) and noting that $|q_1| = \text{sign}(q_1)q_1$ gives

$$\begin{aligned} A &\approx 4 + \frac{2}{15} \frac{q_1 L^2}{EI} \\ B &\approx 2 - \frac{1}{30} \frac{q_1 L^2}{EI} \\ C &\approx 3 + \frac{1}{5} \frac{q_1 L^2}{EI} \end{aligned} \quad (4.37)$$

It turns out that the approximations in (4.37) hold not only for compressive q_1 but also for tensile q_1 . For tensile q_1 the diagonal stiffness coefficients A and C increase, while for compressive q_1 they decrease.

Fig. 4.7 plots the dependence of the stiffness coefficients A , B and C on ψ according to the exact solution of the differential equation in (4.33) and (4.34) and according to the second order approximation with truncation of higher order terms of ψ in (4.37). The first order theory of linear geometry for the element deformation relative to the chord corresponds to the values of A , B and C for $\psi = 0$. Consequently, the dependence of A , B and C on ψ would be represented by a horizontal line passing

through 4, 2, and 3, respectively, if the effect of the axial basic force q_1 on the flexural stiffness coefficients were neglected.

We distinguish three ranges of variable ψ in Fig. 4.7 marked by thick vertical lines:

- 1) **Zone I:** $0 \leq \psi \leq 0.5$. For this range of ψ -values the basic axial force q_1 has little influence on the flexural stiffness coefficients and can be neglected.
- 2) **Zone II:** $0.5 < \psi \leq 2$. For this range of ψ -values the effect of the axial force q_1 on the flexural stiffness coefficients is significant and needs to be included. To this end we use the second order approximation of the flexural stiffness coefficients, which is very close to the exact solution for this range of ψ -values.
- 3) **Zone III:** $2 < \psi$. For this range of ψ -values the second order approximation deviates significantly from the exact solution. To avoid the complexity of the trigonometric expressions for the flexural stiffness coefficients according to (4.33) and (4.34), we should make sure that the ψ -values of the elements of the structural model under compression are smaller than 2. We achieve this by subdivision of the structural members under compression into smaller elements so that $\psi < 2$.

Fig. 4.7 that the flexural stiffness coefficients A and B reach the same value at $\psi = \pi$ so that the basic element stiffness matrix \mathbf{k} becomes singular. \mathbf{k} is singular at the same ψ -value for the element with a moment release, because $C = 0$ at this value. The value $\psi = \pi$ corresponds to the *Euler buckling load* of the basic plane frame element. The corresponding compressive basic force q_1 is equal to

$$\text{from } \pi = \sqrt{\frac{|q_1| L^2}{EI}} \rightarrow |q_1| = \frac{EI\pi^2}{L^2} \quad (4.38)$$

Structural elements with small EI/L^2 ratio have a small Euler buckling load and are, thus, susceptible to the *softening of the flexural stiffness coefficients* under compression that Fig. 4.7 depicts. Such elements are called *slender*.

4.3.4 Summary

We investigated the effect of the axial basic force q_1 on the flexural response of the plane basic frame element. The axial response with respect to the centroidal axis of the element is uncoupled and is assumed to remain unaffected by nonlinear geometry, an inconsistent assumption with the equilibrium equations in the deformed configuration of the infinitesimal element. The error from this inconsistency is, however, very small for the typical range of deformations of structural elements. Accordingly the force-deformation relation of the plane basic frame element is

$$\begin{pmatrix} q_1 \\ q_2 \\ q_3 \end{pmatrix} = \mathbf{q} = \mathbf{k} \mathbf{v} = \left[\begin{array}{c|c} \mathbf{k}_a & \mathbf{0} \\ \hline \mathbf{0} & \mathbf{k}_b \end{array} \right] \begin{pmatrix} v_1 \\ v_2 \\ v_3 \end{pmatrix} \quad (4.39)$$

where \mathbf{k}_a is the axial stiffness

$$\mathbf{k}_a = \frac{EA}{L} \quad (4.40)$$

and \mathbf{k}_b the flexural stiffness

$$\mathbf{k}_b = \frac{EI}{L} \begin{bmatrix} A & B \\ B & A \end{bmatrix} \quad \text{or} \quad \mathbf{k}_b = \frac{EI}{L} \begin{bmatrix} C & 0 \\ 0 & 0 \end{bmatrix} \quad \text{or} \quad \mathbf{k}_b = \frac{EI}{L} \begin{bmatrix} 0 & 0 \\ 0 & C \end{bmatrix} \quad (4.41)$$

for both ends continuous, and for a moment release at end j or i , respectively. The stiffness coefficients A , B and C are functions of ψ defined in (4.35). The exact flexural stiffness coefficients A , B and C are trigonometric functions of ψ for compressive \mathbf{q}_1 in (4.33) and (4.34) or hyperbolic functions of ψ for tensile \mathbf{q}_1 . It is possible to develop approximations of the flexural stiffness coefficients which are linear functions of \mathbf{q}_1 and hold for both tensile and compressive \mathbf{q}_1 according to (4.37).

In the nonlinear analysis of structural models with slender structural members it is important to select the "right" flexural stiffness matrix in accordance with the slenderness of the structural member and the axial compression that it carries. The criterion for this selection is the parameter ψ .

According to Fig. 4.7 we distinguish three cases for the flexural stiffness coefficients depending on the value of parameter ψ :

Zone I: $0 \leq \psi \leq 0.5$. In this case it is sufficiently accurate to neglect the effect of the basic axial force \mathbf{q}_1 on the flexural stiffness coefficients so that the basic flexural stiffness matrix \mathbf{k}_b in (4.39) becomes

$$\mathbf{k}_b = \mathbf{k}_{bl} \quad (4.42)$$

where \mathbf{k}_{bl} is the flexural stiffness matrix under *linear geometry* as the subscript l indicates. We recall that

$$\mathbf{k}_{bl} = \frac{EI}{L} \begin{bmatrix} 4 & 2 \\ 2 & 4 \end{bmatrix} \quad \text{or} \quad \mathbf{k}_{bl} = \frac{3EI}{L} \begin{bmatrix} 1 & 0 \\ 0 & 0 \end{bmatrix} \quad \text{or} \quad \mathbf{k}_{bl} = \frac{3EI}{L} \begin{bmatrix} 0 & 0 \\ 0 & 1 \end{bmatrix} \quad (4.43)$$

depending on whether the plane frame element has both end continuous, or it has a moment release at end j or end i , respectively.

Zone II: $0.5 < \psi \leq 2$. In this case it is sufficiently accurate to represent the effect of the basic axial force \mathbf{q}_1 on the flexural stiffness coefficients by the second order approximation with (4.37). Substituting the second order approximation of the flexural stiffness coefficients A , B and C from (4.37) into (4.39) gives

$$\mathbf{k}_b = \mathbf{k}_{bl} + \mathbf{k}_{P\delta} \quad (4.44)$$

where the flexural stiffness matrix under linear geometry is given by (4.43) and the second order approximation $\mathbf{k}_{P\delta}$ of the flexural stiffness matrix is

$$\mathbf{k}_{P\delta} = \frac{\mathbf{q}_1 L}{30} \begin{bmatrix} 4 & -1 \\ -1 & 4 \end{bmatrix} \quad \text{or} \quad \mathbf{k}_{P\delta} = \frac{\mathbf{q}_1 L}{5} \begin{bmatrix} 1 & 0 \\ 0 & 0 \end{bmatrix} \quad \text{or} \quad \mathbf{k}_{P\delta} = \frac{\mathbf{q}_1 L}{5} \begin{bmatrix} 0 & 0 \\ 0 & 1 \end{bmatrix} \quad (4.45)$$

depending on whether the plane frame element has both end continuous, or it has a moment release at end j or end i , respectively. According to (4.44) the flexural stiffness matrix \mathbf{k}_b of the plane frame element is made up of two contributions: (a) a contribution \mathbf{k}_{bl} equal to the basic stiffness under linear geometry, and (b) a contribution $\mathbf{k}_{P\delta}$ that accounts for the effect of axial basic force \mathbf{q}_1 on the flexural stiffness according to the second order approximation of the stiffness coefficients. It is worth stressing that the second contribution is *linear in the axial basic force \mathbf{q}_1* .

Zone III: $\psi > 2$. To avoid using the trigonometric or hyperbolic expressions for the flexural stiffness coefficients of the exact solution we subdivide the slender structural member carrying a high basic axial force q_1 into several elements. Denoting the structural member length with L_m we assume at first that we make use of one plane frame element for representing the structural member under compression. If the value of ψ exceeds 2, we use two elements for the structural member thus halving the length L_m and with it the value of ψ according to (4.35). We note, in fact, that for a given stiffness EI of the structural member and a given axial compression q_1 the parameter ψ depends linearly on the element length L

$$\psi = \sqrt{\frac{|q_1|}{EI}} L$$

Carrying the preceding argument one step further we realize that we can eliminate the need for including the *nonlinear element geometry effect under the axial basic force q_1 by selecting a small enough element length L to render the parameter ψ smaller than 0.5*. From

$$\sqrt{\frac{|q_1|}{EI}} L \leq 0.5$$

We, therefore, conclude that the selection of an element length L_e such that

$$L \leq \sqrt{\frac{EI}{4|q_1|}} \quad (4.46)$$

ensures that the parameter ψ of the structural element under compression is smaller than 0.5, so that the flexural stiffness coefficients under linear geometry are sufficiently accurate. *This dispenses with the need of developing a sophisticated basic element model, something that proves extremely useful under nonlinear material behavior.*

By controlling the value of parameter ψ through the discretization of the compression member into elements we dispense with the need of including the nonlinear element geometry effect. The discretization length is proportional to the flexural stiffness EI of the structural member and inversely proportional to the compressive force q_1 .

4.4 Corotational Formulation of Plane Frame Element

We turn now our attention to the *nonlinear chord geometry effect, which is critical in the assessment of the nonlinear geometry effects of structures undergoing large displacements*.

4.4.1 Nonlinear Kinematics

The corotational formulation of nonlinear geometry postulates that the large displacement kinematics of the element can be decomposed into the kinematics relative to a reference frame that follows the element chord as it translates and rotates with the relative end translations, and the rigid body translation and rotation of this frame. It is convenient to keep the element kinematics linear, by subdividing a structural member under compression into several elements so as to satisfy equation (4.46). With

linear element kinematics the effect of large displacements is included only in the relation between the intra-node deformations and the element end displacements \mathbf{u} .

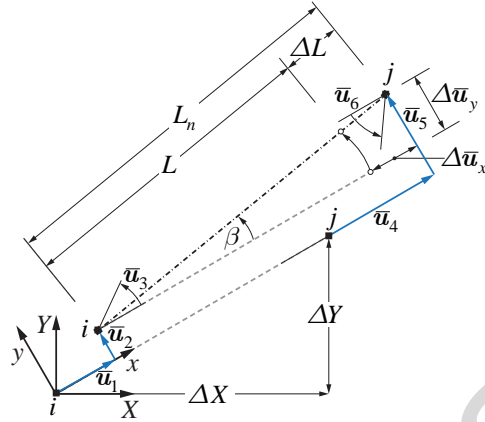


Fig. 4.8: Two dimensional frame element under large displacements

The plane frame element in Fig. 4.8 has three intra-node deformations relative to the corotational reference frame: the change of distance between ends i and j , and the angle between the node director and the chord at each end. Equating these to the element deformations \mathbf{v} gives

$$\begin{aligned} v_1 &= L_n - L \\ v_2 &= \bar{u}_3 - \beta \\ v_3 &= \bar{u}_6 - \beta \end{aligned} \quad (4.47)$$

where L_n is the deformed element length and β is the chord rotation angle relative to the undeformed element orientation.

From (4.47) we conclude that the intra-node deformations depend on two key variables: the deformed element length L_n , and the chord rotation angle β . For large *relative end translations* $\Delta\bar{u}_x = \bar{u}_4 - \bar{u}_1$ and $\Delta\bar{u}_y = \bar{u}_5 - \bar{u}_2$ in the element reference system the deformed element length L_n and the chord rotation angle β are given by

$$\begin{aligned} L_n &= \sqrt{(L + \Delta\bar{u}_x)^2 + (\Delta\bar{u}_y)^2} \\ \beta &= \arctan\left(\frac{\Delta\bar{u}_y}{L + \Delta\bar{u}_x}\right) \end{aligned} \quad (4.48)$$

To express the element deformations \mathbf{v} in terms of the end displacements \mathbf{u} in the global coordinate system we note that $\mathbf{u}_3 = \bar{u}_3$ and $\mathbf{u}_6 = \bar{u}_6$ and use the relation between the local and the global translation components in (2.8)

$$\begin{aligned} \Delta\bar{u}_x &= \frac{\Delta X}{L} \Delta u_x + \frac{\Delta Y}{L} \Delta u_y \\ \Delta\bar{u}_y &= -\frac{\Delta Y}{L} \Delta u_x + \frac{\Delta X}{L} \Delta u_y \end{aligned}$$

Because of (4.48), the element deformations \mathbf{v} in (4.47) are nonlinear functions of the element end displacements \mathbf{u} .

4.4.2 Variation of Deformations

In deriving the equilibrium equations in the deformed configuration with the principle of virtual work we need the variation of the element deformations \mathbf{v} with respect to the end displacements $\bar{\mathbf{u}}$ in the local reference system. From (4.47) we get

$$\delta \mathbf{v}_1 = \frac{\partial L_n}{\partial \bar{\mathbf{u}}} \delta \bar{\mathbf{u}} \quad (4.49a)$$

$$\delta \mathbf{v}_2 = \begin{bmatrix} 0 & 0 & 1 & 0 & 0 & 0 \end{bmatrix} \delta \bar{\mathbf{u}} - \frac{\partial \beta}{\partial \bar{\mathbf{u}}} \delta \bar{\mathbf{u}} \quad (4.49b)$$

$$\delta \mathbf{v}_3 = \begin{bmatrix} 0 & 0 & 0 & 0 & 0 & 1 \end{bmatrix} \delta \bar{\mathbf{u}} - \frac{\partial \beta}{\partial \bar{\mathbf{u}}} \delta \bar{\mathbf{u}} \quad (4.49c)$$

We conclude that the variation of the element deformations depends on two derivatives: (a) the derivative of the deformed element length L_n , and (b) the derivative of the chord rotation angle β with respect to the end displacements $\bar{\mathbf{u}}$ in the local reference system. It is convenient to express these derivatives with the aid of the unit vectors of the corotational reference system.

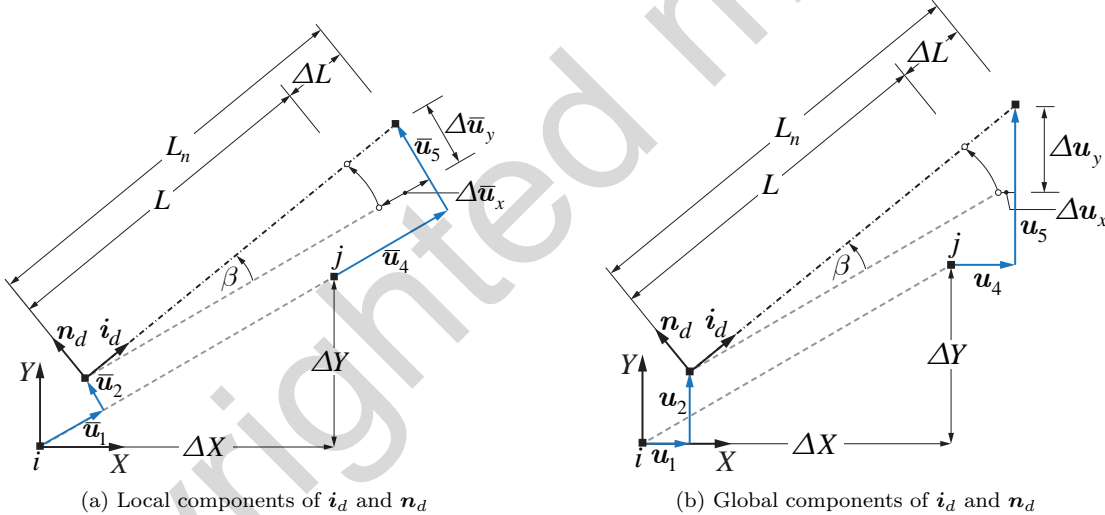


Fig. 4.9: Components of unit vectors for corotational reference frame

The unit vector \mathbf{i}_d lies on the chord of the deformed configuration with components relative to the local reference system x - y in Fig. 4.9(a)

$$\mathbf{i}_d = \begin{pmatrix} \frac{L + \Delta \bar{u}_x}{L_n} \\ \frac{\Delta \bar{u}_y}{L_n} \end{pmatrix} \quad (4.50)$$

while the unit vector \mathbf{n}_d is normal to the chord of the deformed configuration with components relative to the local reference system x - y

$$\mathbf{n}_d = \begin{pmatrix} -\frac{\Delta \bar{u}_y}{L_n} \\ \frac{L + \Delta \bar{u}_x}{L_n} \end{pmatrix} \quad (4.51)$$

We can also define the unit vector \mathbf{i}_d on the chord of the deformed configuration with components relative to the global reference system $X-Y$ in Fig. 4.9(b)

$$\mathbf{i}_d = \begin{pmatrix} \frac{\Delta X + \Delta u_x}{L_n} \\ \frac{\Delta Y + \Delta u_y}{L_n} \end{pmatrix} \quad (4.52)$$

and the unit vector \mathbf{n}_d normal to the chord of the deformed configuration with components relative to the global reference system $X-Y$

$$\mathbf{n}_d = \begin{pmatrix} -\frac{\Delta Y + \Delta u_y}{L_n} \\ \frac{\Delta X + \Delta u_x}{L_n} \end{pmatrix} \quad (4.53)$$

We determine first the derivative of the deformed element length L_n with respect to $\bar{\mathbf{u}}$. Recalling from calculus that $\frac{d(\sqrt{x})}{dx} = \frac{1}{2\sqrt{x}}$ we get

$$\frac{\partial L_n}{\partial \bar{\mathbf{u}}} = \frac{1}{2L_n} [2(L + \Delta \bar{u}_x)] \frac{\partial(\Delta \bar{u}_x)}{\partial \bar{\mathbf{u}}} + \frac{1}{2L_n} [2(\Delta \bar{u}_y)] \frac{\partial(\Delta \bar{u}_y)}{\partial \bar{\mathbf{u}}}$$

with

$$\begin{aligned} \frac{\partial \Delta \bar{u}_x}{\partial \bar{\mathbf{u}}} &= \frac{\partial(\bar{u}_4 - \bar{u}_1)}{\partial \bar{\mathbf{u}}} = \begin{bmatrix} -1 & 0 & 0 & 1 & 0 & 0 \end{bmatrix} \\ \frac{\partial \Delta \bar{u}_y}{\partial \bar{\mathbf{u}}} &= \frac{\partial(\bar{u}_5 - \bar{u}_2)}{\partial \bar{\mathbf{u}}} = \begin{bmatrix} 0 & -1 & 0 & 0 & 1 & 0 \end{bmatrix} \end{aligned}$$

we get

$$\frac{\partial L_n}{\partial \bar{\mathbf{u}}} = \left[-\frac{L + \Delta \bar{u}_x}{L_n} \quad -\frac{\Delta \bar{u}_y}{L_n} \quad 0 \quad \frac{L + \Delta \bar{u}_x}{L_n} \quad \frac{\Delta \bar{u}_y}{L_n} \quad 0 \right]$$

With the definition of the unit vector \mathbf{i}_d for the corotational reference system we express the derivative of the deformed element length L_n in the form

$$\frac{\partial L_n}{\partial \bar{\mathbf{u}}} = \begin{bmatrix} -\mathbf{i}_d^T & 0 & \mathbf{i}_d^T & 0 \end{bmatrix} \quad (4.54)$$

The derivative of the chord rotation angle β with respect to $\bar{\mathbf{u}}$ is

$$\frac{\partial \beta}{\partial \bar{\mathbf{u}}} = \left[\frac{\partial \beta}{\partial(\Delta \bar{u}_x)} \frac{\partial(\Delta \bar{u}_x)}{\partial \bar{\mathbf{u}}} + \frac{\partial \beta}{\partial(\Delta \bar{u}_y)} \frac{\partial(\Delta \bar{u}_y)}{\partial \bar{\mathbf{u}}} \right]$$

Recalling from calculus that

$$\frac{d}{dx} \arctan(x) = \frac{1}{1+x^2}$$

and noting that

$$\frac{1}{1 + \left(\frac{\Delta \bar{u}_y}{L + \Delta \bar{u}_x} \right)^2} = \frac{(L + \Delta \bar{u}_x)^2}{L_n^2}$$

we get

$$\frac{\partial \beta}{\partial \bar{u}} = -\frac{(L + \Delta \bar{u}_x)^2}{L_n^2} \frac{(\Delta \bar{u}_y)}{(L + \Delta \bar{u}_x)^2} \frac{\partial (\Delta \bar{u}_x)}{\partial \bar{u}} + \frac{(L + \Delta \bar{u}_x)^2}{L_n^2} \frac{1}{(L + \Delta \bar{u}_x)} \frac{\partial (\Delta \bar{u}_y)}{\partial \bar{u}}$$

which simplifies to

$$\frac{\partial \beta}{\partial \bar{u}} = \frac{1}{L_n} \begin{bmatrix} \Delta \bar{u}_y & -\frac{L + \Delta \bar{u}_x}{L_n} & 0 & -\frac{\Delta \bar{u}_y}{L_n} & \frac{L + \Delta \bar{u}_x}{L_n} & 0 \end{bmatrix}$$

With the definition of the unit vector \mathbf{n}_d for the corotational reference system we express the derivative of the chord rotation angle β in the form

$$\frac{\partial \beta}{\partial \bar{u}} = \frac{1}{L_n} \begin{bmatrix} -\mathbf{n}_d^T & 0 & \mathbf{n}_d^T & 0 \end{bmatrix} \quad (4.55)$$

We note that

- 1) The derivative of the deformed element length L_n with respect to \bar{u} depends on the unit vector \mathbf{i}_d in the chord direction of the deformed configuration.
- 2) The derivative of the chord angle β with respect to \bar{u} depends on the unit vector \mathbf{n}_d normal to the chord in the deformed configuration and the deformed element length L_n .

4.4.3 Incremental Kinematic Matrix

With the derivative of the element length L_n and of the chord rotation angle β for the deformed configuration we can express the variation of the deformations \mathbf{v} in (4.49) relative to the end displacements \bar{u} in the local coordinate system and derive the kinematic matrix $\mathbf{a}(\bar{u})$ of the plane frame element

$$\delta \mathbf{v} = \frac{\partial \mathbf{v}}{\partial \bar{u}} \delta \bar{u} = \mathbf{a}(\bar{u}) \delta \bar{u}$$

with the kinematic matrix $\mathbf{a}(\bar{u})$ given by

$$\mathbf{a}(\bar{u}) = \begin{bmatrix} \frac{\partial L_n}{\partial \bar{u}} \\ \begin{bmatrix} 0 & 0 & 1 & 0 & 0 & 0 \end{bmatrix} - \frac{\partial \beta}{\partial \bar{u}} \\ \begin{bmatrix} 0 & 0 & 0 & 0 & 0 & 1 \end{bmatrix} - \frac{\partial \beta}{\partial \bar{u}} \end{bmatrix} = \begin{bmatrix} -\mathbf{i}_d^T & 0 & \mathbf{i}_d^T & 0 \\ \mathbf{n}_d^T & 1 & -\frac{\mathbf{n}_d^T}{L_n} & 0 \\ \frac{\mathbf{n}_d^T}{L_n} & 0 & -\frac{\mathbf{n}_d^T}{L_n} & 1 \end{bmatrix}$$

or, explicitly

$$\mathbf{a}(\bar{u}) = \begin{bmatrix} -\mathbf{i}_d^T & 0 & \mathbf{i}_d^T & 0 \\ \frac{\mathbf{n}_d^T}{L_n} & 1 & -\frac{\mathbf{n}_d^T}{L_n} & 0 \\ \frac{\mathbf{n}_d^T}{L_n} & 0 & -\frac{\mathbf{n}_d^T}{L_n} & 1 \end{bmatrix} = \begin{bmatrix} -\frac{L + \Delta \bar{u}_x}{L_n} & -\frac{\Delta \bar{u}_y}{L_n} & 0 & \frac{L + \Delta \bar{u}_x}{L_n} & \frac{\Delta \bar{u}_y}{L_n} & 0 \\ -\frac{\Delta \bar{u}_y}{L_n^2} & \frac{L + \Delta \bar{u}_x}{L_n^2} & 1 & \frac{\Delta \bar{u}_y}{L_n^2} & -\frac{L + \Delta \bar{u}_x}{L_n^2} & 0 \\ -\frac{\Delta \bar{u}_y}{L_n^2} & \frac{L + \Delta \bar{u}_x}{L_n^2} & 0 & \frac{\Delta \bar{u}_y}{L_n^2} & -\frac{L + \Delta \bar{u}_x}{L_n^2} & 1 \end{bmatrix}$$

The significant advantage of expressing the incremental kinematic matrix $\mathbf{a}(\bar{u})$ in terms of the unit vectors \mathbf{i}_d and \mathbf{n}_d is that the transformation to global coordinates simply involves expressing the unit vectors in terms of Δu_x and Δu_y according to (4.52) and (4.53).

Consequently, the incremental kinematic matrix $\mathbf{a}_g(\mathbf{u})$ is

$$\mathbf{a}_g(\mathbf{u}) = \begin{bmatrix} -\mathbf{i}_d^T & 0 & \mathbf{i}_d^T & 0 \\ \frac{\mathbf{n}_d^T}{L_n} & 1 & -\frac{\mathbf{n}_d^T}{L_n} & 0 \\ \frac{\mathbf{n}_d^T}{L_n} & 0 & -\frac{\mathbf{n}_d^T}{L_n} & 1 \end{bmatrix}$$

or, explicitly

$$\mathbf{a}_g(\mathbf{u}) = \begin{bmatrix} -\frac{\Delta X + \Delta u_x}{L_n} & -\frac{\Delta Y + \Delta u_y}{L_n} & 0 & \frac{\Delta X + \Delta u_x}{L_n} & \frac{\Delta Y + \Delta u_y}{L_n} & 0 \\ -\frac{\Delta Y + \Delta u_y}{L_n^2} & \frac{\Delta X + \Delta u_x}{L_n^2} & 1 & \frac{\Delta Y + \Delta u_y}{L_n^2} & -\frac{\Delta X + \Delta u_x}{L_n^2} & 0 \\ -\frac{\Delta Y + \Delta u_y}{L_n^2} & \frac{\Delta X + \Delta u_x}{L_n^2} & 0 & \frac{\Delta Y + \Delta u_y}{L_n^2} & -\frac{\Delta X + \Delta u_x}{L_n^2} & 1 \end{bmatrix} \quad (4.56)$$

It can be readily shown that

$$\mathbf{a}_g(\mathbf{u}) = \frac{\partial \mathbf{v}}{\partial \mathbf{u}} = \frac{\partial \mathbf{v}}{\partial \bar{\mathbf{u}}} \frac{\partial \bar{\mathbf{u}}}{\partial \mathbf{u}} = \mathbf{a}(\bar{\mathbf{u}}) \mathbf{a}_r = \begin{bmatrix} -\mathbf{i}_d^T & 0 & \mathbf{i}_d^T & 0 \\ \frac{\mathbf{n}_d^T}{L_n} & 1 & -\frac{\mathbf{n}_d^T}{L_n} & 0 \\ \frac{\mathbf{n}_d^T}{L_n} & 0 & -\frac{\mathbf{n}_d^T}{L_n} & 1 \end{bmatrix}$$

Under small relative end displacements Δu_x and Δu_y it can be assumed that the unit vectors \mathbf{i}_d and \mathbf{n}_d of the corotational reference system coincide with the undeformed element orientation, so that they not change direction under deformation. In this case

$$\mathbf{i}_d = \mathbf{i} = \begin{pmatrix} \frac{\Delta X}{L} \\ \frac{\Delta Y}{L} \end{pmatrix} \quad \text{and} \quad \mathbf{n}_d = \mathbf{n} = \begin{pmatrix} -\frac{\Delta Y}{L} \\ \frac{\Delta X}{L} \end{pmatrix} \quad (4.57)$$

where \mathbf{i} and \mathbf{n} are the unit vectors in the chord direction and in the direction normal to the chord of the original (undeformed) element orientation, respectively. The linear kinematic matrix \mathbf{a}_g then becomes

$$\mathbf{a}_g = \begin{bmatrix} -\mathbf{i}^T & 0 & \mathbf{i}^T & 0 \\ \frac{\mathbf{n}^T}{L} & 1 & -\frac{\mathbf{n}^T}{L} & 0 \\ \frac{\mathbf{n}^T}{L} & 0 & -\frac{\mathbf{n}^T}{L} & 1 \end{bmatrix}$$

or, explicitly

$$\mathbf{a}_g = \begin{bmatrix} -\frac{\Delta X}{L} & -\frac{\Delta Y}{L} & 0 & \frac{\Delta X}{L} & \frac{\Delta Y}{L} & 0 \\ -\frac{\Delta Y}{L^2} & \frac{\Delta X}{L^2} & 1 & \frac{\Delta Y}{L^2} & -\frac{\Delta X}{L^2} & 0 \\ -\frac{\Delta Y}{L^2} & \frac{\Delta X}{L^2} & 0 & \frac{\Delta Y}{L^2} & -\frac{\Delta X}{L^2} & 1 \end{bmatrix}$$

4.4.4 Nonlinear Statics

We use the principle of virtual work to establish the equilibrium relations between the basic forces \mathbf{q} of the plane frame element and the end forces $\bar{\mathbf{p}}$ in the local reference system or the end forces \mathbf{p} in the global reference system. For the relation between \mathbf{q} and $\bar{\mathbf{p}}$ we get

$$\delta \bar{\mathbf{u}}^T \bar{\mathbf{p}} = \delta \mathbf{v}^T \mathbf{q} = \delta \bar{\mathbf{u}}^T \mathbf{a}^T(\bar{\mathbf{u}}) \mathbf{q}$$

and because this statement holds for arbitrary $\delta \bar{\mathbf{u}}$ we get

$$\bar{\mathbf{p}} = \mathbf{a}^T(\bar{\mathbf{u}}) \mathbf{q}$$

or, explicitly

$$\bar{\mathbf{p}} = \begin{bmatrix} -\mathbf{i}_d & \mathbf{n}_d & \mathbf{n}_d \\ 0 & 1 & 0 \\ \mathbf{i}_d & -\frac{\mathbf{n}_d}{L_n} & -\frac{\mathbf{n}_d}{L_n} \\ 0 & 0 & 1 \end{bmatrix} \mathbf{q} = \begin{bmatrix} -\frac{L + \Delta \bar{\mathbf{u}}_x}{L_n} & -\frac{\Delta \bar{\mathbf{u}}_y}{L_n^2} & -\frac{\Delta \bar{\mathbf{u}}_y}{L_n^2} \\ -\frac{\Delta \bar{\mathbf{u}}_y}{L_n} & \frac{L + \Delta \bar{\mathbf{u}}_x}{L_n^2} & \frac{L + \Delta \bar{\mathbf{u}}_x}{L_n^2} \\ 0 & 1 & 0 \\ \frac{L + \Delta \bar{\mathbf{u}}_x}{L_n} & \frac{\Delta \bar{\mathbf{u}}_y}{L_n^2} & \frac{\Delta \bar{\mathbf{u}}_y}{L_n^2} \\ \frac{\Delta \bar{\mathbf{u}}_y}{L_n} & -\frac{L + \Delta \bar{\mathbf{u}}_x}{L_n^2} & -\frac{L + \Delta \bar{\mathbf{u}}_x}{L_n^2} \\ 0 & 0 & 1 \end{bmatrix} \mathbf{q} \quad (4.58)$$

For the relation between \mathbf{q} and \mathbf{p} we get

$$\delta \mathbf{u}^T \mathbf{p} = \delta \mathbf{v}^T \mathbf{q} = \delta \mathbf{u}^T \mathbf{a}_g^T(\mathbf{u}) \mathbf{q}$$

and because this statement holds for arbitrary $\delta \mathbf{u}$ we get

$$\mathbf{p} = \mathbf{a}_g^T(\mathbf{u}) \mathbf{q}$$

or, explicitly

$$\mathbf{p} = \begin{bmatrix} -\mathbf{i}_d & \mathbf{n}_d & \mathbf{n}_d \\ 0 & 1 & 0 \\ \mathbf{i}_d & -\frac{\mathbf{n}_d}{L_n} & -\frac{\mathbf{n}_d}{L_n} \\ 0 & 0 & 1 \end{bmatrix} \mathbf{q} = \begin{bmatrix} -\frac{\Delta X + \Delta \mathbf{u}_x}{L_n} & -\frac{\Delta Y + \Delta \mathbf{u}_y}{L_n^2} & -\frac{\Delta Y + \Delta \mathbf{u}_y}{L_n^2} \\ -\frac{\Delta Y + \Delta \mathbf{u}_y}{L_n} & \frac{\Delta X + \Delta \mathbf{u}_x}{L_n^2} & \frac{\Delta X + \Delta \mathbf{u}_x}{L_n^2} \\ 0 & 1 & 0 \\ \frac{\Delta X + \Delta \mathbf{u}_x}{L_n} & \frac{\Delta Y + \Delta \mathbf{u}_y}{L_n^2} & \frac{\Delta Y + \Delta \mathbf{u}_y}{L_n^2} \\ \frac{\Delta Y + \Delta \mathbf{u}_y}{L_n} & -\frac{\Delta X + \Delta \mathbf{u}_x}{L_n^2} & -\frac{\Delta X + \Delta \mathbf{u}_x}{L_n^2} \\ 0 & 0 & 1 \end{bmatrix} \mathbf{q} \quad (4.59)$$

Fig. 4.10 shows the basic forces \mathbf{q} of the plane frame element in the corotational reference and the end force components \mathbf{p} in the global coordinate system $X-Y$. The transverse forces are oriented normal to

the chord of the deformed element, thus changing orientation continuously as does the axial basic force \mathbf{q}_1 . With the unit vectors of the corotational reference system the end force components are

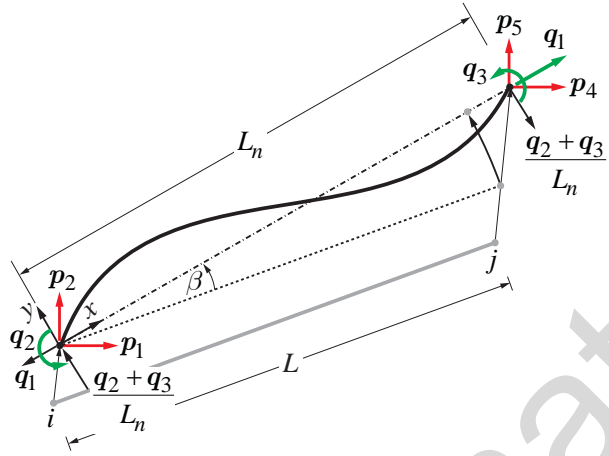


Fig. 4.10: Nonlinear statics of corotational plane frame element

$$\begin{aligned}\begin{pmatrix} \mathbf{p}_1 \\ \mathbf{p}_2 \end{pmatrix} &= -\mathbf{q}_1 \mathbf{i}_d + \frac{\mathbf{q}_2 + \mathbf{q}_3}{L_n} \mathbf{n}_d \\ \begin{pmatrix} \mathbf{p}_4 \\ \mathbf{p}_5 \end{pmatrix} &= \mathbf{q}_1 \mathbf{i}_d - \frac{\mathbf{q}_2 + \mathbf{q}_3}{L_n} \mathbf{n}_d\end{aligned}$$

while, obviously, $\mathbf{p}_3 = \mathbf{q}_2$ and $\mathbf{p}_6 = \mathbf{q}_3$. After inserting the expressions for \mathbf{i}_d and \mathbf{n}_d with the displacement components in the global coordinate system from (4.52) and (4.53) we obtain (4.59).

We conclude that the basic forces \mathbf{q} are defined in a reference system, *the basic system* that translates and rotates with the element chord of length L_n in the deformed configuration. For this reason the reference frame is known as the *corotational frame*. The relations (4.59) transform the basic forces \mathbf{q} from the corotational reference system to the end forces \mathbf{p} in the global coordinate system X - Y of the structural model. The end forces \mathbf{p} can then be directly assembled into the resisting force vector \mathbf{P}_r of the structure.

4.4.5 Tangent stiffness matrix

The tangent stiffness matrix of the corotational plane frame element in global reference is

$$\begin{aligned}\mathbf{k}_e &= \frac{\partial \mathbf{p}}{\partial \mathbf{u}} = \frac{\partial [\mathbf{a}_g^T(\mathbf{u}) \mathbf{q}]}{\partial \mathbf{u}} \\ &= \mathbf{a}_g^T(\mathbf{u}) \frac{\partial \mathbf{q}}{\partial \mathbf{u}} + \frac{\partial [\mathbf{a}_g^T(\mathbf{u})]}{\partial \mathbf{u}} \mathbf{q} \\ &= \mathbf{a}_g^T(\mathbf{u}) \frac{\partial \mathbf{q}}{\partial \mathbf{v}} \frac{\partial \mathbf{v}}{\partial \mathbf{u}} + \frac{\partial [\mathbf{a}_g^T(\mathbf{u})]}{\partial \mathbf{u}} \mathbf{q} \\ &= \mathbf{a}_g^T(\mathbf{u}) \frac{\partial \mathbf{q}}{\partial \mathbf{v}} \mathbf{a}_g(\mathbf{u}) + \frac{\partial [\mathbf{a}_g^T(\mathbf{u})]}{\partial \mathbf{u}} \mathbf{q} \\ &= \mathbf{k}_m + \mathbf{k}_g\end{aligned}$$

where \mathbf{k}_m is the material stiffness matrix and \mathbf{k}_g the geometric stiffness matrix of the corotational plane frame element in the global coordinate system.

The material stiffness matrix of the corotational plane frame element is

$$\mathbf{k}_m = \mathbf{a}_g^T(\mathbf{u}) \frac{\partial \mathbf{q}}{\partial \mathbf{v}} \mathbf{a}_g(\mathbf{u}) \quad (4.60)$$

where

$$\frac{\partial \mathbf{q}}{\partial \mathbf{v}} = \mathbf{k}$$

is the basic element stiffness matrix given by (4.39). Nonlinear element geometry effects are included in \mathbf{k} , if the value ψ falls in the range $0.5 < \psi \leq 2$. Otherwise, if $\psi \leq 0.5$, the basic stiffness matrix \mathbf{k} for linear element geometry is used, and if $\psi > 2$, the structural member is subdivided into smaller elements to make sure that the value of ψ is less than 2.

The geometric stiffness of the corotational plane frame element is

$$\mathbf{k}_g = \frac{\partial [\mathbf{a}_g^T(\mathbf{u})]}{\partial \mathbf{u}} \mathbf{q} = \frac{\partial}{\partial \mathbf{u}} \begin{bmatrix} -\mathbf{i}_d \\ 0 \\ \mathbf{i}_d \\ 0 \end{bmatrix} \mathbf{q}_1 + \frac{\partial}{\partial \mathbf{u}} \begin{bmatrix} \frac{\mathbf{n}_d}{L_n} \\ 1 \\ -\frac{\mathbf{n}_d}{L_n} \\ 0 \end{bmatrix} \mathbf{q}_2 + \frac{\partial}{\partial \mathbf{u}} \begin{bmatrix} \frac{\mathbf{n}_d}{L_n} \\ 0 \\ -\frac{\mathbf{n}_d}{L_n} \\ 1 \end{bmatrix} \mathbf{q}_3 \quad (4.61)$$

The first term on the right hand side of the equation for \mathbf{k}_g represents the frame geometric stiffness contribution from the change of orientation of the axial basic force \mathbf{q}_1 . We call this the truss geometric stiffness \mathbf{k}_{ga}

$$\mathbf{k}_{ga} = \frac{\partial}{\partial \mathbf{u}} \begin{bmatrix} -\mathbf{i}_d \\ 0 \\ \mathbf{i}_d \\ 0 \end{bmatrix} \mathbf{q}_1 = \frac{\mathbf{q}_1}{L_n} \begin{bmatrix} (\mathbf{I} - \mathbf{i}_d \mathbf{i}_d^T) & 0 & -(\mathbf{I} - \mathbf{i}_d \mathbf{i}_d^T) & 0 \\ \mathbf{0} & 0 & \mathbf{0} & 0 \\ -(\mathbf{I} - \mathbf{i}_d \mathbf{i}_d^T) & 0 & (\mathbf{I} - \mathbf{i}_d \mathbf{i}_d^T) & 0 \\ \mathbf{0} & 0 & \mathbf{0} & 0 \end{bmatrix} \quad (4.62)$$

The matrix multiplying $\frac{\mathbf{q}_1}{L_n}$ in (4.62) is a *projection matrix on the plane normal to the unit vector \mathbf{i}_d* , i.e. normal to the element chord in the deformed configuration.

We note that the derivative of the second and third column on the right hand side of (4.61) give the same result, so that the second and the third term can be combined into a single geometric stiffness contribution for the plane frame element, the beam geometric stiffness \mathbf{k}_{gb} . This geometric stiffness contribution arises from the orientation change of the transverse end forces $\frac{\mathbf{q}_2 + \mathbf{q}_3}{L_n}$ noting, however, that there is also a magnitude change of these forces due to the change of the deformed element length L_n

$$\mathbf{k}_{gb} = \frac{\mathbf{q}_2 + \mathbf{q}_3}{L_n^2} \begin{bmatrix} (\mathbf{i}_d \mathbf{n}_d^T + \mathbf{n}_d \mathbf{i}_d^T) & 0 & -(\mathbf{i}_d \mathbf{n}_d^T + \mathbf{n}_d \mathbf{i}_d^T) & 0 \\ \mathbf{0} & 0 & \mathbf{0} & 0 \\ -(\mathbf{i}_d \mathbf{n}_d^T + \mathbf{n}_d \mathbf{i}_d^T) & 0 & (\mathbf{i}_d \mathbf{n}_d^T + \mathbf{n}_d \mathbf{i}_d^T) & 0 \\ \mathbf{0} & 0 & \mathbf{0} & 0 \end{bmatrix} \quad (4.63)$$

The matrix multiplying $\frac{\mathbf{q}_2 + \mathbf{q}_3}{L_n^2}$ in (4.63) is a reflection matrix about the 45° line of the corotational reference system, i.e. the line that bisects the angle between the unit vectors \mathbf{i}_d and \mathbf{n}_d .

In conclusion, the geometric stiffness matrix of the plane frame element *due to the nonlinear chord geometry effect* consists of a truss geometric stiffness \mathbf{k}_{ga} and a beam geometric stiffness \mathbf{k}_{gb}

$$\mathbf{k}_g = \mathbf{k}_{ga} + \mathbf{k}_{gb} \quad (4.64)$$

\mathbf{k}_{ga} is given by (4.62) and \mathbf{k}_{gb} by (4.63). We call \mathbf{k}_{ga} *the truss effect of the nonlinear chord geometry*. It is now worth comparing the corotational form of the truss geometric stiffness in (4.62), with the Green-Lagrange expression for the truss element with nonlinear geometry in (3.47)

$$\mathbf{k}_g = \frac{\mathbf{q}_1}{L} \begin{bmatrix} 1 & 0 & -1 & 0 \\ 0 & 1 & 0 & -1 \\ -1 & 0 & 1 & 0 \\ 0 & -1 & 0 & 1 \end{bmatrix} = \frac{\mathbf{q}_1}{L} \begin{bmatrix} \mathbf{I} & -\mathbf{I} \\ -\mathbf{I} & \mathbf{I} \end{bmatrix}$$

We note that in the corotational formulation L_n takes the place of L and $\mathbf{I} - \mathbf{i}_d \mathbf{i}_d^T$ takes the place of \mathbf{I} in the Green-Lagrange formulation. These stiffness matrices are consistent with the resisting forces of the two truss element formulations, which were discussed in Chapter 2. *For structural engineering applications the two formulations give very similar results.*

In conclusion, the tangent stiffness matrix of the plane frame element with the corotational formulation is given by

$$\mathbf{k}_e = \mathbf{k}_m + \mathbf{k}_g \quad (4.65)$$

with the material stiffness \mathbf{k}_m in (4.60) and the geometric stiffness \mathbf{k}_g in (4.64).

4.5 Truss Effect Approximation of Nonlinear Chord Geometry

4.5.1 Introduction

Structural members that are susceptible to the effect of nonlinear geometry are slender columns and braces carrying high axial compressive forces. The slenderness of these elements implies that the span to depth ratio is relatively large, so that transverse forces due to end moments are several times smaller than the axial forces. Noting that the axial force \mathbf{q}_1 is the direct multiplier of the truss geometric stiffness \mathbf{k}_{ga} in (4.62), while the transverse end force $\frac{\mathbf{q}_2 + \mathbf{q}_3}{L_n}$ is the direct multiplier of the beam geometric stiffness \mathbf{k}_{gb} in (4.63) after leaving out the inverse of the deformed element length L_n in both expressions, we conclude that the truss geometric stiffness \mathbf{k}_{ga} is much more significant than the beam geometric stiffness \mathbf{k}_{gb} . In developing an approximate method for accounting for the geometric stiffness of the frame element we, therefore, *neglect the beam stiffness contribution*.

Consequently, approximations of the nonlinear chord geometry effect neglect the beam geometric stiffness contribution and focus instead on the truss geometric stiffness.

Historic approximate methods of accounting for the truss effect of the nonlinear chord geometry are motivated by the need for calculation simplicity with the calculation tools of the times. In particular,

the convenience of linear structural analysis methods and of the principle of linear superposition for multiple load cases were critical considerations for the development of these approximate methods for the analysis of multi-story frames with typical column compressive load ratios under inter-story sidesway drift ratios smaller than 1%. As long as the application range is respected these approximate methods show impressive accuracy.

With the access to sophisticated analysis software it is not clear that approximate methods of the truss effect of nonlinear chord geometry are as useful today as before. Nonetheless, the approximate methods for the nonlinear geometry of slender frame members provide the best insight into the relative significance of the terms of the corotational theory.

4.5.2 Derivation

The most important approximation for the truss effect of nonlinear chord geometry is based on the simplification of the equilibrium equations in (4.58) between the element end forces $\bar{\mathbf{p}}$ in the local reference system and the basic element forces \mathbf{q} under the following assumptions:

- 1) The terms $\Delta\bar{\mathbf{u}}_x$ and $\Delta\bar{\mathbf{u}}_y$ are very small relative to 1, so that $L_n \approx L$.
- 2) $\Delta\bar{\mathbf{u}}_x$ is so small relative to 1 that it is altogether neglected.
- 3) The term $\Delta\bar{\mathbf{u}}_y/L$ is included only in the first column of the static matrix \mathbf{a}_g^T , because this column multiplies the axial basic force \mathbf{q}_1 , but it is neglected in the second and third column of the static matrix, because these columns multiply the much smaller transverse end forces $\frac{\mathbf{q}_2 + \mathbf{q}_3}{L}$. *Consequently, the truss effect of the nonlinear chord geometry is approximately included, while the beam effect of the nonlinear chord geometry is neglected.*

With these assumptions the equilibrium equations in (4.58) simplify to

$$\bar{\mathbf{p}} = \begin{bmatrix} -\frac{L + \Delta\bar{\mathbf{u}}_x}{L_n} & -\frac{\Delta\bar{\mathbf{u}}_y}{L_n^2} & -\frac{\Delta\bar{\mathbf{u}}_y}{L_n^2} \\ -\frac{\Delta\bar{\mathbf{u}}_y}{L_n} & \frac{L + \Delta\bar{\mathbf{u}}_x}{L_n^2} & \frac{L + \Delta\bar{\mathbf{u}}_x}{L_n^2} \\ 0 & 1 & 0 \\ \frac{L + \Delta\bar{\mathbf{u}}_x}{L_n} & \frac{\Delta\bar{\mathbf{u}}_y}{L_n^2} & \frac{\Delta\bar{\mathbf{u}}_y}{L_n^2} \\ \frac{\Delta\bar{\mathbf{u}}_y}{L_n} & -\frac{L + \Delta\bar{\mathbf{u}}_x}{L_n^2} & -\frac{L + \Delta\bar{\mathbf{u}}_x}{L_n^2} \\ 0 & 0 & 1 \end{bmatrix} \mathbf{q} \approx \begin{bmatrix} -1 & 0 & 0 \\ -\frac{\Delta\bar{\mathbf{u}}_y}{L} & \frac{1}{L} & \frac{1}{L} \\ 0 & 1 & 0 \\ 1 & 0 & 0 \\ \frac{\Delta\bar{\mathbf{u}}_y}{L} & -\frac{1}{L} & -\frac{1}{L} \\ 0 & 0 & 1 \end{bmatrix} \mathbf{q} = \begin{bmatrix} -1 & 0 & 0 \\ 0 & \frac{1}{L} & \frac{1}{L} \\ 0 & 1 & 0 \\ 1 & 0 & 0 \\ 0 & -\frac{1}{L} & -\frac{1}{L} \\ 0 & 0 & 1 \end{bmatrix} \mathbf{q} + \begin{bmatrix} 0 \\ -\frac{\Delta\bar{\mathbf{u}}_y}{L} \\ 0 \\ 0 \\ \frac{\Delta\bar{\mathbf{u}}_y}{L} \\ 0 \end{bmatrix} \mathbf{q}_1$$

In the last expression we split the end forces under linear statics from the contribution of the approximate truss effect of nonlinear chord geometry. Recalling the definition of the static matrix $\mathbf{b} = \mathbf{a}^T$ under linear geometry from linear structural analysis we write the end forces $\bar{\mathbf{p}}$ in the local reference system as

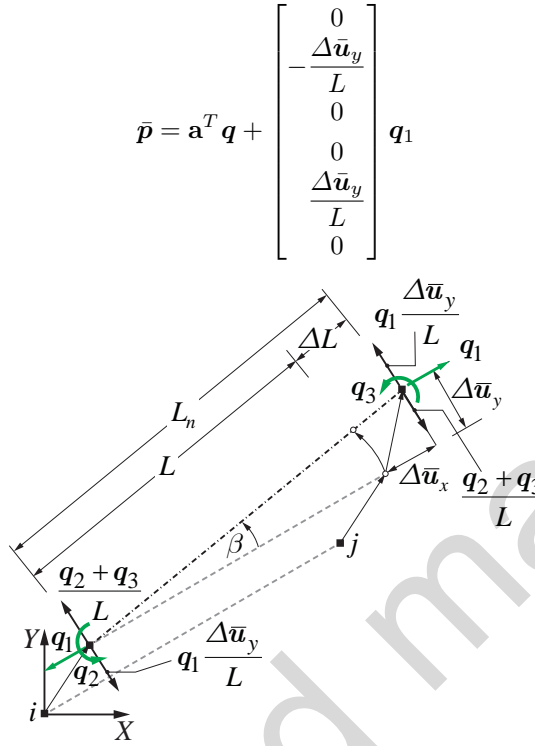


Fig. 4.11: Graphic representation of truss effect approximation of nonlinear chord geometry

Fig. 4.11 shows the graphic representation of the truss effect approximation of nonlinear chord geometry: the basic element forces \mathbf{q} are assumed in a reference system that is oriented in the undeformed element configuration. Consequently, the dependent element end forces are also oriented parallel and normal to the chord direction of the undeformed element. The axial basic force \mathbf{q}_1 at element end j is offset from the corresponding co-directional dependent end force at the opposite end i by the relative end translation $\Delta \bar{u}_y$ normal to the element chord in the undeformed configuration. This gives rise to a moment $\mathbf{q}_1 \Delta \bar{u}_y$ that needs to be resisted by corresponding transverse element end forces. The resulting contribution to the transverse element end forces is

$$\mathbf{q}_1 \frac{\Delta \bar{u}_y}{L}$$

For the case that the element length L is equal to the structural member length L_m , the approximate truss effect of the nonlinear chord geometry is termed the *P-Δ* or *big P-delta effect* in publications and codes of professional practice.

4.5.3 Summary

The truss effect approximation of nonlinear chord geometry is based on the following kinematic and static relations:

- 1) The relation between the element deformations \mathbf{v} and the end displacements \mathbf{u} is linear $\mathbf{v} = \mathbf{a}_g \mathbf{u}$.
- 2) The axial basic force \mathbf{q}_1 is oriented in the chord direction of the undeformed element; the transverse element end forces include the effect of the axial basic force "eccentricity" $\Delta \bar{u}_y$ due to the rotation of the element chord in the deformed configuration. The resulting element end forces \mathbf{p} in the global

coordinate system are

$$\mathbf{p} = \mathbf{a}_g^T \mathbf{q} + \begin{bmatrix} \frac{\Delta \bar{u}_y}{L} \frac{\Delta Y}{L} \\ -\frac{\Delta \bar{u}_y}{L} \frac{\Delta X}{L} \\ 0 \\ -\frac{\Delta \bar{u}_y}{L} \frac{\Delta Y}{L} \\ \frac{\Delta \bar{u}_y}{L} \frac{\Delta X}{L} \\ 0 \end{bmatrix} \mathbf{q}_1 \quad (4.66)$$

- 3) The plane frame stiffness in the global coordinate system is

$$\mathbf{k}_e = \mathbf{k}_m + \mathbf{k}_g = \mathbf{a}_g^T \mathbf{k} \mathbf{a}_g + \frac{\mathbf{q}_1}{L} \begin{bmatrix} (\mathbf{I} - \mathbf{i} \mathbf{i}^T) \mathbf{0} & -(\mathbf{I} - \mathbf{i} \mathbf{i}^T) \mathbf{0} \\ \mathbf{0} & 0 & \mathbf{0} & 0 \\ -(\mathbf{I} - \mathbf{i} \mathbf{i}^T) \mathbf{0} & (\mathbf{I} - \mathbf{i} \mathbf{i}^T) \mathbf{0} \\ \mathbf{0} & 0 & \mathbf{0} & 0 \end{bmatrix} \quad (4.67)$$

where \mathbf{k} is the basic element stiffness matrix that includes the nonlinear element geometry effect, if necessary. The geometric stiffness matrix \mathbf{k}_g represents the truss effect approximation of the nonlinear chord geometry. The components of the unit vector \mathbf{i} are the direction cosines of the element chord in the undeformed configuration according to (4.57).

The stiffness matrix \mathbf{k}_e in (4.67) is not tangent to the element resisting force \mathbf{p} in (4.66). Thus, the use of this approximation with a multi-step nonlinear solution strategy results in slower convergence than with the tangent frame element stiffness matrix in (4.65). The truss effect approximation of nonlinear chord geometry is, however, very useful for the quick estimation of the nonlinear chord geometry effect of frames with a small number of dofs and for the understanding of the methods for including this effect in codes of professional practice, such as the *moment magnification factor*, as will be discussed shortly.

4.6 Linear Stability Analysis

4.6.1 Introduction

The determination of the linear buckling load of a structural model is an interesting problem of structural analysis that occupies several pages of textbooks. Such considerations are reflected in modern design codes in the K -factors for the effective length determination of structural members and in the magnification factors for second order linear analysis of structures.

With the widespread availability of powerful computer hardware and software for conducting non-linear push-over analyses of structures the importance of this problem is significantly reduced.

Because linear buckling analysis offers insight into the behavior of slender structures under high compressive forces, we discuss it in some detail in the following.

4.6.2 Assumptions

The linear buckling load is established *in the undeformed configuration* of the structural model. The elements of the model are assumed to be subjected *only to axial forces* so that the flexural basic forces \mathbf{q}_2 and \mathbf{q}_3 of the element under compression are zero. Moreover, *the compression member is assumed to be inextensible so that its axial force can be determined by static, tributary area considerations even for statically indeterminate structures.*

Because the displacements are zero, and the flexural basic forces are zero, the stiffness matrix of each frame element in the global reference system is given by (4.67)

$$\mathbf{k}_e = \mathbf{a}_g^T \mathbf{k} \mathbf{a}_g + \frac{\mathbf{q}_1}{L} \begin{bmatrix} (\mathbf{I} - \mathbf{i} \mathbf{i}^T) \mathbf{0} & -(\mathbf{I} - \mathbf{i} \mathbf{i}^T) \mathbf{0} \\ \mathbf{0} & 0 & 0 & 0 \\ -(\mathbf{I} - \mathbf{i} \mathbf{i}^T) \mathbf{0} & (\mathbf{I} - \mathbf{i} \mathbf{i}^T) \mathbf{0} \\ \mathbf{0} & 0 & 0 & 0 \end{bmatrix}$$

where \mathbf{k} is the basic element stiffness matrix that includes the nonlinear element geometry effect, if necessary. The element geometric stiffness matrix \mathbf{k}_g represents *the nonlinear chord geometry at the undeformed configuration*. It is important to note that the basic element stiffness matrix *also contains a geometric stiffness matrix contribution when it includes the nonlinear element geometry, or P-δ effect*.

Because the linear buckling analysis investigates the stability of a structural model in the undeformed configuration and considers infinitesimally small displacement increments relative to the undeformed configuration the kinematic matrix \mathbf{a}_g is linear so that

$$\mathbf{a}_g = \begin{bmatrix} -\frac{\Delta X}{L} & -\frac{\Delta Y}{L} & 0 & \frac{\Delta X}{L} & \frac{\Delta Y}{L} & 0 \\ -\frac{\Delta Y}{L^2} & \frac{\Delta X}{L^2} & 1 & \frac{\Delta Y}{L^2} & -\frac{\Delta X}{L^2} & 0 \\ -\frac{\Delta Y}{L^2} & \frac{\Delta X}{L^2} & 0 & \frac{\Delta Y}{L^2} & -\frac{\Delta X}{L^2} & 1 \end{bmatrix}$$

For the same reason the geometric stiffness matrix \mathbf{k}_g depends on the direction cosines of the element chord in the undeformed configuration with the unit vector \mathbf{i} in the direction of the element chord as

$$\mathbf{i} = \begin{pmatrix} \frac{\Delta X}{L} \\ \frac{\Delta Y}{L} \end{pmatrix}$$

4.6.3 Structure Stiffness Contributions

According to Section 4.3.4 the material stiffness contribution $\mathbf{k}_m = \mathbf{a}_g^T \mathbf{k} \mathbf{a}_g$ to the frame element stiffness matrix \mathbf{k}_e can be split into two contributions if the ψ -factor of the frame element lies in Zone II: the first is the linear stiffness matrix \mathbf{k}_l under linear element statics and kinematics, and the second is the $\mathbf{k}_{P\delta}$ stiffness matrix of the second order approximation of the nonlinear element geometry effect. Consequently, the element stiffness matrix \mathbf{k}_e becomes in this case

$$\mathbf{k}_e = \mathbf{a}_g^T \mathbf{k}_l \mathbf{a}_g + \mathbf{a}_g^T \mathbf{k}_{P\delta} \mathbf{a}_g + \frac{\mathbf{q}_1}{L} \begin{bmatrix} (\mathbf{I} - \mathbf{i} \mathbf{i}^T) \mathbf{0} - (\mathbf{I} - \mathbf{i} \mathbf{i}^T) \mathbf{0} \\ \mathbf{0} \quad 0 \quad \mathbf{0} \quad 0 \\ -(\mathbf{I} - \mathbf{i} \mathbf{i}^T) \mathbf{0} \quad (\mathbf{I} - \mathbf{i} \mathbf{i}^T) \mathbf{0} \\ \mathbf{0} \quad 0 \quad \mathbf{0} \quad 0 \end{bmatrix}$$

The direct stiffness assembly of the first contribution gives the structure stiffness matrix \mathbf{K}_l of linear analysis. The direct stiffness assembly of the second gives the $\mathbf{K}_{P\delta}$ contribution to the *geometric stiffness matrix of the structural model*. Finally, the direct stiffness assembly of the third gives the $\mathbf{K}_{P\Delta}$ contribution to the *geometric stiffness matrix of the structural model*. With the Boolean matrix notation we write

$$\begin{aligned}\check{\mathbf{K}}_l &= \sum_{el} \mathbf{A}_b^{(el)T} \mathbf{k}_{el}^{(el)} \mathbf{A}_b^{(el)} \quad \text{with } \mathbf{k}_{el} = \mathbf{a}_g^T \mathbf{k}_l \mathbf{a}_g \\ \check{\mathbf{K}}_{P\delta} &= \sum_{el} \mathbf{A}_b^{(el)T} \mathbf{k}_{eP\delta}^{(el)} \mathbf{A}_b^{(el)} \quad \text{with } \mathbf{k}_{eP\delta} = \mathbf{a}_g^T \mathbf{k}_{P\delta} \mathbf{a}_g \\ \check{\mathbf{K}}_{P\Delta} &= \sum_{el} \mathbf{A}_b^{(el)T} \mathbf{k}_g^{(el)} \mathbf{A}_b^{(el)}\end{aligned}$$

for the stiffness matrix *at all dofs of the structural model*.

Alternatively, for small structural models the structure stiffness matrix *at the free dofs* can be set up with the structure kinematic matrix under linear constraints $\tilde{\mathbf{A}}_f$. For the linear structure stiffness matrix \mathbf{K}_l this gives

$$\mathbf{K}_l = \tilde{\mathbf{A}}_f^T \mathbf{K}_{sl} \tilde{\mathbf{A}}_f \quad \text{with } \mathbf{K}_{sl} = \begin{bmatrix} \mathbf{k}_l^{(a)} & \mathbf{0} & \dots & \mathbf{0} \\ \mathbf{0} & \mathbf{k}_i^{(b)} & \dots & \mathbf{0} \\ \vdots & \vdots & \ddots & \vdots \\ \mathbf{0} & \mathbf{0} & \dots & \mathbf{k}_l^{(ne)} \end{bmatrix} \quad (4.68)$$

and for the $\mathbf{K}_{P\delta}$ structure stiffness matrix it gives

$$\mathbf{K}_{P\delta} = \tilde{\mathbf{A}}_f^T \mathbf{K}_{sP\delta} \tilde{\mathbf{A}}_f \quad \text{with } \mathbf{K}_{sP\delta} = \begin{bmatrix} \mathbf{k}_{P\delta}^{(a)} & \mathbf{0} & \dots & \mathbf{0} \\ \mathbf{0} & \mathbf{k}_{P\delta}^{(b)} & \dots & \mathbf{0} \\ \vdots & \vdots & \ddots & \vdots \\ \mathbf{0} & \mathbf{0} & \dots & \mathbf{k}_{P\delta}^{(ne)} \end{bmatrix} \quad (4.69)$$

For small structural models it is advisable to set up the $\mathbf{K}_{P\Delta}$ structure stiffness matrix directly with the principle of virtual work. We note that this stiffness matrix *affects only the translation dofs*.

4.6.4 Linear Eigenvalue Problem

Noting that there are no applied nodal forces at the free dofs of the structural model with inextensible elements in the undeformed configuration the equilibrium equations at these dofs take the form

$$(\mathbf{K}_l + \mathbf{K}_{P\delta} + \mathbf{K}_{P\Delta}) \mathbf{U}_f = \mathbf{0}$$

We combine the two nonlinear geometry contributions to the structure stiffness matrix into a single *geometric stiffness of the structure* \mathbf{K}_g

$$\mathbf{K}_g = \mathbf{K}_{P\delta} + \mathbf{K}_{P\Delta} \quad (4.70)$$

Noting that both the element stiffness matrix $\mathbf{k}_{P\delta}$ and the element geometric stiffness matrix \mathbf{k}_g depend linearly on the axial basic force \mathbf{q}_1 we conclude that the geometric stiffness of the structure \mathbf{K}_g depends linearly on the magnitude of the axial force distribution in the structure. Because this magnitude is to be determined in the linear buckling analysis problem, we factor out the load factor $\lambda \geq 0$. Because the structural instability in the undeformed configuration arises under compressive element forces we write the equilibrium equations at the free dofs in the form

$$(\mathbf{K}_l - \lambda \mathbf{K}'_g) \mathbf{U}_f = \mathbf{0} \quad (4.71)$$

where \mathbf{K}'_g denotes the geometric stiffness of the structure under the axial force distribution that results from the direction reversal of the applied nodal force pattern.

The solution of the linear eigenvalue problem in (4.71) furnishes as many eigenvalues λ as the number of non-zero terms on the diagonal of the geometric stiffness matrix \mathbf{K}_g of the structure along with the corresponding eigenvectors. We are typically interested only in the lowest eigenvalue λ_e of the linear buckling analysis problem in (4.71).

4.6.5 Examples

Example 4.1 Cantilever Column

Fig. 4.12 shows three variations for the model of a cantilever column of height L . The column is assumed to have infinite axial stiffness EA and is, therefore, treated as inextensible. It carries a downward load λP_v at its tip, with P_v denoting the absolute value of the vertical load. In the first model (a) the column is represented by a Green-Lagrange truss element and is supported laterally with a spring of axial stiffness k_s . In the second model (b) the column has infinite flexural stiffness EI , pivots about the simple support at its base, and is again supported laterally with a spring of axial stiffness k_s . In the third model (c) the column has uniform flexural stiffness EI and is fixed at its base, but does not have a lateral spring at its tip.

We determine the linear buckling load factor λ_e for the three column models. Because the column is assumed to be inextensible, it has only one free dof, the horizontal translation U at the tip. In linear buckling analysis we investigate the column equilibrium at its undeformed position. The equilibrium equation at the free dof is

$$KU = 0 \quad (4.72)$$

where the stiffness K is the sum of the material stiffness K_m and the geometric stiffness K_g . For model (a) the material stiffness consists of only the lateral spring stiffness k_s while the geometric stiffness of the Green-Lagrange truss is given by (3.47). Substituting $-\lambda P_v$ for the axial basic force \mathbf{q}_1 of the truss element gives

$$K = K_m + K_g = k_s - \frac{\lambda P_v}{L} = k_s - \lambda \frac{P_v}{L} = K_m - \lambda K'_g \quad (4.73)$$

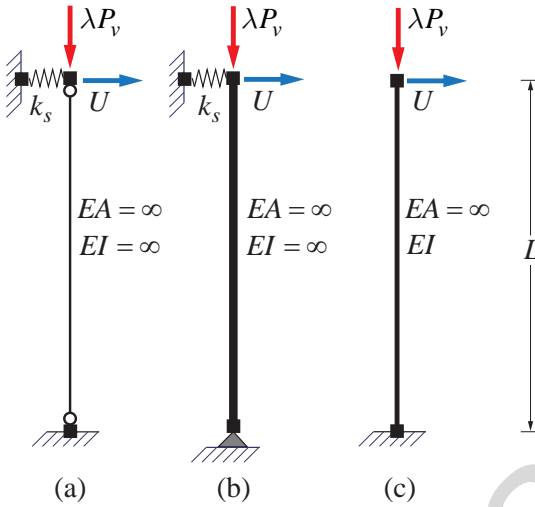


Fig. 4.12: Three cantilever column models under axial load λP ; (a) and (b) have identical response

where K'_g is the geometric stiffness matrix of the Green-Lagrange truss element for a *positive* axial basic force P_v . (4.72) now becomes

$$\left(k_s - \lambda \frac{P_v}{L} \right) U = 0 \quad (4.74)$$

A non-zero horizontal translation U is only possible, if the stiffness becomes zero. This condition renders the structure *unstable* and allows non-zero horizontal translation values of arbitrary magnitude. Theoretically, however, only infinitesimal values of U are consistent with the assumption that the equilibrium is set up in the undeformed, straight column configuration. The zero-stiffness condition at the undeformed configuration is called the *linear buckling condition*, and the corresponding value of the load is called the *linear buckling load* with the load factor $\lambda_e \geq 0$ called the *linear buckling load factor*. From (4.74) we conclude that the linear buckling load for the column model (a) is

$$\lambda_e P_v = k_s L \quad (4.75)$$

The column model (b) has the same material stiffness as the column model (a) and turns out to also have the same geometric stiffness for the following reasons:

- The beam geometric stiffness \mathbf{k}_{gb} in (4.63) for the plane frame element is zero, because \mathbf{q}_2 and \mathbf{q}_3 are equal to zero.
- The truss geometric stiffness \mathbf{k}_{ga} in (4.62) for the plane frame element is equal to

$$k_{ga} = \frac{\mathbf{q}_1}{L}$$

because $L_n = L$ and $\mathbf{id} = \mathbf{i}$ in the undeformed configuration. For the cantilever column the direction cosines of the element axis are $\mathbf{i} = [0 \ 1]^T$, so that the geometric stiffness k_{ga} results.

Consequently, the linear buckling load of the column model (b) is the same as that for model (a).

For the cantilever column model (c) we pursue three solutions following the results of Section 4.3: (1) a solution with the exact flexural stiffness coefficient C of the basic plane frame element with zero moment at one end, (2) a solution with the second order approximation of the flexural stiffness coefficient,

and (3) a solution with a first order (linear) approximation of the flexural stiffness coefficient that does not account for the nonlinear element geometry effect. For all three solutions we use (4.60) to transform the material stiffness of the element to global coordinates, noting that the "material" stiffness includes the nonlinear element geometry effect, because it refers to the transformation of the basic stiffness matrix \mathbf{k} of the plane frame element to global coordinates. Because $\mathbf{u} = 0$ in the undeformed configuration the kinematic matrix \mathbf{a}_g corresponds to linear geometry. For a small structural model we can, therefore, use the expression $\mathbf{A}_f^T \mathbf{K}_s \mathbf{A}_f$ to set up the contribution of the basic stiffness of all structural elements to the global dofs of the model. For the cantilever column model with a single plane frame element a we have

$$v_2^{(a)} = V_1 = \frac{U}{L}$$

so that $\mathbf{A}_f = 1/L$.

(a) *Exact Nonlinear Element Geometry*

The material stiffness contribution to the global dof is

$$K_m = \frac{1}{L} \left(C \frac{EI}{L} \right) \frac{1}{L}$$

The stiffness contribution due to the nonlinear chord geometry effect is the same as for model (b) for the reasons discussed for that model. Consequently, the equilibrium equation at the free dof of the cantilever column is

$$\left(C \frac{EI}{L^3} - \lambda \frac{P_v}{L} \right) U = 0 \quad (4.76)$$

after substituting $-\lambda P_v$ for the axial basic force \mathbf{q}_1 of the plane frame element. Recalling from (4.35) that

$$|\mathbf{q}_1| = \lambda P_v = \psi^2 \frac{EI}{L^2}$$

(4.76) becomes

$$(C - \psi^2) \frac{EI}{L^3} U = 0 \quad (4.77)$$

This gives the following nonlinear equation as the *buckling condition for the cantilever column with flexural stiffness EI*

$$C - \psi^2 = 0 \quad (4.78)$$

Substituting C from (4.34) in the buckling condition (4.78) gives

$$\frac{\psi^2 \sin \psi}{\sin \psi - \psi \cos \psi} - \psi^2 = 0 \quad \rightarrow \quad \frac{\psi^3 \cos \psi}{\sin \psi - \psi \cos \psi} = 0$$

There is an infinite number of solutions for this trigonometric equation, the odd multiples of $\frac{\pi}{2}$. The lowest value corresponds to $\psi = \frac{\pi}{2}$ and the corresponding buckling load is

$$\lambda_{ex} P_v = \frac{\pi^2}{4} \frac{EI}{L^2} = \frac{\pi^2 EI}{(2L)^2} \quad (4.79)$$

The result in (4.79) is the exact linear buckling load for a cantilever column of length L and flexural stiffness EI , which we denote with subscript ex .

(b) *Second Order Nonlinear Element Geometry*

In this case we use the expression for C in (4.37) in the equilibrium equation in (4.76) to get

$$\left(\frac{3EI}{L^3} - \frac{1}{5}\lambda \frac{P_v}{L} - \lambda \frac{P_v}{L} \right) U = 0 \quad (4.80)$$

We note that the basic element stiffness contribution to the global dof stiffness splits into two contributions: (a) the linear contribution $3EI/L^3$, and (b) the second order approximation of the nonlinear element geometry $\lambda P_v/(5L)$. We note that the *second order approximation of the nonlinear element geometry is linear in the axial force of the element, as is the geometric stiffness term due to the nonlinear chord geometry effect*. We can, therefore, combine the two into the *geometric stiffness of the cantilever column K_g* getting

$$K_g = -\frac{1}{5}\lambda \frac{P_v}{L} - \lambda \frac{P_v}{L} = -\lambda \frac{6}{5} \frac{P_v}{L}$$

We note that there are two geometric stiffness contributions to the global dofs by the plane frame element: (a) the P - δ stiffness contribution due to the nonlinear geometry of the *basic frame element* or *nonlinear element geometry*, and (b) the nonlinear chord effect stiffness contribution, which *is the same for all 2-node plane frame elements*. In the following we denote the former with $\mathbf{K}_{P\delta}$ and the latter with $\mathbf{K}_{P\Delta}$ for ease of distinction.

We make the following observations:

- The second order approximation of the flexural stiffness coefficients of the plane frame element under axial compression *separates the linear stiffness contribution from the P - δ contribution*.
- Because the P - δ and the P - Δ contribution depend linearly on the axial force in the element, *they can be combined into the geometric element stiffness contribution $\mathbf{K}_g^{(el)}$ to the structural stiffness matrix \mathbf{K}* .
- Because all geometric element stiffness contributions $\mathbf{K}_g^{(el)}$ appear separately from the linear stiffness matrix, the stiffness matrix \mathbf{K} of the structure is the sum of two stiffness matrices

$$\mathbf{K} = \mathbf{K}_l + \mathbf{K}_g = \mathbf{K}_l + (\mathbf{K}_{P\delta} + \mathbf{K}_{P\Delta})$$

- Because all geometric element stiffness contributions $\mathbf{K}_g^{(el)}$ depend linearly on the axial force of the corresponding element, we factor out the load factor $\lambda \geq 0$ and use a reference axial force distribution *with the absolute value of the basic force q_1 of the corresponding element* to set up a reference geometric stiffness matrix \mathbf{K}'_g . The stiffness matrix of the structure thus becomes

$$\mathbf{K} = \mathbf{K}_l - \lambda \mathbf{K}'_g$$

and the stability condition $\mathbf{KU}_f = \mathbf{0}$ turns into a *linear eigenvalue problem* of the form

$$(\mathbf{K}_l - \lambda \mathbf{K}'_g) \mathbf{U}_f = \mathbf{0}$$

In conclusion we have for the cantilever column

$$K_g = K_{P\delta} + K_{P\Delta} = -\frac{1}{5}\lambda \frac{P_v}{L} - \lambda \frac{P_v}{L} = -\lambda \frac{6}{5} \frac{P_v}{L}$$

and the buckling condition $K = 0$ in (4.80) gives the linear buckling load factor λ_{es}

$$\lambda_{es} P_v = \frac{15}{6} \frac{EI}{L^2} = 2.5 \frac{EI}{L^2} \quad (4.81)$$

The buckling load factor λ_{es} in (4.81) is the exact value for the *second order approximation of the geometric stiffness matrix of the structure* and we denote it with subscript *s*. *Second order approximation* refers to the fact that the $\mathbf{K}_{P\delta}$ and $\mathbf{K}_{P\Delta}$ geometric stiffness contributions to the structure stiffness matrix are *linearly dependent on the axial basic forces of the elements*, as discussed in Section 4.37.

(c) Linear Element Geometry

We neglect the nonlinear element geometry by setting $K_{P\delta} = 0$ thus assuming that the basic flexural stiffness of the frame element without a moment at one end is equal to $3EI/L$. For this case the equilibrium equation in (4.72) becomes

$$\left(\frac{3EI}{L^3} - \lambda \frac{P_v}{L} \right) U = 0 \quad (4.82)$$

and the buckling condition $K = 0$ gives the linear buckling load factor λ_{ec}

$$\lambda_{ec} P_v = 3 \frac{EI}{L^2} \quad (4.83)$$

The buckling load factor λ_{ec} in (4.83) results from including only the nonlinear chord geometry of the frame element, and we denote it with subscript *c*.

(d) Summary

Writing the expression for the buckling load factor in the form

$$\lambda_e = \zeta \frac{EI}{P_v L^2} \quad (4.84)$$

with ζ a numerical coefficient we compare the results for the buckling load factor of the three cases in Table 4.1.

Case	λ_e	ζ	Error
(a)	λ_{ex}	$\frac{\pi^2}{4}$	0
(b)	λ_{es}	2.5	1.3 %
(c)	λ_{ec}	3	21.6 %

Table 4.1: Comparison of the buckling load coefficient ζ for different geometric stiffness models

(e) Further Considerations

Noting that the ψ -factor of the cantilever column for the exact buckling load is equal to $\frac{\pi}{2} = 1.57$ the results of Table 4.1 are not surprising given that the ψ -factor of the frame element lies in Zone II of

Section 4.3.3. We investigate how to improve the buckling load estimate by subdividing the column into two frame elements of equal length without including the nonlinear element geometry effect in the form of the $\mathbf{K}_{P\delta}$ stiffness contribution to the global dofs.

Fig. 4.13 shows the cantilever column model with 2 elements and the independent free dofs. With $L' = L/2$ the linear stiffness matrix \mathbf{K}_l is

$$\mathbf{K}_l = \begin{bmatrix} \frac{15EI}{L'^3} & \frac{3EI}{L'^2} & -\frac{3EI}{L'^3} \\ \frac{3EI}{L'^2} & \frac{7EI}{L'} & \frac{3EI}{L'^2} \\ -\frac{3EI}{L'^3} & \frac{3EI}{L'^2} & \frac{3EI}{L'^3} \end{bmatrix} \quad (4.85)$$

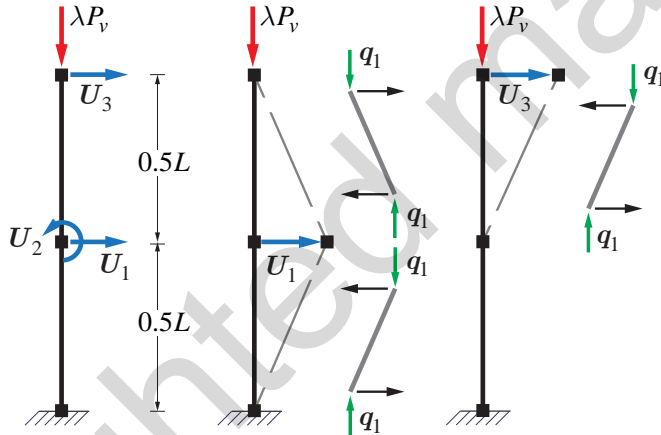


Fig. 4.13: $P\Delta$ stiffness for 2 element discretization of cantilever column

Fig. 4.13 shows the $P\Delta$ forces in the column elements under a unit displacement at the translation dofs \mathbf{U}_1 and \mathbf{U}_3 . The resulting reference geometric stiffness matrix $\mathbf{K}'_{P\Delta}$ is

$$\mathbf{K}'_{P\Delta} = \frac{P_v}{L'} \begin{bmatrix} 2 & 0 & -1 \\ 0 & 0 & 0 \\ -1 & 0 & 1 \end{bmatrix}$$

Because the global rotation dofs are not affected by the $P\Delta$ effect of the column elements, the reference geometric stiffness matrix $\mathbf{K}'_{P\Delta}$ has zero diagonal terms corresponding to the rotation dofs. The solution of the linear eigenvalue problem

$$(\mathbf{K}_l - \lambda \mathbf{K}'_g) \mathbf{U}_f = \mathbf{0}$$

for the buckling load factor determination λ_e is simpler after condensing out the rotation dofs. Condensing out the second dof from the stiffness matrix \mathbf{K}_l in (4.85) gives

$$\mathbf{U}_2 = -\frac{3}{7L'} \mathbf{U}_1 \rightarrow \mathbf{K}_{lc} = \frac{EI}{L'^3} \begin{bmatrix} \frac{96}{7} & -\frac{30}{7} \\ -\frac{30}{7} & \frac{12}{7} \end{bmatrix}$$

where \mathbf{K}_{lc} is the condensed stiffness matrix for the two translation dofs.

An alternative way of determining the condensed stiffness matrix for the two translation dofs is to determine the flexibility matrix \mathbf{F} and then invert it. For the problem in hand this is computationally more onerous, but it becomes advantageous in the presence of more rotation dofs in the stiffness matrix. We, therefore, briefly review the process from Linear Structural Analysis. The flexibility matrix at the two translation dofs is

$$\mathbf{F} = \bar{\mathbf{B}}^T \mathbf{F}_s \bar{\mathbf{B}} \quad \text{with} \quad \bar{\mathbf{B}} = L' \begin{bmatrix} 0 & 1 \\ 0 & -1 \\ 1 & 2 \end{bmatrix} \quad \text{and} \quad \mathbf{F}_s = \frac{L'}{6EI} \begin{bmatrix} 2 & 0 & 0 \\ 0 & 2 & -1 \\ 0 & -1 & 2 \end{bmatrix}$$

This gives the following flexibility matrix and its inverse, the condensed stiffness matrix

$$\mathbf{F} = \frac{L'^3}{6EI} \begin{bmatrix} 2 & 5 \\ 5 & 16 \end{bmatrix} \quad \rightarrow \quad \mathbf{F}^{-1} = \frac{6EI}{7L'^3} \begin{bmatrix} 16 & -5 \\ -5 & 2 \end{bmatrix} = \frac{EI}{L'^3} \begin{bmatrix} \frac{96}{7} & -\frac{30}{7} \\ -\frac{30}{7} & \frac{12}{7} \end{bmatrix}$$

The condensed stiffness matrix is the same as that under condensation of the rotation dof from the stiffness matrix in (4.85). The reference geometric stiffness $\mathbf{K}'_{P\Delta}$ for the two translation dofs is

$$\mathbf{K}'_{P\Delta} = \frac{P_v}{L'} \begin{bmatrix} 2 & -1 \\ -1 & 1 \end{bmatrix}$$

and the linear eigenvalue problem becomes

$$\left(\frac{EI}{L'^3} \begin{bmatrix} \frac{96}{7} & -\frac{30}{7} \\ -\frac{30}{7} & \frac{12}{7} \end{bmatrix} - \lambda \frac{P_v}{L'} \begin{bmatrix} 2 & -1 \\ -1 & 1 \end{bmatrix} \right) \mathbf{U}_f = \mathbf{0} \quad \rightarrow \quad \lambda = \begin{pmatrix} 0.6492 \\ 7.9223 \end{pmatrix}$$

It gives the following eigenvalues λ and eigenvectors \mathbf{U}_b

$$\lambda P_v = \begin{pmatrix} 0.6492 \\ 7.9223 \end{pmatrix} \frac{EI}{L'^2} \quad \mathbf{U}_b = \begin{bmatrix} 0.3827 & 0.9239 \\ 1.3066 & 0.5412 \end{bmatrix}$$

Substituting $L' = L/2$ gives the lowest eigenvalue λ_e in terms of the cantilever column length L

$$\lambda_e P_v = (0.6492)(4) \frac{EI}{L^2} = 2.5967 \frac{EI}{L^2}$$

This value amounts to a 5.2% error relative to the exact buckling load value in Table 4.1.

Fig. 4.14 shows the first and the second buckling mode of the cantilever column for a discretization with 2 and 4 frame elements with the corresponding coefficient ζ in (4.84) with the subscript denoting the buckling mode. The lowest buckling load value for the discretization with 4 elements is

$$\lambda_e P_v = 2.4993 \frac{EI}{L^2}$$

amounting to an error of 0.8%, a rather accurate estimate!

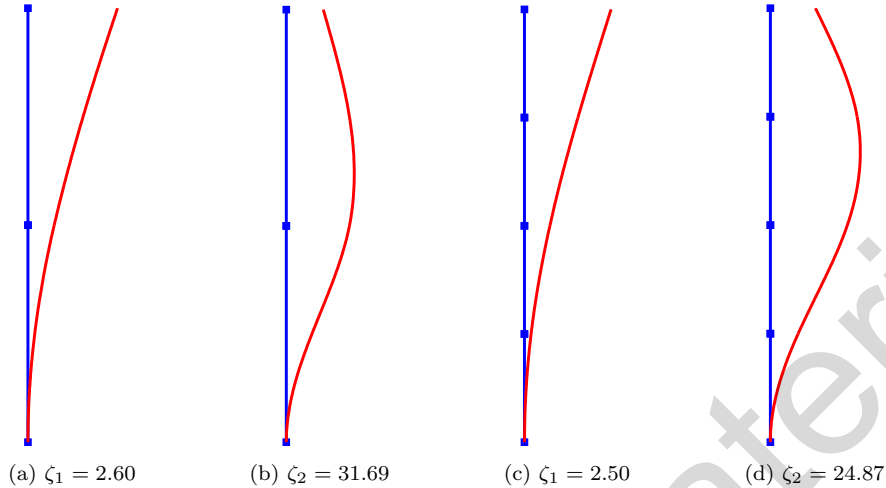


Fig. 4.14: First and second buckling mode of cantilever column with 2 and 4 elements

From the cantilever column example we conclude that a subdivision of the compression member into 2 or, at most, 4 frame elements of equal length suffices for the accurate determination of the linear buckling load of the member with only $\mathbf{K}_{P\Delta}$ geometric stiffness, because the element chords are relatively close to the deformed shape of the structural member under nonlinear geometry. This result is of great significance for the buckling analysis of members with inelastic material response.

Example 4.2 Partially Restrained Cantilever Column

We consider now a cantilever column of height h and flexural stiffness EI_c with its tip restrained against rotation by a girder of length l and flexural stiffness EI_g . Fig. 4.15(a) shows the structural model and the applied vertical force λP_v at node 2. The column-girder assembly constitutes the simplest case of a *sidesway frame*. The task at hand is the determination of the buckling load factor λ_e for the restrained cantilever column.

We define first the ratio η of girder to column stiffness as

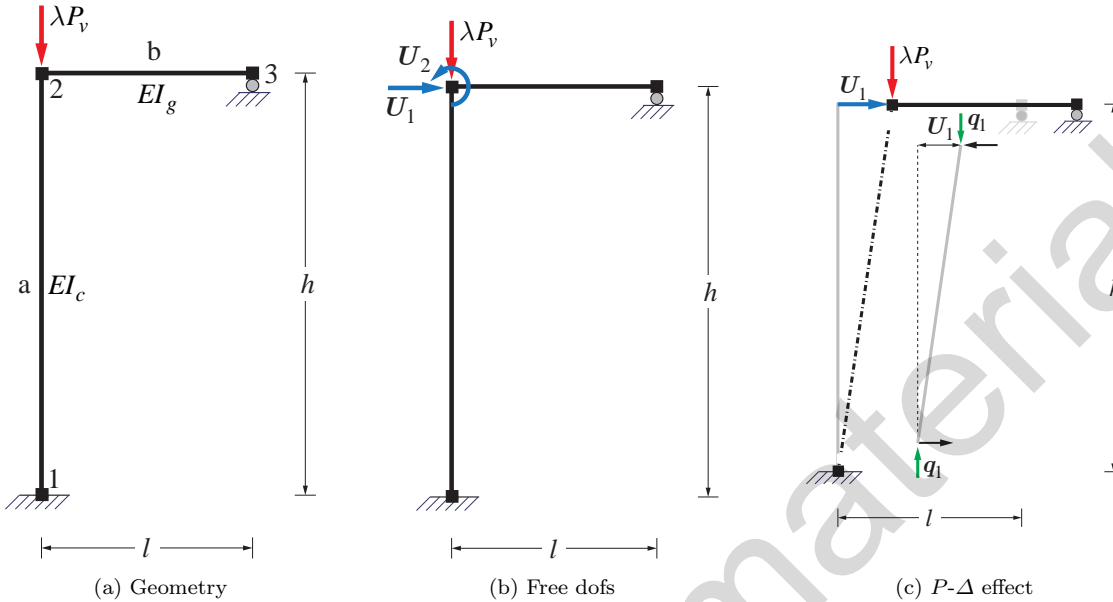
$$\eta = \frac{EI_g}{EI_c} \frac{h}{l}$$

noting that $\eta = 0$ corresponds to a cantilever column without rotation restraint at its tip and a very large value of η corresponds to the case of a fully restrained column.

We assume again that *the frame elements of the structural model are inextensible*. Under this condition the structure has two independent free dofs in Fig. 4.15(b). The linear stiffness matrix \mathbf{K}_l is

$$\mathbf{K}_l = \frac{EI_c}{h^3} \begin{bmatrix} 12 & 6h \\ 6h & (4 + 3\eta)h^2 \end{bmatrix}$$

For the determination of the geometric stiffness matrix of the structure the axial force in the column and in the girder is required. The latter is obviously equal to zero. Under the assumption of inextensibility for column element a its axial force is equal to $-\lambda P_v$. We note that without this assumption the determination of the axial force in the column requires an analysis with the displacement or the force

Fig. 4.15: Restrained cantilever column geometry, dofs and $P\Delta$ effect

method because the structure is statically indeterminate. To illustrate we denote the vertical translation dof with U_v and note that the corresponding equilibrium equation with the displacement method of analysis is uncoupled from the equilibrium equations for dofs #1 and #2. It is

$$-\lambda P_v = \left(\frac{EA}{h} + \frac{3EI_g}{l^3} \right) U_v$$

The axial basic force q_1 in the column then is

$$q_1 = \frac{1}{1 + \frac{h}{EA} \frac{3EI_g}{l^3}} (-\lambda P_v)$$

For $EA \rightarrow \infty$ this equation gives $q_1 = -\lambda P_v$.

The reference geometric stiffness $\mathbf{K}'_{P\delta}$ of the structure is

$$\mathbf{K}'_{P\delta} = \frac{P_v}{30h} \begin{bmatrix} 6 & 3h \\ 3h & 4h^2 \end{bmatrix}$$

The reference geometric stiffness $\mathbf{K}'_{P\Delta}$ of the structure is

$$\mathbf{K}'_{P\Delta} = \frac{P_v}{h} \begin{bmatrix} 1 & 0 \\ 0 & 0 \end{bmatrix}$$

$\mathbf{K}'_{P\delta}$ and $\mathbf{K}'_{P\Delta}$ denote the geometric stiffness contributions under the reference nodal forces \mathbf{P}_{ref} acting in the opposite direction. For the problem at hand \mathbf{P}_{ref} is equal to the nodal force P_v . For setting up $\mathbf{K}'_{P\delta}$ and $\mathbf{K}'_{P\Delta}$ the nodal force P_v acts upward.

The equilibrium equations at the free dofs of the restrained cantilever column are

$$0 = [\mathbf{K}_l - \lambda (\mathbf{K}'_{P\delta} + \mathbf{K}'_{P\Delta})] \mathbf{U}_f \quad (4.86)$$

The solution of the linear eigenvalue problem in (4.86) for a stiffness ratio $\eta = 1$ gives the following buckling load value for the lowest eigenvalue

$$\lambda_e P_v = 0.6166 \frac{EI\pi^2}{h^2} = 0.6166 P_e = \zeta P_e \quad (4.87)$$

where P_e denotes the *Euler buckling load of the basic plane frame element* according to (4.38)

$$P_e = \frac{EI\pi^2}{L^2}$$

with L the length of the compression member, which for the problem in hand is equal to h . The coefficient ζ relates the buckling load of the problem to the Euler buckling load P_e .

The solution of the nonlinear eigenvalue problem with the exact flexural stiffness coefficients A and B in (4.33) gives a buckling load of $0.6110 P_e$ for the lowest eigenvalue. Finally, the solution of the linear eigenvalue problem

$$0 = (\mathbf{K}_l - \lambda \mathbf{K}'_{P\Delta}) \mathbf{U}_f$$

gives a buckling load of $0.6948 P_e$, which overestimates the exact buckling load by 13.7%. It is noteworthy that the linear eigenvalue problem that includes both the $P\text{-}\delta$ and the $P\text{-}\Delta$ geometric stiffness effect gives a buckling load that overestimates the exact value by less than 1%!

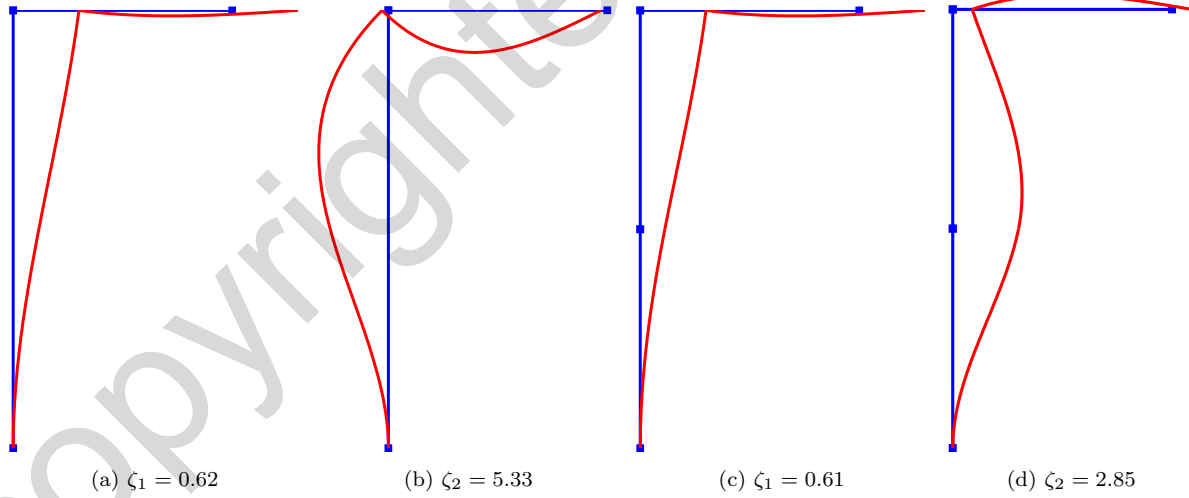


Fig. 4.16: First and second buckling mode of restrained cantilever column with 1 and 2 elements

Fig. 4.16 shows the first and the second buckling mode of the restrained cantilever column for a discretization with 1 and 2 frame elements with the corresponding coefficient ζ in (4.87) with the subscript denoting the buckling mode.

If we include only the reference geometric stiffness matrix $\mathbf{K}'_{P\Delta}$ in the linear eigenvalue problem the buckling load of the restrained cantilever column for different element discretizations is reported in terms of the coefficient ζ in Table 4.2.

ne_c	ζ	Error
1	0.695	13.7 %
2	0.657	7.5 %
4	0.624	2.1 %
8	0.614	0.5 %
16	0.611	0.1 %

Table 4.2: Buckling load coefficient ζ for restrained cantilever column ne_c = number of elements for column subdivision

From the restrained cantilever column example we conclude that a subdivision of the compression member into 4 frame elements of equal length suffices for the accurate determination of the linear buckling load of the member with only $\mathbf{K}_{P\Delta}$ geometric stiffness. *A similar conclusion can be reached for all sidesway moment resisting frames.* The approximate value *always overestimates* the exact buckling load, because the exact solution corresponds to a state of *minimum strain energy* while approximate solutions overestimate the strain energy of the system.

Example 4.3 Simply Supported Column

Fig. 4.17 shows two variations for the model of a simply supported column of height L . The column is assumed to have infinite axial stiffness EA and is, therefore, treated as inextensible. It carries a compressive load λP_v at its tip. The simply supported column belongs to the category of *braced models* with the lateral support at the top provided by a stiff lateral force system such as a braced frame or a shear wall.

In the model (a) the column is represented by Green-Lagrange truss elements and its lateral stiffness is lumped in a spring of axial stiffness k_s . The truss element is assumed to also have infinite flexural stiffness. In the model (b) the column has uniform flexural stiffness EI .

Model (a) of the column with the Green-Lagrange truss elements has one free dof, the lateral translation U_1 at column mid-height in Fig. 4.17(a). Under consideration of the geometric stiffness of the Green-Lagrange truss elements due to the axial force $\mathbf{q}_1 = -\lambda P_v$ in Fig. 4.17(b) the equilibrium equation at the free dof is

$$0 = KU_1 = \left(k_s - 2 \frac{\lambda P_v}{L'} \right) U_1$$

Without the geometric stiffness term the equilibrium equation at the free dof $k_s U_1 = 0$ has only one solution, the undeformed structural configuration $U_1 = 0$. With the inclusion of the geometric stiffness the total stiffness K becomes zero under the load factor λ_e

$$\lambda_e P_v = \frac{k_s L'}{2} = \frac{k_s L}{4} \quad (4.88)$$

For this case U_1 can assume any value, as long as the assumption of infinitesimally small displacements holds. For this reason the equilibrium state is called *indifferent*. In an indifferent equilibrium state the undeformed configuration $U_1 = 0$ is one of infinitely many deformation states. λ_e is the Euler buckling

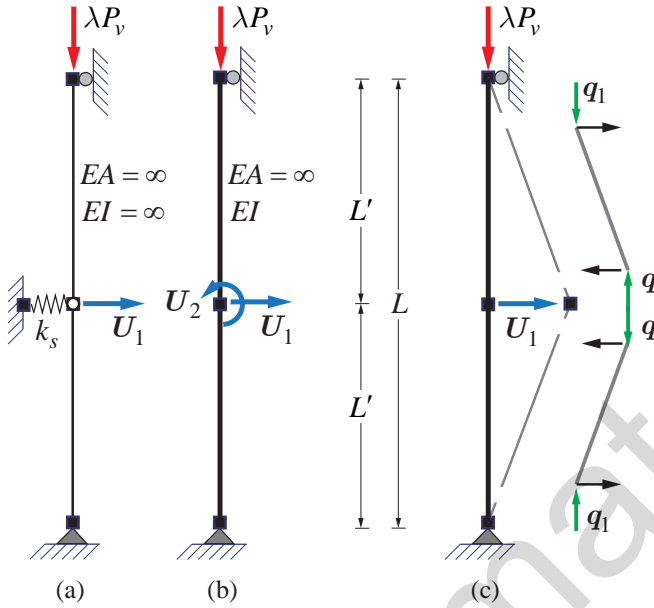


Fig. 4.17: Two models for simply supported column under axial load λP and $P\Delta$ effect

load factor of the column model and $\lambda_e P_v$ its *buckling load*. The buckling load separates stable from unstable equilibrium states of the undeformed structure.

Model (b) of the column in Fig. 4.17 has two free dofs, the lateral translation U_1 and the rotation U_2 at column mid-height.

With the exact flexural stiffness coefficient C under axial compression in (4.34) for the column element of length L' the stiffness matrix of the simply supported column is

$$\mathbf{K} = \begin{bmatrix} \frac{1}{L'} & -\frac{1}{L'} \\ 1 & 1 \end{bmatrix} \frac{EI}{L'} \begin{bmatrix} C & 0 \\ 0 & C \end{bmatrix} \begin{bmatrix} \frac{1}{L'} & 1 \\ -\frac{1}{L'} & 1 \end{bmatrix} + \mathbf{K}_{P\Delta}$$

The reference geometric stiffness $\mathbf{K}'_{P\Delta}$ for the simply supported column in Fig. 4.17(c) is

$$\mathbf{K}'_{P\Delta} = \frac{P_v}{L'} \begin{bmatrix} 2 & 0 \\ 0 & 0 \end{bmatrix}$$

We note that the geometric stiffness term for the translation dof is the same as for the column model with the Green-Lagrange truss elements.

The equilibrium equations at the free dofs of the simply supported column are

$$\mathbf{0} = \mathbf{K} \mathbf{U}_f = \left(\frac{EI}{L'} \begin{bmatrix} \frac{2C}{L'^2} & 0 \\ 0 & 2C \end{bmatrix} - \lambda \frac{P_v}{L'} \begin{bmatrix} 2 & 0 \\ 0 & 0 \end{bmatrix} \right) \mathbf{U}_f$$

The condition that the stiffness matrix \mathbf{K} becomes singular results in a *nonlinear eigenvalue problem*. For the problem in hand the nonlinear problem is rather simple, because the condition that the determinant of the tangent stiffness matrix be zero results in two independent conditions, one for the translation dof

\mathbf{U}_1 and one for the rotation dof \mathbf{U}_2 . The condition for the translation dof is

$$2C \frac{EI}{L'^3} - 2 \frac{\lambda P_v}{L'} = 0 \quad \rightarrow \quad 2(C - \psi^2) = 0$$

noting the definition of ψ from (4.35). We note that the above buckling condition is identical with the buckling condition for the cantilever column model in (4.78). Consequently, the solution involves the odd multiples of $\frac{\pi}{2}$

$$\psi = (2n - 1) \frac{\pi}{2} \quad n = 1, 2, \dots$$

The lowest eigenvalue results for $\psi = \frac{\pi}{2}$ and the corresponding buckling load is

$$\lambda_e P_v = \frac{EI\pi^2}{4L'^2} = \frac{EI\pi^2}{L^2}$$

The expression

$$\lambda_e P_v = \frac{EI\pi^2}{L^2} \tag{4.89}$$

is the buckling load of a simply supported column of length L and is equal to the Euler buckling load of the basic plane frame element according to (4.38). In fact, the simply supported column is equivalent to the basic plane frame element of Section 4.3. We note that the buckling load of a simply supported column is 4-times larger than the buckling load of a cantilever column of the same length L . Stated differently the buckling condition of the simply supported column involves half the column length L' , so that the buckling load of a simply supported column of length L is equal to the buckling load of a cantilever column of length $L' = \frac{L}{2}$. This way of thinking leads to the concept of the effective length factor that will be discussed later.

The buckling condition for the rotation dof \mathbf{U}_2 is $C = 0$ giving $\psi = n\pi$. The lowest eigenvalue then corresponds to $\psi = \pi$ giving a buckling load that is four times larger than the eigenvalue for the translation dof \mathbf{U}_1 . This eigenvalue corresponds to the second buckling mode of the column. Fig. 4.18 shows the first and the second buckling mode of the simply supported column.

We compare now the exact buckling load value of the simply supported column with approximations resulting from the first and second order approximation of the nonlinear element geometry. To this end we set up the linear and the $\mathbf{K}_{P\delta}$ stiffness matrix of the simply supported column. The linear stiffness matrix of the column is

$$\mathbf{K}_l = \frac{EI}{L'^3} \begin{bmatrix} 6 & 0 \\ 0 & 6L'^2 \end{bmatrix}$$

The reference geometric stiffness $\mathbf{K}'_{P\delta}$ of the column is

$$\mathbf{K}'_{P\delta} = \frac{P_v}{5L'} \begin{bmatrix} 2 & 0 \\ 0 & 2L'^2 \end{bmatrix}$$

The first order approximation of the nonlinear element geometry corresponds to linear element geometry by neglecting the $\mathbf{k}_{P\delta}$ geometric stiffness contribution of the basic plane frame element altogether. The linear eigenvalue problem for this case is

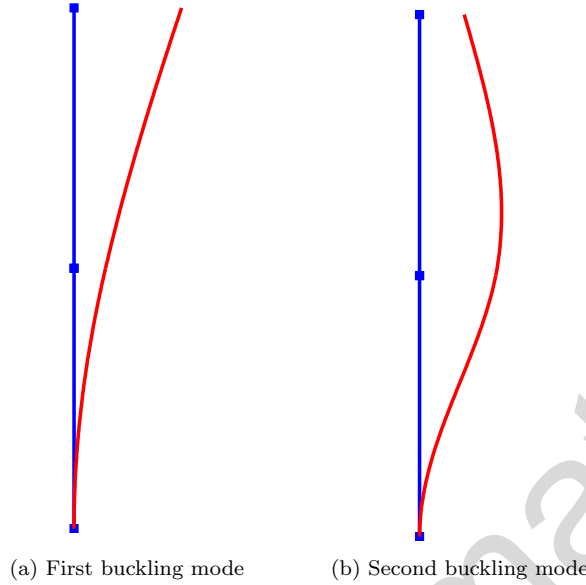


Fig. 4.18: First and second buckling mode of simply supported column

$$\mathbf{0} = \left(\frac{EI}{L'^3} \begin{bmatrix} 6 & 0 \\ 0 & 6L'^2 \end{bmatrix} - \boldsymbol{\lambda} \frac{P_v}{L'} \begin{bmatrix} 2 & 0 \\ 0 & 0 \end{bmatrix} \right) \mathbf{U}_f \quad (4.90)$$

There is only one eigenvalue in this case and it is

$$\lambda_{ec} P_v = \frac{3EI}{L'^2} = \frac{12EI}{L^2}$$

We note again that the result is identical with (4.83) but for half the length of the simply supported column. It is worth noting that the buckling load of the two element model for the simply supported column under consideration only of the $\mathbf{K}_{P\Delta}$ geometric stiffness is the same as the buckling load of the two Green-Lagrange truss element model in (4.88), if the spring stiffness k_s is selected to represent the condensed stiffness for the horizontal translation dof \mathbf{U}_1 at mid-height of the simply supported column. We demonstrate this briefly by determining the lateral flexibility F_m at mid-height of the simply supported column in Fig. 4.19. We have

$$F_m = 2 \left(\bar{\mathbf{B}}^T \frac{L'}{3EI} \bar{\mathbf{B}} \right) = 2 \left(\frac{L'}{2} \frac{L'}{3EI} \frac{L'}{2} \right) = \frac{L'^3}{6EI} = \frac{L^3}{48EI}$$

Substituting $k_s = \frac{1}{F_m}$ in (4.88) gives the buckling load $\lambda_{ec} P_v$. This demonstrates *the equivalence of the nonlinear geometry of the Green-Lagrange truss element with the nonlinear chord geometry effect of the plane frame element under small displacements.*

The second order approximation of the nonlinear element geometry includes the $\mathbf{K}_{P\delta}$ geometric stiffness contribution to the structure stiffness matrix. It gives

$$\mathbf{0} = \left[\frac{EI}{L'^3} \begin{bmatrix} 6 & 0 \\ 0 & 6L'^2 \end{bmatrix} - \boldsymbol{\lambda} \left(\frac{P_v}{L'} \begin{bmatrix} 2 & 0 \\ 0 & 0 \end{bmatrix} + \frac{P_v}{5L'} \begin{bmatrix} 2 & 0 \\ 0 & 2L'^2 \end{bmatrix} \right) \right] \mathbf{U}_f$$

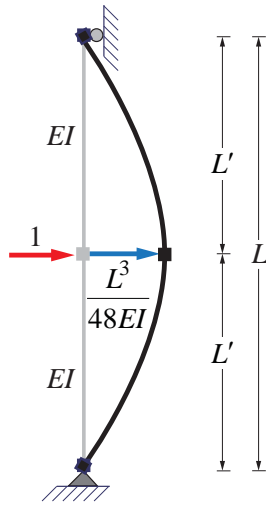


Fig. 4.19: Midspan flexibility of simply supported column

The buckling condition for the translation dof \mathbf{U}_1 is again independent from the condition for the rotation dof \mathbf{U}_2 and two eigenvalues result. The eigenvalue for the translation dof is

$$\lambda_{es} |P| = \frac{2.5EI}{L'^2} = \frac{10EI}{L^2}$$

We note again that the result is identical with (4.81) but for half the length of the simply supported column. The second eigenvalue λ_2 is

$$\lambda_2 |P| = \frac{15EI}{L'^2} = \frac{60EI}{L^2}$$

The second eigenvalue is 6-times larger than the first eigenvalue. Consequently, the error in the estimate of the second eigenvalue is 52%, while the error in the estimate of the first eigenvalue is only 1.3%, as shown in Table 4.1. This discrepancy is associated with the fact that the ψ -value for the second buckling mode is so far removed from $\psi = 0$ that the second order approximation of the nonlinear element geometry effect is rather inaccurate.

Conclusion

The buckling load of the simply supported column of length L is the same as the buckling load of a cantilever column of length $2L$.

4.6.6 Effective Length Factor K

The examples of the preceding section demonstrate the need for expressing the buckling load of a structural model in terms of a reference buckling load. The exact buckling load of a simply supported column serves this purpose. We recall the famous Euler buckling formula for a simply supported column of length L

$$P_e = \frac{EI\pi^2}{L^2}$$

with P_e denoting the Euler buckling load. Instead, however, of expressing the buckling load of a structural model in terms of P_e , it is more expedient to express this buckling load in terms of *the effective length* KL of a simply supported column that has *the same buckling load* as the structural member under consideration. K is known as the effective length factor. We illustrate the concept with the examples of the preceding section.

The buckling load of the cantilever column of Example 4.1 is given by (4.79)

$$\frac{EI\pi^2}{4L^2} = \frac{EI\pi^2}{(2L)^2} = \frac{EI\pi^2}{(KL)^2}$$

with $K = 2$. This means that the buckling load of a cantilever column of length L is equal to the buckling load of a simply supported column with length equal to $2L$.

The buckling load of the restrained cantilever column of Example 4.2 for the stiffness ratio $\eta = 1$ is equal to

$$0.6110 \frac{EI\pi^2}{L^2} = \frac{EI\pi^2}{(1.279L)^2}$$

Accordingly, the effective length factor K of the restrained cantilever column is equal to 1.279 for the stiffness ratio $\eta = 1$. It is easy to show by a parametric analysis that the effective length of a cantilever column that is fully restrained at the top by a very stiff girder is equal to 1.0, while the effective length of a completely unrestrained column is equal to 2.0. These values can be obtained by setting $\eta \rightarrow \infty$ and $\eta = 0$ in the nonlinear eigenvalue problem of Example 4.2, respectively.

Columns in sidesway frames have effective length factors K ranging from 1 to infinity, the latter corresponding to an unrestrained cantilever column with a moment release at its base, which is clearly unstable even before any axial load is applied. Columns in braced frames on the other hand, with negligible sidesway, have effective length factors K ranging from 0.5 to 1, the latter corresponding to a column with a moment release at each end, in other words a simply supported column as in Example 4.3.

While the effective column length concept is useful for compression members in braced frames, a one story or two story, one bay portal frame with two columns of unequal flexural stiffness carrying different axial loads brings to light its limitations, because the stability behavior of a column cannot be investigated in isolation in unbraced frames. Instead, the stability behavior of a story or, better, the stability behavior of the entire frame should be investigated. With today's software this is a rather straightforward task.

4.6.7 Conclusions about Linear Buckling Analysis

The linear buckling analysis of a structural model is useful for the study of its susceptibility to nonlinear geometry effects.

The linear buckling analysis is based on the assumption that the stability of the structural model is studied in the undeformed configuration without external nodal forces causing displacements and, thus, deformations. The only internal forces in the structural elements are the axial basic forces. Because the structural elements are assumed to be axially inextensible, the axial basic force distribution in a statically indeterminate structural model is supplied by the simplest possible static analysis.

Realistically, however, forces causing high axial forces act concurrently with forces causing displacements, and thus, deformations. The latter give rise to flexural basic forces. Moreover, structural members have initial imperfections, either due to crookedness or due to an out-of-plumb position.

To account for these effects an incremental nonlinear analysis is required. A simplification of such analysis is possible, if the chord rotation of the structural elements is smaller than 10^{-2} , and if *the axial forces can be assumed to remain constant during the incremental application of the nodal forces that cause displacements in the independent free dofs of the structural model*. This problem will be discussed in the next section for linear elastic element response, and in the subsequent section for linear elastic, perfectly-plastic element response.

4.7 Second Order Elastic Analysis

In the preceding section on linear stability analysis we noted that the $P\Delta$ and the $P\delta$ stiffness are *linear in the axial basic force q_1 of the structural element*. We also noted that the $P\delta$ effect is an excellent approximation of the nonlinear element geometry, as long as the ψ -factor of the element under the axial basic force q_1 is smaller than 2. Finally, we noted that the $P\Delta$ effect is a relatively accurate approximation of the nonlinear chord geometry effect as long as the chord rotation $\beta = (\Delta \bar{u}_y)/L$ is smaller than 1%.

We turn now our attention to the response of multi-story frames under the simultaneous action of *nodal forces causing high compressive forces in the elements and displacements in the independent free dofs of the structural model*. We assume that the high compressive forces are generated by gravity loads that remain constant during the application of the lateral loads causing the displacements at the free dofs. If we can assume that the axial basic forces of the columns remain constant during the application of the lateral loads the stiffness matrix of the structural model remains constant under the approximation of the nonlinear chord geometry in Section 4.5 and the linear $P\delta$ effect for $\psi \leq 2$. Because the stiffness of the structural model remains constant while the lateral loads are applied, we can determine the response of the structural model under the lateral loads with *a linear analysis without requiring a multi-step incremental analysis*. Most importantly, the principle of linear superposition holds, so that the response under the reference load vector \mathbf{P}_{ref} can be scaled by a load factor and the response under separate lateral force distributions can be factored and combined, as long as the axial compressive forces in the elements remain the same for the different lateral force distributions. This type of analysis is known as *second order elastic analysis*, distinguishing it from the *first order elastic analysis, which refers to the analysis of a linear elastic structural model under linear geometry*.

Example 4.4 Cantilever Column under Vertical and Lateral Force

We study the response of a perfectly straight cantilever column of length L under the action of a vertical force P_v and a horizontal force P_h in Fig. 4.20, noting that P_v denotes the absolute value of the applied vertical force. The cantilever column is assumed to be inextensible with uniform flexural stiffness EI . It has a single independent free dof, the horizontal translation U at the cantilever tip. Noting that U is a scalar we dispense with the subscript for identifying the dof. In the following we determine the horizontal translation U at the column tip with linear second order analysis.

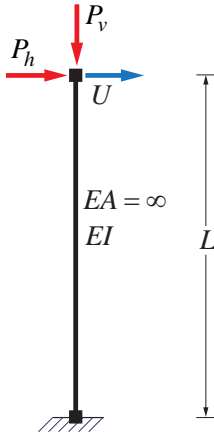


Fig. 4.20: Cantilever column under vertical force P_v and horizontal force P_h

We start with the response under first order elastic analysis. The equilibrium equation of the displacement method for the horizontal translation U gives

$$P_h = K_l U_l \quad \rightarrow \quad U_l = \frac{P_h}{K_l} = P_h \frac{L^3}{3EI} \quad (4.91)$$

where the applied force, the stiffness and the resulting displacement are scalars, and the subscript l denotes *linear first order elastic analysis*.

Under consideration of the truss approximation of the nonlinear chord geometry effect through the $\mathbf{K}_{P\Delta}$ stiffness, the equilibrium equation for the horizontal translation dof gives

$$P_h = K U_\Delta = (K_l + K_{P\Delta}) U_\Delta = \left(\frac{3EI}{L^3} - \frac{P_v}{L} \right) U_\Delta \quad (4.92)$$

with subscript Δ denoting the displacement under second order elastic analysis that includes only the $\mathbf{K}_{P\Delta}$ geometric stiffness contribution.

We note that (4.92) is identical with (4.82) with P_v taking the place of λP_v except for the presence of the lateral nodal force P_h in (4.92). Solving for the horizontal translation U_Δ gives

$$U_\Delta = P_h \frac{L^3}{3EI} \mu_\Delta \quad \text{with} \quad \mu_\Delta = \frac{1}{1 - \frac{P_v}{3EI/L^2}} \quad (4.93)$$

where μ_Δ is a *magnification factor* that accounts for the effect of approximate nonlinear chord geometry on the horizontal translation. The magnification factor μ_Δ depends on the ratio of the vertical force P_v to the buckling load of the cantilever column under inclusion of the geometric stiffness for the $P\Delta$ effect in (4.83). As P_v approaches the buckling load, the horizontal translation grows to infinity.

There is an interesting alternative way of writing (4.92) offering a physical interpretation of the approximate nonlinear chord geometry effect that assists with the extension of the magnification factor μ_Δ to multi-story frames. Starting from (4.92) we move the $\mathbf{K}_{P\Delta}$ term to the loading side of the equation

$$P_h + \frac{P_v}{L} U_\Delta = K_l U_\Delta \quad (4.94)$$

We can treat (4.94) as the prescription of an iterative scheme of the form

$$P_h + \frac{P_v}{L} U_i = K_l U_{i+1} \quad (4.95)$$

where U_i denotes the horizontal translation estimate at iteration i . We start the process with $\mathbf{U}_0 = 0$ on the left hand side of (4.95) to get the linear first order analysis solution

$$P_h + \frac{P_v}{L}(0) = K_l U_1 = K_l U_l \quad (4.96)$$

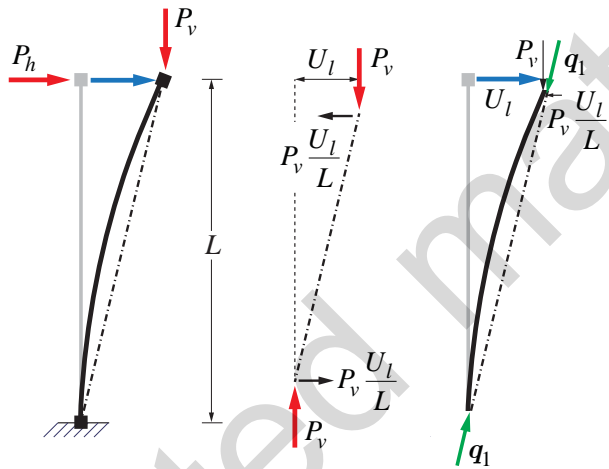


Fig. 4.21: Lateral force due to $P\Delta$ effect of vertical force

We then substitute the horizontal translation U_1 into the left hand side of (4.95) to get

$$\begin{aligned} P_h + \frac{P_v}{L} U_1 &= K_l U_2 \\ \rightarrow P_h + \frac{P_v}{L} U_1 &= K_l (U_1 + \Delta U_1) \\ \rightarrow \frac{P_v}{L} U_1 &= K_l \Delta U_1 \end{aligned} \quad (4.97)$$

where ΔU_1 denotes the change of the horizontal translation under the additional horizontal force on the left hand side of the equilibrium equation. The last relation in (4.97) results under consideration of (4.96). Fig. 4.21 gives the physical interpretation of this horizontal force due to the $P\Delta$ effect of the vertical force P_v . We can treat the $P\Delta$ effect either as the transverse end forces that equilibrate the moment generated by the vertical force P_v acting on the relative horizontal translation U_l of the column ends, or, as the *horizontal end force component of the basic force \mathbf{q}_1* , as Fig. 4.21 shows.

Because the stiffness on the right hand side of (4.97) is the same as (4.96) the correction of the horizontal translation is equal to the translation of the first order analysis in (4.96) after scaling it by the ratio of the applied lateral forces on the left hand side of equations (4.96) and (4.97). It is

$$\Delta U_1 = \left(\frac{1}{P_h} \frac{P_v}{L} U_l \right) U_l = \left(\frac{P_v U_l}{P_h L} \right) U_l \quad (4.98)$$

Repeating the process by substituting U_2 into the left hand side of (4.95) and separating it into the sum of U_l and the translation increment ΔU_1 gives

$$\begin{aligned} P_h + \frac{P_v}{L} U_2 &= K_l U_3 \\ P_h + \frac{P_v}{L} (U_1 + \Delta U_1) &= K_l (U_1 + \Delta U_1 + \Delta U_2) \\ \rightarrow \quad \frac{P_v}{L} \Delta U_1 &= K_l \Delta U_2 \end{aligned} \tag{4.99}$$

From the comparison of the last equations in (4.99) and (4.97) we conclude that the correction of the horizontal translation ΔU_2 is equal to

$$\Delta U_2 = \Delta U_1 \frac{\Delta U_1}{U_1} \tag{4.100}$$

After substituting the last translation correction ΔU_1 from (4.98) into (4.100) we get

$$\Delta U_2 = \left(\frac{P_v}{P_h} \frac{U_l}{L} \right)^2 U_l \tag{4.101}$$

The continuation of the iterative process leads to the expression

$$\Delta U_n = \left(\frac{P_v}{P_h} \frac{U_l}{L} \right)^n U_l \tag{4.102}$$

for iteration n . The horizontal translation, therefore, becomes

$$\begin{aligned} U_\Delta &= U_l + \Delta U_1 + \Delta U_2 + \cdots + \Delta U_n \\ &= U_l + \left(\frac{P_v}{P_h} \frac{U_l}{L} \right) U_l + \left(\frac{P_v}{P_h} \frac{U_l}{L} \right)^2 U_l + \cdots + \left(\frac{P_v}{P_h} \frac{U_l}{L} \right)^n U_l \\ &= U_l \left[1 + \left(\frac{P_v}{P_h} \frac{U_l}{L} \right) + \left(\frac{P_v}{P_h} \frac{U_l}{L} \right)^2 + \cdots + \left(\frac{P_v}{P_h} \frac{U_l}{L} \right)^n \right] \end{aligned}$$

The expression in the square brackets is a geometric series of the form $1 + x + x^2 + \cdots + x^n$ which converges for $|x| < 1$ to $\frac{1}{1-x}$. The horizontal translation U_Δ , therefore, is

$$U_\Delta = U_l \mu_\Delta \quad \text{with} \quad \mu_\Delta = \frac{1}{1 - \frac{P_v}{P_h} \frac{U_l}{L}} \tag{4.103}$$

Substituting the horizontal translation U_l of the cantilever column under P_h from (4.91) gives an alternative expression for the magnification factor μ_Δ as

$$\mu_\Delta = \frac{1}{1 - \frac{\lambda_e |P|}{\lambda_e |P|}} \quad \text{with} \quad \lambda_e |P| = \frac{3EI}{L^2}$$

The expression

$$\mu_\Delta = \frac{1}{1 - \frac{P_v}{P_h} \frac{U_l}{L}} \tag{4.104}$$

is, however, amenable to extension to multi-story unbraced frames, as will be discussed subsequently. We emphasize that the magnification factor in (4.104) *includes only the P-Δ effect*.

We conclude the second order analysis of the cantilever column by including the $P\text{-}\delta$ effect in (4.92) to get

$$P_h = KU_{\Delta\delta} = (K_l + K_{P\Delta} + K_{P\delta})U_{\Delta\delta} = \left(\frac{3EI}{L^3} - \frac{P_v}{L} - \frac{P_v}{5L} \right) U_{\Delta\delta} \quad (4.105)$$

with subscript $\Delta\delta$ denoting the displacement under second order analysis with the inclusion of the approximate nonlinear element geometry effect ($P\text{-}\delta$ effect). We note that (4.105) is identical with (4.80) with P_v taking the place of λP_v except for the presence of the lateral nodal force P_h in (4.105). Solving for the horizontal translation $U_{\Delta\delta}$ gives

$$U_{\Delta\delta} = P_h \frac{L^3}{3EI} \mu_{\Delta\delta} \quad \text{with} \quad \mu_{\Delta\delta} = \frac{1}{1 - \frac{P_v}{2.5EI/L^2}} \quad (4.106)$$

We note that the magnification factor $\mu_{\Delta\delta}$ depends on the ratio of the vertical force P_v to the buckling load of the cantilever column under inclusion of the geometric stiffness for the $P\text{-}\Delta$ and the $P\text{-}\delta$ effect.

Example 4.5 Restrained Cantilever Column under Vertical and Lateral Force

Fig. 4.22(a) shows a restrained cantilever column under the action of a vertical force P_v of 600 units and a horizontal force P_h of 20 units. The column height is $h = 20$ units and the girder length is $l = 10$ units. The flexural stiffness of the column is $EI_c = 2 \cdot 10^5$ and that of the girder is $EI_g = 1 \cdot 10^5$.

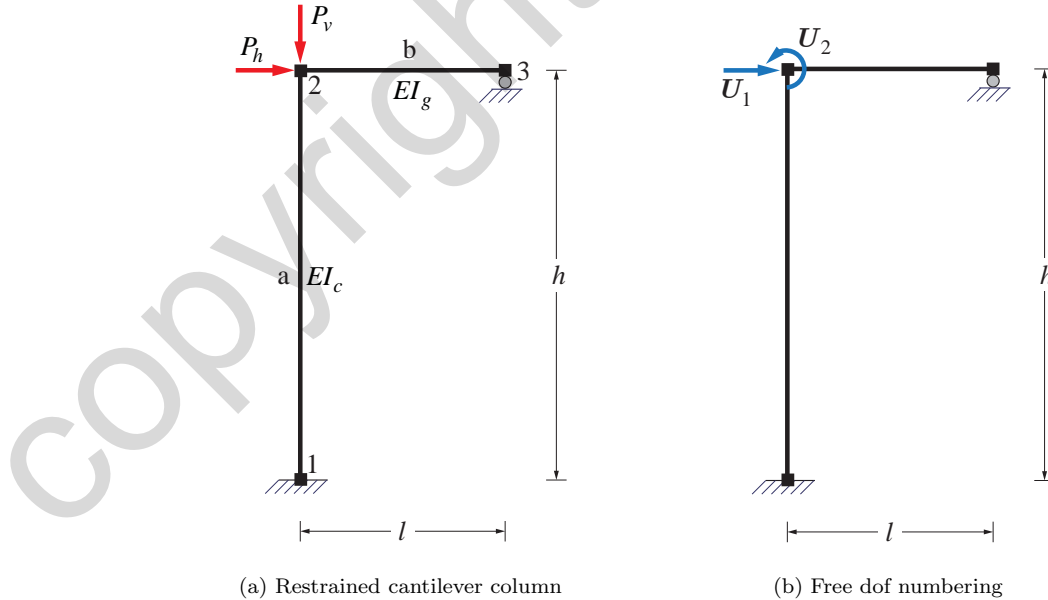


Fig. 4.22: Restrained cantilever column under vertical and horizontal force

Under the assumption that all elements are inextensible there are only two independent free dofs in Fig. 4.22(b). The linear stiffness matrix \mathbf{K}_l is

$$\mathbf{K}_l = \begin{bmatrix} \frac{12EI_c}{h^3} & \frac{6EI_c}{h^2} \\ \frac{6EI_c}{h^2} & \frac{4EI_c}{h} + \frac{3EI_g}{l} \end{bmatrix} \quad (4.107)$$

For determining the geometric stiffness matrices $\mathbf{K}_{P\delta}$ and $\mathbf{K}_{P\Delta}$ it is important to "guess" the axial basic force q_a in column element a. Because the structure is statically indeterminate, "guessing" that the axial load in column a is equal to 600 neglects the overturning moment by the horizontal force of 20 units. Including the overturning moment effect reduces the axial basic force q_a in column a to

$$q_a = -600 + 20 \frac{h}{l} = -560$$

We plan to assess this effect in the following calculations. We start the calculations with the value $q_a = -600$. The $\mathbf{K}_{P\delta}$ geometric stiffness matrix involves only a contribution from column element a. We set it up directly at the global dofs to get

$$\mathbf{K}_{P\delta} = \frac{q_a}{30h} \begin{bmatrix} 6 & 3h \\ 3h & 4h^2 \end{bmatrix} \quad (4.108)$$

The $\mathbf{K}_{P\Delta}$ stiffness matrix is set up directly at the global dofs and affects only the translation dof.

$$\mathbf{K}_{P\Delta} = \frac{q_a}{h} \begin{bmatrix} 1 & 0 \\ 0 & 0 \end{bmatrix} \quad (4.109)$$

Linear first order analysis. The linear first order analysis of the structure gives

$$\mathbf{P}_f = \begin{pmatrix} 20 \\ 0 \end{pmatrix} = \mathbf{K}_l \mathbf{U}_l \quad \rightarrow \quad \mathbf{U}_l = \begin{pmatrix} 11.667 \\ -0.500 \end{pmatrix} 10^{-2} \quad (4.110)$$

We use the slope-deflection equations to determine the basic flexural forces in elements a and b

$\theta = -0.5 \cdot 10^{-2}$ with $\beta_a = -\frac{11.67}{20} \cdot 10^{-2} = -0.5833 \cdot 10^{-2}$	$\mathbf{q}_i^{(a)} = \frac{2EI_c}{h} (\theta - 3\beta_a) = 250$ $\mathbf{q}_j^{(a)} = \frac{2EI_c}{h} (2\theta - 3\beta_a) = 150$	$\mathbf{q}_i^{(b)} = \frac{3EI_g}{l} \theta = -150$
---	---	--

Linear second order analysis with $P\Delta$. The linear second order analysis of the structure with only $P\Delta$ geometric stiffness under $q_a = -600$ gives

$$\mathbf{P}_f = (\mathbf{K}_l + \mathbf{K}_{P\Delta}) \mathbf{U}_\Delta \quad \rightarrow \quad \mathbf{U}_\Delta = \begin{pmatrix} 14.141 \\ -0.606 \end{pmatrix} 10^{-2} \quad (4.112)$$

We confirm the horizontal translation value with the magnification factor μ_Δ from (4.104). It gives

$$\frac{P_v}{P_h} \frac{\mathbf{U}_{1l}}{L} = \frac{600 \cdot 0.1167}{20 \cdot 20} = 0.1751 \quad \rightarrow \quad \mu_\Delta = \left(\frac{1}{1 - 0.1751} \right) = 1.2122$$

Multiplying the horizontal translation value of 0.1167 under first order linear analysis in (4.110) with μ_Δ gives 0.1415. Because the element kinematics remain linear and *the element basic force-deformation relation remains unchanged* we can still use the slope-deflection equations to determine the basic flexural forces in elements a and b

$$\begin{aligned} \theta &= -0.606 \cdot 10^{-2} & q_i^{(a)} &= \frac{2EI_c}{h} (\theta - 3\beta_a) = 303.03 \\ \text{with } \beta_a &= -\frac{14.141}{20} \cdot 10^{-2} = -0.7071 \cdot 10^{-2} & q_j^{(a)} &= \frac{2EI_c}{h} (2\theta - 3\beta_a) = 181.82 \\ & & q_i^{(b)} &= \frac{3EI_g}{l} \theta = -181.82 \end{aligned} \quad (4.113)$$

Linear second order analysis with $P\Delta$ and $P\delta$. The linear second order analysis of the structure with $\mathbf{K}_{P\Delta}$ and $\mathbf{K}_{P\delta}$ geometric stiffness under $q_a = -600$ gives

$$\mathbf{P}_f = (\mathbf{K}_l + \mathbf{K}_{P\Delta} + \mathbf{K}_{P\delta}) \mathbf{U}_{\Delta\delta} \rightarrow \mathbf{U}_{\Delta\delta} = \begin{pmatrix} 14.532 \\ -0.625 \end{pmatrix} 10^{-2} \quad (4.114)$$

The element kinematics are still linear but *the element basic force-deformation relation now changes with the inclusion of the $P\delta$ effect*. We need to add the latter to the slope-deflection equations to determine the basic flexural forces in elements a and b. Using the basic $P\delta$ stiffness for a beam element with continuous ends from (4.45) we have

$$\begin{aligned} q_{i\delta} &= \frac{q_a L}{30} (-4\theta_i - \theta_j - 3\beta) \\ q_{j\delta} &= \frac{q_a L}{30} (-\theta_i + 4\theta_j - 3\beta) \end{aligned} \quad (4.115)$$

We determine the linear basic element contribution first. It is

$$\begin{aligned} \theta &= -0.625 \cdot 10^{-2} & q_i^{(a)} &= \frac{2EI_c}{h} (\theta - 3\beta_a) = 311.03 \\ \text{with } \beta_a &= -\frac{14.532}{20} \cdot 10^{-2} = -0.7266 \cdot 10^{-2} & q_j^{(a)} &= \frac{2EI_c}{h} (2\theta - 3\beta_a) = 186.11 \\ & & q_i^{(b)} &= \frac{3EI_g}{l} \theta = -187.38 \end{aligned} \quad (4.116)$$

We determine the $P\delta$ basic stiffness contribution next.

$$\begin{aligned} \theta &= -0.625 \cdot 10^{-2} & q_{i\delta}^{(a)} &= \frac{q_a L}{30} (-\theta - 3\beta_a) = -11.22 \\ \text{with } \beta_a &= -\frac{14.532}{20} \cdot 10^{-2} = -0.7266 \cdot 10^{-2} & q_{j\delta}^{(a)} &= \frac{q_a L}{30} (4\theta - 3\beta_a) = 1.27 \\ q_a &= -600 & q_{i\delta}^{(b)} &= 0 \end{aligned} \quad (4.117)$$

The combined result is

$$\begin{aligned}
 \mathbf{q}_i^{(a)} + \mathbf{q}_{i\delta}^{(a)} &= 299.81 \\
 \mathbf{q}_j^{(a)} + \mathbf{q}_{j\delta}^{(a)} &= 187.38 \\
 \mathbf{q}_{i\delta}^{(b)} &= -187.38
 \end{aligned} \tag{4.118}$$

We note that the results in (4.118) are not very different from the results of the second order analysis that only includes the $P\Delta$ effect in (4.113). In fact, the horizontal translation is 2.8% larger than the corresponding value with the inclusion of the $P\Delta$ effect only. This is to be expected because the ψ -factor of the restrained cantilever column is

$$\psi = \sqrt{\frac{q_a h^2}{EI}} = \sqrt{\frac{600 \cdot 20^2}{2 \cdot 10^5}} = 1.095$$

It is noteworthy, however, that the basic element forces of the more exact geometric analysis are higher for the girder but smaller for the base of the column.

In the following we determine the support reactions only for the case that we include both the $\mathbf{K}_{P\Delta}$ and the $\mathbf{K}_{P\delta}$ geometric stiffness. The case with only the $P\Delta$ geometric stiffness is completely analogous. We check the global equilibrium with two assumptions and then indicate the method for correcting the discrepancy in these results.

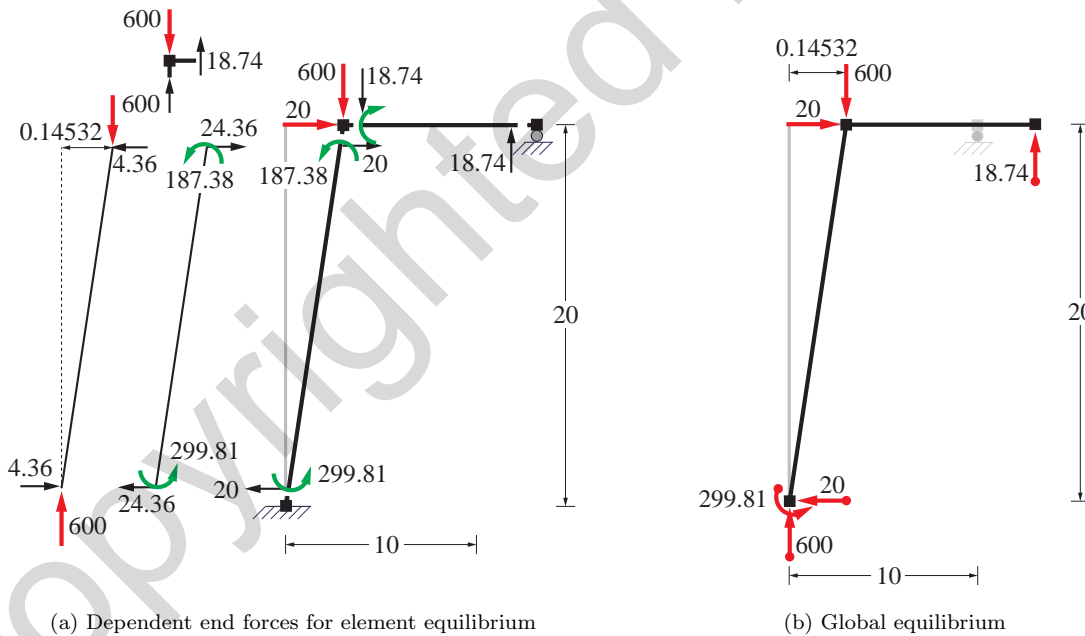


Fig. 4.23: Element and global equilibrium of restrained column for $q_a = -600$

Fig. 4.23(a) shows the determination of the end forces from free body equilibrium of elements a and b for the basic forces in (4.118). The axial force in column element a is assumed equal to -600 consistent with the assumption for the determination of the basic forces in (4.118). We can see that the horizontal force equilibrium is satisfied, but vertical force equilibrium is violated at node 2 with an error of about 3% of the largest term in the equation. The same is true for the global equilibrium with the support reactions in Fig. 4.23(b). Moment equilibrium about the support node 1 gives:

$$\sum M_Z = 299.81 + 18.74 \cdot (10 + 0.14532) - 600 \cdot 0.14532 - 20 \cdot 20 = 2.741 \approx 0 \quad \checkmark$$

with the error equal to approximately 1% of the largest term in the moment equilibrium equation. However, the moment equilibrium about node 2 is satisfied pretty accurately!

$$\sum M_Z = 299.81 + 18.74 \cdot (10) - 600 \cdot 0.14532 - 20 \cdot 20 = 0.018 \approx 0 \quad \checkmark$$

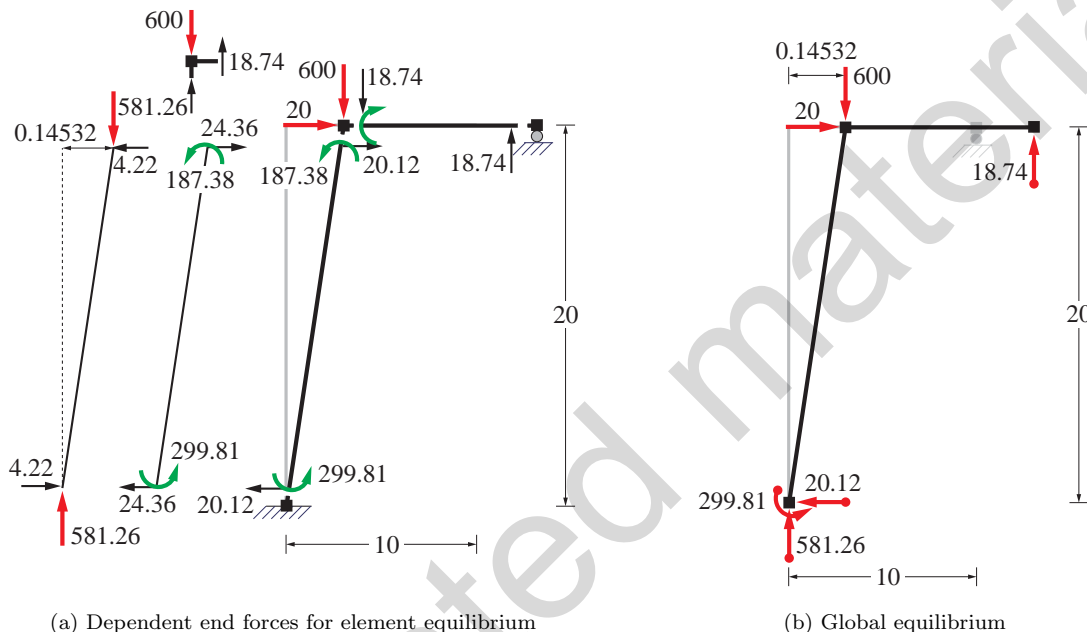


Fig. 4.24: Element and global equilibrium of restrained column for $q_a = -581.3$

Fig. 4.24(a) shows the determination of the end forces from free body equilibrium of elements a and b for the basic forces in (4.118). The axial force in column element a is assumed equal to -581.3 so as to satisfy the vertical force equilibrium at node 2. Because this is inconsistent with the assumption for the determination of the basic forces in (4.118) the horizontal force equilibrium at node 2 is not satisfied. The same is true of the global equilibrium with the support reactions in Fig. 4.24(b). The moment equilibrium about the support node 1 is the same as before. Moment equilibrium about node 2 in Fig. 4.24(b) gives

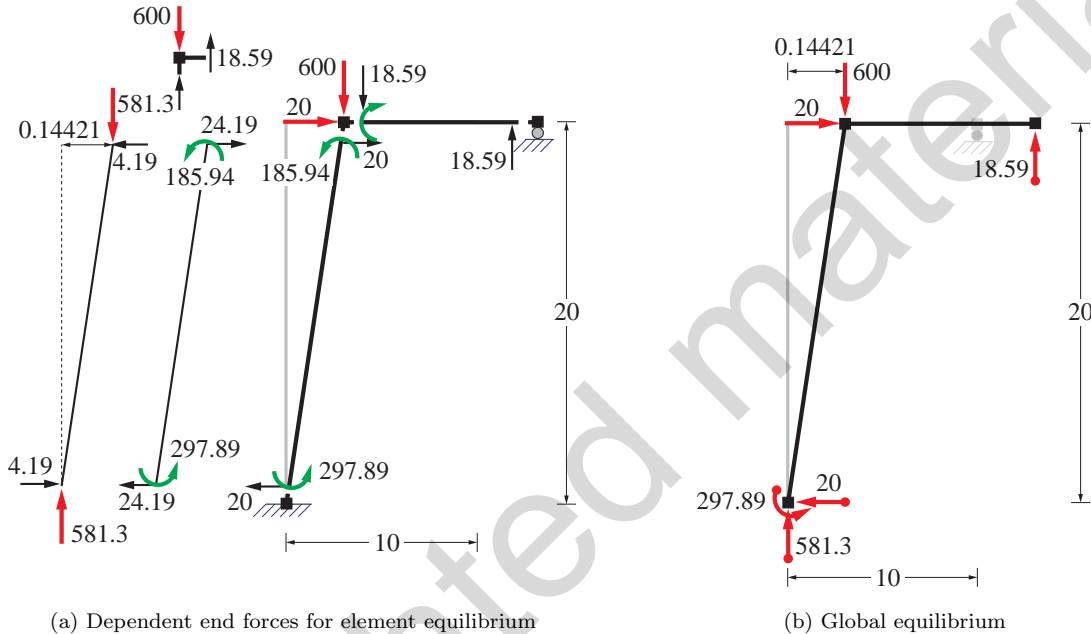
$$\sum M_Z = 299.81 + 18.74 \cdot 10 - 581.26 \cdot 0.14532 - 20.12 \cdot 20 = 0.035 \quad \checkmark$$

Consistent second order analysis. The slight equilibrium violations we encountered stem from the inconsistency in the assumption of the axial force in column element a. It is clear from the second order analysis that the transverse end force in girder element b, *reduces the axial force q_a in column element a*. This reduction is not as high as originally surmised on the basis of the overturning moment with the final basic axial force $q_a = -581.2$. We can now go back and re-analyze the problem with (4.114) to get

$$\mathbf{U}_{\Delta\delta} = \begin{pmatrix} 14.421 \\ -0.620 \end{pmatrix} 10^{-2} \quad \text{for } q_a = -581.3 \quad (4.119)$$

The basic forces from the addition of the basic forces according to (4.116) and (4.117) for the free dof displacement values in (4.119) are

$$\begin{aligned} \mathbf{q}_i^{(a)} + \mathbf{q}_{i\delta}^{(a)} &= 297.89 \\ \mathbf{q}_j^{(a)} + \mathbf{q}_{j\delta}^{(a)} &= 185.94 \\ \mathbf{q}_{i\delta}^{(b)} &= -185.94 \end{aligned} \quad (4.120)$$



(a) Dependent end forces for element equilibrium

(b) Global equilibrium

Fig. 4.25: Element and global equilibrium of restrained column for consistent analysis with $q_a = -581.3$

Fig. 4.25(a) shows the determination of the end forces from free body equilibrium of elements a and b for the basic forces in (4.120) and Fig. 4.25(b) shows the support reactions for the global equilibrium checks. We conclude that horizontal force equilibrium is now exactly satisfied at node 2, while the vertical force equilibrium is satisfied to within 0.1. The moment equilibrium about the support node 1 gives

$$\sum M_Z = 297.89 + 18.59 \cdot (10 + 0.14421) - 600 \cdot 0.14421 - 20 \cdot 20 = -0.056 \quad \checkmark$$

The moment equilibrium about node 2 gives

$$\sum M_Z = 297.89 + 18.59 \cdot 10 - 581.3 \cdot 0.14421 - 20 \cdot 20 = -0.039 \quad \checkmark$$

These results are perfectly acceptable and consistent.

We conclude that at least one iteration is required for determining a consistent axial force in column element a and the corresponding free dof displacements that result in element deformations and basic forces that satisfy element and global free body equilibrium with sufficient accuracy.

In fact, an iterative solution process takes 4 iterations to meet an equilibrium tolerance of 10^{-16} , but already the first iteration has an error norm of only $5.83 \cdot 10^{-5}$. The final result for the horizontal translation is 0.14421 and the final axial basic force in column a is -581.40.

4.7.1 Magnification Factor

The examples for the cantilever column and the restrained cantilever column show that the magnification factor μ_Δ for the first order analysis response produces very accurate estimates of the response under a second order analysis that includes only the $P\text{-}\Delta$ stiffness. The reasons for this are that the vertical force in the compression element remains essentially constant and that the cantilever column models have only a single horizontal translation dof.

For the extension of the magnification factor to a single story multi-column frame we note that there is still a single horizontal translation dof under the assumption that the floor girder elements are inextensible. The $P\text{-}\Delta$ stiffness contribution to the horizontal translation dof of the single story frame is

$$\frac{P_{v1}}{h_1} + \frac{P_{v2}}{h_2} + \cdots + \frac{P_{vn}}{h_n}$$

where the subscript i denotes the i -th column of the frame and h denotes the column height. If all columns in the story have equal height the $P\text{-}\Delta$ stiffness contribution becomes

$$\frac{P_{v1}}{h} + \frac{P_{v2}}{h} + \cdots + \frac{P_{vn}}{h} = \frac{\sum P_v}{h}$$

$\sum P_v$ is the total vertical force on the one-story frame of story height h . Under the application of a lateral force P_h at the free translation dof of the one story frame *the total vertical force does not change due to the overturning moment by the lateral force*. Consequently, the magnification factor for the $P\text{-}\Delta$ stiffness effect becomes

$$\mu_\Delta = \frac{1}{1 - \frac{\sum P_v U_l}{P_h h}}$$

where U_l is the horizontal translation under the horizontal force P_h with linear first order analysis.

The derivation of a magnification factor μ_Δ for multistory sidesway frames is complicated by the fact that the lateral force distribution does not necessarily match the distribution of the $P\text{-}\Delta$ effect, which depends on the total axial force in a story and the relative lateral displacement or story drift. Extensive studies have shown, however, that it is possible to develop a magnification factor on a story-by-story basis. This magnification factor takes the following form for a particular story

$$\mu_\Delta = \frac{1}{1 - \frac{\sum P_v \Delta U_l}{P_h h}} \quad (4.121)$$

where $\sum P_v$ is the total axial force of the story, P_h is *the story shear*, ΔU_l is the relative lateral displacement or lateral drift of the story under linear first order analysis and h is the story height.

To account for the fact that the distribution of the product of the story axial force with the lateral drift deviates over the building height from the lateral force distribution the AISC Specification introduces

a correction factor R_M in the denominator of the magnification factor expression in (4.121). The 2005 AISC code denotes the $P\Delta$ magnification factor μ_Δ with B_2 (consult equation C2-3 and C2-6b in the 2005 AISC code).

The use of the magnification factor is cumbersome and inaccurate when today's software can readily solve the general problem of second order analysis without the limiting approximations that underlie the use of the magnification factor. This approach is allowed in the 2005 AISC Specification under the *Direct Analysis Method* in Appendix 7 of the Specification. The Direct Analysis Method requires the use of a story sway imperfection of $\frac{1}{500}$ of the story height h . It also prescribes a 20% reduction of the axial stiffness EA and the flexural stiffness EI to account for the effect of residual stresses and local inelastic effects.

4.7.2 Summary for Second Order Elastic Analysis

The linear second order analysis method is based on the following assumptions:

- 1) All frame elements are inextensible so that the axial force distribution under vertical forces can be determined by inspection.
- 2) The relative lateral displacements are small enough so that chord rotation of the compression elements does not exceed 1%. Under this condition the truss effect approximation of the nonlinear chord geometry in (4.66) is sufficiently accurate.
- 3) The axial forces in the compression elements *remain constant* on a story-by-story basis under the application of the lateral forces.

With these assumptions the linear second order analysis process consists of a *single load step* under the given lateral forces that involves the following steps:

- 1) Determine the axial forces in the columns under the *factored gravity loads*.
- 2) Determine the parameter ψ for all compression elements and decide whether to include the $P\delta$ effect for nonlinear element geometry. For unbraced frames this is rarely necessary.
- 3) Form the stiffness matrices \mathbf{K}_l , $\mathbf{K}_{P\Delta}$ and $\mathbf{K}_{P\delta}$, as necessary, and the structure stiffness matrix $\mathbf{K} = \mathbf{K}_l + \mathbf{K}_{P\Delta} + \mathbf{K}_{P\delta}$.
- 4) Determine the free dof displacements \mathbf{U}_f under the lateral forces by linear analysis with structure stiffness matrix \mathbf{K} .
- 5) Use linear kinematics to determine the element deformations \mathbf{v} from \mathbf{U}_f .
- 6) Use the $\mathbf{q} - \mathbf{v}$ relation to determine the basic element forces without forgetting to include the $P\delta$ effect, if necessary.
- 7) Determine the dependent element forces by element equilibrium including the nonlinear chord effect with the axial force of each element.
- 8) Determine the support reactions by node equilibrium.
- 9) Check the global equilibrium of the structural model *with the element chord in the deformed position* under the applied vertical and lateral forces and the support reactions.

Example 4.6 Three Story-One Bay Steel Frame under Gravity and Lateral Loads

In this example we demonstrate the use of the consistent second order analysis for a 3-story, one bay steel frame and compare the results with the magnification of the linear first order analysis results according to the 2005 AISC specification.

Fig. 4.26 shows a one-bay, three-story steel frame subjected to gravity loads and lateral forces. All frame elements are assumed inextensible. The cross section properties can be found in the AISC manual. The material is assumed to be Grade 50 steel with $f_y = 50$ ksi and $E = 29,000$ ksi.

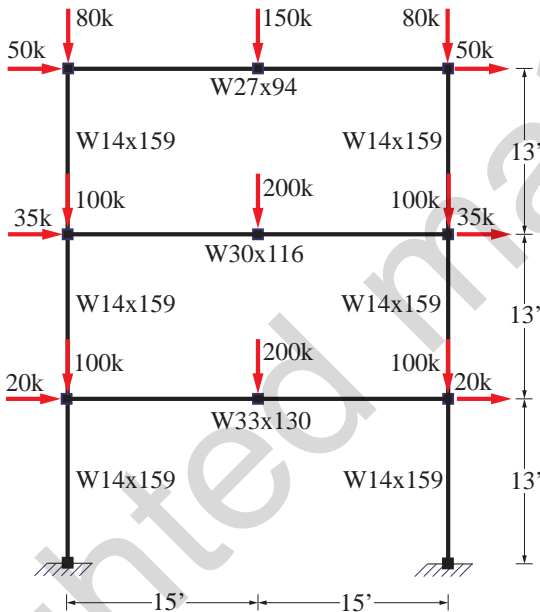


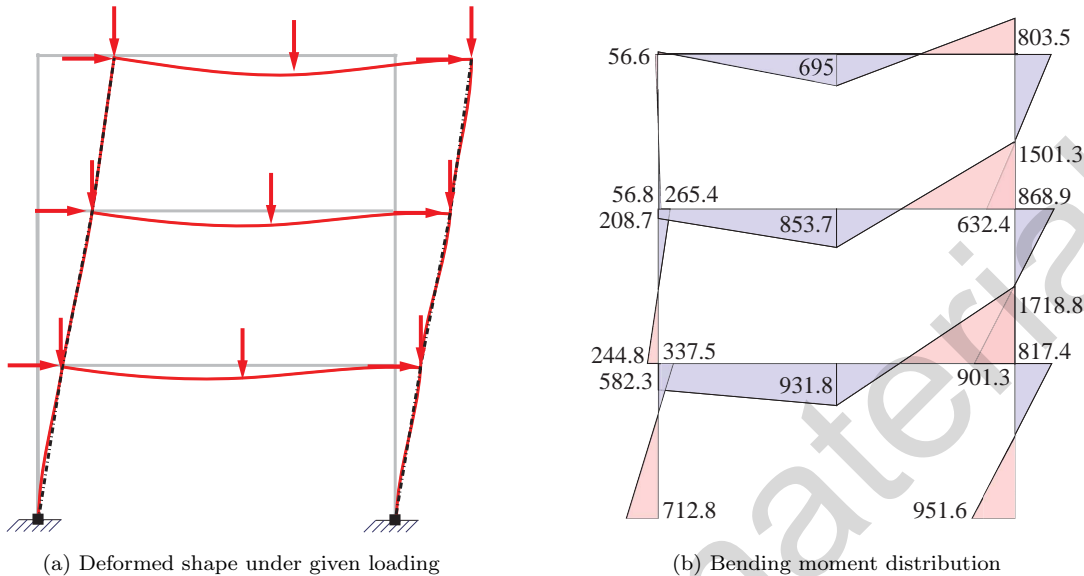
Fig. 4.26: Three story steel frame under gravity and lateral loads

We use **FEDEASLab** with the $P-\Delta$ geometry option for the column elements to determine the consistent second order analysis response under the combined effect of the gravity loads and the lateral forces. Fig. 4.27 shows the deformed shape and the resulting bending moment distribution.

Denoting the horizontal translation of floors 1, 2 and 3 with \mathbf{U}_1 , \mathbf{U}_2 and \mathbf{U}_3 , respectively, the consistent second order analysis gives the following values

$$\mathbf{U} = \begin{pmatrix} 0.9612 \\ 2.1539 \\ 3.0437 \end{pmatrix} \text{ in} \quad (4.122)$$

The magnification factor method of AISC requires that a linear first order analysis be conducted *separately for loads that do not cause sidesway and for loads that do*. For the case in hand this is easy to do because of the symmetry in geometry and loading. Fig. 4.28 shows the deformed shape and bending moment distribution of the 3-story frame under the gravity loads, and Fig. 4.29 shows the deformed shape and bending moment distribution of the 3-story frame under the lateral loads. The corresponding horizontal translations of the floors are

Fig. 4.27: Deformed shape and bending moment distribution of 3-story frame with $P\Delta$ effect

$$\mathbf{U} = \begin{pmatrix} 0.9322 \\ 2.0883 \\ 2.9440 \end{pmatrix} \text{ in} \quad (4.123)$$

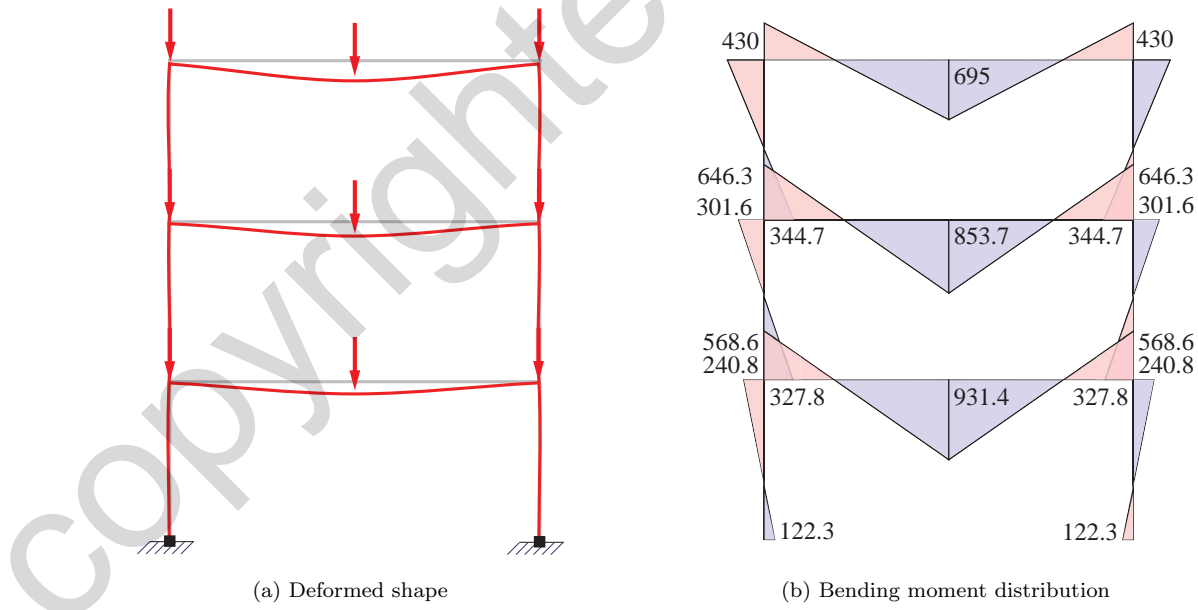


Fig. 4.28: Deformed shape and bending moment distribution of 3-story frame under gravity loads

Fig. 4.30(a) shows the resulting relative story drift values under linear first order analysis and consistent second order analysis. We conclude that the effect of gravity loads is rather small for the case in hand.

We use the formula (C2-3) of the 2005 AISC Specification to determine the magnification factor B_2 for the sway moments under lateral loads in Fig. 4.29(b).

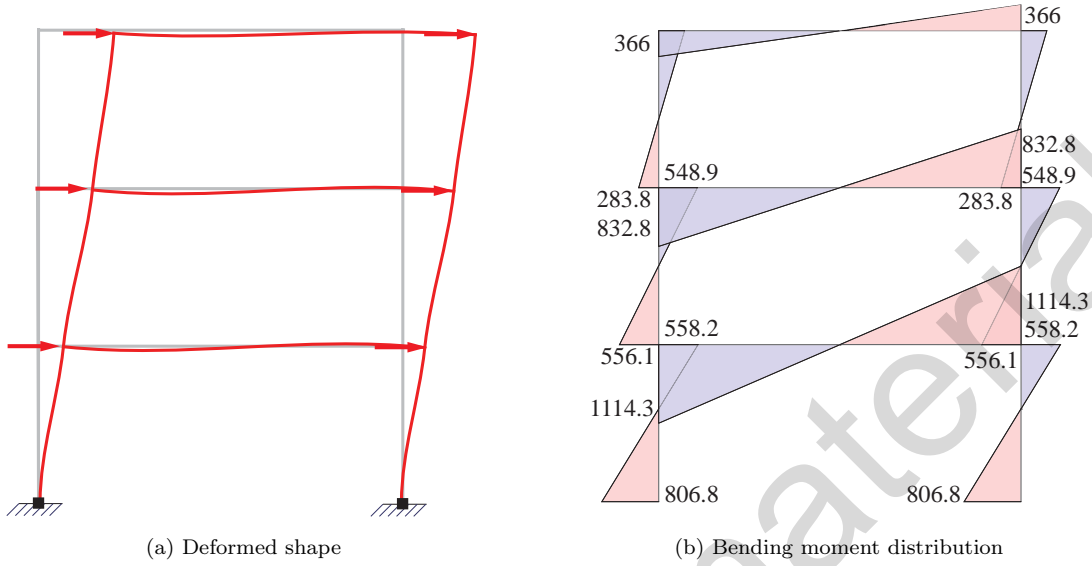


Fig. 4.29: Deformed shape and bending moment distribution of 3-story frame under lateral loads

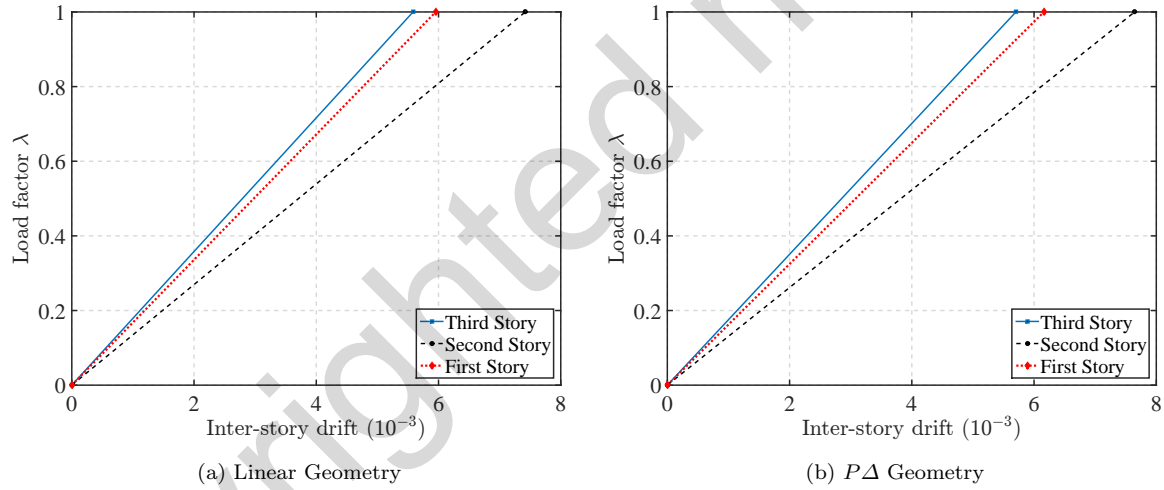


Fig. 4.30: Inter-story drift for three story steel frame

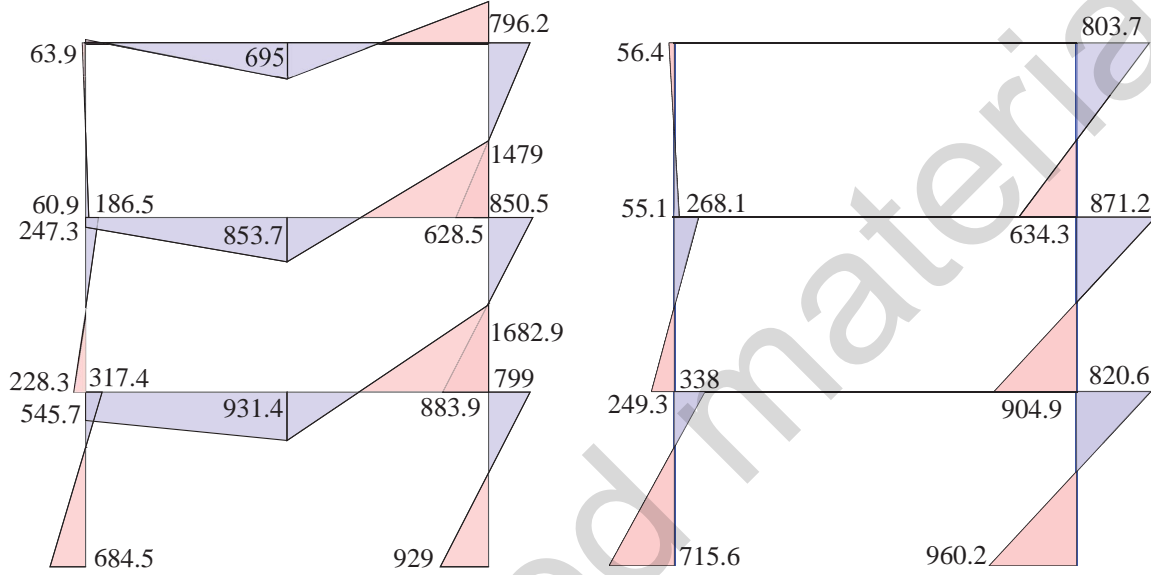
$$B_2 = \frac{1}{1 - \frac{\alpha \sum P_{nt}}{\sum P_{e2}}} \quad (4.124)$$

We set $\alpha = 1.0$ for LRFD design checks. $\sum P_{nt}$ represent the total gravity load on a story and $\sum P_{e2}$ the elastic critical buckling resistance of a story. For the determination of $\sum P_{e2}$ we use the formula (C2-6b) of the 2005 AISC Specification

$$\sum P_{e2} = R_M \frac{\sum H L}{\Delta_H} \quad (4.125)$$

where $R_M = 0.85$ for an unbraced system, $\sum H$ is the story shear, Δ_H is the inter-story drift under first order elastic analysis and L is the story height. The magnification factor is applied story-by-story. Table 4.3 reports the relevant values for the 3-story frame under the gravity and lateral loads in Fig. 4.26.

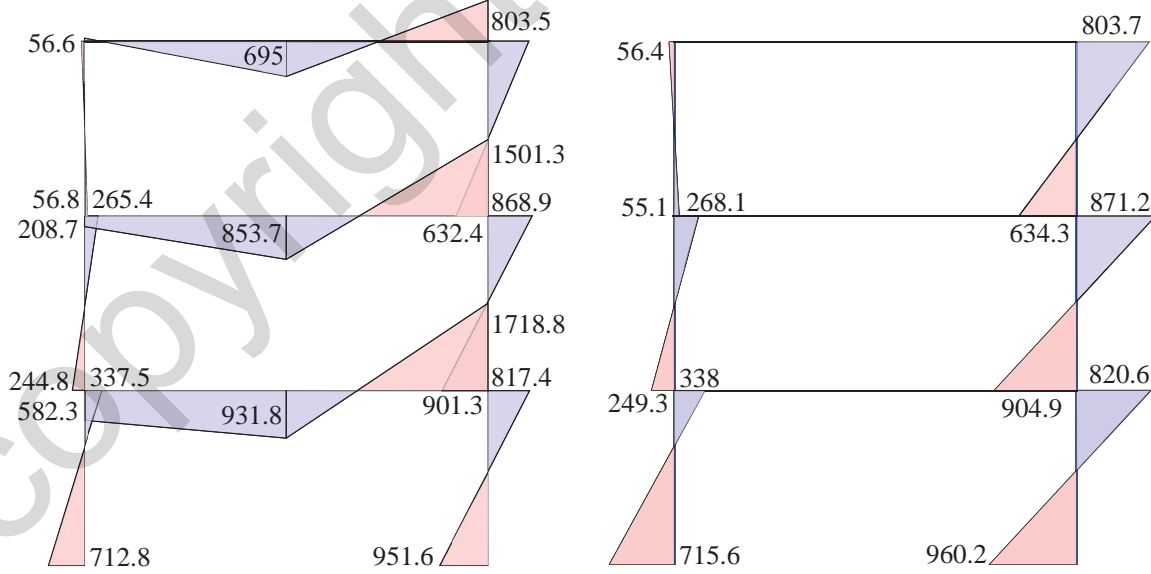
Story	Δ_H (ft)	$\sum P_{nt}$	$\sum H$	B_2
3	0.0713	310	100	1.0204
2	0.0963	710	170	1.0378
1	0.0777	1110	210	1.0386

Table 4.3: Determination of magnification factor B_2 for 3-story frame under loading in Fig. 4.26

(a) Bending moments from linear analysis

(b) Column moment magnification with Table 4.3

Fig. 4.31: Column moment magnification for 2nd order analysis according to 2005 AISC Specification

(a) Bending moments from $P\Delta$ analysis

(b) Column moment magnification with Table 4.3

Fig. 4.32: Comparison of column moment magnification with $P\Delta$ analysis

Fig. 4.31 shows the results of the magnification factor process. Fig. 4.31(a) shows the moment distribution under linear first order analysis and Fig. 4.31(b) shows the magnified *column moments only* with

the factor in Table 4.3. The corresponding girder moments at the girder-column joints should be determined from joint moment equilibrium. The corresponding midspan girder moment should be determined from girder equilibrium under the gravity load at midspan.

From the comparison of the bending moment distribution from $P\Delta$ analysis with the column moment magnification according to the 2005 AISC Specification in Fig. 4.32 we conclude that the accuracy of the latter is very good with the magnified moments slightly on the conservative side.

4.8 Second Order Linear Elastic, Perfectly Plastic Analysis

Noting that the $\mathbf{K}_{P\Delta}$ stiffness for the truss approximation of the nonlinear chord effect is not affected by the element force-deformation behavior of the plane frame element we conclude that we can extend the concepts of plastic analysis from the reader on the Theory of Structures and the event-to-event linear elastic, perfectly plastic analysis from Chapter 1 to consider the $P\Delta$ effect in the equilibrium equations.

Example 4.7 Cantilever Column

Fig. 4.33(a) shows the cantilever column of Example 4.4. The column is subjected to a constant vertical load P_v and a factored horizontal load λP_h . The objective of the following discussion is the determination of the collapse load factor for linear elastic, perfectly plastic force-deformation behavior in flexure with moment capacity M_p under consideration of nonlinear chord geometry effects.

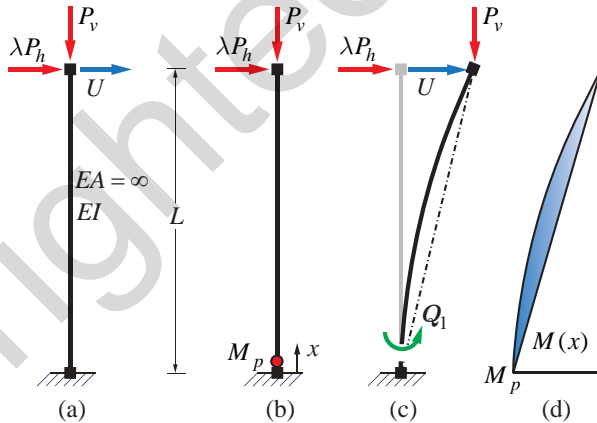


Fig. 4.33: Linear elastic, perfectly plastic cantilever column

The cantilever column has a single independent free dof U , the horizontal translation at the column tip. We start with the determination of the collapse load factor λ_c under the given lateral force P_h from the horizontal translation dof equilibrium in the undeformed configuration in Fig. 4.33(b). It is

$$\lambda P_h = \frac{Q_1}{L}$$

Because the cantilever column is statically determinate, the formation of a single plastic hinge at the column base renders the structure unstable. The corresponding load factor λ_c with $Q_1 = M_p$ is

$$\lambda_c = \frac{M_p}{P_h L} \quad (4.126)$$

We consider now the equilibrium in the deformed configuration in Fig. 4.33(c). The moment generated about the base of the column by the vertical force P_v times the relative horizontal translation U in addition to the moment by the horizontal force λP_h times the column height L gives

$$\lambda P_h + P_v \frac{U}{L} = \frac{Q_1}{L} \quad (4.127)$$

At the instant that the hinge forms at the base of the column the section force-deformation relation is still linear elastic throughout the element axis. Neglecting the nonlinear element geometry effect and assuming that the moment distribution $M(x)$ is linear in Fig. 4.33(d) with maximum moment M_p at the base gives for the horizontal translation U_c at incipient collapse

$$U_c = \frac{M_p L}{3EI} L = \frac{M_p L^2}{3EI} \quad (4.128)$$

Substituting U_c for U in (4.127) gives

$$\lambda_c P_h + P_v \frac{M_p L}{3EI} = \frac{M_p}{L} \rightarrow \lambda_c = \frac{M_p}{P_h L} \left(1 - \frac{P_v L^2}{3EI} \right) \quad (4.129)$$

We note that the second term inside the parentheses is the ratio of the vertical load P_v to the buckling load of the cantilever column under inclusion of only the $\mathbf{K}_{P\Delta}$ stiffness from (4.83). We can, therefore, express the collapse load factor λ_c as

$$\lambda_c = \frac{M_p}{P_h L} \left(1 - \frac{P_v L^2}{3EI} \right) = \frac{M_p}{P_h L} \left(1 - \frac{P_v}{P_{ec}} \right) \quad \text{with} \quad P_{ec} = \frac{3EI}{L^2} \quad (4.130)$$

P_{ec} is the buckling load $\lambda_e |P_v|$ of the cantilever column in (4.83) under the assumption that the geometric stiffness is represented only by the $\mathbf{K}_{P\Delta}$ stiffness.

Before deriving the effect of the nonlinear moment distribution in Fig. 4.33(d) we set up the load-displacement relation of the cantilever column. The displacement method of analysis gives

$$\lambda P_h = KU = (K_l + K_{P\Delta})U = \left(\frac{3EI}{L^3} - \frac{P_v}{L} \right) U = \frac{3EI}{L^3} \left(1 - \frac{P_v}{P_{ec}} \right) U \quad (4.131)$$

The assumption that the moment distribution $M(x)$ is linear corresponds to the assumption that the eccentricity of the vertical force P_v at a section x is measured relative to the element chord. Accounting for the eccentricity of the vertical force P_v relative to the deformed shape of the column requires the inclusion of the P - δ effect in (4.131). We get

$$\lambda P_h = KU = (K_l + K_{P\Delta} + K_{P\delta})U = \left(\frac{3EI}{L^3} - \frac{P_v}{L} - \frac{P_v}{5L} \right) U = \frac{3EI}{L^3} \left(1 - \frac{P_v}{P_{el}} \right) U \quad (4.132)$$

P_{el} is the buckling load $\lambda_e |P_v|$ of the cantilever column in (4.81) under the assumption that the geometric stiffness is represented by the $\mathbf{K}_{P\Delta}$ and the $\mathbf{K}_{P\delta}$ stiffness.

Fig. 4.34 shows the relation between the collapse load factor λ_c and the lateral drift ratio $\frac{U}{L}$ for a W12x336 cantilever column with a height L of 10 ft and a yield strength f_y of 36 ksi. The plastic modulus Z of this section is equal to 603 in³, so that M_p is equal to 21708 k-in. The second area moment I is equal to 4060 in⁴. The horizontal force P_h is equal to 120 kips and the vertical force is equal to 20% of the buckling load P_{ec} .

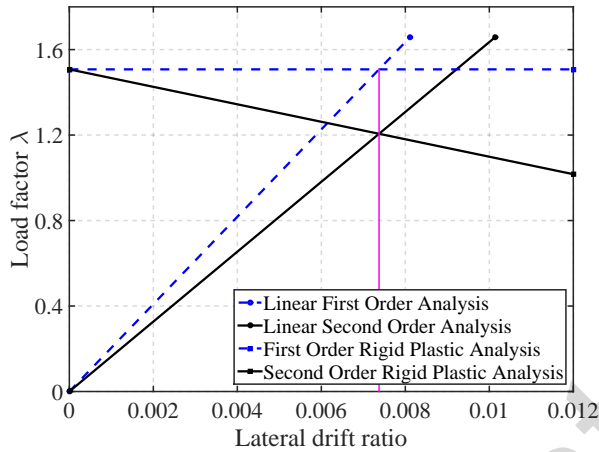


Fig. 4.34: Response of cantilever column under first order and second order linear and rigid plastic analysis

The collapse load factor λ_c under first order plastic analysis is given by (4.126)

$$\lambda_c = \frac{M_p}{P_h L} = \frac{21708}{(120)(10 \cdot 12)} = 1.5075$$

and the horizontal translation at incipient collapse by first order analysis is given by (4.128)

$$U_c = \frac{M_p L^2}{3EI} = \frac{(21708)(120)^2}{3(29000)(4060)} = 0.885 \text{ in}$$

so that the lateral drift ratio at incipient collapse is $\frac{U_c}{L} = 0.0074$. With this information we can trace the first order analysis response shown with a dashed line in Fig. 4.34. The intersection of the horizontal line for the collapse load factor λ_c with the dashed line for the linear first order analysis corresponds to the lateral drift ratio at incipient collapse. The cantilever column with linear elastic section force-deformation response traces the straight line of the linear first order analysis under increasing load factor λ until the latter reaches the collapse load factor λ_c .

The relation between the load factor λ and the horizontal translation U under second order analysis is given by (4.127) for a horizontal translation U past the value at incipient collapse

$$\lambda = \frac{M_p}{P_h L} - \frac{P_v}{P_h} \frac{U}{L}$$

This equation is represented by the sloping solid line in Fig. 4.34 with slope $\frac{P_v}{P_h L}$. The linear second order analysis response of the cantilever column is given by (4.131) under inclusion only of the $\mathbf{K}_{P\Delta}$ geometric stiffness effect. It is represented with a rising solid line in Fig. 4.34. This line intersects the sloping line of the second order plastic analysis response at the same lateral drift value $\frac{U_c}{L}$ at incipient collapse as the first order analysis (can you explain why?). The collapse load factor of the linear elastic, perfectly plastic cantilever column under consideration of the nonlinear chord geometry effect is, therefore, equal to

$$\lambda_c = 1.5075 - \frac{P_v}{P_h} \frac{U_c}{L} = 1.5075 - \frac{4906}{120} \cdot 0.0074 = 1.206$$

Example 4.8 Column-Girder Assembly with Gravity Column

Fig. 4.35 shows a restrained cantilever column-girder assembly formed by elements a and b. The other end of the girder is supported by a *gravity column* represented by a truss element with infinite flexural stiffness EI . The height h in Fig. 4.35 is 15 units and the length l 10 units.

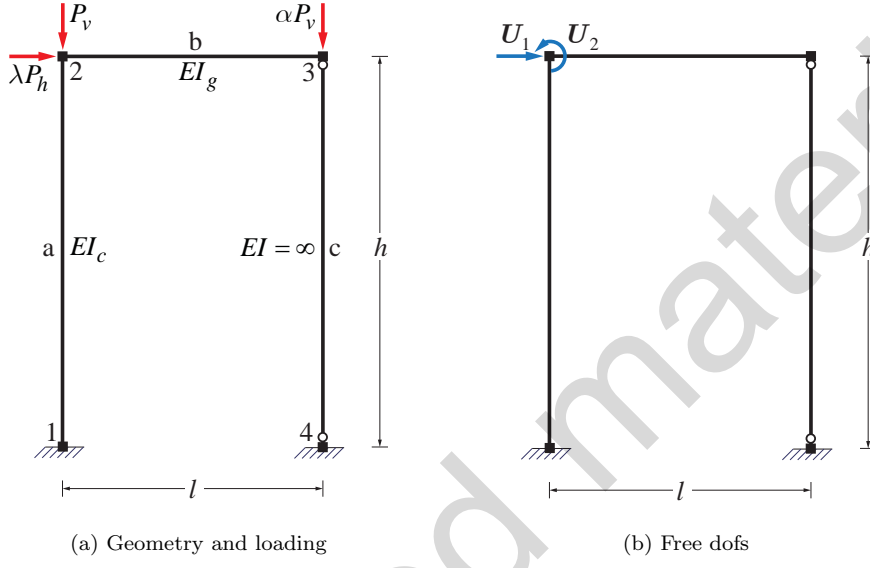


Fig. 4.35: Column-girder assembly with gravity column

All elements of the structural model are assumed inextensible. The column element a has flexural stiffness $EI_c = 2 \cdot 10^5$ and the girder element b has flexural stiffness $EI_g = 10^5$. The force-deformation behavior of these elements is linear elastic, perfectly-plastic with flexural capacity $M_p = 640$ for the column and $M_p = 560$ for the girder.

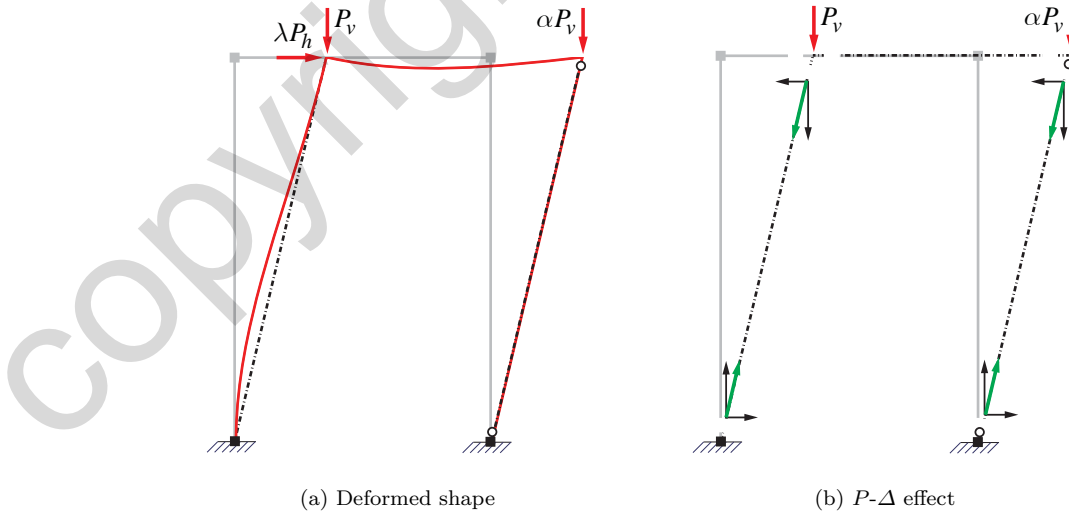


Fig. 4.36: Column-girder assembly with gravity column

The column-girder assembly is subjected to a horizontal force $P_h = 50$ and a vertical force $P_v = -200$. A vertical force of -400 units acts on the gravity column, so that $\alpha = 2$ in Fig. 4.35. The horizontal force increases with load factor λ until collapse, while the vertical forces remain constant.

For the linear elastic, perfectly-plastic *second order* analysis of the column-girder assembly we apply the event-to-event analysis of Chapter 1 and follow Example 1.2. The linear elastic initial stiffness is

$$\mathbf{K}_l = \begin{bmatrix} \frac{12EI_c}{h^3} & \frac{6EI_c}{h^2} \\ \frac{6EI_c}{h^2} & \frac{4EI_c}{h} + \frac{3EI_g}{l} \end{bmatrix} = \begin{bmatrix} 711 & 5333 \\ 5333 & 83333 \end{bmatrix}$$

and the $\mathbf{K}_{P\Delta}$ stiffness matrix is

$$\mathbf{K}_{P\Delta} = \frac{(1+\alpha)P_v}{h} \begin{bmatrix} 1 & 0 \\ 0 & 0 \end{bmatrix} = \begin{bmatrix} -40 & 0 \\ 0 & 0 \end{bmatrix}$$

We note that the $\mathbf{K}_{P\Delta}$ stiffness depends on the *total vertical force*, which does not change under the overturning moment caused by the horizontal force P_h .

With $\mathbf{P}_{ref} = \begin{pmatrix} 50 & 0 \end{pmatrix}^T$ and $\mathbf{K} = \mathbf{K}_l + \mathbf{K}_{P\Delta}$ the free dof displacements \mathbf{U}'_f and the basic forces \mathbf{Q}' under \mathbf{P}_{ref} are

$$\begin{aligned} \mathbf{U}'^{(0)}_f &= \begin{bmatrix} 15.16 & -0.97 \end{bmatrix}^T \cdot 10^{-2} \\ \mathbf{Q}'^{(0)} &= \begin{bmatrix} 549.87 & 291.11 & -291.11 \end{bmatrix}^T \end{aligned}$$

The load factor to the first event is determined from the demand-capacity ratios DC' under \mathbf{P}_{ref}

$$\lambda^{(1)} = \min(1.164, 2.199, 1.924) = 1.164$$

We conclude that the first plastic hinge forms at the column base and scale the free dof displacements \mathbf{U}'_f and the basic forces \mathbf{Q}' with the load factor $\lambda^{(1)}$ to establish the free dof displacements \mathbf{U}_f and the basic forces \mathbf{Q} at the first event

$$\begin{aligned} \mathbf{U}_f^{(1)} &= \lambda^{(1)} \mathbf{U}'^{(0)}_f = \begin{bmatrix} 17.65 & -1.13 \end{bmatrix}^T \cdot 10^{-2} \\ \mathbf{Q}^{(1)} &= \lambda^{(1)} \mathbf{Q}'^{(0)} = \begin{bmatrix} 640 & 338.82 & -338.82 \end{bmatrix}^T \end{aligned}$$

With a hinge at the base of the column the linear stiffness of the structural model changes to

$$\mathbf{K}_l = \begin{bmatrix} \frac{3EI_c}{h^3} & \frac{3EI_c}{h^2} \\ \frac{3EI_c}{h^2} & \frac{3EI_c}{h} + \frac{3EI_g}{l} \end{bmatrix} = \begin{bmatrix} 178 & 2667 \\ 2667 & 70000 \end{bmatrix}$$

The $\mathbf{K}_{P\Delta}$ stiffness is not affected by the hinge formation. Solving for the free dof displacements \mathbf{U}'_f and the basic forces \mathbf{Q}' under \mathbf{P}_{ref} gives

$$\begin{aligned} \mathbf{U}'^{(1)}_f &= \begin{bmatrix} 138.2 & -5.26 \end{bmatrix}^T \cdot 10^{-2} \\ \mathbf{Q}'^{(1)} &= \begin{bmatrix} 0 & 1578 & -1578 \end{bmatrix}^T \end{aligned}$$

The load factor increment to the second event is determined from the demand-capacity ratios DC' under \mathbf{P}_{ref} according to (1.18) after accounting for the residual plastic capacity at end j of the column element a and at end i of the beam element b at the first event

$$\Delta\lambda^{(1)} = \min \begin{pmatrix} - & 0.191 & 0.14 \end{pmatrix} = 0.14$$

We conclude that the second plastic hinge forms at the end i of the girder element b and scale the free dof displacements \mathbf{U}'_f and the basic forces \mathbf{Q}' with the load factor increment $\Delta\lambda^{(1)}$ and add them to those at the first event to establish the free dof displacements \mathbf{U}_f and the basic forces \mathbf{Q} at the second event according to (1.19)

$$\begin{aligned}\lambda^{(2)} &= \lambda^{(1)} + \Delta\lambda^{(1)} = 1.164 + 0.14 = 1.304 \\ \mathbf{U}_f^{(2)} &= \mathbf{U}_f^{(1)} + \Delta\lambda^{(1)} \mathbf{U}'_f^{(1)} = \begin{bmatrix} 37 & -1.87 \end{bmatrix}^T \cdot 10^{-2} \\ \mathbf{Q}^{(2)} &= \mathbf{Q}^{(1)} + \Delta\lambda^{(1)} \mathbf{Q}'^{(1)} = \begin{bmatrix} 640 & 560 & -560 \end{bmatrix}^T\end{aligned}$$

With two plastic hinges the structure is unstable, so that $\lambda_c = 1.304$ is the collapse load factor under *second order linear elastic, perfectly-plastic analysis*.

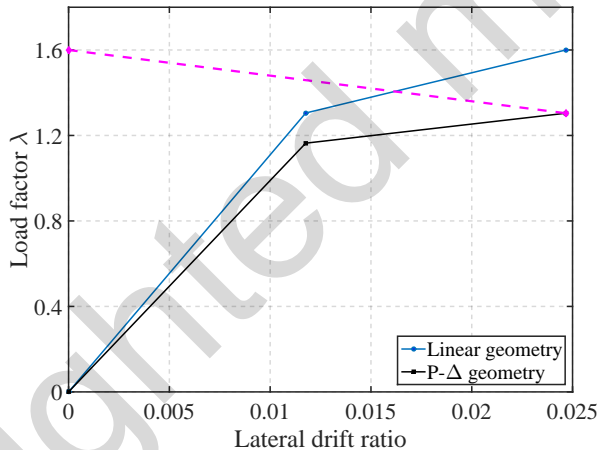


Fig. 4.37: Response of column-girder assembly under first order and second order linear and rigid plastic analysis

Fig. 4.37 shows the results of the analysis along with the results of the first order linear elastic, perfectly-plastic analysis that is left as an exercise for the reader. The latter gives a collapse load factor of 1.6 and the same horizontal translation value at incipient collapse $\mathbf{U}_{1c} = 0.037$ as the second order analysis. With these values we can confirm the collapse load factor with the relation

$$\lambda_c = 1.6 - \frac{P_v}{P_h} \frac{\mathbf{U}_{1c}}{h} = 1.6 - \frac{600}{50} \frac{0.02467}{0.037} = 1.304 \quad \checkmark$$

It is worth noting that we could have included the $\mathbf{K}_{P\delta}$ stiffness in the tangent stiffness of the structure making sure to also include the $\mathbf{k}_{P\delta}$ effect in the calculation of the basic element forces at each event. The $\mathbf{k}_{P\delta}$ column stiffness depends on the axial basic force of the column that is initially equal to P_v . The axial force of the column changes under the increasing horizontal force P_h because of the overturning moment. For the example in hand this change is small and can be accounted for by assuming that the axial column force at the beginning of the event remains constant until the next event. We do not pursue this issue further in this example.

Chapter 5

Path-Independent Nonlinear Material and Section Response

5.1 Introduction

In general, the behavior at a material point is described by a nonlinear relation between the stress and strain tensor

$$\sigma = \hat{\sigma}(\varepsilon, \dot{\varepsilon}, \gamma) \quad (5.1)$$

where ε is the total strain, $\dot{\varepsilon}$ is the strain rate, and γ are internal variables.

Different types of constitutive models are available for the description of material behavior such as linear elastic, linear visco-elastic, perfectly plastic, visco-plastic, and others.

We start with the simplest of nonlinear materials: *a uniaxial, nonlinear elastic or path-independent material*. A linear elastic material is a special case.

For a uniaxial material there is one stress component that depends only on total strain. The material is, therefore, path-independent meaning that it does not have memory of its past and exhibits the same response during loading and unloading, something that is not realistic, but is sufficiently accurate for monotonic response studies without unloading or with limited unloading.

We limit ourselves to this material behavior for now, to establish some fundamental relations between material, section, element and structural response and will return to path-dependent material models later.

5.2 Material State Determination

For path-independent uniaxial material behavior the stress-strain relation is a simple function of one variable, the total strain ε . The stress-strain function should be continuous and, ideally, continuously differentiable resulting in a continuous tangent modulus E_t , which is defined as

$$E_t = \frac{d\sigma}{d\varepsilon} \quad (5.2)$$

for uniaxial material response.

Even though function continuity is readily achievable, slope continuity is rarely present in typical material models for monotonic response. In the absence of a differentiable function for the uniaxial material model, the incremental or initial secant can be used in the place of the tangent modulus.

5.3 Simple Nonlinear Material Models

We introduce three relatively simple models for the simulations of path-independent section and element response in this chapter.

5.3.1 Bilinear Model

The bilinear elastic model has three material parameters: the initial modulus E , the yield strength f_y and the post-yield modulus E_h . The latter may be positive for hardening material response or negative for softening material response, as Fig. 5.1 shows. The behavior in tension and compression is identical.

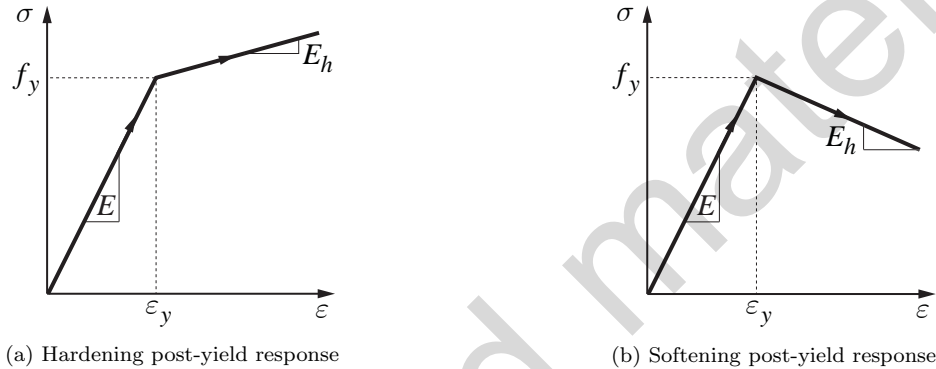


Fig. 5.1: Bilinear stress-strain relation for hardening and softening post-yield response

5.3.2 Giuffré, Menegotto, Pinto (GMP) Model (1970-1973)

Giuffré, Menegotto and Pinto proposed a model with a gradual transition between two straight line asymptotes with slopes E and E_h controlled by the value of a parameter r , as Fig. 5.2 shows.

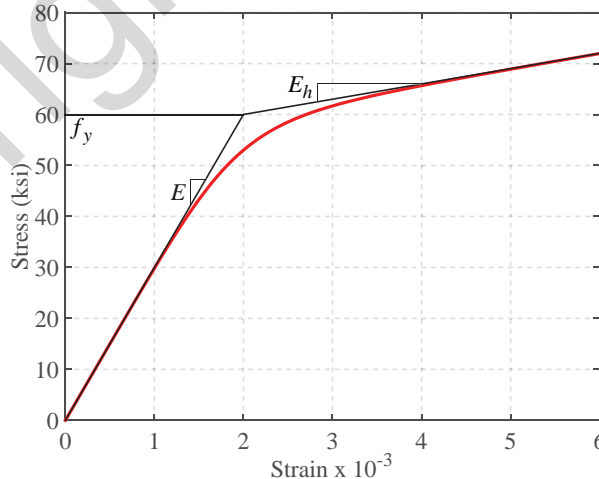


Fig. 5.2: Gradual transition between initial and final asymptote in GMP model

The function is continuous with continuous tangent. The post-yield modulus E_h may be positive or negative, and the model exhibits the same behavior in tension and compression.

The stress-strain relation and tangent modulus of the GMP model are

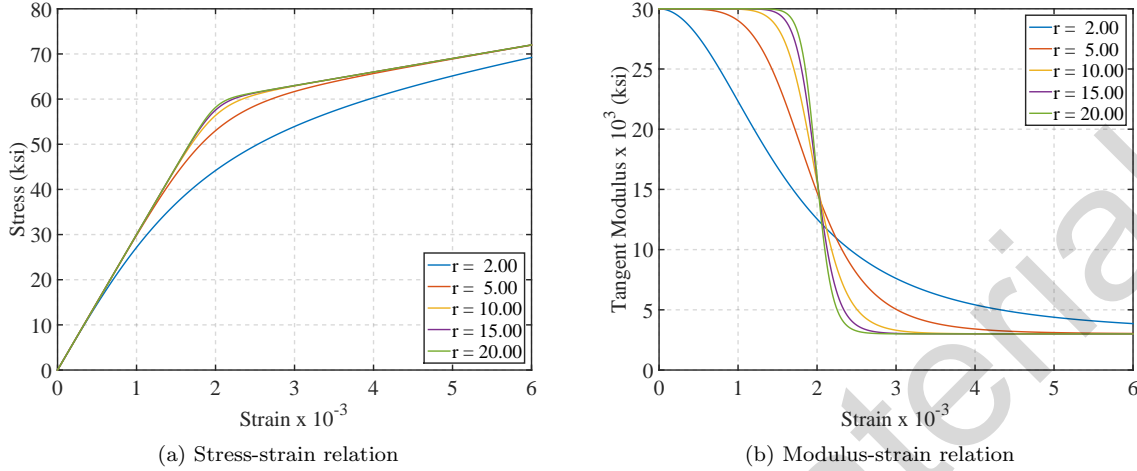


Fig. 5.3: Stress-strain and tangent modulus-strain relation of GMP model for hardening response

$$\begin{aligned}\sigma &= f_y \left[b\xi + \frac{(1-b)\xi}{(1+|\xi|^r)^{\frac{1}{r}}} \right] \\ E_t &= E \left[b + \frac{(1-b)}{(1+|\xi|^r)^{1+\frac{1}{r}}} \right]\end{aligned}\quad (5.3)$$

with

$$\xi = \frac{\varepsilon}{\varepsilon_y} \quad \varepsilon_y = \frac{f_y}{E} \quad b = \frac{E_h}{E}$$

ε_y is the yield strain and b the strain hardening (softening) ratio.

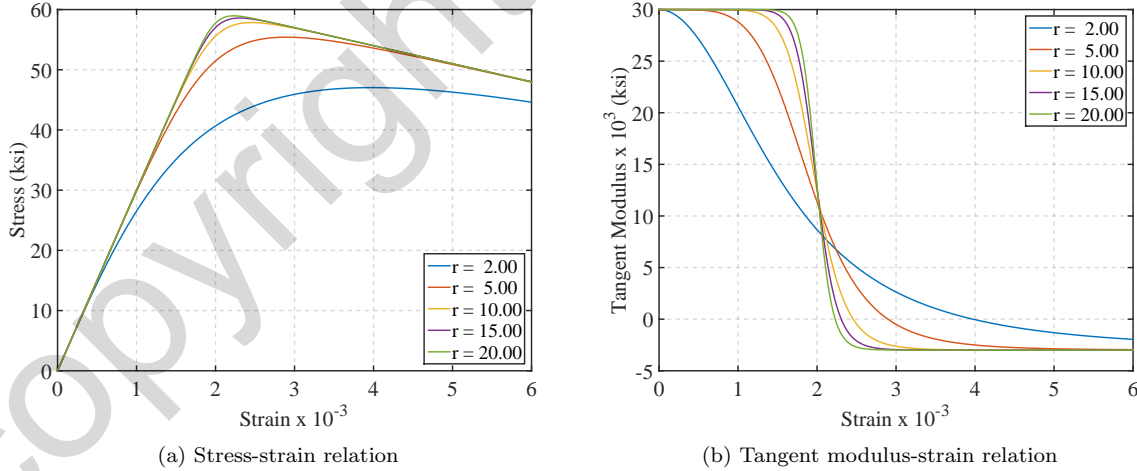


Fig. 5.4: Stress-strain and tangent modulus-strain relation of GMP model for softening response

Fig. 5.3 shows the stress-strain relation of the GMP model and the tangent modulus-strain relation for a material with $f_y = 60$ ksi, $E = 30,000$ ksi and hardening modulus $E_h = 0.1E$. The figures show how the exponent r controls the transition from the initial to the final straight line asymptote. A small value of $r = 2$ produces a very smooth nonlinear curve with the limitation that it departs from the initial

asymptote early and approaches the final asymptote only under large strains. A large value of $r = 20$ approximates the bilinear behavior of cold-formed steel very well and is recommended for the purpose.

Fig. 5.4 shows the stress-strain relation of the GMP model and the tangent modulus-strain relation for a material with $f_y = 60$ ksi, $E = 30,000$ ksi and hardening modulus $E_h = -0.1E$. A negative post-yield modulus describes *strength softening material response*.

The following references provide the original description of the GMP model and a subsequent refinement.

- 1) A. Giuffré and P.E. Pinto, Il comportamento del cemento armato per sollecitazioni cicliche di forte intensità, Giornale del Genio Civile 5 (1970), pp. 391-408.
- 2) M. Menegotto and P.E. Pinto, Method of analysis for cyclically loaded reinforced concrete plane frames including changes in geometry and nonelastic behavior of elements under combined normal force and bending, Proceedings IABSE, Symposium on the Resistance and Ultimate Deformability of Structures Acted on by Well Repeated Loads, Lisbon (1973).
- 3) F.C. Filippou, E.P. Popov, V.V. Bertero, "Effects of Bond Deterioration on Hysteretic Behavior of Reinforced Concrete Joints", Earthquake Engineering Research Center, University of California, Berkeley, Report EERC 1983-19.

5.3.3 Concrete Model by Mander, Priestley, Park (1992)

Mander, Priestley and Park (1992) proposed a nonlinear concrete material model that accounts for the effect of confinement on the stress-strain relation in compression. The model assumes zero stress in tension. It has four material parameters: the concrete compressive strength f_c , the strain ε_{c0} at maximum strength, the secant modulus E_c of the ascending branch, and the confinement factor K_{fc} , which depends on the transverse reinforcement ratio and additional geometric and material properties of concrete section and reinforcement.

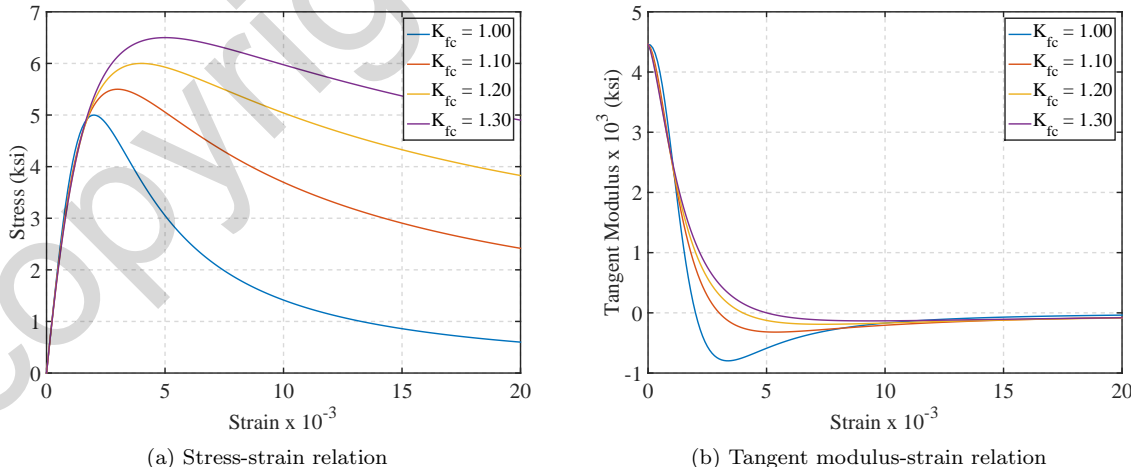


Fig. 5.5: Stress-strain and tangent modulus-strain relation of MPP model

The concrete material model by Mander, Priestley, Park (MPP model) is based on the following continuous stress-strain relation with continuous tangent

$$\sigma_c = \frac{r\eta}{r-1+\eta^r} f_{cc} \quad (5.4)$$

where σ_c is the concrete stress and the concrete strain ε_c appears in the strain ratio η with

$$\eta = \frac{\varepsilon_c}{\varepsilon_{cc0}}$$

The confined concrete strength f_{cc} and corresponding strain ε_{cc0} depend on the respective unconfined concrete values and the confinement factor K_{fc}

$$\begin{aligned} f_{cc} &= K_{fc} f_c \\ \varepsilon_{cc0} &= [5(K_{fc} - 1) + 1] \varepsilon_{c0} \end{aligned} \quad (5.5)$$

Finally, parameter r is defined as follows

$$r = \frac{E_c}{E_c - \frac{f_{cc}}{\varepsilon_{cc0}}} \quad (5.6)$$

Fig. 5.5 shows the effect of the confinement factor K_{fc} on the stress-strain relation and the tangent modulus for the MPP concrete model. A value of $K_{fc} = 1.30$ leads to a compressive strength increase of 30%, but also affects the post-peak behavior of the model that exhibits significant residual strength at a compressive strain of 2%.

The following reference presents the original proposal of the model:

- 1) Mander, Priestley, Park: Theoretical stress-strain model for confined concrete, Journal of the Structural Division, ASCE, 114(8), pp. 1804-1826.

5.4 Section Response

We investigate the force-deformation behavior of sections of arbitrary shape consisting of one or more nonlinear materials. We limit our study to Bernoulli's theory of plane sections remaining plane after deformation, which has proven rather accurate for slender elements whose response depends on flexure and axial force effects.

Extensions of the general concept of section response to the case of shear and torsion are possible with the introduction of appropriate kinematic relations between section deformation variables and normal and shear strains at a material point.

5.4.1 Section Kinematics

Bernoulli's theory assumes that plane sections remain plane after deformation. This assumption works quite well for flexural response, but does not include the effect of shear deformations.

For a section of arbitrary shape in Fig. 5.6 we introduce a reference system $x-y-z$. The location of the system's origin at a point a of the section is arbitrary and will be specified later. The x -axis is normal to the plane of the section and points toward the viewer for a right handed Cartesian coordinate system.

The location of point m in the section is described by coordinates (y, z) . For a section remaining plane after deformation the normal strain ε_m at point m is given by a linear polynomial in y and z .

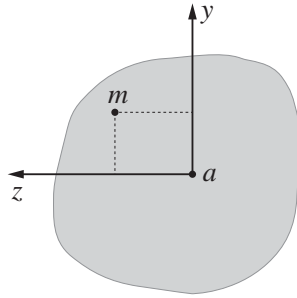


Fig. 5.6: Cross section of arbitrary geometry

$$\varepsilon_m(x, y, z) = \varepsilon_a(x) - y\kappa_z(x) + z\kappa_y(x) \quad (5.7)$$

where ε_a is the normal strain at the origin of the reference axis, κ_z is the curvature about the z-axis, and κ_y is the curvature about the y-axis. The curvatures are rotations per unit of length and their sign is, therefore, defined by the right hand screw rule.

After introducing the section deformation vector e consisting of ε_a , κ_z , and κ_y

$$e(x) = [\varepsilon_a(x) \quad \kappa_z(x) \quad \kappa_y(x)]^T \quad (5.8)$$

we can write (5.7) compactly

$$\varepsilon_m(x, y, z) = \mathbf{a}_s(y, z) e(x) \quad (5.9)$$

$\mathbf{a}_s(y, z)$ is the section kinematic matrix given by

$$\mathbf{a}_s(y, z) = [1 \quad -y \quad z] \quad (5.10)$$

For the case in hand with a single normal strain component $\mathbf{a}_s(y, z)$ is a row vector. With (5.9) the general strain field of the frame element is decomposed into the product of a function $\mathbf{a}_s(y, z)$ over the cross section, and a function $e(x)$ of the location x along the x -axis of the frame element.

5.4.2 Section Equilibrium

What are the work equivalent section forces s for section deformations e ?

We use the principle of virtual work to derive the equilibrium relation: the work done by virtual section deformations $\delta e(x)$ on the real section forces $s(x)$ should be the same as the work done by the virtual normal strain field $\delta \varepsilon_m(y, z)$ on the real normal stress field $\sigma_m(x, y, z)$ over the area of the section.

Expressing this mathematically we get

$$\delta e^T(x) s(x) = \int_A \delta \varepsilon_m^T(y, z) \sigma_m(x, y, z) dA \quad (5.11)$$

where we note that the "summation" of all internal virtual work takes the form of an integral over the cross section area A , since the normal strain and stress are functions of y and z .

In the form of (5.11) the external work is on the left and the internal work on the right of the equal sign, where external and internal work are understood with reference to the section.

For a compatible virtual strain field we take the variation of the real strain field

$$\delta\varepsilon_m(x, y, z) = \mathbf{a}_s(y, z) \delta\mathbf{e}(x) \quad (5.12)$$

Substituting (5.12) into (5.11) we get

$$\delta\mathbf{e}^T(x)\mathbf{s}(x) = \int_A [\mathbf{a}_s(y, z) \delta\mathbf{e}(x)]^T \sigma_m dA = \delta\mathbf{e}^T(x) \int_A \mathbf{a}_s^T(y, z) \sigma_m dA \quad (5.13)$$

Since $\delta\mathbf{e}(x)$ is arbitrary, the only way to satisfy the work equality in (5.13) is

$$\mathbf{s}(x) = \int_A \mathbf{a}_s(y, z)^T \sigma_m dA \quad (5.14)$$

After substitution of $\mathbf{a}_s(y, z)$ from (5.10) into (5.14) we get

$$\mathbf{s}(x) = \int_A \begin{pmatrix} 1 \\ -y \\ z \end{pmatrix} \sigma_m dA \quad (5.15)$$

We conclude that the section force vector is made up of three components, the axial force $N(x)$, the bending moment $M_z(x)$ about the z -axis, and the bending moment $M_y(x)$ about the y -axis with the following definitions

$$\mathbf{s}(x) = \begin{pmatrix} N(x) \\ M_z(x) \\ M_y(x) \end{pmatrix} \quad (5.16)$$

with

$$\begin{aligned} N(x) &= \int_A \sigma_m dA \\ M_z(x) &= \int_A -y \sigma_m dA \\ M_y(x) &= \int_A z \sigma_m dA \end{aligned} \quad (5.17)$$

The section forces \mathbf{s} are also known as stress resultants.

5.4.3 Section Tangent Stiffness

The tangent section stiffness matrix \mathbf{k}_s is the derivative of the section force vector \mathbf{s} with respect to the section deformation vector \mathbf{e} .

After dropping the explicit reference to x for brevity of notation we have

$$\mathbf{k}_s = \begin{bmatrix} \frac{\partial s_1}{\partial e_1} & \frac{\partial s_1}{\partial e_2} & \frac{\partial s_1}{\partial e_3} \\ \frac{\partial s_2}{\partial e_1} & \frac{\partial s_2}{\partial e_2} & \frac{\partial s_2}{\partial e_3} \\ \frac{\partial s_3}{\partial e_1} & \frac{\partial s_3}{\partial e_2} & \frac{\partial s_3}{\partial e_3} \end{bmatrix}$$

By differentiation of (5.14) we get

$$\mathbf{k}_s = \frac{\partial \mathbf{s}}{\partial \mathbf{e}} = \int_A \mathbf{a}_s(y, z)^T \frac{d\sigma_m}{d\varepsilon_m} \frac{\partial \varepsilon_m}{\partial \mathbf{e}} dA = \int_A \mathbf{a}_s(y, z)^T \frac{d\sigma_m}{d\varepsilon_m} \mathbf{a}_s(y, z) dA$$

and after substituting the tangent material modulus for $\frac{d\sigma_m}{d\varepsilon_m}$

$$\mathbf{k}_s = \int_A \mathbf{a}_s(y, z)^T E_m \mathbf{a}_s(y, z) dA \quad (5.18)$$

where E_m is the tangent modulus of the σ - ε relation at point m of the section. We drop subscript t for reference to the tangent value, since it is understood from the derivation. Moreover, it is not important that a tangent modulus for the material be available, since any suitable substitute for it will do (e.g. secant material modulus).

5.4.4 Section Stiffness under Linear Elastic Response

Under nonlinear material response the stress and tangent modulus vary at every point m of the cross section. We are, therefore, faced with the challenge of evaluating the integrals for the section forces \mathbf{s} and the section stiffness matrix \mathbf{k}_s . Because such evaluation is only possible numerically, we will return to the task after first discussing methods of numerical integration.

Under linear elastic material response $\sigma = E\varepsilon$ and $\frac{d\sigma_m}{d\varepsilon_m} = E$, where E is Young's modulus. If the section is homogeneous, then we can factor E out of the area integral in (5.18) to get

$$\mathbf{k}_s = E \int_A \mathbf{a}_s(y, z)^T \mathbf{a}_s(y, z) dA = E \int_A \begin{bmatrix} 1 & -y & z \\ -y & y^2 & -yz \\ z & -yz & z^2 \end{bmatrix} dA$$

The first moments of area

$$\int_A y dA \quad \int_A z dA$$

are zero when the origin of the reference system is at the section centroid.

Similarly, by rotation of the y - z axes (eigenvalue problem) we can ensure that

$$\int_A \tilde{y} \tilde{z} dA = 0$$

where \tilde{y} - \tilde{z} are the principal axes of the cross section.

The section stiffness matrix then becomes simply

$$\mathbf{k}_s = E \begin{bmatrix} A & 0 & 0 \\ 0 & \tilde{I}_z & 0 \\ 0 & 0 & \tilde{I}_y \end{bmatrix} \quad \text{with} \quad \tilde{I}_z = \int_A \tilde{y}^2 dA \quad \tilde{I}_y = \int_A \tilde{z}^2 dA$$

5.4.5 Section Stiffness under Nonlinear Material Response

Under nonlinear material response the section stiffness matrix is fully coupled with the center of gravity and the principal axes loosing their significance because they are continuously changing.

The section forces and stiffness are

$$\mathbf{s} = \int_A \sigma_m \begin{pmatrix} 1 \\ -y \\ z \end{pmatrix} dA \quad (5.19)$$

$$\mathbf{k}_s = \int_A E_m \begin{bmatrix} 1 & -y & z \\ -y & y^2 & -yz \\ z & -yz & z^2 \end{bmatrix} dA \quad (5.20)$$

Despite the loss of any advantage by the center of gravity it still serves typically as reference point of the x - y - z coordinate system of the 2d frame element.

Before discussing the determination of the nonlinear section response we discuss numerical integration for the evaluation of integrals (5.19) and (5.20).

5.5 Numerical Integration

Numerical integration is an important subject of Numerical Analysis. Here we cover just the basics and list a few suitable methods for integral evaluation and limit ourselves to integrals of one independent variable, which can be readily extended to integrals of several variables.

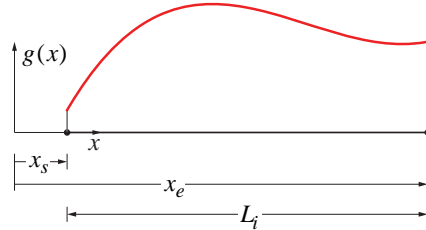


Fig. 5.7: Integral of function $g(x)$ of independent variable x

The task of interest is the evaluation of the integral of the independent variable x in Fig. 5.7

$$I = \int_{x_s}^{x_e} g(x) dx$$

where x_s denotes the beginning of the integration interval and x_e its end with $L_i = x_e - x_s$ denoting the integration length.

We transform the variable x so that the integration interval extends from -1 to 1 with

$$\xi = \frac{2(x - x_s)}{L_i} - 1$$

The inverse relation for the variables and their derivatives is

$$x = x_s + \frac{L_i}{2}(1 + \xi) \quad \text{and} \quad dx = \frac{L_i}{2} d\xi \quad (5.21)$$

The integral then becomes

$$I = \frac{L_i}{2} \int_{-1}^1 \tilde{g}(\xi) d\xi$$

where \tilde{g} is the function obtained from g by substitution of x by the expression in (5.21).

Numerical integration consists of replacing the integral by a sum of the form

$$I = \frac{L_i}{2} \int_{-1}^1 \tilde{g}(\xi) d\xi = \frac{L_i}{2} \sum_{i=1}^{nIP} \tilde{w}_i \tilde{g}(\xi_i) \quad (5.22)$$

where nIP is the number of integration points, ξ_i are the integration locations, and \tilde{w}_i the integration weights.

We can also perform the numerical integration in the original variable as long as we scale the integration weights

$$I = \sum_{i=1}^{nIP} w_i g(x_i) \quad \text{with} \quad w_i = \frac{L_i}{2} \tilde{w}_i \quad (5.23)$$

There are several integration rules. Each integration rule is associated with locations and weights for the integration points. These are tabulated in reference books typically for the integration interval from -1 to 1. To convert the integration locations and weights to the interval from 0 to L we use the transformation

$$x_i = x_s + \frac{L_i}{2}(1 + \xi_i) \quad w_i = \frac{L_i}{2} \tilde{w}_i \quad (5.24)$$

5.5.1 Simpson and Trapezoidal Integration Rules

The first group of integration rules involves the subdivision of the integration interval into segments of equal length Δx and the evaluation of the function to be integrated at the segment ends (Newton-Cotes formulas). There are ways to minimize the amount of work for better accuracy and this is extensively

used in existing software like Mathcad and Matlab®. The interested reader is referred to the software manuals.

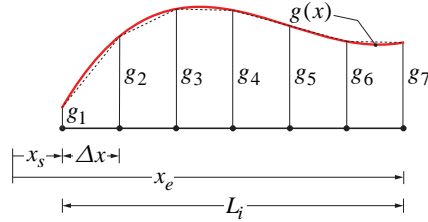


Fig. 5.8: Subdivision of integration interval into segments of equal length for trapezoidal rule

Among the best known Newton-Cotes formulas are the trapezoidal rule and the Simpson rule. The trapezoidal rule in Fig. 5.8 is accurate for quadratic polynomials. Subdividing the integration interval L_i into 6 segments of equal length $\Delta x = \frac{L_i}{6}$ in Fig. 5.8 gives the following numerical approximation I_T of the integral of $g(x)$ with the trapezoidal rule

$$I_T = \frac{L_i}{12} (g_1 + 2g_2 + 2g_3 + 2g_4 + 2g_5 + 2g_6 + g_7)$$

Generalizing to the subdivision into n segments gives

$$I_T = \frac{L_i}{2n} (g_1 + 2g_2 + \dots + 2g_n + g_{n+1})$$

The Simpson integration rule Fig. 5.9 is accurate for cubic polynomials. *It requires subdivision of the integration interval into an even number of segments.* Subdividing the integration interval L_i into 6 segments of equal length $\Delta x = \frac{L_i}{6}$ in Fig. 5.9 gives the following numerical approximation I_S of the integral of $g(x)$ with Simpson's rule

$$I_S = \frac{L_i}{18} (g_1 + 4g_2 + 2g_3 + 4g_4 + 2g_5 + 4g_6 + g_7)$$

Generalizing to the subdivision into an even number n of segments gives

$$I_S = \frac{L_i}{3n} (g_1 + 4g_2 + 2g_3 + \dots + 2g_{n-1} + 4g_n + g_{n+1})$$

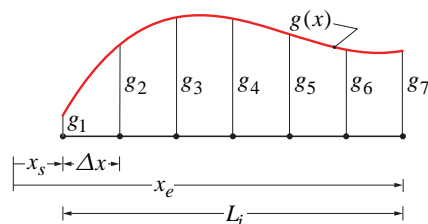


Fig. 5.9: Subdivision of integration interval into even number of segments of equal length for Simpson's rule

These rules are implemented in FEDEASLab functions `Simpson.m` and `Trap.m` with the number `nIP` of integration points as only input argument.

5.5.2 Midpoint integration rule

The midpoint integration rule in Fig. 5.10 is a special case of the Riemann definite integral formula: the integration interval L_i is subdivided into segments of equal length $\Delta x = \frac{L_i}{n}$ and the function to be integrated is evaluated at the midpoint of each segment. In this case the number of integration points is equal to the number of segments n . Because the function value g_i at each midpoint is multiplied by the segment length $\frac{L_i}{n}$, the latter serves as the constant integration weight of this rule. The midpoint rule is exact only for linear functions.

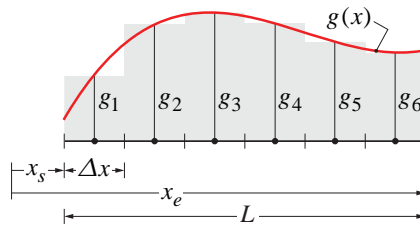


Fig. 5.10: Integration points for midpoint integration rule

Subdividing the integration interval L_i into 6 segments of equal length $\Delta x = \frac{L_i}{6}$ in Fig. 5.10 gives the following numerical approximation I_M of the integral of $g(x)$ with the midpoint rule

$$I_M = \frac{L_i}{6} (g_1 + g_2 + g_3 + g_4 + g_5 + g_6 + g_7)$$

We note that the area under the integral is approximated by the area of the stepped rectangles in the figure. Generalizing to the subdivision into n segments gives

$$I_M = \frac{L_i}{n} \sum_{i=1}^{nIP} g_i$$

where nIP is the number of segments, which is equal to the number of integration points for this rule.

The midpoint rule is implemented in FEDEASLab function `Midpoint.m` with the number `nIP` of integration points as only input argument.

5.5.3 Gaussian Quadrature

If the constraint of evenly spaced integration points is removed, then a new class of numerical integration algorithms arise. These are known as Gaussian quadrature or Gauss integration rules named in honor of Karl Friedrich Gauss (1777-1855) who realized that the integration accuracy for *smooth functions* could be optimized if the location of the integration points as well as their weight are used as parameters.

Among several variants of Gauss quadrature three rules stand out for their importance in linear and nonlinear analysis:

- 1) Gauss-Legendre or simply Gauss quadrature which is accurate for polynomials of order $2nIP-1$ where nIP is the number of integration points
- 2) Gauss-Lobatto or simply Lobatto quadrature which is accurate for polynomials of order $2nIP-3$, because it gives up 2 free parameters to include the function evaluation at the ends of the integration

interval. This rule is especially useful for the integration of the inelastic frame element response with maximum moments and curvatures often arising at the element ends.

- 3) Gauss-Radau or simply Radau quadrature with a function evaluation at only one end of the integration interval. This rule is useful in the integration of response variables over the plastic zone of a frame element.

Gauss quadrature is implemented in FEDEASLab functions `Gauss.m`, `Lobatto.m` and `Radau.m` with the number `nIP` of integration points as only input argument.

Example 5.1 Numerical Evaluation of Integral

The task in hand is the numerical evaluation of the integral

$$I = \int_{-2}^{5} e^{-x}(x^2 - 3x + 5)dx$$

For this problem the exact solution is available: it is equal to 0.6503 to 4 significant digits, but this is not the case for most problems. Most integration rules report locations and weights for a standard interval from -1 to 1. Consequently, we transform the standard interval to the interval of our problem and determine the corresponding integration point locations and weights. With the auxiliary variable ξ covering the standard interval $-1 \leq \xi \leq 1$ the transformation to the integration point location and weight for variable x is given by (5.21).

In the following we demonstrate the numerical evaluation of the integral with the trapezoidal rule and with the Gauss-Legendre quadrature rule.

For the problem in hand the length of the integration interval is $L_i = 3$ and the starting point $x_s = 2$. We make use of $nIP = 7$ integration points. The calculations for the trapezoidal rule are summarized in Table 5.1 and those for the Gauss-Legendre quadrature in Table 5.2.

We note the better accuracy of the Gauss-Legendre quadrature for the same number of integration points. This happens *for smooth integrands* because of the selection of optimum locations for the integration points by the Gauss-Legendre method.

5.6 Section State Determination

The response determination of a section with arbitrary cross section made up of one or more nonlinear materials is an important task of nonlinear analysis, either on its own merit for the determination of moment-curvature relations or axial force-bending moment interaction diagrams of a given section, or as part of the response determination of a nonlinear frame element by integration of the response of control sections over its length, with each section response obtained by integration of the nonlinear material response.

The section state determination constitutes a pivotal step in this process. It requires the determination of the section forces or stress resultants s and the section stiffness \mathbf{k}_s for given section deformations e . Noting explicitly that section variables are functions of x , the distance of the section from end i of the frame element, we summarize the state determination process for a section with given geometry and material constitution:

ξ	\tilde{w}_i	x_i	w_i	$g(x_i)$	$w_i g(x_i)$
-1.0000	0.1667	2.0000	0.25	0.4060	0.1015
-0.6667	0.3333	2.5000	0.50	0.3078	0.1539
-0.3333	0.3333	3.0000	0.50	0.2489	0.1245
0.0000	0.3333	3.5000	0.50	0.2038	0.1019
0.3333	0.3333	4.0000	0.50	0.1648	0.0824
0.6667	0.3333	4.5000	0.50	0.1305	0.0653
1.0000	0.1667	5.0000	0.25	0.1011	0.0253
	$\sum_i \tilde{w}_i = 2.00$		$\sum_i w_i = 3.00$		$\sum_i w_i g(x_i) = 0.6547$

Table 5.1: Organization of calculations for trapezoidal integration rule

ξ	\tilde{w}_i	x_i	$w_i = \frac{L}{2} \tilde{w}_i$	$g(x_i)$	$w_i g(x_i)$
-0.9491	0.1295	2.0763	0.1942	0.3865	0.0751
-0.7415	0.2797	2.3877	0.4196	0.3249	0.1363
-0.4058	0.3818	2.8912	0.5727	0.2601	0.1490
0.0000	0.4180	3.5000	0.6269	0.2038	0.1278
0.4058	0.3818	4.1088	0.5727	0.1570	0.0899
0.7415	0.2797	4.6123	0.4196	0.1235	0.0518
0.9491	0.1295	4.9237	0.1942	0.1052	0.0204
	$\sum_i \tilde{w}_i = 2.00$		$\sum_i w_i = 3.00$		$\sum_i w_i g(x_i) = 0.6503$

Table 5.2: Organization of calculations for Gauss-Legendre quadrature

- 1) Given the section deformations $\mathbf{e}(x)$;
- 2) Determine the strain at point m of the cross section with coordinates y, z

$$\varepsilon_m(x, y, z) = \mathbf{a}_s(y, z) \mathbf{e}(x) \quad \text{with} \quad \mathbf{a}_s(y, z) = \begin{bmatrix} 1 & -y & z \end{bmatrix} \quad \mathbf{e}(x) = \begin{pmatrix} \varepsilon_a \\ \kappa_z \\ \kappa_y \end{pmatrix}$$

- 3) Use the stress-strain relation for the material at point m to determine the stress σ_m and tangent modulus E_m at point m .
- 4) Determine the section forces $\mathbf{s}(x)$ from

$$\mathbf{s}(x) = \int_A \mathbf{a}_s(y, z)^T \sigma_m dA \tag{5.25}$$

and the section stiffness matrix \mathbf{k}_s from

$$\mathbf{k}_s(x) = \int_A \mathbf{a}_s(y, z)^T E_m \mathbf{a}_s(y, z) dA \tag{5.26}$$

with integration over the cross section area A .

For sections with nonlinear material(s) the stress σ_m and modulus E_m in (5.25) and (5.26) vary irregularly over the cross section, as is the case, for example, for a reinforced concrete section with a portion under tension and another under compression. Consequently, the integrals in (5.25) and (5.26) need to be evaluated numerically.

The origin of the y - z axes in point a of Fig. 5.6 is usually taken at the centroid of the cross section, but any other point is equally suitable.

Either way the section stiffness matrix is typically full under nonlinear material response, thus coupling the axial with the flexural response.

In the following we limit ourselves for the sake of simplicity to flexure about the z -axis. For brevity of notation we drop the corresponding subscript from curvature and bending moment. We also refrain from stating explicitly the dependence of section variables on x , which is implied. In this case (5.25) and (5.26) simplify with $\mathbf{a}_s(y, z) = \mathbf{a}_s(y) = [1 - y]$ and $dA = b(y)dy$

$$\mathbf{s} = \begin{pmatrix} N \\ M \end{pmatrix} = \int_A \mathbf{a}_s(y)^T \sigma_m dA = \int_d \mathbf{a}_s(y)^T \sigma_m b(y) dy \quad (5.27)$$

$$\mathbf{k}_s = \int_A \mathbf{a}_s(y)^T E_m \mathbf{a}_s(y) dA = \int_d \mathbf{a}_s(y)^T E_m \mathbf{a}_s(y) b(y) dy \quad (5.28)$$

The integration extends now over the section depth d , and $b(y)$ is the section width at point m , which may vary with y . With $\mathbf{a}_s(y) = [1 - y]$ the integrals become explicitly

$$\mathbf{s} = \begin{pmatrix} N \\ M \end{pmatrix} = \int_d \begin{pmatrix} 1 \\ -y \end{pmatrix} \sigma_m b(y) dy \quad (5.29)$$

$$\mathbf{k}_s = \int_d \begin{bmatrix} 1 & -y \\ -y & y^2 \end{bmatrix} E_m b(y) dy \quad (5.30)$$

The numerical integration converts the integrals to sums of the form

$$\mathbf{s} = \begin{pmatrix} N \\ M \end{pmatrix} = \sum_{i=1}^{nIP} \begin{pmatrix} 1 \\ -y_i \end{pmatrix} \sigma_i b_i w_i \quad (5.31)$$

$$\mathbf{k}_s = \sum_{i=1}^{nIP} \begin{bmatrix} 1 & -y_i \\ -y_i & y_i^2 \end{bmatrix} E_i b_i w_i \quad (5.32)$$

where i is an integer counter ranging from 1 to the number of integration points nIP , $b_i = b(y_i)$ is the section width at y_i , and w_i is the weight of the integration scheme at y_i . σ_i and E_i denotes the stress

and tangent modulus for ε_i , i.e.

$$\sigma_i = \sigma(\varepsilon_i)$$

$$E_i = \left. \frac{d\sigma}{d\varepsilon} \right|_{\varepsilon_i}$$

$$\text{with } \varepsilon_i = \varepsilon_a - y_i \kappa$$

Example 5.2 Section Forces s for Given Deformations e

We determine the section forces s for given section deformations e for the homogeneous rectangular section in Fig. 5.11 with $d = 18$ and $b = 12$. We assume the linear strain distribution of the Euler-Bernoulli plane section remaining plane theory for flexure and axial force with the strain $\varepsilon_b = 2.5 \cdot 10^{-3}$ at the bottom and the strain $\varepsilon_t = -1.5 \cdot 10^{-3}$ at the top of the section. We also assume that the nonlinear material follows the GMP stress-relation with the following material properties: $f_y = 40$, $E = 20,000$, $E_h = 1000$ and $r = 2$.

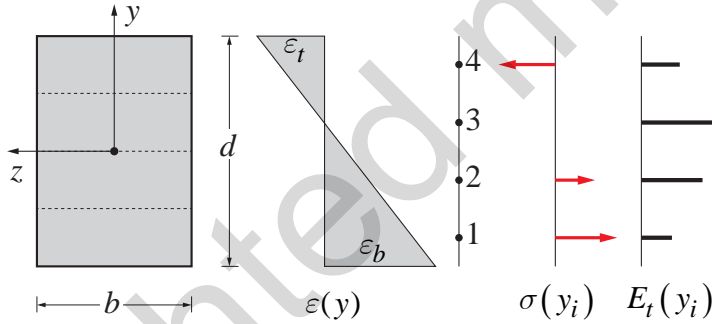


Fig. 5.11: Rectangular section under given linear strain distribution

The first task is the determination of the strain, stress and tangent modulus at each integration point of the integration rule. We use first the midpoint integration rule with 4 integration points numbered from the section soffit, as Fig. 5.11 shows. The strain distribution and the stress and tangent modulus at the integration points are shown schematically in Fig. 5.11. *It is important to realize that the actual distribution of stress and tangent modulus is typically not available.* The strain, the stress and the tangent modulus at each integration point (IP) are given with the corresponding integration weights of the midpoint integration rule in Table 5.3.

IP	ξ_i	\tilde{w}_i	y_i	w_i	ε_i	σ_i	E_i
1	-0.7500	0.50	-6.75	4.50	0.002	28.87	7717.5
2	-0.2500	0.50	-2.25	4.50	0.001	17.99	14595.3
3	0.2500	0.50	2.25	4.50	0.000	0.00	20000.0
4	0.7500	0.50	6.75	4.50	-0.001	-17.99	14595.3

Table 5.3: Material response at midpoint integration points of rectangular section

For the determination of the section forces s we use (5.31) to get

$$\begin{aligned}
 s &= \binom{N}{M} = \sum_{i=1}^{nIP} \binom{1}{-y_i} \sigma_i b_i w_i \\
 s &= \binom{1}{6.75} \cdot (28.87) \cdot (54) + \binom{1}{2.25} \cdot (17.99) \cdot (54) \\
 &\quad + \binom{1}{-2.25} \cdot (0) \cdot (54) + \binom{1}{-6.75} \cdot (-17.99) \cdot (54) = \binom{1.559}{19.267} 10^3
 \end{aligned}$$

For the determination of the tangent section stiffness \mathbf{k}_s we use (5.32) to get

$$\begin{aligned}
 \mathbf{k}_s &= \sum_{i=1}^{nIP} \begin{bmatrix} 1 & -y_i \\ -y_i & y_i^2 \end{bmatrix} E_i b_i w_i \\
 \mathbf{k}_s &= \begin{bmatrix} 1 & 6.75 \\ 6.75 & 6.75^2 \end{bmatrix} \cdot (7717.5) \cdot (54) + \begin{bmatrix} 1 & 2.25 \\ 2.25 & 2.25^2 \end{bmatrix} \cdot (14595.3) \cdot (54) \\
 &\quad + \begin{bmatrix} 1 & -2.25 \\ -2.25 & 2.25^2 \end{bmatrix} \cdot (20000) \cdot (54) + \begin{bmatrix} 1 & -6.75 \\ -6.75 & 6.75^2 \end{bmatrix} \cdot (14595.3) \cdot (54) = \begin{bmatrix} 3.07 & -3.16 \\ -3.16 & 64.35 \end{bmatrix} 10^6
 \end{aligned}$$

The strain, stress and tangent modulus at the integration points of the Gauss-Legendre integration rule are given in Table 5.4.

IP	ξ_i	\tilde{w}_i	y_i	w_i	ε_i	σ_i	E_i
1	-0.8611	0.3479	-7.7502	3.1307	0.0022	30.47	6687.8
2	-0.3400	0.6521	-3.0598	5.8693	0.0012	20.49	13138.9
3	0.3400	0.6521	3.0598	5.8693	0.0002	-3.59	19771.6
4	0.8611	0.3479	7.7502	3.1307	-0.0012	-21.04	12803.6

Table 5.4: Material response at Gauss-Legendre integration points of rectangular section

For the determination of the section forces s we use (5.31) to get

$$\begin{aligned}
 s &= \binom{N}{M} = \sum_{i=1}^{nIP} \binom{1}{-y_i} \sigma_i b_i w_i \\
 s &= \binom{1}{7.75} \cdot 30.47 \cdot 37.57 + \binom{1}{3.06} \cdot 20.49 \cdot 70.43 \\
 &\quad + \binom{1}{-3.06} \cdot (-3.59) \cdot 70.43 + \binom{1}{-7.75} \cdot (-21.04) \cdot 37.57 = \binom{1.545}{20.185} 10^3
 \end{aligned}$$

For the determination of the tangent section stiffness \mathbf{k}_s we use (5.32) to get

$$\mathbf{k}_s = \sum_{i=1}^{nIP} \begin{bmatrix} 1 & -y_i \\ -y_i & y_i^2 \end{bmatrix} E_i b_i w_i$$

$$\mathbf{k}_s = \begin{bmatrix} 1 & 7.75 \\ 7.75 & 7.75^2 \end{bmatrix} \cdot 6687.8 \cdot 37.57 + \begin{bmatrix} 1 & 3.06 \\ 3.06 & 3.06^2 \end{bmatrix} \cdot 13138.9 \cdot 70.43$$

$$+ \begin{bmatrix} 1 & -3.06 \\ -3.06 & 3.06^2 \end{bmatrix} \cdot 19771.6 \cdot 70.43 + \begin{bmatrix} 1 & -7.75 \\ -7.75 & 7.75^2 \end{bmatrix} \cdot 12803.6 \cdot 37.57 = \begin{bmatrix} 3.05 & -3.21 \\ -3.21 & 65.69 \end{bmatrix} 10^6$$

We note that the axial force estimate is close for both integration rules, but the bending moment estimate shows a slight discrepancy. The same is true for the tangent section stiffness term \mathbf{k}_{s22} . This happens because the corresponding integrand is a smooth nonlinear function for which the Gauss-Legendre integration rule gives more accurate results than the midpoint rule for the same number of integration points. We recall that *the midpoint integration rule is exact only for linear polynomials*.

5.7 Section Analysis

The section response constitutes an important intermediate step of the formulation of beam finite element models with nonlinear material response. It is also an important stand-alone problem for the determination of the moment-curvature response of sections of arbitrary geometry comprised of one or more nonlinear materials, and for the determination of the failure surface of such sections under combinations of section force resultants.

Either way, the section response formulation is based on the following steps:

- 1) **Kinematics:** relation between the section deformations and the material strains.
- 2) **Material law:** relation between the material strain and stress.
- 3) **Equilibrium:** relation between the applied and the resisting section forces.

In the preceding section we discussed the determination of the section resultant forces for given section deformations \mathbf{e} with numerical integration.

The determination of the section forces \mathbf{s} and the section stiffness matrix \mathbf{k}_s for given section deformations \mathbf{e} is called the *section state determination*.

5.7.1 Formulation

If the section deformations \mathbf{e} are given, then the determination of the section forces \mathbf{s} and section stiffness matrix \mathbf{k}_s seems straightforward. In the context of a nonlinear beam finite element formulation this requires that the relation between section deformations $\mathbf{e}(x)$ and element deformations \mathbf{v} be defined. This is accomplished with displacement interpolation functions, as will be discussed in later chapters. *Such an approach is known as displacement formulation of finite element analysis.*

What happens, however, if the section forces \mathbf{s} are given and one wishes to determine the section deformations and from these the element deformations \mathbf{v} ? This requires the formulation of the section response analysis as a system of nonlinear equations that need to be solved iteratively. The section

forces \mathbf{s} can be related to the element basic forces \mathbf{q} through element equilibrium in the undeformed configuration. Such an approach is known as force or mixed formulation of finite element analysis.

For the formulation of the section analysis problem we distinguish between applied section forces or resultants \mathbf{s} and resisting section forces or resultants \mathbf{s}_r . The applied section forces depend on the basic element forces \mathbf{q} by means of the element equilibrium relations in the undeformed configuration. The resisting section forces result from the summation of the normal stresses over the cross section corresponding to the normal strains for given section deformations \mathbf{e} . It is, in fact, the resisting section forces \mathbf{s}_r that we set up in the preceding section with (5.19) for the general case of biaxial bending with axial force, and with (5.29) for the case of uniaxial bending with axial force.

We, therefore, rewrite (5.29) with the introduction of subscript r for the section force resultants to denote "resisting" section forces.

$$\mathbf{s}_r = \begin{pmatrix} N_r \\ M_r \end{pmatrix} = \int_d \begin{pmatrix} 1 \\ -y \end{pmatrix} \sigma_m b(y) dy \quad (5.33)$$

where the integration extends over the depth d of the cross section for uniaxial bending.

The section equilibrium, thus, takes the form of 2 nonlinear equations in two unknowns for the problem of uniaxial bending with axial force

$$\mathbf{s}(\mathbf{q}) - \mathbf{s}_r(\mathbf{e}) = \mathbf{0} \quad (5.34)$$

with the dependence of applied and resisting section forces explicitly expressed.

We are not concerned at present with the relation between \mathbf{s} and \mathbf{q} , which was established in the course on Theory of Structures. We will return to it later for the formulation of nonlinear beam finite elements. For now, we concentrate on the solution of the different section analysis problems that we encounter in nonlinear analysis.

5.7.2 Section Analysis Problems

We encounter the following types of section analysis problems:

- 1) Given the section deformations $\mathbf{e}(x)$ determine $\mathbf{s}(x)$.
- 2) Given the section forces $\mathbf{s}(x)$ determine the section deformations $\mathbf{e}(x)$.
- 3) Given one section deformation and one section force determine the corresponding unknowns.

The first section analysis problem appears in the following applications:

- 1) The determination of the failure surface for the interaction of section force resultants under assumed section deformations at failure.
- 2) The determination of the section forces $\mathbf{s}(x)$ for section deformations $\mathbf{e}(x)$ resulting from element deformations \mathbf{v} through displacement interpolation functions.

We have already addressed the solution of this problem in the last section. We plan to discuss the determination of the failure surface of a section later in this chapter.

The second section analysis problem appears in the following applications:

- 1) The determination of the deformation state of statically determinate structures under given nodal forces (e.g. RC cantilever column under eccentric axial force).
- 2) The determination of the failure surface for the interaction of section force resultants under incremental analysis to failure.
- 3) The determination of the section deformations $\mathbf{e}(x)$ for given section forces $\mathbf{s}(x)$ resulting from the element basic forces \mathbf{q} through force interpolation functions.

Finally, the third section analysis problem only appears as a stand-alone problem, but turns out to be nonetheless extremely important, since it leads to the determination of the moment-curvature response of arbitrary cross sections comprised of one or more nonlinear materials under constant axial force.

5.7.3 First Section Analysis Problem

The first section analysis problem consists of the determination of the resisting section forces \mathbf{s}_r for given section deformations \mathbf{e} . We have already addressed the solution of this problem in the last section as part of the section state determination process. We, therefore, just restate the results from the last section. For given section deformations \mathbf{e} we proceed as follows to determine \mathbf{s} :

- 1) For $i = 1 \dots nIP$ determine the strain at integration point i

$$\varepsilon_i = \begin{bmatrix} 1 & -y_i \end{bmatrix} \begin{pmatrix} \varepsilon_a \\ \kappa \end{pmatrix}$$

- 2) Use the material model to determine the stress $\sigma_i = \sigma(\varepsilon_i)$
- 3) Determine the section forces \mathbf{s} from

$$\mathbf{s} = \mathbf{s}_r(\mathbf{e}) = \begin{pmatrix} N_r \\ M_r \end{pmatrix} = \sum_{i=1}^{nIP} \begin{pmatrix} 1 \\ -y_i \end{pmatrix} \sigma_i b_i w_i$$

where $b_i = b(y_i)$ and w_i is the integration weight at i .

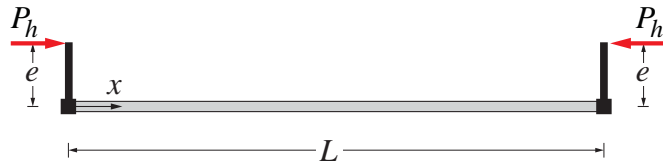
If required, determine the section stiffness \mathbf{k}_s from

$$\mathbf{k}_s = \sum_{i=1}^{nIP} \begin{bmatrix} 1 & -y_i \\ -y_i & y_i^2 \end{bmatrix} E_i b_i w_i$$

Example 5.2 shows the numerical effort for the state determination of a rectangular section under given section deformations \mathbf{e} with 4 integration points.

5.7.4 Second Section Analysis Problem

The second section analysis problem consists of the determination of the section deformations under given section forces \mathbf{s} . Fig. 5.12 shows a beam-column of nonlinear material under an axial load P_h with eccentricity e . Because the axial force and the bending moment distribution in the member is uniform, every section is subjected to an axial compression $N(x) = -P_h$ with eccentricity e , so that the bending moment $M(x) = P_h e$ is also constant. *The internal section forces \mathbf{s} in equilibrium with the applied loads are, therefore, given.*

Fig. 5.12: Beam-column under axial load P with constant eccentricity e

For this type of problem the solution of the nonlinear equation (5.34) is required. We rewrite (5.34) with the unbalanced section force vector \mathbf{s}_u

$$\mathbf{s}_u(\mathbf{e}) = \mathbf{s} - \mathbf{s}_r(\mathbf{e}) = 0 \quad (5.35)$$

We need to determine the section deformations \mathbf{e} that result in resisting section forces \mathbf{s}_r in equilibrium with the applied section forces \mathbf{s} .

The solution of the nonlinear section equilibrium problem in (5.35) is identical with the nonlinear structural equilibrium problem in Chapter 3

$$\mathbf{P}_u(\mathbf{U}) = \mathbf{P}_f - \mathbf{P}_r(\mathbf{U}_f) = 0$$

where the section forces \mathbf{s} take the place of the nodal forces \mathbf{P} and the section deformations \mathbf{e} take the place of the free global dof displacements \mathbf{U}_f . Consequently, we can make use of the nonlinear solution methods of Chapter 3. Here we restate the basic Newton-Raphson (NR) algorithm for a single load step with the variables of this problem.

Given the section forces \mathbf{s} , i.e. the axial force N and bending moment M the equilibrium between applied and resisting section forces is given by (5.35). The NR algorithm for the solution of the system of two nonlinear equations is

- 1) Given the nonlinear equation $\mathbf{s}_u(\mathbf{e}) = 0$ and a guess for the solution \mathbf{e}_0 .
- 2) For $i = 0 \dots n$ determine the function value $\mathbf{s}_u(\mathbf{e}_i)$ and the derivative $\mathbf{k}_s(\mathbf{e}_i)$.
- 3) Determine the correction to the previous solution estimate $\Delta\mathbf{e}_i = \mathbf{k}_s(\mathbf{e}_i) \setminus \mathbf{s}_u(\mathbf{e}_i)$.
- 4) Update the solution estimate $\mathbf{e}_{i+1} = \mathbf{e}_i + \Delta\mathbf{e}_i$.

Return to step 2 until the error norm is smaller than a specified tolerance.

On convergence determine the section forces for the final deformations.

The earlier discussion about nonlinear solution strategies with incrementation, iteration and load factor control can be readily applied to this problem. We show the solution process with a numerical example.

Example 5.3 Section Deformations \mathbf{e} for Given Section Forces \mathbf{s}

Fig. 5.13 shows a rectangular section with a bilinear material. The section has depth $d = 18$ and width $b = 12$. The material properties are: $f_y = 40$, $E = 20,000$, and $E_h = 5,000$. The yield strain ε_y is, therefore, equal to $2 \cdot 10^{-3}$.

The rectangular section is subjected to a normal force $N = 5000$ and a moment $M = 40,000$. It is required to determine the section deformations \mathbf{e} under these section forces \mathbf{s} .

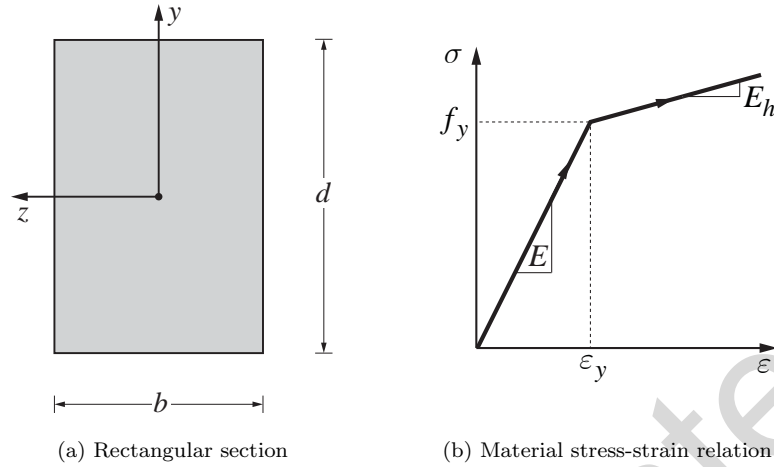


Fig. 5.13: Rectangular section with bilinear stress-strain relation

We plan to use the trapezoidal rule for the numerical evaluation of the section response integrals according to (5.31) and (5.32). We select 4 integration points numbered from the section soffit, as Fig. 5.14 shows.

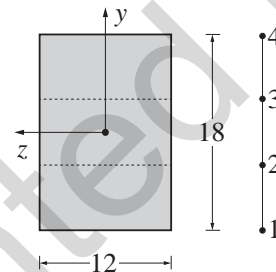


Fig. 5.14: Rectangular section with 4 integration points for trapezoidal rule

Denoting the general integration point with m the normal strain ε_m follows Bernoulli's assumption that plane sections remain plane after deformation. It is

$$\varepsilon_m = \varepsilon_a - y_m \kappa$$

We start the iteration process by assuming $\mathbf{e}_0 = \mathbf{0}$ and determining the unbalanced section forces \mathbf{s}_u and the tangent section stiffness \mathbf{k}_s . For the strain ε_m at each integration point we determine the stress σ_m and the tangent modulus E_m and then use (5.31) and (5.32) to determine the resisting section forces \mathbf{s}_r and the tangent section stiffness \mathbf{k}_s as follows:

$$\mathbf{s}_r = \begin{pmatrix} N \\ M \end{pmatrix} = \sum_{m=1}^4 \begin{pmatrix} 1 \\ -y_m \end{pmatrix} \sigma_m w_m b_m$$

$$\mathbf{k}_s = \sum_{m=1}^4 \begin{bmatrix} 1 & -y_m \\ -y_m & y_m^2 \end{bmatrix} E_m w_m b_m$$

For the numerical integration we organize the calculations in Table 5.5. For $e_0 = \mathbf{0}$ we obtain

IP	y_m	w_m	$w_m b_m$	$\varepsilon_m (10^{-3})$	σ_m	$E_m (10^3)$
1	-9	3	36	0	0	20
2	-3	6	72	0	0	20
3	3	6	72	0	0	20
4	9	3	36	0	0	20

Table 5.5: Strain, stress and tangent modulus at integration points for $e_0 = \mathbf{0}$

$$\mathbf{k}_s = \begin{bmatrix} 4.32 & 0 \\ 0 & 142.56 \end{bmatrix} 10^6 \quad \mathbf{s}_r = \begin{pmatrix} 0 \\ 0 \end{pmatrix} 10^3 \quad \rightarrow \quad \mathbf{s}_u = \mathbf{s} - \mathbf{s}_r = \begin{pmatrix} 5 \\ 40 \end{pmatrix} 10^3$$

We solve for the section deformation increment Δe_0

$$\mathbf{s}_u = \mathbf{k}_s \Delta e_0 \quad \rightarrow \quad \Delta e_0 = \begin{pmatrix} 1.157 \\ 0.281 \end{pmatrix} 10^{-3}$$

and update the section deformations according to

$$\mathbf{e}_1 = \mathbf{e}_0 + \Delta \mathbf{e}_0 = \begin{pmatrix} 1.157 \\ 0.281 \end{pmatrix} 10^{-3}$$

The section deformations \mathbf{e}_1 correspond to the result of a linear solution of (5.35). Stated differently \mathbf{e}_1 is the result at end of the load incrementation step. We now embark on the iterative correction of the equilibrium equations while keeping the applied section forces constant.

For the section state determination for \mathbf{e}_1 we organize the calculations in Table 5.6.

IP	y_m	w_m	$w_m b_m$	$\varepsilon_m (10^{-3})$	σ_m	$E_m (10^3)$
1	-9	3	36	3.683	48.41	5
2	-3	6	72	1.999	39.98	20
3	3	6	72	0.316	6.31	20
4	9	3	36	-1.368	-27.36	20

Table 5.6: Strain, stress and tangent modulus at integration points for e_1

With (5.31) and (5.32) we obtain the resisting section forces \mathbf{s}_r and the tangent section stiffness for \mathbf{e}_1 . It gives

$$\mathbf{k}_s = \begin{bmatrix} 3.78 & -4.86 \\ -4.86 & 98.82 \end{bmatrix} 10^6 \quad \mathbf{s}_r = \begin{pmatrix} 4.09 \\ 31.82 \end{pmatrix} 10^3 \quad \rightarrow \quad \mathbf{s}_u = \mathbf{s} - \mathbf{s}_r = \begin{pmatrix} 0.909 \\ 8.178 \end{pmatrix} 10^3$$

We solve for the section deformation increment Δe_1

$$\mathbf{s}_u = \mathbf{k}_s \Delta e_1 \quad \rightarrow \quad \Delta e_1 = \begin{pmatrix} 0.370 \\ 0.101 \end{pmatrix} 10^{-3}$$

and update the section deformations according to

$$\mathbf{e}_2 = \mathbf{e}_1 + \Delta \mathbf{e}_1 = \begin{pmatrix} 1.157 \\ 0.281 \end{pmatrix} 10^{-3} + \begin{pmatrix} 0.370 \\ 0.101 \end{pmatrix} 10^{-3} = \begin{pmatrix} 1.528 \\ 0.382 \end{pmatrix} 10^{-3}$$

For the section state determination for \mathbf{e}_2 we organize the calculations in Table 5.7.

IP	y_m	w_m	$w_m b_m$	$\varepsilon_m (10^{-3})$	σ_m	$E_m (10^3)$
1	-9	3	36	4.961	54.81	5
2	-3	6	72	2.672	43.36	5
3	3	6	72	0.383	7.66	20
4	9	3	36	-1.906	-38.13	20

Table 5.7: Strain, stress and tangent modulus at integration points for \mathbf{e}_2

With (5.31) and (5.32) we obtain the resisting section forces \mathbf{s}_r and the tangent section stiffness for \mathbf{e}_2 . It gives

$$\mathbf{k}_s = \begin{bmatrix} 2.7 & -8.1 \\ -8.1 & 89.1 \end{bmatrix} 10^6 \quad \mathbf{s}_r = \begin{pmatrix} 4.27 \\ 37.82 \end{pmatrix} 10^3 \quad \rightarrow \quad \mathbf{s}_u = \mathbf{s} - \mathbf{s}_r = \begin{pmatrix} 0.726 \\ 2.178 \end{pmatrix} 10^3$$

We solve for the section deformation increment $\Delta\mathbf{e}_2$

$$\mathbf{s}_u = \mathbf{k}_s \Delta\mathbf{e}_2 \quad \rightarrow \quad \Delta\mathbf{e}_2 = \begin{pmatrix} 0.471 \\ 0.067 \end{pmatrix} 10^{-3}$$

and update the section deformations according to

$$\mathbf{e}_3 = \mathbf{e}_2 + \Delta\mathbf{e}_2 = \begin{pmatrix} 1.528 \\ 0.382 \end{pmatrix} 10^{-3} + \begin{pmatrix} 0.471 \\ 0.067 \end{pmatrix} 10^{-3} = \begin{pmatrix} 1.998 \\ 0.449 \end{pmatrix} 10^{-3}$$

For the section state determination for \mathbf{e}_3 we organize the calculations in Table 5.8.

IP	y_m	w_m	$w_m b_m$	$\varepsilon_m (10^{-3})$	σ_m	$E_m (10^3)$
1	-9	3	36	6.037	60.19	5
2	-3	6	72	3.344	46.72	5
3	3	6	72	0.652	13.04	20
4	9	3	36	-2.041	-40.20	5

Table 5.8: Strain, stress and tangent modulus at integration points for \mathbf{e}_3

With (5.31) and (5.32) we obtain the resisting section forces \mathbf{s}_r and the tangent section stiffness for \mathbf{e}_3 . It gives

$$\mathbf{k}_s = \begin{bmatrix} 2.16 & -3.24 \\ -3.24 & 45.36 \end{bmatrix} 10^6 \quad \mathbf{s}_r = \begin{pmatrix} 5.02 \\ 39.8 \end{pmatrix} 10^3 \quad \rightarrow \quad \mathbf{s}_u = \mathbf{s} - \mathbf{s}_r = \begin{pmatrix} -0.022 \\ 0.198 \end{pmatrix} 10^3$$

We solve for the section deformation increment $\Delta\mathbf{e}_3$

$$\mathbf{s}_u = \mathbf{k}_s \Delta\mathbf{e}_3 \quad \rightarrow \quad \Delta\mathbf{e}_3 = \begin{pmatrix} -0.004 \\ 0.004 \end{pmatrix} 10^{-3}$$

and update the section deformations according to

$$\boldsymbol{e}_4 = \boldsymbol{e}_3 + \Delta \boldsymbol{e}_3 = \begin{pmatrix} 1.998 \\ 0.449 \end{pmatrix} 10^{-3} + \begin{pmatrix} -0.004 \\ 0.004 \end{pmatrix} 10^{-3} = \begin{pmatrix} 1.994 \\ 0.453 \end{pmatrix} 10^{-3}$$

For the section state determination for \boldsymbol{e}_4 we organize the calculations in Table 5.9.

IP	y_m	w_m	$w_m b_m$	$\varepsilon_m (10^{-3})$	σ_m	$E_m (10^3)$
1	-9	3	36	6.070	60.35	5
2	-3	6	72	3.353	46.76	5
3	3	6	72	0.636	12.71	20
4	9	3	36	-2.081	-40.41	5

Table 5.9: Strain, stress and tangent modulus at integration points for \boldsymbol{e}_4

With (5.31) and (5.32) we obtain the resisting section forces \boldsymbol{s}_r and the tangent section stiffness for \boldsymbol{e}_4 .

It gives

$$\mathbf{k}_s = \begin{bmatrix} 2.16 & -3.24 \\ -3.24 & 45.36 \end{bmatrix} 10^6 \quad \boldsymbol{s}_r = \begin{pmatrix} 5.00 \\ 40.0 \end{pmatrix} 10^3 \quad \rightarrow \quad \boldsymbol{s}_u = \boldsymbol{s} - \boldsymbol{s}_r = \begin{pmatrix} 0 \\ 0 \end{pmatrix} 10^3$$

Because of the bilinear stress-strain relation of the material we converged to the exact solution after a finite number of iterations! We were a bit unlucky that at the end of the second iteration with the section deformations at \boldsymbol{e}_3 that material at integration point #4 just exceeded its yield strength requiring an extra iteration to convergence.

The section deformations \boldsymbol{e} for the given section forces \boldsymbol{s} , therefore, are

$$\boldsymbol{e} = \begin{pmatrix} 1.994 \\ 0.453 \end{pmatrix} 10^{-3}$$

and the stresses at the four integration points are given in Table 5.9.

Example 5.4 Incremental Response of Rectangular Section

With the solution algorithms of Chapter 3 we can conduct a multi-step incremental nonlinear analysis for a given cross section under a given reference section force vector \boldsymbol{s}_{ref} . Fig. 5.15 and Fig. 5.16 shows such an example for a rectangular section with $d = 18$ and $b = 12$ consisting of a bilinear material with the following properties: $f_y = 40$, $E = 20,000$, $E_h = 400$ under incremental axial force N with constant eccentricity $e = -\frac{d}{2}$. The section is subdivided into 4 layers with midpoint integration.

During load incrementation the ratio of bending moment M to axial force N is, thus, maintained constant for the section, as Fig. 5.15(a) shows. The load increment is, however, adjusted with a load factor control strategy based on the current stiffness parameter. Fig. 5.15(b) shows that the ratio of the axial strain at the neutral axis ε_a to the curvature κ is piecewise linear with sudden changes of slope on account of the shift in the neutral axis when an integration point experiences yielding. Fig. 5.16(a) shows the relation between axial strain at the neutral axis ε_a and axial force N , and Fig. 5.16(b) the relation between curvature κ and bending moment M . For bilinear material response the abrupt change in stiffness is rather evident. There are three post-yield linear branches corresponding to the 3 integration points experiencing yielding one after the other. The piecewise linear post-yield response in Fig. 5.16(a) and Fig. 5.16(b) relates to the piecewise linear relation of the section deformations in Fig. 5.15(b).

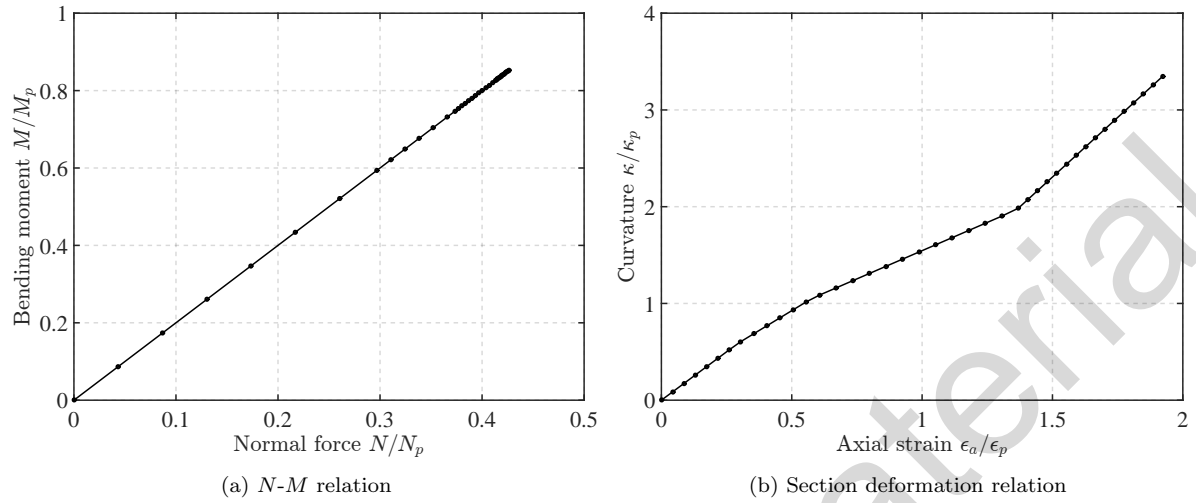


Fig. 5.15: Internal force and section deformation path for rectangular section

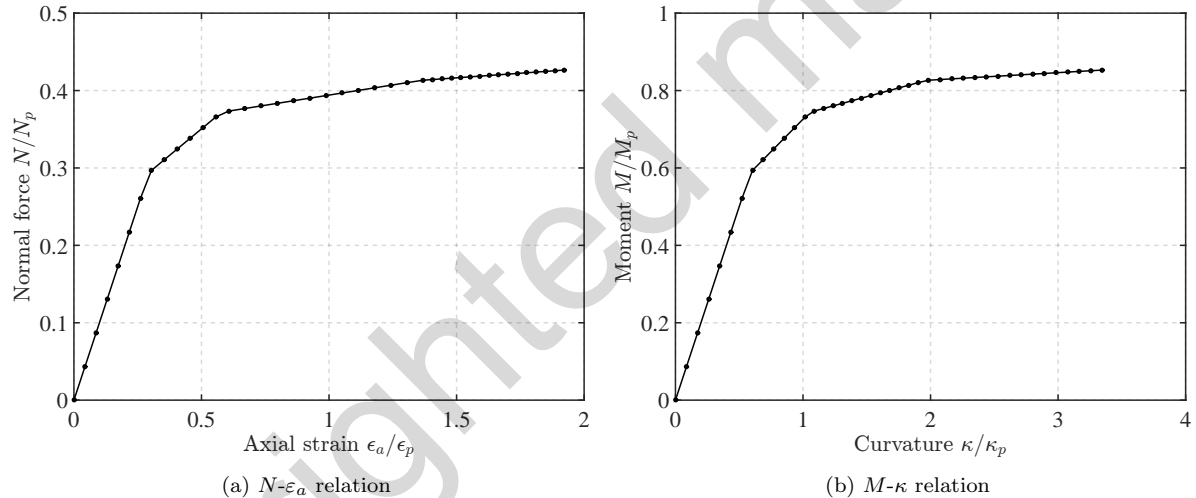


Fig. 5.16: Internal force section deformation relations for rectangular section

5.7.5 Third Section Analysis Problem: Moment-Curvature Analysis

The third section analysis problem is a very important stand-alone problem, because it establishes the moment-curvature diagram of a section under a given axial force that is kept constant while increasing the curvature. It is also interesting for another reason: it is the first problem in this course of mixed type: a force N and a deformation κ is given, while the unknowns of the problem are the deformation ε_a and the bending moment M . The same type of problem for a structural model involves the simultaneous application of forces at the free dofs and displacements at the restrained dofs. Examples for this problem are the imposed support displacements for multi-support earthquake excitation and the imposed displacement history for testing structural members in the laboratory for hybrid simulation of specimen-computer model assemblies.

For the formulation of the solution algorithm for moment-curvature analysis we return to the section equilibrium equations in (5.34) and write these explicitly in terms of the applied section resultant forces

N and M and the resisting section resultants N_r and M_r , which are functions of the axial strain at the reference axis ε_a and the section curvature κ

$$N - N_r(\varepsilon_a, \kappa) = 0 \quad (5.36a)$$

$$M - M_r(\varepsilon_a, \kappa) = 0 \quad (5.36b)$$

With N and κ given, we use the first equation to solve for ε_a and then substitute this value along with the given κ into the second equation to determine the resisting moment M_r that corresponds to the given curvature κ under the given axial force N .

5.7.6 Moment-Curvature Analysis

Expanding the resisting axial force N_r in (5.36a) to a Taylor series and truncating higher than linear terms gives

$$N - \left[N_r(\varepsilon_{a0}, \kappa_0) + \frac{\partial N}{\partial \varepsilon_a} \Delta \varepsilon_a + \frac{\partial N}{\partial \kappa} \Delta \kappa \right] = 0$$

where subscript 0 denotes the initial guess for the solution.

With the given axial force N and curvature increment $\Delta \kappa$, we solve for $\Delta \varepsilon_a$

$$\Delta \varepsilon_a = \left(\frac{\partial N}{\partial \varepsilon_a} \right)^{-1} \left(N_u - \frac{\partial N}{\partial \kappa} \Delta \kappa \right) \quad \text{with} \quad N_u = N - N_r(\varepsilon_{a0}, \kappa_0)$$

For the numerical solution we distinguish the incrementation phase, which consists of the application of the curvature increment, from the equilibrium iterations under constant axial force and curvature. We assume that the axial force is applied in an initial step under zero curvature.

The algorithm for multi-step moment-curvature analysis is as follows (compare with the NR multi-step algorithm on 75):

Given the section geometry and the material properties;
given the axial force N , the curvature increment $\Delta \kappa$, and the number of load steps m .

Incrementation for $k = 1 \dots m$

- 1) Initial guess $\mathbf{e}_0^{(k)} = \mathbf{e}^{(k-1)}$ the solution at $k-1$ with $\mathbf{e}^{(0)} = \mathbf{0}$
- 2) Determine $\mathbf{s}_r^{(k)} = \mathbf{s}_r(\mathbf{e}_0^{(k)})$ and $\mathbf{k}_s^{(k)} = \mathbf{k}_s(\mathbf{e}_0^{(k)})$
- 3) Determine $N_u^{(k)} = N - N_r^{(k)}$ and $\Delta \varepsilon_a^{(k)} = \left(\frac{\partial N}{\partial \varepsilon_a} \right)^{-1} \left(N_u^{(k)} - \frac{\partial N}{\partial \kappa} \Delta \kappa \right)$
where $\frac{\partial N}{\partial \varepsilon_a} = \mathbf{k}_{s,11}^{(k)}$ and $\frac{\partial N}{\partial \kappa} = \mathbf{k}_{s,12}^{(k)}$
- 4) Update solution $\mathbf{e}_1^{(k)} = \mathbf{e}_0^{(k)} + \begin{pmatrix} \Delta \varepsilon_a^{(k)} \\ \Delta \kappa \end{pmatrix}$

Iteration for $i = 1 \dots n$ and constant k (drop superscript)

- 1) Determine $s_r(\mathbf{e}_i)$ and $\mathbf{k}_s(\mathbf{e}_i)$
- 2) Determine $N_{ui} = N - N_{ri}$ and $\Delta\varepsilon_{a_i} = \left(\frac{\partial N_i}{\partial \varepsilon_a}\right)^{-1}(N_{ui})$ where $\frac{\partial N_i}{\partial \varepsilon_a} = \mathbf{k}_{si,11}$
- 3) Update solution $\mathbf{e}_{i+1} = \mathbf{e}_i + \begin{pmatrix} \Delta\varepsilon_{a_i} \\ 0 \end{pmatrix}$
Back to iteration step 1 until the error norm satisfies specified tolerance

On convergence we update the final state thus determining the final resisting axial force N_r and corresponding bending moment M_r . We then proceed to the next curvature increment.

Example 5.5 Section Moment For Given Curvature κ and Normal Force N

We use the rectangular section with the bilinear stress-strain relation in Fig. 5.13 to demonstrate the iterative solution process for determining the moment M for a given curvature under constant axial force N . In the example we assume that the curvature is imposed together with the axial force, so that the initial section state is the undeformed state $\mathbf{e} = \mathbf{0}$. The imposed curvature is $\kappa = 0.4 \cdot 10^{-3}$ and the applied axial force is $N = 5000$.

The determination of the resisting forces and of the tangent stiffness for the rectangular section under $\mathbf{e} = \mathbf{0}$ is given in Table 5.5. We obtain as before

$$\mathbf{k}_s = \begin{bmatrix} 4.32 & 0 \\ 0 & 142.56 \end{bmatrix} 10^6 \quad s_r = \begin{pmatrix} 0 \\ 0 \end{pmatrix}$$

We determine the unbalanced normal force N_u with

$$N_u = N - N_r = 5000 - 0 = 5000$$

The corresponding increment of the axial strain $\Delta\varepsilon_a$ is

$$\Delta\varepsilon_a = \left(\frac{\partial N}{\partial \varepsilon_a}\right)^{-1} \left(N_u - \frac{\partial N}{\partial \kappa} \Delta\kappa\right) = \frac{1}{4.32 \cdot 10^6} (5000 - (0)0.4 \cdot 10^{-3}) = 1.157 \cdot 10^{-3}$$

So that the section deformations \mathbf{e}_1 upon application of the curvature increment $\Delta\kappa = \kappa$ and the normal force N are

$$\mathbf{e}_1 = \begin{pmatrix} 0 \\ 0 \end{pmatrix} + \begin{pmatrix} \Delta\varepsilon_a \\ \Delta\kappa \end{pmatrix} = \begin{pmatrix} 1.157 \\ 0.400 \end{pmatrix} 10^{-3}$$

For the section state determination for \mathbf{e}_1 we organize the calculations in Table 5.10.

IP	y_m	w_m	$w_m b_m$	$\varepsilon_m (10^{-3})$	σ_m	$E_m (10^3)$
1	-9	3	36	4.757	53.79	5
2	-3	6	72	2.357	41.79	5
3	3	6	72	-0.043	-0.85	20
4	9	3	36	-2.443	-42.21	5

Table 5.10: Strain, stress and tangent modulus at integration points for \mathbf{e}_1

With (5.31) and (5.32) we obtain the resisting section forces \mathbf{s}_r and the tangent section stiffness for \mathbf{e}_1 . It gives

$$\mathbf{k}_s = \begin{bmatrix} 2.16 & -3.24 \\ -3.24 & 45.36 \end{bmatrix} 10^6 \quad \mathbf{s}_r = \begin{pmatrix} 3.36 \\ 40.31 \end{pmatrix} 10^3 \quad \rightarrow \quad N_u = 5000 - 3364 = 1636$$

We solve for the axial strain increment $\Delta\varepsilon_a$

$$\Delta\varepsilon_a = \left(\frac{\partial N}{\partial \varepsilon_a} \right)^{-1} (N_u) = \frac{1626}{2.16 \cdot 10^6} = 0.757 \cdot 10^{-3}$$

and update the section deformations to \mathbf{e}_2

$$\mathbf{e}_2 = \begin{pmatrix} 1.157 \\ 0.400 \end{pmatrix} 10^{-3} + \begin{pmatrix} 0.757 \\ 0 \end{pmatrix} 10^{-3} = \begin{pmatrix} 1.915 \\ 0.400 \end{pmatrix} 10^{-3}$$

For the section state determination for \mathbf{e}_2 we organize the calculations in Table 5.11.

IP	y_m	w_m	$w_m b_m$	$\varepsilon_m (10^{-3})$	σ_m	$E_m (10^3)$
1	-9	3	36	5.515	57.57	5
2	-3	6	72	3.115	45.57	5
3	3	6	72	0.715	14.30	20
4	9	3	36	-1.685	-33.70	20

Table 5.11: Strain, stress and tangent modulus at integration points for \mathbf{e}_2

With (5.31) and (5.32) we obtain the resisting section forces \mathbf{s}_r and the tangent section stiffness for \mathbf{e}_2 . It gives

$$\mathbf{k}_s = \begin{bmatrix} 2.7 & -8.1 \\ -8.1 & 89.1 \end{bmatrix} 10^6 \quad \mathbf{s}_r = \begin{pmatrix} 5.17 \\ 36.33 \end{pmatrix} 10^3 \quad \rightarrow \quad N_u = 5000 - 5170 = -170$$

We solve for the axial strain increment $\Delta\varepsilon_a$

$$\Delta\varepsilon_a = \left(\frac{\partial N}{\partial \varepsilon_a} \right)^{-1} (N_u) = \frac{(-170)}{2.7 \cdot 10^6} = -0.063 \cdot 10^{-3}$$

and update the section deformations to \mathbf{e}_3

$$\mathbf{e}_3 = \begin{pmatrix} 1.915 \\ 0.400 \end{pmatrix} 10^{-3} + \begin{pmatrix} -0.063 \\ 0 \end{pmatrix} 10^{-3} = \begin{pmatrix} 1.852 \\ 0.400 \end{pmatrix} 10^{-3}$$

For the section state determination for \mathbf{e}_3 we organize the calculations in Table 5.12.

With (5.31) and (5.32) we obtain the resisting section forces \mathbf{s}_r and the tangent section stiffness for \mathbf{e}_3 . It gives

$$\mathbf{k}_s = \begin{bmatrix} 2.7 & -8.1 \\ -8.1 & 89.1 \end{bmatrix} 10^6 \quad \mathbf{s}_r = \begin{pmatrix} 5.00 \\ 36.84 \end{pmatrix} 10^3 \quad \rightarrow \quad N_u = 5000 - 5000 = 0$$

and the iterative solution process converged in a finite number of iterations to the exact solution of the problem. The bending moment M corresponding to the imposed curvature of $\kappa = 0.4 \cdot 10^{-3}$ under

IP	y_m	w_m	$w_m b_m$	$\varepsilon_m (10^{-3})$	σ_m	$E_m (10^3)$
1	-9	3	36	5.452	57.26	5
2	-3	6	72	3.052	45.26	5
3	3	6	72	0.652	13.04	20
4	9	3	36	-1.748	-34.96	20

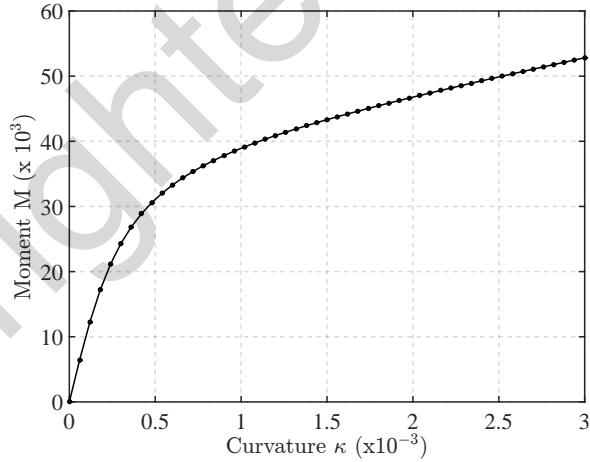
Table 5.12: Strain, stress and tangent modulus at integration points for e_3

an axial force N of 5000 is, therefore, 36,840. The axial strain at the centroid of the cross section is $\varepsilon_a = 1.852 \cdot 10^{-3}$.

Example 5.6 Moment-Curvature Relation of Rectangular Section

By programming the iterative solution process we are able to conduct a multi-step incremental *moment-curvature analysis* under constant normal force N . For the analysis the curvature increment $\Delta\kappa$ and the number of load steps are required, as is information about convergence tolerance and the number of maximum iterations per load step.

Fig. 5.17 shows such an example for the moment-curvature relation of a rectangular section with $d = 18$ and $b = 12$ consisting of a GMP nonlinear material with the properties $f_y = 40$, $E = 20,000$, $E_h = 1000$ and $r = 2$ under constant axial force $N = 0$. The incremental analysis involves 50 steps with curvature increment $\Delta\kappa = 0.06 \cdot 10^{-3}$.

Fig. 5.17: Moment-curvature analysis of rectangular section under constant axial force $N = 0$

5.8 Moment-Curvature Relation

In the following we derive the exact moment-curvature relation for a rectangular section with elastic, perfectly-plastic material and with bilinear elastic material and extend it to the case of an idealized wide-flange section. The Young modulus of the material is E , the yield strength is f_y and the corresponding yield strain is ε_y . The hardening modulus is E_h .

5.8.1 Elastic-Perfectly Plastic Material Response

Fig. 5.18 shows the strain and stress distribution for a rectangular section of depth d and width b at a curvature κ that exceeds the yield curvature κ_y of the section. Consequently, a portion of the section exceeds the yield strain ε_y and has a uniform stress equal to the yield strength f_y of the linear elastic, perfectly plastic material.

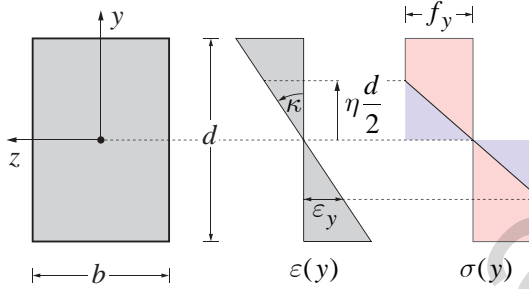


Fig. 5.18: Strain and stress distribution for rectangular section with linear elastic, perfectly plastic material

We determine the corresponding moment from the stress distribution considering the full rectangular block and then subtracting the stress triangle in the figure.

$$M = f_y \left(b \frac{d}{2} \right) \left(\frac{d}{2} \right) - f_y \left(\frac{1}{2} b \frac{\eta d}{2} \right) \left(\frac{\eta d}{3} \right) = f_y \frac{bd^2}{4} \left(1 - \frac{1}{3} \eta^2 \right) \quad (5.37)$$

which holds for $0 \leq \eta \leq 1$.

We note that the largest moment in (5.37) corresponds to $\eta = 0$. It is the section plastic moment M_p . It can be written in the form

$$M_p = f_y Z \quad \text{with} \quad Z = \frac{bd^2}{4}$$

where Z is the plastic section modulus of the section.

The plastic section modulus Z for other shapes is available in reference books. For wide flange shapes it is available in the AISC manual.

We express the variable η in terms of the curvature. Defining the yield curvature κ_y at the instant that the outermost fibers reach the yield strain ε_y of the material we get

$$\eta = \frac{\kappa_y}{\kappa} \quad \text{with} \quad \kappa_y = \frac{2\varepsilon_y}{d}$$

Substituting into (4.5b) we get

$$M = f_y \frac{bd^2}{4} \left[1 - \frac{1}{3} \left(\frac{\kappa_y}{\kappa} \right)^2 \right] \quad (5.38)$$

We observe that for $\eta = 1$, i.e. for $\kappa = \kappa_y$ we get from (5.38)

$$M = f_y \frac{bd^2}{4} \left(1 - \frac{1}{3}\right) = f_y \frac{bd^2}{6} = f_y S = M_y \quad (5.39)$$

S is the elastic section modulus and the yield moment M_y corresponds to κ_y . We also observe that the plastic moment capacity is attained only under infinitely large curvature, i.e. it is approached asymptotically. Noting from (5.39) that $M_y = \frac{2}{3}M_p$ we get for the entire M - κ response

$$\begin{aligned} \text{for } \kappa \leq \kappa_y \quad & \frac{M}{M_p} = \frac{2}{3} \frac{\kappa}{\kappa_y} \\ \text{for } \kappa > \kappa_y \quad & \frac{M}{M_p} = \left[1 - \frac{1}{3} \left(\frac{\kappa_y}{\kappa}\right)^2\right] \end{aligned} \quad (5.40)$$

Fig. 5.19 shows the moment-curvature relation of a rectangular section with linear elastic, perfectly plastic material according to (5.40). The ratio M_p to M_y is equal to the ratio of the plastic section modulus Z to the elastic section modulus S and is known as the shape factor of the section.

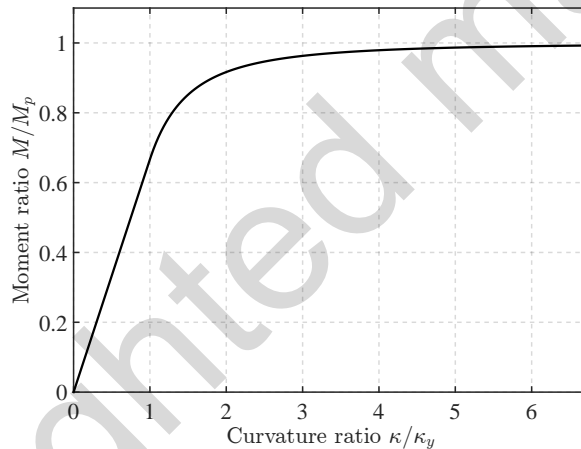


Fig. 5.19: Moment-curvature relation of rectangular section with linear elastic, perfectly plastic material

The shape factor of a rectangular section is thus 1.5. We observe that the shape factor relates to the extent of the transition zone from the linear elastic response to the fully plastic asymptote that the M - κ relation approaches as κ increases. The shape factor is smaller for wide flange sections and ranges from 1.10 to 1.25. This is important for the accuracy of a bilinear approximation of the moment-curvature relation.

Fig. 5.20 shows the shape factor effect on the transition from elastic to plastic response for a heavy wide flange section (W14x426) with a shape factor of 1.23 and for a rectangular section with shape factor of 1.5. We observe that we may be able to approximate the moment-curvature relation, so that we can use it later in the development of simple beam models instead of the significantly more expensive layer discretization of the section. To this end we establish the moment-curvature relation of a rectangular section with bilinear elastic material next.

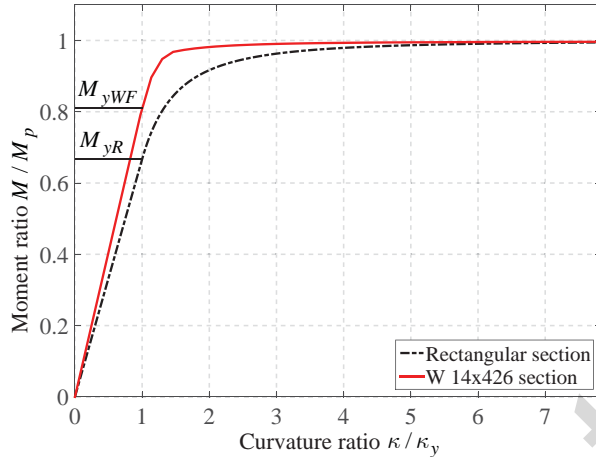


Fig. 5.20: Comparison of moment-curvature relation between rectangular and wide flange section

5.8.2 Bilinear Elastic Material Response

Fig. 5.21 shows the strain and stress distribution for a rectangular section of depth d and width b at a curvature κ that exceeds the yield curvature κ_y of the section. Because the material is now bilinear elastic, as in Fig. 5.1(a), the stress distribution is also bilinear. The additional stress in the yielding portion relative to the yield strength f_y of the material is depicted with a darker triangle in Fig. 5.21.

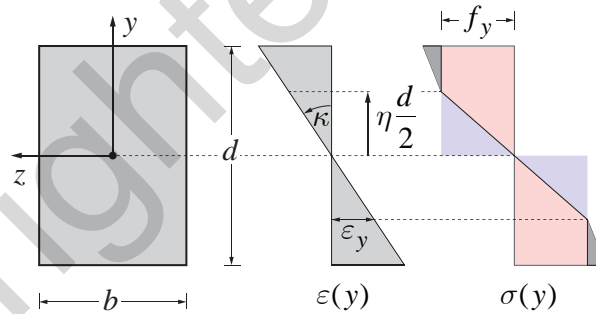


Fig. 5.21: Strain and stress distribution for rectangular section with bilinear elastic material

We modify (5.37) with the contribution of the darker stress triangle in Fig. 5.21 for the post-yield moment-curvature range

$$\text{for } \kappa \leq \kappa_y \quad \frac{M}{M_p} = \frac{2}{3} \frac{\kappa}{\kappa_y} \quad (5.41a)$$

$$\text{for } \kappa > \kappa_y \quad \frac{M}{M_p} = \left(1 - \frac{1}{3}\eta^2\right) + \frac{1}{3}\beta \frac{(1-\eta)^2}{\eta}(2+\eta) \quad (5.41b)$$

where β is the ratio of the hardening modulus E_h of the bilinear material in Fig. 5.1(a) to the initial modulus E , i.e.

$$\beta = \frac{E_h}{E}$$

We differentiate (5.41b) with respect to κ

$$\frac{dM}{d\kappa} = \frac{dM}{d\eta} \frac{d\eta}{d\kappa}$$

and use the following expressions for the derivatives

$$\frac{d\eta}{d\kappa} = -\frac{\kappa_y}{\kappa^2} \quad \text{and} \quad \frac{dM}{d\eta} = \frac{2}{3} M_p \left[(\beta - 1)\eta - \frac{\beta}{\eta^2} \right]$$

to get the moment derivative with respect to curvature

$$\frac{dM}{d\kappa} = \frac{2}{3} M_p \left[(\beta - 1)\eta - \frac{\beta}{\eta^2} \right] \left(-\frac{\kappa_y}{\kappa^2} \right)$$

With $M_p = 1.5M_y$ for a rectangular section and $\eta = \frac{\kappa_y}{\kappa}$ we get

$$\frac{dM}{d\kappa} = \frac{M_y}{\kappa_y} [(1 - \beta)\eta^3 + \beta] = EI [(1 - \beta)\eta^3 + \beta] \quad (5.42)$$

We conclude from (5.42) that with increasing curvature and yielding spreading into the rectangular section η decreases so that the contribution of the first term in the square brackets becomes much smaller than the hardening ratio β .

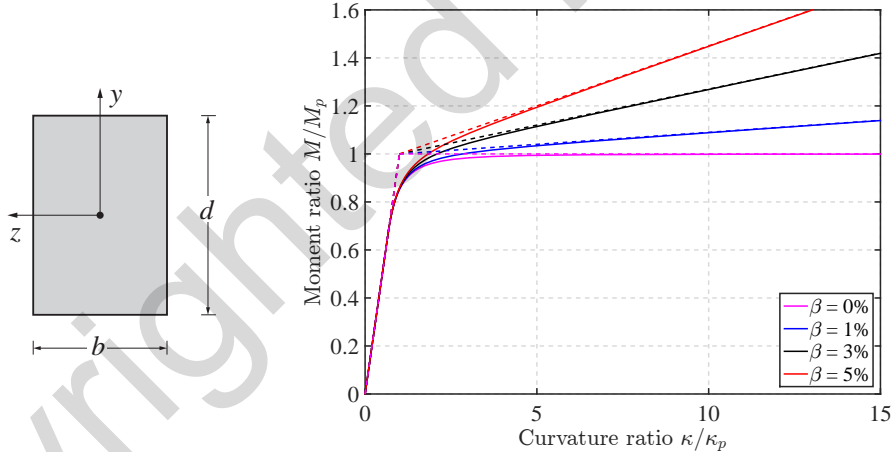


Fig. 5.22: Bilinear approximation of $M\text{-}\kappa$ relation of rectangular section for different material hardening ratios β

For example, when $\kappa = 6\kappa_y$ the expression in the square brackets becomes $0.0046(1 - \beta) + \beta$. For $\beta = 0.03$ the slope of the tangent to the moment-curvature relation at this curvature becomes equal to $0.0345EI$; when $\kappa = 10\kappa_y$ the expression in the square brackets becomes $0.001(1 - \beta) + \beta$ and the slope of the tangent to the $M\text{-}\kappa$ relation at this curvature for the same value of β becomes $0.031EI$. This means that for large curvature ductility values the ratio of the tangent stiffness of the moment-curvature relation of a rectangular section to the elastic stiffness EI is practically equal to the ratio β of the post-yield modulus E_h to the elastic modulus E of the linear elastic, linear hardening material.

Fig. 5.22 shows the accuracy of the approximation of the exact moment-curvature relation of a rectangular section with a bilinear relation with linear stiffness EI and post-yield stiffness βEI for different material hardening ratios β . The curvature κ_p corresponds to the plastic moment M_p , i.e.

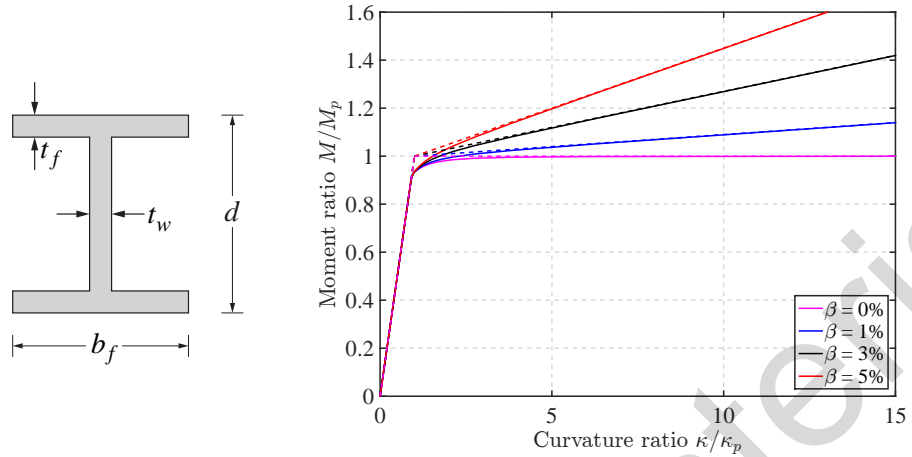


Fig. 5.23: Bilinear approximation of $M-\kappa$ relation of wide flange section W30x173 for different material hardening ratios β

$$\kappa_p = \frac{M_p}{EI}$$

Fig. 5.23 shows the accuracy of the approximation of the exact moment-curvature relation of a wide flange section W30x173 with a bilinear relation with linear stiffness EI and post-yield stiffness βEI for different material hardening ratios β .

It is worth noting that the approximation of the exact moment-curvature relation for a wide flange section neglects the effect of residual stresses which cause a gradual transition from the elastic range to the linear hardening range. In such case the GMP model in the form

$$M = M_p \left(b\xi + \frac{(1-b)\xi}{(1+|\xi|^r)^{\frac{1}{r}}} \right) \quad \text{with} \quad \xi = \frac{\kappa}{\kappa_y} \quad \kappa_y = \frac{M_p}{EI} \quad b = \frac{EI_h}{EI}$$

furnishes a good approximation of the gradual transition from the linear elastic range to the linear hardening or perfectly plastic range for the presence of residual stresses in wide flange sections. Fig. 5.24 shows that suitable exponent r -values for the GMP moment-curvature relation range from 3 to 4.

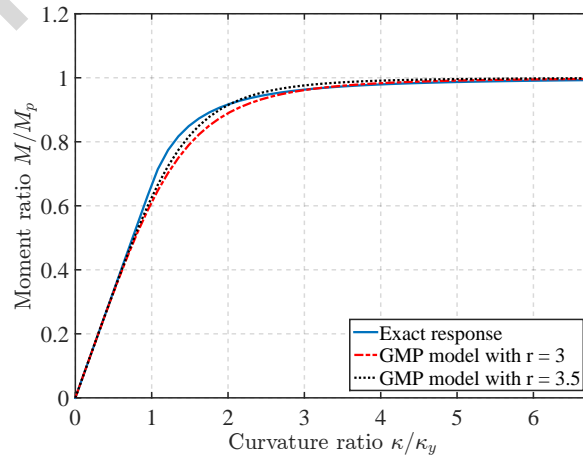


Fig. 5.24: Approximation of residual stress effect in wide flange section with linear elastic, perfectly-plastic material

5.8.3 Numerical Evaluation of Moment-Curvature Response

After establishing the exact moment-curvature relation without normal force for the rectangular and the wide-flange section with linear elastic, perfectly plastic and with bilinear material response we present in the following the numerical evaluation of the section response with the following integration methods: midpoint, trapezoidal and Simpson rule, Gauss-Legendre and Gauss-Lobatto quadrature.

Fig. 5.25-Fig. 5.29 present the numerical moment-curvature relation for a homogenous rectangular section with linear elastic, perfectly plastic material under zero normal force. The response is determined with 4, 5, 6, 8, 10 and 12 integration points, except for Simpson's rule requiring an odd number of integration points, so that 3, 5, 7, 9, 11 and 13 are selected instead.

For wide-flange homogeneous sections it is advisable to take advantage of the section geometry and optimize the distribution of integration points between flange and web. Fig. 5.30 compares the numerical moment curvature relation of a W14x426 wide flange section with linear elastic, perfectly plastic material against the exact result obtained by subtracting the moment-curvature relation of a rectangle of width $b_f - b_w$ and depth $d - 2t_f$ from the moment-curvature of a rectangle of width b_f and depth d , where b_f is the flange width, b_w the web thickness, t_f the flange thickness, and d the section depth (idealized section). It is clear that 8 integration points with two layers for the flange and 4 layers for the web provide excellent accuracy. The short transition from the linear elastic to the plastic range leads to the conclusion that a bilinear approximation with the linear elastic range extending to the plastic moment capacity M_p makes perfect sense.

From the comparison of the numerical results with the exact moment-curvature relation for the rectangular section with linear elastic, perfectly-plastic material in (5.40) we draw the following general conclusions:

- 1) The numerical solution approaches the exact result as the number of integration points increases; 8-10 integration points give satisfactory accuracy for practical purposes.
- 2) The midpoint and trapezoidal rule do not match the exact elastic stiffness, because they do not integrate exactly the quadratic polynomial arising in the flexural stiffness term of (5.30).
- 3) The midpoint rule with an even number of integration points matches the exact plastic moment M_p of the section; the same is true for Simpson's rule with 5, 9, 13, ... integration points.
- 4) Fig. 5.25(a)-Fig. 5.29(a) show that yield initiation is "detected" later than the exact solution for integration rules without a monitoring point at the top or bottom edge of the section. This is true for any number of integration points, but it is harder to detect in Fig. 5.25(b)-Fig. 5.29(b).
- 5) The higher order integration rules of Simpson, Gauss-Legendre and Gauss-Lobatto *do not give results of superior accuracy* than the lower order midpoint integration rule. The reason for this lies in the slope discontinuity of the linear elastic, perfectly plastic stress distribution.

We continue the numerical evaluation of the moment-curvature relation with the response of a homogeneous rectangular section with linear elastic, perfectly plastic material under different normal force levels. These are expressed in terms of the plastic axial capacity $N_p = f_y A$ of the section. The midpoint integration rule with 12 integration points provides excellent agreement with the exact solution in Fig. 5.31, which can be found in the following reference: W.F. Chen, T. Atsuta, "Theory of Beam-Columns,

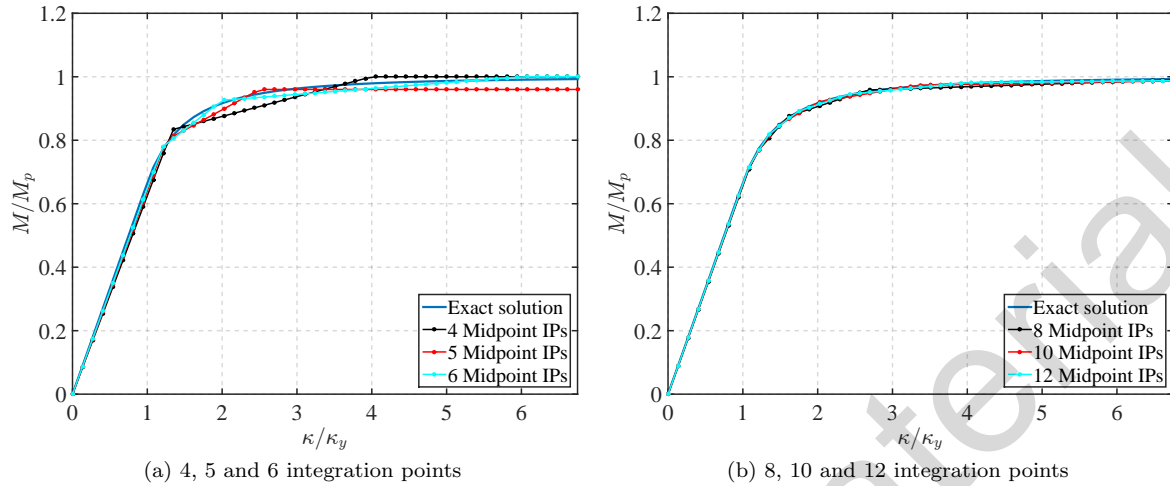


Fig. 5.25: Moment-curvature relation of rectangular section with midpoint rule

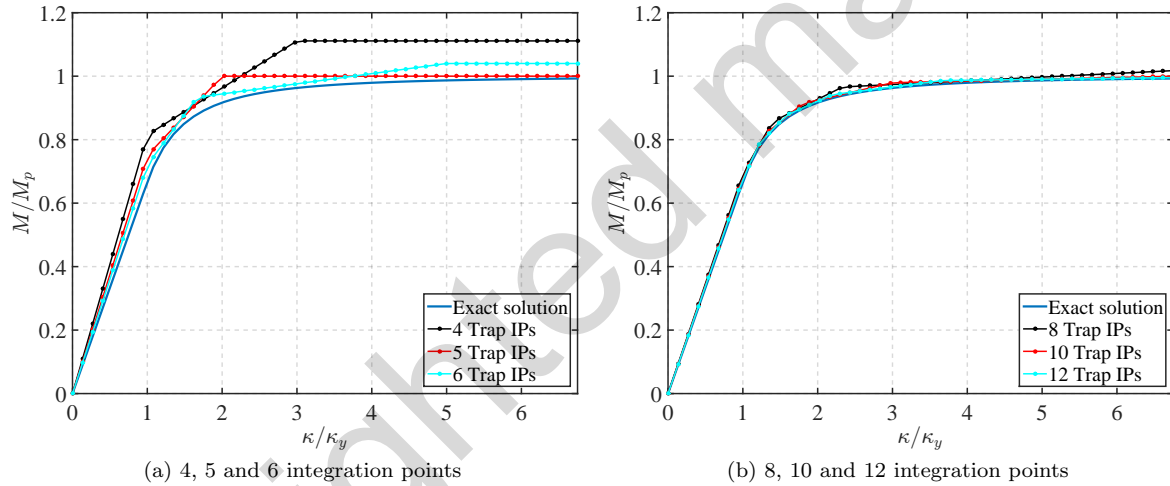


Fig. 5.26: Moment-curvature relation of rectangular section with trapezoidal rule

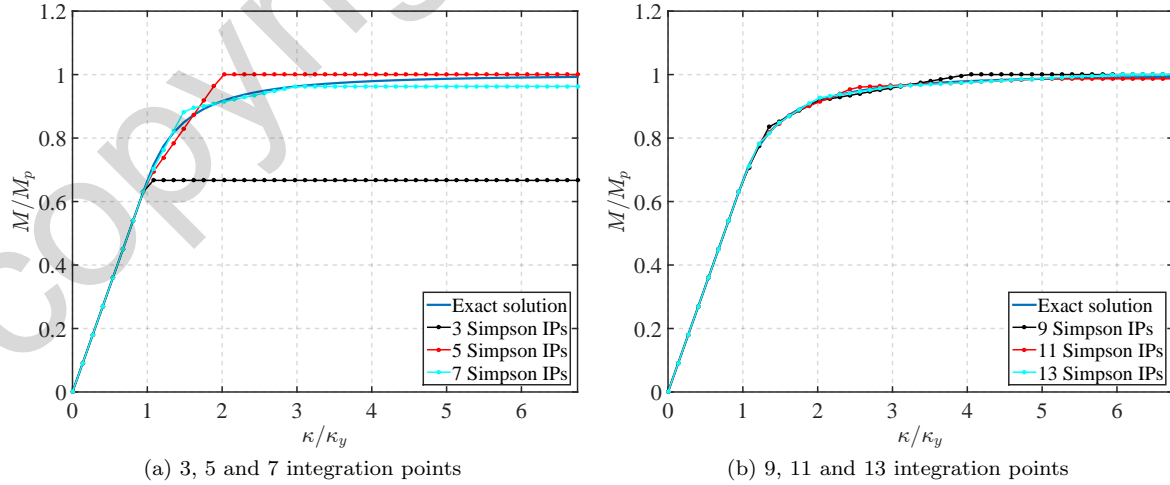


Fig. 5.27: Moment-curvature relation of rectangular section with Simpson rule

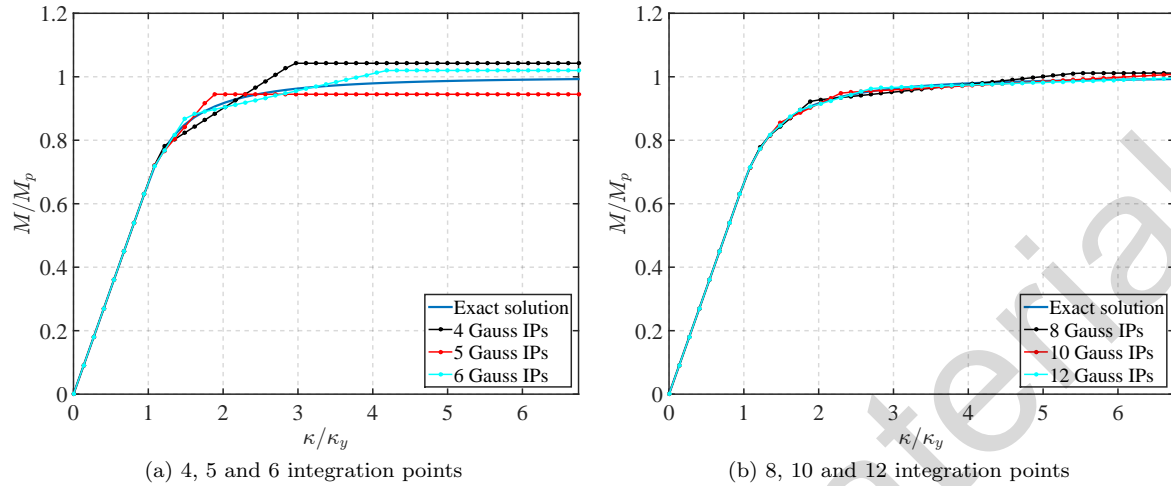


Fig. 5.28: Moment-curvature relation of rectangular section with Gauss-Legendre quadrature

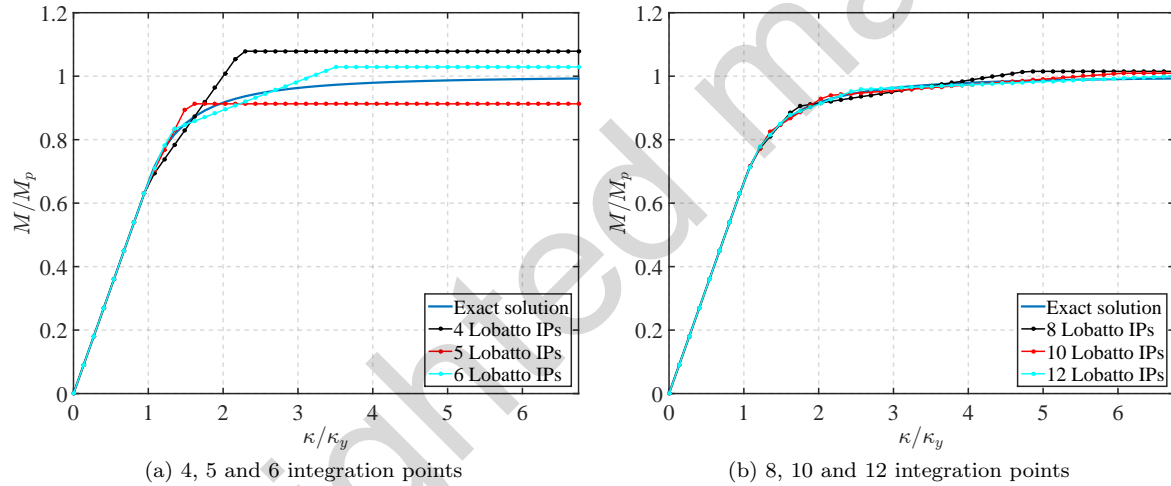


Fig. 5.29: Moment-curvature relation of rectangular section with Gauss-Lobatto quadrature

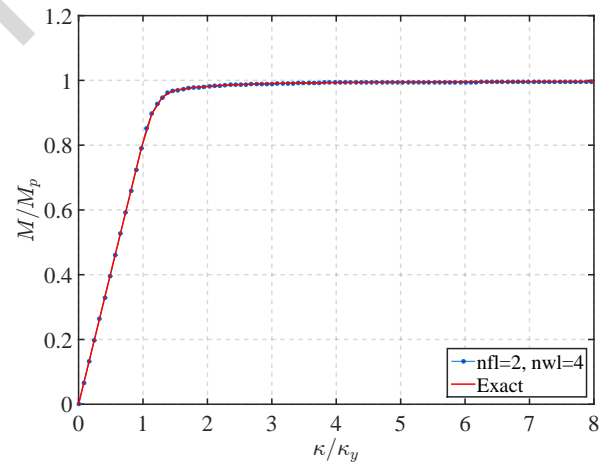


Fig. 5.30: Moment-curvature relation of W14x426 wide flange section with linear elastic, perfectly plastic material

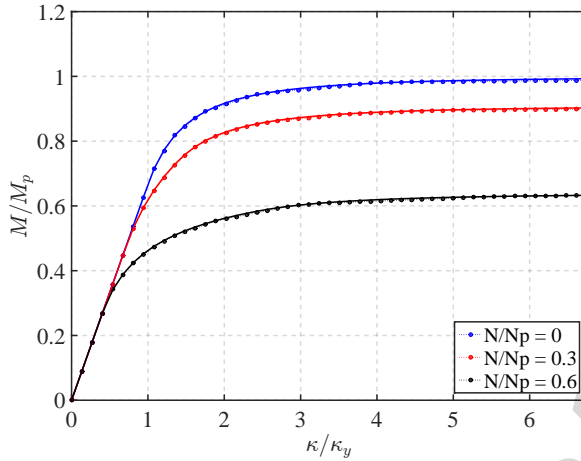
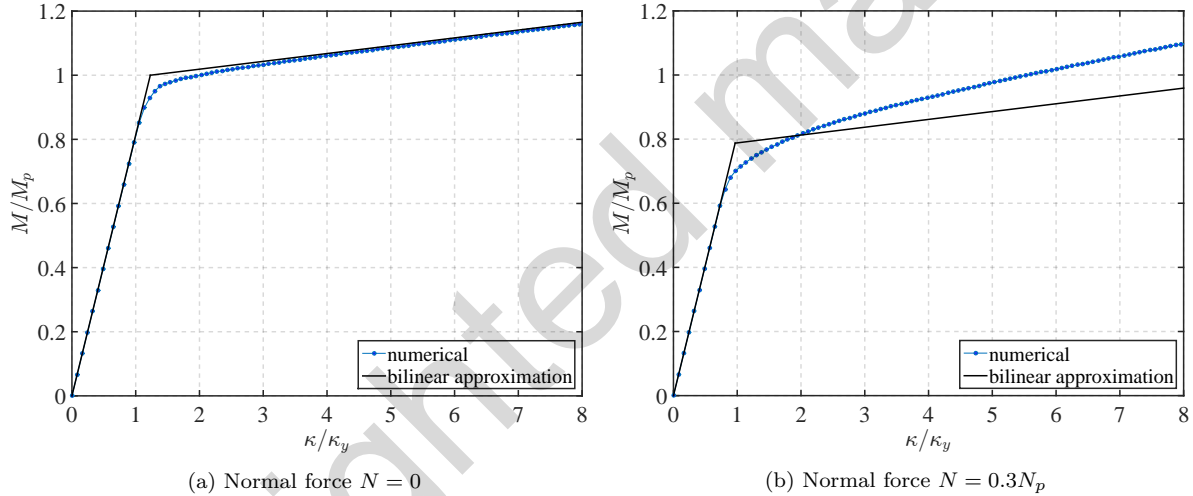


Fig. 5.31: Moment-curvature relation of rectangular section under different normal force levels

Fig. 5.32: Moment-curvature relation of W14x426 section with bilinear material with $E_h = 0.03E$

Vol. 1, In-plane behavior and design”, McGraw Hill, 1976. In Fig. 5.31 the numerical solution is depicted with markers, while the exact solution is depicted with a solid line of the same color.

We conclude this section with the numerical evaluation of the moment-curvature relation for a W14x426 section with bilinear material with strain hardening modulus $E_h = 0.03E$. Fig. 5.32(a) shows the moment-curvature relation under a normal force $N = 0$ and Fig. 5.32(b) shows the moment-curvature relation under a normal force $N = 0.3N_p$. The bilinear approximation with post-yield slope of βEI where $\beta = 0.03$ matches the moment-curvature relation under zero normal force rather well, as already discussed in Section 6.8.2. By contrast, the bilinear approximation of the moment-curvature relation requires a higher post-yield slope, as Fig. 5.32(b) clearly shows. The reason for this is the shift of the neutral axis with increasing curvature.

In summary:

- For the irregular stress distributions that we encounter in steel, reinforced concrete, and composite structures under monotonic, but particularly under cyclic loading conditions, the midpoint integration rule appears to be perfectly suitable and there is no need for higher order integration rules designed for optimizing the integral accuracy for smooth integrands.
- The midpoint integration rule gives rise to the name *layer section model* for y -integration of the section response, and to the name *fiber section model* for y and z integration.
- 8-10 layers give numerical results of sufficient accuracy for the uniaxial bending response of homogeneous rectangular sections with or without normal force. Under biaxial bending the corresponding number requires an 8x8 or 10x10 fiber subdivision of the cross section. Clearly, an optimum selection of the necessary number of fibers and their arrangement is well worth the effort for reducing the computational expense of fiber section models.

Some information about optimum selection of number of fibers for wide flange steel sections and rectangular reinforced concrete (RC) section is available in the following reference: S. Kostic and F.C. Filippou, Section Discretization of Fiber Beam-Column Elements for Cyclic Inelastic Response, Journal of Structural Engineering, ASCE, Vol. 138, No. 5, May 2012, pp. 592-601.

5.8.4 Moment-Curvature Relation of RC Section

Fig. 5.33 shows the numerical moment-curvature relation of a 15 inch square RC column with tension and compression reinforcing steel lumped in a single layer. The reinforcement area amounts to a reinforcing ratio of approximately 1.5% for each layer and the concrete cover is 1.5 inches. The concrete compressive strength f'_c is 5 ksi, the yield strength of the reinforcing steel is 60 ksi with Young modulus of 29,000 ksi. The confinement factor for the Mander, Priestley, Park concrete material model is assumed equal to 1.0 for the unconfined concrete in Fig. 5.33(a) and equal to 1.2 for the confined concrete in Fig. 5.33(b). The GMP model is used for the reinforcing steel with an exponent value r of 20.

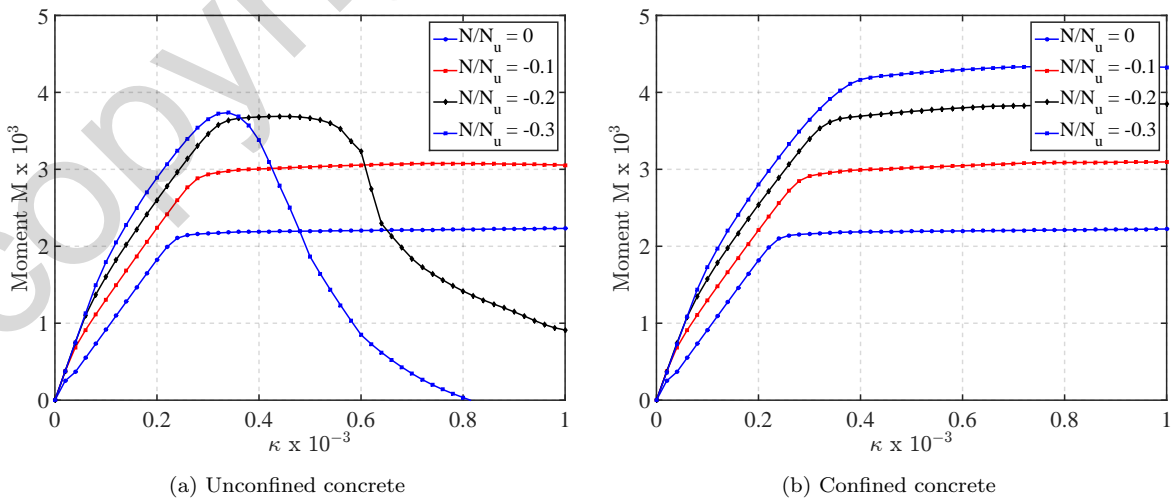


Fig. 5.33: Moment-curvature relation of RC column section with equal top and bottom reinforcement

The section is subjected to a compression force that varies from 0 to 30% of the ultimate axial strength of the column. The moment curvature relation of the RC section with unconfined concrete changes dramatically near the balanced point between 20% to 30% of the ultimate axial strength. Such change is not evident for the section with confined concrete which shows ductile response for the entire range of imposed compression force. The section response in Fig. 5.33 shows that the moment-curvature relation can be approximated with a bilinear curve that neglects the pre-cracking range, or, in general with a trilinear curve with a linear approximation of the pre-cracking response, cracked response, and post-yield response.

5.9 Limit N - M Surface for Perfect Plasticity

In this section we establish the limit surface of steel sections under normal force N and bending moment M for perfectly plastic material response. The limit surface consists of the combinations of N and M resulting under a fully plastic stress state of the section. It is also called the *plastic interaction surface*.

We limit the following discussion to uniaxial bending with normal force of bi-symmetric sections, but the derivation is completely analogous for biaxial bending with normal force of bi-symmetric and other types of cross sections. Similar considerations can be made for other internal forces such as shear and torsion, in which case a *failure criterion* under the biaxial or triaxial stress state of normal stress and shear stress is required. Chapter 3 of the book by M.R. Horne and L.J. Morris on "Plastic Design of Low-Rise Frames" has a concise presentation of the plastic limit surface for steel sections under biaxial bending and under flexure with shear.

5.9.1 Exact Solution for Rectangular Section

We start with the limit surface for a homogeneous rectangular section with depth d and width b with linear elastic-perfectly plastic material of yield strength f_y . Fig. 5.34 shows the stress state of the section under fully plastic conditions. Under the presence of a normal force N with the bending moment M the neutral axis shifts away from the section centroid, so that the difference between the tension stress block and the compression stress block makes up the normal force N . The ideal stress state of Fig. 5.34 is attainable for a linear elastic, perfectly plastic material only in the limit as the curvature of the cross section approaches infinity, as is evident for the case with no normal force in (5.40).

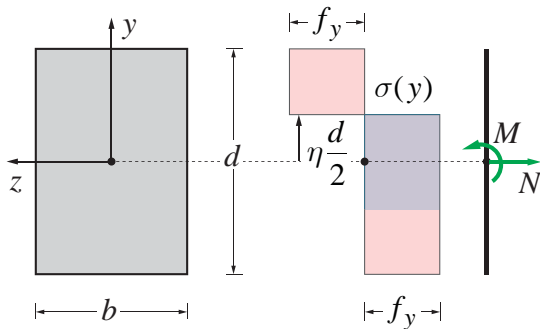


Fig. 5.34: Fully plastic stress state for rectangular cross section under axial force N and bending moment M

The fully plastic stress distribution in Fig. 5.34 can be decomposed into two parts that are symmetric about the centroid of the cross section. The first part consists of a stress block extending over a depth ηd in Fig. 5.34 and not contributing to the bending moment resistance, while the second part consists of a tensile stress block and a compressive stress block and does not contribute to the normal force. We can, therefore, sum up the stresses of the first block to establish the corresponding normal force N , and sum up the moment of the outer stress block pair to find the bending moment M . It gives

$$N = f_y [b(\eta d)] = \eta N_p$$

$$M = f_y 2 \left[b(1 - \eta) \frac{d}{2} \right] \frac{1}{2}(1 + \eta) \frac{d}{2} = f_y \frac{bd^2}{4}(1 - \eta^2) = M_p(1 - \eta^2)$$

where $N_p = Af_y$ and $M_p = Zf_y$ with $A = bd$ and $Z = \frac{bd^2}{4}$. Solving for the depth ratio η of the contiguous stress block in Fig. 5.34 and substituting the result into the equation for the bending moment M gives

$$\frac{M}{M_p} = \left[1 - \left(\frac{N}{N_p} \right)^2 \right]$$

Moving the internal forces to the same side of the equation sign and accounting for positive or negative moment gives

$$\left(\frac{N}{N_p} \right)^2 + \left| \frac{M}{M_p} \right| = 1 \quad (5.43)$$

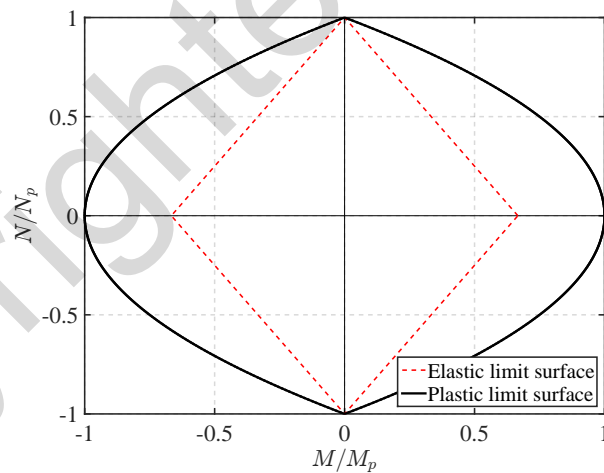


Fig. 5.35: Elastic and plastic limit surface of rectangular section

(5.43) represents the fully plastic limit surface of a rectangular section. With only two internal forces the fully plastic limit "surface" is a curve in the $x-y$ plane with $x = \frac{M}{M_p}$ and $y = \frac{N}{N_p}$, as Fig. 5.35 shows. The figure also shows the elastic limit surface, which is diamond shaped according to

$$\left| \frac{N}{N_y} \right| + \left| \frac{M}{M_y} \right| = 1$$

where $N_y = N_p$, while the yield moment $M_y = \frac{2}{3}M_p$ for a rectangular section.

5.9.2 Numerical Solution for Rectangular Section

The numerical determination of the plastic limit surface of a section can be conveniently performed by selecting nIP integration point locations according to the integration rule and then setting $1 \dots m$ of these integration points at the tensile strength f_y of the material, and the remaining $m + 1 \dots nIP$ integration points at the compressive strength $-f_y$. Varying m from 1 to nIP gives the pairs of normal force N and bending moment M values for one half of the limit surface. The reflection about the N -axis completes the task. The corresponding expressions for a rectangular section with width b are

$$\begin{aligned} N &= f_y b \sum_{i=1}^m w_i - f_y b \sum_{i=m+1}^{nIP} w_i \\ M &= f_y b \sum_{i=1}^m (-y_i w_i) - f_y b \sum_{i=m+1}^{nIP} (-y_i w_i) \end{aligned} \quad \text{with } \sum w_i = d \quad (5.44)$$

The pairs of normal force N and bending moment M values according to (5.44) establish discrete points in the x - y plane with $x = \frac{M}{M_p}$ and $y = \frac{N}{N_p}$. The resulting plastic limit surface is the polygon connecting these points, as Fig. 5.36(a) shows with the midpoint integration rule. With increasing number of integration points the polygon approaches the exact plastic limit "surface", as Fig. 5.36(b) shows with the midpoint integration rule. The number of points of the limit polygon *is equal to twice the number of integration points used in its determination*. We can confirm this with the 4 integration points used for Fig. 5.36(a) and with the 10 integration points for Fig. 5.36(b).

Fig. 5.36-Fig. 5.41 show the resulting polygonal plastic limit surfaces of a rectangular section with the midpoint integration rule, the trapezoidal rule, Simpson's rule, and the Gauss-Legendre and Gauss-Lobatto quadrature rules. These results lead to the following conclusions:

- 1) The midpoint integration rule is an excellent method, particularly, since it gives N - M pairs that lie exactly on the failure surface.
- 2) The trapezoidal rule also yields results of excellent accuracy with an even number of integration points; the numerical results lie slightly outside the exact failure surface and the line connecting the numerical points is tangent to the failure surface.
- 3) An even number of integration points is preferable for any integration method except for Simpson's rule, which requires an odd number.
- 4) The N - M pairs for the midpoint and trapezoidal rule are spaced more uniformly in the area of practical interest, i.e. for N/N_p values less than 0.4, so that the resulting polygonal approximation of the failure surface is more accurate than that for the Gauss-Legendre and Gauss-Lobatto quadrature rules.

5.9.3 Plastic Limit Surface for Wide Flange Section

The exact plastic limit surface of a wide flange section is established by subtracting the plastic limit surface of a rectangle of width $b_f - b_w$ and depth $d - 2t_f$ from the plastic limit surface of a rectangle of width b_f and depth d , where b_f is the flange width, b_w the web thickness, t_f the flange thickness, and

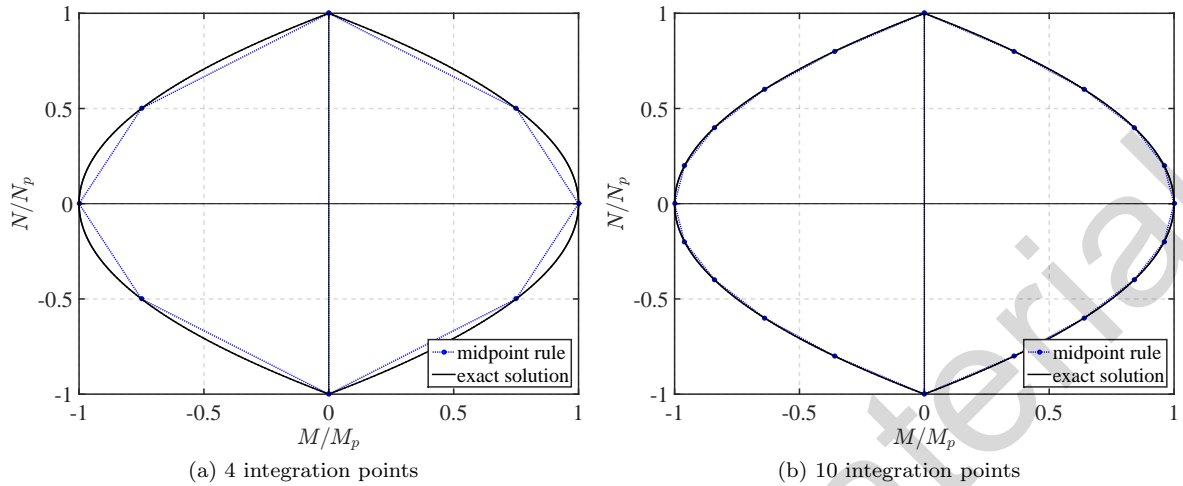


Fig. 5.36: Plastic limit surface of rectangular section with midpoint rule

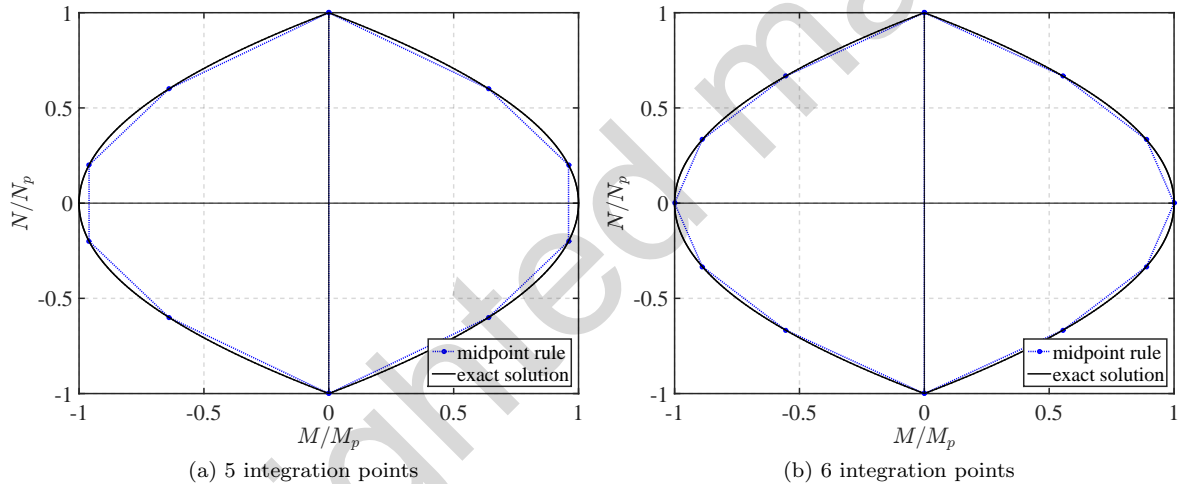


Fig. 5.37: Plastic limit surface of rectangular section with midpoint rule

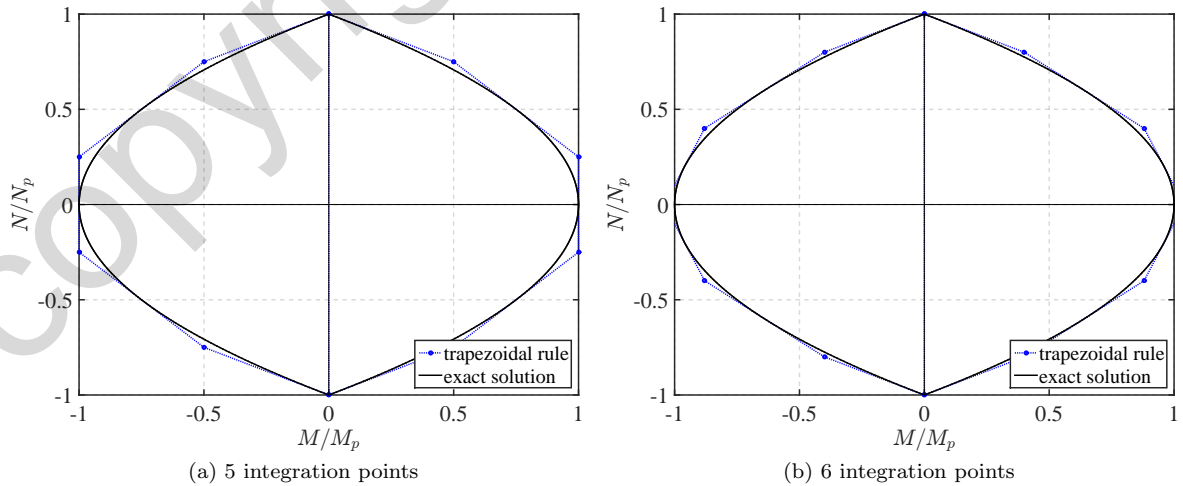


Fig. 5.38: Moment-curvature relation of rectangular section with trapezoidal rule

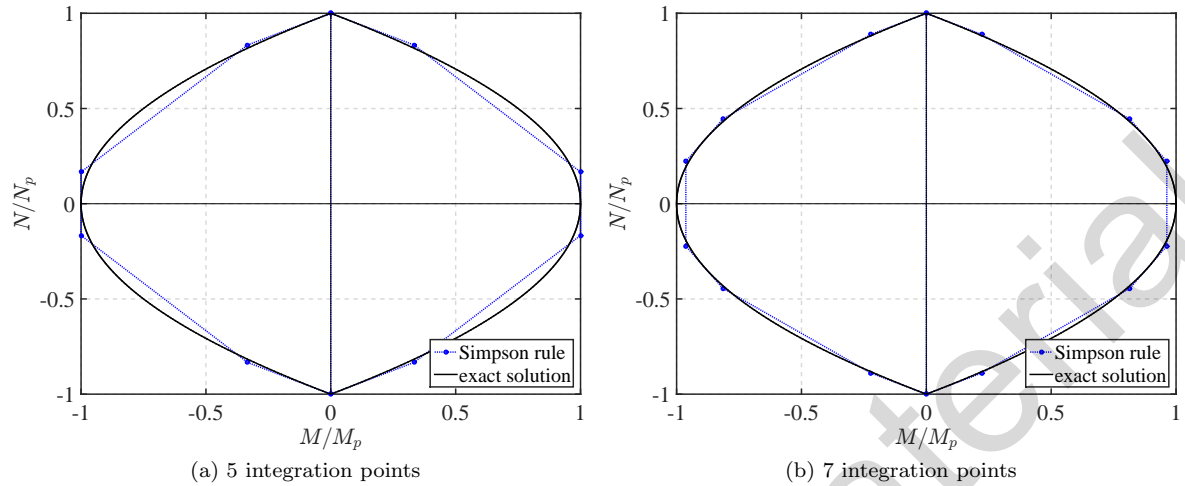


Fig. 5.39: Plastic limit surface of rectangular section with Simpson rule

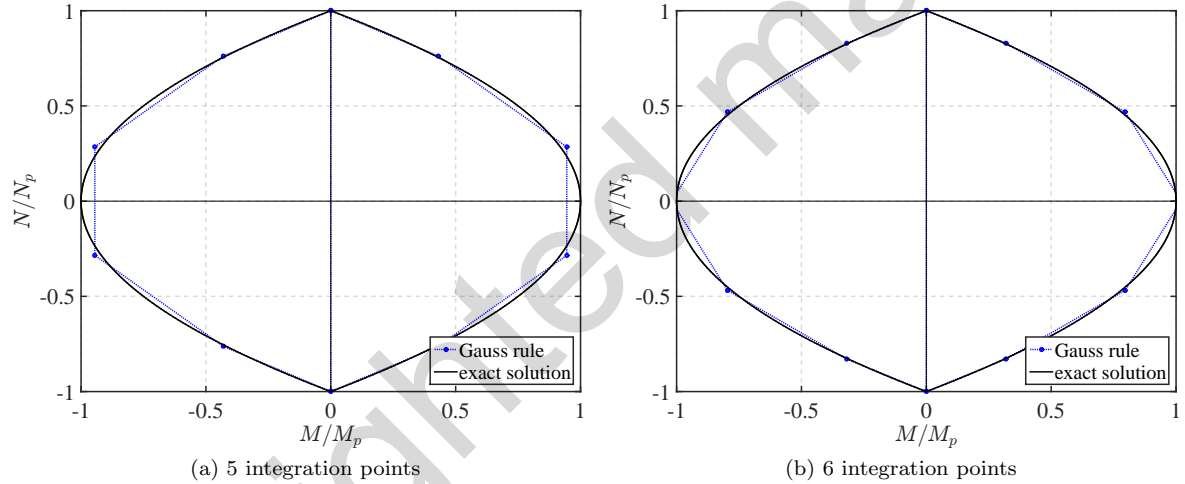


Fig. 5.40: Plastic limit surface of rectangular section with Gauss-Legendre quadrature

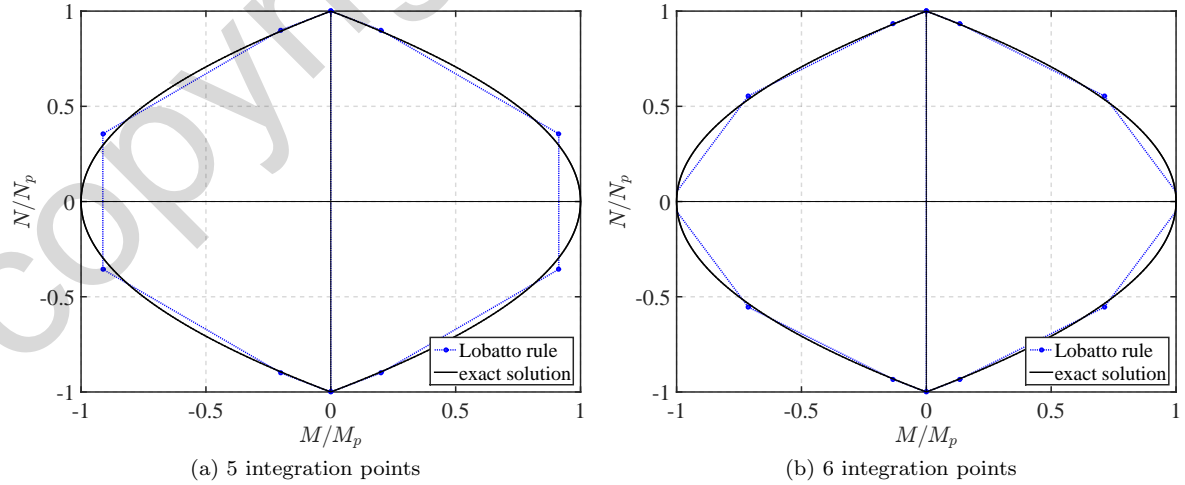


Fig. 5.41: Moment-curvature relation of rectangular section with Gauss-Lobatto rule

d the section depth (idealized section). Fig. 5.42(a) shows the exact plastic limit surface of a W14x426 section and the numerical solution with 4 midpoint integration points in each flange and 4 integration points in the web, which is almost indistinguishable from the exact solution. The figure also shows an approximation of the exact surface with a smooth polynomial that offers excellent accuracy in the range of practical interest. The polynomial equation is

$$\left(\frac{M}{M_p}\right)^2 + 3.5 \left(\frac{M}{M_p}\right)^2 \left(\frac{N}{N_p}\right)^2 + 1.2 \left(\frac{N}{N_p}\right)^2 = 1$$

The smooth polynomial approximation proves suitable for the development of inelastic beam-column elements with concentrated resultant plasticity, as will be discussed later.

It is clear from Fig. 5.42(a) that the plastic limit surface of a wide flange section resembles the diamond shape of the elastic limit surface in Fig. 5.35. In fact, in the limit case of a section with shape factor equal to 1, i.e. $M_p/M_y = 1$ the plastic limit surface is perfectly diamond shaped. Such an ideal section results from two flanges with area equal to half of the cross section area A at distance d from each other, where d is the section depth. Lighter W-sections with a higher proportion of the total area concentrated in the flange with a shape factor of approximately 1.1 approximate this case. Heavier W-sections that are suitable for columns with a shaper factor of 1.2-1.3 have a plastic limit surface in between that of the rectangular section and the diamond shape of an ideal two flange section. The W14x426 section of Fig. 5.42(a) belongs to the latter group.

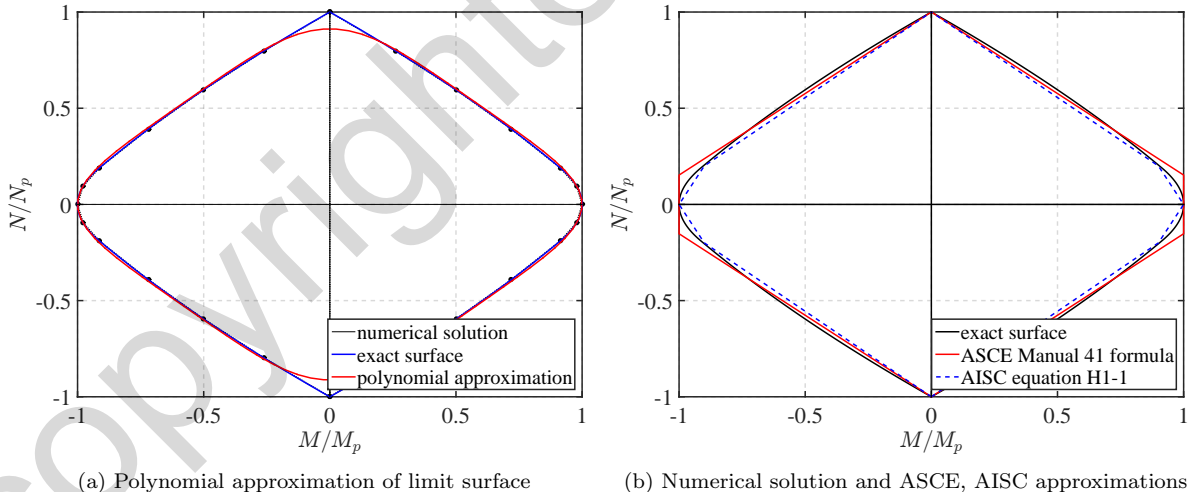


Fig. 5.42: Plastic limit surface of wide flange section with polygonal and smooth approximations

For first and second order plastic analysis under consideration of the interaction between axial force and bending moment a simple polygonal approximation of the plastic limit surface of a wide-flange section suggests itself. This approach is used in design specifications, such as the 2005 AISC specification that is a more accurate evolution of the earlier formula in the ASCE Manual 41 on "Plastic Design in Steel" (1971). The interaction relation for steel beam-columns under uniaxial bending and normal force is given by equation H1-1 of the 2005 AISC specification

$$\begin{aligned} \text{for } \frac{P_r}{P_c} \geq 0.2 & \quad \frac{P_r}{P_c} + \frac{8}{9} \frac{M_r}{M_c} \leq 1 \\ \text{for } \frac{P_r}{P_c} < 0.2 & \quad \frac{P_r}{2P_c} + \frac{M_r}{M_c} \leq 1 \end{aligned} \quad (5.45)$$

For the definition of terms in the above equations consult Section H1.1 of the 2005 AISC Specification. Fig. 5.42(b) compares these polygonal approximations with the exact solution for the W14x426 section. The 2005 AISC Specification approximates the exact surface very well and lies on the inside of it and thus on the safe side for design purposes.

5.9.4 Ultimate Strength Surface for RC Rectangular Section

Reinforced concrete is representative of composite materials with different stress-strain response characteristics. Some of these do not have a well defined plastic strength, others have different strength in tension than in compression, and finally others do not exhibit perfectly plastic response in the post-peak strength range. For these reasons the determination of the ultimate strength surface is computationally intensive. With today's computer hardware and software such determination is not a problem.

Noting that the ultimate strength surface represents the pairs of maximum normal force N and bending moment M that a particular section can resist we adopt the following process for determining the ultimate strength surface of a reinforced concrete section, which is also called the N - M interaction diagram:

- 1) Select a normal force N .
- 2) Determine the moment-curvature response under the normal force N and establish the largest moment M that the cross section resists under this normal force.
- 3) Store the pair of N and M values and repeat the process for a range of normal force values N .

Fig. 5.44 shows the intermediate results and the resulting ultimate strength surface for a rectangular 15 inch square RC section with tension and compression reinforcing steel lumped in a single layer. The reinforcement area amounts to a reinforcing ratio of approximately 1.5% for each layer and the concrete cover is 1.5 inches. The concrete compressive strength f'_c is 5 ksi, the yield strength of the reinforcing steel is 60 ksi with Young modulus of 29,000 ksi. The concrete is assumed unconfined by setting the confinement factor for the Mander, Priestley, Park concrete material model equal to 1.0. The GMP model is used for the reinforcing steel with an exponent value r of 20. The moment-curvature relations in Fig. 5.44(a) correspond to 18 normal force levels from a tensile force of 400 kips to a compression force of 950 kips. For each normal force the maximum moment of the moment-curvature relation is displayed with a round marker in Fig. 5.44(b), where tensile normal forces are negative and compressive normal forces are positive, as is common in RC design. The emerging ultimate strength surface in Fig. 5.44(b) has similar characteristics to the plastic limit surface of a wide flange section, but is centered at the balanced point instead of at $N = 0$ and has a different distance of the ultimate compressive strength from the normal force at the balance point than the distance of the ultimate tensile strength from the normal force at the balance point.

Because the described method for establishing the ultimate strength of a RC section was considered computationally prohibitive in the 1960's and 1970's when modern ultimate strength design specifications

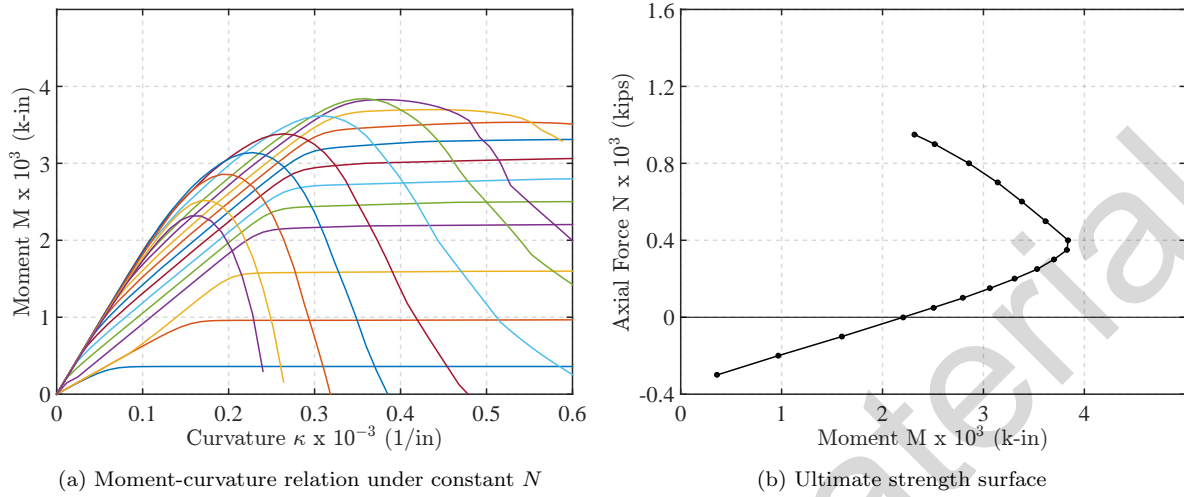


Fig. 5.43: Determination of ultimate strength surface for rectangular RC section with unconfined concrete

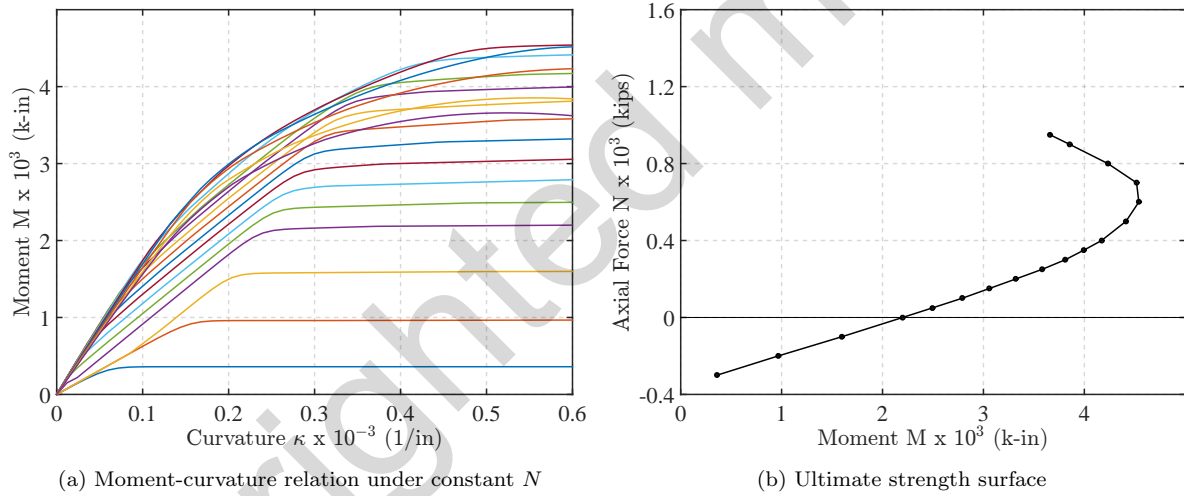


Fig. 5.44: Determination of ultimate strength surface for rectangular RC section with confined concrete

for reinforced concrete were put forward, the following procedure was proposed for establishing the ultimate strength surface of a RC section:

- 1) Consider the following strain distributions for the RC section in Fig. 5.45:
 - a. Uniform tensile strain distribution with yield strain ε_y of reinforcing steel (point P₁). This corresponds to the ultimate tensile strength.
 - b. Strain distribution with compressive strain ε_{cu} at the top of the section and very high tensile strain $10\varepsilon_y$ at the level of the reinforcing steel at the opposite section edge. This corresponds approximately to the moment strength of the section under zero normal force (point P₂).
 - c. Strain distribution with compressive strain ε_{cu} at the top of the section and yield strain ε_y at the level of the reinforcing steel at the opposite section edge. This corresponds to the balanced point of the section (point P₃).

- d. Uniform compressive strain distribution with yield strain $-\varepsilon_y$ of reinforcing steel (point P₄). This corresponds to the ultimate compressive strength.
- 2) Sweep the strain distribution smoothly from point P₁ to point P₂ for Zone A. The strain distribution sweep is represented by the dark gray polygon for Zone A in Fig. 5.45.
 - 3) Sweep the strain distribution smoothly from point P₂ to point P₃ for Zone B. The strain distribution sweep is represented by the dark gray triangle for Zone B in Fig. 5.45.
 - 4) Sweep the strain distribution smoothly from point P₃ to point P₄ for Zone C. The strain distribution sweep is represented by the dark gray polygon for Zone C in Fig. 5.45.

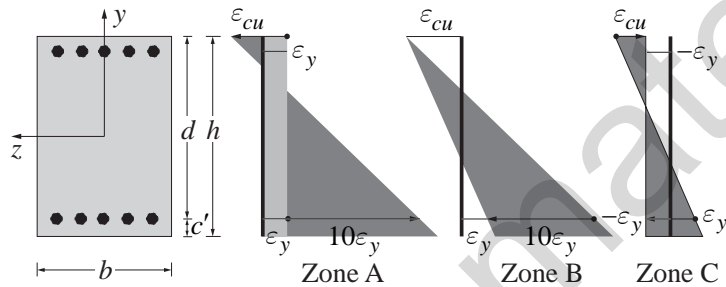


Fig. 5.45: Strain distribution sweeps for zones A, B and C for RC section

For the compressive strain ε_{cu} of unconfined concrete a value of -0.003 is recommended. For confined concrete a value from -0.005 to -0.01 should be used depending on the confinement ratio. Instead of the arbitrary tensile strain value of $10\varepsilon_y$ at the level of the reinforcing steel for determining the moment strength of the section without normal force, the exact value can be established by iteration.

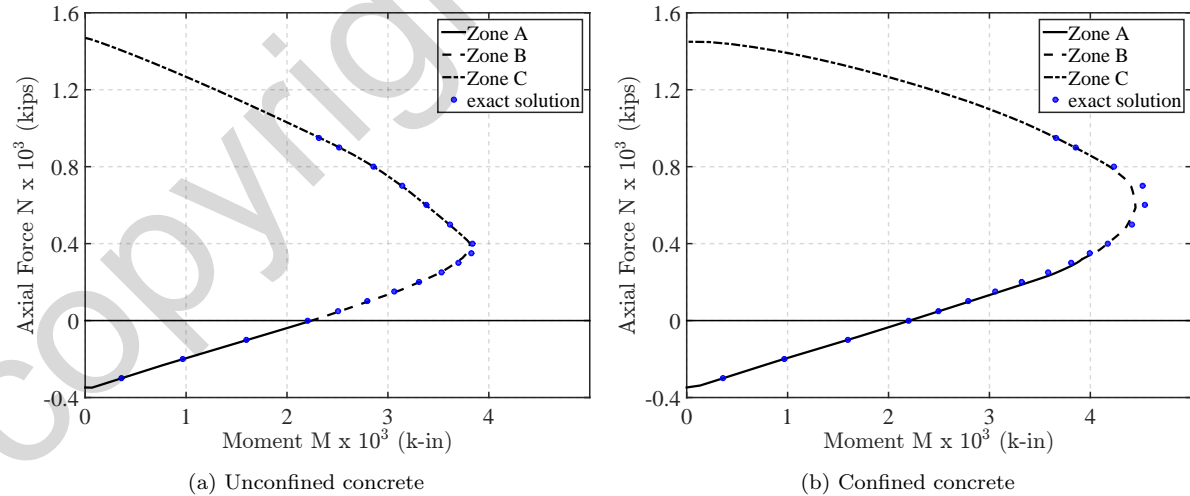


Fig. 5.46: Comparison of exact and approximate method for ultimate strength surface of RC section

Fig. 5.46 shows the comparison of the approximate method with strain distribution sweeps with the exact method of selecting the maximum moment of the moment-curvature relation for a given

normal force level for the 15 inch square RC section. Fig. 5.46(a) shows the ultimate strength surface comparison for unconfined concrete with a confinement factor $K = 1.0$ for the Mander, Priestley, Park concrete material model. The tensile strain value for moment strength of the section is equal to $8.3\varepsilon_y$. Zones A, B and C are denoted in the figure and are clearly delineated by the ultimate tensile strength point P_1 , the moment strength point P_2 , the balance point P_3 , and the ultimate compressive strength point P_4 . The results of the approximate method are impressively accurate, as the markers for the N - M pairs of the exact method reveal.

Fig. 5.46(b) shows the ultimate strength surface comparison for confined concrete with a confinement factor $K = 1.2$ for the Mander, Priestley, Park concrete material model. For this case the compressive strain ε_{cu} is set equal to -0.008. The figure shows that Zone A is not limited to the tensile normal force range in this case, but we do not pursue the detail of improving the assumption for the strain distributions in Fig. 5.45 for confined concrete. The results of the approximate method are still impressively accurate, as the markers for the N - M pairs of the exact method reveal.

Example 5.7 Collapse Load Factor of Column under Eccentric Axial Force

We demonstrate the use of the numerical plastic limit surface with the determination of the collapse load for the cantilever column Fig. 5.47(a) under an axial force P with eccentricity $e = \frac{d}{2}$ relative to the centroidal axis of the rectangular cross section of the column with depth d and width b . The column consists of a linear elastic, perfectly plastic material with yield strength f_y and elastic modulus E . The plastic limit surface in Fig. 5.47(b) is based on the midpoint integration rule with only 4 layers. This is clearly quite approximate but is computationally convenient and suffices for demonstrating the concept. The refinement of the final result will be discussed at the end of the example. The resulting octagon for the failure surface has only 3 distinct pairs of normal force N and bending moment M : the plastic axial capacity at point T_1 , the plastic flexural capacity at point T_3 and the intermediate point T_2 in Fig. 5.47(b). The N - M values for these are:

$$\begin{array}{lll} \text{point } T_1 & N_1 = -N_p = -bd f_y & M_1 = 0 \\ \text{point } T_3 & N_3 = 0 & M_3 = M_p = \frac{bd^2}{4} f_y \\ \text{point } T_2 & N_2 = -0.5 bd f_y = -0.5 N_p & M_2 = 0.25 bd f_y \frac{3d}{4} = \frac{3bd^2}{16} f_y = 0.75 M_p \end{array}$$

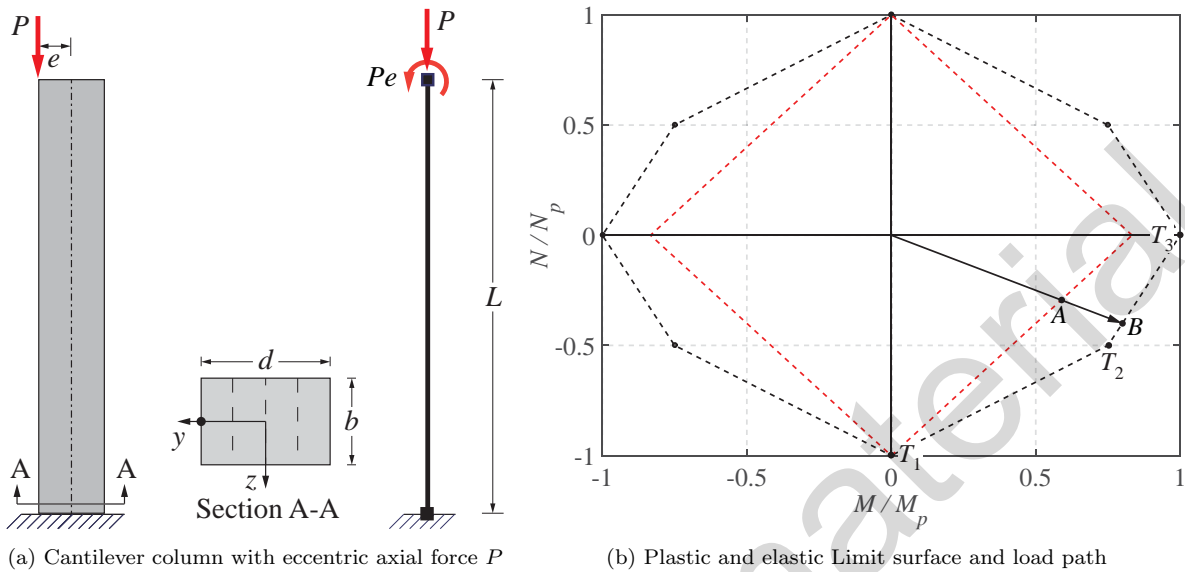
The eccentricity for the axial force P corresponding to point T_2 is:

$$e_2 = -\frac{M_2}{N_2} = 1.5 \frac{M_p}{N_p} = 1.5 \frac{d}{4} = 0.375d$$

The given eccentricity e is larger than e_2 . Thus, we expect the load path of the increasing eccentric axial force P to intersect the edge of the plastic limit surface between points T_2 and T_3 at point B Fig. 5.47(b). The straight line connecting the points T_2 and T_3 has the following equation

$$\frac{N - N_3}{M - M_3} = \frac{N_2 - N_3}{M_2 - M_3} \rightarrow \frac{N}{M - M_p} = 2 \frac{N_p}{M_p} \quad (5.46)$$

Substituting $N = -P$ and $M = N(-e)$ into the above equation gives

Fig. 5.47: Limit surface and failure load of cantilever column under eccentric axial force P

$$-P \left(1 + 2 \frac{N_p}{M_p} e \right) = -2N_p \quad \rightarrow \quad P = 0.4N_p$$

The result is confirmed by geometry in Fig. 5.47(b). The straight line with an arrowhead traces the equation $M = N(-e)$ and represents the load path of N - M values for increasing P with constant eccentricity e . It intersects the edge of the plastic limit polygon at point B with an axial force $N = -0.4N_p$. The cantilever column, therefore, reaches its collapse load at a value of 40% of the plastic axial capacity N_p , because of the eccentricity e of the axial force inducing a moment M_c at incipient collapse equal to

$$M_c = 0.4N_p \frac{d}{2} = 0.8M_p$$

We are now also interested in determining the value of P at yield initiation, i.e. the intersection of the load path with the elastic limit surface at point A in Fig. 5.47(b). To this end we determine first the moment of inertia by midpoint integration to get

$$I = 2 \left(\frac{bd}{4} \right) \left[\left(\frac{d}{8} \right)^2 + \left(\frac{3d}{8} \right)^2 \right] = \frac{5bd^3}{64}$$

We note that the moment of inertia with 4 midpoint integration points shows an error of 6.2% relative to the exact value of $\frac{bd^3}{12}$.

The force P at the initiation of yielding under eccentricity e is determined from the relation

$$\sigma = \frac{N}{A} \pm \frac{My}{I} = \pm f_y$$

$N = -P$ and $M = N(-e)$ gives

$$\frac{-P}{A} - \frac{P \left(\frac{d}{2}\right) \left(\frac{3d}{8}\right)}{\frac{5bd^3}{64}} = -f_y \quad \rightarrow \quad \frac{-P}{A} (1 + 2.4) = -f_y \quad \rightarrow \quad P = 0.294 A f_y = 0.294 N_p$$

and the corresponding moment is

$$M = Pe = 0.294 f_y A \frac{d}{2} = 0.588 M_p$$

The yield moment M_y of the section without normal force is

$$f_y = \frac{M_y}{I} \frac{3d}{8} = M_y \frac{64}{5bd^3} \frac{3d}{8} \quad \rightarrow \quad M_y = \frac{5}{24} f_y bd^2 = \frac{5}{6} M_p$$

which is 25% higher than the exact value of $f_y \frac{bd^2}{6}$. The yield moment with the midpoint integration rule is used to draw the initial yield polygon in Fig. 5.47(b). With it, the preceding answers about the value of the axial force P at the initiation of yielding can be confirmed geometrically in Fig. 5.47(b), which shows that the load path of normal force and bending moment under increasing P pierces the elastic limit surface at the normal force of $-0.294N_p$ with moment equal to $0.588M_p$.

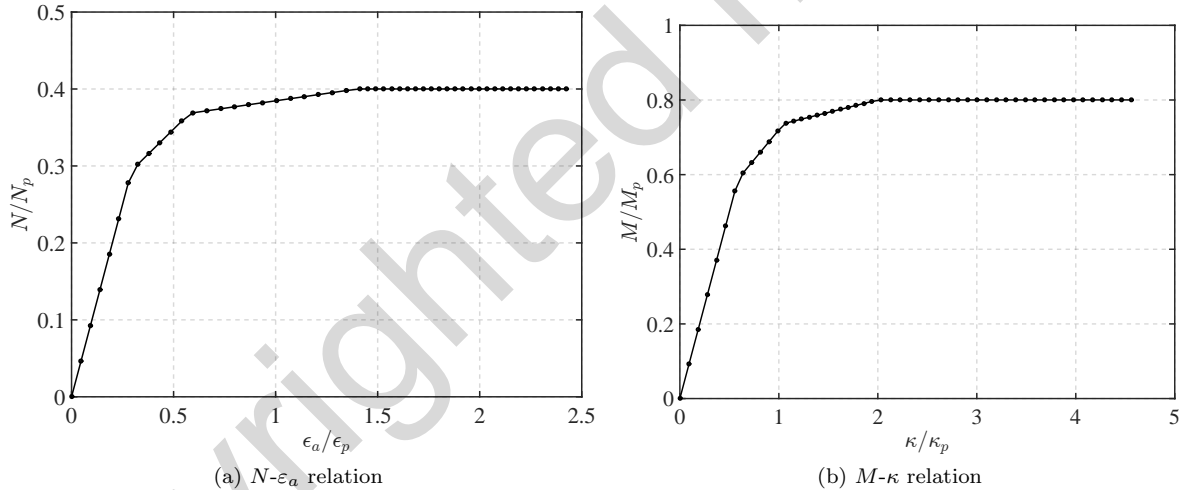


Fig. 5.48: Section force-deformation response for cantilever column

These results are also confirmed from the relation between normal force N and normal strain ϵ_a at the reference axis in Fig. 5.48(a) and from the relation between moment M and curvature κ in Fig. 5.48(b).

We determine now the horizontal translation at the tip of the column at incipient collapse. To this end we need the curvature κ_c at incipient collapse. For this we use the statically determinate stress distribution over the cross section at incipient collapse. The two integration points closest to the compression edge of the section have already yielded. The one closest to the tension edge is about to yield in tension. We, therefore, determine the strain of the one that is elastic. Numbering the integration points from the compression edge, the elastic one is the third. We get

$$-0.25 N_p - 0.25 N_p + \sigma_3(0.25bd) + 0.25 N_p = -0.4N_p \quad \rightarrow \quad \sigma_3 = -0.6f_y \quad \rightarrow \quad \epsilon_3 = -0.6\epsilon_y$$

where ε_y is the yield strain of the linear elastic, perfectly plastic material. The curvature κ_c then is

$$\kappa_c = \frac{\varepsilon_4 - \varepsilon_3}{0.25d} = \frac{\varepsilon_y + 0.6\varepsilon_y}{0.25d} = 6.4 \frac{\varepsilon_y}{d}$$

The horizontal translation U_1 at the cantilever tip then is

$$U_1 = \mathbf{v}_i L = \left(-\frac{1}{2} \kappa_c L \right) L = -\frac{1}{2} \kappa_c L^2$$

where L is the length of the cantilever column. Substituting κ_c we get

$$U_1 = -3.2 \frac{\varepsilon_y}{d} L^2 \rightarrow \frac{U_1}{L} = -3.2 \varepsilon_y \frac{L}{d}$$

indicating that the column tip translates to the left. The ratio $\frac{L}{d}$ is the *span-to-depth* ratio of the cantilever column. For a span-to-depth ratio of 10 the horizontal drift ratio $\frac{U_1}{L}$ is 32 times the yield strain, a rather large value resulting from the fact that the column is yielding over its entire length.

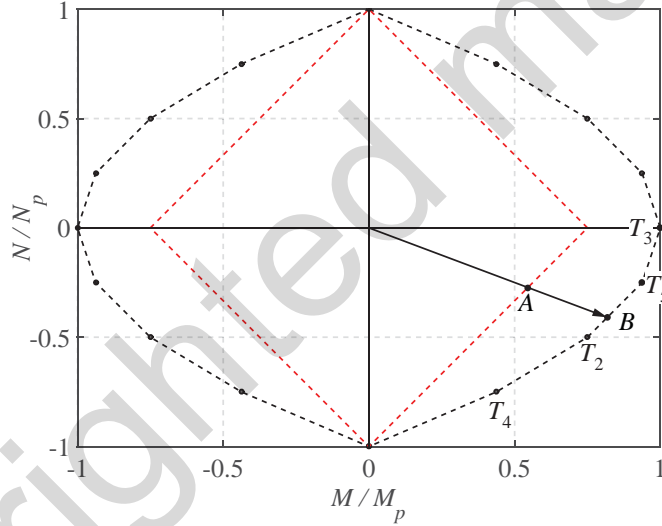


Fig. 5.49: Elastic and plastic limit surface with 8 layers

To increase the accuracy of the initial yield and failure load determination we increase the number of layers for the midpoint rule evaluation of the limit surfaces. With 8 layers the limit surfaces in Fig. 5.49 result. We conclude that the elastic limit surface is now smaller, i.e. initiation of yielding at the outermost integration point takes place *sooner* and point A in Fig. 5.49 corresponds to a smaller normal force N and bending moment $M = Pe$ than point A in Fig. 5.47(b). For the limit plastic surface we realize that point T_2 Fig. 5.49 has the same normal force N and bending moment M as point T_2 Fig. 5.47(b) (can you explain why?). Thus, all that is required for determining the failure load more accurately is to determine the normal force N and bending moment M as point T_5 . These values result from the assumption that 3 layers are at the positive yield strength f_y and 5 layers are at the negative yield strength $-f_y$. Following the determination of N_5 and M_5 we can use the same relation as (5.46) after replacing N_3 with N_5 and M_3 with M_5 to describe the critical edge of the plastic limit polygon that the straight load path will

intersect at point B, the failure load of the cantilever column. The determination of this value is left as an exercise to the reader.

Chapter 6

Path-Independent Nonlinear Frame Elements

6.1 Introduction

This chapter discusses the formulation of the force-deformation relation for a few simple truss and plane beam elements with path-independent material response. The extension of these elements to path-dependent material response will be presented in a later chapter. The force-deformation relation of these elements is described *in the basic system that moves with the element chord as the element displaces and deforms*. With this corotational approach which was presented in Chapter 4 in the context of the nonlinear geometry of linear frame elements, the transformation from the basic system to the global reference system of the structural model *is independent of the force-deformation relation for the basic element*. In the following sections we, therefore, concentrate only on the task of determining the basic element forces \mathbf{q} and the basic stiffness matrix \mathbf{k} for given element deformations \mathbf{v} with the understanding that the relations of Chapter 4 for transforming \mathbf{q} and \mathbf{k} to the global reference system after the addition, if necessary, of the nonlinear geometry contribution hold for the present chapter as well.

6.2 Plane and Space Truss Element

Whether we are dealing with a plane truss or a space truss element the basic force deformation relation is the same. Because the basic truss element has only one deformation and one basic force, we drop the subscript in the following and denote the axial deformation with v and the corresponding basic force with q .

In the following we discuss first the displacement formulation of the basic truss element with nonlinear material, and then the force formulation. We subsequently discuss these formulations in the context of a parallel spring and a series spring model whose formulation are completely analogous to the displacement and force formulation, respectively.

6.2.1 Displacement Formulation of Nonlinear Basic Truss Element

In deriving the force-deformation relation of the basic truss element with nonlinear material we assume linear intra-element geometry, as discussed in Chapter 4.

The development of the force-deformation relation for a homogeneous truss element with variable cross section $A(x)$ (non-prismatic truss element) composed of a material with nonlinear stress-strain

relation is not as straightforward, as it appears at first. The element state determination within the nonlinear incremental analysis of the structural model under applied nodal forces requires the determination of the basic element force q and the tangent stiffness k for given element deformation v . Because the nonlinear basic element response derives from the nonlinear stress-strain relation of the material, a relation between the strain at section x and the element deformation v is required. Unfortunately, however, such relation is directly available only for a prismatic truss element. This can be concluded from the first equation in (4.10)

$$\frac{d}{dx} \left[EA(x) \frac{du_x(x)}{dx} \right] = 0$$

For a homogeneous truss element with variable cross section $A(x)$ this second order differential equation has a closed form solution only for special cases of function $A(x)$. Consequently, the *finite element* analysis uses a polynomial for the solution $u_x(x)$ with the simplest choice being the linear polynomial constituting the exact solution of the prismatic truss element. With

$$u_x(x) = C_{11}x + C_{12} \quad (6.1)$$

we get

$$\varepsilon_a(x) = \frac{du_x(x)}{dx} = C_{11} = \frac{v}{L}$$

noting that $v = u_x$ at $x = L$. $\varepsilon_a(x)$ is the normal strain at the reference axis, but the assumption that plane section remain plane leads to the conclusion that $\varepsilon(x, y, z) = \varepsilon_a(x)$ meaning that the strain field $\varepsilon(x, y, z)$ is uniform over the cross section and only depends on x .

The stress field $\sigma(x)$ is derived from the strain field $\varepsilon(x)$ by satisfying the material constitutive relation

$$\sigma(x) = \hat{\sigma}[\varepsilon(x)]$$

where the symbol $\hat{\sigma}$ denotes the function of the corresponding variable. We conclude that the stress field depends on x on account of $\varepsilon(x, y, z) = \varepsilon_a(x)$.

The principle of virtual displacements gives the basic element force q corresponding to deformation v

$$\delta v^T q = \int_V \delta \varepsilon^T \sigma(x) dV$$

where V is the element volume and δ denotes the virtual fields. Because of $\varepsilon(x, y, z) = \varepsilon_a(x)$, the integral for the internal work simplifies to

$$\int_V \delta \varepsilon^T \sigma(x, y, z) dV = \int_0^L \delta \varepsilon_a^T \sigma(x) \left(\int_A dA \right) dx = \int_0^L \delta \varepsilon_a^T \sigma(x) A(x) dx$$

The Galerkin approach of finite element analysis uses the same approximation for the virtual displacement field as for the real field to get

$$\delta v^T q = \delta v^T \left(\frac{1}{L} \right) \int_0^L \sigma(x) A(x) dx \rightarrow q = \frac{1}{L} \int_0^L \sigma(x) A(x) dx \quad (6.2)$$

The tangent stiffness of the truss element is determined by differentiation of the basic force q with respect to v to give

$$k = \frac{dq}{dv} = \frac{1}{L} \int_0^L \frac{d\sigma}{d\varepsilon} \left(\frac{1}{L} \right) A(x) dx = \frac{1}{L^2} \int_0^L E_t A(x) dx \quad (6.3)$$

where E_t is the tangent material modulus

$$E_t = \frac{d\hat{\sigma}}{d\varepsilon}$$

The preceding approach for the determination of the force-deformation relation for the nonlinear truss element is called *displacement formulation*. It has the shortcoming of using an approximation for the displacement field $u_x(x)$, even though an exact solution for the force field is available, as we see subsequently. It has, however, the significant benefit of directness and ease of implementation. For a homogeneous, linear elastic truss member with variable cross section $A(x)$ a uniform strain field produces a uniform stress field, *but a nonuniform normal force field* $N(x) = \sigma(x)A(x)$. Nonetheless, the subdivision of the member into several finite elements, with a uniform strain field in each, produces results that converge to the exact solution with finer element subdivision.

For an inhomogeneous truss element with constant or variable cross section the displacement formulation has some serious limitations that can be partly overcome with higher order elements and enhanced formulations, but this subject is beyond the scope of this text. Such limitations are particularly noticeable for nonlinear fracturing material response. This issue will be addressed briefly in the following section with the parallel and the series spring model of material response.

Before turning our attention to an alternative determination of the force-displacement relation of the truss element with nonlinear material, we summarize the state determination for the truss element with the displacement formulation. The presence of integrals over the element length L in (6.2) and (6.3) requires numerical integration, as discussed in Section 5.5.

The state determination of each element of the structural model is based on the free global dof displacements $\mathbf{U}_i^{(k)}$ at the iteration i of load step k of the solution strategy for multi-step incremental analysis. It consists of the following operations

- 1) Determine the element deformation v based on linear or nonlinear kinematics. For linear kinematics use $v = \mathbf{a}_g \mathbf{u}$, for nonlinear Green-Lagrange kinematics use (2.9) for the plane truss or (2.10) for the space truss.
- 2) Determine the strain ε_m at integration point m of the numerical integration scheme.

$$\varepsilon_m = \frac{v}{L}$$

where L is the element length.

- 3) Use the material constitutive relation to determine the stress σ_m and the tangent modulus E_m at the integration point m .
- 4) Use numerical integration to evaluate the integrals in (6.2) and (6.3)

$$\begin{aligned} q &= \frac{1}{2} \sum_{nIP} w_m \sigma_m A_m \\ k &= \frac{1}{2L} \sum_{nIP} w_m E_m A_m \end{aligned} \quad (6.4)$$

after first transforming to the integration interval $-1 \leq \xi \leq 1$ and recalling the relation $dx = \frac{L}{2} d\xi$.

- 5) Transform the basic element force q and stiffness k to the global reference system under nonlinear geometry

$$\begin{aligned}\mathbf{p} &= \mathbf{a}_g^T q \\ \mathbf{k}_e &= \mathbf{a}_g^T k \mathbf{a}_g + \mathbf{k}_g\end{aligned}$$

according to (3.44), (3.45), and (3.47) for the Green-Lagrange truss element. For linear geometry the transformation matrix \mathbf{a}_g is related to the direction cosines of the undeformed element x -axis and the geometric stiffness matrix \mathbf{k}_g is zero.

For a homogeneous, prismatic truss element the state determination process simplifies significantly by the direct evaluation of the integrals in (6.2) and (6.3) to give

$$\begin{aligned}q &= \sigma_m A \\ k &= \frac{E_m A}{L}\end{aligned}\tag{6.5}$$

where σ_m is the stress and E_m the tangent modulus of the nonlinear material stress-strain relation for ε_m . The other steps of the state determination process are not affected.

Before discussing the alternative approach for deriving the force-deformation relation of the basic truss element with nonlinear material we present in the following an example of the state determination process for a simple truss with homogeneous, prismatic elements.

Example 6.1 Simple Truss

We present the incremental nonlinear analysis of the simple truss in Fig. 6.1. It consists of 3 elements of unit area $A = 1$. The nonlinear material stress-strain relation follows the GMP model with the following material properties: $f_y = 40$, $E = 20,000$, $E_h = 200$ and $r = 2$. The truss is subjected to the reference forces in Fig. 6.1(a), so that

$$\mathbf{P}_{ref} = \begin{pmatrix} 50 \\ 40 \end{pmatrix}$$

We apply the reference load vector in two steps with constant load factor increment $\Delta\lambda_0 = 0.75$. We follow the Newton-Raphson solution strategy according to Chapter 3.

Before presenting the numerical results of the solution process we summarize the key relations. The tangent stiffness matrix at the free global dofs of the truss *under linear geometry* is

$$\mathbf{K}_t = \mathbf{A}_f^T \mathbf{K}_s \mathbf{A}_f = \begin{bmatrix} \frac{E_{tc}A}{L_c} + \left(\frac{8}{L_b}\right)^2 \frac{E_{tb}A}{L_b} & \left(\frac{8}{L_b}\right) \left(\frac{6}{L_b}\right) \frac{E_{tb}A}{L_b} \\ \left(\frac{8}{L_b}\right) \left(\frac{6}{L_b}\right) \frac{E_{tb}A}{L_b} & \frac{E_{ta}A}{L_a} + \left(\frac{6}{L_b}\right)^2 \frac{E_{tb}A}{L_b} \end{bmatrix}\tag{6.6}$$

where E_t represents the tangent material modulus of the element indicated by the subscript. The equilibrium error \mathbf{P}_u with the resisting element forces *in the undeformed configuration* is

$$\mathbf{P}_u = \mathbf{P}_f - \mathbf{P}_r = \lambda \mathbf{P}_{ref} - \mathbf{A}_f^T \mathbf{Q} = \lambda \mathbf{P}_{ref} - \begin{bmatrix} 0 & 0.8 & 1 \\ 1 & 0.6 & 0 \end{bmatrix} \begin{pmatrix} q_a \\ q_b \\ q_c \end{pmatrix}\tag{6.7}$$

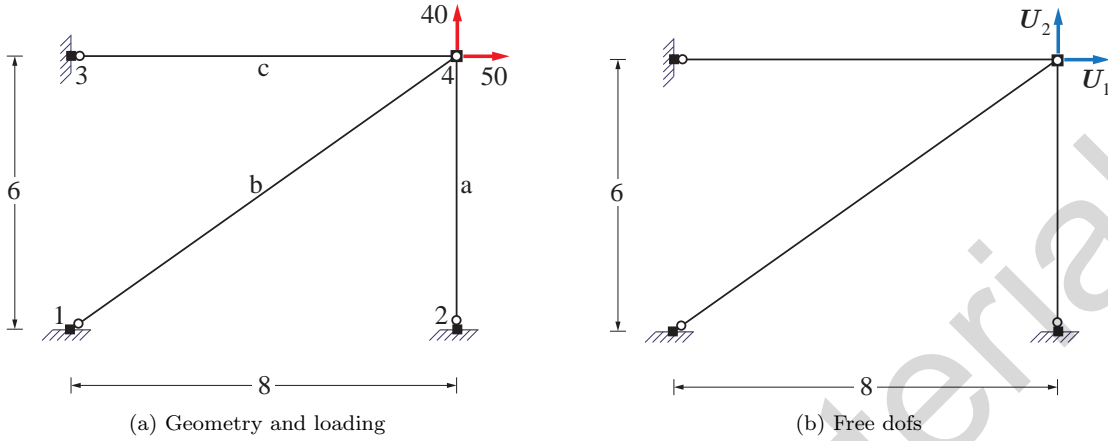


Fig. 6.1: Simple truss with nonlinear material response

where we chose to label the basic forces of each element with a subscript, since each truss element has only one basic force. Under linear kinematics the free dof displacements give the element deformations \mathbf{v} with the relation

$$\mathbf{V} = \begin{pmatrix} v_a \\ v_b \\ v_c \end{pmatrix} = \mathbf{A}_f \mathbf{U}_f = \begin{bmatrix} 0 & 1 \\ 0.8 & 0.6 \\ 1 & 0 \end{bmatrix} \begin{pmatrix} \mathbf{U}_1 \\ \mathbf{U}_2 \end{pmatrix} \quad (6.8)$$

The structure state determination unfolds as follows:

- 1) Given the free dof displacements $\mathbf{U}_i^{(k)}$ at iteration i of load step k , determine the element deformations \mathbf{V} with (6.8).
- 2) Determine the normal strain ε for each truss element with $\varepsilon = \frac{v}{L}$.
- 3) The material state determination gives the stress σ and tangent modulus E_t corresponding to normal strain ε .
- 4) The basic force q and basic stiffness k of each truss element is

$$q = \sigma A + q_0$$

$$k = \frac{E_t A}{L}$$

- 5) With (6.7) determine the equilibrium error \mathbf{P}_u .
- 6) With (6.6) determine the tangent stiffness \mathbf{K}_t at the free global dofs of the structure.
- 7) Use the linear equilibrium equations $\mathbf{P}_u = \mathbf{K}_t \Delta \mathbf{U}_i$ to determine the free dof displacement corrections $\Delta \mathbf{U}_i$.
- 8) Update the free dof displacements and return to the first step until convergence.

In the following we present in detail the calculations for two load steps. We refrain from using superscripts for the load step, since it is clear from the context.

First load step.

With $\Delta \lambda_0 = 0.75$ the applied forces at the free dofs are

$$\mathbf{P}_f = \lambda^{(1)} \mathbf{P}_{ref} = \begin{pmatrix} 37.5 \\ 30 \end{pmatrix} \quad \text{with} \quad \lambda^{(1)} = \lambda^{(0)} + \Delta\lambda_0 = 0 + 0.75 = 0.75$$

with the superscript in parentheses denoting the load step. With the initial guess $\mathbf{U}_0^{(1)} = \mathbf{0}$ and the relations

$$\begin{aligned}\mathbf{P}_u(\mathbf{U}_i) &= \mathbf{P}_f - \mathbf{P}_r(\mathbf{U}_i) \\ \Delta\mathbf{U}_i &= \mathbf{K}_t(\mathbf{U}_i) \setminus \mathbf{P}_u(\mathbf{U}_i) \\ \mathbf{U}_{i+1} &= \mathbf{U}_i + \Delta\mathbf{U}_i\end{aligned}$$

where we use the Matlab® command \ to indicate the solution of the linear system of two equilibrium equations in two unknowns, the results of the NR iteration algorithm for the first load step are summarized in Table 6.1. Because all variables in the table refer to the first load step, we drop the superscript convenience of notation.

Iteration i	$\mathbf{U}_i (\times 10^{-3})$	$\mathbf{P}_u(\mathbf{U}_i)$	$\mathbf{K}_t(\mathbf{U}_i) (\times 10^3)$	$\Delta\mathbf{U}_i (\times 10^{-3})$	$\mathbf{U}_{i+1} (\times 10^{-3})$
0	$\begin{pmatrix} 0 \\ 0 \end{pmatrix}$	$\begin{pmatrix} 37.5 \\ 30 \end{pmatrix}$	3.78 0.96 0.96 4.05	$\begin{pmatrix} 8.56 \\ 5.37 \end{pmatrix}$	$\begin{pmatrix} 8.56 \\ 5.37 \end{pmatrix}$
1	$\begin{pmatrix} 8.56 \\ 5.37 \end{pmatrix}$	$\begin{pmatrix} 4.21 \\ 2.83 \end{pmatrix}$	2.64 0.69 0.69 3.06	$\begin{pmatrix} 1.44 \\ 0.60 \end{pmatrix}$	$\begin{pmatrix} 9.99 \\ 5.98 \end{pmatrix}$
2	$\begin{pmatrix} 9.99 \\ 5.98 \end{pmatrix}$	$\begin{pmatrix} 0.21 \\ 0.10 \end{pmatrix}$	2.37 0.63 0.63 2.87	$\begin{pmatrix} 0.09 \\ 0.02 \end{pmatrix}$	$\begin{pmatrix} 10.08 \\ 5.99 \end{pmatrix}$
3	$\begin{pmatrix} 10.08 \\ 5.99 \end{pmatrix}$	$\begin{pmatrix} 0.00 \\ 0.00 \end{pmatrix}$	2.35 0.62 0.62 2.86	$\begin{pmatrix} 0.00 \\ 0.00 \end{pmatrix}$	$\begin{pmatrix} 10.08 \\ 5.99 \end{pmatrix}$

Table 6.1: Iteration results for the equilibrium solution of the two dof truss in the first load step

The calculations for the structure state determination at each iteration i involve the state determination of all elements. These, in turn, require the material state determination for each element. These calculations are summarized in Table 6.2.

Second load step.

Upon convergence of the Newton-Raphson iterative process to the solution for the first load step we impose the second load increment

$$\mathbf{P}_f = \lambda^{(2)} \mathbf{P}_{ref} = \begin{pmatrix} 75 \\ 60 \end{pmatrix} \quad \text{with} \quad \lambda^{(2)} = \lambda^{(1)} + \Delta\lambda_0 = 0.75 + 0.75 = 1.5$$

With the initial guess

$$\mathbf{U}_0^{(2)} = \mathbf{U}_4^{(1)} = \begin{pmatrix} 10.08 \\ 5.99 \end{pmatrix} 10^{-3}$$

and the relations

$$\begin{aligned}\mathbf{P}_u(\mathbf{U}_i) &= \mathbf{P}_f - \mathbf{P}_r(\mathbf{U}_i) \\ \Delta\mathbf{U}_i &= \mathbf{K}_t(\mathbf{U}_i) \setminus \mathbf{P}_u(\mathbf{U}_i) \\ \mathbf{U}_{i+1} &= \mathbf{U}_i + \Delta\mathbf{U}_i\end{aligned}$$

Iteration i	0	1	2	3
$v_a (\times 10^{-3})$	0	5.37	5.98	5.99
$\varepsilon_a (\times 10^{-3})$	0	0.90	1.00	1.00
σ_a	0	16.37	17.85	17.89
E_{ta}	20,000	15,251	14,400	14,377
q_a	0	16.37	17.85	17.89
k_a	3333.3	2542	2400	2396
$v_b (\times 10^{-3})$	0	10.07	11.58	11.66
$\varepsilon_b (\times 10^{-3})$	0	1.01	1.16	1.17
σ_b	0	18.01	20.07	20.18
E_{tb}	20,000	14,309	13,032	12,967
q_b	0	18.01	20.07	20.18
k_b	2,000	1431	1303	1297
$v_c (\times 10^{-3})$	0	8.56	9.99	10.08
$\varepsilon_c (\times 10^{-3})$	0	1.07	1.25	1.26
σ_c	0	18.89	21.23	21.36
E_{tc}	20,000	13,778	12,281	12,194
q_c	0	18.89	21.23	21.36
k_c	2,500	1722	1535	1524
\mathbf{P}_r	$\begin{pmatrix} 0 \\ 0 \end{pmatrix}$	$\begin{pmatrix} 33.29 \\ 27.17 \end{pmatrix}$	$\begin{pmatrix} 37.29 \\ 29.90 \end{pmatrix}$	$\begin{pmatrix} 37.50 \\ 30.00 \end{pmatrix}$

Table 6.2: State determination of elements a, b and c during the first load step

the results of the NR iteration algorithm for the second load step are summarized in Table 6.3. Because all variables in the table refer to the second load step, we drop the superscript convenience of notation.

Iteration i	$\mathbf{U}_i (\times 10^{-3})$	$\mathbf{P}_u(\mathbf{U}_i)$	$\mathbf{K}_t(\mathbf{U}_i) (\times 10^3)$	$\Delta\mathbf{U}_i (\times 10^{-3})$	$\mathbf{U}_{i+1} (\times 10^{-3})$
0	$\begin{pmatrix} 10.08 \\ 5.99 \end{pmatrix}$	$\begin{pmatrix} 37.5 \\ 30 \end{pmatrix}$	2.35 0.62 0.62 2.86	$\begin{pmatrix} 13.96 \\ 7.44 \end{pmatrix}$	$\begin{pmatrix} 24.04 \\ 13.44 \end{pmatrix}$
1	$\begin{pmatrix} 24.04 \\ 13.44 \end{pmatrix}$	$\begin{pmatrix} 15.44 \\ 10.52 \end{pmatrix}$	0.72 0.21 0.21 1.16	$\begin{pmatrix} 19.85 \\ 5.53 \end{pmatrix}$	$\begin{pmatrix} 43.89 \\ 18.97 \end{pmatrix}$
2	$\begin{pmatrix} 43.89 \\ 18.97 \end{pmatrix}$	$\begin{pmatrix} 6.85 \\ 3.52 \end{pmatrix}$	0.22 0.07 0.07 0.59	$\begin{pmatrix} 31.06 \\ 2.37 \end{pmatrix}$	$\begin{pmatrix} 74.95 \\ 21.34 \end{pmatrix}$
3	$\begin{pmatrix} 74.95 \\ 21.34 \end{pmatrix}$	$\begin{pmatrix} 2.69 \\ 0.99 \end{pmatrix}$	0.08 0.03 0.03 0.44	$\begin{pmatrix} 31.94 \\ 0.26 \end{pmatrix}$	$\begin{pmatrix} 106.89 \\ 21.60 \end{pmatrix}$
4	$\begin{pmatrix} 106.89 \\ 21.60 \end{pmatrix}$	$\begin{pmatrix} 0.54 \\ 0.20 \end{pmatrix}$	0.06 0.02 0.02 0.42	$\begin{pmatrix} 9.69 \\ 0.07 \end{pmatrix}$	$\begin{pmatrix} 116.58 \\ 21.67 \end{pmatrix}$
5	$\begin{pmatrix} 116.58 \\ 21.67 \end{pmatrix}$	$\begin{pmatrix} 0.02 \\ 0.01 \end{pmatrix}$	0.05 0.02 0.02 0.42	$\begin{pmatrix} 0.37 \\ 0.00 \end{pmatrix}$	$\begin{pmatrix} 116.95 \\ 21.68 \end{pmatrix}$

Table 6.3: Iteration results for the equilibrium solution of the two dof truss in the second load step

The calculations for the structure state determination at each iteration i involve the state determination of all elements. These, in turn, require the material state determination for each element. These calculations are summarized in Table 6.4.

Iteration i	0	1	2	3	4	5
$v_a (\times 10^{-3})$	5.99	13.44	18.97	21.34	21.60	21.67
$\varepsilon_a (\times 10^{-3})$	1.00	2.24	3.16	3.56	3.60	3.61
σ_a	17.89	29.98	34.10	35.23	35.34	35.37
E_{ta}	14,377	6052	3225	2530	2467	2450
q_a	17.89	29.98	34.10	35.23	35.34	35.37
k_a	2396	1009	537	422	411	408
$v_b (\times 10^{-3})$	11.66	27.29	46.50	72.77	98.48	106.27
$\varepsilon_b (\times 10^{-3})$	1.17	2.73	4.65	7.28	9.85	10.63
σ_b	20.18	32.49	37.31	39.64	40.78	41.04
E_{tb}	12,967	4288	1421	569	356	325
q_b	20.18	32.49	37.31	39.64	40.78	41.04
k_b	1297	429	142	56.9	35.6	32.5
$v_c (\times 10^{-3})$	10.08	24.04	43.89	74.95	106.89	116.58
$\varepsilon_c (\times 10^{-3})$	1.26	3.01	5.49	9.37	13.36	14.57
σ_c	21.36	33.57	38.30	40.60	41.84	42.15
E_{tc}	12,194	3568	995	380	264	250
q_c	21.36	33.57	38.30	40.60	41.84	42.15
k_c	1524	446	124	47.5	33	31.2
P_r	$\begin{pmatrix} 37.50 \\ 30 \end{pmatrix}$	$\begin{pmatrix} 59.56 \\ 49.48 \end{pmatrix}$	$\begin{pmatrix} 68.15 \\ 56.48 \end{pmatrix}$	$\begin{pmatrix} 72.31 \\ 59.01 \end{pmatrix}$	$\begin{pmatrix} 74.46 \\ 59.80 \end{pmatrix}$	$\begin{pmatrix} 74.98 \\ 59.99 \end{pmatrix}$

Table 6.4: State determination of elements a, b and c during the second load step

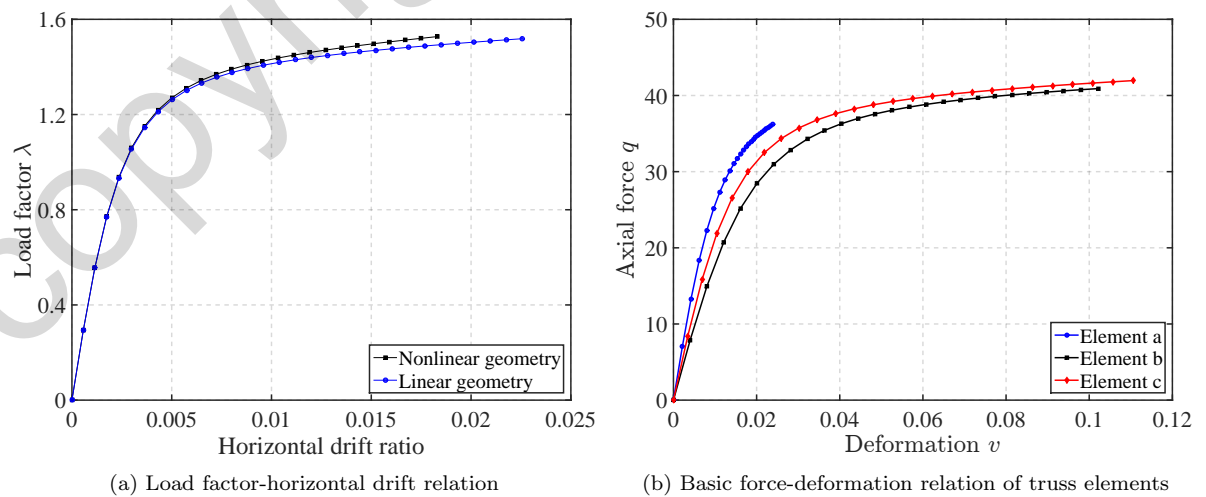


Fig. 6.2: Nonlinear incremental response of simple truss in Fig. 6.1 under linear and nonlinear geometry

Fig. 6.2 shows the nonlinear response of the truss under linear and nonlinear geometry. It consists of 30 load steps with load factor control and initial load factor increment $\Delta\lambda_0 = 0.3$. Because the truss elements are in tension the nonlinear geometry response is stiffer than the response under linear geometry.

6.2.2 Force Formulation of Nonlinear Basic Truss Element

The alternative approach for deriving the force-deformation relation of the basic truss element with nonlinear material uses the integral form of the kinematic relations in (4.2). The kinematic relation for the axial deformation is

$$v = \int_0^L \varepsilon_a(x) dx \quad (6.9)$$

after dropping the vector notation and the subscript noting that the truss element has only one deformation. The solution of the differential equation of element equilibrium leads to (4.3a)

$$N(x) = q$$

Under the assumption that plane sections remain plane after deformation the strain field $\varepsilon(x, y, z)$ and the stress field $\sigma(x, y, z)$ only depend on x so that

$$N(x) = \int_{A(x)} \sigma(x) dA = \sigma(x) A(x) \quad (6.10)$$

With (6.10) and (4.3a) the stress at section x is directly related to the basic force q of the truss element

$$\sigma(x) = \frac{q}{A(x)} \quad (6.11)$$

(6.11) makes clear that the stress field varies with x , if the truss element has variable cross section $A(x)$.

For a homogeneous section with linear elastic material the strain $\varepsilon_a(x)$ can be directly related to the stress $\sigma(x)$ leading first to (4.6a) and then to (4.7a) which can be written in compact form

$$v = f q + v_0 \quad \text{with} \quad f = \int_0^L \frac{1}{EA(x)} dx \quad (6.12)$$

where f is the truss element flexibility. For the general case of $EA(x)$ the determination of the truss element flexibility requires numerical integration which takes the form

$$f = \frac{L}{2} \sum_{nIP} \frac{w_m}{E_m A_m} \quad (6.13)$$

after first transforming to the integration interval $-1 \leq \xi \leq 1$ and recalling the relation $dx = \frac{L}{2} d\xi$.

For a truss element with a homogeneous section with linear elastic material the deformation-force relation in (6.12) can be inverted to give the basic force q in terms of the element deformation v in the form

$$q = k v + q_0 \quad \text{with} \quad k = \frac{1}{f} \quad (6.14)$$

It is worth noting the difference of the resulting truss element stiffness k in (6.14) from (6.4): the truss element stiffness k in (6.14) involves only the approximation of the numerical integration scheme, while the truss element stiffness k in (6.4) involves the approximation of the axial displacement field in (6.1) and the approximation of the numerical integration. There is no difference, of course, for a homogeneous, prismatic truss element, in which case both formulations are exact and lead to the same result.

The challenge of implementing the state determination of the truss element with the force formulation stems from the fact that there is no direct relation between the element deformation v and the basic force q under nonlinear material response, as is the case for the displacement formulation. To see this better we summarize the governing relations of the force formulation

$$\begin{aligned} v &= \int_0^L \varepsilon(x) dx \\ \sigma(x) &= \frac{q}{A(x)} \\ \sigma(x) &= \hat{\sigma}[\varepsilon(x)] \end{aligned} \quad (6.15)$$

where we dropped the subscript a from the strain field in the first equation, because of $\varepsilon(x, y, z) = \varepsilon_a(x)$. Because the state determination of the basic truss element involves the determination of the basic force q and of the stiffness k for given deformation v , it requires the solution of the first equation in (6.15). Noting that the basic force q is the independent variable of the problem for the force formulation, we conclude that the strain field $\varepsilon(x)$ is implicitly dependent on q through the second and the third relation of (6.15). To solve the first equation we write it in the form

$$v - \int_0^L \varepsilon(x) dx = v - v_r(q) = 0 \quad (6.16)$$

We denote the element deformation that is kinematically consistent with the strain field $\varepsilon(x)$ with v_r to distinguish it from the deformation v that depends on the element end displacements \mathbf{u} in accordance with $v = \mathbf{a}_g \mathbf{u}$ for linear kinematics and in accordance with (2.9) or (2.10) for nonlinear Green-Lagrange kinematics of the plane truss or space truss, respectively. We note explicitly the indirect dependence of v_r on q , so as to identify clearly the independent variable of the scalar nonlinear equation. Denoting the difference between v and v_r with v_u we make use of a Taylor series expansion of the function $v_u(q)$ with truncation after the linear term to get

$$v_u(q) = 0 \quad \rightarrow \quad v_{ui} + \left. \frac{dv_u}{dq} \right|_i \Delta q_i + \text{h.o.t} = 0 \quad \rightarrow \quad v_{ui} - \left. \frac{dv_r}{dq} \right|_i \Delta q_i = 0 \quad (6.17)$$

where v_{ui} is the value of $v - v_r(q_i)$ at an approximation q_i of the solution where also the derivative of the v_r is evaluated. (6.17) defines the iterative Newton-Raphson algorithm for the determination of q for a given v as long as the following two issues are addressed: (a) the determination of v_r for given q , and (b) the determination of $\frac{dv_r}{dq}$. The second task is easier; with

$$v_r = \int_0^L \varepsilon(x) dx$$

it follows

$$\frac{dv_r}{dq} = \int_0^L \frac{d\varepsilon(x)}{d\sigma(x)} \frac{d\sigma(x)}{dq} dx = \int_0^L \frac{1}{E_t(x)} \frac{1}{A(x)} dx$$

where

$$E_t(x) = \frac{d\hat{\sigma}(x)}{d\varepsilon(x)}$$

E_t is the tangent modulus of the material stress-strain relation. We conclude that $\frac{dv_r}{dq}$ is the tangent flexibility of the basic truss element with nonlinear material.

The determination of v_r for given q requires the determination of $\varepsilon(x)$ for given q . Because q is directly related to $\sigma(x)$ with the second equation in (6.15), this translates to determining $\varepsilon(x)$ for given $\sigma(x)$. Writing the third equation in (6.15) in the form

$$\sigma(x) - \hat{\sigma}[\varepsilon(x)] = \sigma(x) - \sigma_r[\varepsilon(x)] = \sigma_u[\varepsilon(x)] = 0$$

We conclude that the solution of another nonlinear equation is required for determining $\varepsilon(x)$ for a given $\sigma(x)$ or q ! Dropping the dependence on x from the fields in the interest of compact notation we make use of a Taylor series expansion of the function $\sigma_u(\varepsilon)$ with truncation after the linear term to get

$$\sigma_{ui} + \left. \frac{d\sigma_u}{d\varepsilon} \right|_i \Delta\varepsilon_i = 0 \quad \rightarrow \quad \sigma_{ui} - \left. \frac{d\sigma_r}{d\varepsilon} \right|_i \Delta\varepsilon_i = 0 \quad \rightarrow \quad \sigma_{ui} - E_{ti} \Delta\varepsilon_i = 0 \quad (6.18)$$

where σ_{ui} is the value of $\sigma - \sigma_r(\varepsilon_i)$ at an approximation ε_i of the solution where also the derivative of $\sigma_r = \hat{\sigma}(\varepsilon)$ is evaluated. (6.18) defines the iterative Newton-Raphson algorithm for the determination of ε for a given σ , and thus for a given q .

The state determination of each element of the structural model is based on the free global dof displacements $\mathbf{U}_i^{(k)}$ at the iteration i of load step k of the solution strategy for the multi-step incremental analysis. It consists of the following operations:

- 1) Determine the element deformation v based on linear or nonlinear kinematics. For linear kinematics use $v = \mathbf{a}_g \mathbf{u}$, for nonlinear Green-Lagrange kinematics use (2.9) for the plane truss or (2.10) for the space truss.
- 2) Determine the basic force q for the deformation v through the iterative solution algorithm of (6.17)

$$v_{u,j-1} - f_{j-1} \Delta q_{j-1} = 0 \quad \text{with} \quad \Delta q_{j-1} = q_j - q_{j-1} \quad \text{and} \quad f = \frac{dv_r}{dq} = \frac{L}{2} \sum_{nIP} \frac{w_m}{E_m A_m}$$

where the iteration counter is denoted with j to distinguish it from the load step counter k and the iteration counter i for the structure equilibrium equations in load step k . $j = 1 \dots$ until convergence.

- a. For the basic element force q_j use the stress σ_m at each integration point to determine the corresponding strain ε_m through the iterative solution algorithm of (6.18)

$$\sigma_{u,l-1} - E_{t,l-1} \Delta\varepsilon_{l-1} = 0 \quad \text{with} \quad \Delta\varepsilon_l = \varepsilon_l - \varepsilon_{l-1} \quad \text{and} \quad E_t = \frac{d\hat{\sigma}}{d\varepsilon}$$

noting that the function of the stress error is

$$\sigma_u = \sigma_m - \sigma_r(\varepsilon_m) \quad \text{with} \quad \sigma_m = \frac{q}{A_m}$$

at integration point m . The iteration counter for the solution of the nonlinear stress-strain relation for given σ is denoted with l in order to distinguish it from the iteration counter j for the element state determination, and i for the structure state determination within load step k . $l = 1 \dots$ until convergence.

- b. After establishing ε_{mj} at each integration point m with the iterative solution process of the preceding step determine the element deformation v_{rj} for iteration j with

$$v_{rj} = \frac{1}{2L} \sum_{nIP} w_m \varepsilon_{mj}$$

and the element flexibility f_j with

$$f_j = \frac{L}{2} \sum_{nIP} \frac{w_m}{E_{mj} A_m}$$

and return with $v_{uj} = v - v_{rj}$ to step (2) for determining Δq_j with

$$\Delta q_j = \frac{v_{uj}}{f_j}$$

updating q with $q_{j+1} = q_j + \Delta q_j$ and repeating steps (a) and (b) for q_{j+1} until convergence.

- 3) Upon convergence of the iterative solution algorithm with counter j invert the element flexibility f to get the stiffness k .
- 4) Transform the basic element force q and stiffness k to the global reference system under nonlinear geometry

$$\begin{aligned} p &= \mathbf{a}_g^T q \\ \mathbf{k}_e &= \mathbf{a}_g^T k \mathbf{a}_g + \mathbf{k}_g \end{aligned}$$

according to (3.44), (3.45), and (3.47) for the Green-Lagrange truss element. For linear geometry the transformation matrix \mathbf{a}_g is related to the direction cosines of the undeformed element x -axis and the geometric stiffness matrix \mathbf{k}_g is zero.

It is clear from the above description of the element state determination algorithm for the force formulation that it is much more computationally onerous than the state determination algorithm for the displacement formulation with two nested iterative solutions for each iteration i of the structure state determination algorithm for the solution of global equilibrium equations that is common to both. The significant benefit of the force formulation derives from the fact that the element equilibrium is satisfied in a strict sense in the undeformed basic element configuration, so that the subdivision of a truss member with variable cross section and nonlinear material into several elements is not required for accuracy. The accuracy of the formulation is governed only by the number of integration points for the evaluation of the integrals for the element deformation and the element flexibility. Consequently, a significant portion of the computational cost deficit of the force formulation relative to the displacement formulation is recovered from the use of a single element for each truss member. A more important benefit of the force formulation lies in its numerical robustness under strength softening and under unloading following a load reversal.

6.2.3 Parallel Spring Model

It is possible to combine several springs either in parallel, or in series, or in a combination of the two to create composite material or truss element models. In the following we discuss the parallel spring model first and then the series spring model. In the process we reveal the complete analogy between the parallel spring model and the displacement formulation on the one hand and the series spring model and the force formulation on the other.

6.2.3.1 Description

Fig. 6.3 shows a parallel spring model with three components. For the sake of simplicity we assume that each component has unit area A and unit length L , so that the spring force-deformation relation can be thought of either as a stress σ -strain ε relation or as a basic element force q -deformation v relation. We present the parallel spring model in terms of the latter, but it is straightforward to switch to the more general description of the springs representing the stress-strain relation of a material that can then be scaled up by the area A and scaled down by the element length L .

The parallel model is governed by the kinematic relation between the component deformations and the deformation of the spring assembly. For the simple model in Fig. 6.3 each component deformation is equal with the deformation of the assembly so that

$$v = v_a = v_b = v_c$$

with each component denoted with a letter subscript.

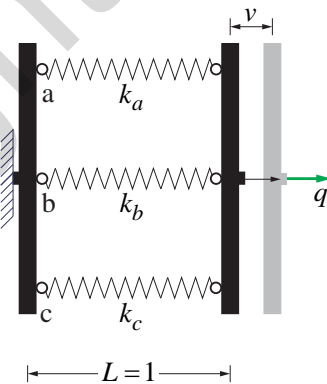


Fig. 6.3: Parallel spring model with three components

The kinematic relation can be written in matrix form, which points the way of generalizing the model for the case that each component deformation is related to the deformation of the assembly with a constant

$$\begin{pmatrix} v_a \\ v_b \\ v_c \end{pmatrix} = \begin{pmatrix} 1 \\ 1 \\ 1 \end{pmatrix} v = \mathbf{a}_v v$$

The static relation of the assembly is established with the principle of virtual work

$$q = \mathbf{a}_v^T \begin{pmatrix} q_a \\ q_b \\ q_c \end{pmatrix} = q_a + q_b + q_c$$

It is clear from Fig. 6.3 that for the simple arrangement in hand the basic force q of the assembly is simply the sum of the component forces.

The stiffness k of the assembly is the derivative of the basic force with respect to the assembly deformation. It is

$$k = \frac{dq}{dv} = \frac{dq_a}{dv_a} \frac{dv_a}{dv} + \frac{dq_b}{dv_b} \frac{dv_b}{dv} + \frac{dq_c}{dv_c} \frac{dv_c}{dv} = k_a + k_b + k_c$$

The stiffness of the parallel spring model can be written in matrix form as

$$k = \mathbf{a}_v^T \begin{bmatrix} \frac{dq_a}{dv_a} & 0 & 0 \\ 0 & \frac{dq_b}{dv_b} & 0 \\ 0 & 0 & \frac{dq_c}{dv_c} \end{bmatrix} \mathbf{a}_v = \mathbf{a}_v^T \begin{bmatrix} k_a & 0 & 0 \\ 0 & k_b & 0 \\ 0 & 0 & k_c \end{bmatrix} \mathbf{a}_v$$

In this form we recognize the analogy between the parallel spring model stiffness k and the structure stiffness matrix \mathbf{K} in the form $\mathbf{A}_f^T \mathbf{K}_s \mathbf{A}_f$. In fact, *any system whose response is based on a kinematic assumption about its component deformations constitutes a parallel model*. The most prominent case is the structural model, which constitutes a parallel spring model of its elements. Another important case is the cross section of a structural member. Under plane section kinematics the section is a parallel spring model of its fibers or material points.

6.2.3.2 State Determination

The state determination of the parallel spring model involves the determination of the resisting force q and the assembly stiffness k for given element deformation v and is practically the same as the state determination for the displacement formulation of the basic truss element. Nonetheless, we restate the complete process in the following for the sake of completeness.

At the outset of the element state determination the free global dof displacements $\mathbf{U}_i^{(k)}$ at the iteration i of load step k of the solution strategy for the multi-step incremental analysis are given. On this basis the state determination involves the following steps:

- 1) Determine the element deformation v based on linear or nonlinear kinematics. For linear kinematics use $v = \mathbf{a}_g \mathbf{u}$, for nonlinear Green-Lagrange kinematics use (2.9) for the plane truss or (2.10) for the space truss.
- 2) Determine the deformation v_m of each component m with $v_m = \mathbf{a}_{v_m} v$.
- 3) The state determination of each component m gives the force q_m and tangent stiffness k_m for the given deformation v_m , where

$$k_m = \frac{d\hat{q}_m}{dv_m}$$

with $q_m = \hat{q}(v_m)$ representing the nonlinear force-deformation relation of spring m .

- 4) Determine the basic force q and the stiffness k of the parallel model by summation of its component forces and stiffnesses according to

$$\begin{aligned} q &= \sum_m \mathbf{a}_{v_m}^T q_m \\ k &= \sum_m \mathbf{a}_{v_m}^T k_m \mathbf{a}_{v_m} \end{aligned} \quad (6.19)$$

- 5) Transform the basic element force q and stiffness k to the global reference system under nonlinear geometry

$$\begin{aligned} \mathbf{p} &= \mathbf{a}_g^T q \\ \mathbf{k}_e &= \mathbf{a}_g^T k \mathbf{a}_g + \mathbf{k}_g \end{aligned}$$

according to (3.44), (3.45), and (3.47) for the Green-Lagrange truss element. For linear geometry the transformation matrix \mathbf{a}_g is related to the direction cosines of the undeformed element x -axis and the geometric stiffness matrix \mathbf{k}_g is zero.

We note the complete analogy of (6.19) with (6.4) after setting $q_m = \sigma_m A_m$ and $k_m = \frac{E_m A_m}{L}$ and noting that the integration weights w_m are equal to 2 for the single midpoint integration of the parallel spring model in the interval $-1 \leq \xi \leq 1$. We, therefore, conclude that the displacement formulation is analogous to a parallel spring model with the stress-strain relation at each integration point m corresponding to a nonlinear spring of the parallel spring model.

6.2.4 Series Spring Model

The springs can also be arranged in series to give a model with different behavior than that of the parallel spring model. The series model plays a very important role in the description of the force-deformation relation of truss and beam elements with nonlinear material response, but has not been given the deserved attention in the literature because of the relative complexity of its state determination. In the following we describe the model for a simple spring arrangement and then discuss its state determination.

6.2.4.1 Description

Fig. 6.4 shows a series spring model with three components. For the sake of simplicity we assume that each component has unit area A and unit length L , so that the spring force-deformation relation can be thought of either as a stress σ -strain ε relation or as a basic element force q -deformation v relation. We present the series spring model in terms of the latter, but it is straightforward to switch to the more general description of the springs representing the stress-strain relation of a material that can then be scaled up by the area A and scaled down by the element length L .

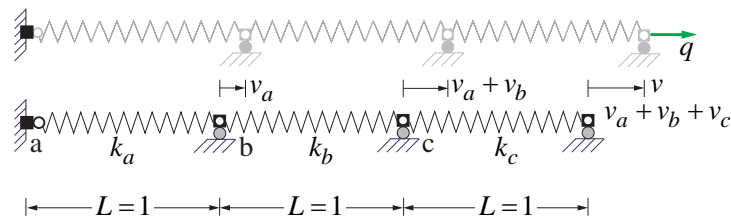


Fig. 6.4: Series spring model with three components

The series spring model is governed by the static relation between the component forces and the force of the spring assembly. For the simple model in Fig. 6.4 each component force is equal with the force of the assembly so that

$$q = q_a = q_b = q_c$$

The static relation can be written in matrix form, which points the way of generalizing the model for the case that each component force is related to the force of the assembly with a constant

$$\begin{pmatrix} q_a \\ q_b \\ q_c \end{pmatrix} = \begin{pmatrix} 1 \\ 1 \\ 1 \end{pmatrix} q = \mathbf{b}_v q$$

The principle of complementary virtual work gives the kinematic relation of the assembly as

$$v = \mathbf{b}_v^T \begin{pmatrix} v_a \\ v_b \\ v_c \end{pmatrix} = v_a + v_b + v_c$$

It is clear that for the simple arrangement of the springs in series in Fig. 6.4 the deformation v of the assembly is simply the sum of the component deformations. The flexibility f of the spring assembly is the derivative of the deformation v with respect to the basic force q . It is

$$f = \frac{dv}{dq} = \frac{dv_a}{dq_a} \frac{dq_a}{dq} + \frac{dv_b}{dq_b} \frac{dq_b}{dq} + \frac{dv_c}{dq_c} \frac{dq_c}{dq} = \frac{dv_a}{dq_a} + \frac{dv_b}{dq_b} + \frac{dv_c}{dq_c}$$

The flexibility of the series spring model can be written in matrix form as

$$f = \mathbf{b}_v^T \begin{bmatrix} \frac{dv_a}{dq_a} & 0 & 0 \\ 0 & \frac{dv_b}{dq_b} & 0 \\ 0 & 0 & \frac{dv_c}{dq_c} \end{bmatrix} \mathbf{b}_v$$

We note, however, that the spring force-deformation relation is only available in the form

$$q_m = \hat{q}(v_m)$$

so that the component flexibility f_m can only be established as the inverse of the component stiffness k_m

$$k_m = \frac{d\hat{q}(v_m)}{dv_m}$$

Consequently, the flexibility of the series spring model is

$$f = \mathbf{b}_v^T \begin{bmatrix} \frac{1}{k_a} & 0 & 0 \\ 0 & \frac{1}{k_b} & 0 \\ 0 & 0 & \frac{1}{k_c} \end{bmatrix} \mathbf{b}_v$$

which for the simple arrangement of the series in hand becomes

$$f = \frac{1}{k_a} + \frac{1}{k_b} + \frac{1}{k_c}$$

With the notation $f_m = \frac{1}{k_m}$ for each spring m we can write the flexibility matrix of the series model in the form

$$f = \mathbf{b}_v^T \begin{bmatrix} f_a & 0 & 0 \\ 0 & f_b & 0 \\ 0 & 0 & f_c \end{bmatrix} \mathbf{b}_v = f_a + f_b + f_c \quad (6.20)$$

In this form we recognize the analogy between the series spring model flexibility f and the structure flexibility matrix \mathbf{F} in the form $\bar{\mathbf{B}}^T \mathbf{F}_s \bar{\mathbf{B}}$. Because of the difficulty of establishing the force influence matrix $\bar{\mathbf{B}}$ for statically indeterminate structures, it is better to limit the analogy of the series spring model with a statically determinate structure for which the force influence matrix $\bar{\mathbf{B}}$ is readily available. The same is true for elements for which the relation between the internal forces $s(x)$ and the basic element forces \mathbf{q} can be readily established from the satisfaction of the element equilibrium. This is the case with all truss and frame elements whose equilibrium is satisfied in the undeformed configuration, as is the case with the force formulation. In fact, the complete analogy of the flexibility f in (6.20) with the flexibility f in (6.13) after setting $f_m = \frac{L}{E_m A_m}$ should be noted. We need to set the integration weights w_m equal to $\frac{2}{3}$ in (6.13) for three midpoint integration in the interval $-1 \leq \xi \leq 1$ noting that the total element length is equal to $3L$.

6.2.4.2 State Determination

The state determination of the series spring model requires the determination of the resisting force q and the tangent stiffness k for given element deformation v and is almost identical to the state determination of the truss element with the force formulation. Nonetheless, we restate the complete process in the following for the sake of completeness.

- 1) Determine the element deformation v based on linear or nonlinear kinematics. For linear kinematics use $v = \mathbf{a}_g \mathbf{u}$, for nonlinear Green-Lagrange kinematics use (2.9) for the plane truss or (2.10) for the space truss.
- 2) The determination of the basic force q for the given deformation v depends on the solution of the kinematic relation

$$v - (v_a + v_b + v_c) = v - v_r(q) = v_u(q) = 0$$

with the implicit dependence of the spring deformations v_m on q noted. This nonlinear relation is solved by *linearization* through truncation of the Taylor series expansion of v_u after the linear term

$$v_{u,j-1} - f_{j-1} \Delta q_{j-1} = 0 \quad \text{with} \quad \Delta q_{j-1} = q_j - q_{j-1} \quad \text{and} \quad f = \frac{dv_r}{dq} = f_a + f_b + f_c$$

with the iteration counter j distinct from the load step counter k and the iteration counter i for the structure equilibrium equations within load step k . $j = 1 \dots$ until convergence.

- a. For the basic element force q_j use the spring force $q_m = q_j$ to determine the deformation v_m of each spring m through the solution of the nonlinear equation

$$q_{m,u} = q_m - \hat{q}(v_m) = 0$$

This nonlinear relation is solved by *linearization* through truncation of the Taylor series expansion of $q_{m,u}$ after the linear term

$$q_{m,l-1} - k_{m,l-1} \Delta v_{m,l-1} = 0 \quad \text{with} \quad \Delta v_{m,l-1} = v_{m,l} - v_{m,l-1} \quad \text{and} \quad k_m = \frac{d\hat{q}(v_m)}{dv_m}$$

The iteration counter l for the solution of the nonlinear spring force-deformation relation for given q_m is distinct from the iteration counter j for the element state determination, and the iteration counter i for the structure state determination within load step k . $l = 1 \dots$ until convergence.

- b. After establishing v_{mj} for each spring m with the iterative solution process of the preceding step determine the element deformation $v_{r,j}$ for iteration j with

$$v_{r,j} = v_{a,j} + v_{b,j} + v_{c,j}$$

and the element flexibility f_j with

$$f_j = f_{a,j} + f_{b,j} + f_{c,j} \quad \text{with} \quad f_m = \frac{1}{k_m}$$

and return with $v_{u,j} = v - v_{r,j}$ to step (2) for determining Δq_j with

$$\Delta q_j = \frac{v_{u,j}}{f_j}$$

updating q with $q_{j+1} = q_j + \Delta q_j$ and repeating steps (a) and (b) for q_{j+1} until convergence.

- 3) Upon convergence of the iterative solution algorithm with counter j invert the element flexibility f to get the stiffness k .
- 4) Transform the basic element force q and stiffness k to the global reference system under nonlinear geometry

$$\mathbf{p} = \mathbf{a}_g^T q$$

$$\mathbf{k}_e = \mathbf{a}_g^T k \mathbf{a}_g + \mathbf{k}_g$$

according to (3.44), (3.45), and (3.47) for the Green-Lagrange truss element. For linear geometry the transformation matrix \mathbf{a}_g is related to the direction cosines of the undeformed element x -axis and the geometric stiffness matrix \mathbf{k}_g is zero.

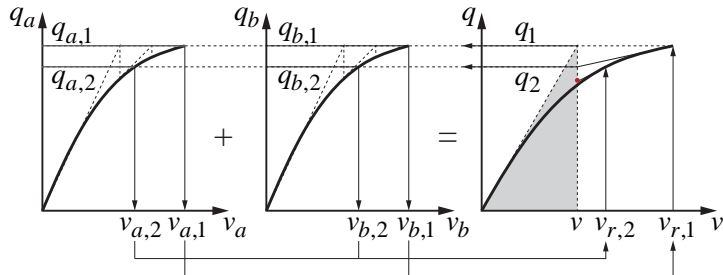


Fig. 6.5: Schematic depiction of two iterations j for the state determination of a series spring model with two components

We conclude that the state determination of the series spring model requires two nested iterations: the outer iteration with counter j is for the kinematic relation $v - v_r(q) = 0$ with independent variable the basic force q , and the inner iteration with counter l is for the spring constitutive force-deformation relation $q_m - \hat{q}(v_m) = 0$ with independent variable the spring deformation v_m . It turns out that we can perform these iterations simultaneously by concurrently solving both governing nonlinear equations, but this is not pursued further in the following.

The nested iterative process for the determination of the basic force q of the series spring model is shown schematically in Fig. 6.5 for the first two iterations j of a series spring model with two components.

Example 6.2 Nonlinear Truss with Series Material

The simple truss in Fig. 6.6 is subjected to a horizontal and a vertical force with reference value of 20 units each. All truss elements have area $A = 1$. The elements a and c consist of a bilinear elastic material with initial modulus $E_1 = 10,000$, yield strength $f_{y1} = 10$, and hardening modulus $E_{h1} = 2,000$. The yield strain of this material is $\varepsilon_{y1} = 1 \cdot 10^{-3}$. The element b consists of a composite material whose stress-strain response can be represented with two nonlinear springs b_1 and b_2 in series, as Fig. 6.8 shows. Both springs of the series material model have initial modulus $E_2 = 50,000$, and hardening modulus $E_{h2} = 5,000$. The yield strength of spring b_1 is $f_y^{(b_1)} = 10$, and that of spring b_2 is $f_y^{(b_2)} = 20$.

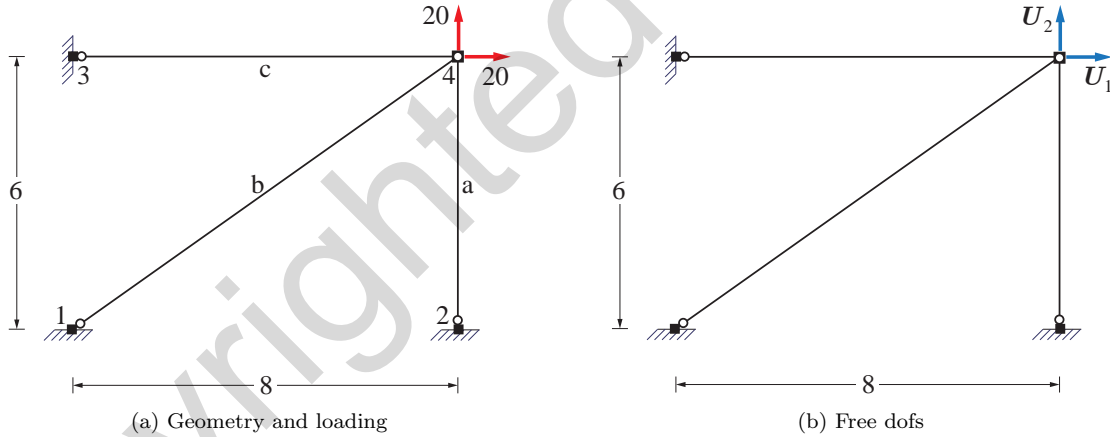


Fig. 6.6: Simple truss with nonlinear series material

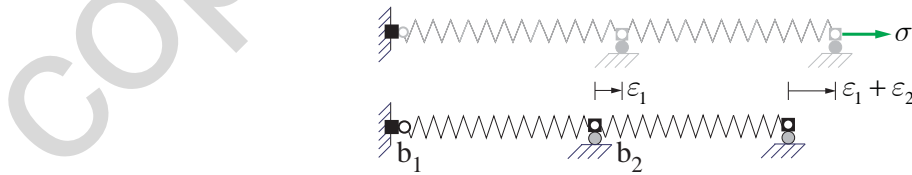


Fig. 6.7: Two spring in series material model for truss element b

It is required to determine the free global dof displacements of the truss under the load factor $\lambda = 1.2$.

We assume that the given reference load is applied in a single load step with $\Delta\lambda_0 = 1.2$. Because the truss geometry is identical with that of Example 6.1 we use the truss stiffness matrix in (6.6), the global

equilibrium error in (6.7), and the kinematic relations in (6.8) for the solution. With the initial guess

$$\mathbf{U}_0 = \begin{pmatrix} U_{1,0} \\ U_{2,0} \end{pmatrix} = \begin{pmatrix} 0 \\ 0 \end{pmatrix}$$

we determine the initial truss stiffness with (6.6). For this we need the initial material modulus of the elements a, b and c. For elements a and c the initial modulus is $E_a = E_c = E_1$. For element b, consisting of a two component series spring material model, with initial spring modulus E_2 we have

$$E_b = \frac{1}{\frac{1}{E_2} + \frac{1}{E_2}} = \frac{1}{\frac{1}{50,000} + \frac{1}{50,000}} = 25,000$$

The initial truss stiffness matrix \mathbf{K}_0 is

$$\mathbf{K}_0 = \begin{bmatrix} \frac{E_c A}{L_c} + \left(\frac{8}{L_b}\right)^2 \frac{E_b A}{L_b} & \left(\frac{8}{L_b}\right) \left(\frac{6}{L_b}\right) \frac{E_b A}{L_b} \\ \left(\frac{8}{L_b}\right) \left(\frac{6}{L_b}\right) \frac{E_b A}{L_b} & \frac{E_a A}{L_a} + \left(\frac{6}{L_b}\right)^2 \frac{E_b A}{L_b} \end{bmatrix} = \begin{bmatrix} 2850 & 1200 \\ 1200 & 2566.67 \end{bmatrix}$$

Under the applied nodal forces

$$\mathbf{P}_f = \lambda \mathbf{P}_{ref} = \begin{pmatrix} 24 \\ 24 \end{pmatrix}$$

the displacement correction $\Delta \mathbf{U}_0$ is

$$\Delta \mathbf{U}_0 = \begin{pmatrix} \Delta U_{1,0} \\ \Delta U_{2,0} \end{pmatrix} = \mathbf{K}_0 \backslash \mathbf{P}_u(\mathbf{U}_0) = \begin{pmatrix} 5.583 \\ 6.740 \end{pmatrix} 10^{-3}$$

noting that

$$\mathbf{P}_u(\mathbf{U}_0) = \mathbf{P}_f - \mathbf{P}_r(\mathbf{U}_0) = \begin{pmatrix} 24 \\ 24 \end{pmatrix} - \begin{pmatrix} 0 \\ 0 \end{pmatrix} = \begin{pmatrix} 24 \\ 24 \end{pmatrix}$$

Consequently, the free global dof displacements at the end of load incrementation are

$$\mathbf{U}_1 = \begin{pmatrix} U_{1,1} \\ U_{2,1} \end{pmatrix} = \mathbf{U}_0 + \Delta \mathbf{U}_0 = \begin{pmatrix} 5.583 \\ 6.740 \end{pmatrix} 10^{-3}$$

We now embark on the determination of the resisting forces \mathbf{P}_r and the tangent truss stiffness matrix for \mathbf{U}_1 . To this end we follow the procedure of Example 6.1 with the caveat that the state determination of the element b is a bit more involved than that for the elements a and c.

1) Element a

$$v_a = \mathbf{U}_{2,1}$$

$$\varepsilon = \frac{v_a}{L_a} = 1.123 \cdot 10^{-3} \rightarrow \text{yielding} \rightarrow \sigma = f_{y1} + E_{h1} (\varepsilon - \varepsilon_{y1}) = 10.247 \quad E_a = E_{h1}$$

$$q_a = \sigma A = 10.247 \quad k_a = \frac{E_a A}{L_a}$$

2) Element c

$$v_c = \mathbf{U}_{1,1}$$

$$\begin{aligned}\varepsilon &= \frac{v_c}{L_c} = 0.698 \cdot 10^{-3} \rightarrow \text{not yielding} \quad \sigma = E_1 \varepsilon = 6.979 \quad E_c = E_1 \\ q_c &= \sigma A = 6.979 \quad k_c = \frac{E_c A}{L_c}\end{aligned}$$

3) **Element b**

$$v_b = 0.8\mathbf{U}_{1,1} + 0.6\mathbf{U}_{2,1}$$

$$\varepsilon_b = \frac{v_b}{L_b} = 0.851 \cdot 10^{-3}$$

Because the material model of element b consists of two springs in series, it is not possible to directly determine the stress σ and tangent modulus E_t of the material. Instead, the iterative state determination of the series spring model is required noting that in the following ε replaces v , E replaces k and σ replaces q in the algorithm of Section 6.2.4.2. Moreover, the spring response variables are identified with number, with 1 referring to spring b_1 and 2 referring to spring b_2 . The steps of the state determination algorithm are:

- a. Assume $\sigma_0 = 0$ and determine the initial stiffness $E_{b,0}$ of the series model

$$E_{b,0} = \frac{1}{\frac{1}{E_2} + \frac{1}{E_2}} = \frac{1}{\frac{1}{50,000} + \frac{1}{50,000}} = 25,000$$

- b. Determine the stress correction $\Delta\sigma_0$ from the equation

$$\varepsilon_{u,0} - \frac{1}{E_{b,0}} \Delta\sigma_0 = 0 \rightarrow \Delta\sigma_0 = E_{b,0} \varepsilon_{u,0} = 21.277$$

Noting that with $\varepsilon_{r,0} = 0$, $\varepsilon_{u,0} = \varepsilon = 0.851 \cdot 10^{-3}$. We update the stress $\sigma_1 = \sigma_0 + \Delta\sigma_0 = 21.277$.

- c. We conclude that both components of the series material model are yielding under the stress σ_1 . Because the material of the components is bilinear, *an iteration is not required for the determination of the component strains under this stress*. Instead we can directly determine these from the corresponding linear branch to get

$$\begin{aligned}\varepsilon_{1,1} &= \frac{f_y^{b_1}}{E_2} + \frac{\sigma_1 - f_y^{b_1}}{E_{h2}} = 2.455 \cdot 10^{-3} \\ \varepsilon_{2,1} &= \frac{f_y^{b_2}}{E_2} + \frac{\sigma_1 - f_y^{b_2}}{E_{h2}} = 0.655 \cdot 10^{-3}\end{aligned}$$

- d. Determine the strain $\varepsilon_{r,1}$ of the series model under the stress σ_1

$$\varepsilon_{r_1} = \varepsilon_{1,1} + \varepsilon_{2,1} = 3.111 \cdot 10^{-3}$$

- e. Determine the strain error

$$\varepsilon_{u,1} = \varepsilon - \varepsilon_{r,1} = 0.851 \cdot 10^{-3} - 3.111 \cdot 10^{-3} = -2.26 \cdot 10^{-3}$$

and the stiffness $E_{b,1}$ of the series material model

$$E_{b,1} = \frac{1}{\frac{1}{E_{h2}} + \frac{1}{E_{h2}}} = \frac{1}{\frac{1}{5,000} + \frac{1}{5,000}} = 2,500$$

- f. Determine the stress correction $\Delta\sigma_1$ from the equation

$$\varepsilon_{u,1} - \frac{1}{E_{b,1}} \Delta\sigma_1 = 0 \quad \rightarrow \quad \Delta\sigma_1 = E_{b,1} \varepsilon_{u,1} = -5.649$$

and update the stress $\sigma_2 = \sigma_1 + \Delta\sigma_1 = 15.628$.

- g. We conclude that only the first component of the series material model is yielding under the stress σ_2 . We determine the corresponding strain for both components

$$\begin{aligned}\varepsilon_{1,2} &= \frac{f_y^{b_1}}{E_2} + \frac{\sigma_2 - f_y^{b_1}}{E_{h2}} = 1.326 \cdot 10^{-3} \\ \varepsilon_{2,2} &= \frac{\sigma_2}{E_2} = 0.313 \cdot 10^{-3}\end{aligned}$$

- h. Determine the strain $\varepsilon_{r,2}$ of the series model under the stress σ_2

$$\varepsilon_{r_2} = \varepsilon_{1,2} + \varepsilon_{2,2} = 1.638 \cdot 10^{-3}$$

- i. Determine the strain error

$$\varepsilon_{u,2} = \varepsilon - \varepsilon_{r,2} = 0.851 \cdot 10^{-3} - 1.638 \cdot 10^{-3} = -0.787 \cdot 10^{-3}$$

and the stiffness $E_{b,2}$ of the series material model

$$E_{b,2} = \frac{1}{\frac{1}{E_{h2}} + \frac{1}{E_2}} = \frac{1}{\frac{1}{5,000} + \frac{1}{50,000}} = 4,545.45$$

- j. Determine the stress correction $\Delta\sigma_2$ from the equation

$$\varepsilon_{u,2} - \frac{1}{E_{b,2}} \Delta\sigma_2 = 0 \quad \rightarrow \quad \Delta\sigma_2 = E_{b,2} \varepsilon_{u,2} = -3.577$$

and update the stress $\sigma_3 = \sigma_2 + \Delta\sigma_2 = 12.05$.

- k. We conclude that only the first component of the series material model is yielding under the stress σ_3 . Because the state of both spring components did not change relative to the preceding iteration, the process has converged, and the subsequent steps are not necessary. Nonetheless, we include them for the sake of completeness. The strain of each component of the series material model under σ_3 is

$$\begin{aligned}\varepsilon_{1,3} &= \frac{f_y^{b_1}}{E_2} + \frac{\sigma_3 - f_y^{b_1}}{E_{h2}} = 0.610 \cdot 10^{-3} \\ \varepsilon_{2,3} &= \frac{\sigma_3}{E_2} = 0.241 \cdot 10^{-3}\end{aligned}$$

- l. Determine the strain $\varepsilon_{r,3}$ of the series model under the stress σ_3

$$\varepsilon_{r_3} = \varepsilon_{1,3} + \varepsilon_{2,3} = 0.851 \cdot 10^{-3}$$

- m. Determine the strain error

$$\varepsilon_{u,3} = \varepsilon - \varepsilon_{r,3} = 0.851 \cdot 10^{-3} - 0.851 \cdot 10^{-3} = 0 \cdot 10^{-3}$$

n. The final stress and tangent modulus of element b are: $\sigma = 12.05$ and $E_b = 4,545.45$

With these values the basic force q_b and stiffness k_b of the element b are

$$q_b = \sigma A = 12.05 \quad k_b = \frac{E_b A}{L_b}$$

This completes the process of the element state determination for the free global dof displacements \mathbf{U}_1 .

For the structure equilibrium error we determine the resisting forces $\mathbf{P}_r(\mathbf{U}_1)$ with $\mathbf{A}_f^T \mathbf{Q}$ to get

$$\mathbf{P}_u(\mathbf{U}_1) = \mathbf{P}_f - \mathbf{P}_r(\mathbf{U}_1) = \begin{pmatrix} 24 \\ 24 \end{pmatrix} - \begin{pmatrix} 16.619 \\ 17.477 \end{pmatrix} = \begin{pmatrix} 7.381 \\ 6.523 \end{pmatrix}$$

The tangent truss stiffness matrix \mathbf{K}_1 is

$$\mathbf{K}_1 = \begin{bmatrix} \frac{E_c A}{L_c} + \left(\frac{8}{L_b} \right)^2 \frac{E_b A}{L_b} & \left(\frac{8}{L_b} \right) \left(\frac{6}{L_b} \right) \frac{E_b A}{L_b} \\ \left(\frac{8}{L_b} \right) \left(\frac{6}{L_b} \right) \frac{E_b A}{L_b} & \frac{E_a A}{L_a} + \left(\frac{6}{L_b} \right)^2 \frac{E_b A}{L_b} \end{bmatrix} = \begin{bmatrix} 1540.9 & 218.2 \\ 218.2 & 497 \end{bmatrix}$$

and the displacement correction $\Delta\mathbf{U}_1$ is

$$\Delta\mathbf{U}_1 = \mathbf{K}_1 \setminus \mathbf{P}_u(\mathbf{U}_1) = \begin{pmatrix} 3.126 \\ 11.753 \end{pmatrix} 10^{-3}$$

The free global dof displacement estimate becomes

$$\mathbf{U}_2 = \mathbf{U}_1 + \Delta\mathbf{U}_1 = \begin{pmatrix} 5.583 \\ 6.740 \end{pmatrix} 10^{-3} + \begin{pmatrix} 3.126 \\ 11.753 \end{pmatrix} 10^{-3} = \begin{pmatrix} 8.709 \\ 18.484 \end{pmatrix} 10^{-3}$$

For the determination of the resisting forces \mathbf{P}_r and the tangent truss stiffness matrix for \mathbf{U}_2 we need to repeat the earlier state determination process for the three truss elements, but we refrain from such undertaking, because it does not add anything further to the understanding of the example. Clearly, the process needs to be repeated until the norm of the structure equilibrium error \mathbf{P}_u is smaller than a specified tolerance. Because the material response of the truss elements is bilinear for the problem in hand, the process converges to the exact solution after two more iterations. The final answer for the free global dof displacements is

$$\mathbf{U} = \begin{pmatrix} 10.301 \\ 17.795 \end{pmatrix} 10^{-3}$$

6.2.5 Applications

The parallel spring model is used for describing perfectly plastic or strain hardening, multi-linear material stress-strain relations. Noting that the stress of the assembly is *the sum of the component stresses* and the stiffness is *the sum of the component stiffnesses* it is easy to calibrate several bilinear

springs to obtain a multi-linear stress-strain relation, as Fig. 6.8 shows. Alternatively, several bilinear truss elements can be connected to the same two nodes to give a multi-linear force-deformation response.

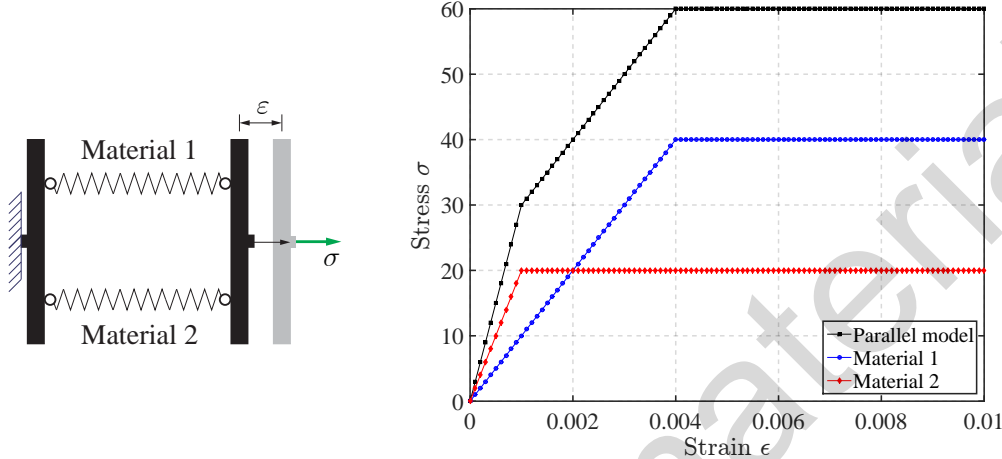


Fig. 6.8: Trilinear stress-strain relation by combination of bilinear models in parallel

The parallel model in Fig. 6.8 consists of two linear elastic, perfectly plastic materials with the following properties: $f_{y1} = 40$, $E_1 = 10,000$, $f_{y2} = 20$, $E_2 = 20,000$. For the calibration of the trilinear stress-strain relation in Fig. 6.8 it is worth noting that the initial stiffness of the stronger material is equal to the second stiffness of the target trilinear stress-strain relation, *because the weaker material does not add to the stiffness of the parallel model past its yield strength*.

The series model is used for the representation of multi-linear stress-strain relations that are characterized by fracturing or "pinching".

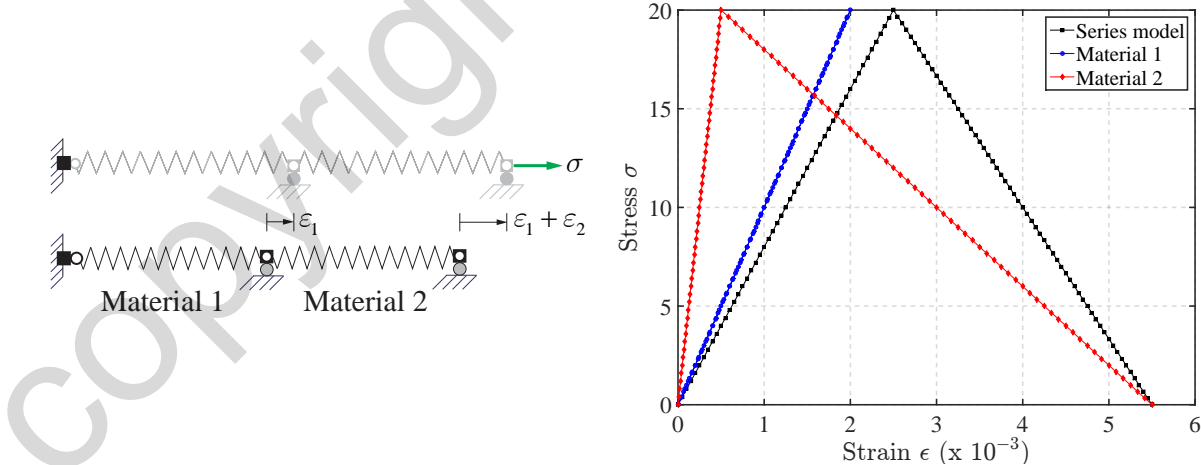


Fig. 6.9: Trilinear stress-strain relation with fracturing component through combination of bilinear models in series

Fig. 6.9 shows an example of a two component series material model with fracture of the weaker material component that is characterized by strength loss after reaching its tensile strength. The stronger material component in the series model in Fig. 6.9 is linear elastic, or, simply has tensile strength that is slightly higher than that of the fracturing component. For the case in Fig. 6.9 the material properties

of the bilinear components are: $f_{y1} = 30$, $E_1 = 10,000$, E_{h1} is irrelevant, $f_{y2} = 20$, $E_2 = 40,000$, $E_{h2} = -4,000$. Because the stress in each component of the series model is the same, the fracture of the weaker material prevents the stronger material from ever reaching its yield strength. The strength loss of the weaker material component under increasing deformation causes the stronger material component to unload. This is characteristic of the cracking process in brittle tension members when a crack forms at the weakest point of the element.

The strength softening slope of the series model depends on the relative stiffness of the elastic component with respect to the strength softening slope of the fracturing component. In fact, "snap-back" of the series model stress-strain relation during strength softening is possible when the elastic zone has higher flexibility (smaller stiffness) than the inverse of the slope of the fracturing component. This happens at the formation of the initial cracks in long, brittle, tensile members. For the two series spring model in Fig. 6.9 this happens for $E_{h2} < -10,000$. The state determination algorithm breaks down in this case and a special path-tracing iterative solution strategy is required.

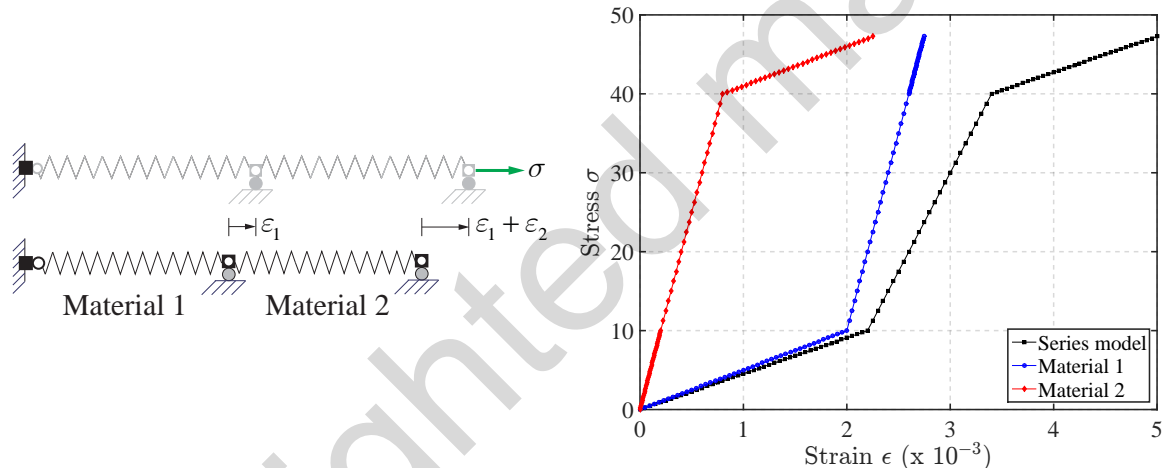


Fig. 6.10: Trilinear stress-strain relation with "pinching" through combination of bilinear models in series

The series model is also used for the stress-strain relation of a material that initially exhibits a soft response, but subsequently stiffens until reaching its yield strength, as Fig. 6.10 shows. The initial soft response is associated with slip or friction. In Fig. 6.10 the two components making up the series model have the same stiffness values, but the weaker component starts out with the small stiffness and then stiffens, while the stronger component starts out with the high stiffness and then softens. For the case in Fig. 6.10 the material properties of the bilinear components are: $f_{y1} = 10$, $E_1 = 5,000$, $E_{h1} = 50,000$, $f_{y2} = 40$, $E_2 = 50,000$, $E_{h2} = 5,000$. This type of force-deformation behavior arises in restraining cables for bridges or electrical substation equipment that are initially slack and then "engage" to prevent the bridge span or equipment from rolling off the support or toppling during a major ground excitation.

6.2.6 Conclusions

From the preceding discussion of the parallel and serial spring model and their state determination we reach the following conclusions:

- 1) The series model is more computationally intensive, since it requires two nested iteration loops for each value of the truss element deformation v .
- 2) Without any memory of the preceding step, the serial spring components start the iteration for their state determination from $v_m = 0$. This is a serious limitation requiring an ever increasing number of iterations for each component state determination as the imposed deformation v increases. This problem is easily resolved for path-dependent material behavior. For such behavior the material memory stores the last converged state.
- 3) Whereas the state determination of the parallel model works for perfectly-plastic component response, the state determination of the series model in Section 6.2.4.2 breaks down in this case, because perfectly plastic behavior implies infinite flexibility. It is possible to remedy the situation by modifying the state determination process, but it is often expedient to simply supply a small hardening or softening stiffness value for the series spring component instead of zero.

6.3 Beam Elements

6.3.1 Introduction

In a beam element with nonlinear material we concentrate on the description of the flexural response and neglect the axial response, either because the element is inextensible or because the axial response can be assumed to remain linear elastic and uncoupled from the flexural response. We deal with the coupling of the axial and the flexural response in the following chapter.

The force-deformation relation of a beam element with nonlinear material is complex, even in the absence of an axial force. In the following we use the bilinear approximation of the moment-curvature relation from Chapter 5 to derive the exact force-displacement response of a cantilever beam with bilinear moment-curvature and show that a bilinear approximation of this response is also possible, albeit with some limitations. With the force-displacement relation of a cantilever beam with bilinear moment-curvature as reference we proceed to develop a few simple beam element models of increasing complexity. Finally, we investigate the ability of these models to represent the nonlinear behavior of beams for the general case of a nonlinear moment-curvature relation under general bending moment distribution along the element.

6.3.2 Force-Displacement Response of Cantilever Beam

We turn our attention to the determination of the nonlinear force-displacement response of the homogeneous, prismatic cantilever beam of length L with a force P_v at its tip in Fig. 6.11. The beam has rectangular section of depth d and width b .

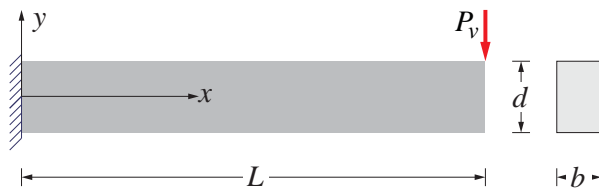


Fig. 6.11: Homogeneous, prismatic cantilever beam under tip load

This study is significant because the cantilever beam is used in experimental setups to represent the response of girders in multi-story frames under the assumption that the point of inflection under lateral loads lies at girder midspan.

The cantilever is a statically determinate structure for which the load-displacement response can be readily established, as will be shown in detail in the following.

It is first worth recalling the following general relations for the flexural element deformations $\mathbf{v}_{\varepsilon_2}$ and $\mathbf{v}_{\varepsilon_3}$ under the assumption of linear geometry in the basic system:

$$\begin{aligned}\mathbf{v}_{\varepsilon_2} &= - \int_0^L \left(1 - \frac{x}{L}\right) \kappa(x) dx \\ \mathbf{v}_{\varepsilon_3} &= \int_0^L \left(\frac{x}{L}\right) \kappa(x) dx\end{aligned}\tag{6.21}$$

For the statically determinate cantilever the force-displacement response can be established in the following way:

- 1) For any value of the tip load set up the linear moment distribution $M(x)$.
- 2) Determine the curvature distribution $\kappa(x)$ for $M(x)$ using the moment-curvature relation of the cross-section according to Chapter 5.
- 3) Integrate $\kappa(x)$ to determine the displacement U_{tip} at the cantilever tip with

$$U_{tip} = -\mathbf{v}_{\varepsilon_2} L = \int_0^L \kappa(x)(L-x) dx\tag{6.22}$$

Note that the deformation $\mathbf{v}_{\varepsilon_2}$ at the root of the cantilever is equal to $\frac{U_{tip}}{L}$, while the basic force \mathbf{q}_2 at the same location is equal to $P_v L$. Consequently, the cantilever tip force-displacement relation is equivalent to the basic force-deformation relation $\mathbf{q}_2 \cdot \mathbf{v}_2$ under anti-symmetric flexure after appropriate scaling.

We apply the process first to a linear elastic, perfectly plastic material for which the exact moment-curvature relation of a rectangular section is according to (5.40)

$$\begin{aligned}\text{for } \kappa \leq \kappa_y \quad \frac{M}{M_p} &= \frac{2}{3} \frac{\kappa}{\kappa_y} \\ \text{for } \kappa > \kappa_y \quad \frac{M}{M_p} &= \left[1 - \frac{1}{3} \left(\frac{\kappa_y}{\kappa}\right)^2\right]\end{aligned}$$

Once the moment at the root of the cantilever exceeds M_y the curvature $\kappa(x)$ in the zone where $M(x) \geq M_y$ needs to be determined from (5.40). Solving this equation for the curvature $\kappa(x)$ corresponding to a moment $M(x)$ gives the curvature distribution in the yield zone at the root of the cantilever

$$\kappa(x) = \frac{\kappa_y}{\sqrt{3}} \sqrt{\frac{M_p}{M_p - M(x)}}\tag{6.23}$$

which stretches over length L_y , as Fig. 6.12 shows. The length L_y is

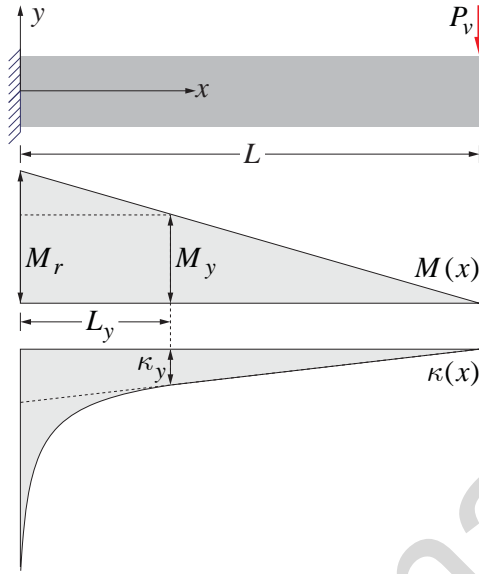


Fig. 6.12: Curvature distribution along cantilever under $M_r > M_y$ for linear elastic, perfectly plastic material response

$$L_y = L \left(1 - \frac{M_y}{M_r} \right) \quad (6.24)$$

where M_r is the moment at the root of the cantilever under the applied force P_v .

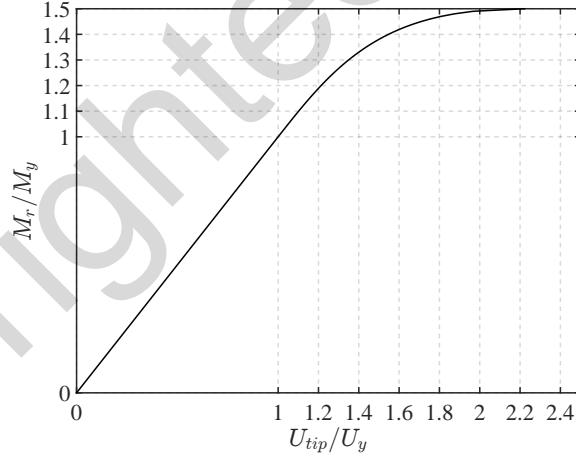


Fig. 6.13: Relation between moment M_r at the cantilever root and tip translation U_{tip}

With the curvature distribution $\kappa(x)$ we can determine the tip displacement with (6.22). For an analytical solution the integral is split in two integrals, one over the yield zone L_y for which the curvature is given by (6.23) and another over the zone from L_y to L with a linear curvature distribution.

The analytical solution in Fig. 6.13 can be found on pp. 90-93 of the book by Philip G. Hodge "Plastic Analysis of Structures" (McGraw Hill, 1959).

Fig. 6.15 shows the distribution of moments, curvatures, and transverse displacements of the cantilever beam along with the spread of the yield zone at the root of the cantilever. The distributions are shown for 6 load stages corresponding to a moment at the root of the cantilever equal to

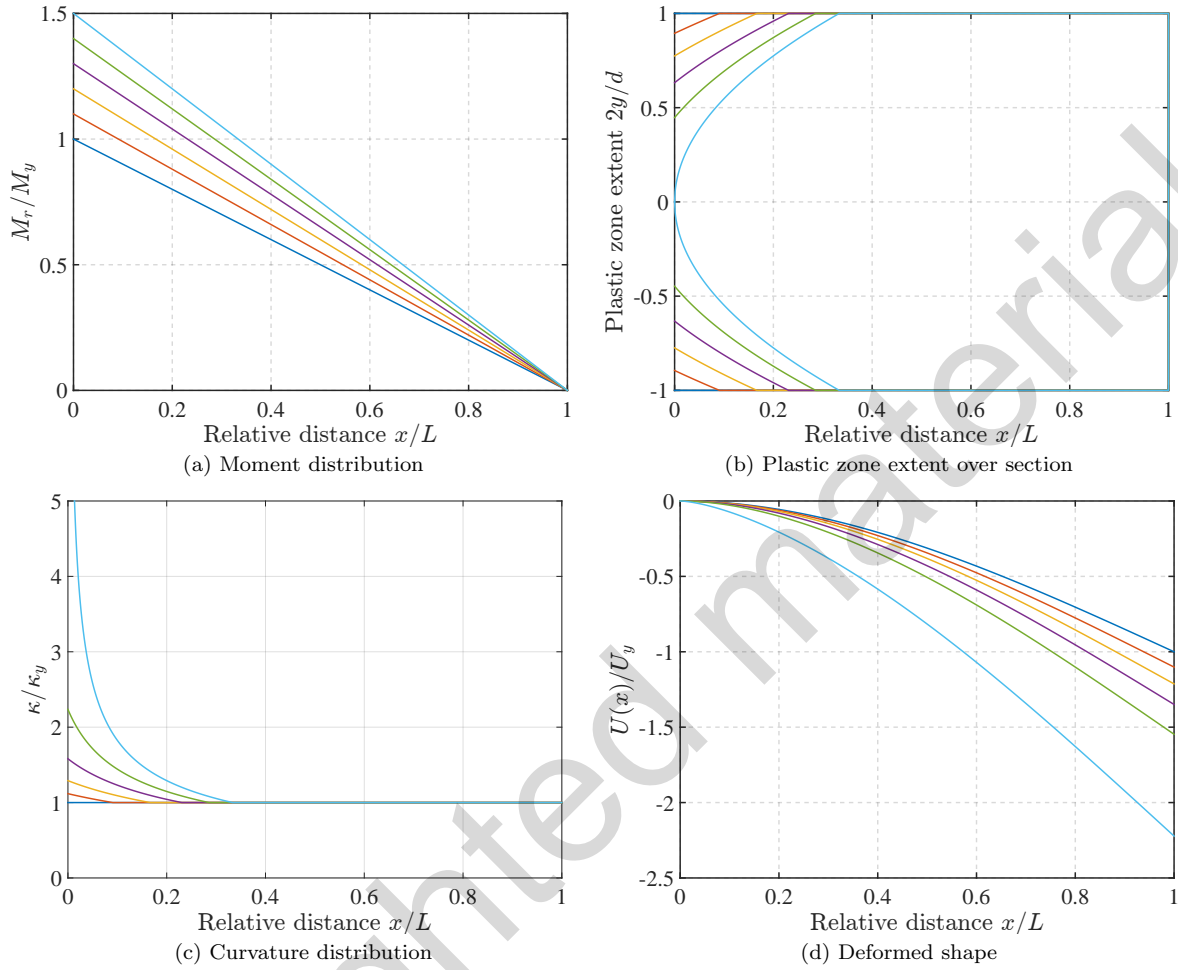


Fig. 6.14: Spread of yielding and deformed shape of cantilever under increasing tip load

$1.0, 1.1, 1.2, 1.3, 1.4$ and $1.5M_y$. All values are scaled with respect to the corresponding values at the initiation of yielding. The spread of the yield or plastic zone over the depth of the beam with increasing value of the applied force P_v are evident. The largest extent of the plastic zone is equal to $L/3$, as is evident from (6.24). This happens when the root moment reaches the plastic moment capacity M_p , at which instant a plastic hinge forms at the root section, as is clear from the infinite curvature in Fig. 6.15(c) and the deformed shape of the cantilever in Fig. 6.15(d).

We establish next the response of the cantilever beam in Fig. ?? for bilinear elastic hardening material.

Following the results in Fig. 5.22 and Fig. 5.23 we approximate the exact moment-curvature relation of the section with a bilinear curve with linear elastic slope EI up to the plastic moment capacity M_p , followed by a linear hardening branch with slope βEI , where β is the ratio between the hardening modulus E_h and the elastic modulus E of the material. The results in Fig. 5.22 for a rectangular section and in Fig. 5.23 for a wide flange section show that this approximation is very accurate, particularly for curvature ductility values greater than 4.

Fig. ?? shows the moment and curvature distribution of the cantilever beam with bilinear elastic hardening material for the case that the bending moment at the root of the cantilever exceeds the plastic

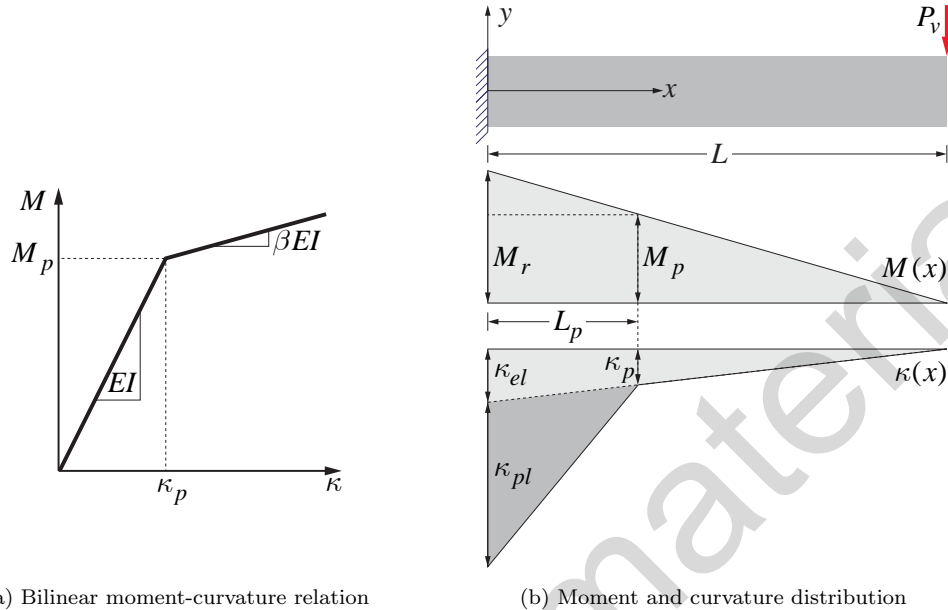


Fig. 6.15: Moment and curvature distribution of cantilever under $M_r > M_p$ for bilinear moment-curvature relation

moment capacity M_p . The extent of the plastic zone L_p can be determined from similar triangles of the moment distribution to give

$$L_p = L \left(1 - \frac{M_p}{M_r} \right) \quad (6.25)$$

The tip displacement can be determined by integration of the curvature distribution according to (6.22). The curvature distribution is bilinear following the bilinear moment-curvature relation. We identify two triangles: one extending over the entire cantilever length L , and the other extending over the plastic zone L_p . The curvature κ_r at the root of the cantilever is made up of two contributions: the elastic curvature κ_{el} , and the plastic curvature κ_{pl} . We write

$$\kappa_r = \kappa_{el} + \kappa_{pl} \quad (6.26)$$

The curvature integral in (6.22) becomes the sum of two terms

$$U_{tip} = \frac{1}{2} \kappa_{el} L \left(\frac{2L}{3} \right) + \frac{1}{2} \kappa_{pl} L_p \left(L - \frac{L_p}{3} \right) = \frac{M_r L^2}{3EI} + \frac{\kappa_{pl} L^2}{2} \frac{L_p}{L} \left(1 - \frac{L_p}{3L} \right) \quad (6.27)$$

We use the moment-curvature relation to express the curvature κ_r in terms of the moment at the root of the cantilever

$$\kappa_r = \kappa_p + \frac{M_r - M_p}{\beta EI} = \frac{M_p}{EI} + \frac{M_r - M_p}{\beta EI} \quad (6.28)$$

where we made use of $\kappa_p = \frac{M_p}{EI}$.

We use (6.26) and (6.28) to solve for κ_{pl} and get

$$\kappa_{pl} = \frac{M_r - M_p}{\beta EI} + \frac{M_p}{EI} - \frac{M_r}{EI} = \frac{M_r - M_p}{EI} \frac{1 - \beta}{\beta} \quad (6.29)$$

where we made use of $\kappa_{el} = \frac{M_r}{EI}$.

After substitution of the plastic curvature κ_{pl} from (6.29) into (6.27) we get the following relation between the moment at the root of the cantilever M_r and the tip displacement U_{tip}

$$\begin{aligned} U_{tip} &= \frac{M_r L^2}{3EI} + \frac{L^2}{2} \frac{M_r - M_p}{EI} \frac{1-\beta}{\beta} \left(1 - \frac{M_p}{M_r}\right) \left[1 - \frac{1}{3} \left(1 - \frac{M_p}{M_r}\right)\right] \\ &= \frac{M_r L^2}{3EI} + \frac{L^2}{2EI} \frac{1-\beta}{\beta} M_r \left(1 - \frac{M_p}{M_r}\right)^2 \left(\frac{2}{3} + \frac{1}{3} \frac{M_p}{M_r}\right) \\ &= \frac{M_r L^2}{3EI} + \frac{M_r L^2}{3EI} \frac{1-\beta}{\beta} \left(1 - \frac{M_p}{M_r}\right)^2 \left(1 + \frac{1}{2} \frac{M_p}{M_r}\right) \\ &= \frac{M_r L^2}{3EI} + \frac{M_r L^2}{3EI} \frac{1-\beta}{\beta} \left[1 - \frac{3}{2} \frac{M_p}{M_r} + \frac{1}{2} \left(\frac{M_p}{M_r}\right)^3\right] \end{aligned}$$

In conclusion

$$U_{tip} = \frac{M_r L^2}{3EI} + \frac{M_r L^2}{3EI} \frac{1-\beta}{\beta} \left[1 - \frac{3}{2} \frac{M_p}{M_r} + \frac{1}{2} \left(\frac{M_p}{M_r}\right)^3\right] \quad (6.30)$$

The end moment-tip displacement relation in (6.30), which holds for $M_p \geq M_r$, shows that the cantilever beam with bilinear material is a series model consisting of an elastic component and a plastic hardening component.

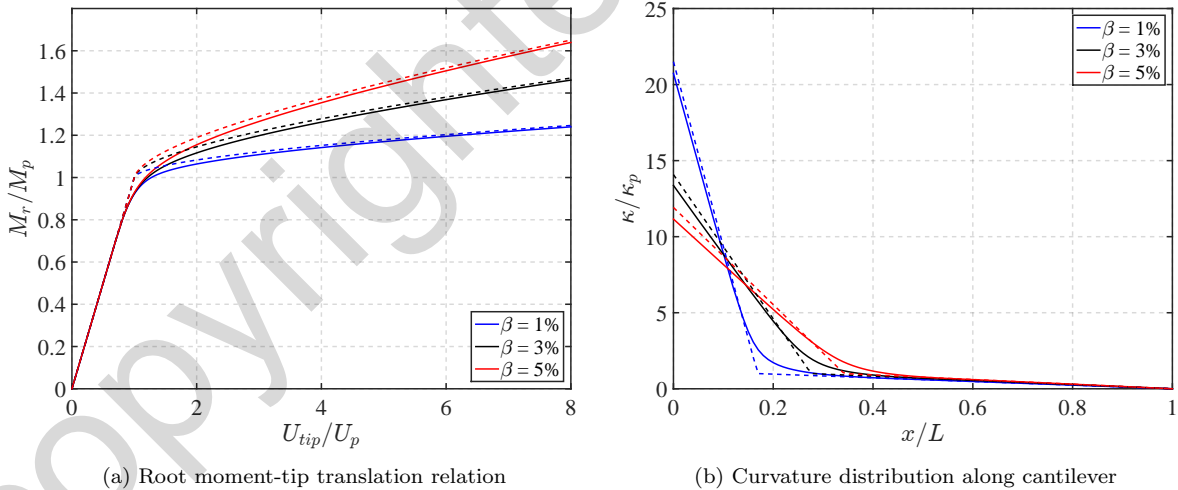


Fig. 6.16: Root moment-tip translation relation and curvature distribution for different hardening ratios β

Fig. 6.16(a) plots the root moment-tip displacement relation of (6.30) for three hardening ratios β and compares the response with the exact solution that involves the integration of the nonlinear moment-curvature relation for bilinear elastic hardening material. The right figure shows the curvature distribution at a displacement ductility $U_{tip}/U_p = 6$. The exact solution for each hardening ratio is shown with a solid line, while the solution for a bilinear moment-curvature relation is shown with a dashed line of the corresponding color.

We are interested in establishing the relation between the slope of the post-yield tangent of the basic force-deformation relation and the hardening ratio β . To this end we determine the tangent flexibility by differentiating the element deformation with respect to the basic force. We get

$$\frac{\partial \mathbf{v}_2}{\partial \mathbf{q}_2} = \frac{1}{L} \frac{\partial U_{tip}}{\partial \mathbf{q}_2} = \frac{1}{L} \frac{\partial U_{tip}}{\partial M_r} \quad (6.31)$$

The first term on the right hand side of (6.30) is straightforward to differentiate. The second term involves the differentiation of

$$M_r \left[1 - \frac{3}{2} \frac{M_p}{M_r} + \frac{1}{2} \left(\frac{M_p}{M_r} \right)^3 \right]$$

with respect to M_r , which with the introduction of the parameter $\xi = M_r/M_p$ becomes

$$M_p \left(\xi - \frac{3}{2} + \frac{1}{2\xi^2} \right)$$

so that the derivative with respect to ξ is simply

$$M_p \left(1 - \frac{1}{\xi^3} \right)$$

and the derivative with respect to M_r becomes

$$\left(1 - \frac{1}{\xi^3} \right)$$

Substituting this result into (6.31) gives

$$\frac{\partial \mathbf{v}_2}{\partial \mathbf{q}_2} = \mathbf{f}_{22} = \frac{L}{3EI} + \frac{L}{3EI} \frac{1-\beta}{\beta} \left(1 - \frac{1}{\xi^3} \right) \quad (6.32)$$

The flexibility \mathbf{f}_{22} of the basic beam deformation-force relation is, thus, the sum of two contributions: the elastic flexibility f_{el} and the plastic flexibility f_{pl} where

$$\mathbf{f}_{el} = \frac{L}{3EI} \quad \text{and} \quad \mathbf{f}_{pl} = \frac{L}{3EI} \frac{1-\beta}{\beta} \left(1 - \frac{1}{\xi^3} \right) \quad (6.33)$$

In the last expressions we left out the flexibility subscript for brevity of notation.

Now we determine the stiffness of the basic force-deformation relation by inverting the flexibility term in (6.32) which gives

$$\mathbf{k}_{22} = \frac{3\beta EI}{L} \frac{\xi^3}{\xi^3 - (1-\beta)} = \frac{3\beta EI}{L} c_1 \quad (6.34)$$

which holds for the post-yield tangent stiffness for which $\xi \geq 1$, whereas the elastic stiffness is $\mathbf{k}_{22} = 3EI/L$ corresponding to $\xi < 1$.

The ratio between the tangent post-yield stiffness and the elastic stiffness of the cantilever beam force-deformation relation is thus equal to $c_1 \beta$.

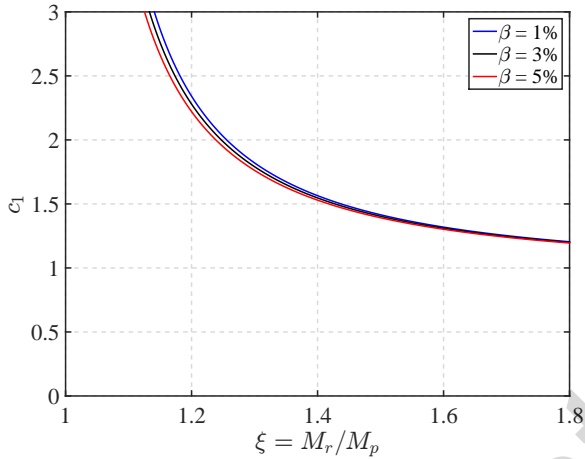


Fig. 6.17: Dependence of coefficient c_1 on M_r/M_p for different hardening ratios β

Fig. 6.17 shows the dependence of parameter c_1 on ξ for different material hardening ratios β . Its dependence on β is so small, that a single approximate relation may be used for beam hardening parameter calibration. In the range of practical interest for metallic structures, $1.1 \leq \xi \leq 1.5$, the value of parameter c_1 is strongly dependent on the end moment value M_r with values ranging from more than 3 to 1.5. The value of ξ depends on the material hardening ratio β and on the displacement ductility value according to Fig. 6.16(a).

6.3.3 Approximation of Load-Displacement Response of Cantilever Beam

Before turning our attention to some simple nonlinear beam models and their calibration we demonstrate that we can approximate the load-displacement response of the cantilever beam with a bilinear relation. Fig. 6.18(a) shows the approximation for a rectangular section and Fig. 6.18(b) shows the bilinear approximation for a W30x173 wide flange section for different strain hardening ratios β . The exact response of each case is depicted with a solid line, and the bilinear approximation with a dashed line of the same color for each hardening ratio.

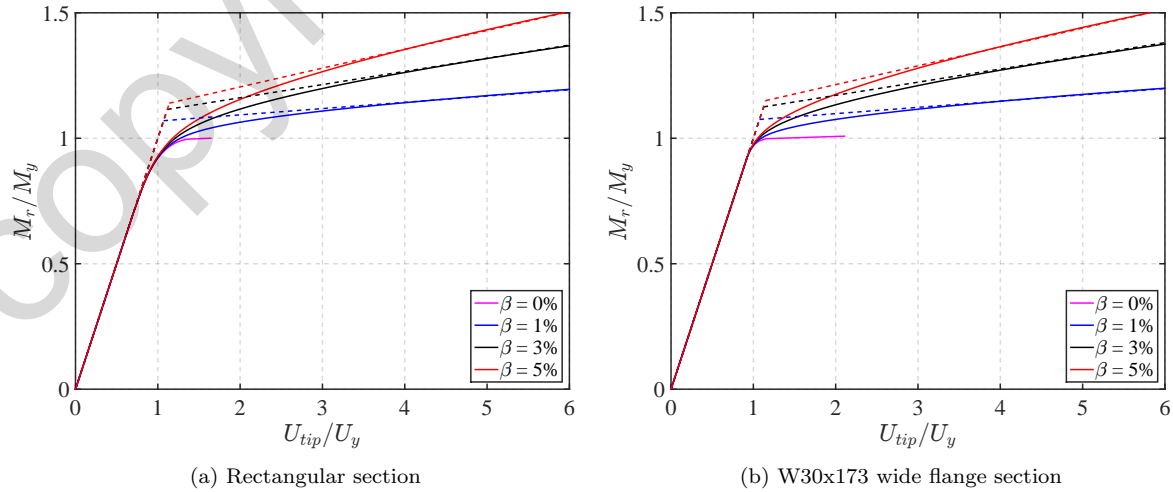


Fig. 6.18: Bilinear approximation of load-displacement response

The figures lead to the conclusion that a bilinear approximation of the force-displacement relation of the cantilever beam is quite satisfactory for displacement ductilities greater than 3. However, the bilinear approximation needs to use a fictitious plastic moment M'_p that is higher than the plastic moment capacity M_p of the section. The ratio M'_p/M_p depends on the material hardening ratio β . The post-yield slope of the bilinear approximation is equal to $c_1 \beta$ with c_1 values ranging from 1.5 to 2.5, with smaller values corresponding to higher material hardening ratio β .

We conclude this section with the following observations from the load-displacement response of a homogeneous, prismatic cantilever beam with either a rectangular or a wide flange cross section composed of a bilinear elastic material:

- 1) The cantilever beam with bilinear elastic material is a series model consisting of an elastic component and a plastic hardening component.
- 2) A bilinear approximation of the exact response of the cantilever beam under a bilinear moment-curvature relation is possible with the assumption of a fictitious plastic moment that is higher than the plastic moment capacity M_p of the section, and with a constant post-yield stiffness whose ratio to the elastic stiffness depends on the material hardening ratio β and on a parameter c_1 that depends on β and on the *target displacement ductility*.

6.3.4 Some Simple Nonlinear Beam Models

We turn now our attention to the development of suitable simple nonlinear beam models. The force-displacement response of the cantilever beam serves as reference for their assessment and the calibration of their parameters.

The following discussion is limited to the determination of the force-deformation relation of the beam element *in the basic reference system*, with the subsequent transformation to the global coordinates following the transformation relations in (4.59) for the element end forces \mathbf{p} and in (4.65) for the element stiffness matrix \mathbf{k}_e under nonlinear geometry. Under linear geometry these relations simplify to $\mathbf{p} = \mathbf{a}_g^T \mathbf{q}$ and $\mathbf{k}_e = \mathbf{a}_g^T \mathbf{k} \mathbf{a}_g$. Similarly, the element deformations \mathbf{v} are related to the element end displacements \mathbf{u} either by the linear kinematic relation $\mathbf{v} = \mathbf{a}_g \mathbf{u}$, or, by the nonlinear kinematic relations of the corotational formulation in (4.47). As was the case for the truss element, we discuss first the formulation of each element and then present the element state determination process which consists in the determination of the basic forces \mathbf{q} and tangent stiffness matrix \mathbf{k} for given element deformations \mathbf{v} .

6.3.5 Linear Elastic, Perfectly Plastic Beam Element

The simplest nonlinear beam model is the linear elastic, perfectly plastic (LEPP) beam element schematically shown in Fig. 6.19. The element of length L is based on the following assumptions:

- 1) The element has uniform axial and flexural stiffness, EA and EI , respectively.
- 2) The flexural response is uncoupled from the axial response. The axial response is linear elastic.
- 3) When an end moment reaches the plastic flexural capacity M_p , a concentrated hinge forms at that location and the moment at that location no longer changes.

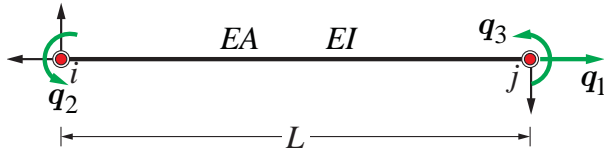


Fig. 6.19: Linear elastic, perfectly plastic beam element

We have, in fact, already encountered this element in the lower and upper bound theorems of plastic analysis in Theory of Structures, and in the event-to-event analysis for linear elastic, perfectly plastic element response in Chapter 1. Because all these problems were formulated directly in terms of the collection of basic element forces \mathbf{Q} and of the element deformations \mathbf{V} , the state determination of an isolated beam element was not discussed. Nor was it possible, as a result, to accommodate the nonlinear geometry under large displacements, which can be readily accounted for with the corotational formulation of Chapter 4. Consequently, the following discussion and implementation of the LEPP beam element opens new applications for its use that were heretofore inaccessible.

6.3.5.1 State Determination of LEPP Beam Element

The state determination for the basic LEPP beam element involves the determination of the basic forces \mathbf{q} and stiffness matrix \mathbf{k} for given element deformations \mathbf{v} .

There are three distinct outcomes for the element state under given deformations \mathbf{v} :

- 1) The frame element remains elastic.
- 2) One end reaches the plastic flexural capacity M_p .
- 3) Both ends reach the plastic flexural capacity M_p .

We use the event-to-event analysis to determine \mathbf{q} and \mathbf{k} for the given deformations \mathbf{v} noting that each element state determination involves zero, one, or, at most, two events. Since the element does not possess memory, the event-to-event state determination starts from the elastic state for each deformation vector \mathbf{v} regardless of the multi-step incremental application of the applied nodal forces onto the structural model.

With the given element deformations \mathbf{v} we determine trial basic forces \mathbf{q}_{tr} under the assumption of linear elastic response

$$\mathbf{q}_{tr} = \mathbf{k}_{el}\mathbf{v} \quad \text{with} \quad \mathbf{k}_{el} = \begin{bmatrix} \frac{EA}{L} & 0 & 0 \\ 0 & \frac{4EI}{L} & \frac{2EI}{L} \\ 0 & \frac{2EI}{L} & \frac{4EI}{L} \end{bmatrix}$$

Since the axial response is linear elastic and uncoupled from the flexural response, we only need check the basic forces \mathbf{q}_{tr_2} and \mathbf{q}_{tr_3} . To this end we determine the event factor η for end i and end j of the beam by comparing the trial end forces against the plastic flexural capacity M_p under the assumption that the beam has the same positive and negative plastic flexural capacity

$$\begin{aligned}\eta_i &= \frac{M_p}{|q_{tr_2}|} \\ \eta_j &= \frac{M_p}{|q_{tr_3}|}\end{aligned}\quad (6.35)$$

If the positive and negative plastic flexural capacity are different, we compare the end force at each end against the plastic flexural capacity for the corresponding sign of the bending moment.

If both η values in (6.35) are larger than one, neither basic force exceeds the flexural plastic capacity M_p ; in such case we set the basic forces equal to the trial force values and the stiffness \mathbf{k} equal to the elastic stiffness \mathbf{k}_{el} , thus completing the state determination of the basic element. The frame element then transforms the basic element forces \mathbf{q} and the basic stiffness \mathbf{k} to the global coordinates, which are assembled for all elements of the structural model by the structural assembly process to give the resisting forces \mathbf{P}_r and the stiffness matrix \mathbf{K}_t of the structure for the current free global dof displacements \mathbf{U}_f .

If at least one event factor is less than one, we select the smaller of the two η values. It supplies the factor of the deformation increment to the first event, the yielding of the corresponding end. We denote events with superscripts in parentheses to avoid confusion with the subscripts of the basic force and deformation vector. We have

$$\eta^{(1)} = \min(\eta_i, \eta_j)$$

We scale the given element deformations to the first event and determine the corresponding basic forces with the elastic stiffness matrix

$$\begin{aligned}\mathbf{v}^{(1)} &= \eta^{(1)} \mathbf{v} \\ \mathbf{q}^{(1)} &= \mathbf{k}_{el} \mathbf{v}^{(1)}\end{aligned}$$

At the first event we update the tangent basic stiffness matrix k_t to the new state. If yielding takes place at end node i , the tangent basic stiffness k_t is

$$\mathbf{k}_t = \begin{bmatrix} \frac{EA}{L} & 0 & 0 \\ 0 & 0 & 0 \\ 0 & 0 & \frac{3EI}{L} \end{bmatrix}$$

If yielding takes place at end node j , the tangent stiffness k_t is instead

$$\mathbf{k}_t = \begin{bmatrix} \frac{EA}{L} & 0 & 0 \\ 0 & \frac{3EI}{L} & 0 \\ 0 & 0 & 0 \end{bmatrix}$$

With the remaining deformation increment $(1 - \eta^{(1)}) \mathbf{v}$ we determine new trial basic forces according to

$$\Delta \mathbf{q} = \mathbf{k}_t (1 - \eta^{(1)}) \mathbf{v} \quad (6.36)$$

$$\mathbf{q}_{tr} = \mathbf{q}^{(1)} + \Delta \mathbf{q} \quad (6.37)$$

Because an event already took place at either end node i or end node j , it is necessary to check the new trial basic force value only at the other node against the plastic flexural capacity M_p to decide whether another event takes place. Under the assumption that the first event took place at end node i it is only necessary to check the event factor at end node j according to the following equation

$$\eta^{(2)} = \frac{\text{sign}(q_{tr_3})M_p - q_3^{(1)}}{\Delta q_3}$$

If $\eta^{(2)} \geq 1$, no other event takes place. In such case we set the basic forces equal to the last trial force values in (6.37) and the stiffness \mathbf{k} equal to the last tangent stiffness \mathbf{k}_t and consider the state determination of the basic element complete.

If $\eta^{(2)}$ is less than one, then we determine the final basic forces from

$$\begin{aligned}\Delta \mathbf{q} &= \mathbf{k}_t \eta^{(2)} \left(1 - \eta^{(1)}\right) \mathbf{v} \\ \mathbf{q} &= \mathbf{q}^{(1)} + \Delta \mathbf{q}\end{aligned}$$

and return from the state determination with these basic forces and the new tangent stiffness matrix

$$\mathbf{k}_t = \begin{bmatrix} \frac{EA}{L} & 0 & 0 \\ 0 & 0 & 0 \\ 0 & 0 & 0 \end{bmatrix}$$

The plastic deformations of the beam element are of particular interest for post-processing. We determine these with the final basic forces for the given element deformations \mathbf{v} according to

$$\mathbf{v}_{pl} = \mathbf{v} - \mathbf{v}_\varepsilon \quad \text{where} \quad \mathbf{v}_\varepsilon = \mathbf{f}_{el} \mathbf{q} \quad \text{with} \quad \mathbf{f}_{el} = \begin{bmatrix} \frac{L}{EA} & 0 & 0 \\ 0 & \frac{L}{3EI} & -\frac{L}{6EI} \\ 0 & -\frac{L}{6EI} & \frac{L}{3EI} \end{bmatrix}$$

Example 6.3 State Determination for LEPP Beam

The portal frame in Fig. 6.20 consists of inextensible linear elastic frame elements for the columns and of an inextensible LEPP beam element for the girder. The girder element b and the right column element c have flexural stiffness EI , while the left column element a has flexural stiffness $1.78 \cdot EI$ with $EI = 300,000$. The plastic flexural capacity of the girder is $M_p = 400$.

We are interested in determining the horizontal translation under a load factor $\lambda = 1.47$ with the Newton-Raphson iterative process for the solution of the free global dof equilibrium equations.

We assume that the nodal forces are applied in a single load step, so that the applied force vector \mathbf{P}_f for this analysis is

$$\mathbf{P}_f = \lambda \mathbf{P}_{ref} = 1.47 \begin{pmatrix} -200 \\ 0 \\ 0 \end{pmatrix} = \begin{pmatrix} -294 \\ 0 \\ 0 \end{pmatrix}$$

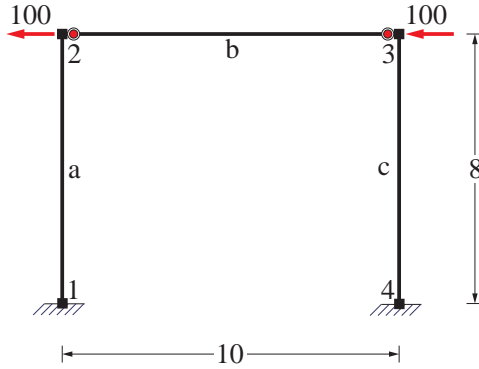


Fig. 6.20: Portal frame with LEPP girder element

with dof #1 corresponding to the horizontal translation, dof #2 to the rotation at the left girder end, and dof #3 to the rotation at the right girder end. Under the initial guess for the free global dof displacements $\mathbf{U}_0 = \mathbf{0}$ the initial portal frame stiffness is

$$\mathbf{K}_0 = \begin{bmatrix} \frac{12EI_l}{h^3} + \frac{12EI_r}{h^3} & \frac{6EI_l}{h^2} & \frac{6EI_r}{h^2} \\ \frac{6EI_l}{h^2} & \frac{4EI_l}{h} + \mathbf{k}_{g_{22}} & \mathbf{k}_{g_{23}} \\ \frac{6EI_r}{h^2} & \mathbf{k}_{g_{32}} & \frac{4EI_r}{h} + \mathbf{k}_{g_{33}} \end{bmatrix} \quad (6.38)$$

where EI_l is the stiffness of the left column, EI_r the stiffness of the right column, and \mathbf{k}_g the basic flexural stiffness of the girder. The girder stiffness coefficients are numbered under consideration of the axial effect, which for the problem in hand is of no interest. h is the column height and L is the girder length. The initial girder stiffness is the linear elastic stiffness

$$\mathbf{k}_g = \frac{2EI}{L} \begin{bmatrix} 2 & 1 \\ 1 & 2 \end{bmatrix}$$

Noting that the equilibrium error $\mathbf{P}_{u,0}$ is

$$\mathbf{P}_{u,0} = \mathbf{P}_f - \mathbf{P}_{r,0} = \begin{pmatrix} -294 \\ 0 \\ 0 \end{pmatrix} - \begin{pmatrix} 0 \\ 0 \\ 0 \end{pmatrix} = \begin{pmatrix} -294 \\ 0 \\ 0 \end{pmatrix}$$

the displacement correction $\Delta\mathbf{U}_0$ is

$$\Delta\mathbf{U}_0 = \mathbf{K}_0 \backslash \mathbf{P}_{u,0} = \begin{pmatrix} -25.61 \\ 3 \\ 2 \end{pmatrix} 10^{-3}$$

and the free global dof displacements \mathbf{U}_1 become

$$\mathbf{U}_1 = \mathbf{U}_0 + \Delta\mathbf{U}_0 = \begin{pmatrix} 0 \\ 0 \\ 0 \end{pmatrix} + \begin{pmatrix} -25.61 \\ 3 \\ 2 \end{pmatrix} 10^{-3} = \begin{pmatrix} -25.61 \\ 3 \\ 2 \end{pmatrix} 10^{-3}$$

We need to determine the resisting forces $\mathbf{P}_{r,1}$ and the new stiffness matrix \mathbf{K}_1 of the structural model for the displacements \mathbf{U}_1 so as to proceed with the first equilibrium iteration of the NR solution process.

The state determination of the linear elastic columns is straightforward: the stiffness does not change, and the resisting force contribution $\mathbf{P}_{r,l}$ for the left column and $\mathbf{P}_{r,r}$ for right column are

$$\mathbf{P}_{r,l} = \begin{pmatrix} \frac{12EI_l}{h^3}\mathbf{U}_1 + \frac{6EI_l}{h^2}\mathbf{U}_2 \\ \frac{6EI_l}{h^2}\mathbf{U}_1 + \frac{4EI_l}{h}\mathbf{U}_2 \\ 0 \end{pmatrix} \quad \mathbf{P}_{r,r} = \begin{pmatrix} \frac{12EI_r}{h^3}\mathbf{U}_1 + \frac{6EI_r}{h^2}\mathbf{U}_3 \\ 0 \\ \frac{6EI_r}{h^2}\mathbf{U}_1 + \frac{4EI_r}{h}\mathbf{U}_3 \end{pmatrix}$$

The state determination of the LEPP beam element for $v_2 = 3 \cdot 10^{-3}$ and $v_3 = 2 \cdot 10^{-3}$ requires the following steps:

- 1) We denote the flexural deformations of the girder element with \mathbf{v} leaving out the axial deformation v_1 , which is of no interest, but retaining the basic force numbering of the general derivation for the flexural basic forces.

$$\mathbf{v} = \begin{pmatrix} 3 \\ 2 \end{pmatrix} 10^{-3}$$

- 2) The trial basic forces \mathbf{q}_{tr} are

$$\mathbf{q}_{tr} = \begin{bmatrix} \frac{4EI}{L} & \frac{2EI}{L} \\ \frac{2EI}{L} & \frac{4EI}{L} \end{bmatrix} \begin{pmatrix} 3 \\ 2 \end{pmatrix} 10^{-3} = \begin{pmatrix} 480 \\ 420 \end{pmatrix}$$

- 3) Because the end forces exceed the plastic flexural capacity, we determine the scale factor to the first event

$$\eta^{(1)} = \min\left(\frac{M_p}{480}, \frac{M_p}{420}\right) = \min(0.83, 0.95) = 0.83$$

indicating that the hinge at end i forms first. The corresponding deformations and basic forces are

$$\begin{aligned} \mathbf{v}^{(1)} &= \eta^{(1)}\mathbf{v} = \begin{pmatrix} 2.50 \\ 1.67 \end{pmatrix} 10^{-3} \\ \mathbf{q}^{(1)} &= \mathbf{k}_{el} \mathbf{v}^{(1)} = \begin{pmatrix} 400 \\ 350 \end{pmatrix} \end{aligned}$$

and the tangent stiffness becomes

$$\mathbf{k}_t = \begin{bmatrix} 0 & 0 \\ 0 & \frac{3EI}{L} \end{bmatrix}$$

- 4) We impose the remaining element deformation increment $\Delta\mathbf{v} = (1 - \eta^{(1)})\mathbf{v}$ to find out whether end j also yields under the given element deformations \mathbf{v} . The remaining element deformation increment $\Delta\mathbf{v}$ is

$$\Delta\mathbf{v} = (1 - \eta^{(1)})\mathbf{v} = \begin{pmatrix} 0.50 \\ 0.33 \end{pmatrix} 10^{-3}$$

and the corresponding basic force increment $\Delta\mathbf{q}$ is

$$\Delta\mathbf{q} = \mathbf{k}_t \Delta\mathbf{v} = \begin{bmatrix} 0 & 0 \\ 0 & \frac{3EI}{L} \end{bmatrix} \begin{pmatrix} 0.50 \\ 0.33 \end{pmatrix} 10^{-3} = \begin{pmatrix} 0 \\ 30 \end{pmatrix}$$

5) Because

$$\eta^{(2)} = \frac{\text{sign}(q_{tr_3})M_p - q_3^{(1)}}{\Delta q_3} = \frac{400 - 350}{30} = 1.67$$

is greater than 1, no other event takes place. Thus, the final basic forces \mathbf{q} are

$$\mathbf{q} = \mathbf{q}^{(1)} + \Delta\mathbf{q} = \begin{pmatrix} 400 \\ 350 \end{pmatrix} + \begin{pmatrix} 0 \\ 30 \end{pmatrix} = \begin{pmatrix} 400 \\ 380 \end{pmatrix}$$

and the corresponding tangent stiffness is the last tangent stiffness \mathbf{k}_t we determined. This completes the LEPP beam state determination for the given deformations \mathbf{v} !

6) The corresponding plastic deformations are most conveniently determined from

$$\mathbf{v}_{pl} = \mathbf{v} - \mathbf{v}_{el} = \mathbf{v} - \mathbf{f}\mathbf{q}$$

for the case in hand this becomes

$$\mathbf{v}_{pl} = \begin{pmatrix} 3 \\ 2 \end{pmatrix} 10^{-3} - \frac{L}{6EI} \begin{bmatrix} 2 & -1 \\ -1 & 2 \end{bmatrix} \begin{pmatrix} 400 \\ 380 \end{pmatrix} = \begin{pmatrix} 0.67 \\ 0 \end{pmatrix} 10^{-3}$$

We conclude that resisting flexural basic forces \mathbf{q} and basic stiffness matrix \mathbf{k}_g of the girder under the deformations \mathbf{v} are

$$\begin{pmatrix} \mathbf{q}_2 \\ \mathbf{q}_3 \end{pmatrix} = \begin{pmatrix} 400 \\ 380 \end{pmatrix} \quad \mathbf{k}_g = \begin{bmatrix} 0 & 0 \\ 0 & \frac{3EI}{L} \end{bmatrix} \quad (6.39)$$

so that the resisting force contribution $\mathbf{P}_{r,g}$ of the girder to the resisting forces \mathbf{P}_r of the structure is

$$\mathbf{P}_{r,g} = \begin{pmatrix} 0 \\ 400 \\ 380 \end{pmatrix}$$

The unbalanced force vector $\mathbf{P}_{u,1}$ is

$$\mathbf{P}_{u,1} = \mathbf{P}_f - \mathbf{P}_{r,1} = \mathbf{P}_f - (\mathbf{P}_{r,l} + \mathbf{P}_{r,r} + \mathbf{P}_{r,g}) = \begin{pmatrix} 0 \\ 80.35 \\ 40.17 \end{pmatrix}$$

and the tangent stiffness matrix \mathbf{K}_1 is given by (6.38) with \mathbf{k}_g from (6.39). The displacement correction under the equilibrium error $\mathbf{P}_{u,1}$ is

$$\Delta\mathbf{U}_1 = \mathbf{K}_1 \setminus \mathbf{P}_{u,1} = \begin{pmatrix} -2.88 \\ 0.84 \\ 0.50 \end{pmatrix} 10^{-3}$$

and the free global dof displacements are

$$\mathbf{U}_2 = \mathbf{U}_1 + \Delta\mathbf{U}_1 = \begin{pmatrix} -25.61 \\ 3 \\ 2 \end{pmatrix} 10^{-3} + \begin{pmatrix} -2.88 \\ 0.84 \\ 0.50 \end{pmatrix} 10^{-3} = \begin{pmatrix} -28.49 \\ 3.84 \\ 2.51 \end{pmatrix} 10^{-3}$$

The process of element state determination is now repeated for \mathbf{U}_2 and so on, until the error \mathbf{P}_u of the free dof equilibrium equations becomes smaller than a specified tolerance. For the case in hand with piecewise linear element response the process converges in a small number of steps to the exact solution. Because the LEPP beam element has no memory of the events from the last state determination, it starts the new state determination process for the deformations \mathbf{v} under \mathbf{U}_2 with the trial basic forces \mathbf{q}_{tr} under the assumption of linear elastic response.

We do not complete the process in the following and leave it as an exercise to the reader. Instead, we demonstrate the state determination process of the LEPP beam element for a different set of flexural deformations \mathbf{v} .

- 1) Assume that the flexural deformations of the girder element at the end of the load application on the portal frame are equal to

$$\mathbf{v} = \begin{pmatrix} 3 \\ 2.4 \end{pmatrix} 10^{-3}$$

What are the corresponding basic forces \mathbf{q} and girder tangent stiffness matrix \mathbf{k}_g for this case?

- 2) The trial basic forces \mathbf{q}_{tr} are

$$\mathbf{q}_{tr} = \begin{bmatrix} \frac{4EI}{L} & \frac{2EI}{L} \\ \frac{2EI}{L} & \frac{4EI}{L} \end{bmatrix} \begin{pmatrix} 3 \\ 2.4 \end{pmatrix} 10^{-3} = \begin{pmatrix} 504 \\ 468 \end{pmatrix}$$

- 3) Because the end forces exceed the plastic flexural capacity, we determine the scale factor to the first event

$$\eta^{(1)} = \min \left(\frac{M_p}{504}, \frac{M_p}{468} \right) = \min(0.79, 0.85) = 0.79$$

which means that the hinge at end i forms first. The corresponding deformations and basic forces are

$$\begin{aligned} \mathbf{v}^{(1)} &= \eta^{(1)} \mathbf{v} = \begin{pmatrix} 2.38 \\ 1.9 \end{pmatrix} 10^{-3} \\ \mathbf{q}^{(1)} &= \mathbf{k}_{el} \mathbf{v}^{(1)} = \begin{pmatrix} 400 \\ 371.4 \end{pmatrix} \end{aligned}$$

and the tangent stiffness matrix becomes

$$\mathbf{k}_t = \begin{bmatrix} 0 & 0 \\ 0 & \frac{3EI}{L} \end{bmatrix}$$

- 4) We impose the remaining element deformation increment $(1 - \eta^{(1)}) \mathbf{v}$ to find out whether end j also yields under the given element deformations \mathbf{v} . The remaining element deformation increment $\Delta\mathbf{v}$ is

$$\Delta \mathbf{v} = \left(1 - \eta^{(1)}\right) \mathbf{v} = \begin{pmatrix} 0.62 \\ 0.50 \end{pmatrix} 10^{-3}$$

and the corresponding basic force increment $\Delta \mathbf{q}$ is

$$\Delta \mathbf{q} = \mathbf{k}_t \Delta \mathbf{v} = \begin{bmatrix} 0 & 0 \\ 0 & \frac{3EI}{L} \end{bmatrix} \begin{pmatrix} 0.62 \\ 0.50 \end{pmatrix} 10^{-3} = \begin{pmatrix} 0 \\ 44.6 \end{pmatrix}$$

5) Because

$$\eta^{(2)} = \frac{\text{sign}(q_{tr_3}) M_p - q_3^{(1)}}{\Delta q_3} = \frac{400 - 371.4}{44.6} = 0.64$$

is less than 1, a hinge also forms at end j . The basic forces \mathbf{q} at the next event are determined from the last deformation increment

$$\Delta \mathbf{v} = \eta^{(2)} \left(1 - \eta^{(1)}\right) \mathbf{v} = \begin{pmatrix} 0.40 \\ 0.32 \end{pmatrix} 10^{-3}$$

The corresponding basic force increment $\Delta \mathbf{q}$ is

$$\Delta \mathbf{q} = \mathbf{k}_t \Delta \mathbf{v} = \begin{pmatrix} 0 \\ 28.6 \end{pmatrix}$$

The basic forces at the next event become

$$\mathbf{q}^{(2)} = \mathbf{q}^{(1)} + \Delta \mathbf{q} = \begin{pmatrix} 400 \\ 371.4 \end{pmatrix} + \begin{pmatrix} 0 \\ 28.6 \end{pmatrix} = \begin{pmatrix} 400 \\ 400 \end{pmatrix}$$

The corresponding deformations $\mathbf{v}^{(2)}$ are

$$\mathbf{v}^{(2)} = \mathbf{v}^{(1)} + \Delta \mathbf{v} = \begin{pmatrix} 2.38 \\ 1.9 \end{pmatrix} 10^{-3} + \begin{pmatrix} 0.40 \\ 0.32 \end{pmatrix} 10^{-3} = \begin{pmatrix} 2.78 \\ 2.22 \end{pmatrix} 10^{-3}$$

and the corresponding tangent stiffness is

$$\mathbf{k}_t = \begin{bmatrix} 0 & 0 \\ 0 & 0 \end{bmatrix}$$

- 6) The last deformation increment to reach the given deformations occurs without further basic force increments, since $\mathbf{k}_t \Delta \mathbf{v} = \mathbf{0}$. This is also clear from the fact that both ends reach the plastic capacity at the second event.
- 7) The plastic deformations are most conveniently determined from

$$\mathbf{v}_{pl} = \mathbf{v} - \mathbf{v}_{el} = \mathbf{v} - \mathbf{f} \mathbf{q}$$

for the case in hand this becomes

$$\mathbf{v}_{pl} = \begin{pmatrix} 3 \\ 2.4 \end{pmatrix} 10^{-3} - \frac{L}{6EI} \begin{bmatrix} 2 & -1 \\ -1 & 2 \end{bmatrix} \begin{pmatrix} 400 \\ 400 \end{pmatrix} = \begin{pmatrix} 0.78 \\ 0.18 \end{pmatrix} 10^{-3}$$

The state determination of the LEPP beam element can be programmed in Matlab® and used to establish the basic forces \mathbf{q} for element deformations \mathbf{v} that are imposed in several increments. Fig. 6.21 shows the resulting basic-force deformation response for end i and end j of the LEPP beam element for Example 7.3 for two ratios α of the imposed deformations \mathbf{v}_2 and \mathbf{v}_3 with

$$\alpha = \frac{\mathbf{v}_3}{\mathbf{v}_2}$$

The deformations are imposed in 30 increments with the corresponding \mathbf{q} - \mathbf{v} pairs depicted with round markers. We note from Fig. 6.21(a) for $\alpha = \frac{2}{3}$ and Fig. 6.21(b) for $\alpha = 0.8$ that the \mathbf{q}_2 - \mathbf{v}_2 relation differs from the \mathbf{q}_3 - \mathbf{v}_3 relation with the end that experiences yielding first displaying a bilinear elastic, perfectly plastic response, while the end that yields second displays a trilinear response. The initial slope of the \mathbf{q}_2 - \mathbf{v}_2 basic force-deformation relation is $\mathbf{k}_{22} + \alpha \mathbf{k}_{23}$, whereas the initial slope of the \mathbf{q}_3 - \mathbf{v}_3 basic force-deformation relation is $\frac{\mathbf{k}_{32}}{\alpha} + \mathbf{k}_{33}$. The second slope of the trilinear basic force-deformation relation is equal to $\frac{3EI}{L}$. The results of the state determination for Example 7.3 correspond to the last marker of the \mathbf{q} - \mathbf{v} relations in Fig. 6.21(a) for $\mathbf{v}_2 = 3 \cdot 10^{-3}$ and $\mathbf{v}_3 = 2 \cdot 10^{-3}$, and in Fig. 6.21(b) for $\mathbf{v}_2 = 3 \cdot 10^{-3}$ and $\mathbf{v}_3 = 2.4 \cdot 10^{-3}$.

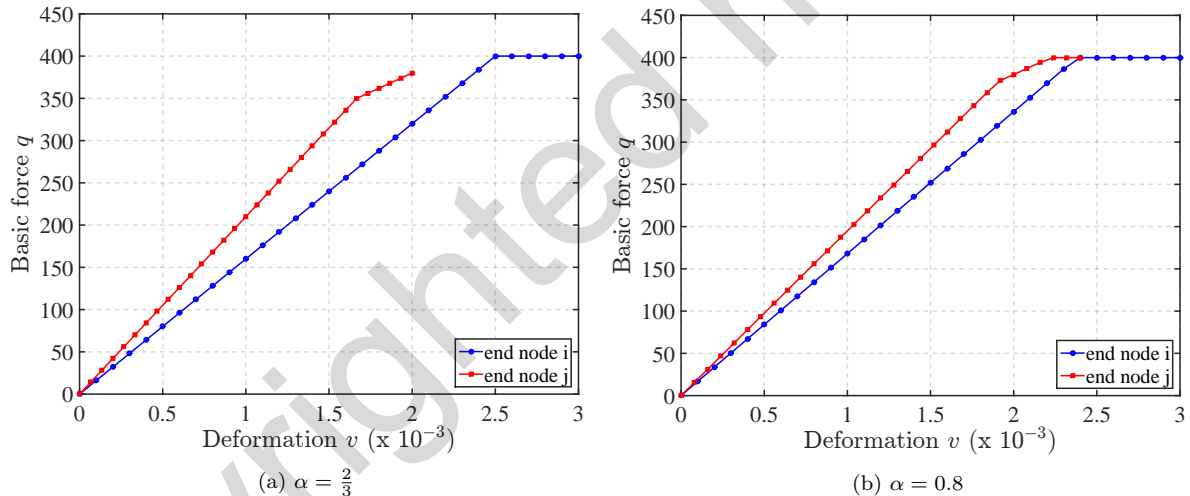


Fig. 6.21: LEPP beam basic force-deformation response for two deformation ratios α

The two basic force-deformation relations are identical only for the case that $\alpha = 1$, so that $\mathbf{v}_2 = \mathbf{v}_3$. This case corresponds to anti-symmetric bending with point of inflection at midspan and with initial stiffness of the basic force-deformation relation equal to $\frac{6EI}{L}$.

6.3.6 Two (Parallel) Component Beam Model

Because of the importance of including the hardening response of metallic structures in nonlinear structural analysis, the first model proposals appeared in the mid 1960's, once computers were powerful enough to handle building models of sufficient size. The first model to be introduced was the so called two-component model by Clough, Benuska and Wilson of UC Berkeley in 1965¹. It consists of two components

¹ Inelastic Earthquake Response of Tall Buildings, Proceedings of 3rd World Conference in Earthquake Engineering, NZ

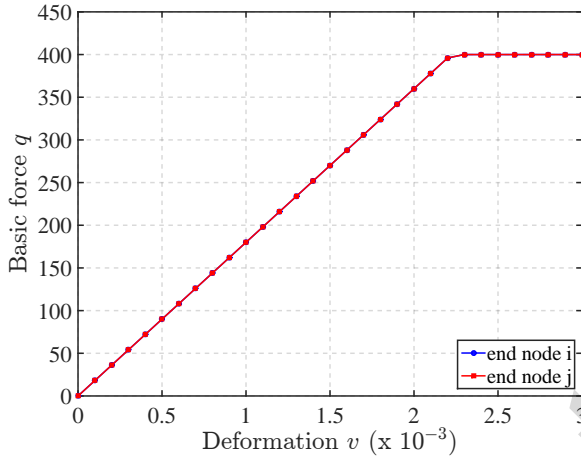


Fig. 6.22: Beam basic force-deformation response for deformation ratio $\alpha = 1$ (anti-symmetric bending mode)

in parallel, one linear elastic-perfectly plastic and the other linear elastic. Both components have linear axial stiffness that is uncoupled from the flexural response. Fig. 6.23 gives a schematic representation of the flexural components of the two-component model.

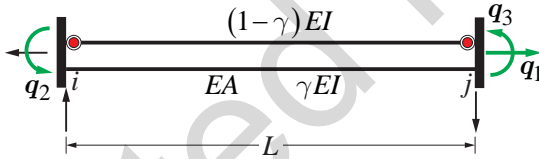


Fig. 6.23: Two (parallel) component beam model

The ratio of the stiffness of the linear elastic flexural component to the flexural stiffness EI of the element is denoted with γ . This component represents the linear hardening behavior of the element. Because the stiffness matrix of a parallel model is the sum of the stiffness matrices of its components, the elastic stiffness of the linear elastic, perfectly plastic element is set equal to $(1 - \gamma)EI$, so that the total stiffness before yielding takes place at either end is equal to EI .

If the plastic flexural capacity of the member to be modeled is M_p , then the plastic capacity of the linear elastic, perfectly plastic component is set equal to $(1 - \gamma)M_p$.

In the original proposal the parameter γ was set equal to the stiffness ratio β of the bilinear approximation of the moment-curvature relation of the member. With this assumption the two-component model matches the exact response of the member only under uniform curvature, a rare case in moment resisting frames under gravity and lateral loads. For this case Fig. 6.24 shows the contribution of the linear elastic and the linear elastic, perfectly plastic component.

For the linear moment distribution of a cantilever beam or a girder under anti-symmetric bending the selection $\gamma = \beta$, where β is the hardening ratio of the bilinear moment-curvature relation of the member results in rather poor agreement of the hardening response of the two-component beam model with the exact cantilever response, as Fig. 6.25 shows.

As discussed in Sections 6.3.2 and 6.3.3, the nonlinear nature of the hardening response of the cantilever beam reflects the gradual spread of the plastic zone that depends on the magnitude of the

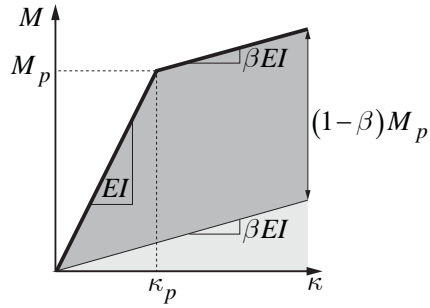


Fig. 6.24: Identification of linear elastic and linear elastic, perfectly plastic component of beam model

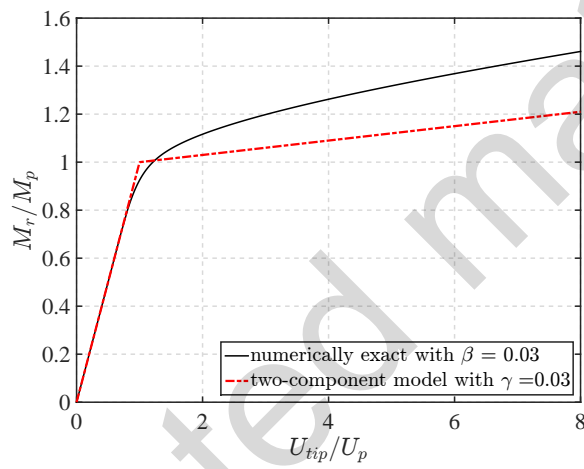


Fig. 6.25: Comparison of two-component beam model with exact cantilever response for $\gamma = \beta$

moment M_r at the root of the cantilever. It is, therefore, important to select the parameter γ of the two-component beam model by calibration of its force-deformation relation against the exact cantilever response. We address this subsequently after first briefly stating the state determination process for the model.

6.3.6.1 State Determination

The governing relations for the flexural components of the two-component model are the same as for the parallel spring model of Section 6.2.3 noting, however, that the parallel beam model has two flexural deformations and corresponding basic forces under the assumption that the uncoupled linear elastic axial response is simply added to the flexural response at the end. Denoting with subscript el the elastic component and with subscript ep the elastic, perfectly plastic component of the beam model we have the following relation between the component deformations and the deformations of the beam model

$$\boldsymbol{v} = \boldsymbol{v}_{el} = \boldsymbol{v}_{ep}$$

The basic forces \boldsymbol{q} are related to the basic forces of the components with

$$\boldsymbol{q} = \boldsymbol{q}_{el} + \boldsymbol{q}_{ep}$$

In this case the stiffness matrix of the beam model is equal to *the sum of the stiffness matrices of the components*

$$\mathbf{k} = \mathbf{k}_{el} + \mathbf{k}_{ep}$$

As discussed in Section 6.2.3, the state determination of the parallel spring model is straightforward. For the two component beam model the bulk of the work deals with the state determination of the elastic, perfectly plastic component, which follows the event-to-event strategy of the LEPP beam model in Section 6.3.5.1.

6.3.6.2 Parameter Calibration

The selection of the parameter γ for the two-component beam model has a significant effect on the accuracy of the results relative to the exact response of a cantilever with bilinear material response or bilinear moment-curvature relation. Fig. 6.25 leads to the conclusion that the value of the parameter γ for the two-component model has to be greater than the stiffness ratio β of the bilinear moment-curvature relation in order to represent the gradual spread of the plastic zone.

Section 6.3.2 shows that the hardening behavior of a cantilever beam with rectangular or wide flange cross section is dependent not only on the hardening ratio β of the bilinear material response, but also on a target displacement ductility, which affects the spread of the plastic zone. Moreover, the nonlinear load-displacement response of the cantilever beam reveals that the best bilinear approximation in Section 6.3.3 is obtained with a fictitious plastic capacity for the element that is higher than the plastic capacity of the member. We, therefore, pursue two methods for calibrating the parameter γ against the exact response of the cantilever beam:

- 1) Equating the bending moment of the model with the bending moment of the exact cantilever response at a particular tip translation.
- 2) Matching the hardening slope of the model with the hardening slope of the exact cantilever response at a particular tip translation.

With the first calibration method we match the moment value of the two-component beam model with the exact solution of a cantilever beam at a target displacement ductility μ_u . The cantilever beam and the two-component beam model are assumed to have the same length L . Noting that the deformation v_i of the two-component beam model is equal to $\frac{U_{tip}}{L}$ we conclude that the displacement ductility ratio $\mu_u = \frac{U_{tip}}{U_p}$ is equal to the deformation ductility ratio $\mu_v = \frac{v_i}{v_p}$ where $v_p = \frac{M_p L}{3EI}$. Matching the moment of the two-component beam model with the moment M_r of the exact cantilever response means

$$\gamma \frac{3EI}{L} v_i + (1 - \gamma) M_p = M_r \quad \rightarrow \quad \gamma \left(\frac{3EI}{L} v_i - M_p \right) = M_r - M_p$$

Dividing both sides by M_p and recalling that $\xi = \frac{M_r}{M_p}$ gives

$$\gamma (\mu_v - 1) = \xi - 1 \quad \rightarrow \quad \gamma = \frac{\xi - 1}{\mu_u - 1} \quad (6.40)$$

recalling that $\mu_u = \mu_v$ for the cantilever beam. Because of the equivalence of the cantilever beam of length L with a girder of length $2L$ under anti-symmetric bending, the displacement ductility μ_u is equal to the rotation ductility of the girder under anti-symmetric bending.

If we select to match the moment M_r of the exact response of the cantilever beam for a displacement ductility $\mu_u = 5$, we read from Fig. 6.16(a) that $\xi \approx 1.33$. With these values $\gamma \approx 0.08$ from (6.40). Fig. 6.26(a) compares the moment-tip translation response of the two-component beam model with the exact response of the cantilever beam for this calibration of parameter γ .

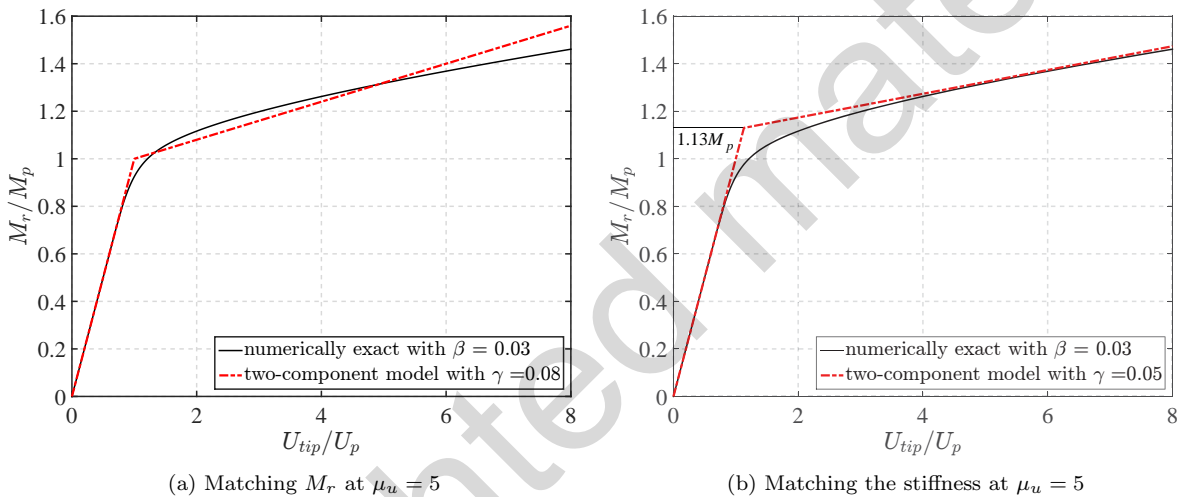


Fig. 6.26: Comparison of two-component beam model with the exact cantilever response for different calibration schemes

With the second calibration method we match the hardening slope of the two-component beam model with the slope of the exact response of the cantilever beam at a target displacement ductility μ_u . Selecting again a displacement ductility of $\mu_u = 5$ gives a maximum moment M_r at the root of the cantilever of approximately $1.33M_p$ in Fig. 6.16(a), so that $\xi \approx 1.33$. From Fig. 6.17 or (6.34) we determine $c_1 = 1.7$ for $\xi = 1.33$. Consequently, the hardening parameter γ of the two-component beam model according to (6.34) is

$$\gamma = \beta c_1 = 0.03 \cdot 1.7 \approx 0.05$$

Once we determine the hardening parameter γ of the two-component beam element, we determine the intersection of the line with slope γ in the moment-tip translation relation of Fig. 6.26(b) with the initial elastic stiffness. The two lines intersect at a fictitious plastic flexural capacity M'_p which can be derived from the relation

$$\begin{aligned} \gamma \frac{3EI}{L} v_i + (1 - \gamma) M'_p &= M_r \\ \gamma \mu_v + (1 - \gamma) \frac{M'_p}{M_p} &= \xi \end{aligned}$$

Noting that $\mu_v = \mu_u$ this gives the fictitious plastic capacity M'_p with

$$\frac{M'_p}{M_p} = \frac{\xi - \gamma\mu_u}{1 - \gamma} \quad \rightarrow \quad M'_p = \frac{\xi - \gamma\mu_u}{1 - \gamma} M_p$$

With the values $\mu_u = 5$, $\xi = 1.33$, and $\gamma = 0.05$ we get $M'_p \approx 1.13 M_p$.

The comparison of Fig. 6.26(a) with Fig. 6.26(b) shows that the second calibration method gives much better results for displacement ductilities from 3 to 8.

In conclusion, the two-component model is suitable for representing the nonlinear response of a girder under anti-symmetric bending, *as long as the hardening parameter γ is calibrated against the actual response of the member*. The calibration method was described with reference to the exact response of a cantilever beam with bilinear stress-strain or bilinear moment-curvature relation, but can be used in exactly the same way with reference to experimental measurements of the nonlinear response of steel and concrete members.

6.3.7 One-Component (Series) Beam Model

In 1967 Giberson proposed the one-component (series) beam model in his doctoral thesis at CalTech and compared it with the two-component beam model².

The one-component model consists of a linear elastic beam element *in series with nonlinear springs at its ends*. The springs have rigid plastic, linear hardening force-deformation behavior, so as to activate only after the corresponding end reaches the plastic flexural capacity M_p of the member. The name choice of the model was intended in contrast to the two-component beam model, but is confusing, since the element consists of three components in series, the elastic beam and two nonlinear springs. Consequently, we adopt the name series beam model in the following. Fig. 6.27 depicts the series beam model consisting of the linear elastic beam element with axial stiffness EA and flexural stiffness EI and two rotation springs at its ends.

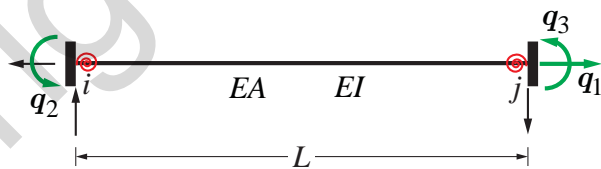


Fig. 6.27: Linear elastic beam with linear or nonlinear rotation springs in series

Before embarking on the description of the series beam model with nonlinear springs at its ends, we discuss briefly the properties of the model *for the case that the rotation springs are linear*. Such a model represents the behavior of girders *with flexible or semi-rigid connections to the column*.

The governing relations of the series beam model are the same as for the series spring model of Section 6.2.4 noting, however, that the series beam model in Fig. 6.27 has two flexural deformations and corresponding basic forces under the assumption that the uncoupled linear elastic axial response is simply added to the flexural response at the end. We denote the elastic beam contribution with *el* and the linear rotation spring contribution with *sr*.

² Two Beam Models with Definitions of Ductility, Proceedings of the Structural Division of ASCE, vol. 95, No. 2, Feb. 1969

For a series beam model the flexural flexibility \mathbf{f}_b is equal to the sum of the component flexibilities so that

$$\mathbf{f}_b = \mathbf{f}_{el} + \mathbf{f}_{sr} = \frac{L}{6EI} \begin{bmatrix} 2 & -1 \\ -1 & 2 \end{bmatrix} + \frac{L}{6EI} \begin{bmatrix} \frac{1}{\zeta_i} & 0 \\ 0 & \frac{1}{\zeta_j} \end{bmatrix}$$

where we have selected to express the rotation spring stiffness in terms of $\frac{6EI}{L}$, the flexural stiffness under anti-symmetric bending, so that we can combine the two flexibility contributions with facility. For the general case we assume that the end springs have different rotational stiffness.

The stiffness matrix of the basic beam element with flexible or semi-rigid connections is the inverse of the flexibility matrix \mathbf{f}_b

$$\mathbf{k}_b = \frac{6EI}{L} \frac{1}{D} \begin{bmatrix} 2 + \bar{\zeta}_j & 1 \\ 1 & 2 + \bar{\zeta}_i \end{bmatrix} \quad \text{with } D = (2 + \bar{\zeta}_i)(2 + \bar{\zeta}_j) - 1 \quad (6.41)$$

where $\bar{\zeta} = \frac{1}{\zeta}$. For a beam with rigid end connections we substitute $\bar{\zeta}_i = \bar{\zeta}_j = 0$ into (6.41) to get the flexural stiffness matrix for the linear elastic beam.

The series beam model with nonlinear rotation springs by Giberson can be obtained from the beam with linear flexible connections with the following modifications:

- 1) Noting that the nonlinear spring activates only after the corresponding end reaches the plastic flexural capacity M_p of the member we introduce an activation switch r which is equal to either 0 or 1, the former when the corresponding end is elastic, and the latter when it is active.
- 2) The rotation spring stiffness represents the *post-yield stiffness* of the corresponding end. We express this stiffness again in terms of $\frac{6EI}{L}$ and denote the ratio with η . Fig. 6.28 shows the rigid plastic, linear hardening force-deformation behavior of the nonlinear spring at end i or end j with the corresponding variables denoted with subscript pl .

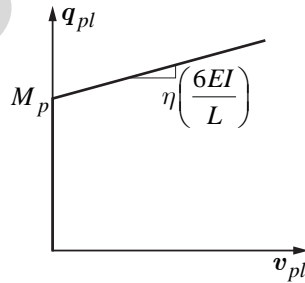


Fig. 6.28: Rigid plastic, linear hardening behavior of nonlinear spring in series beam model

With these modifications the flexural flexibility of the series beam model of Giberson becomes

$$\mathbf{f}_b = \mathbf{f}_{el} + \mathbf{f}_{pl} = \frac{L}{6EI} \begin{bmatrix} 2 & -1 \\ -1 & 2 \end{bmatrix} + \frac{L}{6EI} \begin{bmatrix} \frac{r_i}{\eta_i} & 0 \\ 0 & \frac{r_j}{\eta_j} \end{bmatrix} \quad (6.42)$$

noting that r_i and r_j are equal to 1 only when the corresponding basic forces \mathbf{q}_2 and \mathbf{q}_3 , respectively, are greater than the plastic flexural capacity M_p of the member.

We derive the beam stiffness matrix \mathbf{k}_b of the series beam model for the special case that $\eta_i = \eta_j$. If both ends are active it is

$$\mathbf{k}_b = \mathbf{f}_b^{-1} = \frac{6EI}{L} \frac{1}{(\eta+1)(3\eta+1)} \begin{bmatrix} \eta(2\eta+1) & \eta^2 \\ \eta^2 & \eta(2\eta+1) \end{bmatrix} \quad (6.43)$$

with $r_i = 1$ and $r_j = 1$ in (6.42). If only end i is active, the beam stiffness matrix \mathbf{k}_b is

$$\mathbf{k}_b = \mathbf{f}_b^{-1} = \frac{6EI}{L} \frac{1}{(3\eta+2)} \begin{bmatrix} 2\eta & \eta \\ \eta & (2\eta+1) \end{bmatrix} \quad (6.44)$$

If only end j is active, the beam stiffness matrix \mathbf{k}_b results from the exchange of the diagonal stiffness coefficients in (6.44).

6.3.7.1 State Determination

The state determination of the series beam model follows the state determination for the series spring model of Section 6.2.4.2 noting that the series beam model in Fig. 6.27 has two flexural deformations \mathbf{v}_2 and \mathbf{v}_3 and corresponding basic forces \mathbf{q}_2 and \mathbf{q}_3 under the assumption that the uncoupled linear elastic axial response is simply added to the flexural response at the end. Consequently, the kinematic relation in the second state of the state determination process of Section 6.2.4.2 is a system of two nonlinear equations in two unknowns. The equations are

$$\mathbf{v}_u(\mathbf{q}_b) = \mathbf{v} - (\mathbf{v}_{el} + \mathbf{v}_{pl}) = 0 \quad (6.45)$$

and the unknowns are the flexural basic forces \mathbf{q}_2 and \mathbf{q}_3 collected in vector \mathbf{q}_b . We note, however, that the bilinear rigid, hardening behavior of the rotation springs dispenses with the need for the iteration with counter l in Section 6.2.4.2. Moreover, because the resulting force-deformation response of the series beam model is bilinear, the iterative solution of (6.45) converges in one or two iterations.

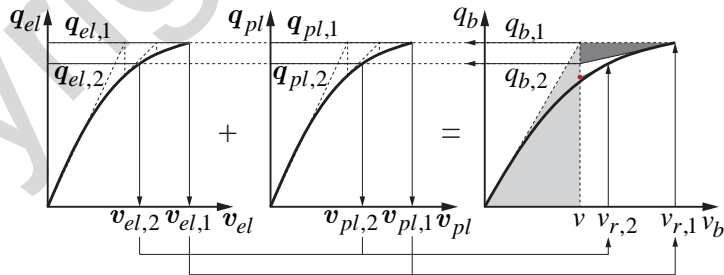


Fig. 6.29: Schematic depiction of one iteration for the state determination of the series beam model

Fig. 6.29 shows a schematic representation of the state determination process for the series beam model with the elastic beam element variables denoted with subscript el and the rotation spring variables denoted with subscript pl . It is important to note the schematic nature of Fig. 6.29 for the series beam model whose component response *depends on two independent variables*, thus requiring a representation of the iterative process in three dimensions. The scheme in Fig. 6.29 assumes that both rotation springs yield under the initial guess for the basic forces $\mathbf{q}_{b,1}$ and that is still true after the correction of the

basic forces to $\mathbf{q}_{b,2}$ so that the iterative process for the solution of element kinematic relations in (6.45) converges with one iteration.

We summarize the state determination process for the series beam model in the following. It determines the basic forces \mathbf{q} and the tangent stiffness matrix \mathbf{k} of the series beam model for given element deformations \mathbf{v} .

We assume that the axial response is linear elastic and uncoupled from the flexural response, so that for given $v_a = \mathbf{v}_1$, the axial basic force q_a and the axial stiffness k_a are

$$\mathbf{q}_a = \frac{EA}{L} v_a \quad \text{and} \quad k_a = \frac{EA}{L}$$

In the following presentation of the steps for the state determination algorithm we use \mathbf{v} to denote the given values of the flexural element deformations \mathbf{v}_b . The steps are:

Incrementation

- 1) Assume

$$\mathbf{q}_{b,0} = \mathbf{0} \quad \mathbf{v}_{el,0} = \mathbf{0} \quad \mathbf{v}_{pl,0} = \mathbf{0} \quad \mathbf{f}_{el} \quad \mathbf{f}_{pl,0} = \mathbf{0}$$

- 2) The initial deformation residual \mathbf{v}_u is

$$\mathbf{v}_{u,0} = \mathbf{v}$$

- 3) Use the initial flexibility \mathbf{f}_b

$$\mathbf{f}_{b,0} = \mathbf{f}_{el} + \mathbf{f}_{pl,0}$$

to determine the initial stiffness $\mathbf{k}_{b,0} = \mathbf{f}_{b,0}^{-1}$ and determine the basic force correction

$$\Delta\mathbf{q}_{b,0} = \mathbf{k}_{b,0} \mathbf{v}_{u,0}$$

The basic force correction is represented by the gray triangle in Fig. 6.29.

- 4) Update the basic forces

$$\mathbf{q}_{b,1} = \mathbf{q}_{b,0} + \Delta\mathbf{q}_{b,0}$$

Iteration

- 1) Use

$$\mathbf{q}_{el,i} = \mathbf{q}_{pl,i} = \mathbf{q}_{b,i}$$

to determine the deformations $\mathbf{v}_{el,i}$ and $\mathbf{v}_{pl,i}$ and the flexibility matrices \mathbf{f}_{el} (constant) and $\mathbf{f}_{pl,i}$.

- 2) Determine the deformation residual

$$\mathbf{v}_{u,i} = \mathbf{v} - (\mathbf{v}_{el,i} + \mathbf{v}_{pl,i})$$

- 3) Update the flexibility matrix

$$\mathbf{f}_{b,i} = \mathbf{f}_{el} + \mathbf{f}_{pl,i}$$

Use it to update the basic stiffness $\mathbf{k}_{b,i} = \mathbf{f}_{b,i}^{-1}$ and determine the basic force correction

$$\Delta\mathbf{q}_{b,i} = \mathbf{k}_{b,i} \mathbf{v}_{u,i}$$

The basic force correction is represented by the green triangle in Fig. 6.29.

4) Update the basic forces

$$\mathbf{q}_{b,i+1} = \mathbf{q}_{b,i} + \Delta \mathbf{q}_{b,i}$$

5) Set $i = i+1$ and go to step 1 until $\mathbf{v}_{u,i} = \mathbf{0}$: with rigid, linear hardening springs the process converges after the second iteration at the latest.

Upon convergence set up the basic forces of the series beam element

$$\mathbf{q} = \begin{pmatrix} q_a \\ \mathbf{q}_b \end{pmatrix}$$

and the tangent stiffness matrix \mathbf{k}

$$\mathbf{k} = \begin{bmatrix} k_a & \mathbf{0} \\ \mathbf{0} & \mathbf{k}_b \end{bmatrix}$$

and transform these to the global reference system under linear or nonlinear geometry considerations.

Example 6.4 State Determination of One Component Model

We demonstrate the state determination process for the flexural response of a series beam model with length $L = 10$, $EI = 300,000$, $M_p = 400$, and stiffness ratio of the rotation springs $\eta = 0.05$.

The given flexural deformations are denoted with \mathbf{v}

$$\mathbf{v} = \begin{pmatrix} 3 \\ 2 \end{pmatrix} 10^{-3}$$

With $\mathbf{f}_{b,0} = \mathbf{f}_{el}$ and $\mathbf{k}_{b,0} = \mathbf{f}_{b,0}^{-1}$ we get for the basic force correction

$$\Delta \mathbf{q}_{b,0} = \mathbf{k}_{b,0} \mathbf{v}_{u,0} = \frac{2EI}{L} \begin{bmatrix} 2 & 1 \\ 1 & 2 \end{bmatrix} \begin{pmatrix} 3 \\ 2 \end{pmatrix} 10^{-3} = \begin{pmatrix} 480 \\ 420 \end{pmatrix}$$

and update the basic forces

$$\mathbf{q}_{b,1} = \mathbf{q}_{b,0} + \Delta \mathbf{q}_{b,0} = \begin{pmatrix} 0 \\ 0 \end{pmatrix} + \begin{pmatrix} 480 \\ 420 \end{pmatrix} = \begin{pmatrix} 480 \\ 420 \end{pmatrix}$$

This completes the incrementation phase of the iterative solution of the element kinematic relations.

During the iteration phase we use the basic forces in each component

$$\mathbf{q}_{el,1} = \mathbf{q}_{pl,1} = \mathbf{q}_{b,1}$$

to determine the corresponding deformations under $\mathbf{q}_{b,1}$. For the elastic component we get

$$\mathbf{v}_{el,1} = \mathbf{f}_{el} \mathbf{q}_{el,1} = \frac{L}{6EI} \begin{bmatrix} 2 & -1 \\ -1 & 2 \end{bmatrix} \begin{pmatrix} 480 \\ 420 \end{pmatrix} = \begin{pmatrix} 3 \\ 2 \end{pmatrix} 10^{-3}$$

and for the plastic component

$$\mathbf{v}_{pl,1} = \mathbf{f}_{pl,1} \mathbf{q}_{pl,1} = \frac{L}{6\eta EI} \begin{bmatrix} 1 & 0 \\ 0 & 1 \end{bmatrix} \begin{pmatrix} 480 - M_p \\ 420 - M_p \end{pmatrix} = \begin{pmatrix} 8.89 \\ 2.22 \end{pmatrix} 10^{-3}$$

The corresponding flexural tangent flexibility matrix is

$$\mathbf{f}_{b,1} = \mathbf{f}_{el} + \mathbf{f}_{pl,1} = \frac{L}{6EI} \begin{bmatrix} 2 & -1 \\ -1 & 2 \end{bmatrix} + \frac{L}{6\eta EI} \begin{bmatrix} 1 & 0 \\ 0 & 1 \end{bmatrix} = \frac{L}{6EI} \begin{bmatrix} 2 + \frac{1}{\eta} & -1 \\ -1 & 2 + \frac{1}{\eta} \end{bmatrix}$$

and the corresponding flexural tangent stiffness \mathbf{k}_b is given by (6.43)

$$\mathbf{k}_{b,1} = \mathbf{f}_{b,1}^{-1} = \frac{6EI}{L} \frac{1}{(\eta+1)(3\eta+1)} \begin{bmatrix} \eta(2\eta+1) & \eta^2 \\ \eta^2 & \eta(2\eta+1) \end{bmatrix} = \begin{bmatrix} 8199 & 373 \\ 373 & 8199 \end{bmatrix}$$

With the deformation residual $\mathbf{v}_{u,1}$

$$\mathbf{v}_{u,1} = \mathbf{v} - (\mathbf{v}_{el,1} + \mathbf{v}_{pl,1}) = \binom{3}{2} 10^{-3} - \left[\binom{3}{2} 10^{-3} + \binom{8.89}{2.22} 10^{-3} \right] = -\binom{8.89}{2.22} 10^{-3}$$

we determine the basic force correction $\Delta\mathbf{q}_{b,1}$

$$\Delta\mathbf{q}_{b,1} = \mathbf{k}_{b,1} \mathbf{v}_{u,1} = - \begin{bmatrix} 8199 & 373 \\ 373 & 8199 \end{bmatrix} \begin{pmatrix} 8.89 \\ 2.22 \end{pmatrix} 10^{-3} = \begin{pmatrix} -73.71 \\ -21.53 \end{pmatrix}$$

and update the flexural basic forces \mathbf{q}_b

$$\mathbf{q}_{b,2} = \mathbf{q}_{b,1} + \Delta\mathbf{q}_{b,1} = \begin{pmatrix} 480 \\ 420 \end{pmatrix} + \begin{pmatrix} -73.71 \\ -21.53 \end{pmatrix} = \begin{pmatrix} 406.3 \\ 398.5 \end{pmatrix}$$

This completes the first iteration.

At the start of the second iteration we use the basic forces in each component

$$\mathbf{q}_{el,2} = \mathbf{q}_{pl,2} = \mathbf{q}_{b,2}$$

to determine the corresponding deformations under $\mathbf{q}_{b,2}$. For the elastic component we get

$$\mathbf{v}_{el,2} = \mathbf{f}_{el} \mathbf{q}_{el,2} = \frac{L}{6EI} \begin{bmatrix} 2 & -1 \\ -1 & 2 \end{bmatrix} \begin{pmatrix} 406.3 \\ 398.5 \end{pmatrix} = \begin{pmatrix} 2.3 \\ 2.17 \end{pmatrix} 10^{-3}$$

and for the plastic component

$$\mathbf{v}_{pl,2} = \mathbf{f}_{pl,2} \mathbf{q}_{pl,2} = \frac{L}{6\eta EI} \begin{bmatrix} 1 & 0 \\ 0 & 0 \end{bmatrix} \begin{pmatrix} 406.3 - M_p \\ 398.5 - M_p \end{pmatrix} = \begin{pmatrix} 0.7 \\ 0 \end{pmatrix} 10^{-3}$$

The corresponding flexural tangent flexibility matrix \mathbf{f}_b is

$$\mathbf{f}_{b,2} = \mathbf{f}_{el} + \mathbf{f}_{pl,2} = \frac{L}{6EI} \begin{bmatrix} 2 & -1 \\ -1 & 2 \end{bmatrix} + \frac{L}{6\eta EI} \begin{bmatrix} 1 & 0 \\ 0 & 0 \end{bmatrix} = \frac{L}{6EI} \begin{bmatrix} 2 + \frac{1}{\eta} & -1 \\ -1 & 2 \end{bmatrix}$$

and the corresponding flexural tangent stiffness \mathbf{k}_b is given by (6.44)

$$\mathbf{k}_{b,2} = \mathbf{f}_{b,2}^{-1} = \frac{6EI}{L} \frac{1}{(3\eta+2)} \begin{bmatrix} 2\eta & \eta \\ \eta & (2\eta+1) \end{bmatrix} = \begin{bmatrix} 8372 & 4186 \\ 4186 & 92093 \end{bmatrix}$$

With the deformation residual $\mathbf{v}_{u,2}$

$$\mathbf{v}_{u,2} = \mathbf{v} - (\mathbf{v}_{el,2} + \mathbf{v}_{pl,2}) = \begin{pmatrix} 3 \\ 2 \end{pmatrix} 10^{-3} - \left[\begin{pmatrix} 2.3 \\ 2.17 \end{pmatrix} 10^{-3} + \begin{pmatrix} 0.7 \\ 0 \end{pmatrix} 10^{-3} \right] = - \begin{pmatrix} 0 \\ 0.17 \end{pmatrix} 10^{-3}$$

we determine the basic force correction $\Delta\mathbf{q}_{b,2}$

$$\Delta\mathbf{q}_{b,2} = \mathbf{k}_{b,2} \mathbf{v}_{u,2} = - \begin{bmatrix} 8372 & 4186 \\ 4186 & 92093 \end{bmatrix} \begin{pmatrix} 0 \\ 0.17 \end{pmatrix} 10^{-3} = \begin{pmatrix} -0.71 \\ -15.68 \end{pmatrix}$$

and update the flexural basic forces \mathbf{q}_b

$$\mathbf{q}_{b,3} = \mathbf{q}_{b,2} + \Delta\mathbf{q}_{b,2} = \begin{pmatrix} 406.3 \\ 398.5 \end{pmatrix} + \begin{pmatrix} -0.71 \\ -15.68 \end{pmatrix} = \begin{pmatrix} 405.58 \\ 382.79 \end{pmatrix}$$

This completes the second iteration. Because there is no change in the state of either nonlinear spring, these are the final basic forces \mathbf{q}_b and the stiffness matrix $\mathbf{k}_{b,2}$ is the corresponding flexural tangent stiffness of the series beam element under the deformations \mathbf{v} .

6.3.7.2 Parameter Calibration

The calibration of the stiffness ratio η for the nonlinear rotation springs of the series beam model is rather straightforward. Recalling the flexibility coefficient \mathbf{f}_{22} in (6.32) for the exact response of the cantilever beam with bilinear moment-curvature relation we simply equate the flexibility of the plastic component of the series beam model with the plastic flexibility contribution of the cantilever beam response in (6.33) to get

$$\frac{L}{\eta 6EI} = \frac{L'}{3EI} \frac{1-\beta}{\beta} \left(1 - \frac{1}{\xi^3} \right)$$

where L is the length of the series beam model and $L' = \frac{L}{2}$ is the length of the cantilever beam. Consequently, the stiffness ratio η for the rotation springs of the series beam model is

$$\eta = \frac{\beta}{1-\beta} \frac{\xi^3}{\xi^3 - 1} \quad (6.46)$$

Because the plastic flexibility contribution of the cantilever beam response is a nonlinear function of ξ , i.e. of the maximum moment M_r at the root of the cantilever, a nonlinear rotation spring for the series beam model would be the ideal solution. Before embarking on a complex undertaking, however, it is advisable to evaluate the capabilities of the bilinear rigid, hardening rotation spring proposal in the original paper. Under the assumption that both rotation springs have the same hardening stiffness ratio η there is only one parameter available for calibration, unless one is willing to adjust the plastic flexural capacity of the rotation spring.

With a single parameter η available for calibration (6.46) can be used to determine this parameter for a specific value of $\xi = M_r/M_p$. This value depends on the target displacement ductility μ_u , as already discussed for the calibration of the two component beam model. To demonstrate we select $\mu_u = 5$ and use the exact nonlinear response in Fig. 6.16(a) to conclude $\xi \approx 1.33$ for a hardening ratio $\beta = 0.03$ of

the bilinear moment-curvature relation. Substituting these values into (6.46) gives $\eta = 0.054$. With this approach the series beam model matches the slope of the exact nonlinear response of the cantilever beam at a specific value of the moment M_r at the root of the cantilever. Fig. 6.30(a) compares the response of the series beam model with the exact nonlinear response of the cantilever beam for the hardening ratios $\beta = 1\%$, $\beta = 3\%$ and $\beta = 5\%$ of the bilinear moment-curvature relation. The values of the hardening ratio η of the series beam model for each case are listed in the legend of the plot. It is clear that simply matching the slope at a target displacement ductility μ_u without adjusting the plastic flexural capacity of the nonlinear rotation springs does not give very satisfactory results.

For a better match of the nonlinear response of the cantilever beam with a *bilinear rotation spring* in the series beam model we adjust the plastic flexural capacity of the rotation spring to M'_p so as to match not only the slope at a displacement ductility μ_u but also the corresponding moment value M_r at the root of the cantilever. Considering the deformation-force behavior of the series beam model

$$\frac{M_r L}{6EI} + \frac{L}{\eta 6EI} (M_r - M'_p) = v_2$$

and noting that $\mu_u = \mu_v$ and $v_p = \frac{M_p L}{6EI}$ gives

$$\frac{M'_p}{M_p} = \xi(1 + \eta) - \eta \mu_u \quad \rightarrow \quad M'_p = [\xi(1 + \eta) - \eta \mu_u] M_p \quad (6.47)$$

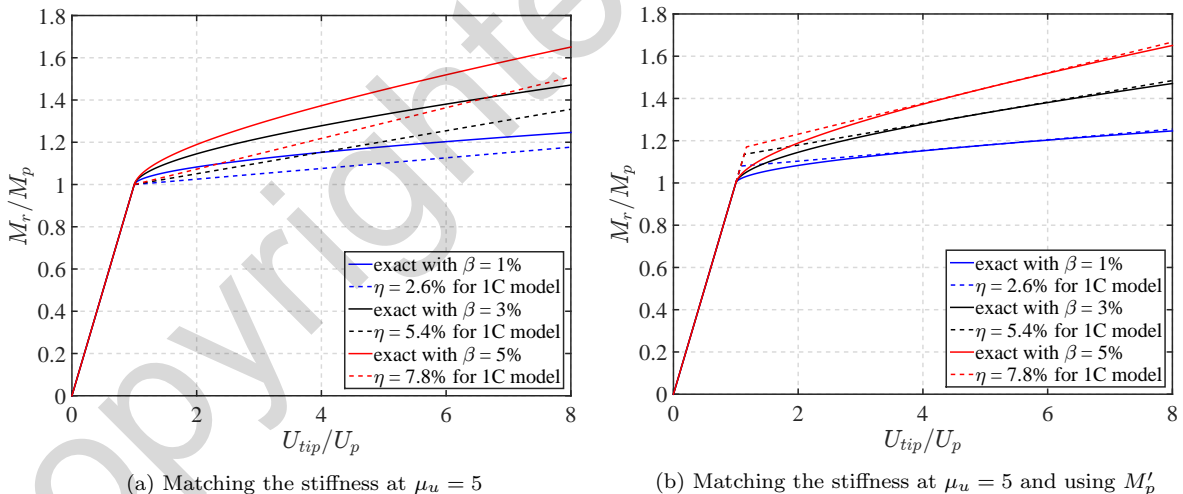


Fig. 6.30: Comparison of series beam model with the exact cantilever response for different calibration schemes

Fig. 6.30(b) compares the resulting response of the series beam model with the exact nonlinear response of the cantilever beam for the hardening ratios $\beta = 1\%$, $\beta = 3\%$ and $\beta = 5\%$ of the bilinear moment-curvature relation. The values of the hardening ratio η of the series beam model for each case are listed in the legend of the plot, while the corresponding values of M'_p are determined from (6.47). They are $M'_p = 1.08M_p$, $M'_p = 1.135M_p$ and $M'_p = 1.17M_p$ for $\beta = 1\%$, $\beta = 3\%$ and $\beta = 5\%$, respectively. We conclude from the comparison that matching the slope of the exact response at a target displacement ductility μ_u and adjusting the plastic flexural capacity of the rotation springs to M'_p allows

the series beam model to represent the exact response of the cantilever beam with very good accuracy for displacement ductilities from 3 to 8.

6.3.8 Series Beam Model with Offset Nonlinear Springs

In this section we generalize the series beam model by placing the nonlinear rotation springs in the interior of the beam element at a distance c_i from the ends in Fig. 6.31.

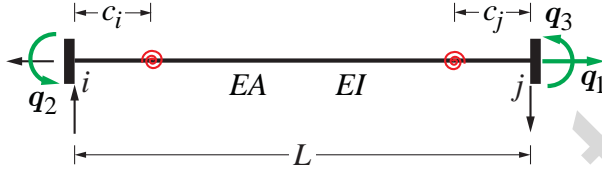


Fig. 6.31: Linear elastic beam with nonlinear rotation springs in series that are offset from the beam ends

Fig. 6.32 shows that the series beam model with offset nonlinear rotation springs is composed of a linear elastic component with axial stiffness EA and flexural stiffness EI in series with a rigid component with two bilinear rigid, linear hardening rotation springs. The rotation springs are placed in the interior of the component at a distance c_i and c_j from ends i and j , respectively. Typically we assume that $c_i = c_j$, but keep the following formulation general so as to facilitate later extensions of the model.

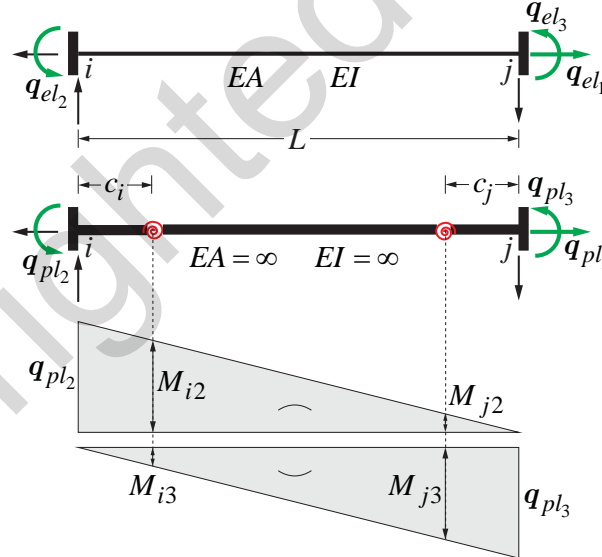


Fig. 6.32: Components of series beam model with offset nonlinear springs and moment distribution

The rigid, linear hardening rotation springs activate only when the moment $M(x)$ exceeds the plastic flexural capacity M_p at the spring location. The linear hardening response of each rotation spring is described with the hardening stiffness ratio η relative to the stiffness $\frac{6EI}{L}$ of the linear elastic beam element under anti-symmetric bending. We assume that the rotation springs have the same hardening stiffness ratio η .

The governing relations for the flexural contribution of the series beam model with offset nonlinear springs are the same as for any series model

$$\begin{aligned}\mathbf{q}_{el} &= \mathbf{q}_{pl} = \mathbf{q}_b \\ \mathbf{v}_b &= \mathbf{v}_{el} + \mathbf{v}_{pl} \\ \mathbf{f}_b &= \mathbf{f}_{el} + \mathbf{f}_{pl}\end{aligned}$$

with subscript *el* denoting the variables of the elastic component, subscript *pl* the variables of the plastic component, and subscript *b* the flexural variables of the beam model. As was the case with the series beam model of the preceding section, the axial response is linear elastic and uncoupled from the flexural response. It is denoted with subscript *a*.

The governing relations of the plastic component depend on setting up an equilibrium relation between the moments M_i and M_j at the rotation springs closest to end *i* and end *j*, respectively, and the basic forces \mathbf{q}_{pl} of the component with bilinear rotation springs. Because the moment distribution is linear in the absence of element loading, this equilibrium relation can be readily set up with the help of Fig. 6.32. It is

$$\begin{aligned}M_i &= (\chi_i - 1)\mathbf{q}_{pl_2} + \chi_i\mathbf{q}_{pl_3} & \rightarrow \begin{pmatrix} M_i \\ M_j \end{pmatrix} &= \mathbf{b}_{pl}\mathbf{q}_{pl} \\ M_j &= -\chi_j\mathbf{q}_{pl_2} + (1 - \chi_j)\mathbf{q}_{pl_3}\end{aligned}$$

with the force influence or internal force interpolation matrix \mathbf{b}_{pl} equal to

$$\mathbf{b}_{pl} = \begin{bmatrix} (\chi_i - 1) & \chi_i \\ -\chi_j & (1 - \chi_j) \end{bmatrix} \quad \text{with} \quad \chi_i = \frac{c_i}{L} \quad \chi_j = \frac{c_j}{L} \quad (6.48)$$

The kinematic relation for the component with bilinear rotation springs is then set up with the principle of complementary virtual work

$$\mathbf{v}_{pl} = \mathbf{b}_{pl}^T \begin{pmatrix} \theta_{ri} \\ \theta_{rj} \end{pmatrix}$$

where θ_r is the rotation of the bilinear spring that depends on the bending moment $M(x)$ at the location.

The flexibility matrix of the component with bilinear rotation springs then becomes

$$\mathbf{f}_{pl} = \mathbf{b}_{pl}^T \begin{bmatrix} \frac{r_i L}{6\eta EI} & 0 \\ 0 & \frac{r_j L}{6\eta EI} \end{bmatrix} \mathbf{b}_{pl}$$

where the activation switch r is 1 only when the moment $M(x)$ exceeds the plastic flexural capacity M_p at the location of the corresponding rotation spring. Substituting the force interpolation matrix \mathbf{b}_{pl} from (6.48) gives for the flexibility matrix \mathbf{f}_{pl}

$$\mathbf{f}_{pl} = \frac{r_i L}{6\eta EI} \begin{bmatrix} (\chi_i - 1)^2 & (\chi_i - 1)\chi_i \\ \chi_i(\chi_i - 1) & \chi_i^2 \end{bmatrix} + \frac{r_j L}{6\eta EI} \begin{bmatrix} (-\chi_j)^2 & -\chi_j(1 - \chi_j) \\ -(1 - \chi_j)\chi_j & (1 - \chi_j)^2 \end{bmatrix}$$

Setting $c_i = c_j = c$ simplifies the flexibility matrix to

$$\begin{aligned}\mathbf{f}_{pl} &= \frac{r_i L}{6\eta EI} \begin{bmatrix} (\chi - 1)^2 & (\chi - 1)\chi \\ \chi(\chi - 1) & \chi^2 \end{bmatrix} + \frac{r_j L}{6\eta EI} \begin{bmatrix} (-\chi)^2 & -\chi(1 - \chi) \\ -(1 - \chi)\chi & (1 - \chi)^2 \end{bmatrix} \\ &= \frac{r_i L}{6\eta EI} \begin{bmatrix} (1 - \chi)^2 & (1 - \chi)\chi \\ \chi(1 - \chi) & \chi^2 \end{bmatrix} + \frac{r_j L}{6\eta EI} \begin{bmatrix} \chi^2 & \chi(\chi - 1) \\ (\chi - 1)\chi & (1 - \chi)^2 \end{bmatrix}\end{aligned}$$

The flexural flexibility matrix \mathbf{f}_{pl} of the component with bilinear rotation springs is now coupled so that yielding of the spring near end i affects the deformation at the opposite end j and vice versa. This improves the accuracy of the series beam model under bending moment distributions that are not anti-symmetric, as will be shown in the evaluation studies of the different beam models. *By contrast, the flexibility matrix \mathbf{f}_{pl} of the plastic component of the series beam with nonlinear springs at its ends is uncoupled*, as is readily concluded from (6.42).

The tangent flexural flexibility matrix of the series beam with offset nonlinear rotation springs is

$$\mathbf{f}_b = \mathbf{f}_{el} + \mathbf{f}_{pl} = \frac{L}{6EI} \begin{bmatrix} 2 & -1 \\ -1 & 2 \end{bmatrix} + \frac{r_i L}{6\eta EI} \begin{bmatrix} (1-\chi)^2 & (\chi-1)\chi \\ \chi(\chi-1) & \chi^2 \end{bmatrix} + \frac{r_j L}{6\eta EI} \begin{bmatrix} \chi^2 & \chi(\chi-1) \\ (\chi-1)\chi & (1-\chi)^2 \end{bmatrix} \quad (6.49)$$

under the assumption that $c_i = c_j = c$. The flexural stiffness matrix \mathbf{k}_b is the inverse of \mathbf{f}_b .

6.3.8.1 Calibration

The series beam model with offset nonlinear springs has two parameters for calibration: the hardening ratio η and the relative offset value χ of the nonlinear spring. We can, therefore, select the parameters by matching the end moment value M_r and the tangent slope of the exact force-deformation relation for a given displacement ductility μ_u .

The equation for matching the maximum moment M_r is

$$M_r = \frac{M_p}{1-2\chi} + \left(\mu_u - \frac{1}{1-2\chi} \right) \frac{L}{6EI} \left[1 + \frac{1-\beta}{\beta} \left(1 - \frac{1}{\xi^3} \right) \right]^{-1}$$

which upon division of both sides by M_p gives a linear equation for χ

$$\xi = \frac{1}{1-2\chi} + \left(\mu_u - \frac{1}{1-2\chi} \right) \frac{\beta \xi^3}{\xi^3 - 1 + \beta} \quad (6.50)$$

The equation for matching the slope at a particular value of ξ is

$$\eta = \frac{\beta}{1-\beta} \frac{\xi^3}{\xi^3 - 1} (1-2\chi)^2 \quad (6.51)$$

For given target displacement ductility μ_u we determine the value of M_r and, therefore, ξ from Fig. 6.16(a). With these values we solve the linear equation in (6.50) for χ and use it along with the other two values in (6.51) to determine the hardening ratio η .

For a target displacement ductility of $\mu_u = 5$ we get the offset values of 0.037, 0.060, 0.073 for χ for a hardening ratio β of the moment-curvature relation of the exact response equal to 1%, 3%, 5%, respectively. The corresponding hardening ratio values for the nonlinear hardening spring are listed in the legend of Fig. 6.33, which compares the response of the series beam model with offset nonlinear springs with the exact nonlinear response of the cantilever of length $L' = \frac{L}{2}$, where L is the length of the series beam element. The agreement of the series beam model with offset nonlinear springs with the exact response of a cantilever beam with bilinear moment-curvature relation in Fig. 6.33 is excellent.

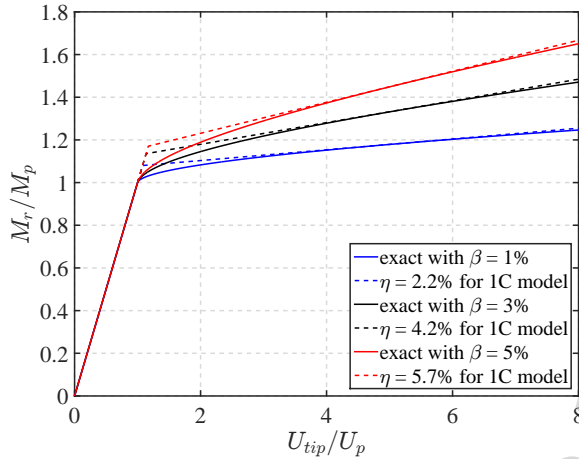


Fig. 6.33: Comparison of series beam model with offset nonlinear springs with the exact cantilever response

6.3.9 Conclusions about Beam Models

The series model is the most rational way of representing the inelastic behavior of frame members without interaction of axial force and bending moment. This conclusion results from the fact that the exact inelastic response of the cantilever beam was shown to consist of an elastic and an inelastic contribution *in series*.

In the simplest form of the series model with a rotation spring at each element end, it has a single parameter, the hardening ratio η . The ratio is expressed with respect to the elastic stiffness $\frac{6EI}{L}$ of an elastic beam *under anti-symmetric curvature distribution*. The comparison of this beam with the exact response reveals its limited accuracy. Much better results can be obtained by introducing a second parameter, the offset c of the nonlinear spring location relative to the corresponding element end. With the second parameter we can match the slope and the end moment value at a target displacement ductility, and thus obtain results of very good accuracy *under anti-symmetric bending*.

The series beam model with a spring at each end is very economical and shows good agreement with the actual response of hardening members, if the location of the nonlinear spring is offset by a certain amount from the end. An additional nonlinear spring can be inserted at the end to represent the nonlinear effect of a semi-rigid connection and the pull-out of anchored reinforcing bars from the beam-to-column joint. The state determination of such a model with an elastic element and four nonlinear springs is the same as for the simple series model.

A significant benefit of the series beam model over the parallel beam model is that the former can account for the effect of element loading, but this subject is beyond the scope of this text.

The main limitation of the series model with a single offset spring at each element end is the need for calibration. Since the calibration is performed for the ideal case of anti-symmetric flexure, the response of the model may not match the exact behavior of a member under non-antisymmetric bending. To this end we evaluate the response of the parallel beam model and the series beam model with offset nonlinear springs by comparing it with the exact response of a girder under general moment distribution.

6.3.10 Evaluation of Beam Models under General Moment Distributions

In this section we evaluate the ability of the two-component beam model and the series beam model with nonlinear rotation springs to represent the exact nonlinear response of a girder with bilinear moment-curvature relation under general bending moment distributions.

The parameters of each model are first calibrated against the exact nonlinear response of the girder of length L under anti-symmetric bending. Because this case is identical with the response of a cantilever beam of length $L' = \frac{L}{2}$, we can directly use the calibration results from the preceding sections. For a bilinear moment-curvature relation with hardening ratio $\beta = 0.03$ the parameters of the two beam models are selected so as to match the slope and moment of the exact force-deformation relation under anti-symmetric bending for a target displacement ductility μ_u of 5. They are:

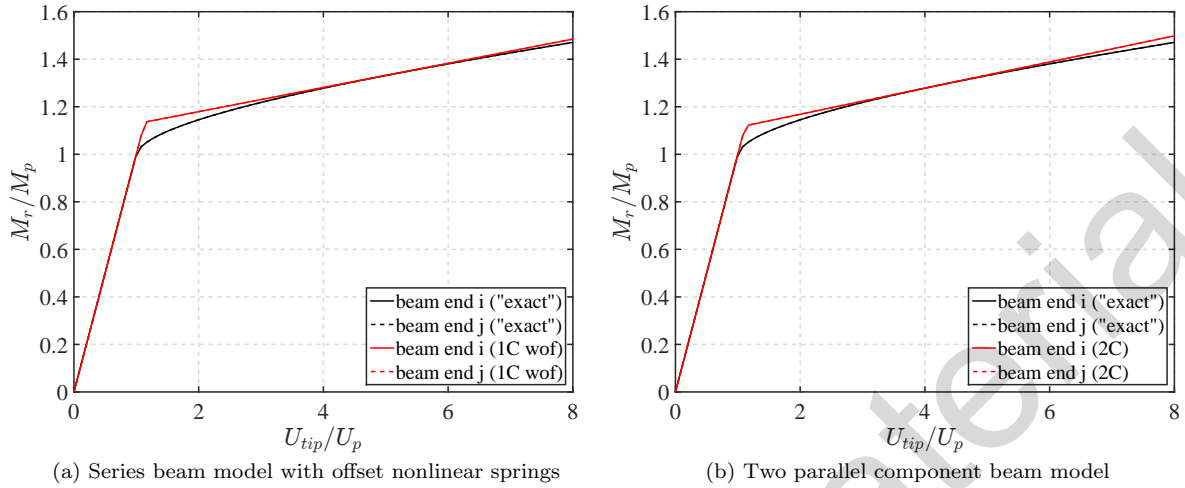
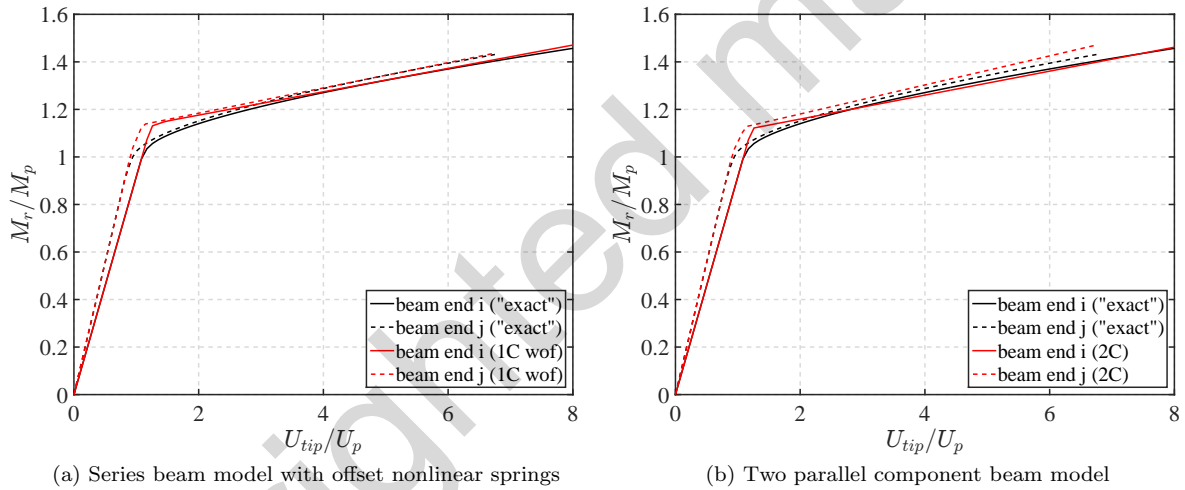
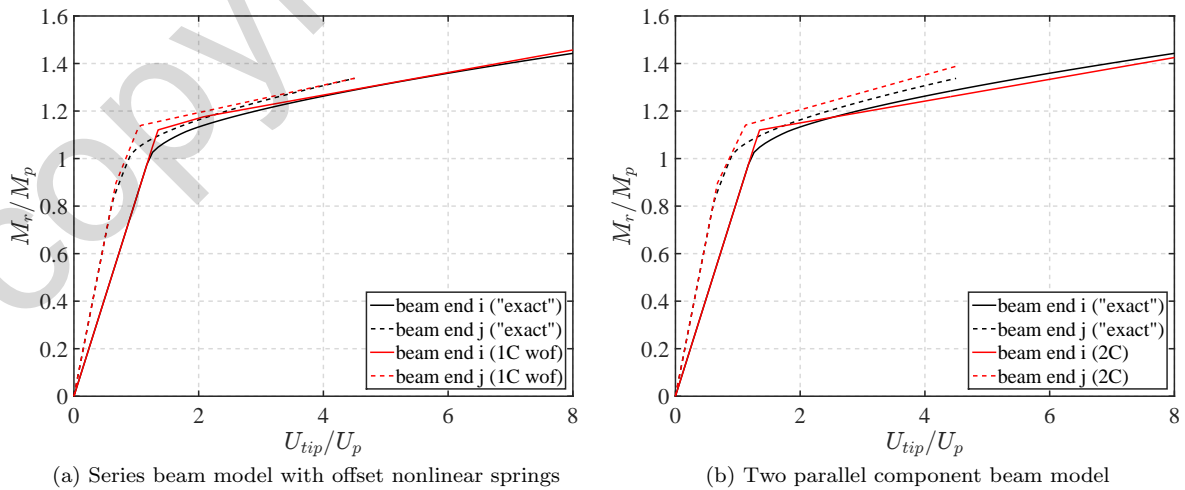
- 1) The two (parallel) component beam model is assigned a plastic moment capacity M'_p equal to $1.13M_p$ and a stiffness hardening ratio γ equal to 0.055 (see Fig. 6.26(b)).
- 2) The series beam model with offset bilinear rotation springs is assigned a stiffness hardening ratio η equal to 0.042. The springs are offset from the ends by the distance $c = 0.060L$ (see Fig. 6.33).

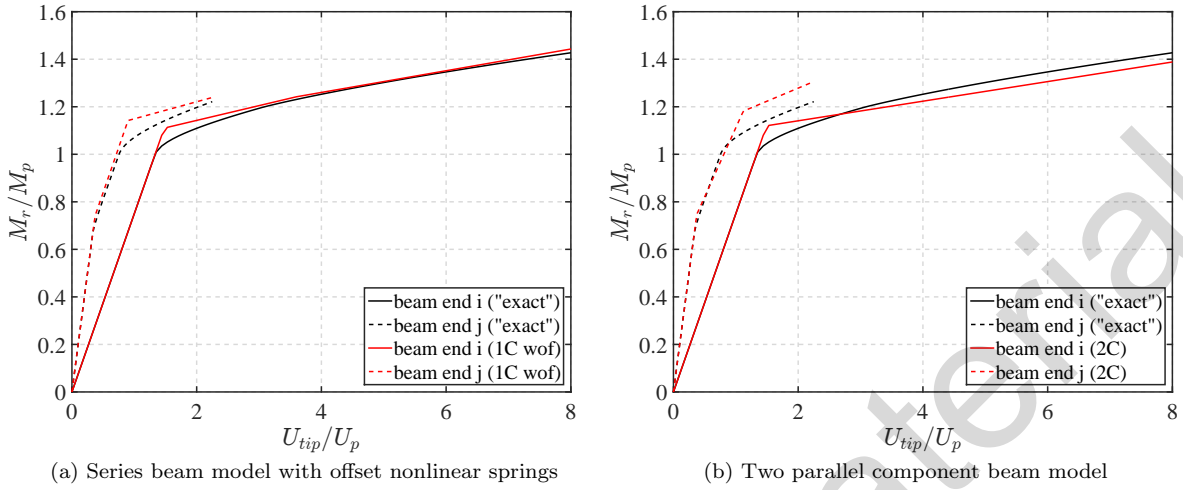
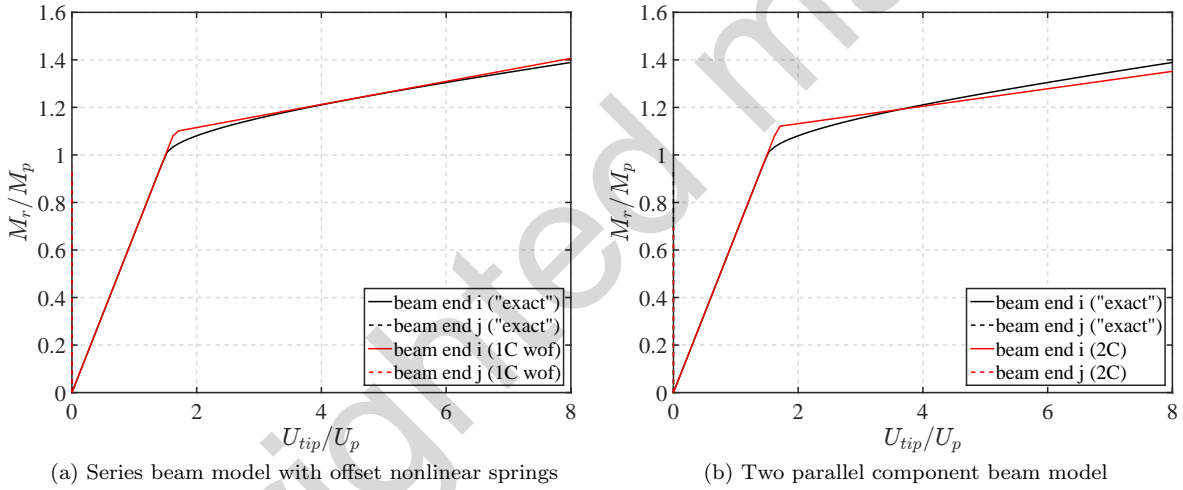
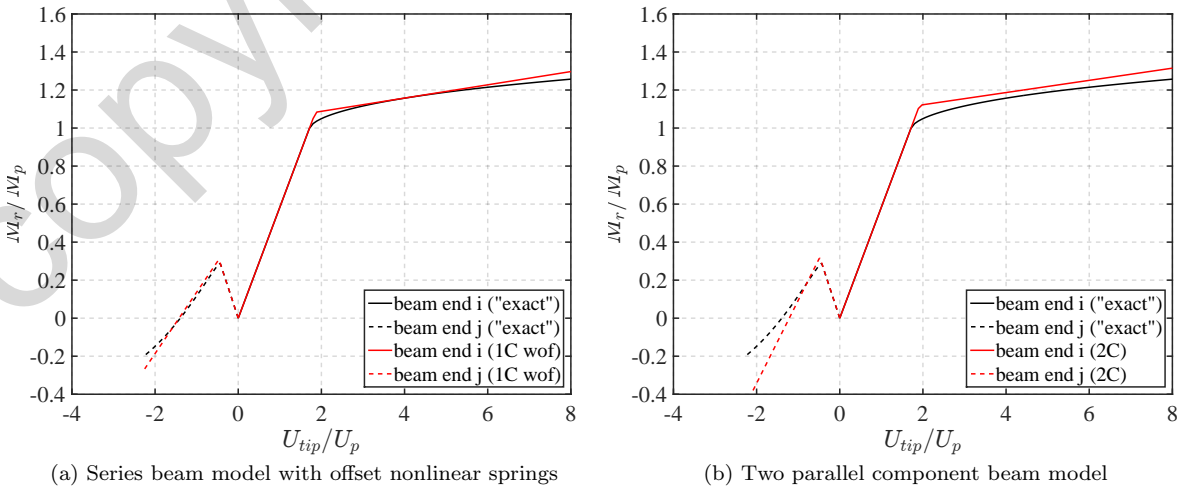
The exact response of the girder with bilinear moment-curvature with hardening ratio $\beta = 0.03$ is then established by integration of the curvature distribution that results from imposed flexural deformations v_i and v_j at the girder ends i and j , respectively. The process uses the state determination of the series model with a linear bending moment distribution. Instead of an analytical solution, a numerical solution with 100 integration points is used for the solution of the kinematic relations in (6.21).

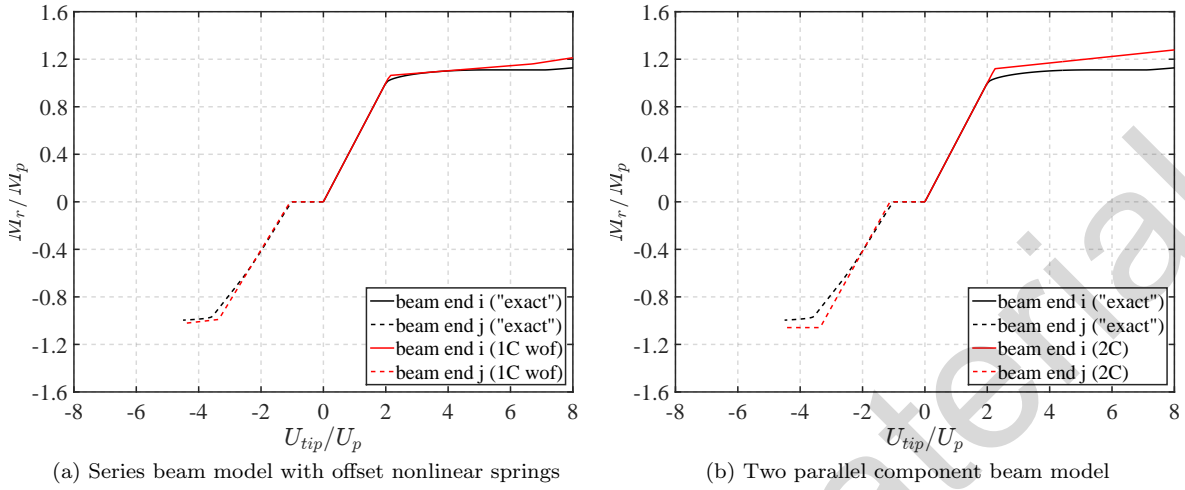
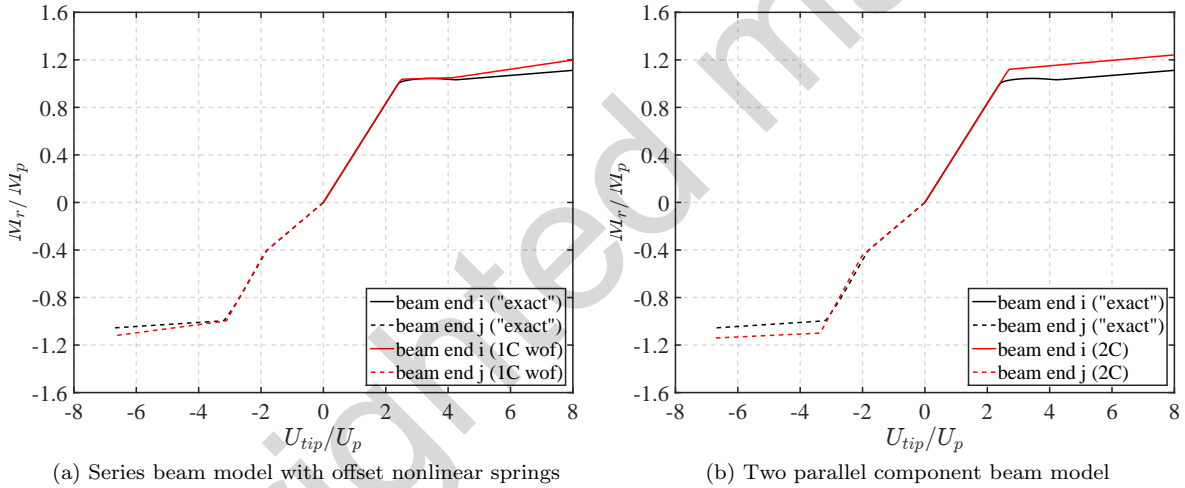
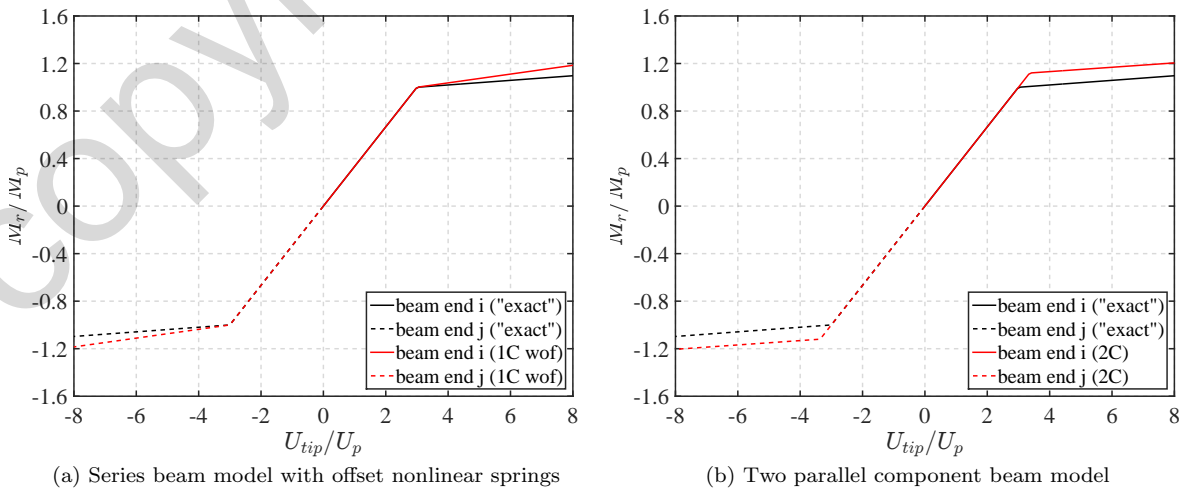
The response of the two beam models is compared with the exact response in Fig. 6.34-Fig. 6.42 for deformation ratios $\rho = v_j/v_i$ ranging from 1 to -1 in increments of 0.25. $\rho = 1$ corresponds to anti-symmetric bending, and $\rho = -1$ corresponds to a uniform moment and curvature distribution.

From the comparison of the two models with the exact response we conclude that while both models agree relatively well with the numerically exact response of the girder with a bilinear moment-curvature relation, the series beam model with offset bilinear springs does consistently much better as the deformation ratio ρ changes from the anti-symmetric bending condition to the uniform moment and curvature distribution. In fact, the accuracy of the series beam model is rather impressive on consideration of its simplicity and relative computational efficiency. An important reason for this is the coupling of the plastic response of the model through the offset of the nonlinear rotation springs from the element ends, which the two parallel component beam model cannot account for.

It is worth noting the post-yield force overestimation by the two component beam model for negative values of the deformation ratio ρ . This is caused by assigning a fictitious plastic moment M'_p to the two-component model for improving its accuracy under anti-symmetric bending. Because M'_p is larger than the actual plastic flexural capacity M_p of the girder, the two component model overestimates the strength by 10-15% under end deformations that induce moments of the same sign along the entire girder.

Fig. 6.34: Comparison of beam models with exact response for $\rho = v_j/v_i = 1$ Fig. 6.35: Comparison of beam models with exact response for $\rho = v_j/v_i = 0.75$ Fig. 6.36: Comparison of beam models with exact response for $\rho = v_j/v_i = 0.50$

Fig. 6.37: Comparison of beam models with exact response for $\rho = v_j/v_i = 0.25$ Fig. 6.38: Comparison of beam models with exact response for $\rho = v_j/v_i = 0$ Fig. 6.39: Comparison of beam models with exact response for $\rho = v_j/v_i = -0.25$

Fig. 6.40: Comparison of beam models with exact response for $\rho = v_j/v_i = -0.50$ Fig. 6.41: Comparison of beam models with exact response for $\rho = v_j/v_i = -0.75$ Fig. 6.42: Comparison of beam models with exact response for $\rho = v_j/v_i = -1$

copyrighted material